RTO-MP-36
AC/323(AVT)TP/17

RTO-MP-36

NORTH ATLANTIC TREATY ORGANIZATION

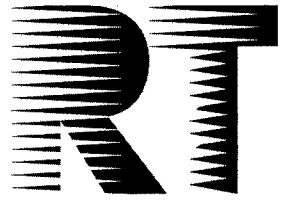

RESEARCH AND TECHNOLOGY ORGANIZATION
BP 25, 7 RUE ANCELLE, F-92201 NEUILLY-SUR-SEINE CEDEX, FRANCE

RTO MEETING PROCEEDINGS 36

Structural Aspects of Flexible Aircraft Control

(les Aspects structuraux du contrôle actif et flexible des aéronefs)

Papers presented at the Specialists' Meeting of the RTO Applied Vehicle Technology Panel (AVT) held in Ottawa, Canada, 18-20 October 1999.

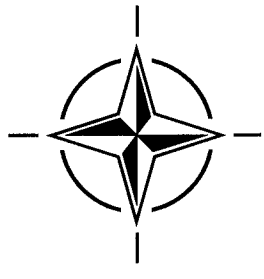

Published May 2000

Distribution and Availability on Back Cover

The Research and Technology Organization (RTO) of NATO

RTO is the single focus in NATO for Defence Research and Technology activities. Its mission is to conduct and promote cooperative research and information exchange. The objective is to support the development and effective use of national defence research and technology and to meet the military needs of the Alliance, to maintain a technological lead, and to provide advice to NATO and national decision makers. The RTO performs its mission with the support of an extensive network of national experts. It also ensures effective coordination with other NATO bodies involved in R&T activities.

RTO reports both to the Military Committee of NATO and to the Conference of National Armament Directors. It comprises a Research and Technology Board (RTB) as the highest level of national representation and the Research and Technology Agency (RTA), a dedicated staff with its headquarters in Neuilly, near Paris, France. In order to facilitate contacts with the military users and other NATO activities, a small part of the RTA staff is located in NATO Headquarters in Brussels. The Brussels staff also coordinates RTO's cooperation with nations in Middle and Eastern Europe, to which RTO attaches particular importance especially as working together in the field of research is one of the more promising areas of initial cooperation.

The total spectrum of R&T activities is covered by 7 Panels, dealing with:

- SAS Studies, Analysis and Simulation
- SCI Systems Concepts and Integration
- SET Sensors and Electronics Technology
- IST Information Systems Technology
- AVT Applied Vehicle Technology
- HFM Human Factors and Medicine
- MSG Modelling and Simulation

These Panels are made up of national representatives as well as generally recognised 'world class' scientists. The Panels also provide a communication link to military users and other NATO bodies. RTO's scientific and technological work is carried out by Technical Teams, created for specific activities and with a specific duration. Such Technical Teams can organise workshops, symposia, field trials, lecture series and training courses. An important function of these Technical Teams is to ensure the continuity of the expert networks.

RTO builds upon earlier cooperation in defence research and technology as set-up under the Advisory Group for Aerospace Research and Development (AGARD) and the Defence Research Group (DRG). AGARD and the DRG share common roots in that they were both established at the initiative of Dr Theodore von Kármán, a leading aerospace scientist, who early on recognised the importance of scientific support for the Allied Armed Forces. RTO is capitalising on these common roots in order to provide the Alliance and the NATO nations with a strong scientific and technological basis that will guarantee a solid base for the future.

Published May 2000

ISBN 92-837-0014-7

Printed by Canada Communication Group Inc.
(A St. Joseph Corporation Company)
45 Sacré-Cœur Blvd., Hull (Québec), Canada K1A 0S7

Structural Aspects of Flexible Aircraft Control

(RTO MP-36)

Executive Summary

The papers presented at this meeting dealt with the state-of-the-art, underlying theory of the influencing factors and characteristics, and existing capabilities of Nations to integrate various factors during the design stage while observing the effects on aircraft layout and behaviour.

Aircraft are inherently flexible and flexibility can be used to advantage as a design feature for improved performance. Flexible aircraft are subject to interaction between flight mechanics, structural dynamics, and flight control system dynamics. Aeroservoelastic instability can lead to disastrous failures in aircraft as was recently the case for several fighter aircraft. These problems are very similar to flutter accidents which occurred two decades ago. Limit cycle oscillations could restrict fighter aircraft performance particularly those with various store configurations. This problem is most relevant to air-to-ground attack and fighter aircraft.

Flight control systems increasing the stability, or the active control of low damped or unstable aircraft with rigid or flexible modes, have additional coupling effects on flight mechanics and structural responses. These interactions must be considered when designing the airframe structure, flight control systems, and elastic alleviation systems in order to avoid bad handling qualities and bad ride comfort.

An integral analysis of flight mechanics, flight control, static and dynamic loads, flutter and aeroservoelasticity has to be carried out. Therefore, a compatible mathematical model of the coupled dynamics of flight mechanics, flight control, and structural dynamics must be established. Such models (using the time and frequency domain descriptions) are available in the military aircraft industry to assist in the design and clearance of flight control systems. However, the design of flight control systems and structures is usually performed separately. As such, an integrated interdisciplinary design of flight control systems is generally not feasible due to its complexity. At present, it is only used to improve the control system and the structural capability of components in critical areas.

How to improve the design methods used in the development of military fighter aircraft, and its use in transport aircraft design applications was an outcome of this meeting.

les Aspects structuraux du contrôle actif et flexible des aéronefs

(RTO MP-36)

Synthèse

Les communications présentées lors de cette réunion ont examiné l'état actuel des connaissances dans ce domaine, les théories régissant les facteurs déterminants et les caractéristiques et les capacités actuelles des pays membres de l'OTAN à incorporer ces différents facteurs dans le processus de conception, ainsi que les effets sur la configuration et le comportement des aéronefs.

Les aéronefs sont intrinsèquement flexibles et cette flexibilité peut être mise à profit au stade de la conception pour améliorer leurs performances. Les aéronefs flexibles sont sujets à des interactions entre la mécanique du vol, la dynamique structurale et la dynamique des systèmes de pilotage. L'instabilité aéroservoélastique peut conduire à une défaillance catastrophique de l'avion, comme il a été démontré récemment pour plusieurs avions de combat. Ces problèmes ressemblent aux accidents dûs au flottement, survenus il y a deux décennies. Il se peut que le rayon d'action des avions de combat soit limité par les oscillations limites, et surtout dans le cas de certaines configurations d'emports. Ce problème affecte particulièrement les avions de combat d'attaque au sol.

Les systèmes de pilotage privilégiant l'augmentation de la stabilité, ou le contrôle actif d'aéronefs instables ou aux oscillations faiblement amorties ayant des modes rigides ou flexibles peuvent créer des effets de couplage supplémentaires affectant la mécanique du vol et les réponses structurales. Ces interactions doivent être prises en compte lors de la conception de la cellule, des systèmes de commande de vol et des systèmes d'allègement élastique afin d'éviter la détérioration des qualités de vol et du confort du pilote.

Il y a lieu de procéder à une analyse intégrale de la mécanique du vol, des systèmes de pilotage, des charges statiques et dynamiques, du flottement et de l'aéroservoélasticité. Il est, par conséquent, nécessaire d'établir un modèle mathématique compatible de la dynamique couplée de la mécanique du vol, des systèmes de pilotage et de la dynamique structurale. De tels modèles (qui intègrent la description du domaine du temps et du domaine de fréquence), sont à la disposition de l'industrie aéronautique militaire pour la conception et l'homologation des systèmes de pilotage. Cependant, les systèmes de commande de vol et les structures sont, en principe, conçus séparément. Par conséquent, la conception interdisciplinaire intégrée des systèmes de commande de vol n'est en général guère faisable en raison de sa complexité. A l'heure actuelle, cette approche est utilisée uniquement pour améliorer le système de commande et la capacité structurale de certains composants critiques.

Les conclusions de cette réunion permettent d'envisager l'amélioration des méthodes de conception mises en œuvre dans le développement des avions de combat et de les appliquer à la conception des avions de transport militaires.

Contents

SESSION II: ACTIVE CONTROL OF FLEXIBLE STRUCTURE I

SESSION III: ACTIVE CONTROL OF FLEXIBLE STRUCTURE II

† Paper not available at time of printing.

Theme

Aircraft are inherently flexible and flexibility can be used to advantage as a design feature for improved performance. Aeroservoelastic instability can also lead to a catastrophic failure of the aircraft as was shown lately on a F117 stealth aircraft accident similar to flutter accidents two decades ago. Limit cycle oscillations may placard fighter airplanes especially with various store configurations. This is most true to military transport and fighter aircraft. Flexible aircraft are subject to interactions between flight mechanics, structural dynamics and flight control system dynamics. The Meeting will look into the state of the art treating as well the underlying theory of the influencing factors and characteristics as also the existing capabilities of Nations for integrating the various factors in the design stage and the effects on aircraft layout and behaviour.

Flight control systems for the augmentation of stability or for the active control of low damped or unstable aircraft with rigid or flexible modes have additional coupling effects on flight mechanics and structural responses. These interactions have to be taken into consideration for the design of the airframe structure, flight control system and elastic alleviation systems in order to avoid bad handling qualities as well as bad ride comfort.

An integral analysis of flight mechanics, flight control, static and dynamic loads, flutter and aero-servo-elasticity has to be carried out. Therefore, a compatible mathematical model of the coupled dynamics of flight mechanics, flight control, and structural dynamics must be established. Such models (using the time and frequency domain description) are available in the military aircraft industry to assist in the design and clearance of flight control systems. However, the design of flight control systems and structures is in principle performed separately and integrated interdisciplinary design of flight control systems is in general not yet feasible due to its complexity. At present, it is used only to improve the control system and the structural capability of components in critical areas.

How the design methods used in the development of military fighter aircraft can be improved, and applied to transport aircraft design applications will be an outcome of this meeting.

Thème

Les aéronefs sont par nature flexibles et cette flexibilité peut être mise à profit au stade de la conception pour améliorer les performances. L'instabilité aéroservoélastique peut également conduire à une défaillance catastrophique de l'avion, comme il a été démontré récemment par l'accident du bombardier furtif F117, qui ressemble aux accidents dûs au flottement, survenus il y a deux décennies. Il se peut que le rayon d'action des avions de combat soit limité par les oscillations limites, et surtout dans le cas de certaines configurations d'emports. Ces phénomènes affectent particulièrement les avions de combat et de transport militaires. En raison de leur flexibilité, ces aéronefs sont sujets à des interactions entre la mécanique du vol, la dynamique structurale et la dynamique des systèmes de commande de vol. La réunion examinera l'état actuel des connaissances dans ce domaine, et traitera également des théories régissant les facteurs déterminants et les caractéristiques. Elle étudiera également les capacités actuelles des pays membres de l'OTAN à incorporer ces différents facteurs dans le processus de conception, ainsi que les effets sur la configuration et le comportement des aéronefs.

Les systèmes de commande de vol privilégiant soit l'augmentation de la stabilité, soit le contrôle actif d'aéronefs instables ou aux oscillations faiblement amorties ayant des modes rigides ou flexibles, peuvent créer des effets de couplage supplémentaires affectant la mécanique du vol et les réponses structurales. Ces interactions doivent être prises en compte lors de la conception de la cellule, des systèmes de commande de vol et des systèmes d'allègement élastique afin d'éviter la détérioration des qualités de vol et du confort du pilote.

Il y a lieu de procéder à une analyse intégrale de la mécanique du vol, des systèmes de pilotage, des charges statiques et dynamiques, du flottement et de l'aéroservoélasticité. Il est, par conséquent, nécessaire d'établir un modèle mathématique compatible de la dynamique couplée de la mécanique du vol, des systèmes de commande de vol et de la dynamique structurale. De tels modèles (qui intègrent la description du domaine du temps et du domaine de fréquence), sont à la disposition de l'industrie aéronautique militaire pour la conception et l'homologation des systèmes de commande de vol. Cependant, les systèmes de commande de vol et les structures sont, en principe, conçus séparément, et la conception interdisciplinaire intégrée des systèmes de commande de vol n'est guère encore faisable en raison de sa complexité. A l'heure actuelle, cette approche est utilisée uniquement pour améliorer le système de commande et la capacité structurale de certains composants critiques.

Les conclusions de cette réunion devraient permettre d'améliorer les méthodes de conception mises en œuvre dans le développement des avions de combat et de les appliquer à la conception des avions de transport militaires.

Publications of the RTO Applied Vehicle Technology Panel

MEETING PROCEEDINGS (MP)

Design for Low Cost Operation and Support
MP-37, Spring 2000

Structural Aspects of Flexible Aircraft Control
MP-36, May 2000

Aerodynamic Design and Optimization of Flight Vehicles in a Concurrent Multi-Disciplinary Environment
MP-35, Spring 2000

Gas Turbine Operation and Technology for Land, Sea and Air Propulsion and Power Systems (Unclassified)
MP-34, Spring 2000

New Metallic Materials for the Structure of Aging Aircraft
MP-25, April 2000

Small Rocket Motors and Gas Generators for Land, Sea and Air Launched Weapons Systems
MP-23, April 2000

Application of Damage Tolerance Principles for Improved Airworthiness of Rotorcraft
MP-24, January 2000

Gas Turbine Engine Combustion, Emissions and Alternative Fuels
MP-14, June 1999

Fatigue in the Presence of Corrosion
MP-18, March 1999

Qualification of Life Extension Schemes for Engine Components
MP-17, March 1999

Fluid Dynamics Problems of Vehicles Operation Near or in the Air-Sea Interface
MP-15, February 1999

Design Principles and Methods for Aircraft Gas Turbine Engines
MP-8, February 1999

Airframe Inspection Reliability under Field/Depot Conditions
MP-10, November 1998

Intelligent Processing of High Performance Materials
MP-9, November 1998

Exploitation of Structural Loads/Health Data for Reduced Cycle Costs
MP-7, November 1998

Missile Aerodynamics
MP-5, November 1998

EDUCATIONAL NOTES

Measurement Techniques for High Enthalpy and Plasma Flows
EN-8, April 2000

Development and Operation of UAVs for Military and Civil Applications
EN-9, April 2000

Planar Optical Measurements Methods for Gas Turbine Engine Life
EN-6, September 1999

High Order Methods for Computational Physics (published jointly with Springer-Verlag, Germany)
EN-5, March 1999

Fluid Dynamics Research on Supersonic Aircraft
EN-4, November 1998

Integrated Multidisciplinary Design of High Pressure Multistage Compressor Systems
EN-1, September 1998

TECHNICAL REPORTS

Recommended Practices for Monitoring Gas Turbine Engine Life Consumption
TR-28, April 2000

Verification and Validation Data for Computational Unsteady Aerodynamics
TR-26, Spring 2000

A Feasibility Study of Collaborative Multi-facility Windtunnel Testing for CFD Validation
TR-27, December 1999

Specialists' Meeting Programme Committee

Programme Committee Chairmen

Prof.Dr. O. SENSBURG
DaimlerChrysler Aerospace AG
Military Aircraft MT2
P O Box 80 11 60
81663 Munich
E/mail: wolfgang.luber@m.dasa.de

Mr. J. CHOPLIN
Dassault Aviation
Direction Générale Technique
78, Quai Marcel Dassault, Cedex 300
92550 Saint-Cloud
E/M:jean.choplin@dassault.aviation.fr

BELGIUM
Prof. Dr. Ing. J. VANTOMME
Royal Military Academy (RMA)
Avenue de la Renaissance, 30
1000 Brussels

CANADA
Mr. C. PERRON
Bombardier Inc. Canadair
Military Aircraft Division
10,000 Cargo A-4 Street
Montreal International Airport
Mirabel, Québec I7N 1H3

FRANCE
Mr. J. GROUAS
Aérospatiale
316, route de Bayonne
31060 Toulouse Cedex

Mr. M. LABARRERE
ONERA/CERT/DSAC
BP 4025
2, Avenue Edouard Belin
31055 Toulouse Cedex 4

GERMANY
Dr. J. BECKER
DaimlerChrysler Aerospace AG
Military Aircraft MT2
Postfach 80 11 60
81663 Munich

Dr. Ing. P. HAMEL
PO Box 3267
38022 Braunschweig

Dr. H. HÖNLINGER
DLR, Institut für Aeroelastik
Bunsenstrasse 10
D-37073 Göttingen

ITALY
Prof. A. SALVETTI
Universita di Pisa, Dipartimento di
Ingegneria Aerospaziale
Via Diotisalvi 2
56126 Pisa

NETHERLANDS
Ir. J. MEIJER
National Aerospace Lab. NLR
Dept. AE
Anthony Fokkerweg 2
1059 CM Amsterdam

SPAIN
Dr. E. SANCHIZ
Div. de Estructuras y Materiales
Laboratorio de Diseno y Analisis
Estructural – INTA
Carretera Torrejon Ajalvir, Km.4
28850 Torrejon de Ardoz (Madrid)

TURKEY
Prof. Dr. E. SELÇUK
Metallurgical Eng. Dept.
Middle East Technical University
06531 Ankara

UNITED KINGDOM
WG CDR Chamberlain
W.G.A.S.I., B Block, Room B009
RAF Wyton, P.O. Box 7, Huntington
Cambridgeshire PE17 2EA

UNITED STATES
Mr. K.G. BHATIA
Aeroelasticity & Multidisciplinary
Optimization
Boeing Company Airplane Group
P O Box 3707 MS 6H-CJ
Seattle, WA 98124-2207

Mr. J.A. ELLIS
LMTAS
P O Box 748 Mail Zone 2851
Fort Worth, TX 76101

Dr. D. PAUL
Chief Scientist Air Vehicles
Air Force Research Laboratory
AFRL/VA, Bldg 45
2130 8th St., Suite 1
Wright Patterson AFB, OH 45433-7542

Technical Evaluation Report

Terrence A. Weisshaar
Purdue University
1282 Grissom Hall
West Lafayette, IN 47907-3783, USA

This meeting displayed a rich diversity of efforts, projects and people. It is to the credit of the organizers that the sessions were judged to be an overwhelming success. Aeroelasticity has a long and distinguished research and practitioner history dating as far back to at least the early 1920's and perhaps even before. Since then aeronautical history has been strewn with the skeletons of failed aircraft due to aeroelastic problems. Early on, researchers in Britain, France and Germany combined the areas of structures, structural dynamics and unsteady aerodynamics to solve and anticipate problems of flexible aircraft in high-speed flight. Later, others from many nations joined these early efforts, primarily at national laboratories, to solve aeroelastic problems in high-speed flight. Aeroelastic research and contributions have been not only multi-disciplinary but also multi-national. This theme was particularly evident in this conference where twenty-five papers were presented in a program that spanned two days. These papers brought together recognized experts from all RTO members and provided a perspective on current and future problems related to the design and control of flexible aircraft.

Aeroelastic design depends on anticipating and controlling the interaction between the motion of flight vehicles, aerodynamic forces generated by this motion and the relative flexibility of the vehicle compared to the forces generated. The quest for higher speeds, more maneuverability and active control with feedback loops between the control surfaces and measured response has increased the need for accurate design assessment before design plans are finalized. New technology has also brought additional opportunities to intentionally couple together this interaction rather than diminish it to increase some measures of aircraft performance.

There are many classic examples of problems arising because of neglect of coupling between aircraft flexible response and traditional aircraft flight mechanics. These will not be recited here, except to say that until recently, it has not been convenient to treat the fully coupled problem soon enough in the design cycle to defeat design problems or to take advantage of design opportunities. This condition is changing rapidly due to new analytical capabilities such as high-speed analysis and the development of numerical techniques that take advantage of this high speed computing. One has only to look at the development of state-space aerodynamic representations that have largely replace frequency domain techniques, such as the venerable V-g approach as the mainstay of flutter analysis.

However, no matter how good the computational capabilities may be, it still takes a trained specialist to identify problems and ask the proper questions to be answered by analytical treatments. The past decade has brought about a decline in activity related to design of military systems. This decline has resulted in a "graying" of experts in this area and the retirement of many more. The evaluator recently made a list of at least two dozen distinguished contributors who have retired in the United States during the past decade alone. Many of the experts who have retired have not been replaced. Once dominant research establishments have even eliminated aeroelasticity as a major core competency. It was comforting to see that this meeting brought to it several younger practitioners who have distinguished themselves in research in a short time and hold promise for the future.

Three sessions were held and thoughtfully chaired by Messrs. Christian Petiau, Ed Pendleton and Anthony Morris. Although the sessions had the titles Aeroservoelasticity and Active Control of Flexible Structure, the papers presented addressed three distinct themes related to aeroelasticity and control of aeroelastic phenomena: 1) lessons learned, where interesting experiences and valuable learning were discussed; 2) analysis papers with new methods for computing and new results obtained from these methods; and, 3) discussions of new technology that has not yet impacted designs, but which may be valuable for advancing future concepts. In the future we may expect to provide design decision makers with comprehensive, timely information on aeroelastic details of advanced, high performance designs at an earlier time in the design cycle and with considerably higher fidelity than is now possible. Because the papers are available to reader, we will not reproduce abstracts here, but simply summarize the results.

A key feature of several papers was unification of aeroelasticity with flight mechanics and active control. Ed Pendleton observed that flight controls needs to "buy into" aeroelasticity and although the gulf between the two disciplines has been narrowing during the past few years, there is still a major difference between the areas, despite the

fact that they essentially deal with the same type of response phenomena. The theme of encouraging connectivity between flight controls and aeroelasticity was amply illustrated with the paper "Unified Flight Mechanics and Aeroelasticity for Accelerating, Maneuvering, Flexible Aircraft" by Dr. James Olsen. He used his broad experience and keen perspective to formulate simple but useful problems whose solution help to understand the interconnectivity so prevalent in aeroelasticity. Other papers used developments to transform unsteady aerodynamics from the frequency domain to the state-space domain and have blurred the separation between traditional flight control mechanics, structural vibration and unsteady aerodynamics. Emerging technologies such as Unmanned Air Vehicles (UAV's) and smart aircraft provide an opportunity to use aeroelasticity as an asset, not a constraint. With this as a promising theme, it was also noted that aeroelasticity is declining as a core competency at many locations as people retire and are not replaced or replaced by less experienced personnel. One participant observed that there were very few "young faces" in the audience.

The paper "A Unique Design for the Diverging Flexible Vertical Tail" by Sensburg, Schneider, Tishcler and Venkayya presented innovative results for the design of a flexible vertical tail surface. This paper illustrated what can happen if conventional design tradition is challenged by formal optimization and human creativity is then allowed to evolve a design with less weight but with advantageous flexibility. It also provided an excellent example of how two international groups can collaborate on innovative design. Similarly, the paper "The Impact of Active Aeroelastic Wing Technology on Conceptual Aircraft Design" by Flick, Love and Zink describes the use of static aeroelastic controlled deformations to improve maneuverability. This Active Aeroelastic Wing concept represents an example of creative use of aeroelasticity, as does the paper "Active Aeroelastic Aircraft and its Impact on Structure and Flight Control Systems Design" by Schweiger and Krammer. The latter paper was an excellent review to focus attention on fundamental problem and payoffs and describe the history of this area.

Both of these papers provided valuable insights into uses and strategies for acceptance and exploitation of flexibility and aeroelasticity into the design arena. The paper "NASA's Aircraft Morphing Research for Active Aeroelastic Control" by McGowan, Horta, Harrison and Raney provided a glimpse into the future when active materials will be used for control of small designs for special purposes. This paper reviewed an area called "smart wing research" that promises to produce creative new concepts. These researchers are recognized as among the most forward looking individuals in the active aeroelasticity advocacy community. Finally, "Design Aspects of the Elastic Trailing Edge for an Adaptive Wing" by Monner, Sachau and Breibach reviews the use of camber control to create lift for maneuvering flight. It presents a novel alternative to articulated control surfaces.

Later, during a panel session, a participant observed that "legacy projects provide income, but won't use new ideas unless there is a compelling reason." New developments face barriers to acceptance; overcoming these barriers requires understanding by non-expert users about how theoretical developments can benefit their commercial products. It is also a major task to certify a new concept and have it make an impact on the commercial product.

Several papers amply demonstrated the state of improved, advanced modeling capabilities. "Aeroelastic Modeling, Analysis and Design Techniques for Transport Aircraft" by Baker, Goggin and Winther demonstrated how far we have come during the past two decades in reliable modeling of aeroelastic aircraft. They surveyed the techniques used at the Boeing Company to develop aeroservoelastic math models for control system design of transport aircraft. Similarly, the paper "Flutter Analysis Method in the Presence of Mechanical Play and Experimental Verification" by Journee, Petiau and Nicot showed the degree to which we can now model complex phenomena and verify accuracy. They also shared a valuable lesson learned for the certification of the Falcon jet aircraft. After all these years, free-play of surfaces continues to be an important problem in aircraft design and operation.

Petiau, Garrigues and Nicot discussed the extraction of information from flight tests for verification and understanding in their paper "Method of Mathematical Identification of Unsteady Airloads from Flight Measurements, Experimental Verification." This discussion was based on features developed at Dassault within the framework of ELFINI. These analytical methods provide benchmarks to judge other developments. Anna McGowan, a panelist at the conclusion of the sessions observed that "more flexible can also be more nonlinear." In the paper "Nonlinear Effects of Loads and Large Deformations on Complete Aircraft Normal Modes" Oliver, Climent and Rosich showed the accurate depiction of nonlinear effects for large aircraft. They address the difficulties of assessing the validity of ground vibration test (GVT) when nonlinearities are present. The differences between in-flight conditions and test conditions are sometimes important. Their results, for a large transport, show that the influence of large loads and large deformations can result in misinterpretation of GVT results and corrections to the finite element model (FEM). Their results also show the increasing importance of Spanish researchers to the aeroelastic field. Meijer addressed another traditionally difficult problem - predicting flutter of aircraft with external stores – in "Aeroelastic Methods for Flexible Aircraft Including Flight Control System on Wing/Store Flutter and Dynamic Loads."

Several authors addressed active control of aeroelastic phenomena, the development of active control laws and the assessment of the effects of aeroelastic/control coupling. The paper "The Interaction of Flight Control System and Aircraft Structure" by Becker, Vaccaro and Caldwell discussed these interactions. "Ground Structural Coupling Testing and Model Updating in the Aeroservoelastic Qualification of a Combat Aircraft" by Vaccaro, Caldwell and Becker discussed the important role played by ground structural coupling tests and their essential role in updating the aeroservoelastic model in a qualification test of an advanced canard configuration aircraft.

Luber and Becker showed an analytical procedure to encompass both flight mechanics and unsteady aerodynamic forces in their paper "An Integrated Design Procedure for Aircraft Structure Including the Influence of Flight Control System on Aircraft Flutter." These results were presented for an example aircraft. They show the importance of linking analysis to reliable ground vibration tests. In their paper "Integral Control of Large Flexible Aircraft" Koenig and Schuler addressed the problem of integral control of a large flexible aircraft, disciplines that have worked largely independently of one another for decades. They described the development of an integral model that is capable of describing both the flight mechanics and aeroelastic response of the aircraft and the couplings between each. This type of approach is particularly important to new designs that are non-traditional.

The paper "Integrated Flight Mechanics and Aeroelastic Modeling and Control of a Flexible Transport Aircraft" by Teufel, Hanel and Well addressed the same type of problem for gust response. The purpose of their study was to reduce gust sensitivity. An added feature was that flight maneuvers do not then excite elastic reactions. The novel use of flight controls to reduce fuselage response and improve ride quality was carefully discussed by Kubica and Fath in their paper "Passenger Comfort Improvement by Integrated Control Law Design." Integrated control was also addressed in an interesting study by Prudhomme, Alazard, Bucharles, Ferreres and Magni in their paper "An Integrated Methodology for Flexible Aircraft Control."

Characterization of nonlinear aeroservoelastic behavior was the subject of a paper by Cooper and Dimiriadis entitled "Characterization of Nonlinear Aeroservoelastic Behavior." These nonlinearities were due to such effects as friction damping in the system. The relationship to their work and limit cycle oscillations was also presented. These effects are an important potential source of limit cycle oscillations and this paper is a contribution to this complicated area.

Lessons learned included three interesting papers. The first, the paper "F-22 Structural Coupling-Lessons Learned" by Wray of Lockheed-Martin, addressed the lessons learned in structural coupling on the F-22 aircraft. The F-22 is a complex design requiring a robust flight control system. This paper reviewed agreement between ground testing and aeroservoelastic (ASE) analysis. Britt, Volk, Dreim and Applewhite discussed ASE problems related to the B-2 bomber in their paper "Aeroservoelastic Characteristics of the B-2 Bomber and Implications for Future Large Aircraft." They recommended the lessons learned from this project be applied to large flexible future aircraft. Among these lessons were a multidisciplinary approach to designing the flight control system. This paper was extraordinary on at least one count. It shows that integrated design problems are often encountered and solved in the "black world" where little assistance is available, but where advanced design creates aeroelastic problems.

Buffet continues to be an important research area and a development issue. "Contributions to Active Buffeting Alleviation Programs" by Moses, a recognized expert in this area, from NASA Langley Research Center reported on continuing buffet response research. This research is essential for the design of twin tail advanced fighters. Suppression of the loads through selective stiffening and active control is required to qualify the design.

Two papers discussed nonflight design where lessons learned could be applied to aircraft. Hoenlinger and Glauch discussed controlled suspension systems and their design for ride quality in their paper "Mobility Analysis of a Heavy Off Road Vehicle Using a Controlled Suspension." Krueger and Kortuem discussed the design of control laws for alleviation of ground-induced vibrations in their paper "Design of Control Laws for Alleviation of Ground Induced Vibrations." This paper covered active landing gears for aircraft where ground induced vibrations are important.

After the papers were presented, Otto Sensburg chaired a panel session. He and others summarized the presentations on the review panel as being novel, creative and essential to progress in a still important area of aeroelastic research. Several themes were addressed. One of these was the hope that in the future we will be able to address flexibility issues earlier in the design process, in the conceptual stage, rather than the preliminary design stage where less design freedom is available. The point was made that we need not only multi-disciplinary analysis, but also multi-disciplinary thinking. It was further mentioned that aeroelasticity and multi-disciplinary thinking were essential to both ordinary design and revolutionary designs. Earlier comments about the loss of core competency were reinforced.

The discussion of applications of aeroelasticity and related fields to advanced designs was met with notes of caution. For instance, new concepts such as smart structures are not to be universally applied. There needs to be a new realism about where some of these concepts should be applied. The essential question is "where and when do we use new technology?" Only when practitioners are encouraged to work alongside theoreticians will be have acceptance of new ideas and modification of the original idea to fit the need.

Finally, there was a feeling by many at the presentations that sensor placement was also an important problem in controlling aeroelastic phenomena. Numbers required and placement of sensors is both a practical and a theoretical issue.

The organizers of these sessions displayed an excellent understanding of who to bring together. These papers, presented by leading figures in the European community and America provoked lively discussion and will furnish a valuable archival source for other researchers for years to come.

Air Vehicle Design – New Horizons?

Dr. Terrence A. Weisshaar
Professor, Purdue University
1282 Grissom Hall
West Lafayette, IN 47907-1282
United States

Keynote talk – Structures and Materials

My outline is shown in Figure 1. I am aware that this is a Structures and Materials keynote, but I also know that a theme of this meeting is multidisciplinary design and optimization (MDO). Structures and materials considerations play a key role in this MDO process. I want to explore the future for modeling and simulation as a contributor to innovation during the early parts of the product development and design process. This involves the computer.

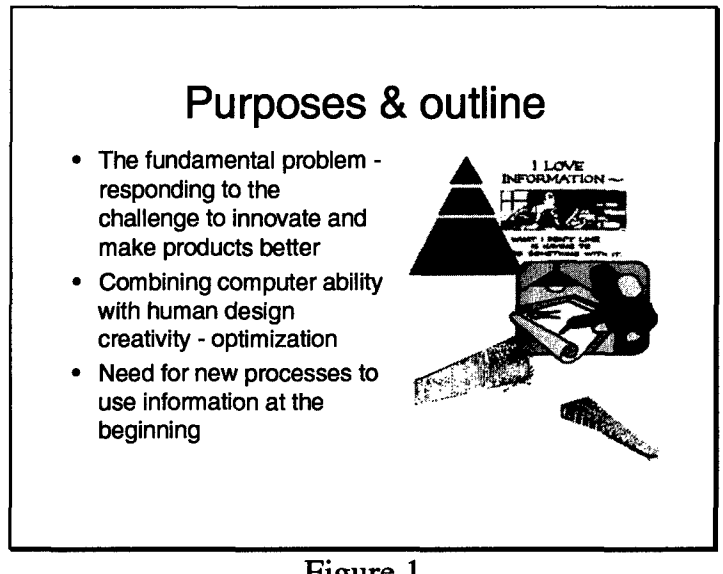

Figure 1

It is taken for granted that computer speed is the key to future success – but just to do it quicker does not assure that everything will change for the better.

We not only have to be faster, but we need to be smarter and that involves knowing when and where to insert information into our processes.

Let me give you my conclusions before I even begin. These conclusions are addressed in Figure 2. The cartoon by Ashley Brilliant sums up a fear we all have – doing something that is interesting, but worthless, just as the gentleman shown loves twirling a plate on a string. Another problem is how to increase productivity of a smaller group of engineers and designers and product developers with less experience. How do we keep up with the stockpile of new

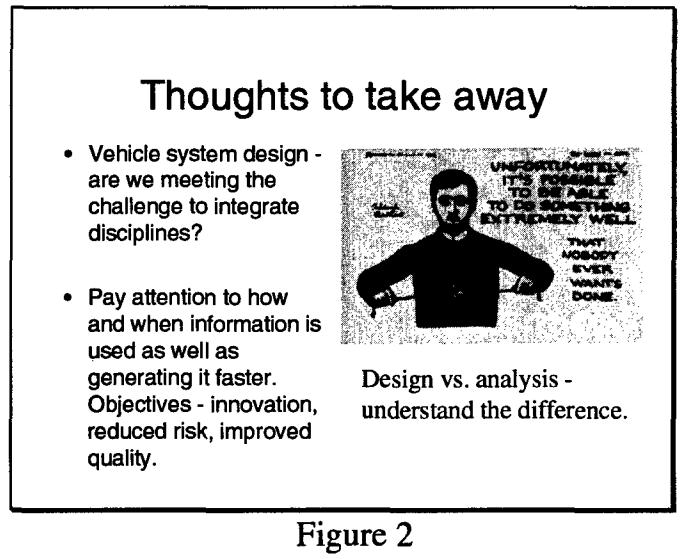

Figure 2

Paper presented at the RTO AVT Specialists' Meeting on "Structural Aspects of Flexible Aircraft Control", held in Ottawa, Canada, 18-20 October 1999, and published in RTO MP-36.

technology and convert it into products that help us improve our lives? We also have to decide what we need to develop at a time when we have few clear, centralized military challenges.

Let's make sure that our reduced resources are placed wisely and that we don't end up like the fellow shown in Figure 2. What he does, he does very well, in a timely affordable manner, but no one wants it.

Computers are an essential ingredient for improved product development processes. Figure 3 illustrates a visionary view of the times we live in, although the comment was first made in 1964. Technological revolution always involves the addition of an active ingredient that has been in place for years, but has been underused until it reaches a level where it triggers a revolution. I believe that computational and simulation technologies now give us a new opportunity to enhance innovation – but only if new tools and processes are integrated with human cognitive abilities to encourage creativity and reduce development risk. One name applied to this is Simulation Based R&D and its vision is one where we work in a virtual development world.

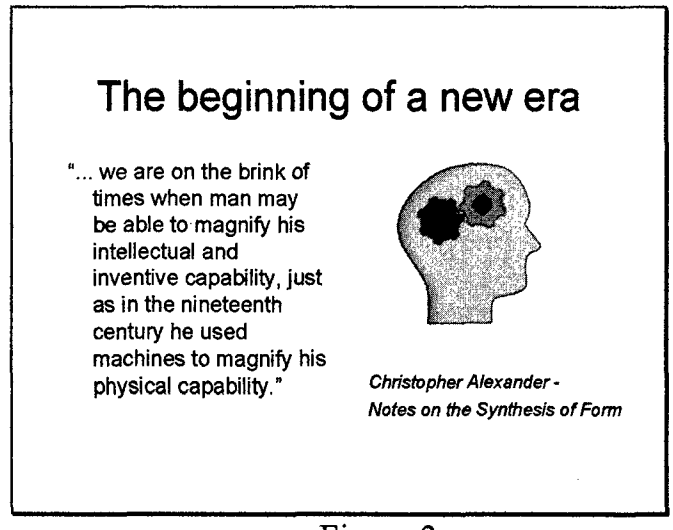

Figure 3

We need to begin with a look at the big picture. The pyramid in Figure 4 describes the hierarchy and flow of product development. It also shows major interfaces that are more like walls and wide chasms than conduits for information. This pyramid exists and it is a challenge to the developer and innovator to bridge those gulfs quickly and efficiently.

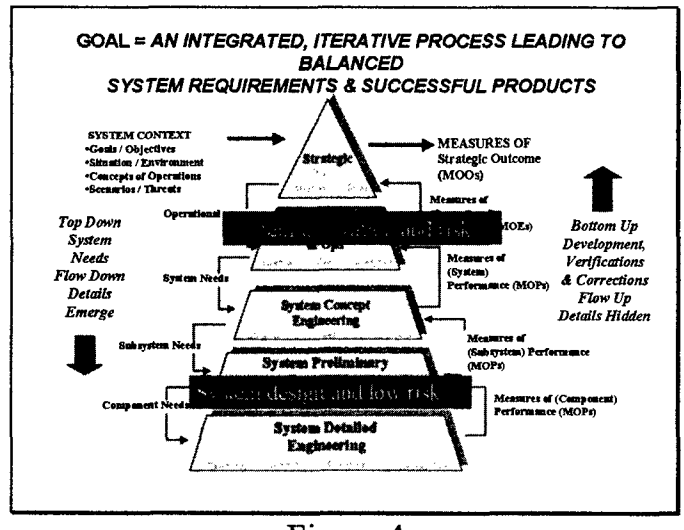

Figure 4

Many different, complex iterative processes take place within and between each of the elements. A good example of how this pyramid works in a modern setting is our Joint Strike Fighter development where some requirements were, at first, negotiable; high fidelity answers were used to trade cost and performance. Requirements were adjusted by product teams working with virtual models.

In reality the process represented by this pyramid is complex and relatively unorganized; communication between upper layers where authority, resources and power reside and the lower levels where technology and ingenuity reside is expensive and uncertain.

An often heard complaint is that it takes 30 years to get a material from a laboratory at the lowest level to a vehicle operating as part of a system at the highest level. Is that a surprise?

Product development begins with a need advocated at the upper level of the pyramid. That idea can come from anywhere within the pyramid. Figure 5 shows one example of how UAV's are used to fight wars. At this point in the development of the UAV enterprise many believe that UAV's will drastically change warfare - the problem is that we don't have real requirements for the design community to attack nor do we understand which technologies need further work.

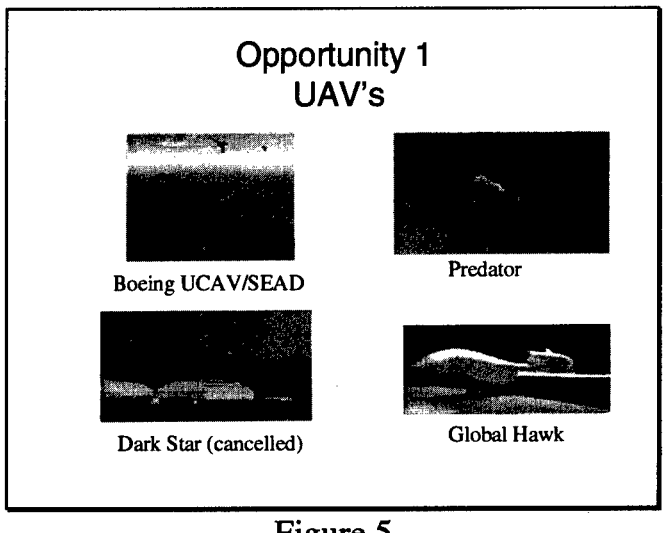

Figure 5

A second development opportunity is Space, as indicated in Figure 6. After 40 years, commercial and military Space operation is still a new enterprise; we do not fully understand the best use or payoffs. Also, technology at the bottom is moving fast and is outstripping ideas at the top. Wouldn't it be nice if we had foresight rather than hindsight? This is a particularly good opportunity for modeling and simulation as well as optimization.

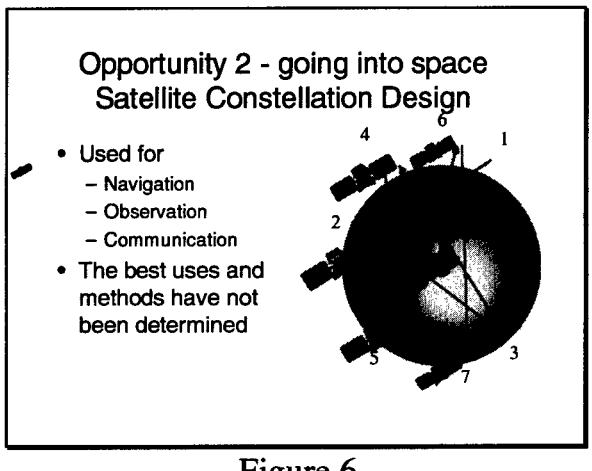

Figure 6

There are many computational algorithms being used to solve these types of upper level problems. Figure 7 shows a method for gaining insight into this problem. I am intrigued in the use of Genetic algorithms because learning from Nature is always useful - new methods are being explored to help us understand these new enterprises. Some of these uses will be discussed at this meeting.

As indicated in Figure 8, we already have had success with these algorithms; some of these appear to have commercial advantage. We could not have considered these

problems a decade ago because the computer intensive nature of this work would have made it difficult to place into a design environment. This enterprise is a model for the way we can use intensive computer capabilities to help in our thinking and discovery.

Figure 9 shows another beneficial feature of computer simulation to consider and to appreciate. We can make very interesting and sometimes useful mistakes, but at a low cost. We do not need a technology readiness level of 6 or 7 to try an idea. I could not resist using this quote about the Langley project to make a point. I fact, Langley did have a good idea, if only he had a user's license for NASTRAN.

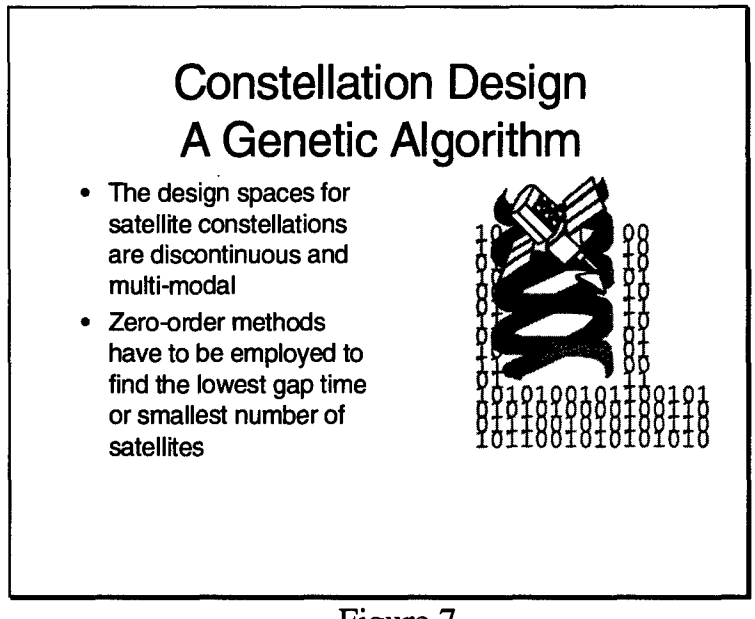

Figure 7

The second thought on Figure 9 is more serious – it is one from Donald G. Reinertsen in his book *Managing the Design Factory.* At the top of the pyramid when we are in the innovative portion of product development we must learn rapidly and we do so only if there is a significant chance of failure. Remember that there is a difference between testing and validation.

We also need an organization that will not be penalized if the product innovation effort fails at an early level. Technology and computer codes with no organization challenged to use them are not likely to result in innovation or discovery. The Air Force Research Laboratory has a broad mission in the area of science and technology. Words like "lead" and "discovery" are prominent in our mission statement.

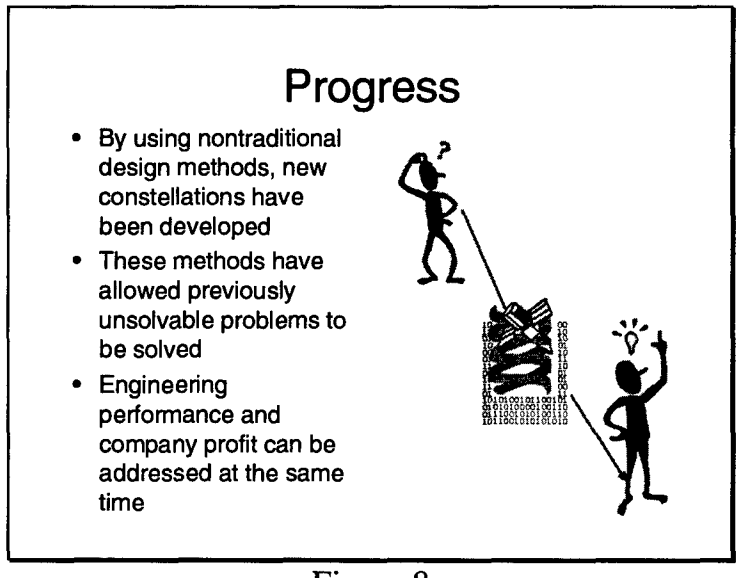

Figure 8

Figure 10 shows the U. S. Air Force Research Lab/Air Vehicles Directorate vision - to put together a small group of people to tackle the innovation problem and to develop tools and experiment with bringing computer technology and analysis closer together with experienced designers. The challenge is not just to develop a better bow and arrow, or to optimize a musket; it is to move to the machine gun and find technologies that,

when placed together, will revolutionize warfare itself and - I hope - deter those who would be so foolish to attack others.

Let's move down the product development pyramid in Figure 4 and look at component design and how it is affected by the presence of "smart" simulation. Innovation at this level is needed to satisfy requirements demanded at the higher levels.

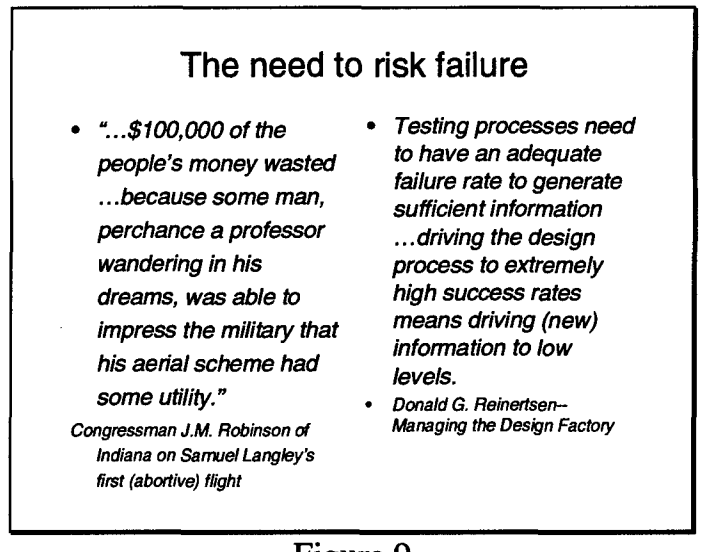

Figure 9

Figure 11 shows a complicated finite element model of a wing box with a 1-g load and a tip twist applied. This example is from a commercial wing project; it illustrates how structural design can support multidisciplinary design. The purpose of this simulation exercise is not to generate the actual final structure – that will be done by an experienced design team – but rather to give them insight into issues that arise from design requirements. Among these issues is where to place spars and how to identify interdisciplinary interactions early.

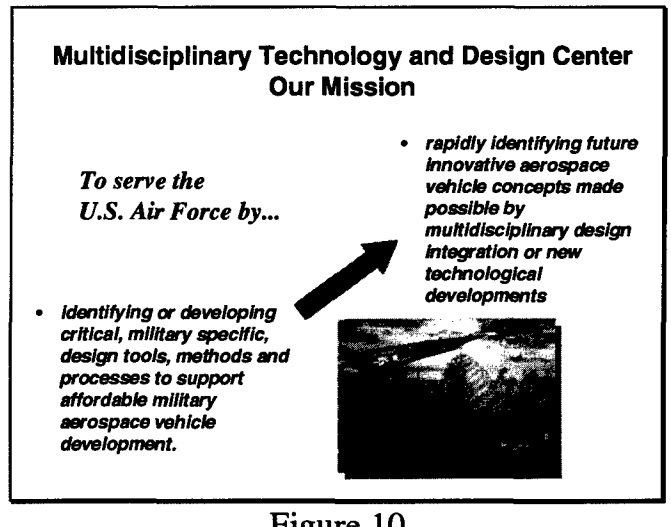

Figure 10

The aerodynamic surface extends around this box and the design space is completely filled with material. We use an optimization method to remove material when it carries little internal stress; we can watch a structure evolve, courtesy of an optimization algorithm. The time to create this design and run it is of the order of minutes, not days or weeks.

I have chosen this example because we couldn't do this efficiently 5 or 10 years ago. I also chose it because it adds to the fidelity of the conceptual design effort and it is a personal interest of mine. By taking several snapshots as the design optimization process iterates and progresses, we can watch the evolution of a primary wing structure from a solid block of material to this final form.

Figure 12 shows the side view of the final optimized structure, while Figure 13 gives a top view of the optimized load-bearing structure. Notice that there is a requirement for a very dense structure – shown in red - near the mid-span. This is the result of the decision

by the aerodynamic designers to place a discontinuity in the wing chord there. This design feature will produce increased wing weight. We have uncovered an issue here that may be important to bring to the attention of the configuration designers.

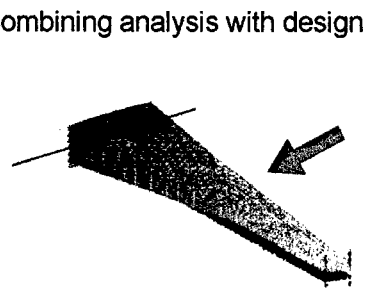

Figure 11

There are two other observations. First, this mathematical optimization result confirms our suspicion that the best structure does have a short load path associated with it. The loads are fed aft, not forward. The second observation is that this is the wrong structure for the task, based on our design experience of 70 years with semi-monocoque structures. Does this mean that this computer code is wrong?

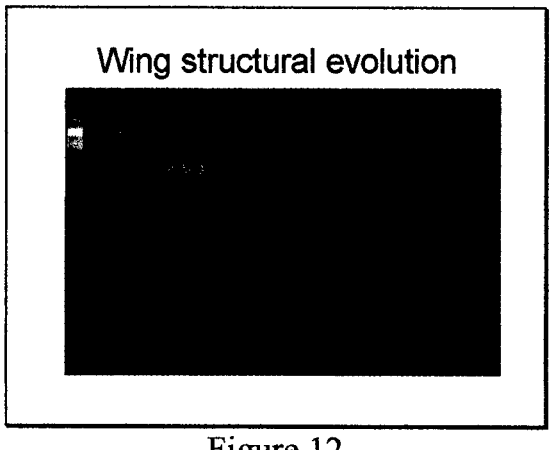

Figure 12

No! Our conceptual design model of the structure was too restrictive and could not develop into a shell. A more complex model with more finite elements through the thickness, shown in Figure 14, gave the type of results we would expect from experience. This new model illustrates that we must be smart users of tools and also be careful not to exclude experienced designers. This is what I mean by matching cognitive abilities to the computer.

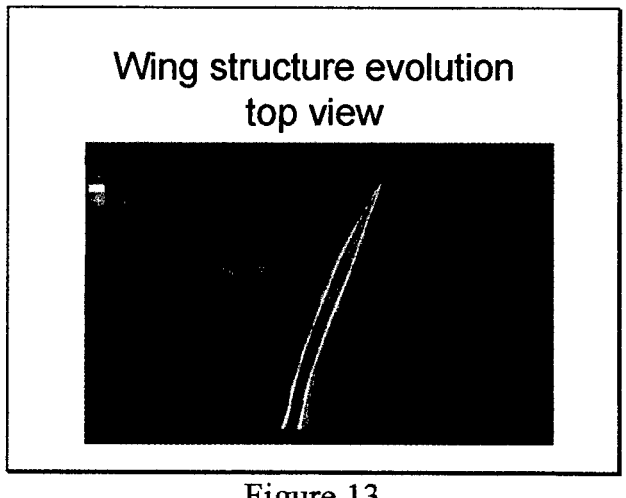

Figure 13

What other lessons were learned? This exercise took 20 minutes of PC computation (the shell model took 2 hours). Computational capabilities are said to be doubling every 18 months. Computers are faster and cheaper. We see them in every aspect of our lives, from the supermarket to the entertainment industry. Much has been promised, but the fact remains, we do not know how to properly use computer technology in the aircraft system design process. This reminds me of UAV's where we are asking robots to fight wars, but are not sure how to talk to them or control them at critical moments. This is what I mean by integration of our tools with cognitive abilities. We must make the computer work for us, not the other way around.

Let's think about the product development and design enterprise. Consider the points in Figure 15. High quality products will always require experienced designers and computational simulation. Some software tools have failed to have the desired impact on product innovation, cost reduction or quality. Part of this failure is due to the unwillingness or inability of design and product development organizations to use new tools or to change as much as our analytical technology has changed. Additional blame must be given to tool developers who do not understand or are unwilling to understand the needs of the pyramidal product development process.

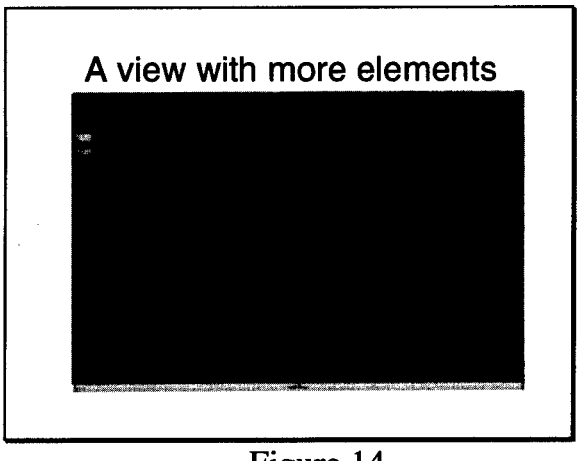

Figure 14

Let's look at the product design process in the lower levels of the pyramid in Figure 4 and think about where we might make contributions in the area of structures. We can look anywhere, but my interest is in the conceptual design - Phase 1 - effort depicted as the first block on the left of Figure 16 and shown in greater detail in Figure 17. Phase 1 results determine, like the genetic code placed at human conception, the final outcome of product development.

During Phase 1 design activities, optimization methods are mostly directed towards defining external configuration details such as wing shape and size, but not concerned with internal features such as structural layout or materials selection.

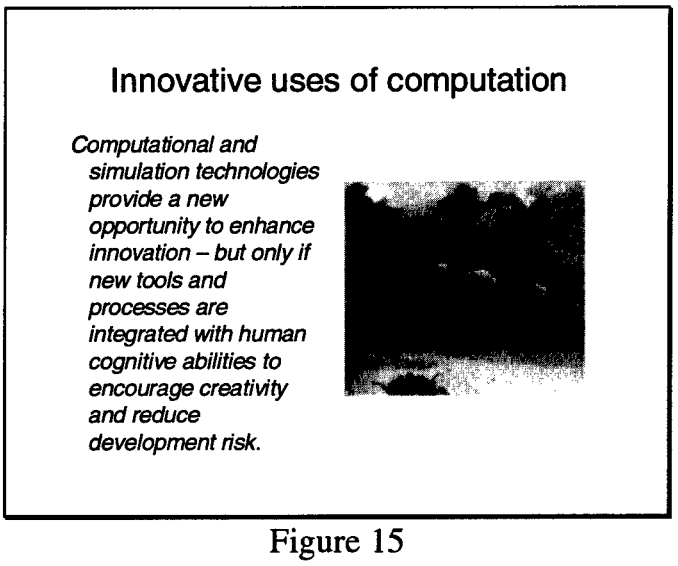

Figure 15

It is discomforting to think that the merits of structural concepts are discussed using terms like "I think" rather than "I know." Mistakes - whether the result of stupidity or just bad luck - are more expensive to fix as the process goes along. The best way to avoid them is to have appropriate information available. I am an advocate to have the structure represented early in the process to turn "I think" into "I know" and I understand." The examples just shown provide this type of structural information about "ideal" structural arrangements that, while not necessarily practical, nevertheless give us knowledge of the load transfer, topology design process.

The need for more structural information is clear when we look at the requirements at the end of a general conceptual design effort - summarized in Figure 17 as "Phase 1" - and realize that a majority of these requirements impact the design of the undesigned internal

structure. These structures related requirements are shown on the right of Figure 17. These preliminary results will be the basis of the company's decision to go forward or to abandon ship. They will also be the starting points from which the detailed design, down to the last rivet, will evolve. A key problem is that the moldline generation capabilities coupled with CFD and CAD tools such as CATIA are able to move rapidly ahead of the internal structural design features.

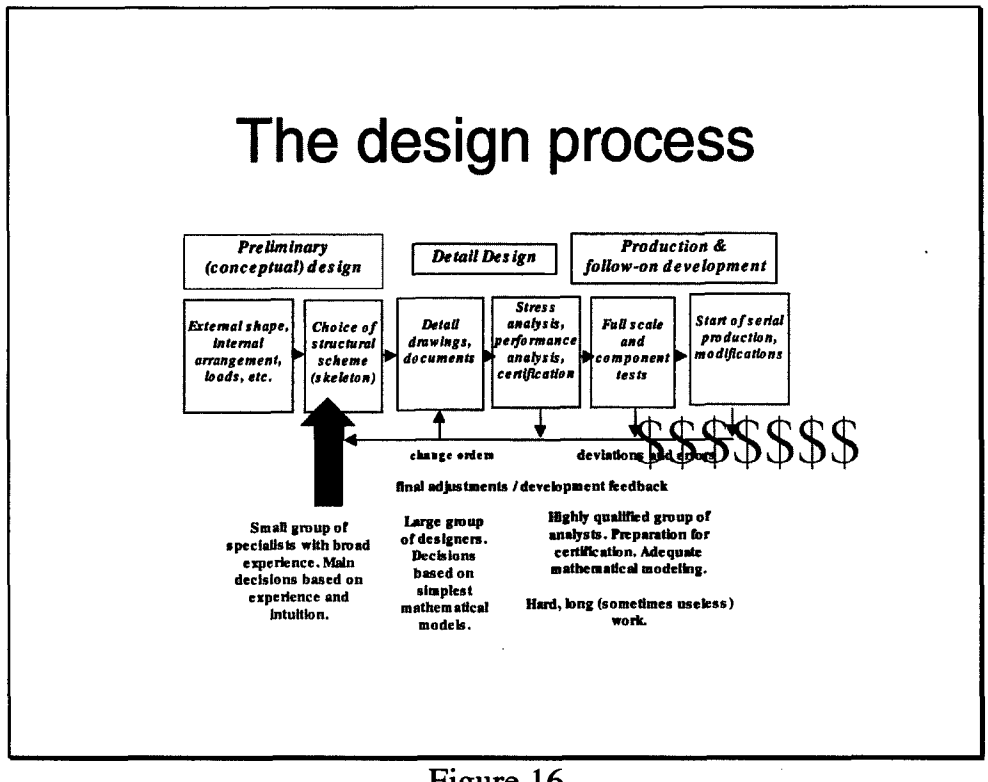

Figure 16

This means that structural design, although important to every operational and cost feature of an aircraft system, is muzzled at the conception of the design and is subservient to aerodynamics. Is this necessary today or even a good idea? I don't think so.

Let's talk about information for a moment. The points listed in Figure 18 (including another Ashley Brilliant cartoon) are not new or profound, but they remind us to think about what we compute and who we share it with. I am an analyst and must admit that I have at times been more fascinated by my ability to generate plots and figures than mundane efforts like worrying about who will use the results.

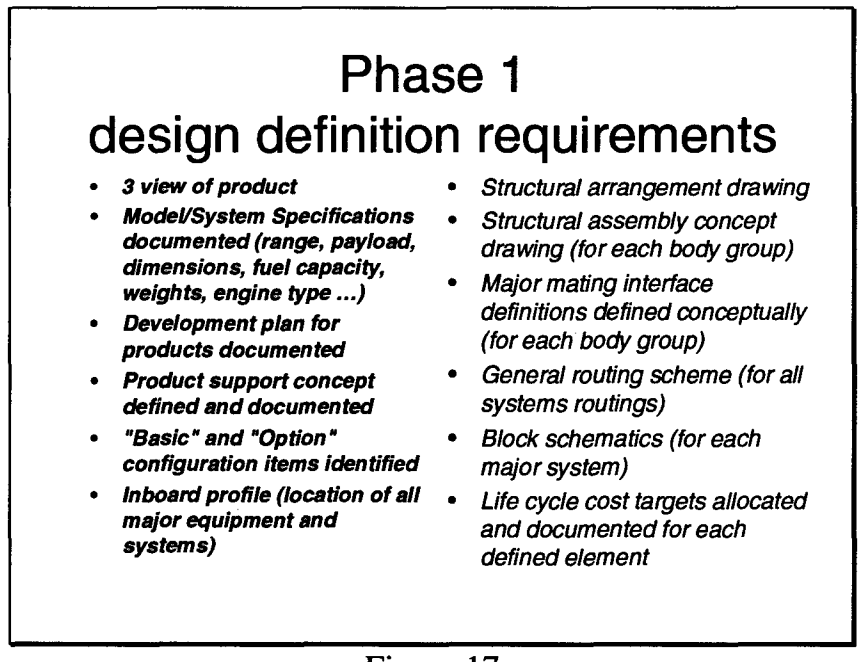

Figure 17

On the other hand we must always remember that there is a progression

of data generation to information to knowledge. If you have developed a computer code or an algorithm, think of the question "So what?" What differences will your results make to the product development enterprise? The key value of computer aided design programs is the ability to generate information that leads to new knowledge. It may seem like splitting of hairs on definitions, but we must realize that the difference between data and information depends on human cognitive abilities. This is the ability to think, recognize and associate reality with figures and drawings, not with numbers and digits. This is a link between the machine and the brain. It requires a rethinking of the design and development process.

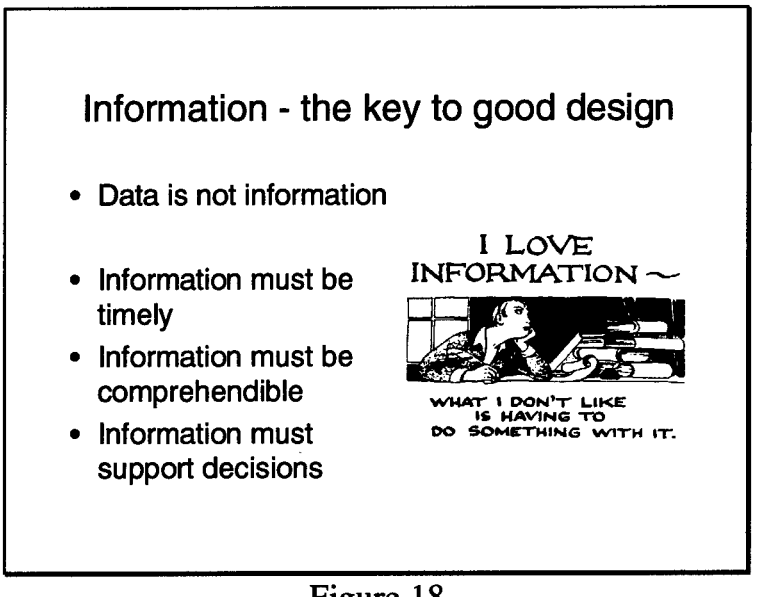

Figure 18

Let me give an example of turning data into information. Figure 19 shows a top view of the same wing structural box model as we saw previously. Instead of beginning with a solid that turned into a shell, we used a different procedure. This procedure is part of an object based design tool called AML, developed by Technosoft, Inc. with Air Force Research Laboratory sponsorship; this design code uses special sandwich elements together with a proven optimization algorithm. The new feature in this AML code is the ability to insert high fidelity structural analysis and optimization techniques early. The result is a new process, including how structural optimization information is used. Let me explain.

Figure 19 introduces the concept of "force flow." These force flows show up as small arrows in the figure and are the products of principal stresses and wing skin thickness. This is information that everyone talks about - getting the load paths right- but few do anything about finding them before a design is solidified. To understand their importance, think of placing a large building at

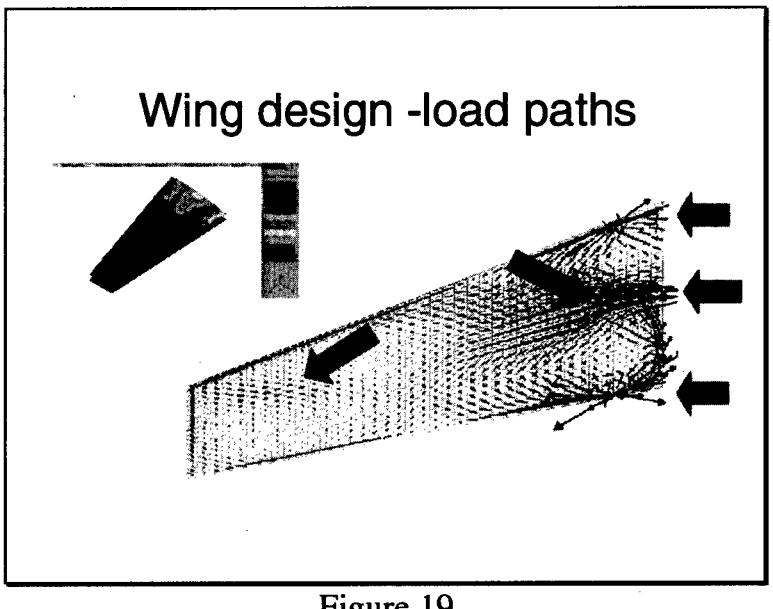

Figure 19

its site, but without sidewalks or delivery roads. After a month, the users would beat down paths and ruts that would identify how the people – the loads – prefer to get into and out of the building. We would then tailor our sidewalks and delivery roads as closely to the users as possible. We can also do this for structures with this procedure.

This type of information lets the experienced designers understand where to place load-bearing items and what type of elements – plates, stiffeners, spar caps - are to be used. It also alerts them to special features of the design that may come back to cause trouble. I have indicated areas where loads are coming into the skin and changing direction and also where material is crucial to resist loads. These areas will be the locations of spars and stiffeners when the design work is finished.

MDO example
supersonic control effectiveness

- Wing center of pressure shifts aft during transition from subsonic to supersonic flight
- more elevon displacement is required for pitch trim
- wing flexibility requires more elevon
- problem is solved by fuel shifting
- problem is solved with a larger engine
- problem is solved by selective stiffening

Figure 20

So – a final word about this – we have used finite element methods and optimization at a point early in the design process that is nontraditional. Until recently, we could not even think about using these methods within the short time frame dictated by conceptual design. That is no longer true. The example in Figure 19 can be done in a morning and the results discussed in the afternoon. It shows that thoughtful collaboration between designers and analysts yields productive results. The end product is an actual structure, different than that shown, with spars and ribs, but with approximately the same load paths.

I also will mention that this information makes good designers into excellent designers, but poor designers will still be poor designers because they will not be able to define the right questions, search for an answer or understand the results.

One theme of this RTO meeting is optimization and design – there will be many papers presented during the next three days. Let me end my presentation by showing you an MDO opportunity to identify structural problems early in design if we have modern, easy-to-use multidisciplinary design tools. This example is structural design, but the problem involves stability and control, propulsion,

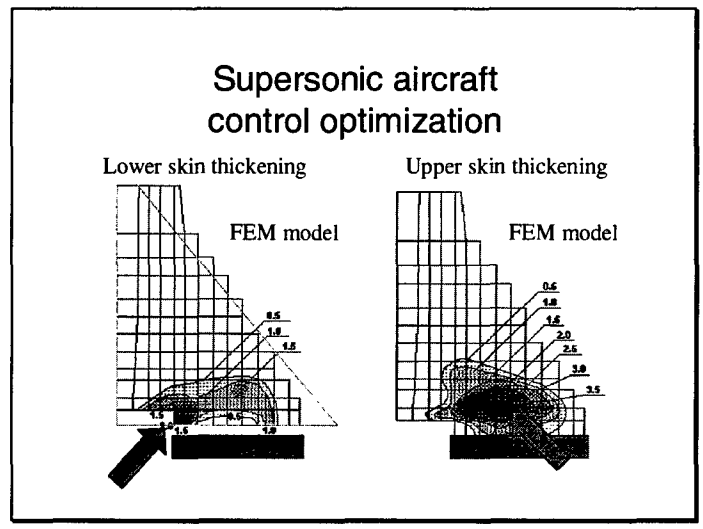

Figure 21

performance and aerodynamics. Figure 20 shows the issues addressed.

Figure 21 shows an SST wing from a generic supersonic wing model. Configurations of this type can have control effectiveness problems that lead to excessive trim drag. The model is a coarse structural finite element model that can run on laptop computers. The wing and control surface loads are approximations to those placed on the wing by control surface movement and lift of the wing.

The original wing design, using strength considerations alone, has excessive trim drag. We are allowed 100 lbs. of material to place into the upper and lower skins and we want to reduce trim drag. Figure 21 shows the best locations to place material to maximize stiffness that, in turn, will reduce the trim drag. Computing more detailed loads with CFD or panel codes can enhance the model. The fact remains that it is appropriate and beneficial to use a structural finite element model for this purpose and would not have been considered until well into the design process when a change would be expensive. In fact, for the class of aircraft represented, these problems were never considered early, to their detriment.

New computational methods and the types of information that they can quickly bring to the process affect the organization of the design and development process itself. In particular, the level of analysis that we think is "old" is also very efficient and can be placed early in the process. Figure 22 suggests the change that I would like to see. Here I have placed a new step in the conceptual process to help the design team. By the way – this idea is not unique to me – several others from around the world have advocated this approach.

The new process made possible by modeling and simulation has high fidelity structural and optimization procedures applied early in the process, but only to a level of detail consistent

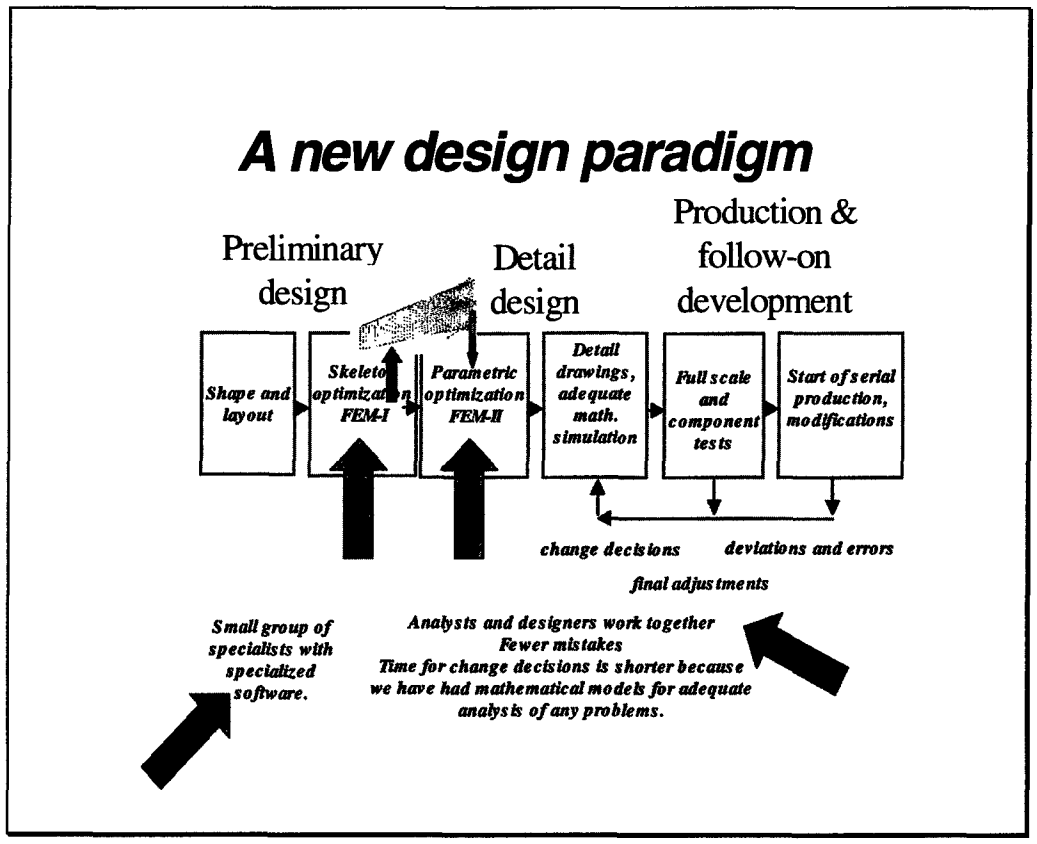

Figure 22

with the decisions addressed and the design definition available. For instance, I enjoy flutter analysis, but flutter speed constraints need not be addressed early, although aeroelastic issues such as changes in wing load distribution due to wing flexibility are important. We can also anticipate problems created by access openings in fuselages. We can also estimate weight of unusual components for which there are no reliable databases.

Let me state my points again in a slightly different form, as shown in Figure 23. The issue is not only to improve productivity; it is to improve both productivity and innovation. We have to decide what we need to develop in a time when we have few clear, centralized military challenges. Then we have to come up with new system components to do the mission. This involves modeling and simulation coupled together with human minds.

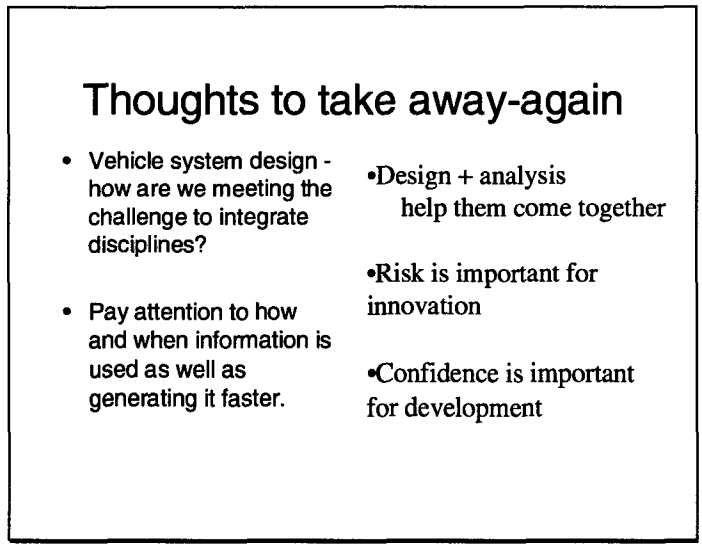

Figure 23

Modeling and simulation efforts are occurring all over the world. If, within 10 years, we are not living in a more creative world filled with better products that match our needs then we will not have fulfilled the vision being able to magnify our intellectual and inventive capability. Fulfilling that vision is the responsibility of all stakeholders - producers, designers, analysts and researchers. I urge you to help to link the virtual world to a better real world.

A UNIQUE DESIGN FOR A DIVERGING FLEXIBLE VERTICAL TAIL

O. Sensburg, G. Schneider
DaimlerChrysler Aerospace, Military Aircraft MT24
P.O. Box 80 11 60
81663 Munich, Germany

V. Tischler, V. Venkayya
Wright Patterson Air Force Base
WL/FIBAD Bldg. 45
2130 Eighth Street, Ste. 1
Dayton, Ohio 45433-7542, United States

Summary

A method is developed which allows to use the flexible behaviour of aircraft structures to enhance aerodynamic derivatives. A vertical tail analytical model was used to show these effects and by exploiting the aeroelastic deflections it is possible to reduce the area of this surface up to thirty percent. Numerous applications are possible including fighter and transport airplanes. Since composite structures are involved it is absolutely necessary to use a multidisciplinary optimisation program code such as the US-Airforce ASTROS-code.

1. Introduction

Vertical tails designed for high speed aircraft suffer from reduced stability and control effectiveness at high dynamic pressures due to aeroelasticity. Therefore, adequate tail performance requires large tail area with high aspect ratios, and stiff and heavy structures. These large tails are also subject to burst vortex or shock induced buffet which causes fatigue problems. Their size and structural constraints cause weight, drag, and radar cross section penalties. These penalties can be significantly reduced by the application of divergent flexible technologies to the vertical tail design problem, which results in a lighter structure and potentially smaller size to reduce buffet, drag and observables. In same cases the smaller size requirement could remove the necessity of two vertical tails.

Although active flexible technology is currently being developed for wing structures under other programs [1,2] application of this technology to vertical tails requires a different design process and results in a different design solution due to the different design requirements between the tail and wing.

The vertical tail is a stiffness design because flight loads are much lower than on the wings of fighter airplanes. Therefore there is a wider variation of CFC-layers available than on wings where a lot of the stiffness is defined by strength constraints.

In this work the objective was to demonstrate increased tail effectiveness at high speeds. This could lead to decreased tail size and structural weight that meets or exceeds all tail performance and observables goals.

The reason why it is called „diverging" is that a surface design with greater efficiency than one must diverge at some speed. Our aim must be that the divergence does not occur in the required speed range of the air vehicle.
The technology applied is called Active Flexible Technology which is a multi-disciplinary, synergistic technology that integrates aerodynamics, controls, and

Paper presented at the RTO AVT Specialists' Meeting on "Structural Aspects of Flexible Aircraft Control", held in Ottawa, Canada, 18-20 October 1999, and published in RTO MP-36.

structures together to maximize air vehicle performance shapes for optimum performance. This was first described extensively in [3].

For high speed the vertical tail is designed to provide a minimum value of the directional static stability derivative. For low speed the rudder power unit must be adequate to hold a sideslip of ß = 11,5° at the approach speed for a cross wind landing. It also must cover the one engine out case. This low speed requirement may reduce the possibility to cut the fin span and area commensurate with positive high speed aeroelastics.

2. Description of Work

A generic aircraft design was selected and the vertical tail was designed (at the conceptual design level) with conventional and with active flexible technologies. The weight, performance, and observables benefits of DFVT were then determined relative to the conventional design.

A FEM model for a generic fin was available which was used in the Dasa Lagrange optimisation code [4]. This model was modified to serve for the USAF-ASTROS optimisation code. The finite element model could be very useful for future work as a benchmark. Therefore all comparisons with Dasa results are well documented.

Because of the low aspect ratio of the chosen vertical tail design - AR = 1.2 - this is an ideal candidate for applying aeroelastic tailoring for carbon fibre composite structure (Figure I). As can be seen in this figure the higher the aspect ratio is the higher the weight penalties to meet the performance goals.

The design of aircraft and space structures requires the marshalling of large teams of engineers to select a design which satisfies all requirements. Typically this design goes through further refinement or modification as more knowledge is gained about requirements or as new conditions are imposed. Much of this effort presently consists of applying laborious „cut and try" procedures wherein the design is perturbed and reanalysed many times. This redesign frequently is required because two or more disciplines have conflicting demands that require compromise.

Therefore it is necessary to have an automated design and analysis tool that performs the trade-off and synthesis tasks in a systematic way. The ASTROS (Automated Structural Optimisation System) is such a computer code [5].

3. ASTROS Concepts

ASTROS is a finite element-based software system that has been designed to assist, to the maximum practical extent, in the preliminary design of aerospace structures. A concerted effort has been made to provide the user with a tool that has general capabilities with flexibility in their application.

A vital consideration in software of this type is that the key disciplines that impact the design must be included in the automated design task. This multidisciplinary aspect of the program has been implemented in an integrated way so that all the critical design conditions are considered simultaneously.

In addition to the interaction of several disciplines, ASTROS can treat multiple boundary conditions, and, within each boundary condition, multiple subcases. The system is not arbitrarily restricted by problem size, and it conforms to the current environment for performing structural analysis in the aerospace industry. The practical limitations on problem size are available disk space and data processing time.

Compatibility with the current aerospace environment is addressed because the ASTROS procedures resemble those of NASTRAN in terms of user input and pre- and post-processor interfaces. While the ASTROS program does not contain many of the specialised capabilities available in NASTRAN, the basic structural analysis features have been included. Most importantly, from a user point-of-view, the Bulk Data formats have been taken directly from NASTRAN and modified only if the design considerations required such a modification in the data or, in a few cases, if minor changes result in superior capability. New Bulk Data entries have been created to input design information and data needed to run the steady aerodynamics and other analyses specifics to ASTROS.

3.1 ASTROS Capabilities

This section gives a brief overview of the capabilities that are included in the code. The basic disciplines that are implemented within this code are as follows:

1. Static analysis
2. Modal and flutter analysis
3. Aerodynamic Analysis
4. Dynamic Response Analysis
5. Optimisation

The statics analysis methodology is based on a finite element representation of the structure, as are all the structural analysis disciplines in ASTROS. The static analysis compute responses to statically applied mechanical (e.g. discrete forces and moments), thermal and gravity loadings. Static deformations and their resultant stresses are among the computed responses. An extensive design capability is provided for the static analysis discipline. It provides the capability to analyse- and design linear structures subjected to time invariant loading.

The modal analysis feature in ASTROS provides the capability to analyse and design linear structures for their modal characteristics; i.e., eigenvalues and eigenvectors. The design aspect of ASTROS places limits on the frequencies of the structures. The modal analysis is not only useful in its own right, but also provides the basis for a number of further dynamic analysis. Flutter and blast response analyses in ASTROS are always performed in modal co-ordinates.
Transient and frequency response analyses can be performed in either modal or physical co-ordinates, at the selection of the user.

Steady aerodynamics are used for the computation of external loads an aircraft structures.

The static aeroelastic analysis features in ASTROS provide the capability to analyse and design linear structures in the presence of steady aerodynamic loading. This provides the ASTROS user with a self-contained capability to compute loads

experienced by a manoeuvring aircraft and to redesign the structure based on these loads. The capabilities available for steady aerodynamics design include specifying limits on

- allowable stress or strain response due to a specified trimmed manoeuvre,
- flexible to rigid ratio of the aircraft's life curve slope,
- flexible roll control effectiveness of any antisymmetric control surface and
- values of flexible stability derivatives and trim parameters.

Flutter analysis in ASTROS provides the capability to assess the aeroelastic stability characteristics of the designed structure and to correct any deficiencies in a systematic fashion. Both subsonic and supersonic analyses are available and, reflecting the multidisciplinary character of the procedure, the design task can be performed with any number of boundary conditions and flight conditions. In this way, all critical flutter conditions can be analysed and designed for simultaneously.

Dynamic analysis is performed for loadings which are a function of time or frequency.

The final discipline listed above is that of optimisation. If only stress, or strain, constraints are included in the design task, the fully stresses design option may be used. For more general design tasks, a mathematical programming approach has been implemented.

3.2 Structural constraints for Vertical Tail layout

- Strength or strain allowable must not be exceeded. Five load cases were used in our case

- Static aeroelastic efficiencies for vertical tail and rudder were required. These terms are defined as flexible coefficients divided by rigid coefficients.

- Flutter or divergence speed requirements: for this case 530 m/sec, Ma 1,2

In addition there are some specific composite requirements such as minimum ply thickness and maximum amount of one layer.

4. Structural description of Fin and Rudder

The overall geometry of the fin is given in figure 2. The surface area is 5.46 m^2 and the leading edge sweep angle is 45°. The fin box has one shear pick-up in the front and one bending attachment at the rear. The rudder actuator is connected with two rods for control actuation. Fin box and rudder skins are built as carbon fibre laminates. A quasi isotropic glass fibre laminate is used for the tip structure which contains avionic equipment. Fin box and rudder are coupled by three hinges.
These are the four materials which were used: CFC, GFC, Aluminium, Titanium

- Fin Box Skin - Four Layer CFC Laminate
- Rudder Skin - Three Layer CFC Laminate
- Tip Skin - Quasi Isotropic GFC
- Fin Box Rear Spar - Four Layer CFC Laminate
- Rudder Main Spar - Four Layer CFC Laminate
- Remaining Spars - Aluminium

- Fin Box End Rib - Titanium
- Rudder End Ribs - Titanium
- Remaining Ribs - Isotropic CFC

5. Comparison of NASTRAN and ASTROS Results with existing Dasa Data

In order to become familiar with the Dasa model of fin and rudder several NASTRAN and ASTROS analysis were performed and results were compared with existing Dasa data. Correlation was found to be excellent. After that exercise the Dasa-model was changed. To allow different attachment conditions the general stiffness element (GENEL, giving the effect of the fuselage stiffness) was removed and replaced with single attachment springs. These springs were tuned so that the model would give the original Dasa results. ASTROS and NASTRAN results are identical because the ASTROS-code uses the finite element description of NASTRAN.
Results of this comparison can be found in table 1.

6. Results of Optimisation Runs with ASTROS

Several computer runs were performed with
- strength constraints
- flutter speed 530m/sec at Ma 1.2 / S.L.
- areoelastic efficiency

trying to first match the Dasa results for fin efficiency of 0.814 at M 1.8, 102 kPa. The rudder efficiency was fallout at 0.3799.
The ASTROS code reduced the weight for this configuration to

81.1 kg.

The weight of the initial design was 99.4 kg. When all constraints were fulfilled the weight was 95.1 kg for a fin efficiency of 0.814.

Higher fin efficiency was requested and the weights for these designs are plotted in figure 3. Whilst 0.9 can be reached with very little extra weight higher efficiencies need excessive weight penalties. When rudder efficiency was treated as fallout, then the weight reduces considerably and efficiency of 1.0 can be reached when flutter is fallout too. The fallout's are quite reasonable and sufficient for a feasible design.
From figure 3 it can be seen that a fin efficiency of 1.0 can only be achieved with infinite weight.
The picture changes completely when Ma 0.9 subsonic air forces are used (Figure 4). Now we reach higher efficiencies than 1.0. As can be seen with very little additional weight 1.3 can be reached for a high pressure of 102 KPa which is not possible for air. The highest possible q is 57 KPa for Ma 0.9, sea level in air.

This trend is also verified in figure 5 which clearly shows that the wash-in angle increases for higher efficiencies which simulates basically a forward swept fin behaviour (diverging!) and in figure 6 which shows a positive wash-in angle despite that it is a swept back surface.

7. Physical Explanation of the Basic Mechanism of the Diverging Flexible Vertical Tail (DFVT)

In order to understand the elastic behaviour of the fin an equivalent beam is assumed which contains the stiffness of the fin. This beam would be located at the elastic axis which is a spanwise line through the shear centres of each cross section. The shear centre of each cross section is computed by establishing the point in the plane of the section at which a normal load can be applied without twisting the section or whereas torsion moment can be applied to the section without producing a deflection at the shear centre. An effective elastic axis was defined by using the deflection of two points fore and aft on the chord where a moment was applied at the tip assuming small angles and that the deflection vary linearly along the chord. Figure 7 shows the elastic axis location. From this figure one can assess why it is impossible to get a wash-in effect (diverging) for the supersonic Ma 1.8 case. The centre of pressure - at 30% span and 50% chord - just reduces any initial angle attack of the fin, and therefore the best fin efficiency which can be reached with aeroelastic tailoring is 1.0 which is the rigid behaviour and needs a lot of structural weight. At the subsonic case, Ma 0.9, there exists some possibilities for wash-in, because the aeroelastic tailoring also shifts the so called elastic axis. This behaviour is shown in figure 4 and also in figure 8 for an optimised case of Ma 0.9, 102 kPA and fin efficiency of 1.3.

8. Results for shifting the attachments back

The behaviour changes drastically when the fin attachments are shifted back. The x-position for the forward attachment was shifted back from x = 450mm to x = 950mm. The x-position for the rear attachment was shifted from x = 1750mm to x = 2300mm. The new positions can be seen figure 9.
Now the centres of pressure are forward of the elastic axis and wash-in behaviour can be expected for both subsonic and supersonic cases (figure 10). For Ma 0.9, 57 KPa a fin efficiency of 1.3 can be reached with practically no weight increase. Also the rudder efficiency increases from 0.5 to about 0.7. This can be seen in figure 11. For the supersonic case Ma 1.8, 102 kPa the behaviour is similar (Figure 12), and 1.3 can also be reached with an optimised laminate. The rudder efficiency is now reduced to 0.5. The flutter speed is 530m/sec.. As an item of interest an analysis was performed (no optimisation) to find the fin and rudder efficiency at Ma 0.9, 57 kPa for the laminate of Ma 1.8 102 kPa. This shows a fin efficiency of 1.3 and a rudder efficiency of 0.8.
Figures 13 to 16 show the thicknesses of the different CFC layers for Ma 1.8, 102 kPa and an effectiveness of 1.3.

9. Conclusions and Recommendations

A list of possible benefits is presented below:

- The reduced tail size reduces the CD_0 drag.

- The reduced span and area reduces the exposure to upstream induced burst vortex and separated flow unsteady pressure fields which increases tail buffet fatigue life. The increase in life reduces repair and replacement life cycle costs.

- The reduced planform size reduces observable signatures to increase stealth mission capability and reduce detectability.

- Because of the possible size reduction one vertical tail would be sufficient even for Navy airplanes.

- With proper multidisciplinary optimisation a carbon fibre vertical tail can be made 30% more efficient than a rigid surface at the same weight.

- If the low speed requirement is not relevant the area of the vertical tail can be reduced by 30% together with the structural weight.

- An all moveable vertical tail could be the optimum solution for a fighter aircraft because the yaw axis would be brought very far to the rear. It would also be a solution for a subsonic aircraft because moving the whole tail would fulfil the low speed requirement. This was discussed in [6].

- A wind tunnel model should be built and tested to prove the concept experimentally. An analytical method to lay out and fabricate a low cost wind tunnel model is available.

10. References

[1] Pendleton, E., Bessette, D., Field, P., Miller, G., and Griffin, K.,
"The Active Aeroelastic Wing Flight Research Program"
39th AIAA/ASME/ASCE/AHS/ASC Structures, Structural Dynamics, and Materials Conference, April 1998

[2] Flick, P., Love, M.,
"The Impact of Active Aeroelastic Wing Technology Conceptual Aircraft Design"
AVT PANEL MEETING Proceedings OTTAWA, CANADA, FALL 1999

[3] Shirk, M. H., Hertz, T.J., Weisshaar, T.A.,
A Survey of Aeroelastic Tailoring Theory, Practice, Promise,
AIAA Paper AIAA-84-0982-CP, 25th Structures, Structural Dynamics and Materials Conference, Palm Springs, California, 1984

[4] G. Schneider, J. Krammer, H.R.E.M. Hörnlein
"First Approach to an Integrated Fin Design"
AGARD Report 784
Integrated Design Analysis and Optimisation of Aircraft Structures

[5] ASTROS THEORETICAL MANUAL

D.J. Neill, D.L. Herendeen, V.B. Venkayya
US-Airforce WL-TR-95-3006

[6] J. Schweiger, J. Krammer
"Active Aeroelastic Aircraft and its Impact on Structure and Flight Control System Design"
AVT PANEL MEETING Proceedings OTTAWA, CANADA, FALL 1999

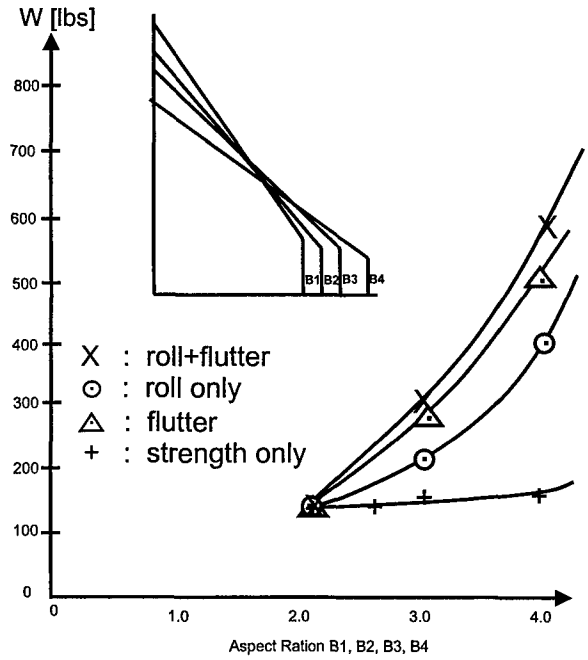

Fig. 1. Structural Weight for Various Constraints vs. Aspect Ratio

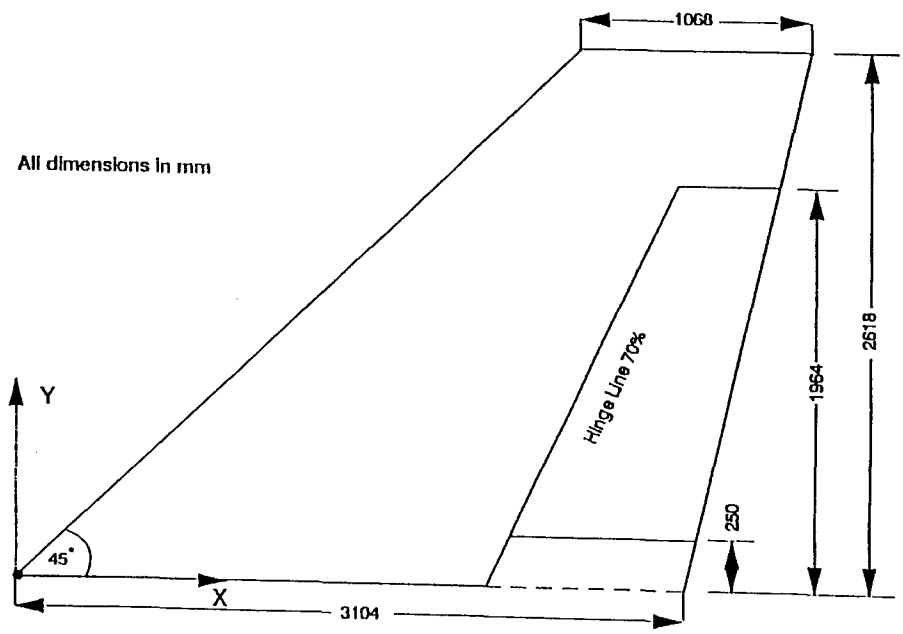

Fig. 2. Fin Geometry

	Initial Design ASTROS	Initial Design Dasa	With Single Springs	Optimum Design	
				ASTROS	Dasa
Weight [kg]					
Structure	99.4	99.4	99.4	95.1	92.9
Non Structure	53.6	53.6	53.6	53.6	53.6
Total	153.0	153.0	153.0	148.7	146.5
Deflections [mm]					
Load Case 1	304	291			
Load Case 2	384	367			
Load Case 3	148	154			
Load Case 4	220	231			
Load Case 5	146	159			
Frequences [Hz]					
f_1	9.1	8.9	9.0	9.0	9.2
f_2	30.5	29.8	30.0	29.1	30.2 (f+a)
f_3	32.5 (fore + aft)	31.2 (f+a)	43.9 (f+a)	42.7 (f+a)	30.6
f_4	41.4	40.0	41.6	41.1	41.08
f_5	55.7	54.9	57.6	60.0	58.31
Ma 1.2, S.L.					
Flutter Frequency – f_F [Hz]	20.2	21.2	20.0		
Speed - v_f [m/s]	493.4	495.0	534.0	530.0	530.0
Ma 1.8, 750 kts – Aeroelastics					
Fin	0.753		0.740	0.814	0.814
Rudder	0.441		0.423	0.500	0.500
Aeroelatic Deflections [mm]					
Fin 1°	65.34	53.7			
Rudder 1°	8.88	8.29			

Table 1: Comparison of DASA-Lagrange and ASTROS Results

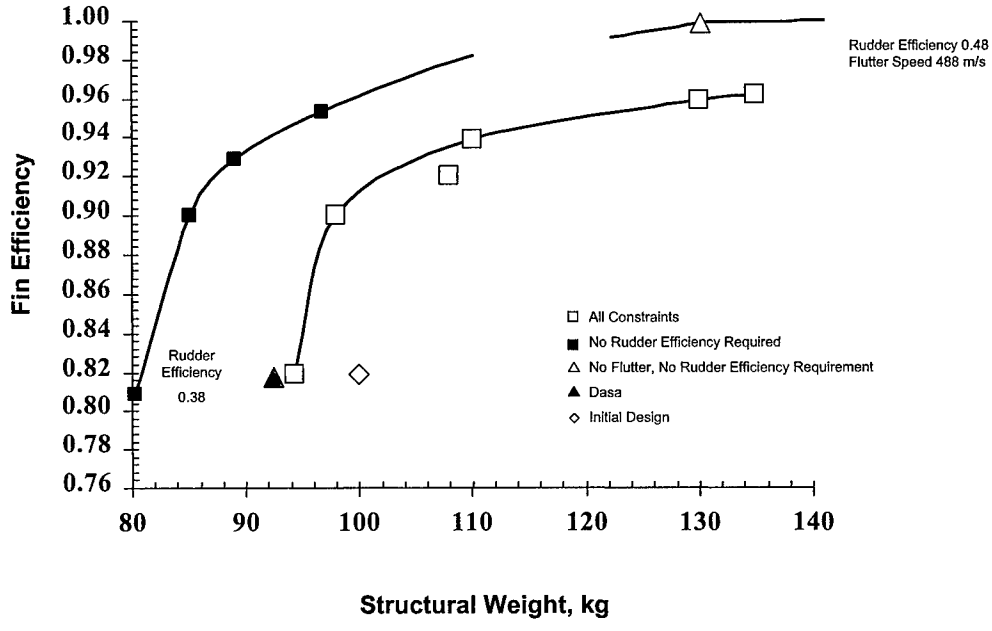

Fig. 3. Fin Efficiency vs. Structural Weight for Ma 1.8, 102 KPa

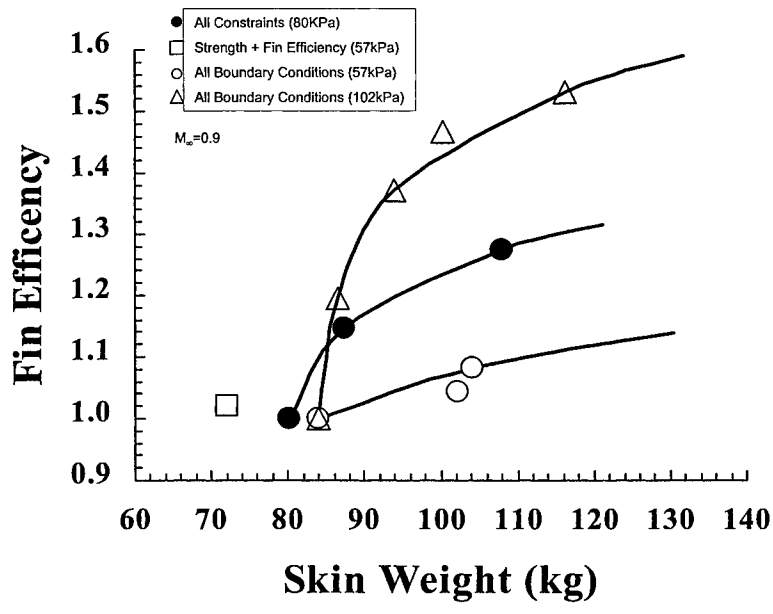

FIG. 4 Fin Efficiency vs. Structural Weight for Ma 0.9

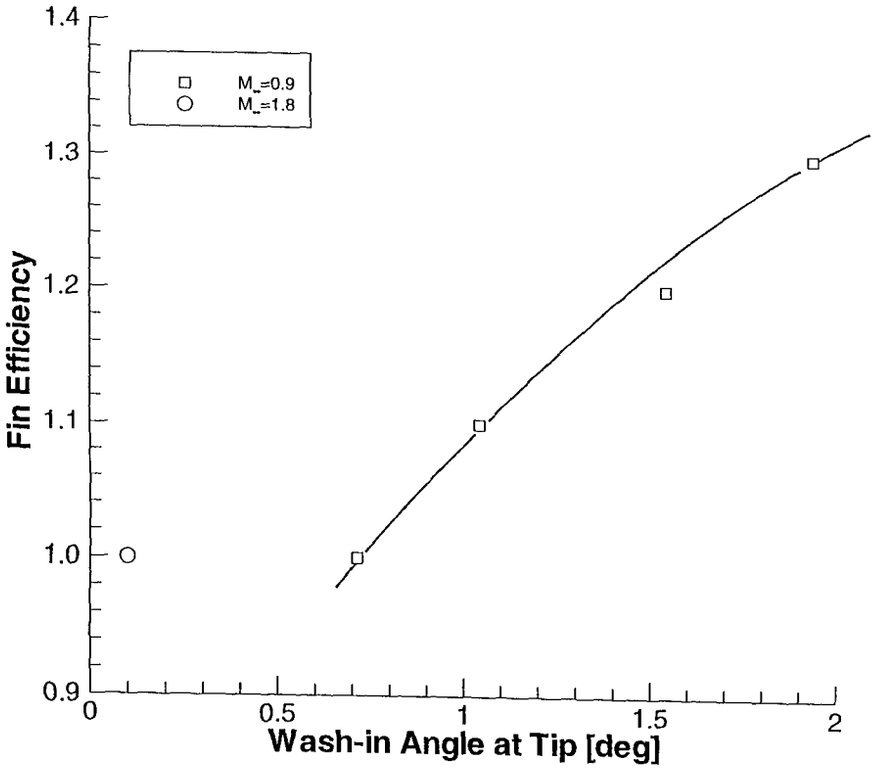

FIG. 5 Fin Efficiency vs. Wash-in angle at Tip

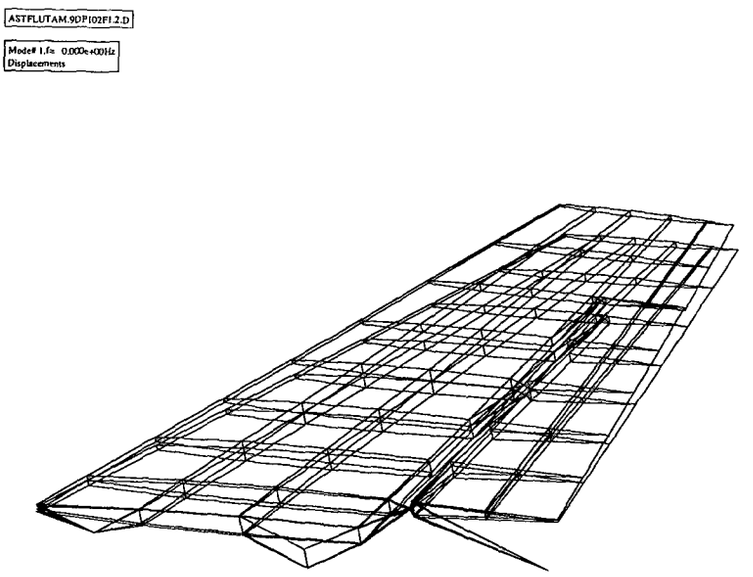

FIG. 6 Displacement in Aeroelastic Case Side Slip for Fin Efficiency 1.2, MA 0.9, 102 kPa

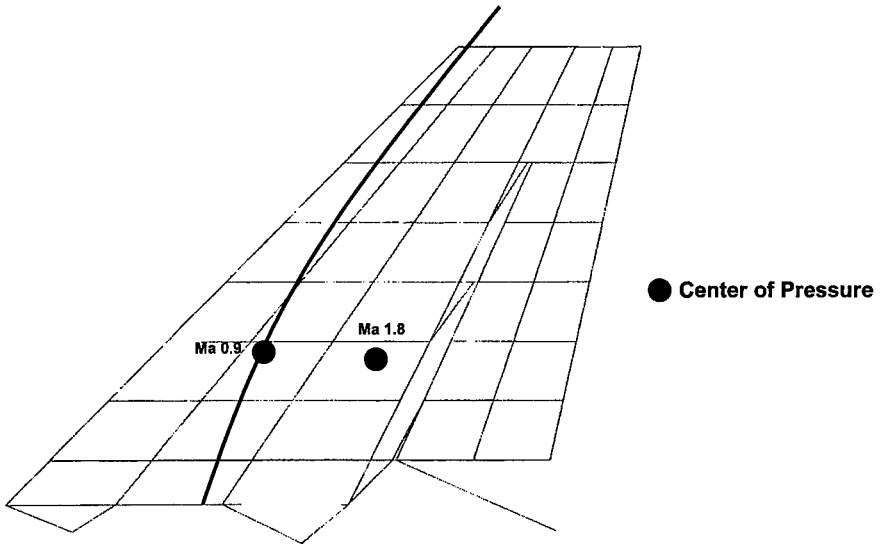

FIG. 7. Elastic Axis Location
(Original Attachments and DASA Skin Thicknesses)

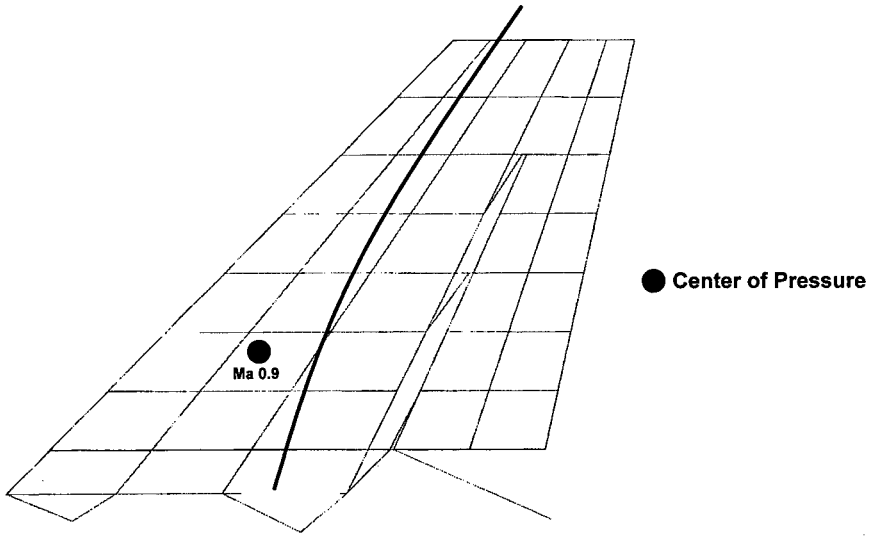

FIG. 8. Elastic Axis Location for Ma 0.9, 102 KPa, Fin Efficiency 1.3

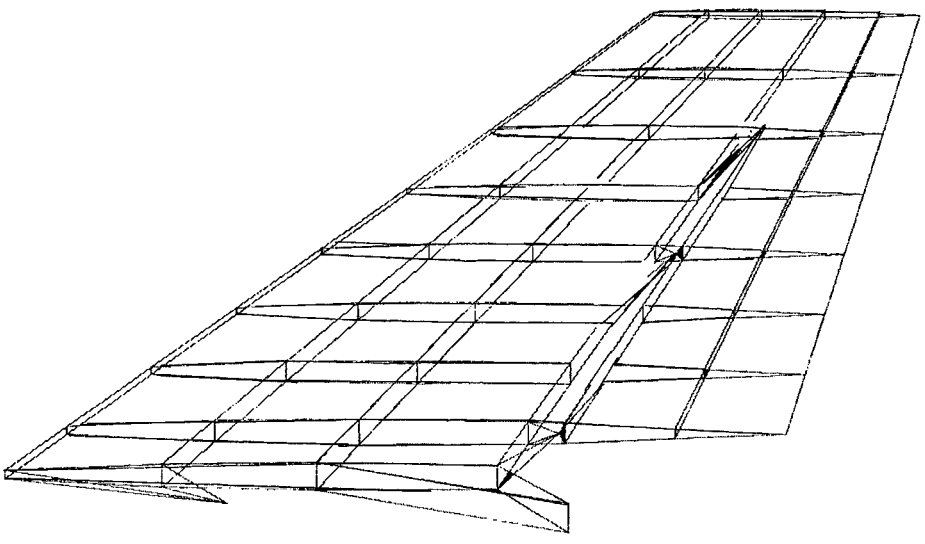

FIG. 9. Rear Attachment Location

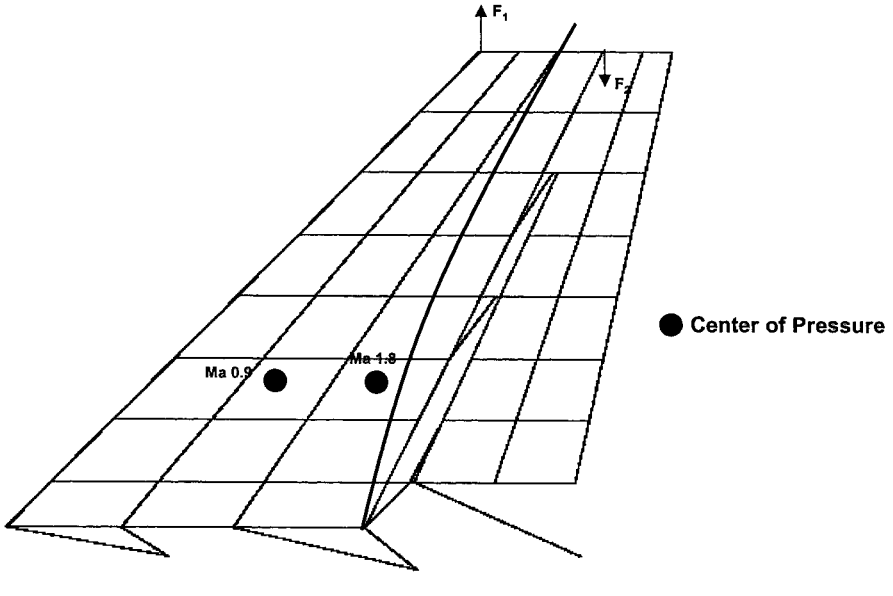

FIG. 10. Elastic Axis Location (Rear Attachments)

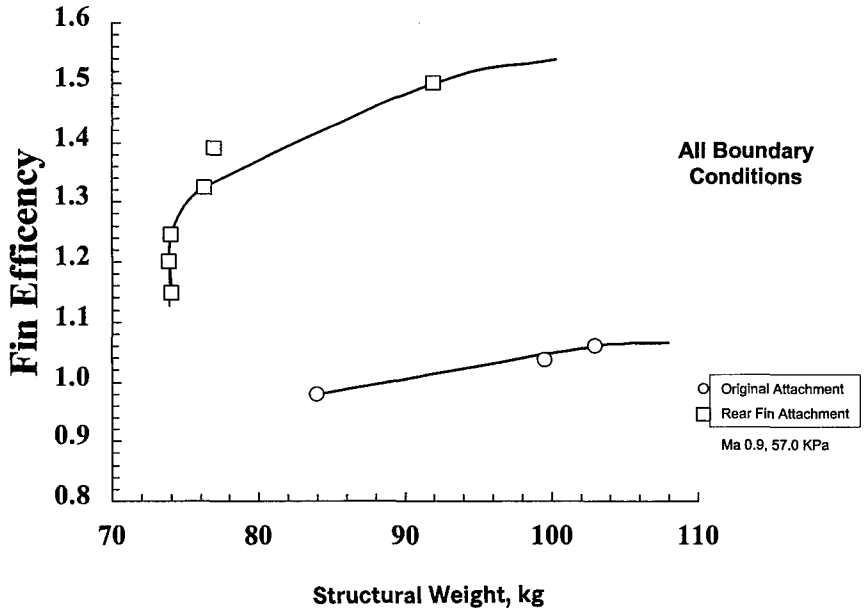

FIG. 11. Fin Efficiency vs Structural Weight for Ma 0.9, 57.0 KPa

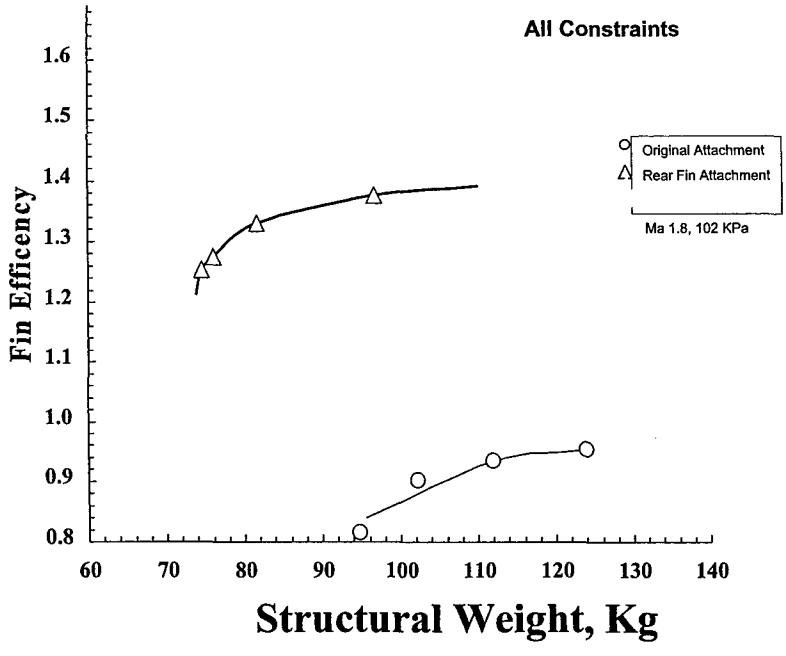

FIG. 12. Fin Efficiency vs. Structural Weight for Ma 1.8, 102 KPa

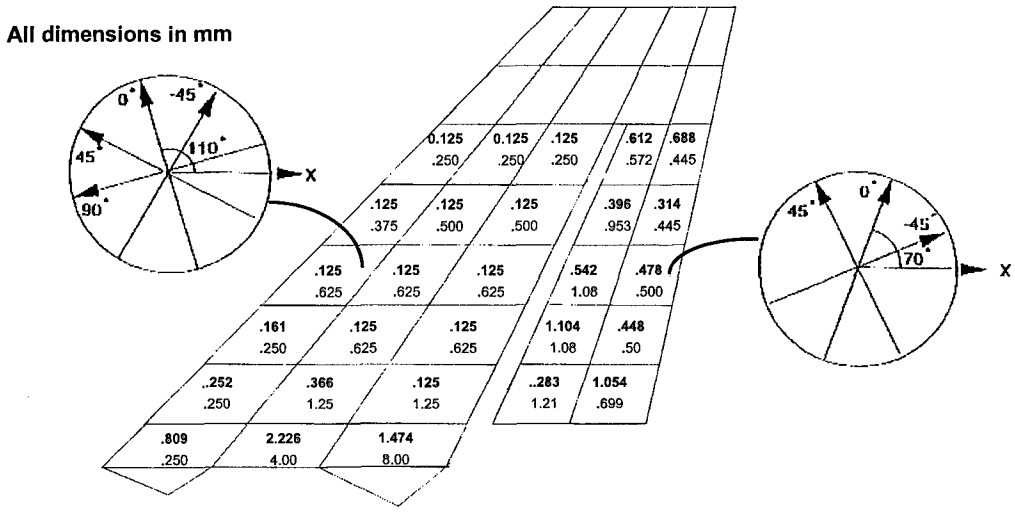

FIG. 13 Thickness of Layer 1 After Optimization (Ma 1.8, 102 Kpa, 1.3 Efficiency)

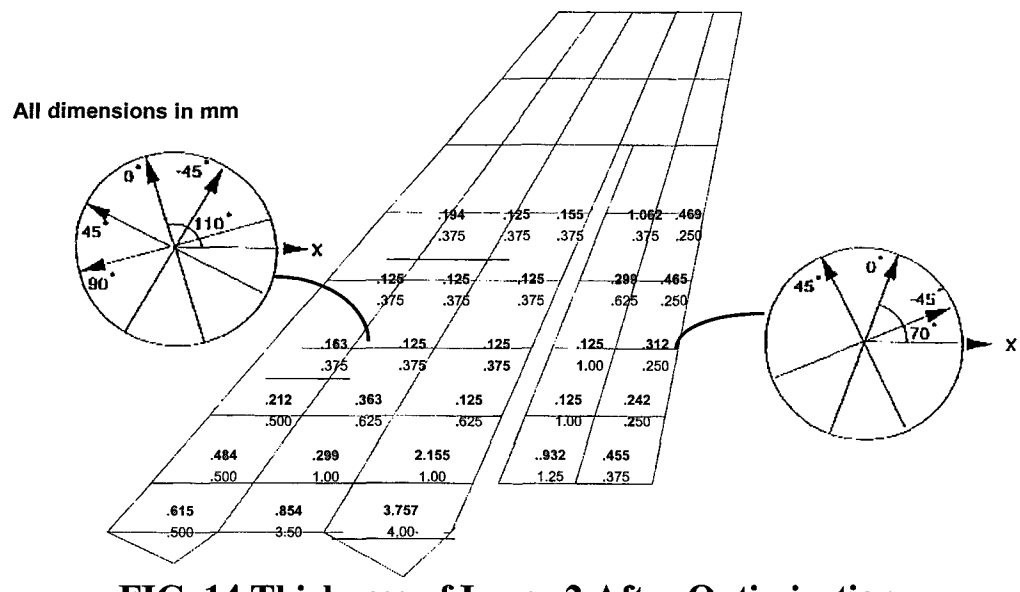

FIG. 14 Thickness of Layer 2 After Optimization (Ma 1.8, 102KPa, 1.3 Efficiency)

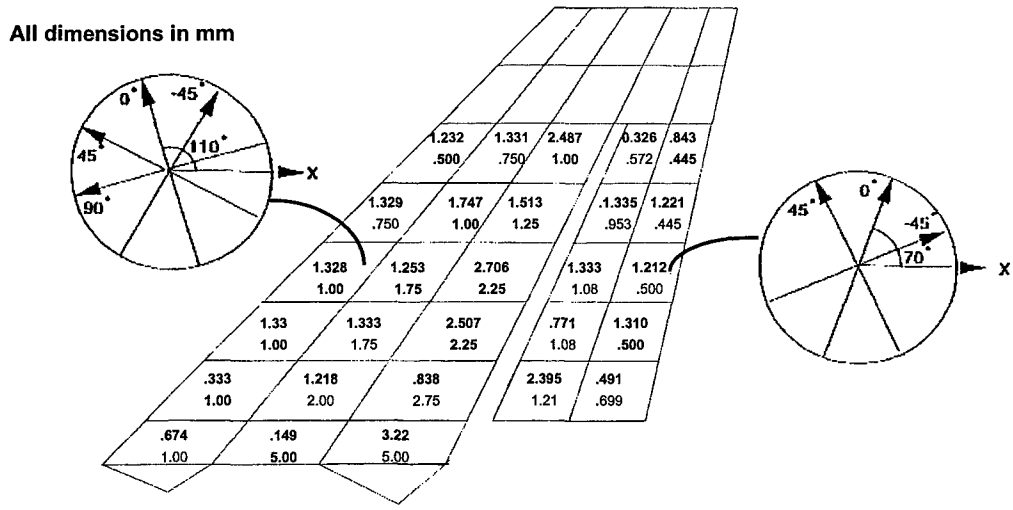

FIG 15. Thickness of Layer 3 After Optimization (Ma 1.8, 102KPa, 1.3 Efficiency)

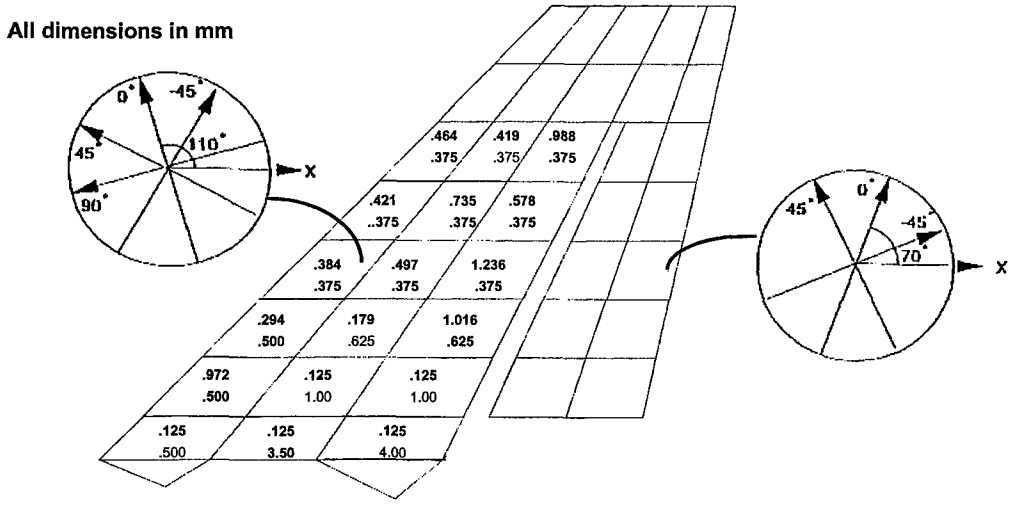

FIG. 16 Thickness of Layer 4 After Optimization (Ma 1.8, 102 Kpa, 1.3 Efficiency)

F-22 Structural Coupling Lessons Learned

William R. Wray, Jr.
F-22 Structural Dynamics
Lockheed Martin Tactical Aircraft Systems
P.O. Box 748, Mail Zone 4272
Forth Worth, TX 76101
United States

Abstract

A survey of current F-22 aeroservoelastic analysis and testing activity shows that valuable insight has been gained into several structural coupling and ride quality problems. The aeroservoelastic (ASE) analysis results agree well with flight and ground test measurements. Examples from a recent structural coupling test will be used to illustrate some recent F-22 ASE issues.

Introduction

The nature of the F-22's mission requires a flight control system (FLCS) which is robust at many different flight conditions. The combination of flexible structure, high bandwidth actuators, and high gains in the FLCS guarantees some structural coupling difficulties. Figure 1 shows a picture of the aircraft and its control surfaces. The horizontal tails and thrust vectoring nozzles are used for pitch control. The tails, ailerons, flaperons, and rudders are used in the lateral and directional axes. The FLCS accelerometers are near the cockpit and the rate gyros are about 150 inches aft of the cockpit.

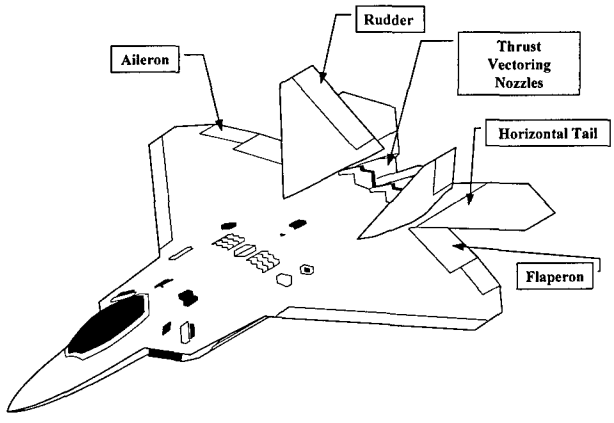

Figure 1 F-22 Aircraft Control Surfaces

Figure 2 shows the F-22 in flight with the Stabilization Recovery Chute (SRC) installed. This is also called the spin chute. It is required for high angle of attack flight testing until adequate spin stability can be shown. A recent structural coupling test was conducted to evaluate the effect of this 1100 pound structure on the critical fuselage bending modes. An additional justification for the test was the loading of a new operational flight program (OFP) with control law changes that had structural coupling ramifications.

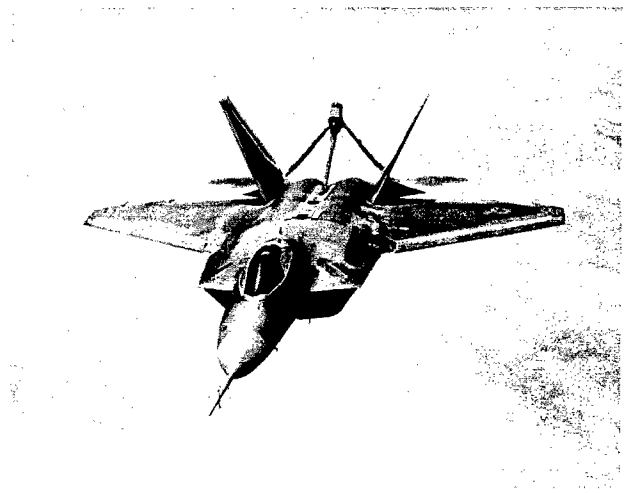

Figure 2 F-22 with Stabilization Recovery Chute (SRC)

Analysis Issues

The lessons learned in the analysis area will be reviewed before proceeding to specific test cases. The analysis issues encountered to date fall into two obvious categories: 1) Modeling the FLCS control laws, and 2) Modeling the structural transfer functions.

The aeroservoelastically sensitive modes on the F-22 are in the 8 to 18 Hz frequency range. There are structural filters on all rate gyro sensor feedback signals and on the vertical and lateral acceleration signals. The goal is to eliminate interaction from the structural modes without causing degradation to the flying qualities due to phase loss and associated time delay.

Modeling the Flight Control Laws

The pitch axis FLCS is fairly easy to model in the analysis. It is essentially a single input, single output system. There are other paths in various parts of the envelope but these have been found to contribute very little to structural coupling. The frequency response bandwidth of the thrust vectoring nozzle is so limited that it can be neglected for the most part. It is necessary to maintain a lookup table for the current pitch

Paper presented at the RTO AVT Specialists' Meeting on "Structural Aspects of Flexible Aircraft Control", held in Ottawa, Canada, 18-20 October 1999, and published in RTO MP-36.

axis gains as a function of Mach, altitude, and other parameters, but this data is readily available.

The lateral-directional analysis requires a different approach. Figure 3 is a diagram of the multi-input, multi-output lateral-directional FLCS. The lateral-directional FLCS gains change mainly as a function of angle of attack and speed. There are interconnects between the lateral and directional axes to remove roll due to yaw and yaw due to roll. At some angles of attack, surfaces are removed completely from the system. Initial efforts to model this complex system for all flight conditions were not successful.

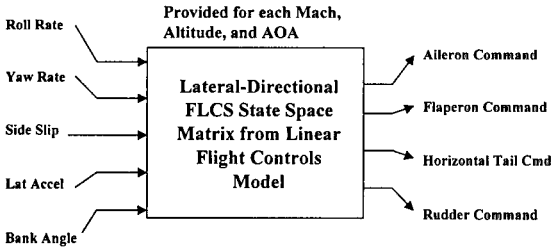

Figure 3 Lateral Directional FLCS for ASE Analysis

Tasking the Flight Controls group with providing state space matrices for each analysis flight condition solved the problem. This requires planning and coordination but it has been quite successful. Figure 4 shows a comparison of the analysis model of the lateral FLCS for a particular path, versus lab test and aircraft ground test for a recent structural coupling test condition. We have found that it is a good 'sanity' check to measure the control law frequency response in the ground simulator and compare this to analysis and aircraft test transfer functions.

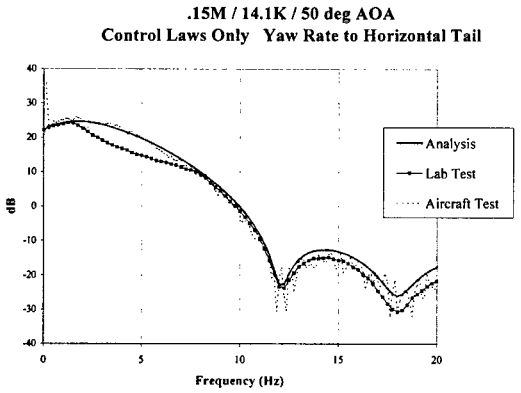

Figure 4 Control Law for Yaw Rate to Tail

Modeling the Structural Transfer Functions

Assuming the control laws are well known, the structure's contribution is the main unknown in structural coupling analysis. The finite element model (FEM) gives estimates of this contribution, but test data is necessary to prove (or disprove) the accuracy of the FEM.

Pitch Axis Structural Transfer Functions

Figure 5 shows the structural transfer function between the horizontal tail and Qb, body axis pitch rate and Nz, the normal acceleration. The strong peak on the charts is the vertical fuselage bending mode. This mode is affected by the overall weight of the configuration. The clean wing condition can have a vertical fuselage bending mode of 10.3 Hz to 11.7 Hz depending on the presence of the spin chute and fuel state.

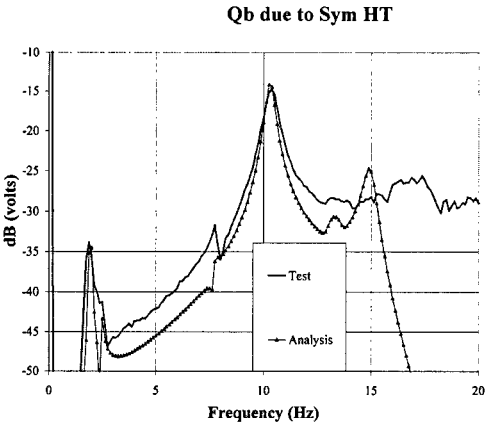

Figure 5a Pitch Rate Structural Transfer Function

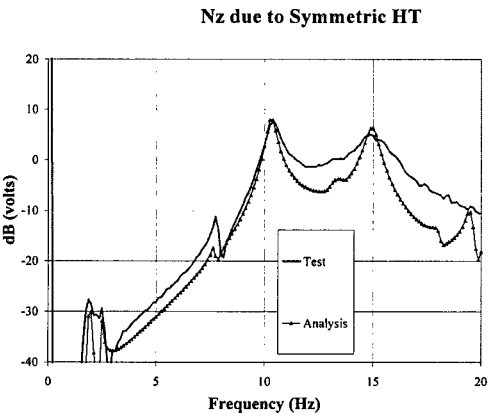

Figure 5b Normal Acceleration Structural Transfer Function

The structural filters for pitch rate and normal acceleration have their maximum effectiveness at 11 Hz. If the fuselage mode is higher or lower by even 1 Hz, the effectiveness is reduced by as much as 10 dB. This will have consequences as the aircraft proceeds through its development program. However, if the structural model has been verified by test, the analyst can make confident predictions about future configuration changes. The analysis matches the test data for the pitch axis cases fairly well. The analysis has been tuned with regard to frequency and damping to achieve this result.

Lateral Axis Structural Transfer Functions

The lateral axis structural transfer functions are shown in Figure 6. Typically, the modes of primary importance for the lateral axis are the wing bending mode at 9 to 10 Hz, and the lateral fuselage bending mode at 14 to 16 Hz.

The analysis predicts the wing bending mode fairly well. The amplitude is close and the frequency is only slightly low. The good analysis correlation allowed the accurate prediction of several roll rate problems that will be discussed in the next section.

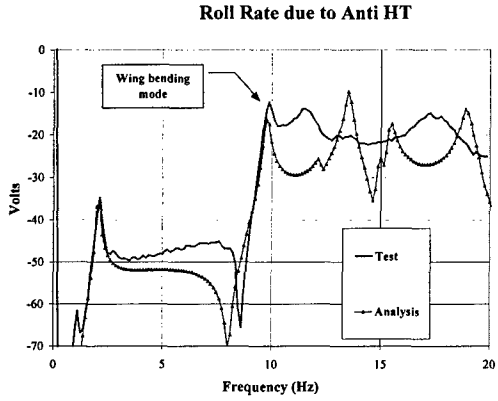

Figure 6a Roll Rate Structural Transfer Function

The analysis is less successful in predicting the amplitude of the lateral fuselage bending mode. This mode is over-predicted by 10 to 20 dB in terms of horizontal tail to Ny, the lateral acceleration at the pilot's seat. This is not the major problem it once was since due to a change in the control laws. The FLCS now uses the lateral acceleration sensor only when the angle of attack is below 16 degrees. When it is important to correctly model the lateral fuselage bending mode for an analysis, the typical practice is to substitute test data in the place of FEM predictions.

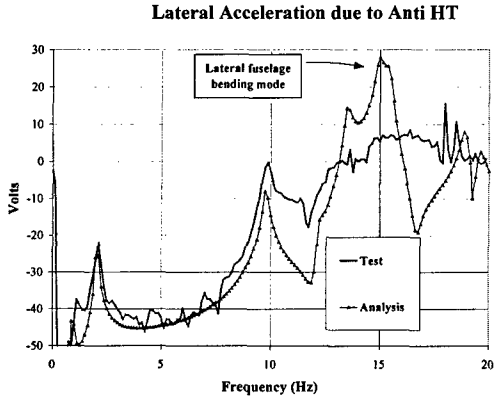

Figure 6b Lateral Acceleration Structural Transfer Function

The lateral and directional axes are controlled using the rudders, flaperons, and ailerons, as well as the horizontal tails. These transfer functions are not shown here but, in general, trends for the other surfaces are similar. The wing bending mode is predicted well and the lateral fuselage bending mode is over-predicted.

Discussion of Specific Case Studies

A recent structural coupling test offers examples of F-22 ASE issues that are of current interest. The main purpose of the test was to provide structural coupling flight safety clearance for the F-22 with stabilization recovery chute (SRC) attached. This 1100 lb installation on the aft part of the aircraft changes the fuselage bending modes slightly. Note that the F-22 structural coupling tests are conducted with the airplane on the landing gear.

The F-22 convention for displaying structural coupling information may not be standard so an explanation is appropriate. Transfer function plots are in dB versus frequency. For test data the Y axis is dB (Volts). The conversion to dB (engineering units) is a constant dB value.

Phase data is not generally reported in the classic Bode style. In general phase considerations have been de-emphasized on the F-22 program. Many feel that the frequencies where problems tend to occur are so high (10 to 20 Hz) that phase predictions are unreliable. The analysis has been tuned to match phase fairly well in the pitch axis, but the lateral-directional still has problems, as will be seen later.

For stability considerations, the first plot shown is generally the open loop transfer function in magnitude form. This plot is dB (dimensionless) on the Y axis, since it is a ratio of output due to an input in the same units. The F-22 has a goal for 6 dB of margin on the open loop transfer function plot, without regard to phase.

When phase is important to show stability, the Nyquist plot is used. The –1 point on the horizontal axis is the neutral stability point and gain margin and phase margin are referenced to this point. The requirement is 6 dB of gain margin and 60 degrees of phase margin.

During a structural coupling test, stability is also shown with closed loop testing. This amounts to simply adding gain to the nominal closed loop system to show required margins.

Discussion of Pitch Axis Test Cases

Pitch Axis Condition #1 "Gravel Road" 160KCAS/1000ft/12deg/Power Approach (Flaps down)

Since the initial flights of the Engineering and Manufacturing Development (EMD) program, the pilots have reported a feeling of light turbulence on approach even in calm air. This has been given the colorful name of Gravel Road, since it feels like the plane is being driven over a rough surface. The dominant frequency is around 12 Hz, the vertical fuselage bending mode. The possibility existed that this rough ride was caused by a structural coupling with the flight control system. Dynamic content was clearly seen in the commands to the actuators but was it cause or effect?

Since the flight test program is currently limited in its ability to measure in-flight stability margins, an experiment was devised to check the level of control system interaction. A switchable filter was created to deepen the pitch rate structural filter on command from the pilot. The idea is that if the control system is causing the Gravel Road, then a deeper filter would improve the ride quality. Figure 7 shows a plot of the flight test aid filter versus the nominal pitch rate filter.

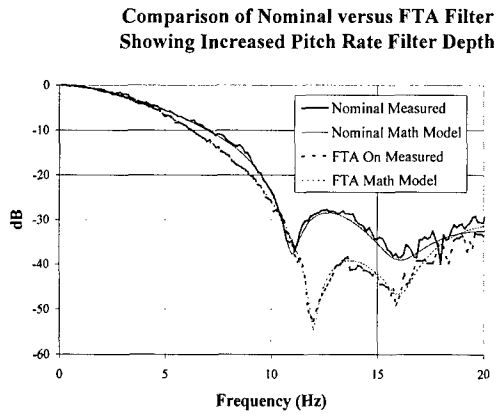

Figure 7 Gravel Road Structural Filter versus Nominal

Figure 8 shows an acceleration time history during the transition from nominal to deeper, flight test aid (FTA) filter. No measurable differences were seen. The prevailing opinion is that the rough ride is caused by separated flow impacting the horizontal tails. However, this issue continues to receive such visibility within the program that every structural coupling test revisits this condition to reiterate that it is not a coupling problem.

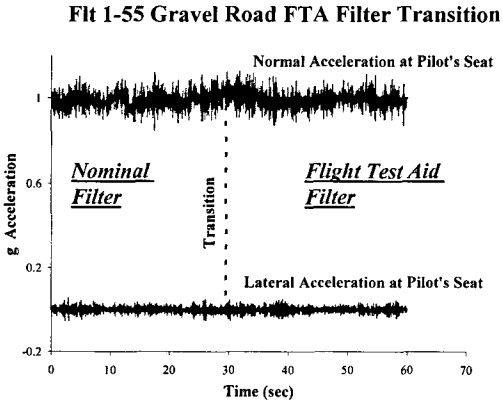

Figure 8 Time History of Pilot Seat Acceleration
Shows no difference with deeper pitch rate filter.

The installation of the 1100 pound spin chute structure causes the vertical fuselage bending mode to go down in frequency by about .7 Hz thus missing the optimal part of the structural filter. Figure 9 shows the magnitude of open loop transfer function with the input at the horizontal tail actuator and the feedback signal to the actuator as the output. The spin chute condition is barely 6 dB down from a magnitude perspective for the Gravel Road condition.

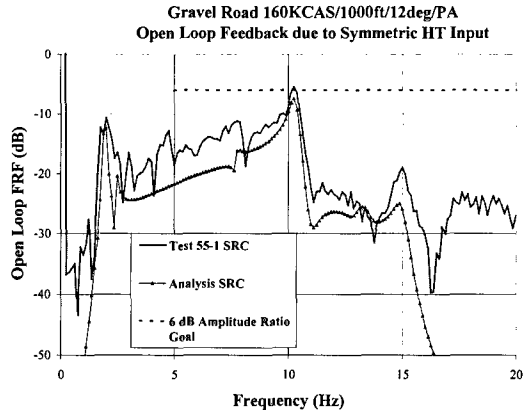

Figure 9 Gravel Road with Spin Chute Open Loop FRF
Shows barely adequate margin

It should be noted that when phase is considered – that is, when a true gain margin is calculated - the actual margin is much greater than the 6 dB shown in the magnitude plot. Figure 10 illustrates this point with a Nyquist plot of the same case.

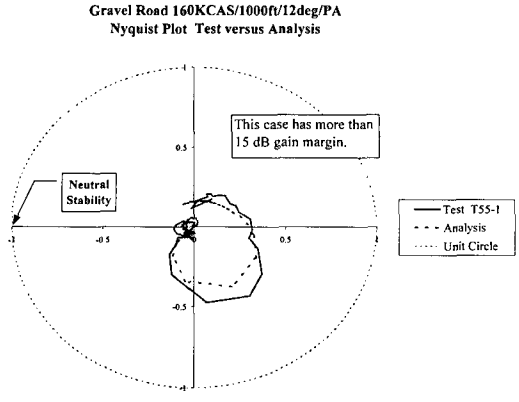

Figure 10 Nyquist Plot for Gravel Road Case
Shows large stability margins.

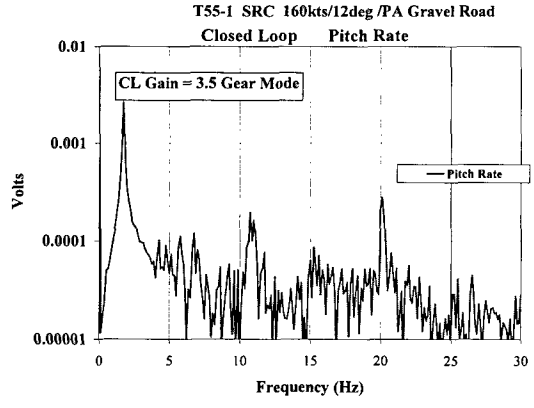

Figure 11 Gravel Road Closed Loop Pitch Rate
With gain of 3.5, only gear mode at 2 Hz is unstable. No problem with fuselage bending mode.

Closed loop testing of this condition also showed a large margin. Figure 11 shows the closed loop pitch rate signal with a gain of 3.5 inserted into the critical path. The next pitch rate case will show the importance of phase considerations.

Pitch Axis Condition #2 .4M/40K/0deg Vector Off

This condition has been tested on every structural coupling test done on the F-22. With vectoring off, all the pitch axis feedback gain is taken by the tail. This results in a 6 dB increase in FLCS gains and a possible decrease in stability margin. Switching vectoring off is a flight test technique only. It will not be possible on production aircraft. It is meant to test the flying qualities where vectoring is inhibited due to an engine anomaly. Also, the vectoring is switched off for parameter identification testing. Analysis predicted that the 6 dB amplitude ratio goal (amplitude margin without regard to phase) would not be met and the test results shown in Figure 12 bear this out.

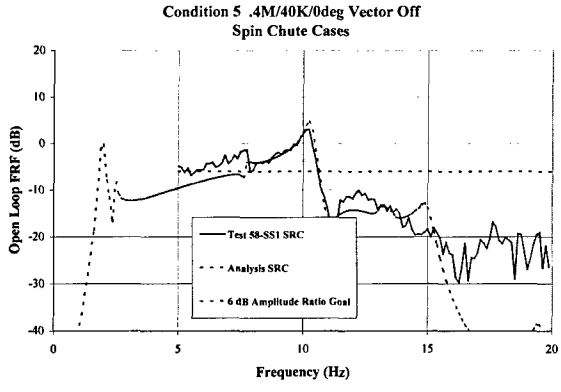

Figure 12 .4M/40K/Vector Off Open Loop FRF

Figure 13 shows the Nyquist plot which accounts for the phase of the open loop frequency response. This plot shows that the high magnitude response is phased such that it will be stable when the loop is closed. This was confirmed with closed loop testing. Despite all testing and analysis showing stability, the vector off case is still approached with caution during flight test. The pilot is briefed that there is potential for a problem and how to respond. So far, the vector off condition has been very stable in flight.

Pitch Axis Condition #3 .95M/High Altitude/0deg Nz Command and Roll Rate Surprise

This condition is called Nz Command because it is the worst case condition for the part of the flight envelope where the Nz sensor is the dominant feedback sensor in the pitch axis. This condition has been tested on all F-22 structural coupling tests.

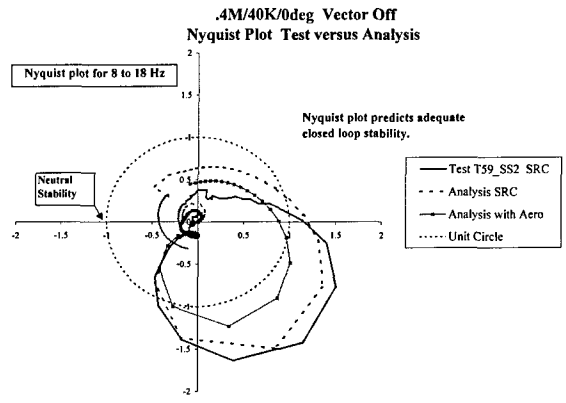

Figure 13 Nyquist Plot of Vector Off Case Showing predicted closed loop stability.

As seen in Figure 14, the spin chute case has a large peak which does not meet the 6 dB magnitude margin goal. This is due to the previously discussed issue of missing the 'sweet spot' of the Nz structural filter because of a lower fuselage bending mode frequency.

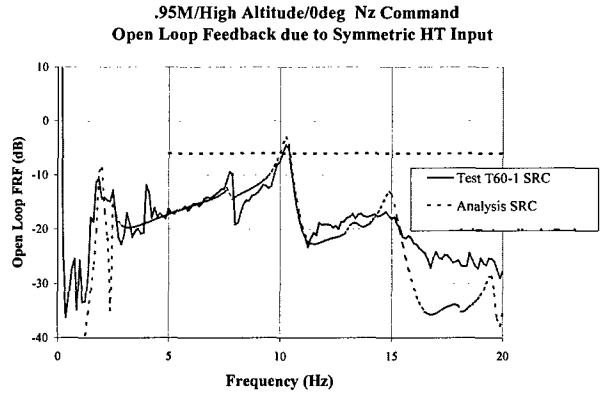

Figure 14 Magnitude Plot for Nz Command Case

The Nyquist plot and the closed loop testing show this mode to be stable. See Figure 15.

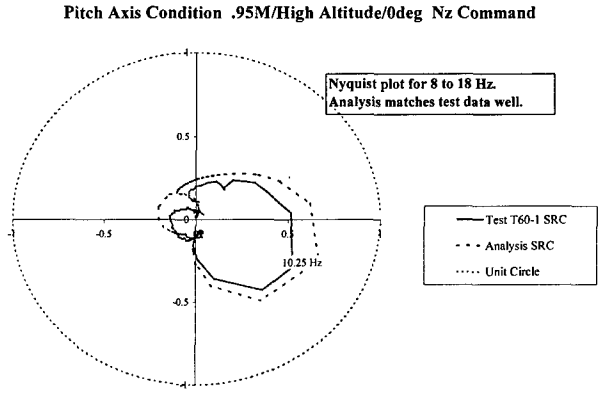

Figure 15 Nyquist Plot for Nz Command

During closed loop testing, an unexpected antisymmetric roll rate instability at 10 Hz was apparent when the gain to the tails was increased. The data was recorded and subjected to post-test analysis. Indeed, the roll rate to horizontal tail loop was only marginally stable at this condition. Figure 16 is the Nyquist plot for roll rate constructed in the post-test analysis.

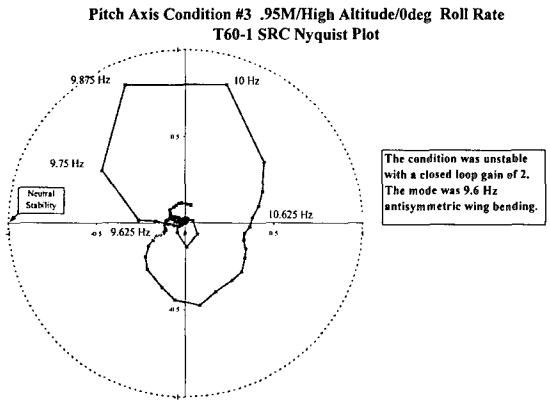

Figure 16 Nyquist plot for Roll Rate at Pitch Condition #3

Figure 17 is the closed loop roll rate signal measured after a gain of 2 was inserted into the horizontal tail actuator path. The large peak is antisymmetric wing bending. The coupling mechanism is horizontal tail exciting roll of the fuselage, which excites the antisymmetric wing bending mode, which generates roll rate feedback, which generates more horizontal tail motion.

After the problem was understood, the next question was: "How did this condition slip by the ASE Analysis certification process?". Discussions with the flight controls engineers revealed that there is a local peak in the roll rate to tail feedback gains at the .95M/High Altitude condition. The .90M/High Altitude condition had been analyzed and found stable as part of the ASE certification process, but the .95M gains were 9 to 12 dB higher. In addition, the gain is increased by the 0 deg angle of attack of the test condition with respect to a trim alpha condition. The problem is

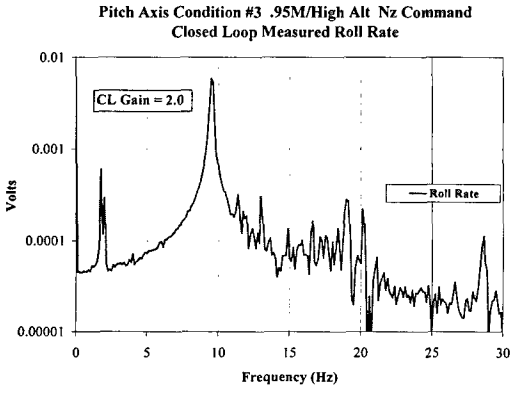

Figure 17 Closed Loop Roll Rate at Pitch Condition #3 Shows unexpected roll rate response.

exacerbated by the fact that in this low alpha flight regime, a shallow 2nd order roll rate filter is employed. In retrospect, this is a very good test condition for roll rate.

The flight controls engineers agreed to reduce the roll rate gains at .95M/High Alt to arrive at values which yield 6 dB of stability margin. This was accomplished with a software change request. In addition, the .95M condition will be added to the ASE Analysis Certification plan.

Pitch Axis Condition #4 Pilot in the Loop

During early flights of the first two development aircraft a "pilot in the loop" structural coupling was observed. This was seen during turns when the pilot was applying aft stick while being subjected to a load factor of about 2 g's. One pilot reported that he could feel himself coupling with the aircraft's structural mode. Figure 18 shows flight test data illustrating this coupling. The frequency is about 13 Hz, slightly higher than the vertical fuselage bending frequency.

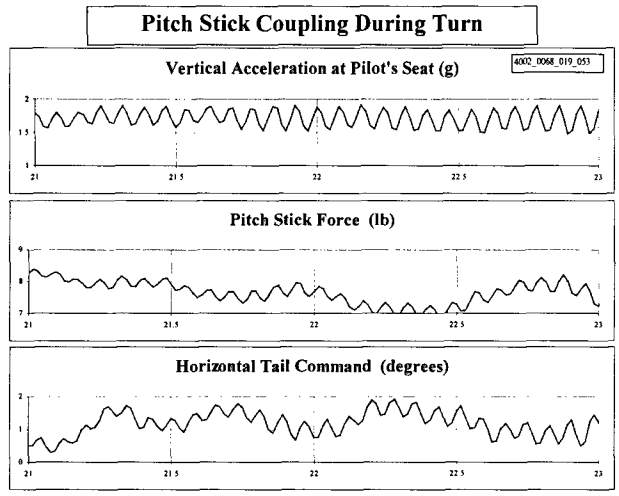

Figure 18 Time History of Stick Coupling

A simple analysis model was constructed to understand the problem. A pilot "gain" was estimated by computing the transfer function between the acceleration at the pilot's seat and the resulting stick force. For the case above, the pilot exerted about .3 lb for every g of acceleration at the 13 Hz frequency. The analysis model confirmed that a problem existed for a portion of the flight envelope.

A structural filter was designed for the pitch stick path that created adequate margin for all test and analysis cases. The filter design had to be coordinated closely with the flight control engineers since the response of the stick is very important to the way an airplane feels to the pilot. Certain overall system time delay requirements dictated a filter with very little phase loss. Throughput requirements set a limit on the filter order. A simple notch filter design met all requirements.

The pitch stick filter was tested to demonstrate its adequacy during the structural coupling test. A volunteer was placed in the cockpit and instructed to apply about 5 lb of aft stick. Data for the unfiltered condition existed from a previous test.

Figure 19a shows the open loop transfer function for the filtered design versus the unfiltered for a worst case condition. The filtered design still has a large response at the fuselage bending mode.

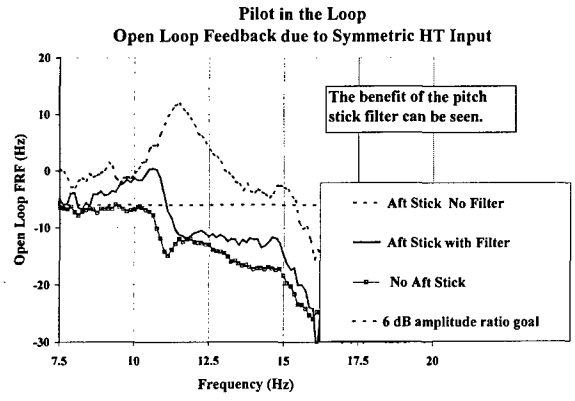

Figure 19a Pilot in the Loop Transfer Function

Figure 19b shows the Nyquist plot for the filtered versus unfiltered test data. This solves the mystery as to why the frequency of the instability was higher than the fuselage bending frequency. The phase of the response caused the instability to be shifted away from the peak response frequency. The plot also demonstrated that the filtered design has more than 90 degrees of phase margin. No "pilot in the loop" problems have been reported in flight testing since the installation of the filter.

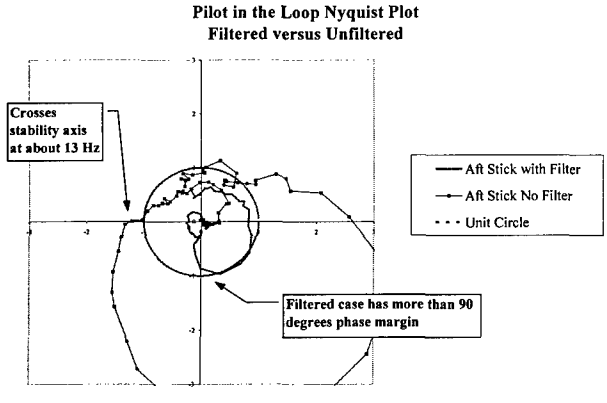

Figure 19b Nyquist Plot for Pilot in the Loop Case

Lateral Directional Test Cases

Lateral Directional Condition #1 .3M/30K/26deg 26 Alpha Concern

Previous structural coupling testing with an older set of flight control laws showed a potential problem at this flight condition due to the contribution of the Ny (lateral acceleration) sensor. When the Ny sensor was opened during testing, the problem went away entirely. The gains at this condition are a strong function of angle of attack. The new operational flight program (OFP) eliminates the Ny sensor for feedback when the angle of attack is greater that 16 degrees. Analysis shows the new FLCS to be very stable at this condition. The test was designed to demonstrate this stability so aircraft limitations could be lifted.

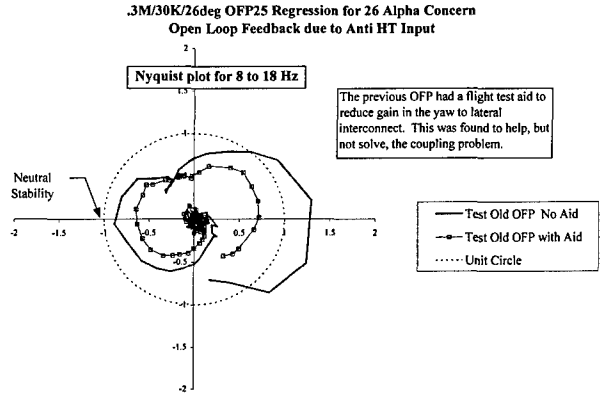

Figure 20a Nyquist Plot for Previous Control Laws Shows beneficial effect of flight test aid.

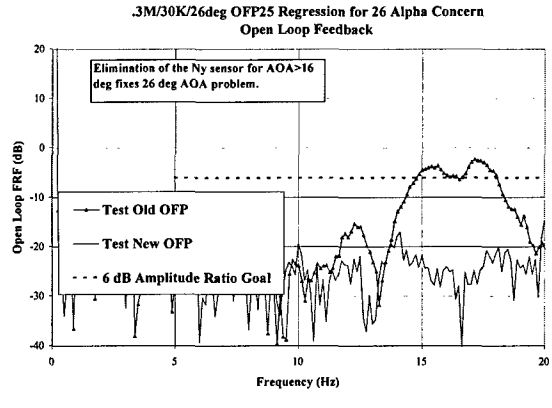

Figure 20b Stability Improvement due to OFP Change

Figure 20a shows a Nyquist plot of previous results. A flight test aid was used to improve the stability as a temporary solution. As expected, the new OFP results are a great improvement over the previous results. See Figure 20b for a magnitude comparison of new versus old control laws at this condition. The 26 degree AOA condition is very stable now.

Flight testing at the 26 degree AOA condition has been marked by a rough ride which has led to pilot comments. At first some thought the entire problem was due to the ASE sensitivity with the old control laws. Certainly, the Ny sensor was feeding significant dynamic content to the actuators. At the time of testing, it was not possible to do an in-flight evaluation of ASE stability margins. Figure 21 shows that the rough ride at the 26 alpha condition has not improved with the new control laws. Apparently, there is considerable buffet at this condition that is not related to the control system.

This rough ride seems to be confined to the 26 degrees and 20000 feet altitude region. If the aircraft goes higher in angle of attack or altitude, the buffet at the pilot's station subsides. At lower altitudes, the buffet does not increase. The bufet has been linked to a vertical tail mode which is excited by separated flow coming from the nose of the aircraft. This vertical tail mode is at about 17 Hz which is very close to the lateral fuselage bending mode. Figure 22 shows the difference in the amount of dynamic content being fed to the actuators due to this buffet-induced signal.

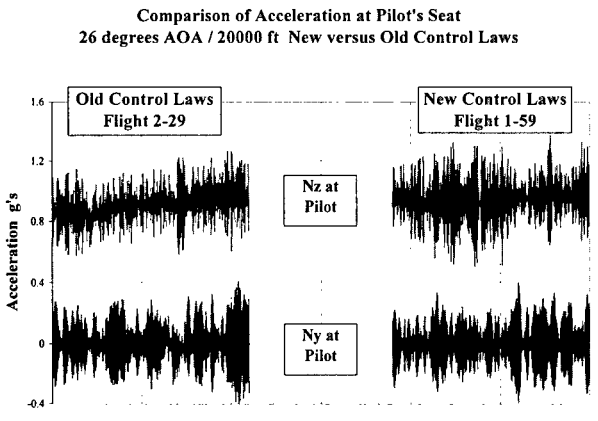

Figure 21 Pilot Seat Acceleration at 26 degrees AOA New versus Old Control Laws

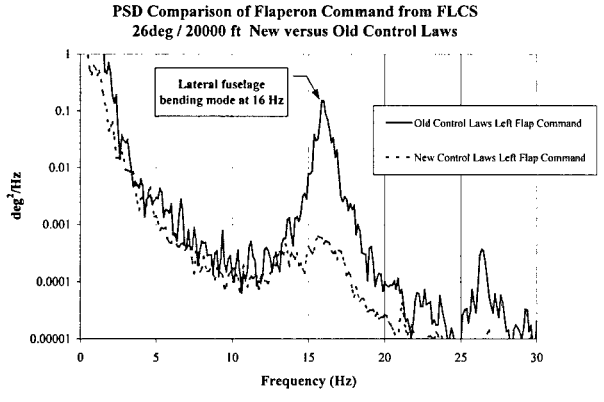

Figure 22 PSD Comparison of Flaperon Command New versus Old Control Laws

Figure 23 shows the hydraulic pressure in two of the control surface actuators at the 26 degree condition. The time slices shown are the same as in Figure 21. Whether the previous FLCS had an ASE problem or not is still debated, but there is no doubt that the pressure fluctuations seen by the actuators have been reduced dramatically due to the elimination of the lateral acceleration sensor. This is bound to be beneficial to their service life.

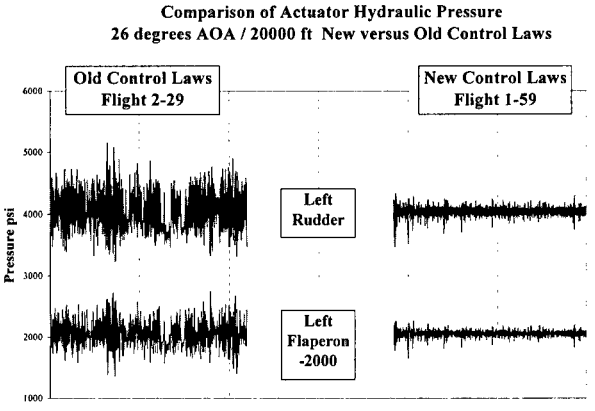

Figure 23 Comparison of Actuator Hydraulic Pressures New versus Old Control Laws for 26 degree AOA

Lateral Directional Condition #2
.25M/26K/60deg Max Roll Rate to HT

This condition was chosen by a survey to determine the worst case roll rate gains for the flight controls update. Pre-test analysis showed the case to be marginally stable. The critical mode is 10 Hz wing bending. The horizontal tail gets the airplane rolling, which excites the antisymmetric wing bending, which imparts roll rate to the roll rate sensor, which commands more horizontal tail.

Figure 24 shows an example of the control laws correlation for this case. Extreme high AOA cases are more difficult to simulate on the F-22 because the flight data is being received from the inertial reference system. This requires good test technique on the part of the control system hardware engineers.

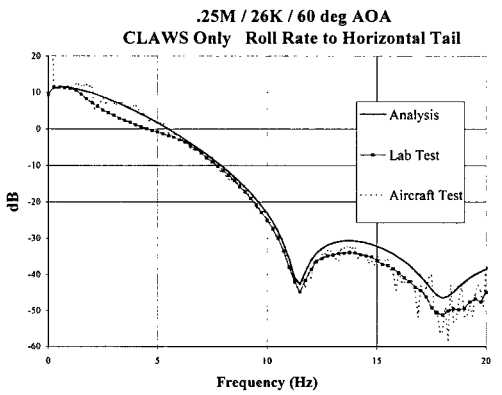

Figure 24 Controls Laws Correlation for Max Roll Rate Case

The test results for the spin recovery chute (SRC) case, shown in Figure 25, agree well with pre-test predictions with regard to the critical 10 Hz wing bending mode. Figure 25 is an example of sensor input test data. The loop was opened at the roll rate sensor and the transfer function is ratio of the output to the random input.

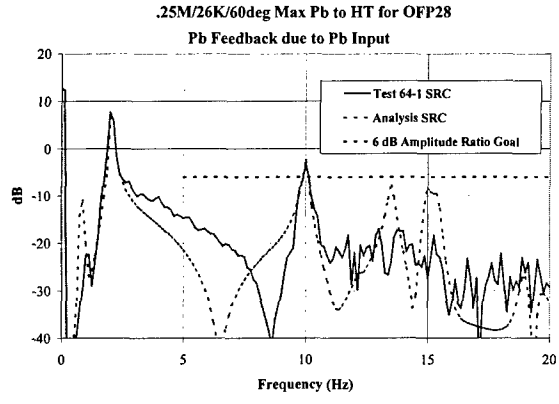

Figure 25 Max Roll Rate Case Magnitude Plot

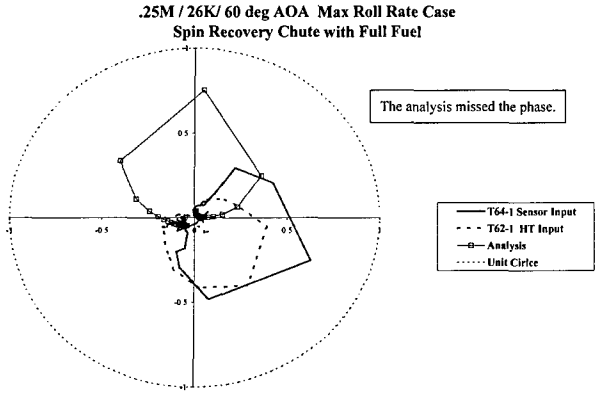

Figure 26 Nyquist Plot for Max Roll Rate Case
Comparison of Sensor versus Surface Input and Analysis.

The Nyquist plot in Figure 26 also shows that the analysis missed the phase. The analysis will be tuned to predict the phase more accurately for cases of this type.

It is helpful to simplify a multi-input, multi-output system to a single-input, single-output system. Pre-test analysis indicated that this flight condition was dominated by the horizontal tail to roll rate sensor path.

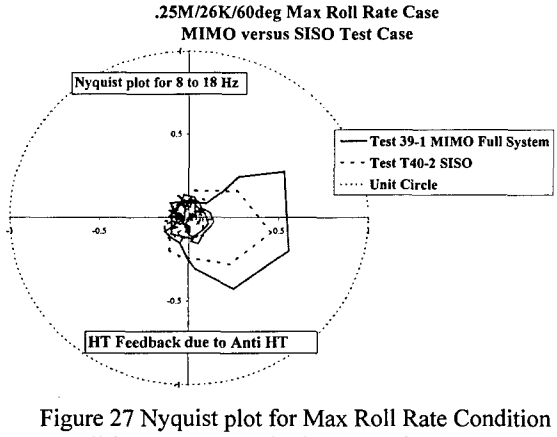

Figure 27 Nyquist plot for Max Roll Rate Condition
Full System versus Single Input, Single Output

To show this, the test case was run in a single input, single output (SISO) condition. In this test, the roll rate sensor is the only active sensor and the horizontal tail is the only active surface. The results are within 1.5 dB of the fully functional FLCS result. The Nyquist plot for the SISO system versus the full system is shown in Figure 27.

The closed loop testing for this condition was not possible in the conventional sense. The horizontal tails were being nearly saturated using artificial pitch rate to keep the FLCS on condition. This left no margin for applying more gain in the horizontal tail path. Though it was not possible to increase the gain, the nominal closed loop case was shown to be stable as expected.

Summary

The F-22 ASE methodology has evolved to a level of maturity that is adequate to show safe flight. The ground and flight testing confirms and agrees with the analytical models. The foundation of results obtained to date will help solve new problems as the aircraft continues through its development program.

Acknowledgements

The author would like to acknowledge the helpful support and advice from colleagues here at Lockheed Martin Tactical Aircraft Systems including Jack Ellis and Mike Bernens. Will Thomas at the F-22 Systems Program Office offered excellent suggestions for improving the content and readability of this paper. Jeff Harris consulted on the stick coupling problem. The Flutter and Dynamics group at Lockheed Martin Aeronautical Systems in Marietta, Georgia furnishes excellent modal and aerodynamic data that is essential to the ASE modeling task. David Layton, Bill Anderson, Nick Radovcich, David Denner, Shahram Parvani, Dave Bougine, John Babb, Bobby Williams, Bob Eller, Chris Economy, Andy Stevenson, Darrell Carney, Keith Edgell, Linda Showers, Vin Sharma, and Alex Tzetzo have all contributed to the structural coupling work described here. The remarkable talents of the Engineering Test Lab at LMTAS including Chi Le and Bryan Jones are much appreciated. The author's management including Mike Woodward, Art Wikoff, and David Lloyd have provided the supportive environment that makes the job enjoyable. In addition, the author expresses gratitude for the assistance of the Structural Analysis core group, including Dave Gibson and Joe Morrow, who made this paper possible.

Aeroservoelastic Modeling, Analysis, and Design Techniques for Transport Aircraft

Myles L. Baker, Patrick J. Goggin, and Bertil A. Winther

Boeing Phantom Works

2401 E. Wardlow Road

Long Beach, California 90807, USA

Abstract

Piloted and batch simulations of the aeroservoelastic response of flight vehicles are essential tools in the development of advanced flight control systems. In these simulations the number of differential equations must be sufficiently large to yield the required accuracy, yet small enough to enable real-time evaluations of the aircraft flying qualities and rapid batch simulations for control law design. The challenge of these conflicting demands is made especially difficult by the limited accuracy of the analytical modeling techniques used, nonlinearities in the quasi-steady equations of motion and by the complex characteristics of the unsteady aerodynamic forces. In this paper, a brief survey of some of the techniques that have been used at Boeing to develop aeroservoelastic math models for control system design and evaluation are presented, along with a discussion of the strengths and weaknesses of the various techniques. The modeling techniques discussed include frequency response fitting methods, rational function approximation methods, and the P-Transform technique. Integration of the aeroservoelastic structural dynamic model with a nonlinear flight simulation is also discussed.

Introduction

Historically, flight control laws have been designed based on the quasi-steady, mean axis flying qualities of an aircraft. However, as airplanes get larger and larger, flexibility and structural dynamics become more and more important. In order to address the influence of aeroservoelastic interactions in large aircraft, it is necessary to include structural dynamic and aeroelastic effects in the simulation tools used for control law design. This results in the generation of a dynamic ASE model with a large number of degrees of freedom for many flight conditions, which creates significant challenges for both the structural and flight controls engineers.

An additional difficulty in aeroservoelastic analysis stems from the fact that the modeling and analysis techniques that are most applicable to aeroelastic loads or flutter analysis are not necessarily those that are most useful for control law design. Traditionally, aeroelasticians have modeled the flexible aircraft in the frequency domain using modal degrees of freedom and generalized mass, generalized stiffness, and frequency dependent generalized aerodynamic matrices. On the other hand, modern control theory is based primarily on the state-space approach, in which the aeroelastic airplane must be modeled as a first-order system of linear ordinary differential equations in the time domain. In addition, the aeroelastician typically works in a mean flight path coordinate system, and the flight controls engineer in a body axis coordinate system.

The final challenge is to ensure that throughout the transformations from frequency domain to time domain, and from one axis system to another, the models remain consistent. This ensures that when a control law is designed based on the time domain state-space model, the same control law can be input into the aeroelastician's frequency-domain analysis and comparable results can be expected.

Modeling of Structural Dynamics & Unsteady Aerodynamics

Three main classes of time domain mathematical modeling techniques are discussed, including the P-transform [1,2,3], frequency response fitting techniques [4], and use of rational function approximations [5,6,7,8,9,10,11,12]. In addition, the application of promising aerodynamic model reduction techniques to the aeroservoelastic model reduction problem are discussed [13,14,15,16,17,18]. Integration of these time domain aeroelastic modeling techniques with nonlinear rigid body and static aeroelastic equations of motion to develop a universal aeroelastic simulation model for use by both aeroelasticians and flight control designers will also be addressed.

P-Transform Technique

Heimbaugh [1] developed a formulation of the aircraft equations of motion (EOM) that provides an accurate modeling of the flexible aircraft (including the unsteady aerodynamic forces) without aerodynamic lag terms. The formulation is analogous to the process that is employed in structural dynamics to reduce the number of degrees of freedom (DOF) and transform the equations into modal coordinates using the Galerkin approach. Essentially, it can be expressed as:

1. Write the frequency-domain equations of motion of the aircraft:

$$\left[Ms^2 + \left(B - \frac{\rho c V}{4} A^{i/k}\right) + \left(K - \frac{\rho V^2}{2} A^{r}\right)\right] x(s) = F(s)$$

where M, B, and K are the mass, damping, and stiffness matrices, A is the generalized Aerodynamic

Paper presented at the RTO AVT Specialists' Meeting on "Structural Aspects of Flexible Aircraft Control", held in Ottawa, Canada, 18-20 October 1999, and published in RTO MP-36.

Influence Coefficient (AIC) matrix (real and imaginary parts), x is the generalized deflection, F is the generalized force, and s is the Laplace variable.

2. Compute the "important" eigenvalues & eigenvectors using a standard flutter solution technique. Here it is assumed that the eigenvalues found in the flutter solution are those important in the response.

3. Construct a time domain state-space model (A, B, C, D Matrices) based on the known eigenvalues & eigenvectors.

The assembly of the state matrices and associated input/output matrices from the aeroelastic eigensolution is roughly equivalent to the generation of a "quasi-unsteady" aerodynamic fit for each aeroelastic mode. For low damped modes (sharp modal peaks) this is a very good approximation. For lightly damped modes (more gradual, wider peaks) the quasi-unsteady aerodynamic fit is only exact at the peak of the mode, thus the accuracy is reduced. This technique has been shown to be extremely accurate when the input excitation is a control surface deflection. For gust inputs, the P-Transform was augmented with aerodynamic lag states based on a Rational Function Approximation (RFA) originally developed by Sevart [8] and Roger [5]. The p-transform technique was used to generate aeroelastic models for production aircraft programs and advanced design studies at Boeing in Long Beach for many years. Some of the applications of this technique include an advanced design of a DC-10 stretch aircraft, the C-17 program, and the MD-11 program.

These models were generated using beam structural models, unsteady aerodynamics from the Doublet Lattice Method (DLM) [19,20], and small perturbation assumptions. Typically, it is difficult to accurately model many of the rigid body aeroelastic modes of the aircraft using these types of modeling techniques. In particular, neglecting drag and other "second order" aerodynamic effects can significantly effect several of the modes (Dutch Roll and Phugoid for example). An example of the sensitivity of the Dutch Roll frequency and damping to a 10% change in global aircraft weight, inertia, and aerodynamic forces is shown in Figure 1. The nomenclature in this Figure is consistent with that used in [21]. Heimbaugh accounted for these effects in a simplified manner by adding modal stiffness and damping terms to the equations of motion to account for the neglected terms. These terms were locally linearized based upon the trimmed aircraft attitude and had to be recomputed for each flight condition.

In summary, there were many advantages to this type of approach. These advantages included:

- Elastic aircraft formulation is consistent with that used in the flutter and dynamic loads analyses. Roots from Aeroservoelastic models will be consistent with those generated from analytical flutter models.
- The technique could accurately capture the correct mode shapes, frequency, and damping values of both the rigid body and flexible modes.
- The technique provided a high level of accuracy for low-damped modes.
- Additive increments used to accurately represent the rigid body motion of the aircraft also were used directly in the generation of physical DOF responses since they are generated from the modal responses.
- Models could be reduced further while retaining the accuracy through the Guyan reduction.

Disadvantages of this approach included the following:

- Due to the nature of the RFA used in this technique for the gust forces, the gust fit was only accurate for lower frequency gust excitations.
- The technique was very cumbersome to use because there were many convergence problems associated with the p-k type of flutter solution.
- Due to the linear nature of the analysis, there was difficulty in some cases to generate locally linear additive corrections that were appropriate. There are many terms that significantly influence the rigid body motion of the aircraft that can only realistically be accommodated in a nonlinear manner.
- Supplemental corrections that were applied in an additive manner to the generalized equations of motion were never distributed and thus were not reflected directly in the distributed loads.
- An unknown amount of error existed for aeroelastic modes with a high level of damping.

Typical results from this analysis technique are included in Table 1 and Figure 2. Table 1 compares phugoid and short period frequency and damping values for a large commercial transport aircraft. This table lists both the result that was obtained using the traditional stability and control analysis equations (Target) and that obtained using the additive correction terms in the structural equations of motion (P-Transform). This comparison illustrates that the accuracy of the augmented equations of motion were within 1-2% in frequency and 2-4% in damping.

Figure 2 shows the magnitude of the inboard wing bending moment due to a vertical gust for the same commercial aircraft at another flight condition. The graph compares frequency responses from two analyses, one performed using a traditional transcendental frequency domain analysis approach (solid line) and another using the P-Transform technique (dashed line). It is observed that the results are fairly close for the short period mode (~0.3 Hz.) and for the first and third elastic mode (~1.3 and ~3.0 Hz.). Thedata for the second flexible mode are not as accurate asfor the first and third. As indicated above, this is due to the representation of the gust forces using the Sevart/Rogers RFA.

FAMUSS

Pitt and Goodman [4] developed the Flexible Aircraft Modeling Using State Space (FAMUSS) technique at Boeing in St. Louis in the late 80's and early 90's. This tool was used in Long Beach for development of maneuver and gust load alleviation, vibration control, and flutter suppression systems in several advanced design studies on both commercial and military aircraft projects.

This tool required input of frequency response data from an outside source (i.e. a transcendental frequency-domain analysis) and used a linear least squares fit to generate a rational polynomial representing the frequency response function. These polynomials were then converted to state space (in block-diagonal form) using simple algebraic techniques. An option was available that allowed the poles of the system to be pre-defined and constrained. A nonlinear least squares approach was also available to improve the polynomial representation as well as an option for frequency dependent weighting to improve the fit in a specific frequency band.

At that time, the preferred process used by Boeing in Long Beach was to generate frequency response data for each input/output pair included in the final state-space model. These frequency responses were computed using the traditional frequency-domain tools that were used for flutter or dynamic loads. Aeroelastic roots (frequency and damping) were calculated using a traditional p-k type of flutter solution. These frequency responses and aeroelastic roots were then input into FAMUSS. The aeroelastic roots were used to generate the denominator terms in the polynomials in a manner analogous to pole-placement techniques. The numerator terms (which result in the input and output matrices) were then generated using the linear least squares approach.

Accuracy of this technique for computing loads responses to gust inputs was limited. Aircraft physical responses due to gusts are computed through the superposition of the modal responses. The aircraft loads, however are a result of both external forces and forces developed due to aircraft rigid body or flexible motion. It was speculated at that time that the inaccuracies were primarily due to a poor representation of the extrenal force. It was further speculated that this inaccuracy was caused either by delays introduced into the equations of motion from the gradual penetration of the aircraft into the stationary gust field, or by inaccuracies at frequencies where the external forces were prevalent. Through a trial and error fashion, it was finally concluded that the introduction of an additional three aerodynamic roots that were not constrained or preselected significantly increased the accuracy of the state-space model with gust inputs. The location of the additional roots was determined through a linear least squares technique.

In summary, there were many advantages to this type of approach. These advantages included:

- The procedure was simple and very robust. The code was very user friendly and included many graphical techniques to review the accuracy and restart capabilities to further improve the model.
- Due to an improved formulation of the iterative P-K solver [22], we were able to obtain solutions for conditions in which the early P-Transform technique has failed to converge.
- Frequency responses could be computed for the entire system and the user could select the model size inside of FAMUSS based upon the needs of the control analysis being performed.

Disadvantages of this approach included the following:

- The accuracy of the rigid body modes in the procedure as illustrated above was subject to the accuracy of the RB mode in the analysis that produced the transfer function. The technique had not been integrated with a more accurate technique for defining or modifying the rigid body response.
- The accuracy of the aeroelastic model for systems where there were a large number (>5-10) of inputs or outputs was significantly reduced. As the number of inputs/outputs is increased the accuracy is decreased unless the number of states (roots) is increased. Ultimately, for many of the practical problems experienced, the number of roots required to obtain an acceptable level of accuracy was very large.

Example frequency responses from this analysis technique are included in Figures 3-4. These responses resulted from a study of gust load alleviation on a large commercial transport aircraft. Due to the large number of control studies performed at that time on this aircraft, a relatively small aeroelastic model was requested to allow for a number of control configurations to be rapidly evaluated. Since the primary interest in this analysis was the low frequency response (including the first couple of wing elastic modes), the number of modes retained in the analysis was kept to a minimum (~6 modes total).

Figure 3 illustrates a comparison of the aircraft CG pitching response due to elevator deflection. In this Figure, the response from the traditional frequency domain analysis is represented by the solid line. The dashed line illustrates the frequency response resulting from the FAMUSS aeroelastic model. As illustrated in this Figure, the short period mode and the first two flexible modes are accurately represented. Accuracy was limited for some of the higher aeroelastic modes in this model.

Figure 4 shows the CG Pitching response due to a vertical gust. Once again, the solid line represents the traditional frequency domain analysis and the dashed line illustrates FAMUSS model. For this response the model was much more accurate and fairly accurately represented the modal characteristics for all of the aeroelastic modes in the model.

Rational Function Approximation (RFA) Techniques

Over the past 25 years, many researchers have investigated the use of RFA techniques to represent unsteady aerodynamic forces in aeroelastic analytical models. The aircraft equations of motion have generally been formulated using a modal approach to represent the structural dynamics. The unsteady aerodynamic forces are also generated in modal coordinates and are represented by a rational function in frequency. Since the aerodynamics are represented by a rational function, they can be analytically transformed into the time domain using Laplace transform techniques. A final set of time domain equations can then be formulated and cast in state-space form.

Some of the initial studies included Sevart [8], Roger [5], Edwards [9], and Vepa [10]. These approaches differ in the

form of rational function that is used to represent the aerodynamic forces. All of these techniques added a large number of aerodynamic states to the aeroelastic equations of motion. Generally researchers have predefined the poles of the rational function and the numerator coefficients have been determined using linear least squares techniques. Researchers have also investigated optimization of the pole location and other techniques to improve the aerodynamic representation and reduce the number of equations that are required to achieve the required level of accuracy.

The state-space form of the equations of motion using the RFA techniques listed above result in large partitions of null value coefficients. To reduce the size of the aeroelastic system, Karpel [11] developed a form of RFA that reduces the sparse nature of the matrices and the number of states accordingly. This method used convergent iteration techniques to optimize the aeroelastic models given a reduced number of states. This method was named the "Minimum State Method".

Boeing Long Beach has investigated the use of RFAs in the generation of aeroelastic modeling for many years and has kept abreast of changes in this area. Although there was great desire to reduce the size of these aeroelastic models, robustness issues associated with the convergence of accurate minimum state models were never quite resolved. Boeing research included the usage of RFA approximations for both motion-induced unsteady aerodynamic forces as well as the gust induced external forces. Research results concluded that in order to obtain the robustness required in a production engineering environment, the usage of a method such as that developed by Roger [5] was required. The research also concluded that in order to accurately model gust forces on large transport aircraft, an RFA that explicitly captured the time lag associated with the penetration of the aircraft into the gust field, was required. Some of the latest elements of this work are published in technical reports and papers from Dykman [6] and Goggin [7].

In summary, there were many advantages to this type of approach. These advantages included:

- The accuracy of the resulting aeroelastic model is very high.
- The robustness associated with the use of some of the RFA techniques is very good. Aeroelastic models can be generated without a significant amount of user intervention.

Disadvantages of this approach included the following:

- The resulting aeroelastic model is very large and could prohibit quick studies and real-time simulation.
- The accuracy of the rigid body modes was subject to the accuracy of the aerodynamics used in generation of the RFA. The technique had not been integrated with a more accurate technique for defining or modifying the rigid body response.

As stated above, accuracy of these RFA techniques for state space models is very good. For the examples shown here, a Rogers RFA with 4 aerodynamic lag states per mode was used to represent the motion dependent aerodynamic forces. A Dykman [6] gust fit was used with a total of 12 gust aerodynamic states (for the complete model, not per mode) to represent the external gust forces. In the gust RFA, the 12 states are comprised from an RFA with three explicit time delays and four repeated roots per delay. An example of the external gust force representation is included here in Figure 5.

Figures 6 and 7 also illustrate the accuracy that can be obtained from a model of this type. Frequency responses comparing the traditional transcendental frequency response technique (dots) is compared to that using the RFA state space model (solid line). Figure 6 illustrates a bending moment response in the wing due to a gust input. Figure 7 illustrates a horizontal tail root shear due to the same gust input. As shown in these Figures the correlation is excellent.

Figure 8 illustrates a time history of the horizontal tail root shear due to a very short 1-cosine vertical gust. This is a case where the gust force representation developed by Dykman was critical. This was a challenge due to the aft location of this component load on this large transport, and the high frequency excited by these types of gust patterns that are specified in the commercial aircraft criteria.

Other Reduced Order Modeling Techniques

All of the techniques described above can essentially be viewed as model reduction techniques where a dynamic system with a high order (due to the transcendental frequency-domain aerodynamics) is approximated by an "equivalent" low order system. Since the unsteady aerodynamic models used by aeroelasticians (and therefore, by aeroservo-elasticians) have traditionally been frequency domain methods based on the linear potential equations (such as the doublet-lattice method), the model reduction techniques that have received most of the attention in the past are the frequency domain methods described above. However, the exponential growth of computer capability (coupled with the exponential decay of computer cost) is paving the way for using nonlinear unsteady aerodynamic tools based on the finite difference (or finite volume/finite element) method in aeroelasticity. This has the potential for improving the accuracy of the dynamic aeroelastic models used in aeroservoelasticity, but introduces some significant problems in formulating reduced order models suitable for control law design and real time simulation.

Recently, several researchers have started to consider the problem of forming reduced order unsteady aerodynamic models based on unsteady CFD models. Three approaches that have received considerable attention recently are (1) eigenvalue based methods, (2) balanced reduction methods, and (3) system identification methods.

In the eigenvalue based model reduction methods, the eigenvalues and eigenvectors of the unsteady flowfield are computed and used as a basis for model reduction [15]. Those eigenmodes that are "important" (usually quantified by the low frequency or lightly damped eigenvalues) are then retained while the "unimportant" modes are truncated or residualized. This approach is almost identical to the modal truncation approach to model reduction that has been applied for many years in structural dynamics, and has shown great

promise for model reduction of unsteady aerodynamic systems.

The balanced reduction methods, on the other hand, are based on the concepts of controllability and observability of the unsteady aerodynamic model. In these techniques, the aerodynamic states that are highly controllable (i.e. those that are easily excited by airplane control surface, rigid body, or structural deflections) and at the same time highly observable (i.e. those that, once excited, induce significant loads on the structure) are retained. The balanced reduction approach is less physically intuitive than the eigenvalue based techniques, but has the potential for producing smaller and more accurate reduced order models [13,14].

Both the eigenvalue based methods and the balanced reduction methods suffer from a serious drawback in that they require extensive modifications to the CFD code in order to generate reduced order models. This difficulty is avoided if a system identification approach is used in which the CFD code develops time histories of the unsteady aerodynamics, and an external code is used to process the time history data and generate a reduced order model of the unsteady aerodynamics. The K-L method [16,17] is one such technique that develops an eigenvalue-based reduced order model using a system identification approach. Another approach under development are the impulse response based techniques [18], which directly identify impulse responses of the unsteady aerodynamics. The impulse response approach has not been shown to develop models of low enough order to be useful for control law design. However, this approach has been shown to capture some of the aerodynamic nonlinearities inherent in transonic flow, which could substantially increase the range of applicability of the reduced order models.

Boeing has investigated several of the advanced model reduction techniques described in this section, and has applied them to several configurations with good success. However, none of these techniques is mature enough for use in a production environment. Each of the techniques described has its own advantages and disadvantages, and it is not yet clear which approach is best. It is safe to say, however, that they will probably change the face of aeroservoelasticity as they mature, and as the affordability of computational power increases.

Recent Improvements

New transport aircraft designs like the High Speed Civil Transport (HSCT) and the Blended Wing Body (BWB) are more challenging from an aeroservoelastic perspective than conventional configurations. In the case of the HSCT, there is not only the possibility of gaining benefits from load alleviation systems for minimizing gust and maneuver loads, but significant benefits could also be realized through using flutter suppression. In addition, significant ride quality/flying qualities issues arise due to the long, slender fuselage with its associated low bending frequencies. For the new class of BWB configurations, pitch control is obtained by deflecting trailing edge control surfaces (in contrast to a conventional transport configuration, where pitch control comes from a horizontal tail). It is therefore important to include the interaction between the pitch command and the wing bending modes in control law design.

In order to address these new aeroservoelastic challenges and to improve accuracy on conventional configurations, some recent improvements have been made to the ASE modeling techniques described above. The recent modeling improvements have focused on the P-Transform method for two main reasons: (1) acceptable accuracy can be obtained with very low order P-Transform ASE models, and (2) the poles of the P-Transform model are consistent with the P-K flutter results (which is especially important in configurations with lightly damped modes such as the HSCT).

The enhancements that have been made to the P-Transform method in recent years reduce or eliminate many of the disadvantages highlighted above. The most significant improvements are:

- Integration with Nonlinear Simulation. A large portion of the labor required to generate P-Transform ASE models was associated with generating the additive corrections necessary to accurately model the rigid body modes. This problem has been solved by separating the equations of motion into two parts; one describing the linear quasi-steady response and the other containing the dynamic increment. The quasi-steady equations are then discarded in favor of the more accurate nonlinear 6 DOF simulation typically used in flight controls. The resulting ASE models include the best possible (fully nonlinear) model of the rigid body modes, while including linearized structural dynamics and unsteady aerodynamics through the P-Transform technique.

- Integration with improved P-K Solvers. The convergence problems that caused difficulty in using the P-Transform technique were due to the state of the art in P-K flutter solvers at that time. A tight integration of the P-Transform process with the P-K flutter solver in MSC/NASTRAN [22] has significantly improved this situation.

- Modification of the P-Transform technique to compute structural loads (i.e. wing bending moments or hinge moments) in a manner consistent with the quasi-steady nonlinear simulation.

- Improved modeling of gust aerodynamic forces. An improved RFA technique using explicit time lags [6] for the gust aerodynamics has been implemented, significantly improving the accuracy of responses due to gust excitation.

Several tests were performed to verify that the improved P-transform technique was implemented correctly in the simulation. One such test compared the roots of the linear model with roots obtained from the simulation when it was linearized about the trim point. In addition, various mean-axis response variables were computed at the static trim condition to demonstrate that they were unaffected by the superimposed dynamic increments. Figure 9, showing the roots associated with longitudinal motion, confirms that eigenvalues of the flexible modes in the linear analysis are close to the ones obtained for the simulation model at a banked turn as well as at a level flight condition. The nonlinearity of the 6-DOF simulation can be observed in the changes in the rigid body eigenvalues for different trim conditions. A similar

correlation was obtained for roots associated with lateral motion.

The improved P-transform was validated in several other ways. Time response comparisons were made with a version of the RFA technique developed in [12]. Representative results are shown in Figure 10 for an advanced transport aircraft at a Mach number of 0.65. The illustrated response was computed for a horizontal tail doublet input of ± 2 degrees amplitude and a period of 5.0 seconds starting at 2.5 sec. We note that correlation between the two methods is excellent.

The improved method was also evaluated through comparison with MSC/NNASTRAN frequency domain solutions. Figure 11 shows magnitude and phase of the acceleration responses for an advanced transport aircraft flying at sea level and at a Mach number of 0.4. We observe that the two solution techniques yield practically identical magnitude results up to a frequency of 7.0 Hz. Discrepancies above that frequency are explained by differences in the modeling of the elevator surface. A rigid control surface mode is used to generate the P-Transform input whereas a more realistic, flexible elevator model provides the excitation force in the MSC/NASTRAN analysis.

Conclusions

Experiences derived from several transport aircraft programs at Boeing led to a continuous search for, and development of, accurate techniques for ASE modeling and simulation. All of the methods discussed here have several advantages as well as disadvantages. We found that some of the disadvantages of the early P-Transform technique could be removed by separation of the EOMs into two parts, one describing the quasi-steady motion and the other involving the structural dynamics of the aircraft. This development allowed the model to be linked to the nonlinear 6DOF simulation used for analysis and design of advanced flight control systems.

The refined P-transform technique is based on a unique formulation that preserves the roots of the dynamic aeroelastic system and eliminates the need for auxiliary state variables to describe the unsteady aerodynamics. It has provisions for control surface as well as atmospheric gust inputs. Comparisons with other solution techniques were used to validate the method. Our analytical results demonstrate excellent correlation with structural response data (accelerations, rates and displacements) obtained from the transcendental frequency-domain solution. Further work is required to evaluate the accuracy of external loads generated by turbulence.

References

1. Heimbaugh, R. M., "Flight Controls Structural Dynamics IRAD", McDonnell Douglas Report MDC-J2303, March 1983.

2. Winther, B. A., Goggin, P. J. and Dykman, J. R., "Reduced Order Dynamic Aeroelastic Model Development and Integration with Nonlinear Simulation", AIAA/ASME/ASCE/AHS/ASC 39th Conference on Structures, Structural Dynamics and Materials, Paper AIAA-98-1897, Long Beach, California, April 1998.

3. Winther, B. A. and Baker, M. L., "Reduced Order Aeroelastic Model for Rapid Dynamic Loads Analysis", AIAA/ASME/ASCE/AHS/ ASC 40th Conference on Structures, Structural Dynamics and Materials, Paper AIAA-99-1265, St. Louis, MO, April 1999.

4. Pitt, D. M. and Goodman, C. E., "FAMUSS: A New Aeroservoelastic Modeling Tool", Proceedings of the AIAA/ASME/ASCE/AHS/ ASC 33rd Conference on Structures, Structural Dynamics and Materials, Paper AIAA-92-2395. Dallas, Texas, April 1992.

5. Roger, K. L., "Airplane Math Modeling Methods for Active Control Design", AGARD-CP-228, Aug 1977.

6. Dykman, J., "An Approximate Transient Gust Force Derived from Phase Shifted Rational Function Approximations to the Doublet-Lattice Harmonic Gust Coefficients", McDonnell Douglas Report MDC-92-K0283, Feb 1992.

7. Goggin, P. J., "A General Gust and Maneuver Load Analysis Method to Account for the Effects of Active Control Saturation and Nonlinear Aerodynamics", AIAA Dynamics Specialist Conference Paper No. 92-2126, Dallas, Texas, April 1992.

8. Sevart, F. D., "Development of Active Flutter Suppression Wind Tunnel Testing Technology", Air Force Flight Dynamics Laboratory TR-74-126, Jan 1975.

9. Edwards, J. W., "Unsteady Aerodynamic Modeling and Active Control." SUDAAR 504, Stanford University, 1977.

10. Vepa, R., "On the Use of Pade Approximants to Represent Aerodynamic Loads for Arbitrary Small Motions of Wings," AIAA 14th Aerospace Sciences Meeting, Washington, D.C., 1976.

11. Karpel, M., *Design for Active and Passive Flutter Suppression and Gust Alleviation*, Ph.D. Dissertation, Stanford University, 1980.

12. Tiffany, S. H. and Adams, W. H., "Nonlinear Programming Extensions to Rational Function Approximation Methods for Unsteady Aerodynamic Forces", NASA Technical Paper 2776, July 1988.

13. Baker, M. L., *Model Reduction of Large, Sparse Dynamic Systems with Application to Unsteady Aerodynamics*, Ph.D. Dissertation, UCLA, Los Angeles, CA, 1996.

14. Baker, M. L., Mingori, D. L., and Goggin, P. J., "Approximate Subspace Iteration for Constructing Internally Balanced Reduced Order Models of Unsteady Aerodynamic Systems", 37th AIAA/ASME/ASCE/AHS/ASC Structures, Structural Dynamics, and Materials Conference, Salt Lake City, UT, April, 1996.

15. Hall, K. C., "Eigenanalysis of Unsteady Flows About Airfoils, Wings, and Cascades," *AIAA Journal*, Vol. 32, No. 12, pp. 2426-2432, Dec. 1994.

16. Romanowski, M.C., "Reduced-Order Unsteady Aerodynamic and Aeroelastic Models Using Karhunen-Loeve Eigenmodes," Proceedings of the AIAA Symposium on Multidisciplinary Analysis and Optimization (Bellevue, WA), AIAA, Reston, VA, 1996, pp. 7-13 (AIAA Paper 96-3981).

17. Kim, T., "Frequency-Domain Karhunen-Loeve Method and Its Application to Linear Dynamic Systems,", AIAA Journal, Vol.36, No. 11, November 1998.

18. Silva, W.A., "Reduced-Order Models Using Linear and Nonlinear Aerodynamic Impulse Responses," 40th AIAA/ASME/ASCE/AHS/ ASC Structures, Structural Dynamics, and Materials Conference, Paper No. AIAA-99-1474, April 12-15, 1999, St. Louis, MO.

19. Albano, E. and Rodden, W. P., "A Doublet-Lattice Method for Calculating Lift Distributions on Oscillating Surfaces in Subsonic Flow". *AIAA Journal*, Vol. 7, pp. 279-285, Feb 1969.

20. Giesing, J. P., Kalman, T. P. and Rodden, W. P., "Subsonic Unsteady Aerodynamics for General Configurations". Air Force Flight Dynamics Laboratory Report AFFDL-TR-71-5, Nov 1971.

21. Etkin, B., *Dynamics of Flight*. John Wiley & Sons, 1959.

22. Rodden, W. P. (ed.), "MSC/NASTRAN Handbook for Aeroelastic Analysis", MacNeal-Schwendler Corp., MSR-57, Los Angeles, CA, Nov 1987.

Root	Natural Frequency (Hz)		Damping (% Critical)	
	Target	P-Transform	Target	P-Transform
Phugoid	0.0115	0.0114	39.13%	40.41%
Short Period	0.2585	0.2638	31.69%	32.72%

Table 1: Accuracy of P-Transform in Matching Rigid Body Modes of a Transport Aircraft.

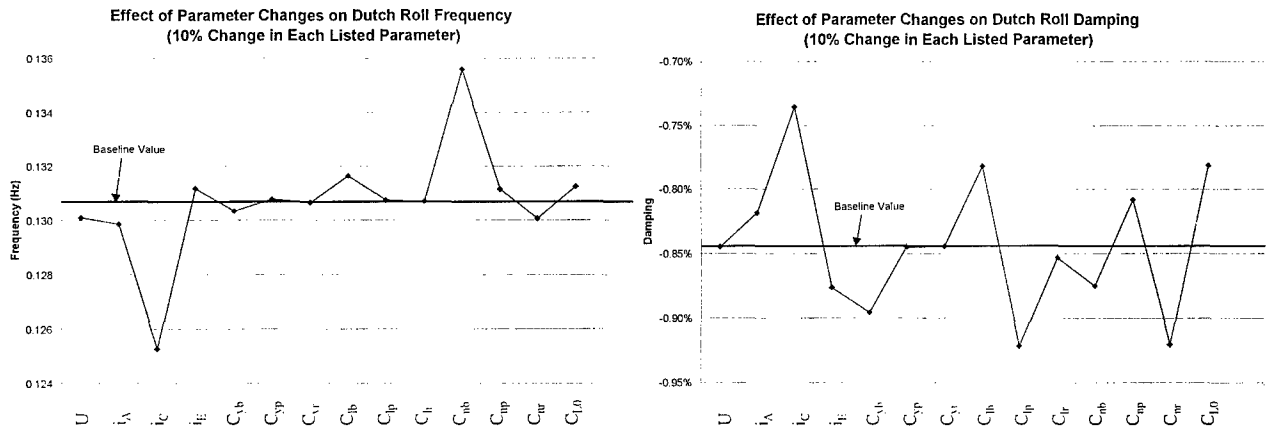

Figure 1: Variation in Dutch Roll Rigid Body Mode Frequency and Damping With 10% Changes in Various Parameters.

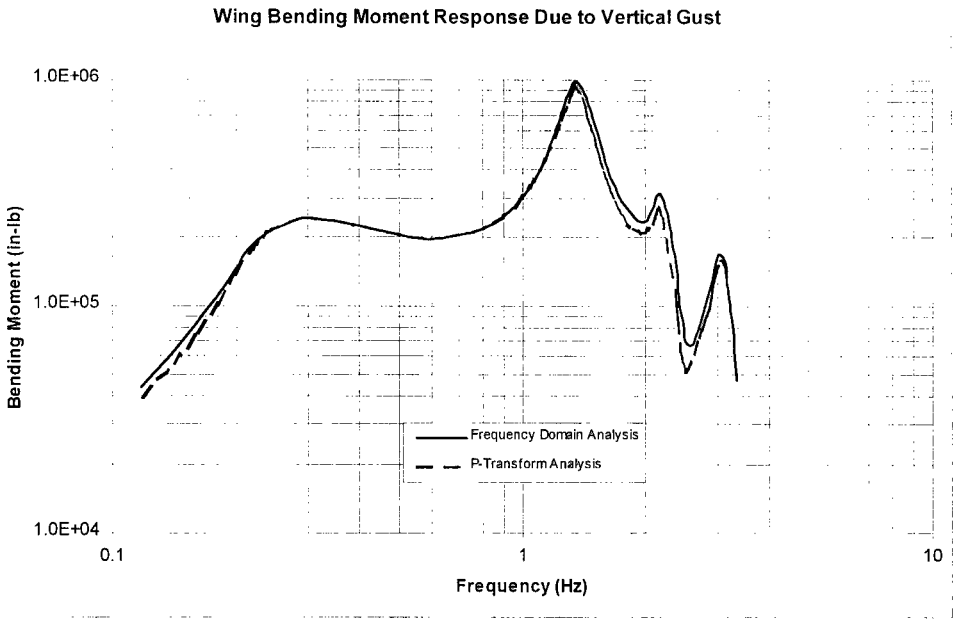

Figure 2: Accuracy of the P-Transform Method for Computing Wing Bending Moments Due to Vertical Gust.

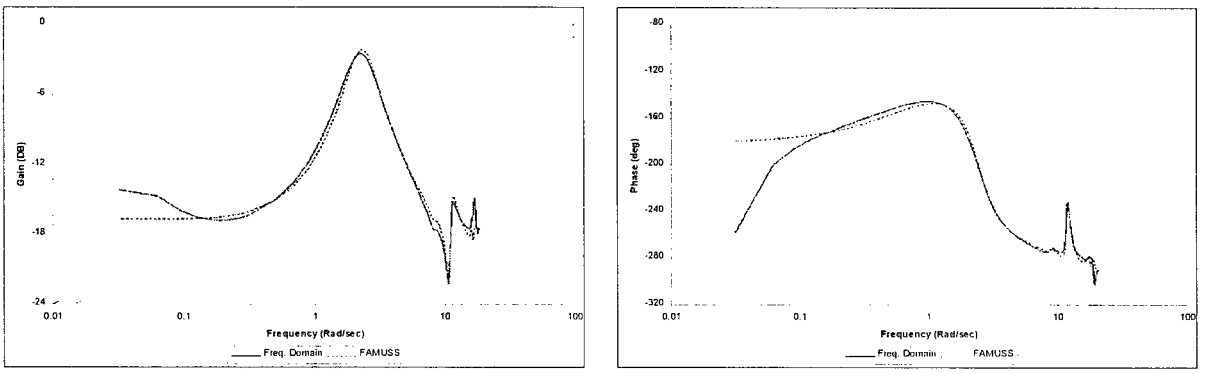

Figure 3: Application of the FAMUSS process to compute CG Acceleration Due to Elevator Excitation.

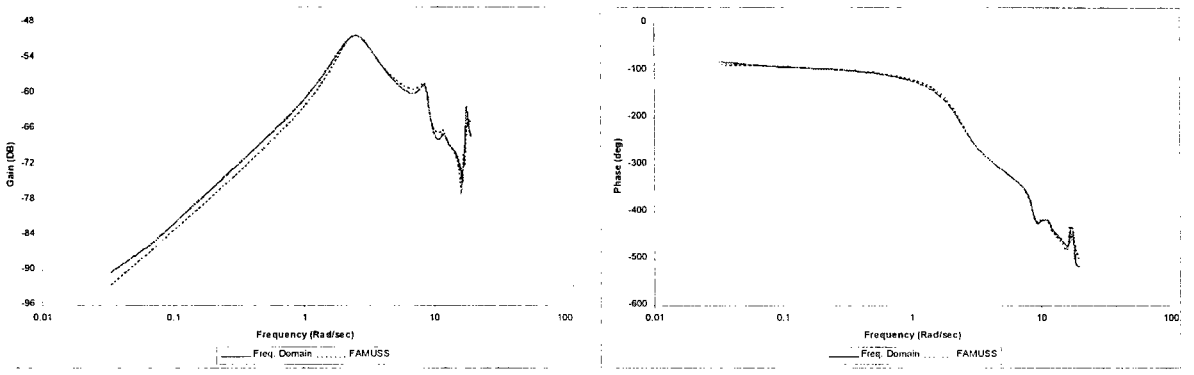

Figure 4: Application of the FAMUSS process to compute CG Acceleration Due to Gust Excitation.

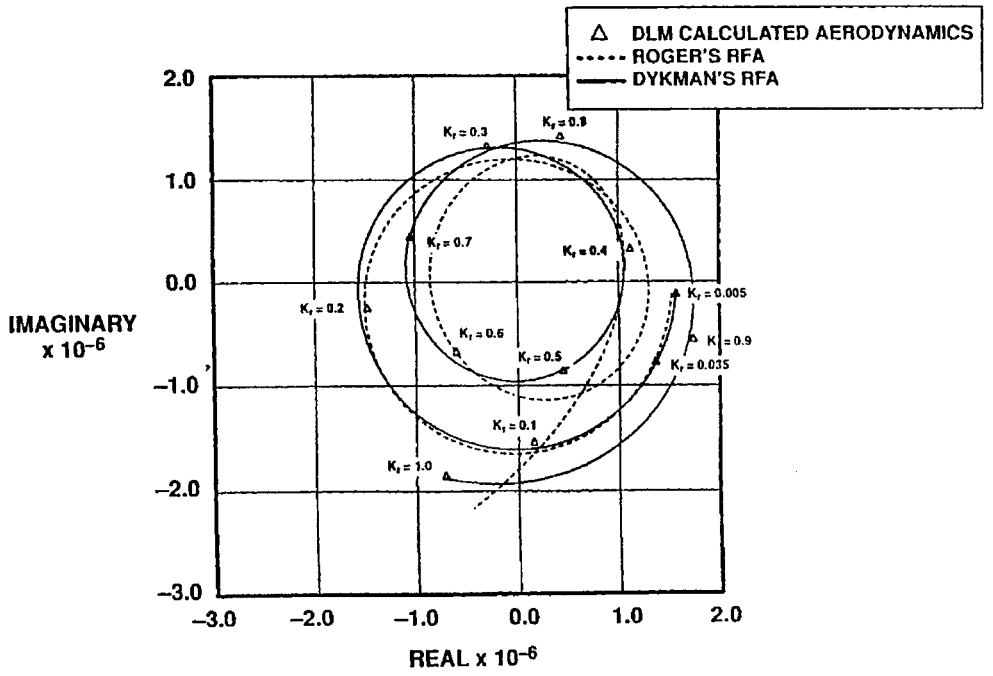

Figure 5: Typical Gust Force Representation.

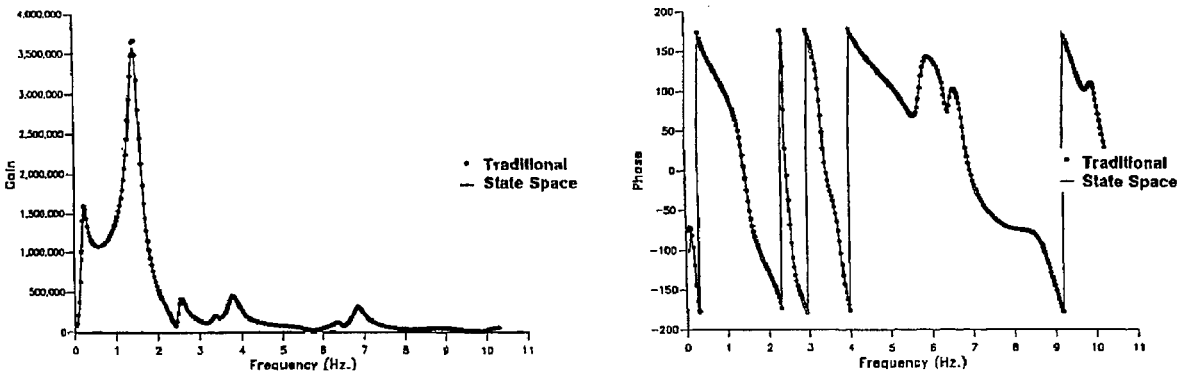

Figure 6: Wing Bending Moment Response Due to Gust Excitation (RFA).

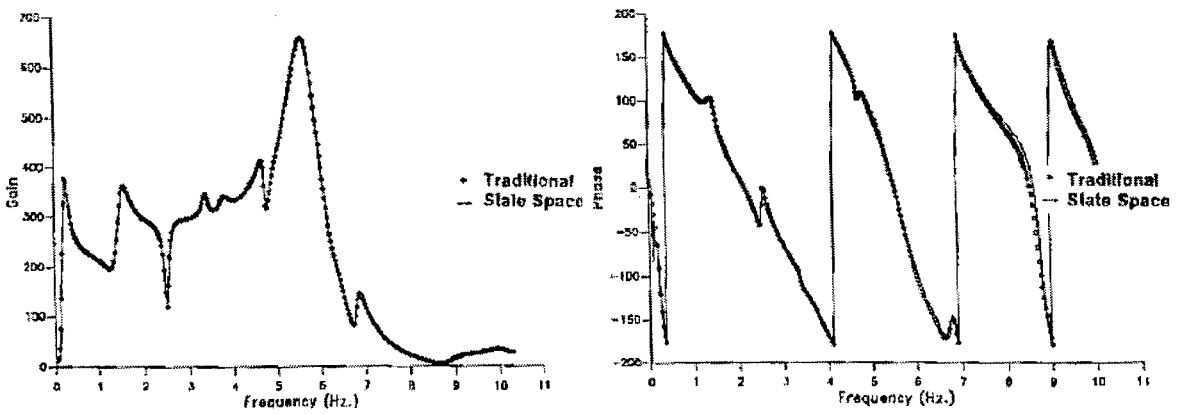

Figure 7: Horizontal Tail Shear Due to Gust Excitation (RFA).

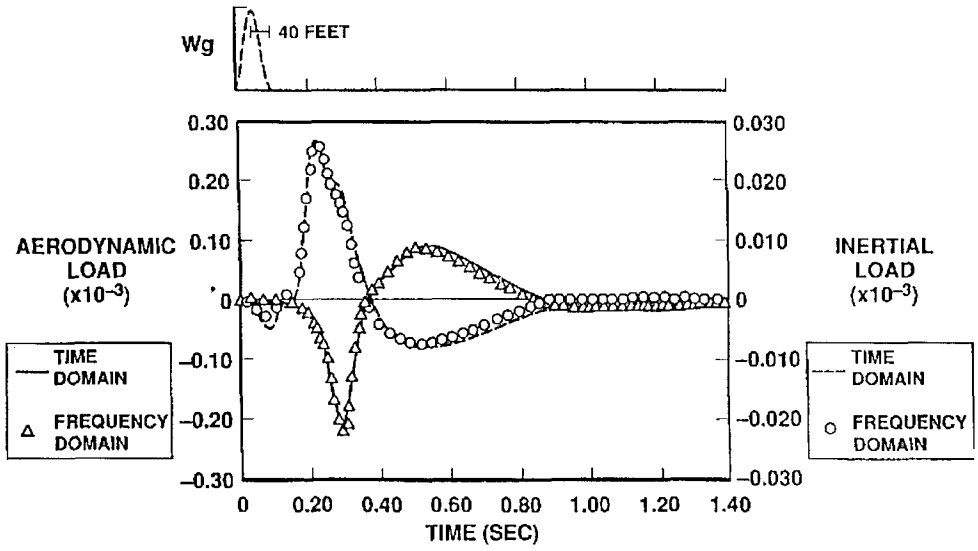

Figure 8: Time-Domain Response: Horizontal Tail Shear Due to 1-Cos Gust Input.

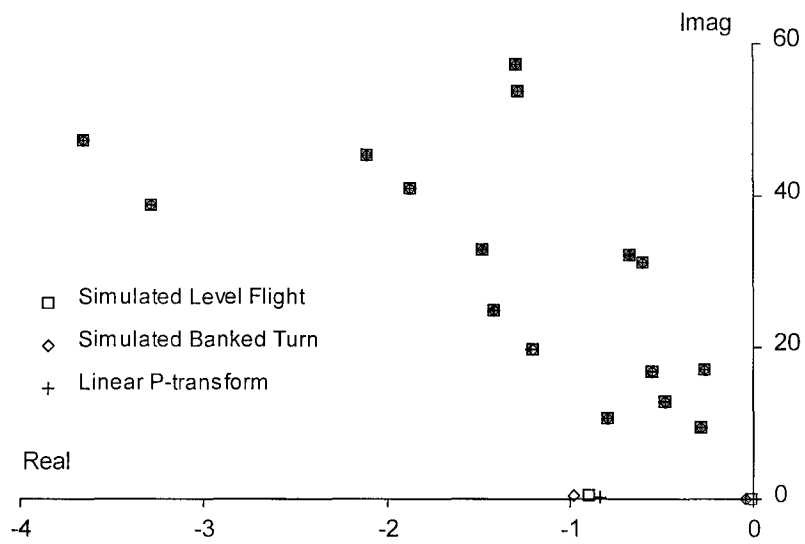

Figure 9: Root Locations for Linear P-transform Analysis and Two Simulated Conditions.

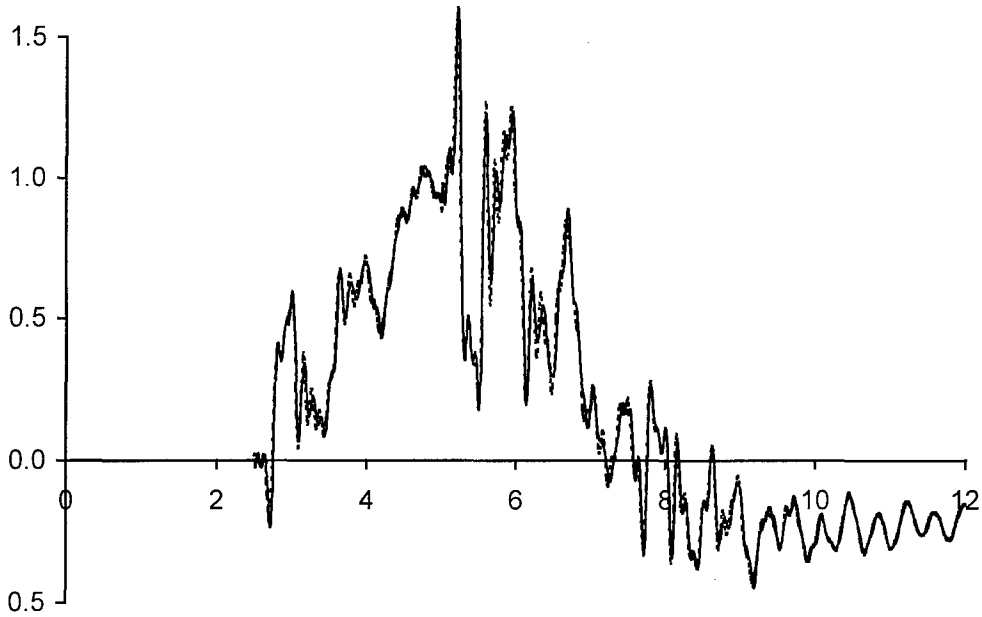

Figure 10: Comparison of Vertical Load Factor Versus Time (sec) at Pilot Station due to Pitch Maneuver. Solid line = P-transform, Dotted line = RFA technique.

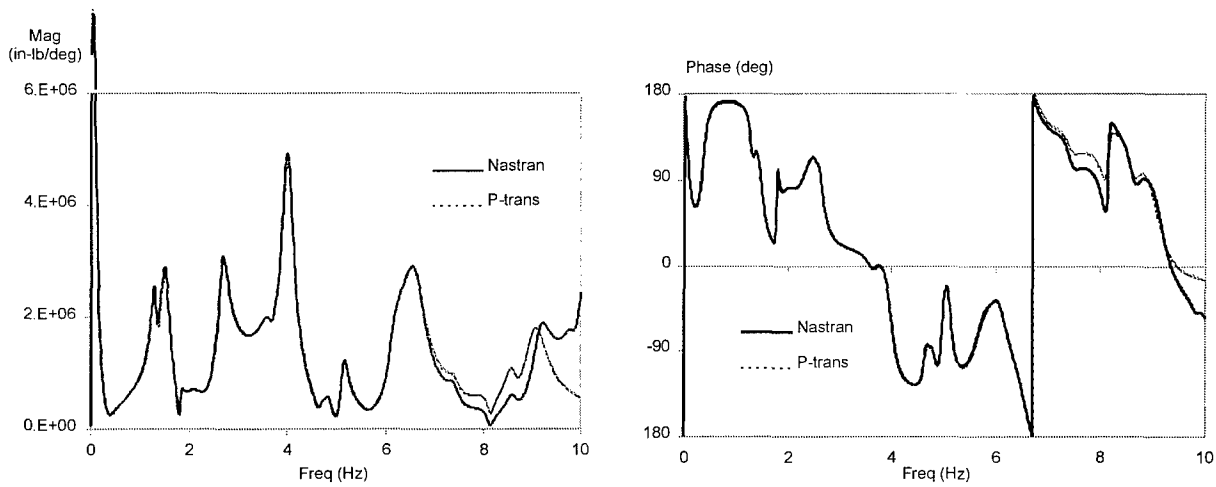

Figure 11: Magnitude and Phase of Wing Bending Moment due to Elevator Excitation

THE INTERACTION OF FLIGHT CONTROL SYSTEM AND AIRCRAFT STRUCTURE

J. Becker
Daimler-Benz Aerospace AG
Military Aircraft Division LMT2
P. O. Box 80 11 60
D-81663 Munich, Germany
Juergen.Becker@m.dasa.de

B. Caldwell
BAe MA&A
W310C Warton Aerodrome,
Preston, PR4 1AX, UK
Brian.Caldwell@BAe.co.uk

V. Vaccaro
Defence Aircraft Engineering
Alenia Aeronautica
Corso Marche 41, Turin, Italy
Dynamics@alnto.finmeccanica.it

ABSTRACT

Results from structural coupling investigations are presented which include the design and verification of structural filters for a flight control system. The advantages of an integrated interdisciplinary flight control system (FCS) design on the basis of the coupled dynamic model of the structural dynamic model and the flight dynamic model of the aircraft are described.

The design strategy of the Flight Control System development is improved through the integrated design optimisation procedure which includes the modelling of the coupled system of the flight dynamics, the structural dynamics, the actuators and sensors as well as the effects of the digital system.

Different examples are demonstrated which document the advantages of the integrated, interdisciplinary design. Methods to avoid structural mode-flight interaction are described. Especially the design of filters to minimise interaction is outlined, which is based upon a model of the aircraft describing the coupled flight dynamic, flight control dynamics and structural dynamic behaviour and on ground and in flight structural coupling tests. The paper explains design procedures, design and clearance requirements, correlation between model predictions and structural coupling tests and model update for on ground and in flight.

1. INTRODUCTION

The development of advanced digital flight control systems for a modern military aircraft, for example Figure 1, is strongly influenced by aeroservoelastic effects. The flexible aircraft behavior, especially for this artificially stabilised aircraft configuration with outer wing missiles, tip pods and heavy under wing stores and tanks, has significant effects on the flight control system. The signals from the Aircraft Inertial Measurement Unit (IMU) - the gyro platform – contain, in addition to the necessary information of rigid aircraft rates and accelerations, flexible aircraft rates and accelerations at the frequencies of the aircraft elastic modes. The flexible aircraft rates and accelerations measured by the IMU are passed through the flight control system control paths, multiplied by the FCS gains and FCS filters, and summed into the control surface actuator inputs, which then drive the controls at the frequencies of the elastic modes of the aircraft. The flexible aircraft is excited by the high frequency control deflections and therefore may experience aeroservoelastic instability i.e. flutter or limit cycle oscillations, and dynamic load and fatigue load problems may arise. The FCS design therefore has to minimize all structural coupling effects through all available means, including optimum sensor positioning, notch filtering and additional active control. This paper describes the major aspects and problem areas to be considered in the FCS design with respect to aeroservoelastic effects, as also previously described in References 1-6, and outlines an integrated design of FCS gains and phase advance filters together with notch filters, see also Reference 8. The integrated design process has been followed for the current project since independent design of notch filters or FCS has not led to a satisfactory solution for stabilization of rigid aircraft or elastic modes.

2. INTEGRATED DESIGN FOR ADVANCED FLIGHT CONTROL SYSTEMS

2.1 Design philosophy

Within the integrated process, structural coupling influences are minimised by the traditional means of notch filtering, but here an optimum solution is reached by exchanging notch attenuation and phase lag with FCS gain and phase advance filtering. The scope of the integrated design therefore covers FCS gains, phase advance and notch filtering across the full rigid and flexible aircraft frequency range, addresses both aircraft rigid mode and structural coupling stability requirements, and encompasses all possible aircraft configurations and configuration changes, (missiles on, off, tanks on and off etc.). Thus all structural coupling

Paper presented at the RTO AVT Specialists' Meeting on "Structural Aspects of Flexible Aircraft Control", held in Ottawa, Canada, 18-20 October 1999, and published in RTO MP-36.

changes with configuration etc will be covered by a single, fixed set of notch filters, avoiding the system complexity associated with configuration switches for different sets of notch filters, and avoiding any scheduling of notch filters with flight conditions.

In order to simplify the design process wherever possible, the basic stability criteria for the flexible modes were based on gain margin only, with no phase margin specification. In practice this principle was not wholly practicable for the pitch axis, where high levels of FCS stability augmentation were required and the integrated design task was particularly difficult. Here, 'gain stabilisation' was applied only to the higher frequency modes, with phase and gain margins taken fully into account ('phase stabilisation') for the lower frequency regime.

For 'phase stabilisation', the notch filter design utilised an analytical model of the aircraft structure incorporating a linear representation of the FCS. In this application, the analytical model was subject to extensive verification against results both from ground resonance and structural coupling testing, and from in-flight flutter and structural coupling testing. Where necessary, the model was updated to improve the match to the test results.
Due to restrictions in the absolute accuracy of the analytical model predictions at higher frequencies, design for gain stabilised elastic modes was based on ground measured data, augmented where necessary with aerodynamic effects derived from the model.

To cover all of the possible sets of aircraft store configurations required under the weapon system specification, those that were critical to the filter design were established by analytical model investigation in advance. These were then treated in test and analysis.

2.2 Design Requirements

2.2.1 Stability Requirements

The design requirements are primarily linear stability margin specifications covering all flight control rigid / flexible aircraft modes, and were developed from the Military Specification MIL-F-9490D.
The open loop frequency response requirements are demonstrated in Figure 2 for two cases, A and B.

Case A describes (in a Nichols diagram) the gain and phase margin requirement for early prototype flying, and indicates that all elastic modes shall be 'gain stabilized'.

Case B describes gain and phase margins applicable following model validation through structural coupling ground and flight tests. The low frequency flexible modes are phase stabilized while higher frequency modes remain gain stabilized.

2.2.2 Vibration / Dynamic Load Requirements

In addition to the stability requirements for structural coupling, unacceptable vibration levels must be avoided. The vibration levels induced by poor structural coupling stability might create high fatigue loads to actuators and to aircraft structure. The notch filters have to be designed with specific vibration requirements accounted for.

2.2.3 Flutter Requirements

The FCS / notch filter design solution has to fulfill the same flutter requirements as the aircraft without FCS. The aircraft with FCS must meet the 15% flutter speed margin as well as the minimum elastic mode damping requirements as described in Military Specification MIL-A-8870 B.

2.3 Design Tools

The integrated FCS design for the flexible aircraft is possible with the assumption that the aircraft characteristics are predictable to the necessary accuracy. The characteristics of the controlled flexible aircraft are described in the form of open loop frequency transfer functions of the FCS/flexible aircraft control path feedback loops to a sufficiently high frequency; see block diagram in Figure 3. For the longitudinal control system, the pitch rate, normal acceleration and flow sensor α open loop signals at the control loop break point have to be known. For the lateral system, the roll rate -, yaw rate-, lateral acceleration - and flow sensor signal β open loop signals are required. The open loop signal consists of the transfer function of the aircraft response to control surface input, sensed at the IMU (rates and accelerations) and flow sensors, combined with the transfer functions of the FCS from the sensor to the opening point and from the opening point to the actuators.
The individual transfer functions are composites covering gain stabilised and phase stabilised modes. As noted, phase stabilised modes use the analytical dynamic model calculation directly, while the gain stabilised modes use on ground measured sensor response to actuator input transfer functions superimposed with calculated magnitudes of unsteady aerodynamic transfer functions.
The applicability of the analytical dynamic model calculation depends on the accuracy of the modeling and its verification. Both methods depend on the accuracy of the unsteady aerodynamic transfer functions, which are in both methods derived from linear potential flow theoretical predictions of unsteady

aerodynamics for elastic modes and control surface deflection.

2.3.1 Analytical Model of the Flexible Aircraft with Flight Control System

The analytical model of the flexible aircraft –plus- FCS consists of a linear dynamic description of the flight mechanic equations of motion, flexible aircraft, and FCS. The flexible aircraft is represented in a modal description, using generalized coordinates, generalized masses, stiffness and structural damping and generalized aerodynamic forces of the flexible modes. Generalized control surface inertia and unsteady aerodynamic terms provide the link to the FCS. The FCS is described through linear differential equations, covering both hardware and software, i.e. all sensors, actuators, computer characteristics and control laws.

The equations of motion for the forced dynamic response of the aeroelastic system can be written in matrix differential equation form:

$$m_r b_r^2 \begin{bmatrix} M_{qq} & M_{q\delta} \\ M_{\delta q} & M_{\delta\delta} \end{bmatrix} \begin{Bmatrix} \ddot{q} \\ \ddot{\delta} \end{Bmatrix} +$$

$$+ \frac{s_R}{kV} \left\{ \omega_r^2 m_r b_r^2 \begin{bmatrix} gK_{qq} & 0 \\ 0 & K''_{\delta\delta} \end{bmatrix} + \frac{\rho}{2} V^2 F s_R \frac{b_r}{S_R} \begin{bmatrix} C''_{qq} & C''_{q\delta} \\ C''_{\delta q} & C''_{\delta\delta} \end{bmatrix} \right\} \begin{Bmatrix} \dot{q} \\ \dot{\delta} \end{Bmatrix} +$$

$$+ \left\{ \omega^2 m_r b_r^2 \begin{bmatrix} K_{qq} & 0 \\ 0 & K'_{\delta\delta} \end{bmatrix} + \frac{\rho}{2} V^2 F s_R \frac{b_r}{s_R} \begin{bmatrix} C'_{qq} & C'_{q\delta} \\ C'_{\delta q} & C'_{\delta\delta} \end{bmatrix} \right\} \begin{Bmatrix} q \\ \delta \end{Bmatrix} = \{Q(t)\}$$

Equation 1

where m_r b_r and ω_r are the reference mass, length and frequency and M, K and C are referred to as the generalized mass, stiffness and aerodynamic matrices, which are non-dimensional. The generalized mass and stiffness matrices are calculated using a finite element mode (FEM) of the total aircraft. For dynamic response calculations, the FEM is reduced to representative generalized dynamic degrees of freedom. The true airspeed V, and semi-span s_R of the reference plane are used to form the reduced frequency $k = (\omega s_R)/V$. F is the area of reference plane and g is the structural damping of the elastic modes. The generalized forces Q(t) are equal to zero for the conventional flutter problem. The generalized coordinate 'q' describes the amplitude of the elastic airplane modes, including elastic control surface modes, whereas 'δ_0' (subscript omitted above) denotes the rotation of the rigid control surface according to the complex actuator stiffness represented by the impedance function of equation (2).

$$K_{\delta_0\delta_0} = K'_{\delta_0\delta_0} + iK''_{\delta_0\delta_0} \qquad \textbf{Equation 2}$$

For the controlled aircraft, the FCS-commanded control deflection '$\Delta\delta$' has to be introduced as an additional degree of freedom for each control surface. The generalized forces generated by the servo induced control deflections ($\Delta\delta$) can be described as the right-hand term of equation (1) by

$$\{Q(t)\} = -m_b b_r^2 \begin{Bmatrix} M_{q\Delta\delta} \\ M_{\delta_0\Delta\delta} \end{Bmatrix} \Delta\ddot{\delta} - \frac{\rho}{2} V^2 F s_R \frac{b_r^2}{s_R^2} \frac{s_R}{k \cdot V} \begin{Bmatrix} C''_{q\Delta\delta} \\ C''_{\delta_0\Delta\delta} \end{Bmatrix} \Delta\dot{\delta}$$

$$- \frac{\rho}{2} V^2 F s_R \frac{b_r^2}{s_R^2} \begin{Bmatrix} C'_{q\Delta\delta} \\ C'_{\delta_0\Delta\delta} \end{Bmatrix} \Delta\delta$$

Equation 3

Assuming normalized rigid control surface modes δ_0 and $\Delta\delta$, the rotation of each control surface can be superimposed by

$$\delta = \delta_0 + \Delta\delta \qquad \textbf{Equation 4}$$

δ here represents foreplane, inboard and outboard flap or for rudder, and differential inboard and outboard flap. The state-space-description of (1) is as follows:

$$\{\dot{x}\} = [A]\{x\} + [B]\{x\} \qquad \textbf{Equation 5}$$

As already described, the matrix equation (1) describes the flexible aircraft, FCS and linearized rigid flight mechanic equations, and thus the state vector for longitudinal control includes the rigid aircraft state variables, as follows:

$$X = \left\lfloor \Delta V/V; \Delta\alpha; \Delta\omega; \Delta\theta; \dot{q}; \dot{\delta}_0; \Delta\dot{\delta}; q; \delta_0; \Delta\delta \right\rfloor$$

The flight mechanic equations may, in a first approximation, contain elastified aerodynamic derivatives as function of incidence and Mach number. For low frequency the flight mechanic equations may be assumed to be decoupled from the flexible aircraft equations. Alternatively, the fully rigid flight mechanic equations are introduced, and theoretical inertia and unsteady aerodynamic coefficients may be used.

The flight mechanic equations for longitudinal control are described below, including rigid aircraft equations with flexible coupling terms.

Normal Force equations:

$$\sum Z = -\frac{\rho}{2} V^2 F \left[C'_{z\alpha}(\omega) \cdot \alpha + C''_{z\alpha}(\omega)/\omega \cdot \dot{\alpha} \right]$$

$$- mV \cos(\alpha\omega_y) - \frac{\rho}{2} V^2 F \cdot \bar{c} \left[C'_{zq}(\omega) \cdot \omega_y + C''_{zq}(\omega) \cdot \dot{\omega}_y \right]$$

$$- mg \sin(\alpha\theta)$$

$$- \frac{\rho}{2} V^2 F \left[C'_{z\delta}(\omega) \cdot \delta + C''_{z\delta}(\omega)/\omega \cdot \dot{\delta} \right] - Z_{m\delta} \cdot \ddot{\delta}$$

$$- \frac{\rho}{2} V^2 F \left[\sum_j C'_{zqj}(\omega) q_j + \sum_j C''_{zqj}(\omega) q_j \right] = 0$$

Elastified normal force 'rigid' aircraft equations

$$\sum Z = -\frac{\rho}{2} V^2 F \cdot C_{zq}(\alpha)\alpha - mV \cos(\alpha\omega_y)$$

$$- \frac{\rho}{2} V^2 F \cdot \bar{c} C_{zq} \omega_y - mg \sin(\alpha\theta) - \frac{\rho}{2} V^2 F \cdot C_{z\delta}(\alpha)\delta = 0$$

Pitching moment equation with flexible coupling terms

$$\sum M = -\frac{\rho}{2}V^2 F \cdot \bar{c}\left[C'_{m\alpha}(\omega)\alpha + C''_{m\alpha}(\omega)\dot{\alpha}\right]$$

$$-I_y\dot{\omega}_y - \frac{\rho}{2}V^2 F \cdot \bar{c}^2\left[C'_{mq}(\omega)\omega_y + C''_m(\omega)\dot{\omega}_y\right]$$

$$-\frac{\rho}{2}V^2 F \cdot \bar{c}\left[C'_{m\delta}(\omega)\delta + C''_{m\delta}(\omega)/\omega \cdot \dot{\delta}\right] - M_{m\delta}\ddot{\delta}$$

$$-qFs\left[\sum_j C'_{mqj}(\omega)q_j + C''_{mqj}(\omega)/\omega \cdot q_j\right] = 0$$

Elastified Pitch Moment 'rigid' aircraft equations

$$\sum M = -\frac{\rho}{2}V^2 F \cdot \bar{c}C_{m\alpha} + \alpha + I_y\dot{\omega}_y - \frac{\rho}{2}V^2 F \cdot \bar{c}C''_{m\delta}(\alpha)\delta$$

$$-\frac{\rho}{2}V^2 F \cdot \bar{c}^2 C_{mq}\omega_y - \frac{\rho}{2}V^2 F \cdot \bar{c}^2 C_{m\dot{\alpha}} \cdot \dot{\alpha} = 0$$

C'	Real part of calc. aerodynamic coefficient
C''	Imag. part of calc. aerodynamic coefficient
$\rho/2\,V^2$	Dynamic pressure
F	Reference area
$\bar{c}, s$	Reference length
q_j	Generalized coordinate

2.3.2. Modelling and Analysis Assumptions

Particularly where the analytical model is being used directly, to predict characteristics for phase stabilised modes, the assumptions be made in dynamic model formulation and subsequent analyses have to be conservative in order to cover, for example, system failures. Particular considerations are outlined below.

Actuator Characteristics

The actuator model transfer function should follow the actuator specification upper gain boundary. When tuning the actuator model phase characteristics, both minimum and maximum phase lag boundaries need to be considered, since either case may be critical for phase stabilised modes. In general, actuator non-linearities reduce gain and structural coupling, and therefore linear characteristics may be modelled.

Inertial Measurement Unit (IMU)

The transfer function of the sensor platform should to describe the upper gain boundary and the minimum and maximum phase boundary. Only the upper linear boundary is necessary to be represented.

Flow Sensors

Measured flow sensor transfer functions must be used.

Structural Modeling

Consideration of the full variation of the flexible mode frequencies with flight condition, fuel contents and actuator failure cases is necessary, and separate models may be created for the critical store cases. In order to be accurate, the analytical model has to be updated from ground test results, principally with respect to mode frequencies, but also considering response amplitude. The model update must consider the effects of structural non-linearity, notably the variation of mode frequency with excitation amplitude.

The minimum measured structural damping must be applied.

Unsteady Aerodynamic Modeling

The unsteady forces used in the dynamic model calculation shall be represented in a conservative manner.

The predicted magnitude (modulus) of the unsteady forces of the flexible modes and control surface deflection represents a high (i.e. conservative) value for all Mach numbers and incidences, since, in practice, flow separation at higher incidences leads to reduction in the motion induced pressure distributions compared with pure linear theory. Special attention has to be paid to transonic effects, however.

Since the predicted criticalities in structural coupling conditions are at high incidence conditions, because of FCS gain scheduling, the adoption of linear unsteady subsonic and supersonic aerodynamics derived by linear theory or numerical Euler code calculations in the linear range (Reference [10].) is believed to be conservative throughout the full flight envelope.

The unsteady forces must be calculated for a number of reduced frequencies to cover the full frequency range.

For the phase stabilization of low frequency flexible modes such as the first wing bending, the unsteady aerodynamic phase is again derived directly from the application of linear theory. Experience for different wing configurations indicates that at high incidence and high FCS gains, the aerodynamic damping is increased compared to low incidence. In terms of phase stability margin, Reference [3] explains the difference in a Nichols diagram, linear theory showing the more critical condition.

For the gain stabilised, higher frequency modes, only the magnitude of the unsteady aerodynamic forces is needed for the design of the notch filters, because only a gain margin is required, and phase is excluded from the analysis.

FCS Control Laws Model

In order to design in a robust manner the calculation of open loop transfer functions shall consider the worst FCS gain conditions. The highest end to end trimmed gain conditions have to be included into the model calculations. Special consideration shall be also given to

the maximum out of trim gain conditions with respect to structural coupling criticality.

2.3.3 Ground Test Result - Update of Dynamic Model

Ground vibration test results and structural coupling tests are needed to verify or update the calculated results from dynamic model. In general the total aircraft structural dynamic model consists of subcomponents. Sub-component models can be refined by updating the sub-component stiffness and damping, using the results from component ground resonance tests. Updating of the total aircraft model then uses overall aircraft ground resonance and structural coupling tests. The update of the analytical model is described in Reference [6].

In Reference [8] a typical result was demonstrated for the comparison of predicted and measured IMU open loop response due to control surface input, showing that dynamic inertia coupling modelling has to be updated with on ground measured results. Both the sensor signal in each aircraft normal mode, and the control surface inertia coupling terms in each mode, have to be tuned to test results.

2.3.4 Flight Test Results - Update of Control Surface Unsteady Aerodynamics

Flight test results from structural coupling/flutter tests are needed to verify or update the predicted results of open loop frequency response functions, by the update of unsteady aerodynamic forces used in the dynamic model. This can be achieved through the comparison of predicted open loop frequency response functions and flight test-measured closed loop converted into open loop frequency response functions.

The flight test results are derived through frequency sweep excitation of the control surfaces, which is possible through special software in the FCC's.

In Reference [8] a typical result for the comparison of predicted and measured IMU open loop response due to control surface input is documented, showing that unsteady aerodynamic coupling modelling has to be updated with in flight measured results both for low and high angle of attack α. From the flight test results it is concluded that the theoretical control surface unsteady aerodynamic coupling terms used in the total dynamic model have to be tuned to test results for low up to high incidences.

The flight test results also shown in Reference [8] demonstrate the alleviation effect resulting from application of the phase stabilisation concept to the first wing bending mode compared to gain stabilisation. Alleviation of IMU pitch rate is found to be at least 3dB.

2.4 FCS Design with Optimization of Structural Decoupling

Different procedures are available to minimize structural coupling effects in the Flight Control System. The practical tools are to minimize structural coupling are:

- Optimum sensor location
  The IMU shall be put to the anti node of the first fuselage bending mode, since the elastic pitch-yaw angle/pitch-yaw rate is minimum at this location. Optimum sensor location is meaningless for first wing bending mode coupling since the fuselage counteracts wing bending with a linear pitch motion.
- Stiffening of the IMU platform
  A very high stiffness of the sensor platform is favorable, since local medium-to-high frequency elastic modes will then be eliminated.
- Actuator transfer function
  A strong decay in the actuator transfer function at medium to high frequencies would minimize coupling effects. Actuator frequencies at medium frequencies (10 - 30 Hz) shall be well damped. Actuator phase shifts at low elastic mode frequencies shall be known for the absolute minimum and maximum value.
- Minimum weight/inertia of control surfaces
  High frequency 20 - 80 Hz structural coupling effects are small using light weight controls.
- Notch Filter Configuration Optimization
  Figure 3 demonstrates schematically the feedback paths for the longitudinal stabilization. Signals from the FCS sensors are filtered in the IMU initially, by notch filters that minimize the high frequency flexible aircraft signal components. The remaining signals are then modified by the FCC notch and phase advance filters. After multiplication with the FCC gains the signals are passed to the different control surface actuators. Upstream of the actuator input, the signals are filtered by flap, foreplane and rudder notch filters. This combination of IMU, FCC and actuator input filters, leads to a better minimization of phase shifts at low frequency, which is necessary to meet the handling criteria.
- Optimization of phase advance filters
  Phase advance filters used in the FCS maximise rigid stability margins by counteracting the low frequency phase shifts due to notch filtering and other delays. However the high frequency gain increase associated with the phase advance exacerbates structural coupling. The optimization of phase advance filter should therefore be combined with the notch filter optimization. This might be performed in a iterative manner, or preferably in a combined optimization with the notch design

frequency response functions covering the rigid aircraft frequency regime.

- Optimization of notch filter
  The notch filter optimization is the major tool for decoupling the aircraft control from aeroservoelastic influences. Since the coupling has a severe impact on the FCS on the current aircraft project, a mathematical filter optimization had to be developed in order to achieve flight dynamic stability requirements. The optimization is described below.

In order to optimize the filters it is necessary to establish the open loop frequency response functions at the opened summation points of the longitudinal and lateral control S_{L1}, S_{L2} and S_{A1}, S_{A2}.
For example, the open loop frequency response function at the longitudinal open loop point S_{L1} of Figure 3 can be formulated using the separate transfer functions of the loop response without notch filters due to flap and foreplane excitation (S_{L2} closed), and by sequentially setting each separate flap or foreplane loop gain to zero.

a) $G_{nz} = 0,\ G_\alpha = 0,\ G_q \pm 0$
a_1) flap excitation only to generate F_F^q at S_{L1}
a_2) foreplane excitation only to generate F_c^q at S_{L1}
b) $G_{nz} = 0,\ G_\alpha \pm 0,\ G_q = 0$
b_1) flap excitation only to generate F_F^α at S_{L1}
b_2) foreplane excitation only to generate F_c^α at S_{L1}
c) $G_{nz} = 0,\ G_\alpha = 0,\ G_q = 0$
c_1) flap excitation only to generate F_F^{nz} at S_{L1}
c_2) foreplane excitation only to generate F_c^{nz} at S_{L1}

The total open loop transfer function F at S_{L1} can be formulated to:

$$F_{Total} = G_q \left\{ F^q_{\delta_0} F_{NF_{O1}} F_{NF_{O2}} + F^q_{\delta_i} F_{NF_i} + F^q_\eta F_{NF_{FP}} \right\}$$
$$\cdot F^q_{NF1_{FCC}} \cdot F^q_{NF2_{FCC}} \cdot F^q_{NF3_{FCC}} \cdot F^q_{NF1_{IMU}} \cdot F^q_{NF2_{IMU}} \cdot F^q_{NF3_{IMU}} \cdot F^q_{Ph.adv}$$
$$+ G_\alpha \left\{ F^\alpha_{\delta_O} \cdot F_{NF_{O1}} \cdot F_{NF_{O2}} + \frac{G_I/G_\alpha}{s} \left[F^\alpha_O \cdot F_{NF_{O1}} \cdot F_{NF_{O2}} \right] + \right.$$
$$+ F^\alpha_{\delta_i} \cdot F_{NF_i} + \frac{G_I/G_\alpha}{s} \left[F^\alpha_{\delta_i} \cdot F_{NF_i} \right] +$$
$$\left. + F^\alpha_\eta \cdot F_{NF_{FP}} + \frac{G_I/G_\alpha}{s} \left[F^\alpha_\eta \cdot F_{NF_{FP}} \right] \right\}$$

G_q pitch rate gain
G_α flow sensor signal α gain
G_I integrated α gain
$F^q_{\delta_O}$ pitch rate frequency response function due to outboard flap
$F^q_{\delta_i}$ pitch rate frequency response function due to inboard flap
F^q_η pitch rate frequency response function due to foreplane
F^α_δ α frequency response function due to outboard flap
$F^\alpha_{\delta_i}$ α frequency response function due to inboard flap
F^α_η α frequency response function due to foreplane
$F_{NF_{FCC}}$ Flight Control Computer notch filter
$F_{NF_{IMU}}$ ASMU notch filter
$F_{NF_{FP}}$ Foreplane notch filter
F_{NF_O} Outboard flap notch filter
F_{NF_i} Inboard flap notch filter
s Reference length

A similar formulation can be derived for all other summation points S_{L2}, and lateral S_{A1} S_{A2}.
The open loop frequency response functions F_{Total} can be calculated at arbitrary frequency steps as described in the previous sections.

Since the FCS of the current project is digitally implemented, digital effects must be accounted for in the notch filter design
The notch filter transfer functions are designed and specified as second order numerator and denominator functions in the continuous Laplace domain but take into account frequency warping effects.

$$\omega_Z = \frac{2}{T} \tan \frac{\omega_L \cdot T}{2}$$

ω_L Laplace domain frequency
ω_Z digital domain frequency
T sample period

The frequency in the continuous domain corresponds to a downward frequency warping in the digital domain.
For the phase stabilised modes, the digital effects caused by IMU sensor signal processing transmission delay and sampling of the IMU output by the FCC's is represented in the dynamic model by IMU hardware assumptions using a defined transfer function. For gain stabilised modes, these effects are implicit in the measured results on which the filter design data are based. The effect of aliasing is included in the analysis by a folding back procedure.

Having assembled the required frequency response function data, the notch filter coefficients are optimized using a notch filter optimization program. The computer program is based on the FORTRAN subroutine of

solving constrained non-linear programming problems from K. Schittkowski, see Reference [9] . A finite difference gradient approach is applied.
From the total open loop frequency response function, the phase shift at low frequency due to notch filters can be derived which is the primary variable to be minimized:

min Phase (F(f = 1 Hz))

The total open loop frequency response function including optimized notch filters shall meet the stability requirements, -9 dB for gain stabilization or the gain/phase requirements described in 2.2.
With these requirements the constraints of the optimization can be formulated. The number of frequencies at which the requirement has to be fulfilled defines the total number of constraints.

The number of variables is known from the number of notch filters. An initial guess of the solution is prescribed in the input, and used in initial optimization runs. Lower and upper bounds of the variables are prescribed.
Notch filter numerator, denominator frequencies are selected using the frequencies response peak characteristic for the selection of numerator frequencies, the asymptotic behavior of the notch filters at high frequencies for the denominator frequency, and the denominator critical damping for each notch filter. The notch filter critical damping for IMU filters is prescribed to be > 0.25 for FCC filters, with the minimum value prescribed to be 0.1. A scaling matrix is used for the variables.
Figure 4 demonstrates the results derived from notch filter optimization. Figure 4 upper part shows the open loop frequency response with optimized notch filters in pitch for the design.
Figure 4 below is showing by open loop frequency response functions with the designed notch filters the case where during notch filter design the design information for additional structural configurations or flight conditions was not available and therefore the requirements are not met.

Figure 5 demonstrates the advantages of integrated FCS design in a Nichols diagram of open loop frequency response.

- Case A shows the pure 'rigid' A/C design (flight mechanics design)
- Case B presents the result on open loop frequency response function of using separate, independent, notch filter design (elastic design), applying a full gain stabilization concept for elastic modes, leading to a higher phase shift at the rigid aircraft frequencies, and conflict with the requirements.
- Case C demonstrates the advantages of phase stabilization on the 1st wing bending (WB1) and rigid A/C motion.
- Case D shows the profits of integrated design; both the rigid A/C and elastic modes have sufficient phase and gain margins.

3. DESIGN AND CLEARANCE PROCEDURE

Figure 6 shows the design and clearance procedure, which is based upon a series of on-aircraft and rig tests for identification and clearance, and consequently a series of dynamic model updates from testing and from updated FCS definitions.
Initial design will be made without the benefit of full-aircraft testing. Following the tests, an update phase of the FCS gains, phase advance filters and of notch filters may be necessary depending on the criticality of mismatch between design assumptions and test, for example, if:

- the structural coupling test on ground shows different frequencies of the elastic modes than assumed in the design (for instance a special configuration was not included in the design etc.).
- the in flight structural coupling test shows different dB's and different phase of the low frequency elastic modes than assumed during design
- the on aircraft actuator characteristics are different from design assumptions.
- redesign of structural parts local weight changes, change of pylon stiffness' etc. during development phase.

It is the task of the structural coupling/notch filter design and clearance procedure to treat this situation.

4. CONCLUSIONS

From the results of structural coupling investigations performed for an advanced fighter aircraft, the following lessons have been learned:
Dynamic modelling of the fuselage response and the essential sensor response due to control surface inputs is limited to a certain low frequency range due to the total aircraft finite element model representation, being extremely complex and due to unsteady control surface aerodynamic representation.
An extensive series of structural coupling tests on ground are therefore necessary to update dynamic fuselage modelling, for and control surface inertia coupling terms. Structural coupling in-flight tests are

necessary to update the unsteady aerodynamic control surface coupling terms.
The integrated design of FCS gains, phase advance filters and of structural coupling/notch filter design and clearance procedure has shown advantages in comparison to the classical, separate FCS and notch filter design. The profits of integrated design are mainly found to be:

- less degradation effects on rigid aircraft stability margins
- improvements of elastic mode stability
- improvement of phase advance filters combined with lower high frequency end to end gains

A robust FCS design has to be adopted which includes the description of all worst case assumptions for the structure, the FCS gains and FCS minimum and maximum phase at low elastic mode frequencies, together with worst case assumptions for actuator and sensor hardware. Digital effects have to be fully included.

5. REFERENCES

(1) J. Becker, W. Luber
Flight control design optimization with respect to flight- and structural dynamic requirements
AIAA Seattle 1996

(2) J. Becker, V. Vaccaro
Aerservoelastic Design, Test Verification and Clearance of an Advanced Flight Control System
AGARD - CP- 566
paper presented at the SMP Meeting Àdvanced Aeroservoelastic Testing and Data Analysis', Rotterdam 8-10 May 1995

(3) J. Becker
Aeroservoelastic Stability of Aircraft at High Incidence.
68th AGARD Fluid Dynamics Panel Specialist Meeting, Toulouse France; May 1991

(4) B.D. Caldwell
The FCS-Structural Coupling Problem and its Solution.
AGARD Conference Proceedings on Active Control Technology, FMP Symposium held at Turin, Italy, May 1994

(5) H. Hönlinger, H. Zimmermann, O. Sensburg, J. Becker
Structural Aspects of Active Control Technology
AGARD Conference Proceedings on Active Control Technology, FMP Symposium held at Turin, Italy, May 1994

(6) V. Vaccaro, J. Becker
Ground Structural Coupling Testing and Model Updating in the Aeroservoelastic Qualification of a Combat Aircraft.
AGARD SMP Meeting on Advanced Aeroservoelastic Testing and Data Analysis, Rotterdam, 8-10 May 1995.

(7) J. Becker, W. Luber
Unsteady Aerodynamic Forces at High Incidence and their Application in Structural- and Flight Control Design. International Forum on Aeroelasticity and Structural Dynamics; Manchester, UK; 26-28 June 1995

(8) J. Becker
The structural coupling resulting from interaction of flight control system and aircraft structure
International Forum on Aeroelasticity and Structural Dynamics, Rome,Italy, June 1997

(9) Schittkowski, K.,
NLPQL: A FORTRAN Subroutine Solving Constraint Non-linear Programming Problems. Annuals of Operations, 5, 485-1 00 (edited by Clyde L. Mouna)

(10) G. Heller, E. Kreiselmaier
Eulerluftkräfte für Klappenschwingungen.
TUM-FLM-96/05, Lehrstuhl für Fluidmechanik, Technische Universität München

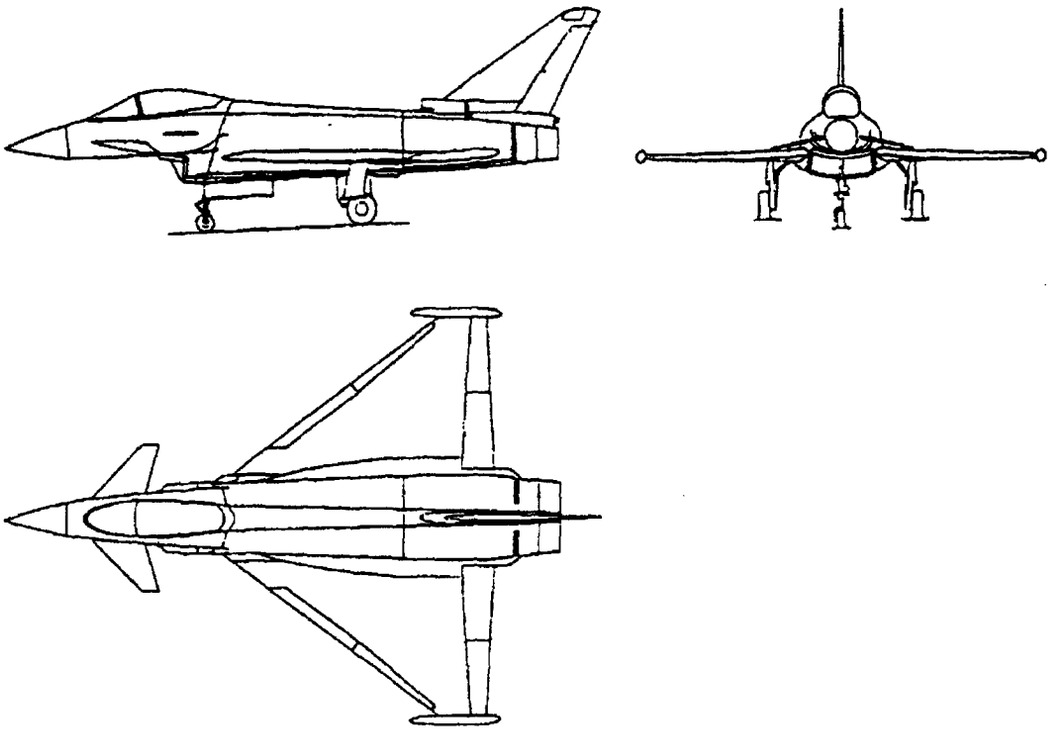

FIG.: 1 MODERN MILITARY AIRCRAFT

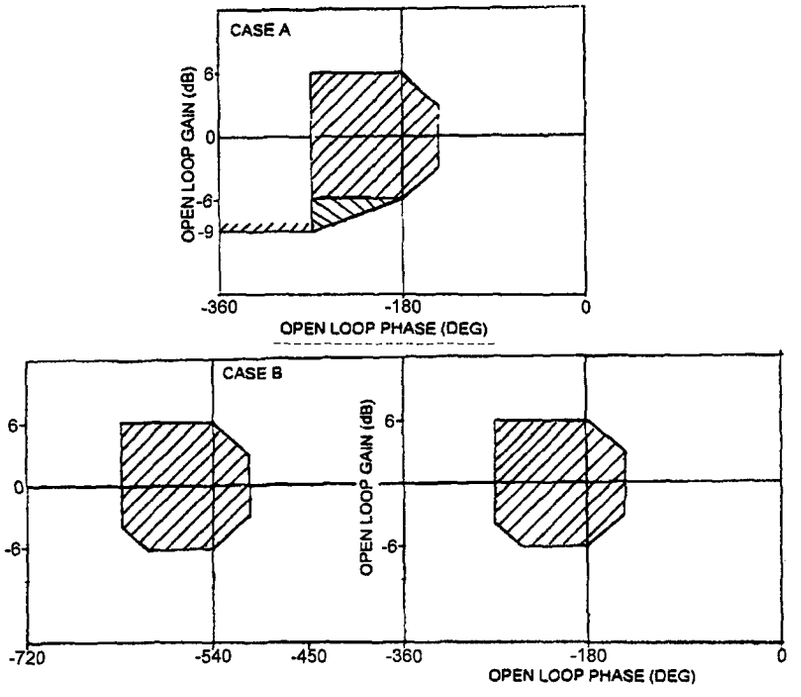

FIG.: 2 STABILITY REQUIREMENTS FOR OPEN LOOP FREQUENCY RESPONSE FUNCTIONS (NICHOLS DIAGRAM)
CASE A: EARLY PROTOTYPE FLYING
CASE B: PRODUCTION AIRCRAFT

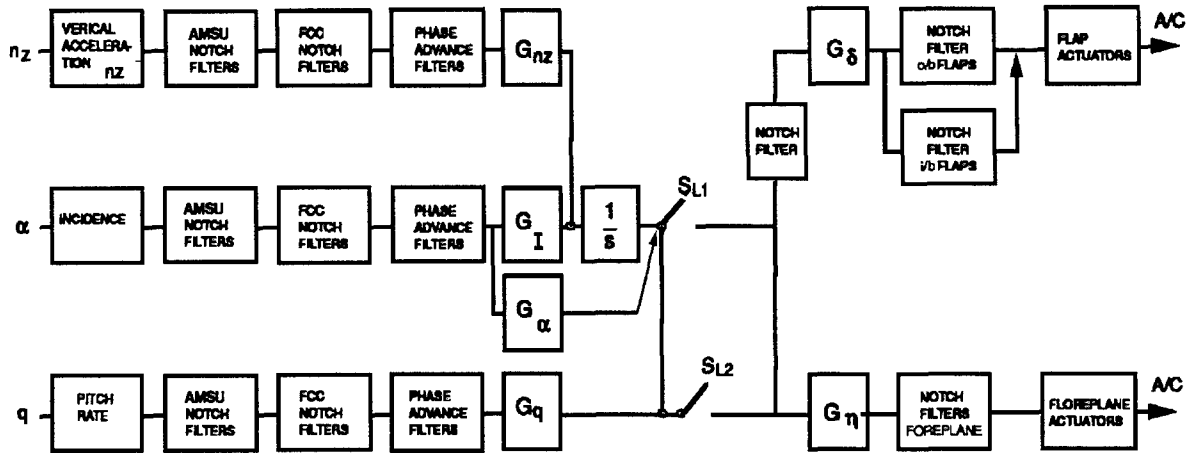

FIG.: 3 FLOWCHART OF LONGITUDINAL CONTROL

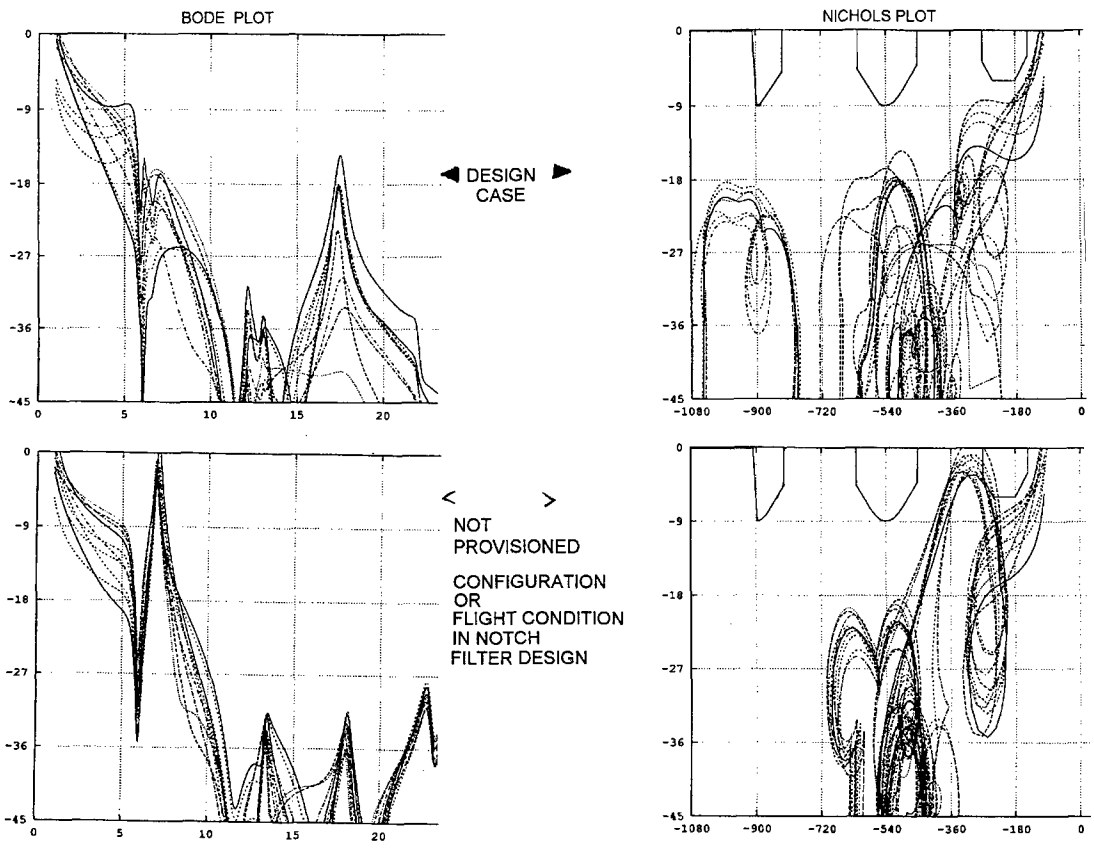

FIG.: 4 OPEN LOOP FREQUENCY RESPONSES WITH NOTCH FILTERS

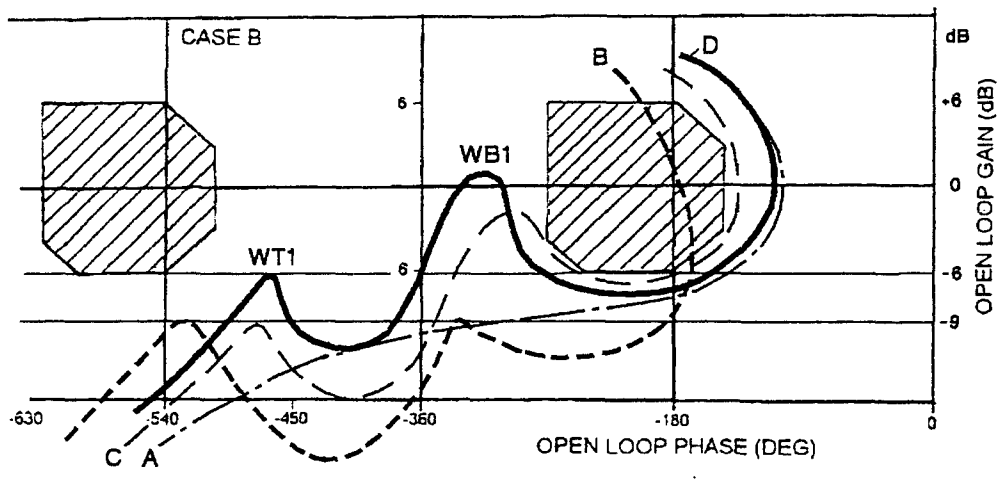

FIG.: 5 COMPARISON OF INTEGRATED TO CLASSICAL

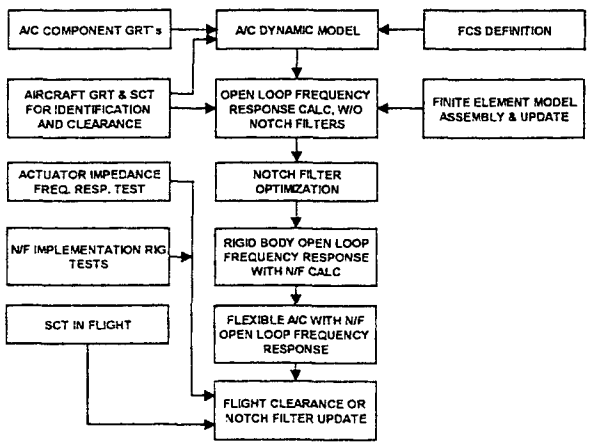

FCS DESIGN

FIG.: 6 DESIGN AND CLEARANCE PROCEDURE

GROUND STRUCTURAL COUPLING TESTING AND MODEL UPDATING IN THE AEROSERVOELASTIC QUALIFICATION OF A COMBAT AIRCRAFT

V. Vaccaro
Aircraft Engineering
Alenia Aeronautica
Corso Marche 41, Turin, Italy
dynamics@alnto.finmeccanica.it

B. Caldwell
British Aerospace BAe
EF2000 Airframe Qualification W310c
Warton Aerodrome
Preston PR41AX
Lancashire, UK
brian.caldwell.@bae.co.uk

J. Becker
Military Aircraft Division
Daimler-Benz Aerospace
Hugo Junkers Strasse, Ottobrunn, Germany
juergen.becker@m.dasa.de

1. SUMMARY

This paper is concerned with the role played by the ground Structural Coupling Test (SCT) and the update of the aeroservoelastic model in the qualification process of a modern combat aircraft. It represents the completion of Reference 1, after several improvements introduced in the Notch Filter (NF) design procedure, numerous ground test campaigns and the confirmation of flight trials.

Most of modern combat aircraft are equipped with fly-by-wire and digital flight control systems (FCS). The problem of interaction between the dynamic response of the airframe and the FCS is usually solved through an appropriate set of notch filters, designed to attenuate the level of structure vibrations picked up by the FCS sensors. Fundamental part of the qualification of the notch filter set is the ground testing activity, generally known as ground Structural Coupling Test.

The main subjects of this paper are:

- Test Procedure
- Model update
- Describe how ground test data is used to augment model predictions in areas where the model on its own is not considered adequate for notch filter design.

2. NOTATION

ATE	Automatic Test Equipment
CG	Centre of Gravity
DOF	Degree of Freedom
FCC	Flight Control Computer
FCS	Flight Control System
FEM	Finite Element Model
FRF	Frequency Response Function
GRT	Ground Resonance Test
IMU	Inertial Measuring Unit
LMS	Loads Monitoring System
NF	Notch Filter
OLFRF	Open Loop Frequency Response Function
PC	Personal Computer
SC	Structural Coupling
SCT	Structural Coupling Test
TBD	To Be Defined
TFA	Transfer Function Analyser
U/W	Under Wing

3. INTRODUCTION

The new generation of high performance fighter aircraft relies upon digital controls, which improve their handling and manoeuvre capabilities, and allow unstable aeroplanes to fly. To achieve these functions the aircraft FCS is designed to generate a feedback based on the analysis of signals coming from IMU sensors. Since the IMU is fitted to the elastic airframe, its sensors, besides the aircraft rigid body motion parameters, pick up also the structure vibrations. The concept of system stability must be therefore extended to the full system, including the aerodynamic and mass characteristics of the aircraft, the FCS and the structural dynamics of the airframe.

Among the forces that cause the airframe dynamic response, the aerodynamic and inertial forces induced by oscillating control surfaces play a fundamental role. They in fact give rise to a very dangerous loop when exciting the structure near a resonance. This can occur when signals from IMU are not appropriately filtered to remove structure vibration contents,

Paper presented at the RTO AVT Specialists' Meeting on "Structural Aspects of Flexible Aircraft Control", held in Ottawa, Canada, 18-20 October 1999, and published in RTO MP-36.

inducing, through the feedback to control surface actuators, those oscillations that must be avoided.

SC is the discipline developed to study the coupling between the dynamic response of the airframe and the FCS, and plays a very important role in the qualification of aircraft with digital controls. The usual solution to SC problems is to implement a set of NF in the FCC and IMU control laws, in order to attenuate to a safe level the airframe vibration contents in the signals running in the FCS. Reference 2 illustrates the procedure developed and applied for the design and qualification of NF. A fundamental step of this procedure is the ground SCT stage, the aim of which is to identify the SC characteristics of the aircraft. Data from SCT are required for the updating of the aeroservoelastic model to be used for the NF upgrade. Ground test data are also essential to improve the design in the high frequency range, where the model predictions are not considered adequate.

4. GROUND STRUCTURAL COUPLING TEST

The main objectives of the ground SCT are to provide data for:

- Model validation
- Investigation of unmodelled aspects
- Coverage of the frequency range where the model alone is not considered to be an adequate basis for production of filter design information.

The amount of analysis to be carried out using the aeroservoelastic model is really huge. Calculations are in fact required for NF design and optimisation, and subsequently for flight clearance and qualification purposes. Considering the wide possibility of combinations of external stores for a military multirole aircraft, which strongly influence the dynamic response characteristics of the airframe, it is evident that only a limited set of external store configurations can be tested on ground, the rest being studied only through calculations. The consequence is the need of an adequate mathematical model for SC analysis and methods to augment the model predictions using a limited set of test data.

The main objective of the ground SCT is therefore to get all information needed to evaluate how the model simulates the SC characteristics of the aircraft in absence of aerodynamics, and then to update the model and the preliminary NF, if necessary. The other important objective is to collect enough experimental data in the high frequency range. It is well-known, in fact, that the quality of the model predictions above a certain frequency is rather poor. Since the NF are to be implemented in a digital system the frequency range that must be covered in their design depends on the sampling rate of the FCS and, as a consequence, the analysis is to be extended usually beyond the model capabilities. During the Identification Test the measurement of transfer functions is performed also covering the frequency range where the model is not satisfactory. The relevant experimental data will feed a procedure developed to augment model predictions, based on the direct usage of experimental data combined with model predictions, as more fully described in section 6.

Additionally, the test is very important to assess the influence on the aircraft response of structure non-linearity, hydraulic failures, control surface trim position, actuator hinge backlash, undercarriage support, etc., not implemented in the linear model.

Essentially the test consists in measuring the IMU signals in response to the excitation of the aircraft, obtained by means of sinusoidal rotation of control surfaces about their hinge axes. This gives rise to inertial forces due to the surface CG offset with respect to the hinge axis, and makes the structure respond at the same frequency of the surface oscillation. The relevant vibration levels are picked up by the IMU sensors, measured and then used to calculate the transfer functions corresponding to those employed for the preliminary NF design. The test is carried out in open loop, to avoid IMU signals being sent to the FCC and therefore to the control surface actuators. This stage of testing is referred as the *Identification Test*, because it serves to identify the SC aircraft characteristics and it must be performed quite early with respect to the flight date, depending on the time required for the updating of notch filters.

A further SCT stage is usually foreseen in the route to clearance just before the first flight, called *confirmatory test*, the aim of which is to verify that the updated NF satisfy the requirement for the aircraft in the pre-flight standard. This test is necessary when significant structural changes are introduced, above all in the mass distribution, between pre-flight and identification test aircraft standard.

The following paragraphs will be devoted to describe more in detail all the aspects which are typical of ground SCT.

4.1 Aircraft Build Standard

The aircraft to be tested must be representative of the flight standard with regard to the mass distribution and the airframe stiffness. Since the identification test is usually carried out several months prior to the first flight, it might be that some equipment are missing or not available at that time. Appropriate ballast should be fitted to substitute the missing items, which with their weight can influence the aircraft response. One of this is, for instance, the pilot with his flight equipment. It is particularly important that mass of equipment located at the extremities of flying surfaces - for example the wing tip pods on Eurofighter – is correctly represented since these have a significant effect on the aircraft flexible mode frequencies and structural coupling characteristics.

Concerning with the stiffness, it is essential that all panels and doors carrying loads must be closed and fixed. Since during the test it is required the access to some equipment for cable connection (FCC, IMU), power supply and inspection, it might be necessary to build spare structural panels with stiffened holes, in order to maintain the stiffness characteristics and fulfil the access requirements.

The peculiarity of the SCT is the excitation, that is obtained by means of the oscillation of the control surfaces. For this reason it is necessary to have the hydraulic and electrical plant perfectly functioning and the flight actuators installed. The power supply to these systems is obtained by means of external devices that will be connected to the aircraft.

Other essential components needed for the test are the FCC and the IMU, each one with the appropriate hardware and software standard. The FCC at this stage is only needed to manage the excitation signal generated from the test equipment, driving it to the actuators. Since the control laws are not involved in the test procedure a preliminary FCC software version can be accepted.

4.2 Aircraft Suspension

The aircraft must be tested in free-free condition, and this can be accomplished using an elastic suspension or pneumatic supports. The suspension must be designed with a response frequency quite below the lowest modal frequency of the aircraft, in order to avoid any interference with the airframe response.

Some test runs might also be repeated on undercarriage, to evaluate the influence of this system on the aircraft response. This approach can result to be very helpful for the confirmatory test phase, when very few runs are required and therefore the test could be carried out, in order to save time, using the undercarriage support. The aircraft response in free-free condition can then be derived from the differences between free-free and on-undercarriage responses measured during the identification test.

4.3 Special Requirements

During the SCT some parameters must be kept under control, in order to avoid damage to the aircraft. For instance, control surface actuators are driven in a manner which is quite different compared with normal operation during the flight for the aircraft control, and some actions are to be undertaken to avoid an excessive drying of actuator ram seals. The risk is in fact that these parts are not lubricated as required, because of the small amplitude of motion of the ram at high frequency. The solution to the problem is to interrupt the test after that the actuator rams have performed a certain number of cycles, fixed by the relevant specification, and lubricate the sealing carrying out a run characterised by few cycles at wide amplitude and very low frequency. Considering that the number of cycles allowed between two lubricating cycles is reached quite rapidly, above all at high frequency, the lubricating cycles are carried out rather frequently during the SCT. This of course slows down the test and compels to split it into several runs.

Engines are other items that need attention during the test, in order to distribute effects of vibration wear on bearings and rotating parts, that during the test are obviously at rest. This is usually accomplished by rotating periodically the shafts of the engine during the test, using crank systems or any other device that allows the rotation of the engine shafts.

During the SCT high vibration levels might be reached in some parts of the airframe and maintained for several cycles. For this reason it is necessary to monitor these levels by means of a set of accelerometers and strain gauges, located at aircraft structure critical points. These sensors send the signals to a device, which automatically cuts out the excitation when it realises a dangerous situation for the aircraft. In particular, each channel is set to the level of acceleration or stress, that must not be exceeded at the relevant airframe point and a continuos comparison is performed between these thresholds and the signals coming from the sensors. Whenever a threshold is exceeded, the device generates a signal which causes the cut-out of the excitation. Usually the thresholds correspond to the *fatigue negligible limits* of the elements of the structural component: if they are not exceeded during the test no fatigue damage is caused to the structure. If the excitation is not high enough to obtain an adequate response of the structure it is necessary to increase the excitation level beyond these limits: in this case the signals coming from the sensors must be recorded for subsequent evaluations on the fatigue damage caused to the structure. The thresholds in this case are increased up to a certain percentage of the negligible limits, never exceeding the *maximum limits*, provided together with the negligible limits.

4.4 Excitation Procedures

SCT is unusual in the manner in which the dynamic response is excited. The inertial forces which excite the aircraft are generated making the control surfaces oscillate about their hinge axis. To do this a sinusoidal signal is generated by the test equipment and then sent to the control surface actuators through an appropriate setting of FCC. The control surfaces are not moved all at the same time, but they operate in couple or single, depending whether they are symmetrically located on both sides of the aeroplane or not (rudder). Two different types of excitation can be considered: symmetric, sending the same signal to the two surfaces of the couple; anti-symmetric, sending signals with same amplitude but shifted in phase of 180 degree. With this approach it is possible to excite separately the symmetric and anti-symmetric modes of the airframe. Figure 1 shows the different combinations of control surfaces and the relevant IMU signals measured to calculate the OLFRFs.

The aim of the test is to identify how the principal modes of the aircraft respond to this kind of excitation To fulfil this task a sine step sweep procedure has been adopted, changing the frequency of the signal with discrete steps and maintaining the same signal for a certain number of cycles, during which signals from IMU are measured. The Sine Step method has shown to be more appropriate than a sine continuous sweep with logarithmic frequency variation, because it allows to gather data for more cycles at each frequency and consequently a better average of the aircraft response.

The amplitude of the oscillation must be set sufficiently high to obtain the level of forces needed for a proper response of

the aircraft, while avoiding actuator non-linear effects. In general, excitation amplitude is high at low frequency, and diminishes as frequency increases, in order to respect the LMS constraints. The approach normally followed to obtain the best response of the structure is to maintain the level of the excitation amplitude as high as allowed by the LMS constraints. Some preliminary runs are dedicated to optimise the amplitude of the sine sweep: starting from a TBD value at low frequency, the run is repeated increasing every time the level of amplitude, until the LMS cuts off the input signal. On the basis of this level an appropriate amplitude profile versus frequency can be defined, following two opposite necessities: to keep the amplitude as high as possible and to avoid a continuos interruption of the test by the LMS

4.5 Preliminary Checks

Many checks must be carried out prior to start with the SCT, in order to verify that all test equipment and instrumentation items are working in accordance to the SCT specifications.

An assessment of the mass characteristics of the aircraft is required in order to update the representation of mass in the mathematical model. This will require a measurement of the total weight and cg position of the aircraft. A check is necessary to ensure that the mass of equipment located at the extremities of flying surfaces - for example the wing tip pods on Eurofighter –is correctly represented since these have a significant effect on the aircraft flexible mode frequencies and structural coupling characteristics. A detailed monitoring of the aircraft build standard up to the time of the tests is therefore needed.

Control surface actuator hinge backlash tests are required prior and after the test, to verify that the surface oscillations have not caused any damage to the hinges.

It must be verified that the FCC feedback loops are opened, and this can be done by simply *hand rocking* the aircraft in pitch, yaw and roll. From the analysis of FCC signals that indicate the position of control surfaces it can be deduced whether they are moving or not: of course, since no external signal is sent to the actuators, a movement of the surfaces would mean that a feedback signal is sent by the FCC to them, and that therefore the loop is closed. Since the test must be carried out in open loop, the FCC setting has to be reviewed and the check repeated if the open loop condition is not verified.

Another important check regards the by-pass of the IMU NFs. Preliminary NFs are in fact implemented in the FCC and IMU control laws and all facilities provided for their by-pass must be activated. To verify the effectiveness of the by-pass procedure, some runs must be repeated in the frequency range where IMU NFs are active, with the by-pass on/off: if the NFs are correctly by-passed the appropriate attenuation has to be found when comparing the OLFRF measured with the by-pass active with respect to the one without by-pass.

The last stage before starting the SCT consists in measuring the transfer function of each actuator, to verify that the relevant performances are in accordance with previous rig tests.

4.6 Aircraft Identification Test

The OLFRFs to be measured are defined by the procedure for the NF design , and can be deduced from the sketches reported in Figure 1. They must be measured in a frequency range extended up to the sampling rate which characterises FCC digital signals. This is necessary to take into account the folding-back effect of the high frequency range due to digitalisation.

To carry out the SCT it is necessary to exchange data with the FCC and this function is performed by the ATE, a device designed for pre-flight FCC checks and able to perform the following operations during SCT:

– set up and read/write FCC parameters
– injection of the excitation signal into the FCC
– reading of IMU sensor signals from FCC facilities
– real time presentation of FCC signals.

The excitation signal is generated by a TFA, incorporated in the ATE and interfaced with an external PC. The same TFA performs the calculation of the OLFRFs and sends the relevant data to the PC for storing and subsequent analysis. Figure 2 illustrates the layout of the test, showing the links among the test items and the exchanged data. During the test measured OLFRFs are compared with theoretical predictions, in order to check whether unexpected or unwanted effects are influencing the test.

It is very important to verify the degree of non linearity of the aircraft response during the test, looking at the shape of IMU and LMS sensor time histories traced in real time by a brush recorder. More detailed information are obtained repeating some runs, usually for the most important normal modes, at different amplitude levels. The lesson learnt from the SCT is that the highest amplitude levels compatible with LMS constraints should be used, to keep non linearity effects to a minimum level. Figure 3 shows the same OLFRF measured at different amplitude levels in the first wing bending frequency range, highlighting that the main effect of non linearity is on the amplitude of the peak, with small influence on the frequency.

Besides the influence of amplitude other test runs are to be carried out, in order to investigate the influence of failures of one or two of the four redundant hydraulic systems and FCCs. These checks are needed since in this case the actuator performances can present significant changes, influencing the OLFRFs and thus the NF design.

4.7 Confirmatory Test

The *identification test* covers all the aspects necessary to identify the SC characteristics of the aircraft required for the NF design. It is very detailed and carried out for different aircraft configurations, regarding both external stores and internal fuel. This is done to verify the theoretical predictions

relevant to the influence of mass characteristics on the aircraft response.

On the contrary, the *confirmatory test* is intended to be a very short test, with the aim of verifying that the aircraft in the ready-to-fly standard does not present significant changes in the response with respect to the *identification test*. The test is therefore to be carried out when the aircraft is in the flight configuration. The verification test is normally limited to modes that are very sensitive to mass distribution changes and that play a leading role in the NF design. It consists in a short *identification test*, limited to few modes, selected as most critical from the NF design point of view.

The confirmatory test is the last step in the NF qualification route before flying the configuration investigated. It is needed to issue the SC flight clearance: from the analysis of the test results it will come out whether the NFs, based on data from the *identification test*, can be confirmed for flight or not, and a reassessment for worst flight conditions can be necessary. In the worst case flight limitations might result for some regions of the flight envelope.

5. UPDATING OF THE AEROSERVOELASTIC MODEL

To accomplish the NF design procedure the OLFRFs relevant to external store configurations are required. Considering the number of configurations and the possible sub-configurations deriving from store release, it is essential the development of a reliable aeroservoelastic model to perform the amount of calculations required for the NF design.

Among the components of the aeroservoelastic model there is the aircraft structural dynamic model, the updating of which is discussed in this paper. The basis of this model is the Nastran Superelement Technique, which allows to design simpler models and then to assemble the final model with a linking procedure. In the case of the Eurofighter the airframe has been divided in the following superelements:

– wing, including flaperons and slats
– fuselage
– foreplane
– fin and rudder
– U/W pylons

Each superelement consists in a mass and stiffness matrix, calculated using the relevant FEM and applying a reduction to a set of DOFs. The dynamic reduction of the model is a very important stage, since it allows a drastic reduction in the number of DOFs, leading to a simplified model. The DOFs selection must be performed following the guideline that the reduced model has to simulate adequately the structural dynamic characteristics of the component in a certain frequency range. Some trials might be required before a satisfactory result can be achieved.

5.1 Model Updating on the Basis of GRT Results

The GRT results represent the basis for the updating of the dynamic model. All the remarks that follow about the model updating, are based on the activity performed after the GRT and SCT campaigns carried out on the first U/W stores configurations to be cleared.

Considering that component GRT for wing, fin, foreplane and pylons, had already been carried out and the relevant superelements updated, the GRT on the assembled aircraft was required to gather data for the updating mainly of the fuselage superelement and of all the elastic elements used to simulate, in the assembled model, the links among the superelements. Figure 4 is a sketch of the superelement model updating activity performed before the GRT on the aircraft. At this stage a preliminary updated model was available and it was used to predict the response of the aircraft during GRT and SCT. It was also employed to carry out all calculations required for the preliminary NF design. Figure 5 illustrates the next step, carried out after the GRT and concerning with the delivery of the final updated model, including all the effects not covered during previous superelement GRTs.

From a first rough look at the aircraft GRT results it came out that the model had the general trend to predict lower modal frequencies. The differences between test results and predictions indicated that a model adjustment was necessary. The correction was obtained applying factors to the superelement stiffness matrices and updating the mass distribution of the model, the latter based on the assessment of the aircraft mass distribution carried out before starting the test. Several trials were needed to find a set of factors for the superelement stiffness matrices, but eventually this approach demonstrated to be adequate to obtain satisfactory results. The factors were all greater than one, the greatest being applied to the fuselage, and the updated stiffness matrices were obtained multiplying all their elements for the relevant factor.

Before starting with the updating procedure it was necessary to manipulate the experimental data, transforming the GRT modal shapes in perfectly symmetric and anti-symmetric modes. This step was needed since the aircraft model is a representation of half aircraft. The main problems with asymmetry in modal shapes came from modes characterised by external stores and control surfaces wide motion. For these cases the approach was to consider data coming only from the accelerometers located on the side of the aircraft which showed a better *phase index*.

The correction procedure was iterative, starting with an initial set of factors. The new model was assembled using the factored superelement matrices and modal characteristics compared with those ones measured during the GRT. From this comparison a new set of factors would be defined and the process repeated until a satisfactory comparison could be found. The modal characteristics monitored during the iterative procedure to establish when the process could be stopped were the modal frequencies, the generalised masses and the modal shapes.

Regarding the frequency, the comparison was based on the percentage difference between test and model data. Figure 6 shows the situation for some modes at the end of the procedure, pointing out to the improvement obtained for this parameter with respect to the GRT predictions.

For the comparison of the generalised masses and the modal shapes it was necessary to renormalize the theoretical modes, in order to make them homogeneous with the measured ones. In general the location of the accelerometer with the highest response level was chosen as reference point. This step was repeated for different points, depending on the modal shape and the accelerometer phase index measured during the acquisition of the mode. The aim of this repetition was to understand how the selection of the reference point could influence the calculated generalised mass. To perform these checks without problems the GRT accelerometer map was designed making the accelerometer locations coincide with model grids whenever it was possible. This approach could be easily followed for components like wings, foreplane and fin, but for the fuselage an interpolation of sensor data was necessary. For the comparison of modal shapes the following index was calculated:

$$\frac{\left(\Phi_{theory} \bullet \Phi_{GRT}\right)^2}{\left|\Phi_{theory}\right|^2 \times \left|\Phi_{GRT}\right|^2}$$

where Φ_{theory} and Φ_{GRT} are the two eigenvectors to be compared.

In the updating procedure a special attention was dedicated to the most significant modes, namely those ones that in the previous analyses had shown to have a considerable influence on flutter, SC and dynamic loads. This approach allowed to obtain a model that can be considered adequate for general dynamic analyses, the modes represented by the model with less precision being not essential for the study of aeroservoelastic criticality.

Since the issue of Reference 1 several GRT and SCT campaigns have been performed, each one devoted to investigate a set of critical store configurations, followed by further updates. As expected, the corrections were necessary only to those items, like pylons and launchers, not tested before and there was no need to touch the baseline aircraft model updated after the first GRT campaign.

5.2 Model Updating on the Basis of SCT Results

Progressing with the development of the aircraft the necessity to cover more stores configurations with the same set of filters became the most challenging problem to solve. This is also the final target: a unique set of NF able to guarantee the required gain and phase margins for all configurations. It was immediately evident that this was a difficult task, and a less conservative approach was necessary, starting from a better correlation of the Structural Coupling model with SCT results. Moreover, the introduction in the design procedure of the Phase Stabilisation concept (Reference 2) required also to validate the phase predicted by the model for the low frequency modes, extending the comparison also to the phase of the OLFRFs.

The SCT is in general performed in parallel to the GRT, but not necessarily on the same configurations. The aim of the GRT is in fact to collect enough data for the modal identification of the aircraft, and in particular for specific items like pylons and launchers. In this case single store configurations are acceptable. For the SCT, since the high frequency measurements are used directly in the notch filter design, the configurations must be representative of the most critical ones, previously identified by the model.

Immediately after the release of the model updated on the basis of GRT, the next step is the simulation of the SCT runs carried out on ground, using initially the modal damping values measured during the GRT. At this stage a further improvement is introduced in the aeroservoelastic model, replacing the actuator transfer functions with the frequency functions measured during the preliminary phase of the SCT. These frequency functions are thus compared with the test data.

In general the correction is needed only to match the amplitude of the main modes responses, the frequency being already corrected during the GRT updating. No attempt is made to correct the phase, but simply a monitoring of main modes to confirm the applicability of the Phase Stabilisation concept.

The first step in the correction of the SC model is to identify the possible source of errors in the model and next to find a procedure simple enough to obtain a satisfactory result across all of the several configurations to be covered. The source of errors considered for the model correction are the following:

- Fuselage model and IMU location.
- Modal shapes.
- Non linearity effects.

The first point is very important, but difficult to address. The superelement representing the fuselage is in fact reduced to a limited number of grid points along the longitudinal axis representing the main structural stations, and other grid points located at the position of main equipment items to simulate their mass and inertia characteristics. Among the latter there is the IMU grid point, but trying to match the SCT results changing the elements of the stiffness and mass matrices was not considered practical. Another approach was tried, applying appropriate factors to the modal deformations of the IMU grid point, but a satisfactory solution was not found, principally because the factor affected all OLFRFs whereas the error in each mode is different for each control surface / sensor combination. This result confirms that the correction of only the fuselage modal shape is not enough and, since the inertial excitation induced by the oscillating surface depends on the modal response of the aircraft, a more general correction is needed. However, in order to generate a

reliable model, the location of sensors and the fuselage model must be considered with great care. Concerning with the modal shapes, the matching of the main modal frequencies was considered a success, since the optimisation of the model with the modes as constraints at the current state of the art is feasible only using very simple dynamic models.

Another aspect to be considered in the model updating is the effect of non linearity on the test results. As explained in the description of the SCT procedure, excitation amplitude varies with frequency. This means that, if the effect of the non linearity of the system is significant, the comparison with the model is affected by an error distribution that depends on the frequency. For the most important modes this effect is assessed repeating the surface excitation at different input levels. In general the effect on the frequency of the mode is small, but on the amplitude of the response is significant, and should be taken into account. The general approach is to consider the amplitude associated to the highest level of excitation and to change the original GRT modal damping values according to SCT data.

On the basis of the above discussion it has been decided to adopt a data base of frequency dependent response-amplitude correction functions, to be applied to the OLFRFs calculated by the model. The data base is generated according to the following procedure:

- The data base contains several sets of correction functions, one set for each store configuration tested on ground during the SCT.
- Each set contains one correction function for each OLFRFs, calculated comparing the measured and the related analytical OLFRFs.
- The data base contains also a set where each correction function is the envelope of the corresponding functions calculated for the tested configurations. This set will be used for configurations not tested during the SCT.

The OLFRF correction process consists in performing the product of each OLFRF for the associated correction function before the filter optimisation phase. This approach allows the correction of the structural uncertainties of the model. Figure 7 is an example of how this method is applied. The picture shows the typical situation encountered during the correction procedure: a very good matching of the model for the first modes and the necessity to introduce a correction for the modes close to the frequency limits of application of the model.

A further correction can be implemented after the structural coupling flight trials have been completed. This correction is much simpler, being associated to the efficiency of control surfaces, generally overestimated by the model. A factor can be identified for each significant mode and applied for all configurations, since the effect of stores on these factors can be accepted as negligible. The main difference between the structural and the aerodynamic correction is that the first is represented, generally speaking, by an amplification factor, the second by an alleviation factor. Figure 8 illustrates this characteristic from the comparison of model predictions with flight test data. It gives an idea of the degree of conservatism of the model, from which the aerodynamic alleviation factors can be derived.

The procedure described, even though complex, is very practical and easy to be implemented in a global automatic procedure for the generation of the OLFRFs needed for the NF design. Its weak side is represented by the management of a data base with data associated to several stores configurations and the necessity to identify the most critical configurations to be tested on ground. The number of critical configurations can be significant and the dependency on ground testing is a heavy burden in the qualification of a multirole aircraft. For future aircraft an improvement in the structural and aerodynamic modelling techniques is necessary, in order to reduce the cost and the risks inherent in the design and qualification of notch filters.

6. REPRESENTATION OF HIGHER FREQUENCY RANGE

Under the current Eurofighter notch filter design philosophy and procedure (Reference 2), the OLFRFs derived as described in Section 5, i.e. wholly from the flexible aircraft model, are used only for representation of the lower frequency modes, which are critical for notch filter design and which have the most significant impact on the notch filter phase lag.

For higher frequency modes the model is not considered reliable enough for use in a 'stand alone' manner, and an alternative approach is taken which combines ground test-measured frequency response functions with model-predicted aerodynamic effects and calculated FCS control law gains to form a conservative representation of the overall system.

This approach avoids the difficulties associated with a model update that aims to;

- be rational and physically meaningful, and
- lead to a single model able to reproduce measured responses in several different sensor / excitation combinations.

In the applying the method, it is assumed that the predicted aerodynamic effects, in terms of gain change as a function of airspeed, are correctly predicted by the model, and that it is fundamentally the zero-speed characteristics which are in error when compared with ground test results. Thus the method effectively substitutes the measured zero speed characteristics for the predicted, producing a composite FRF which, when the FCS gain is included, can be used for Notch Filter design.

6.1 Aerodynamic Effects

Flexible aircraft response to control surface excitation is calculated across a range of flight conditions, covering the desired flight envelope (extended to encompass Mach and height overshoots). The combinations of sensor output and

control surface input required are determined by the control law configuration. These combinations are identical to those defined for ground SCT, Figure 1.

Aerodynamic effects are derived from the FRFs in the form of increments in predicted response-peak gain and frequency, relative to the corresponding zero-speed characteristics. This results in a presentation of response gain and frequency trends for each mode and sensor / control surface combination, which, when combined with the corresponding FCS gain schedules, gives a clear and concise view of the variation of overall response, and by implication gain margin, with speed.

The calculation can be made with a preliminary, pre-SCT, model standard, facilitating early progress with notch filter design, but careful checks must be made where the actual (SCT measured) modal frequency separation is found to vary significantly from prediction, implying differences in mode shape and hence in the unsteady aerodynamics.

6.2 Zero Speed Characteristics

Clearly, successful application of the method will depend on both the quality of the ground structural coupling test data and the correct identification of the correspondence between modes excited in the ground test with those predicted by the model. Particular attention must be paid to both of these aspects in the conduct of the ground test, implying close involvement of structural coupling specialists in the tests.

7. CONCLUSIONS

The test procedure followed for the SC identification test of a delta-canard aircraft has been described. The need for an accurate aeroservoelastic model, in order to limit the testing activity to a reduced number of external store configurations, selected on the basis of SC criticality, has been pointed out. The way followed to update the theoretical model using Ground Resonance and SC Test results has been presented. The aeroservoelastic model, updated with test data, can be considered a reliable tool for the FCS NF design in the low frequency range, where the most critical modes can be found. For the high frequency range a method, based on a combination of test and model data, has been described. Its application allows to contain the model deficiency in this frequency range.

The updating procedure described in this paper is based on two steps: the first mainly on the correction of the stiffness characteristics of the model, using data gathered during GRTs carried out on a limited number of external store configurations. This set of configurations of course must be selected so to cover the stiffness characteristics of all pylons and launchers which can significantly influence the airframe dynamic response. The second step refers to the generation of a data base of correction FRFs derived from the comparison of model predictions with SCT data.

Following this approach all not tested combinations of stores can be studied using the mathematical model, by the simulation of the appropriate mass distribution, and thus limiting to a limited number of critical configurations the very expensive test activities. For the high frequency range it is essential that the configurations tested on ground are the most critical for SC aspects, and therefore the measured data can be used also for the remaining configurations.

8. REFERENCES

1. V.Vaccaro, J.Becker, "Ground Structural Couplign Testing and Model Updating in the Aeroservoelastic Qualification of a Combat Aircraft", AGARD SMP Meeting on Advanced Aeroservoelastic Testing and Data Analysis, Rotterdam, 8-10 May 1995.
2. J.Becker, V.Vaccaro, B. Caldwell, "The Interaction of Flight Control System and Aircraft Structure", AVT Panel: Specialist Meeting on Structural Aspects of Flexible Aircraft Control, Ottawa 18-20 October 1999
3. J.Becker, V.Vaccaro, "Aeroservoelastic Design, Test Verification And Clearance of an Advanced Flight Control System", AGARD 80th SMP Meeting on Advanced Aeroservoelastic, 5/1995
4. V.Vaccaro, J.Becker, "Ground Structural Couplign Testing and Model Updating in the Aeroservoelastic Qualification of a Combat Aircraft", AGARD SMP Meeting on Advanced Aeroservoelastic Testing and Data Analysis, Rotterdam, 8-10 May 1995.
5. B.D.Caldwell, "The FCS-Structural Coupling Problem and Its Solution", AGARD FMP 4/94
6. M.G.Allen, S.J.Pollock, "AFTI/F-16 Aeroservoelastic Analysis and Ground Test with a Digital Flight Control System", AIAA Paper No.83-0994
7. T.D.Smith, C.J.Yeo, R.E.W.Marshall, "Ground and Flight Testing on the Fly-By-Wire Jaguar Equipped with a Full Time Quadruplex Digital Integrated Control System", AGARD CP-321
8. MSC/NASTRAN-HANDBOOK FOR SUPERELEMENT ANALYSIS
9. B.D.Caldwell, R.Felton, "Validation of FCS Structural Coupling Stability Characteristics Through in-Flight Excitation", CEAS International Forum on Aeroelasticity and Structural Dynamics, Rome, 17-20 June 1997

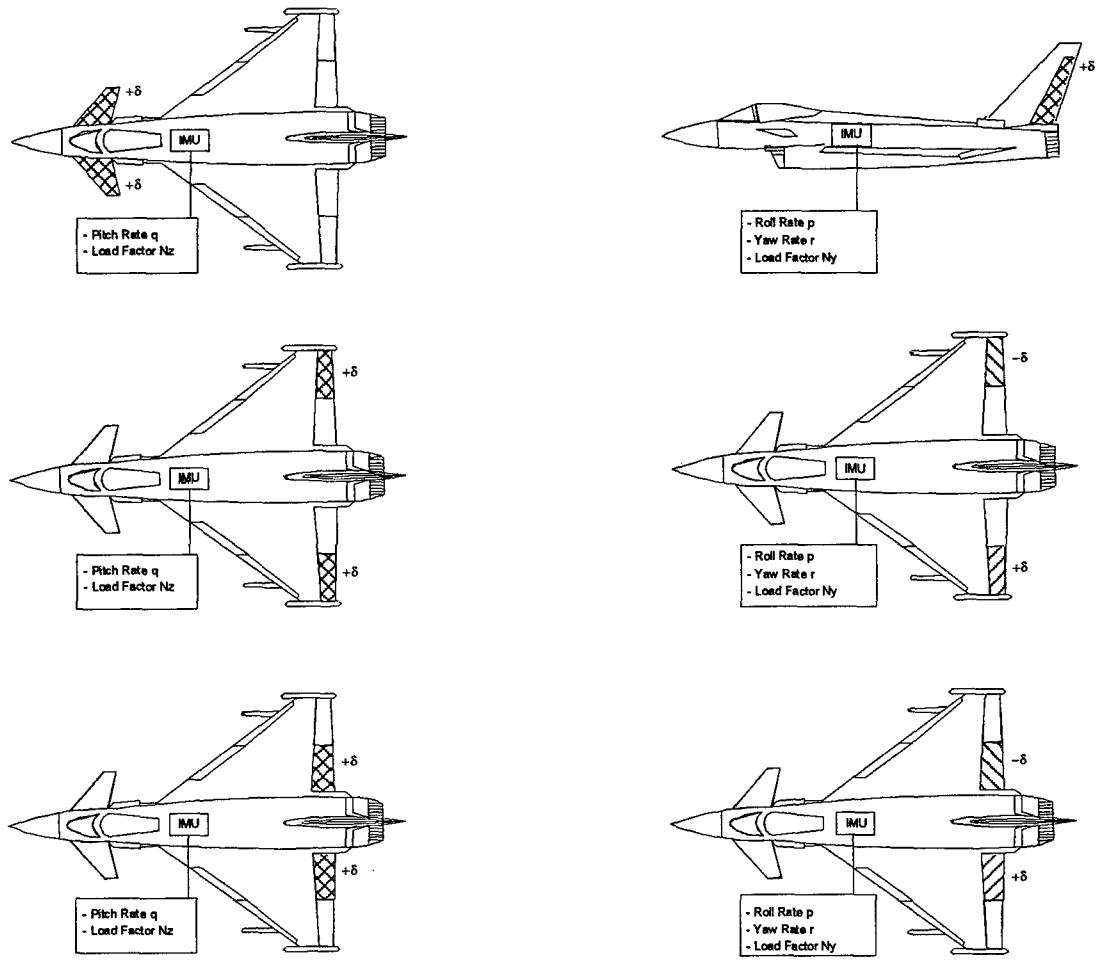

Figure 1: SCT and Antisymmetric Symmetric Excitations and Measurements

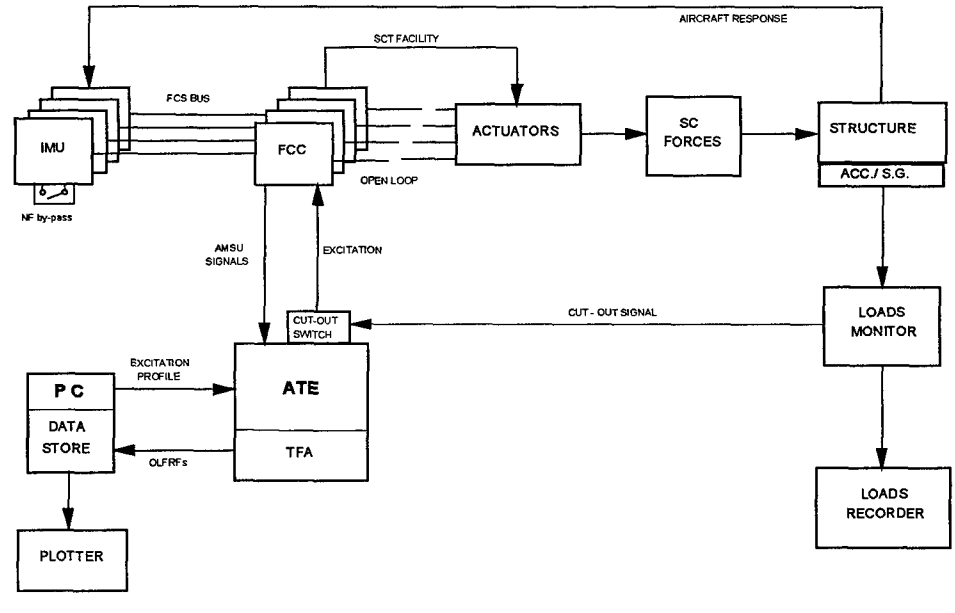

Figure 2: SCT Layout

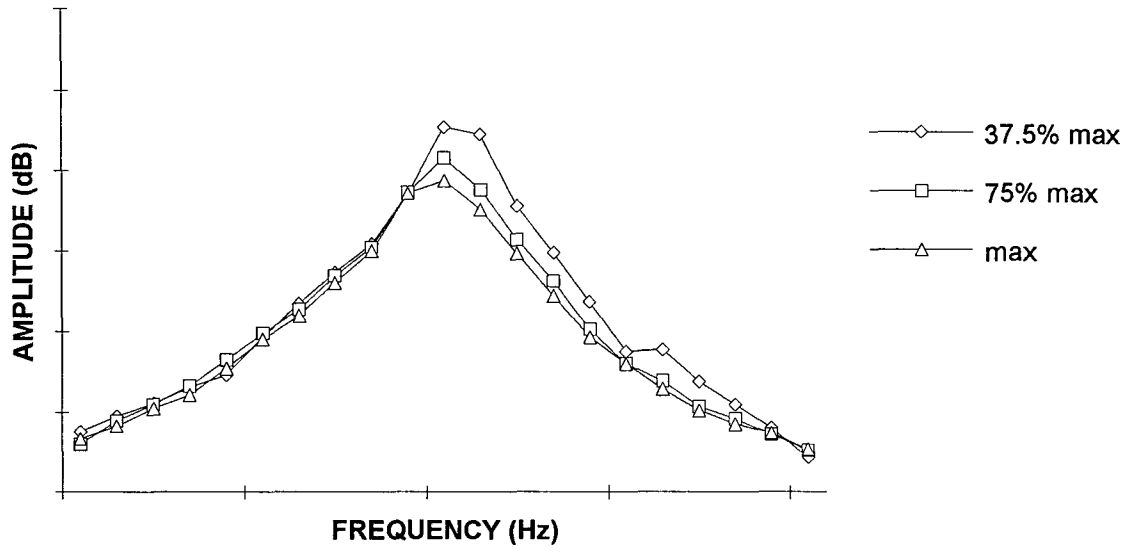

Figure 3: Influence of Excitation Amplitude on OLFRF

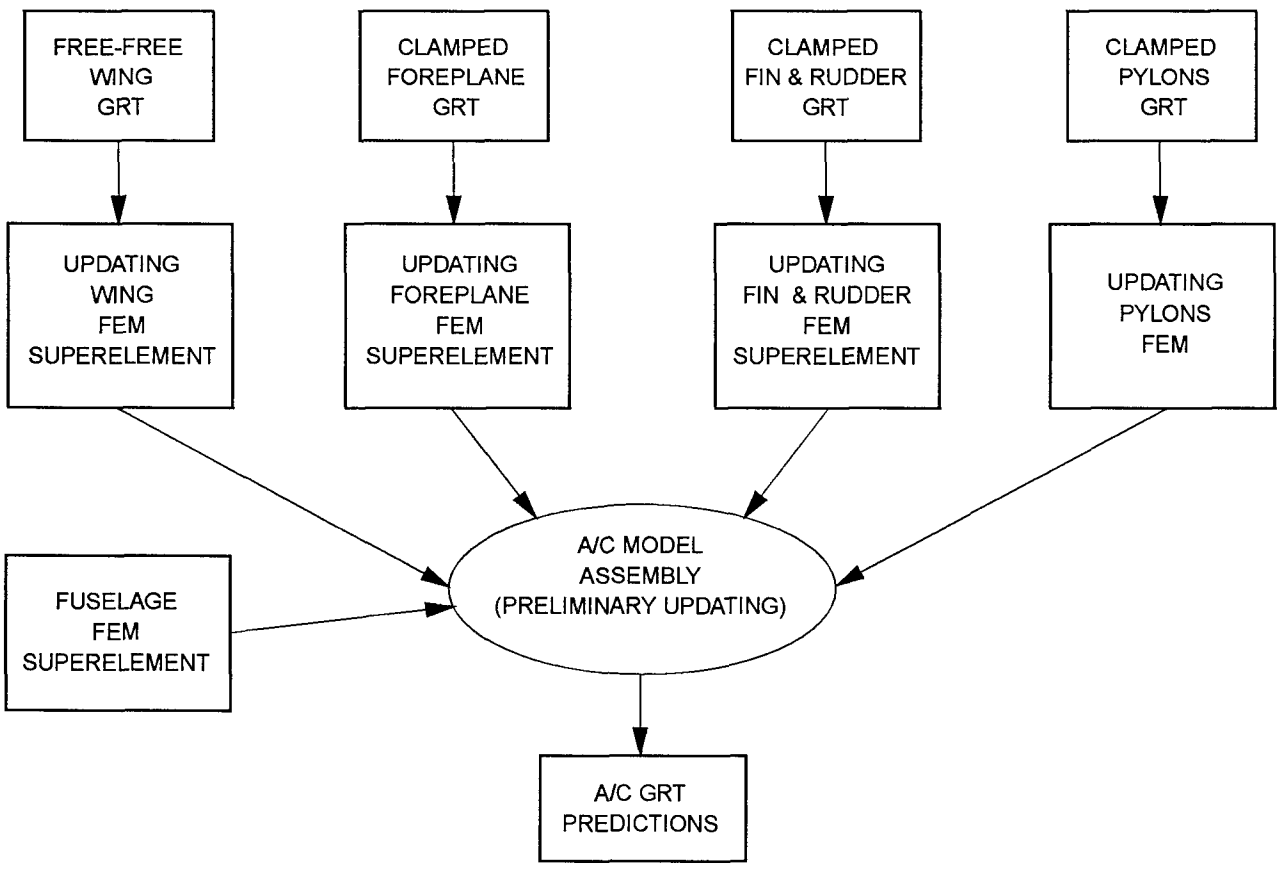

Figure 4: Model Preliminary Update Procedure (Components)

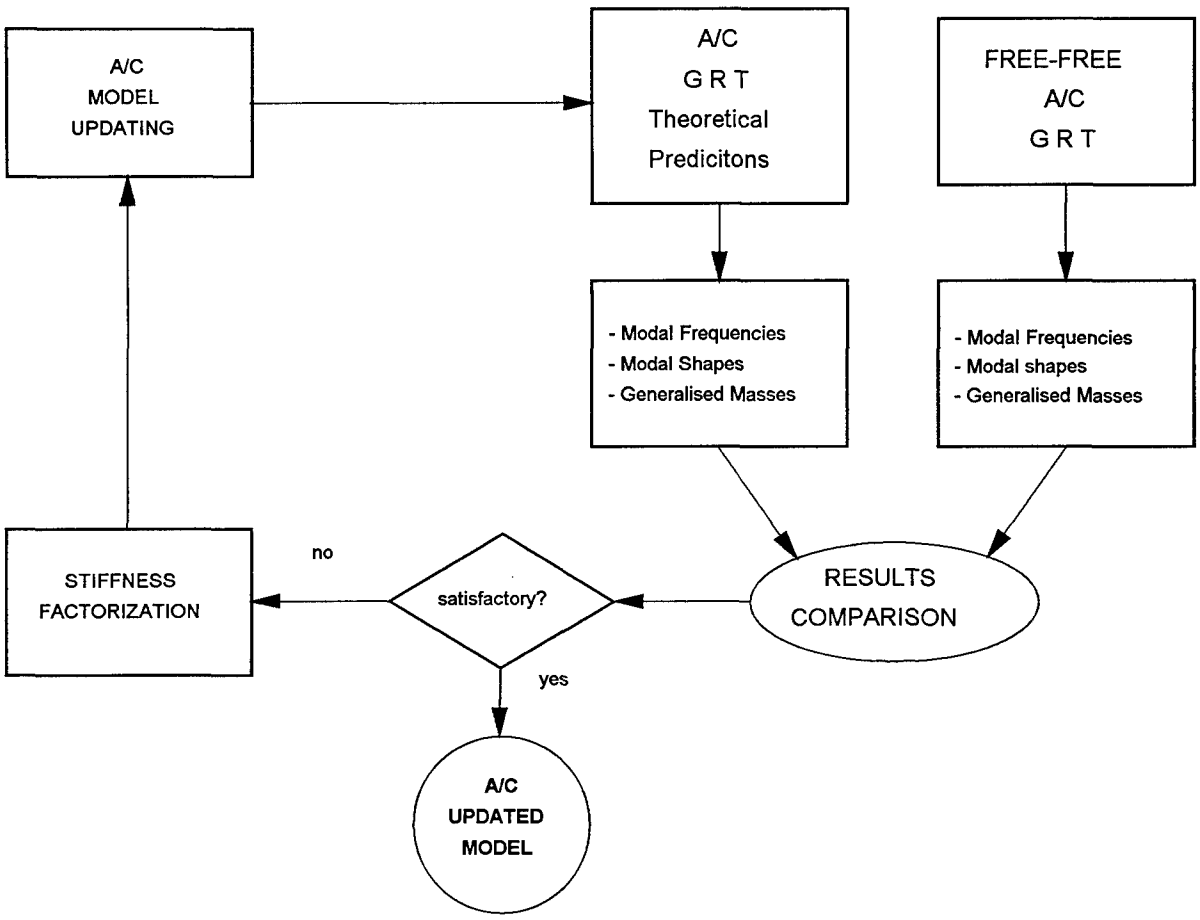

Figure 5: Aircraft Dynamic Model Updating Procedure Based on GRT

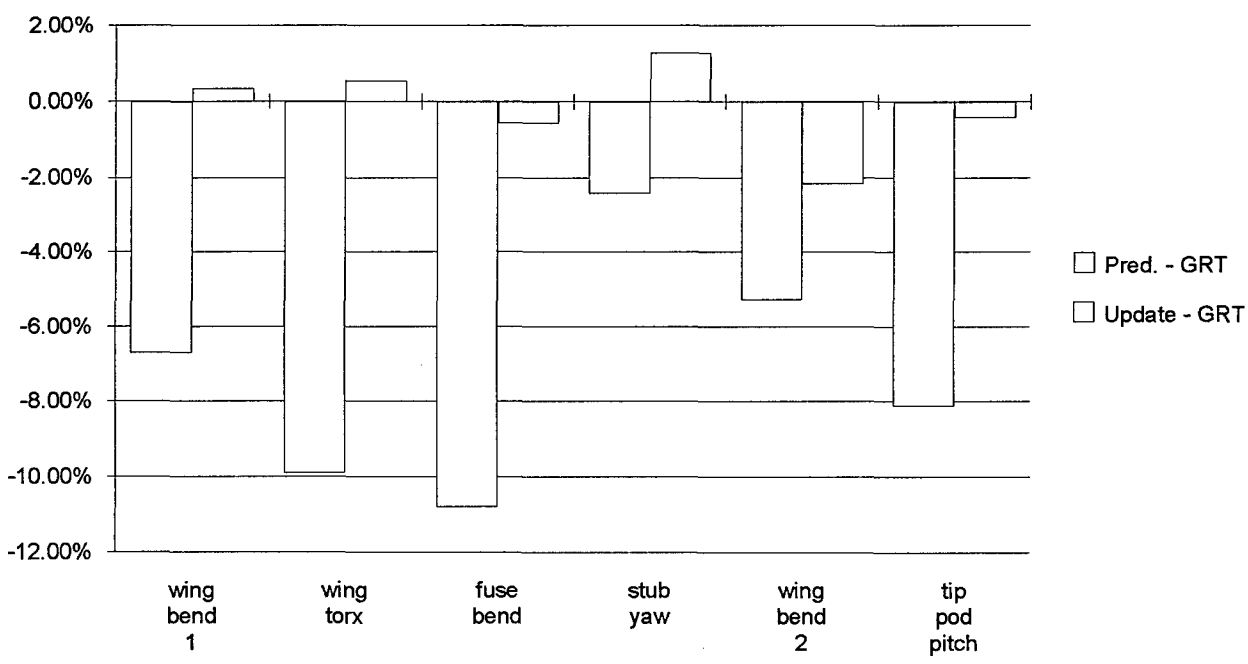

Figure 6: Modal Frequency Percentage Differences

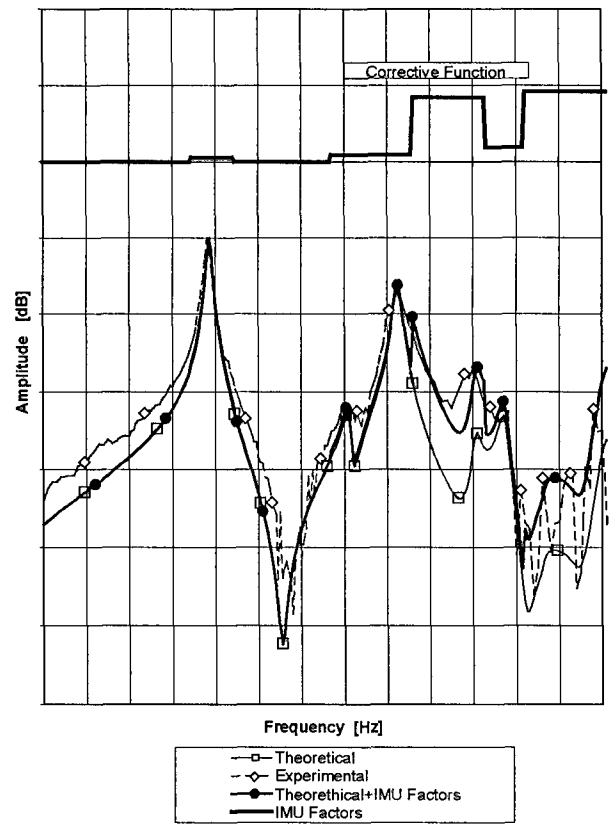

Figure 7:Example of application of a Correction Function

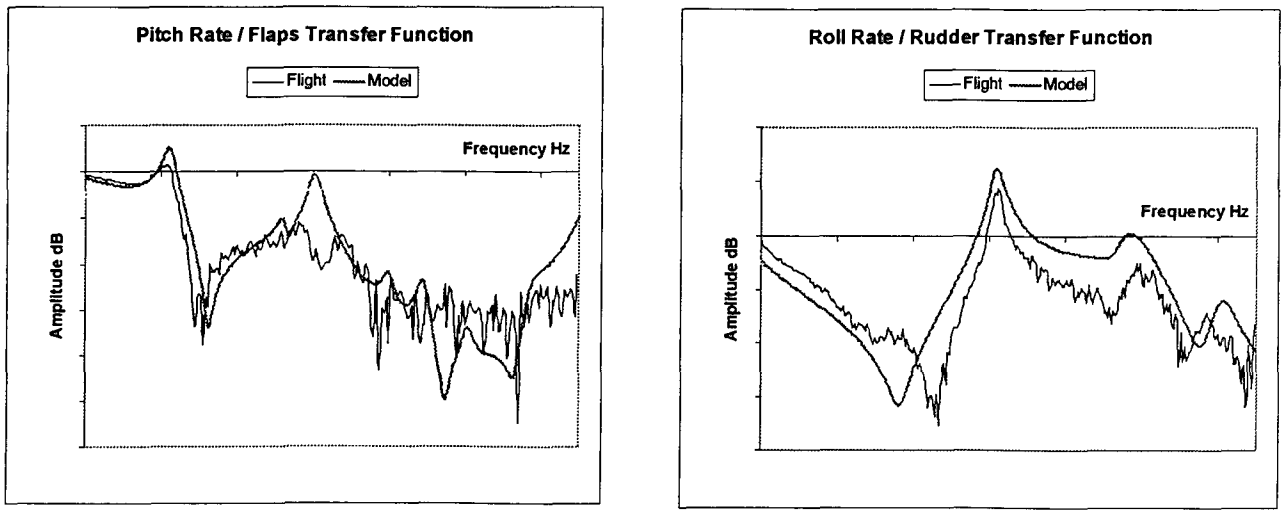

Figure 8: Example of comparison of SCT Flight test data with model predictions

Unified " Flight Mechanics and Aeroelasticity for Accelerating, Maneuvering, Flexible Aircraft

Dr. James J. Olsen
Olsen Engineering Consulting
1186 Tralee Trail
Dayton, Ohio 45430-1219
United States

Abstract

This paper reveals new insights in the aeroelasticity and flight mechanics of flexible aircraft by obtaining and solving the equations of motion for a flexible, accelerating, rotating aircraft. We illustrate the approach for three cases of increasing complexity: The first case is a "sprung" pendulum. It shows when rigid body angular velocities can be important in the flexibility equations as they approach as the flexible frequencies. The second case is a typical section airfoil on an accelerating, rotating fuselage. It applies Lagrange's equations to a longitudinal problem in inertial coordinates, then transforms the equations to noninertial, body - fixed coordinates for solution. It also shows when rigid body rotations and longitudinal accelerations must be included in the flexibility equations. The third case is the general longitudinal/lateral motion of an accelerating, rotating, flexible vehicle. Rather than setting up the general problem in inertial coordinates and then transforming to body - fixed coordinates, instead we use the idea of "quasi - coordinates". We establish a general form for Lagrange's equations in the noninertial, body - fixed coordinates. The paper gives the general equations and reduces them to a special case of a "flat" airplane. It also gives guidelines as to when the rigid body rotations and accelerations are important factors in the flexibility equations.

1. Introduction

For many years there has been a search for a practical set of "unified" equations of motion that can be used in all of the disciplines of aerodynamics, structures and stability and control of flexible aircraft. Such an approach would allow the customary determination of the effects of structural flexibility on aircraft performance, stability and air loads. An added benefit is that it would also allow us to determine the effects of the "rigid body" motions on aeroelastic characteristics such as control - effectiveness, divergence and flutter. Further (and most importantly), it would allow all of those engineering problems to be treated by subsets of a single set of "unified" equations. In effect we want to convert the aeroelastic problems into coordinate systems and equations that are conventional for aircraft flight mechanics, stability and control.

In many aircraft applications, the mutual coupling of rigid body and flexible motions has been small because the vehicle angular velocities and flexible frequencies were well separated. However, there have been recent examples of large aircraft where flexible frequencies (say 2 Hz) begin to approach the rigid body angular velocities (say 1 Hz). Other cases have been known where the aerodynamic forces can drive the structural frequencies and the rigid body frequencies close together. In both cases the coupling effects should be accounted for in the lowest order equations of motion to obtain the correct modeling.

To develop the necessary equations we must account for the fact that the aircraft's body - fixed coordinate system is not (in general) an inertial system. Dusto et al [1], Bekir et al [2] and Waszak and Schmidt [3] are a few examples of earlier attempts which have had to leave out crucial terms or were difficult to implement. This paper shows that a practical set of equations for general problems is available through the use of energy methods, Lagrange's equations and "quasi - coordinates".

We illustrate the approach for three cases of increasing complexity: The first case is a "sprung" pendulum. It shows when rigid body angular velocities can be important in the flexibility equations as they approach as the flexible frequencies. The second case is a typical section airfoil on an accelerating, rotating fuselage. It applies Lagrange's equations to a longitudinal problem in inertial coordinates, then transforms the equations to noninertial, body - fixed coordinates for solution. It also shows when rigid body rotations and longitudinal accelerations must be included in the flexibility equations. The third case is the general longitudinal/lateral motion of an accelerating, rotating, flexible vehicle. Rather than setting up the general problem in inertial coordinates and then transforming to body - fixed coordinates, instead we use the idea of "quasi - coordinates". We establish a general form for Lagrange's equations in the noninertial, body - fixed coordinates. The paper gives the general equations and reduces them to a special case of a "flat" airplane. It also gives guidelines as to when the rigid body rotations and accelerations are important factors in the flexibility equations.

The equations become somewhat more complicated, and it is useful to examine them in three stages. First, some

Paper presented at the RTO AVT Specialists' Meeting on "Structural Aspects of Flexible Aircraft Control", held in Ottawa, Canada, 18-20 October 1999, and published in RTO MP-36.

insight is available via a simplification which considers the rigid body motions merely as constant parameters. There the rigid body motions alter the flexible frequencies of vibration, thereby altering aeroelastic stability. Second, a more exact approach is to recognize that the flexibility equations have some of the characteristics of Mathieu's classical ordinary differential equation. The similarity to Mathieu's equation introduces the possibility that the coupled rigid - body/flexible motions can be unstable within narrow ranges of frequencies and amplitudes, even without aerodynamic forces. Third, the ultimate procedure is always available - the simultaneous solution (perhaps numerically) of the fully coupled, non - linear, rigid body and flexibility equations of motion in body - fixed coordinates.

2. Lagrange's Equations

If the inertial coordinates of a dynamic system can be represented in terms of N independent generalized coordinates:

$$X = X(q_i) \quad Y = Y(q_i) \quad Z = Z(q_i)$$

Lagrange's equations [4] can describe the motion of the system:

$$\frac{d}{dt}\left(\frac{\partial L}{\partial \dot{q}_i}\right) - \frac{\partial L}{\partial q_i} = Q_i$$

where:

L = Lagrangian, $T - U$

Q_i = Generalized Force

T = Kinetic Energy

U = Potential Energy

For simple geometries, it usually is a straightforward matter to write down the inertial coordinates, inertial velocities, kinetic and potential energies, the Lagrangian, and the various derivatives. For complicated geometries, the process can become tedious, but Whittaker[5] showed that, if the kinetic energy can be expressed in terms of the coefficients m_{ij}

$$T = \frac{1}{2}\sum_{i=1}^{n}\sum_{j1}^{n} m_{ij}\dot{q}_i\dot{q}_j$$

Then the equations of motion can be written

$$\sum_{j=1}^{n} m_{ij}\ddot{q}_j + \sum_{j=1}^{n}\sum_{k=1}^{n}\begin{bmatrix} j\ k \\ i \end{bmatrix}\dot{q}_j\dot{q}_k = Q_i + \frac{d}{dt}\left(\frac{\partial U}{\partial \dot{q}_i}\right) - \frac{\partial U}{\partial q_i}$$

where the Christoffel symbol is:

$$\begin{bmatrix} j\ k \\ i \end{bmatrix} = \frac{1}{2}\left(\frac{\partial m_{ji}}{\partial q_k} + \frac{\partial m_{ki}}{\partial q_j} - \frac{\partial m_{jk}}{\partial q_i}\right)$$

Olsen[6] showed a related (and sometimes) simpler approach, noting that if we could write the partial derivatives:

$$X_i = \frac{\partial X}{\partial q_i} \quad Y_i = \frac{\partial Y}{\partial q_i} \quad Z_i = \frac{\partial Z}{\partial q_i}$$

$$X_{ij} = \frac{\partial^2 X}{\partial q_i \partial q_j} \quad Y_{ij} = \frac{\partial^2 Y}{\partial q_i \partial q_j} \quad Z_{ij} = \frac{\partial^2 Z}{\partial q_i \partial q_j}$$

We don't need the often tedious expressions for the kinetic energy, and the equations of motion take the form:

$$\sum_{j=1}^{n} m_i\ddot{q}_j + \sum_{j=1}^{n}\sum_{k=1}^{n} m_{ijk}\dot{q}_j\dot{q}_k = Q_i + \frac{d}{dt}\left(\frac{\partial U}{\partial \dot{q}_i}\right) - \frac{\partial U}{\partial q_i}$$

where:

$$m_{ij} = \int_{mass}\left(X_iX_j + Y_iY_j + Z_iZ_j\right)dm$$

$$m_{ijk} = \int_{mass}\left(X_iX_{jk} + Y_iY_{jk} + Z_iZ_{jk}\right)dm$$

Even though Whittaker's and Olsen's expressions look simple in principle, in practice their implementation can be quite lengthy for complicated geometries with many degrees of freedom. The development of the required expressions can be greatly assisted by symbolic algebra software.

3. Example of Coupled Rigid - Flexible Motions, The "Sprung" Pendulum

In the first case we want to determine when "rigid body" motions can have important effects on the flexible motions. Consider the "sprung" pendulum which is free to rotate or oscillate about the origin in the x, y (or r,θ) plane, but which also contains a radial spring of linear stiffness k (Figure 1). We will refer to the angular motion as the "rigid body" motion and the radial motion as the "flexible" motion. Proceeding through the usual process[4] of the inertial coordinates, inertial velocities, virtual displacements, kinetic energy, potential energies (due to stiffness and gravity), the Lagrangian is:

$$L = \frac{1}{2}m\left(\dot{r}^2 + r^2\dot{\theta}^2\right) - \frac{1}{2}k\left(r - r_k\right)^2 - mg\left(r\sin\theta - Y_g\right)$$

From Lagrange's equations the radial differential equations is:

$$\boxed{\ddot{r} + \left(\omega_0^2 - \dot{\theta}^2\right)r = \frac{F_r}{m} + \frac{k}{m}r_k - g\sin\theta}$$

We also can obtain the angular equation, but we can always interpret it as the angular force required to produce the stipulated motions.

3.1 Rotation at Constant Angular Velocity

In the first case we stipulate that the pendulum moves through a complete circular motion at a constant angular velocity of ω. Then $\theta = \omega t$, and the radial differential equation is:

$$\ddot{r} + \left(\omega_0^2 - \omega^2\right) r = \frac{F_r}{m} + \frac{k}{m}\eta_k - g\sin\omega t$$

Regardless of the radial force, the radial response acts as if the natural frequency in the radial direction was

$$\omega_{effective} \rightarrow \sqrt{\omega_0^2 - \omega^2}$$

3.2 Simple Harmonic Rotation

In the second case we stipulate that the pendulum oscillates through an amplitude θ_0 with a constant frequency ω. Then $\theta = \theta_0 \sin\omega t$, and the radial differential equation is:

$$\ddot{r} + \left[\omega_0^2 - \frac{\omega^2\theta_0^2}{2}(1 + \cos 2\omega t)\right] r = \frac{F_r}{m} + \omega_0^2 \eta_k$$

The complete solution of the radial equation depends on the LHS, RHS and initial conditions. The LHS can be converted, with a change of variables,

$$\tau = \omega t \quad a = \frac{\omega_0^2}{\omega^2} - \frac{1}{2}\theta_0^2 \quad b = \frac{1}{4}\theta_0^2$$

to the classical Mathieu's equation.

$$r'' + (a - 2b\cos 2\tau) r = 0$$

Mathieu's equation applies to the vibrations of spinning satellites, buckling of beams with periodic end forces, the saturation of loudspeakers, tides in circular bodies of water and many other problems. In our application, if the radial force does not depend on **r** then the stability of the solutions depends only on the frequency ratio $\frac{\omega_0}{\omega}$ and the angular amplitude θ_0

Intuitively, one would expect that the effects on stability would be small unless the angular amplitude is large or the frequency ratio is near 1. Figure 2 (from McLachlan[7]) shows the classical plot of the regions of stability/instability for periodic solutions of Mathieu's equation. Regions of instability are shown to be emanating from the points

$$a = \left(\frac{\omega_0}{\omega}\right)^2 - \frac{1}{2}\theta_0^2 = 1, 2^2, 3^2, \ldots n^2$$

So a question becomes - what practical values of **a, b** put the solutions into the stable or unstable regions. For instance, in the neighborhood of **a=1**, we can use McLachlan's[7] boundaries to obtain a region for instability for small **b**. Figure 3 shows the lower and upper bounds of the narrow unstable region for frequency ratios near 1 and for angular amplitudes up to 10 degrees. The instability range continues to widen for higher values of the angular amplitude. For frequency ratios near 2, 3, 4,..., the instability ranges exist, but over ever narrower ranges of angular amplitude.

We also can integrate the equation numerically. Figure 4 shows typical time histories for a frequency ratio of 1.1, damping of 0.02 and amplitudes of 0.53, 0.54 and 0.55 radians. The solutions are stable for 0.53 radians and unstable for 0.54 and 0.55 radians. Figure 5 gives a general pattern for the smallest amplitudes to produce instability for damping of 0.02 and frequency ratios up to 2.

In summary, the problem of the "sprung" pendulum shows that rigid body motions can affect the flexible motions:

a. Constant angular velocity reduces the "effective" radial natural frequency;

b. Forced sinusoidal angular motion can produce radial instability near integer values of the frequency ratio as the angular amplitudes grow large.

4. Typical section Airfoil on an Accelerating, Rotating Fuselage

The second case is a problem that is closer to practical interest - a typical section airfoil on an accelerating, rotating fuselage. We will apply Lagrange's equations in inertial coordinates, then transform the equations to noninertial, body - fixed coordinates for solution. We want to show when rigid body rotations and longitudinal accelerations must be included in the flexibility equations.

Consider a slender airfoil which is mounted on a slender fuselage. (Figure 6). The fuselage has inertial coordinates $X_0 = q_1$, $Y_0 = q_2$ and pitch angle $\theta = q_3$. The airfoil is located at fuselage position $x = x_w$ and has its own degrees of freedom in vertical translation $h = q_4$ and rotation $\delta = q_5$.

4.1 Equations of Motion

For a general point on the slender fuselage and airfoil the inertial coordinates are:

$$\text{Fuselage} \quad X = q_1 + xc_3 \quad Y = q_2 + xs_3$$

$$\text{Airfoil} \quad \begin{aligned} X &= q_1 + x_w c_3 - q_4 s_3 + \xi c_{35} \\ Y &= q_2 + x_w s_3 + q_4 c_3 + \xi s_{35} \end{aligned}$$

Proceeding through the usual process of the inertial coordinates, inertial velocities, virtual displacements, kinetic and potential energies (due to stiffness and gravity) and the Lagrangian for the complete fuselage/airfoil system, we establish the complete nonlinear equations in inertial coordinates. Then, it is more convenient to actually solve the problem in a body - fixed coordinate system. So we define the "apparent" body - fixed components of the vehicle's velocities and accelerations by

$$\dot{q}_x = \dot{q}_1 c_3 + \dot{q}_2 s_3 \qquad \dot{q}_y = \dot{q}_2 c_3 - \dot{q}_1 s_3$$

$$\ddot{q}_x = \ddot{q}_1 c_3 + \ddot{q}_2 s_3 \qquad \ddot{q}_y = \ddot{q}_2 c_3 - \ddot{q}_1 s_3$$

We simplify further by dropping second order terms in q_4, q_5 to obtain the linearized equations in terms of noninertial, body - fixed coordinates.

$$\begin{bmatrix} M_{11} & 0 & -\tilde{M}_{334} & 0 & -\tilde{M}_{435} \\ 0 & M_{11} & \tilde{M}_{y3} & M_{44} & \tilde{M}_{45} \\ -\tilde{M}_{334} & \tilde{M}_{y3} & \tilde{M}_{33} & \tilde{M}_{34} & \tilde{M}_{35} \\ 0 & M_{44} & \tilde{M}_{34} & M_{44} & \tilde{M}_{45} \\ -\tilde{M}_{435} & \tilde{M}_{45} & \tilde{M}_{35} & \tilde{M}_{45} & M_{55} \end{bmatrix} \begin{Bmatrix} \ddot{q}_x \\ \ddot{q}_y \\ \ddot{q}_3 \\ \ddot{q}_4 \\ \ddot{q}_5 \end{Bmatrix} - \dot{q}_3 \begin{bmatrix} \tilde{M}_{y3} & 2M_{44} & 2\tilde{M}_{45} \\ \tilde{M}_{334} & 0 & 0 \\ 0 & 0 & 0 \\ \tilde{M}_{334} & 0 & 0 \\ \tilde{M}_{335} & 0 & 0 \end{bmatrix} \begin{Bmatrix} \dot{q}_3 \\ \dot{q}_4 \\ \dot{q}_5 \end{Bmatrix}$$

$$+ \begin{bmatrix} 0 & 0 \\ 0 & 0 \\ 0 & 0 \\ k_4 & 0 \\ 0 & k_5 \end{bmatrix} \begin{Bmatrix} q_4 \\ q_5 \end{Bmatrix} + g \left(c_3 \begin{Bmatrix} 0 \\ M_{11} \\ \tilde{M}_{y3} \\ M_{44} \\ \tilde{M}_{45} \end{Bmatrix} + s_3 \begin{Bmatrix} M_{11} \\ 0 \\ -\tilde{M}_{334} \\ 0 \\ -\tilde{M}_{435} \end{Bmatrix} \right) \approx \begin{Bmatrix} Q_3 c_3 + Q_2 s_3 \\ Q_2 c_3 - Q_1 s_3 \\ Q_3 \\ Q_4 \\ Q_5 \end{Bmatrix} + \begin{Bmatrix} 0 \\ 0 \\ 0 \\ k_4 q_{4_{ref}} \\ k_5 q_{5_{ref}} \end{Bmatrix}$$

where

$$m_w = \int_{wing} dm$$

$$S_w = \int_{wing} \xi dm$$

$$I_w = \int_{wing} \xi^2 dm$$

$$\tilde{M}_{33} = I_f + I_w + m_w x_w^2 + 2 S_w x_w$$

$$\tilde{M}_{34} = m_w x_w + S_w$$

$$\tilde{M}_{35} = I_w + S_w x_w$$

$$\tilde{M}_{45} = S_w$$

$$\tilde{M}_{334} = m_w q_4 + S_w q_5$$

$$\tilde{M}_{335} = S_w (q_4 - x_w q_5)$$

$$\tilde{M}_{435} = S_w q_5$$

$$\tilde{M}_{y3} = S_f + x_w m_w + S_w$$

4.2 Separate Rigid and Flexible Equations - Body Coordinates

The total solution requires the solution of the five coupled equations. It can be convenient to separate the complete equations into separate rigid equations and flexible equations. If we separate the purely rigid body terms, coupling terms and purely flexible terms - the linearized flexibility equations, in body - fixed coordinates, (with damping added) are :

$$\begin{bmatrix} m_w & S_w \\ S_w & I_w \end{bmatrix} \begin{Bmatrix} \ddot{q}_4 \\ \ddot{q}_5 \end{Bmatrix} + \begin{bmatrix} c_4 & 0 \\ 0 & c_5 \end{bmatrix} \begin{Bmatrix} \dot{q}_4 \\ \dot{q}_5 \end{Bmatrix}$$

$$+ \left(\begin{bmatrix} k_4 & 0 \\ 0 & k_5 \end{bmatrix} - \dot{q}_3^2 \begin{bmatrix} m_w & S_w \\ S_w & -x_w S_w \end{bmatrix} - S_w (\ddot{q}_x + g s_3) \begin{bmatrix} 0 & 0 \\ 0 & 1 \end{bmatrix} \right) \begin{Bmatrix} q_4 \\ q_5 \end{Bmatrix}$$

$$\approx \begin{Bmatrix} Q_4 \\ Q_5 \end{Bmatrix} - \begin{bmatrix} m_w & m_w x_w + S_w \\ S_w & I_w + x_w S_w \end{bmatrix} \begin{Bmatrix} \ddot{q}_y \\ \ddot{q}_3 \end{Bmatrix} - g c_3 \begin{Bmatrix} m_w \\ S_w \end{Bmatrix} + \begin{bmatrix} k_4 & 0 \\ 0 & k_5 \end{bmatrix} \begin{Bmatrix} q_{4_{ref}} \\ q_{5_{ref}} \end{Bmatrix}$$

4.3 Vibration Solutions

Immediately we can see hints of the effects of the pitch rate $\dot{q}_3$ and the acceleration along the body axis $\ddot{q}_x$ as they alter the "effective stiffness" in the flexibility equation. Assuming $\dot{q}_3, \ddot{q}_x$ are constants, figures 7 and 8 show the effects of aircraft pitch rate on the coupled (unbalance not equal zero) airfoil frequencies of translation and rotation for the airfoil slightly aft and slight forward (1 chord) of the aircraft axis.

In the case of the unbalance equal zero, the vibration equations are uncoupled and the translation mode just acts as if the "effective" stiffness is

$$k_{4_{eff}} = k_4 - m_w \dot{q}_3^2 = k_4 \left[1 - \left(\frac{\dot{q}_3}{\omega_4} \right)^2 \right]$$

In the case where the $\dot{q}_3 = 0$ but the unbalance is not zero, the equations remain coupled, but the torsion equation acts with an "effective" stiffness

$$k_5 - S_w \ddot{q}_x = k_5 \left(1 - \frac{\hat{x}_w}{\hat{r}_w^2} \frac{g}{c\omega_5^2} \frac{\ddot{q}_x}{g} \right)$$

Whether the effective torsional stiffness is slightly larger or smaller depends on the sign of the unbalance and whether the aircraft is accelerating or decelerating.

4.4 Aeroelastic (Hypersonic) Equations

We use (for convenience) hypersonic aerodynamics from piston theory[8], to obtain the hypersonic flexibility equations.

$$\begin{bmatrix} 1 & \hat{x}_w \\ \hat{x}_w & \hat{r}_w^2 \end{bmatrix} \begin{Bmatrix} \ddot{q}_3 \\ \ddot{q}_5 \end{Bmatrix} + \left(2 \begin{bmatrix} \lambda_4 s_4 & 0 \\ 0 & \hat{r}_w^2 \lambda_5 s_5 \end{bmatrix} + \frac{4\mu}{M_\infty} \begin{bmatrix} 1 & \hat{r}_1 \\ \hat{r}_1 & \hat{r}_2 \end{bmatrix} \right) \begin{Bmatrix} \dot{q}_4 \\ \dot{q}_5 \end{Bmatrix}$$

$$+ \left(\begin{bmatrix} \lambda_4^2 & 0 \\ 0 & \hat{r}_w^2 \lambda_5^2 \end{bmatrix} - \frac{4\mu}{M_\infty} \begin{bmatrix} 0 & 1 \\ 0 & \hat{r}_1 \end{bmatrix} - \dot{q}_3^2 \begin{bmatrix} 1 & \hat{x}_w \\ \hat{x}_w & -x_w^* \hat{x}_w \end{bmatrix} - \hat{x}_w (\ddot{q}_3 + g s_3) \begin{bmatrix} 0 & 0 \\ 0 & 1 \end{bmatrix} \right) \begin{Bmatrix} q_4 \\ q_5 \end{Bmatrix}$$

$$= \frac{4\mu}{M_\infty} \begin{bmatrix} 1 & -(\hat{x}_w^* + \hat{r}_1) \\ \hat{r}_1 & -(x_w^* \hat{r}_1 + \hat{r}_2) \end{bmatrix} \begin{Bmatrix} a \\ q_3 \end{Bmatrix} - \begin{bmatrix} 1 & \hat{x}_w^* + \hat{x}_w \\ \hat{x}_w & \hat{r}_w^2 + x_w^* \hat{x}_w \end{bmatrix} \begin{Bmatrix} \dot{q}_3^* \\ q_3^* \end{Bmatrix} - g c_3 \begin{Bmatrix} 1 \\ \hat{x}_w \end{Bmatrix} + \begin{bmatrix} \lambda_4^2 & 0 \\ 0 & \hat{r}_w^2 \lambda_5^2 \end{bmatrix} \begin{Bmatrix} q_{4_{ref}} \\ q_{5_{ref}} \end{Bmatrix}$$

where the nondimensional variables are defined by:

lengths
c=chord l=span

positions/coordinates $x_w = cx_w^* \quad \xi_{le} = c\hat{\xi}_{le}$

$q_4 = c\hat{q}_4 \quad q_x = c\hat{q}_x \quad q_y = c\hat{q}_y$

inertias

$S_w = m_w c\hat{x}_w \quad I_w = m_w c^2 \hat{r}_w^2$

stiffnesses

$k_4 = m_w\omega_4^2 \quad k_5 = I_w\omega_5^2 = m_w c^2\hat{r}_w^2\omega_5^2$

dampings

$c_4 = 2m_w\omega_4\varsigma_4 \quad c_5 = 2m_w c^2\hat{r}_w^2\omega_5\varsigma_5$

time and frequency

$$t = \tau\, c/V_\infty \quad \lambda = \frac{c\omega}{V_\infty}$$

time derivative

$$\dot{f}(t) = f'(\tau)\frac{V_\infty}{c} \quad \ddot{f}(t) = f''(\tau)\left(\frac{V_\infty}{c}\right)^2$$

air density and gravity

$$\mu = \frac{\rho_\infty l c^2}{2m_w} \quad \hat{g} = \frac{gc}{V_\infty^2}$$

aerodynamic coefficients

$$Q_4 = N_w = \frac{\rho V_\infty^2 lc}{2} C_{N_w} \quad Q_5 = M_w = \frac{\rho V_\infty^2 lc^2}{2} C_{M_w}$$

Geometry integrals

$$\hat{F}_1 = \hat{\xi}_{le} - 0.5 \quad \hat{F}_2 = \hat{\xi}_{le}^2 - \hat{\xi}_{le} + 0.333...$$

As usual, the damping is modified with the aerodynamic damping and the stiffness is modified with the aerodynamic stiffness. However, the stiffness also has terms that are proportional to the nondimensional pitch rate q_3' and the nondimensional acceleration q_x''.

4.5 Rigid Body Motions as Constant Parameters in the Aeroelastic Equations

Now again consider the pitch rate and the aircraft acceleration as constant parameters. From the differential equation and the vibration solutions, we know that the rigid body pitch rate will decrease the bending frequency (even if only slightly), and that the rigid body acceleration (or deceleration) along the body axis can increase or decrease the torsional frequency. Therefore those rigid body motions also can alter the aircraft speeds for aeroelastic divergence and flutter. For example, under the assumed conditions we can obtain an approximate expression for the μ required for aeroelastic divergence:

$$\mu_{Div} = \frac{M_\infty}{4}\frac{\lambda_5^2\hat{r}_w^2}{\hat{F}_1}\left[1 - \varepsilon^2\frac{\hat{x}_w}{\hat{r}_w}\left(\frac{\hat{r}_w}{\hat{F}_1} - \frac{x_w^*}{\hat{r}_w}\phi^2\right) - \frac{\hat{x}_w}{\hat{r}_w}\left(\frac{\hat{q}_x'' + \hat{g}\cdot\mathfrak{B}}{\lambda_5^2\hat{r}_w}\right)\right]$$

where

$$\varepsilon = q_3'/\lambda_4 \quad \phi = \lambda_4/\lambda_5$$

which shows the importance on the divergence speed of:

a. ε, the ratio of the pitch rate to the uncoupled translation frequency;

b. $\frac{\hat{q}_x''}{\lambda_5^2\hat{r}_w}$, the relationship of the acceleration to the torsional frequency and the radius of gyration

c. ϕ, the ratio of the uncoupled translation and rotation frequencies

d. $\frac{\hat{x}_w}{\hat{r}_w}$, the relationship of the unbalance to the radius of gyration.

We also can use the hypersonic aeroelastic equation to do an eigenvalue calculation (dropping the RHS) to obtain flutter solutions. Figures 9 and 10 show representative effects of pitch rate and acceleration on hypersonic divergence and flutter boundaries.

4.6 Forced Rigid Body Motions in the Aeroelastic Equations

Rather than assume that the rigid body motions are constant parameters, we can assume representative forms for their time dependent motions and then plug them into the flexible equations of motion. We need the terms $\alpha, \dot{q}_3, \dot{q}_3^2, \ddot{q}_x, \ddot{q}_y$ and $\ddot{q}_3$. Following Etkin's[9] notation we can assume the time dependent forms for the oscillatory, damped speed, pitch angle and angle of attack, wherein each expression the terms **a** and **b** are assumed constants:

$$\dot{q}_x = u_0 + E(a_u S_1 + b_u C_1)$$

$$\theta = q_3 = \theta_0 + E(a_\theta S_1 + b_\theta C_1)$$

$$\alpha = \alpha_0 + E(a_\alpha S_1 + b_\alpha C_1)$$

where

$$S_n = \sin n\omega_{rb}t \quad C_n = \cos n\omega_{rb}t \quad E = e^{-\omega_{rb}\varsigma_{rb}t}$$

ω_{rb} = assumed "rigid body" frequency

ς_{rb} = assumed "rigid body" damping

Noting that $\dot{q}_y \approx \dot{q}_x\alpha$ and combining angles where possible, we obtain the "forcing terms" to be included

in the equations of motion. The terms $\dot{q}_3^2, \ddot{q}_x$ appear on the LHS of the equation and influence stability:

$$\ddot{q}_x = \omega_{rb} E\left(a^{*}_{\ddot{q}_x} S_1 + b^{*}_{\ddot{q}_x} C_1\right)$$

$$\dot{q}_3^2 = \tfrac{1}{2}\omega_{rb}^2 E^2\left(K^{*}_{\cdot 2_{q_3}} + a^{*}_{\cdot 2_{q_3}} S_2 + b^{*}_{\cdot 2_{q_3}} C_2\right)$$

The major point is that terms $S_2 = \sin 2\omega_{rb} t$ and $C_2 = \cos 2\omega_{rb} t$ on the LHS introduce behavior like that of Mathieu's equation.

5. The General Case - Three Dimensional Motion of a Flexible Vehicle

5.1 Geometry

We start with an inertial X, Y, Z coordinate system and a noninertial x, y, z system that can accelerate and rotate in the X, Y, Z system (Figure 11). The origin of the x, y, z is located in the inertial system at:

$$X = X_0 = q_1 \quad Y = Y_0 = q_2 \quad Z = Z_0 = q_3$$

The orientation of the x, y, z system is given by the conventional sequence of Euler rotations:

$$\psi = q_4 \quad \theta = q_5 \quad \phi = q_6$$

5.2 Inertial Coordinates

Then inertial coordinates of a general point in x, y, z are:

$$\{X, Y, Z\} = \{q_1, q_2, q_3\} + [\tau]\{x, y, z\}$$

where $[\tau]$, the Euler transformation[9], is the product of three transformations that depend on the Euler angles:

$$[\tau] = [\tau_4][\tau_5][\tau_6]$$

$$[\tau_4] = \begin{bmatrix} c_4 & -s_4 & 0 \\ s_4 & c_4 & 0 \\ 0 & 0 & 1 \end{bmatrix} \quad [\tau_5] = \begin{bmatrix} c_5 & 0 & s_5 \\ 0 & 1 & 0 \\ -s_5 & 0 & c_5 \end{bmatrix} \quad [\tau_6] = \begin{bmatrix} 1 & 0 & 0 \\ 0 & c_6 & -s_6 \\ 0 & s_6 & c_6 \end{bmatrix}$$

$$s_i = \sin q_i \quad c = \cos q_i$$

We also write the "local" coordinates in terms of additional generalized coordinates $q_7, q_8 \ldots q_n$:

$$\{x, y, z\} = \sum_{i=7}^{n} \{x_i, y_i, z_i\} q_i(t)$$

to obtain the inertial coordinates in terms of the generalized coordinates:

$$\{X, Y, Z\} = \{q_1, q_2, q_3\} + [\tau] \sum_{i=7}^{n} \{x_i, y_i, z_i\} q_i(t)$$

The kinetic energy, in terms of the inertial coordinates is a lengthy expression which shows why it can be useful to use Olsen's[6] form of the equations of motion (which doesn't require the kinetic energy), rather than Whittaker's[5] form which does require the kinetic energy.

5.3. Overcoming the Tedious Aspects - Quasi Coordinates

Again, we could use Lagrange's equations on the Lagrangian in inertial coordinates to obtain the equations of motion for the flexible system. We would be accurately accounting for all of the inertia couplings that arise from the fact that the noninertial x, y, z system is accelerating and rotating in the inertial X, Y, Z system. We could solve the problem in terms of the inertial translations q_1, q_2, q_3 and the Euler angles q_4, q_5, q_6 and then transform the results to the translations along the body axes q_x, q_y, q_z and the instantaneous angular velocities $\omega_x, \omega_y, \omega_z$, using the transformations:

$$\{q_x, q_y, q_z\} = [\tau]^T \{q_1, q_2, q_3\}$$

$$\{\omega_x, \omega_y, \omega_z\} = [\alpha]\{\dot{q}_4, \dot{q}_5, \dot{q}_6\}$$

where

$$[\alpha] = \begin{bmatrix} -s_5 & 0 & 1 \\ c_5 s_6 & c_6 & 0 \\ c_5 c_6 & -s_6 & 0 \end{bmatrix}$$

The approach is correct in principal. However, it works easiest for special cases like rotation about one axis (where the time derivative of the appropriate Euler angle is indeed the angular velocity). However, it suffers from two shortcomings in the general case of three dimensional motions.

First, the generalized coordinates q_1, q_2, q_3 are the translations in the directions of the inertial coordinates. We would like to replace them with the translations in directions of the noninertial, body - axis coordinates q_x, q_y, q_z.

Second, the generalized coordinates q_4, q_5, q_5 are the Euler angles. Their time derivatives $\dot{q}_4, \dot{q}_5, \dot{q}_5$ may not be the physical angular velocities of the x, y, z system for general motions. We would like to replace them with the physical angular velocities of the noninertial, body - axis coordinates, $\omega_x, \omega_y, \omega_z$.

However, a much more elegant and simple method is available, the method of quasi - coordinates due to Hamel[10] and Boltzmann[11]. The term "quasi - coordinates" refers to the fact that we cannot (in the general case of three dimensional motions) directly integrate the angular velocities to get the generalized coordinates. Actually all we are doing is performing the transformations before we apply Lagrange's equations to obtain the differential equations, rather than after we get them.

Whittaker[5] and Meirovitch[12] explain the method of quasi - coordinates for the special case of rotational motions. Several others, among them Nayfeh and Mook[13], give applications.

The basic idea is that we want to write Lagrange's equations in a form that treats directly the body axis translations q_x, q_y, q_z and the true angular velocities $\omega_x, \omega_y, \omega_z$. We start with the usual form of Lagrange's equations in terms of the original, independent generalized coordinates $q_1, q_2 \ldots q_n$ and their time derivatives $\dot{q}_1, \dot{q}_2 \ldots \dot{q}_n$:

$$\frac{d}{dt}\left(\frac{\partial L}{\partial \dot{q}_i}\right) - \left(\frac{\partial L}{\partial q_i}\right) = Q_i$$

The Lagrangian can be written in the usual form in the original inertial coordinates:

$$L = L\begin{pmatrix} q_1, q_2, q_3, q_4, q_5, q_6, q_7, \ldots q_n; \\ \dot{q}_1, \dot{q}_2, \dot{q}_3, \dot{q}_4, \dot{q}_5, \dot{q}_6, \dot{q}_7, \ldots \dot{q}_n \end{pmatrix}$$

If we note that:

$$\{\dot{q}_4, \dot{q}_5, \dot{q}_6\} = [\beta]\{\omega_x, \omega_y, \omega_z\}$$

where

$$[\beta] = [\alpha]^{-1} = \begin{bmatrix} 0 & c_5^{-1} s_6 & c_5^{-1} c_6 \\ 0 & c_6 & -s_6 \\ 1 & t_5 s_6 & t_5 c_6 \end{bmatrix}$$

we can obtain the equivalent form of the Lagrangian in the quasi - coordinates:

$$\tilde{L} = \tilde{L}\begin{pmatrix} q_x, q_y, q_z, q_4, q_5, q_6, q_7, \ldots q_n; \\ \dot{q}_x, \dot{q}_y, \dot{q}_z, \omega_x, \omega_y, \omega_z, \dot{q}_7, \ldots \dot{q}_n \end{pmatrix}$$

Then, following Whittaker[5] we can obtain the equations for:

Translation DOFs:

$$\boxed{\frac{d}{dt}\begin{Bmatrix} \frac{\partial \tilde{L}}{\partial \dot{q}_x} \\ \frac{\partial \tilde{L}}{\partial \dot{q}_y} \\ \frac{\partial \tilde{L}}{\partial \dot{q}_z} \end{Bmatrix} - \begin{Bmatrix} \frac{\partial \tilde{L}}{\partial q_x} \\ \frac{\partial \tilde{L}}{\partial q_y} \\ \frac{\partial \tilde{L}}{\partial q_z} \end{Bmatrix} + [\Omega]\begin{Bmatrix} \frac{\partial \tilde{L}}{\partial \dot{q}_x} \\ \frac{\partial \tilde{L}}{\partial \dot{q}_y} \\ \frac{\partial \tilde{L}}{\partial \dot{q}_z} \end{Bmatrix} = [\tau]^T \begin{Bmatrix} Q_1 \\ Q_2 \\ Q_3 \end{Bmatrix}}$$

Rotation DOFs:

$$\boxed{\frac{d}{dt}\begin{Bmatrix} \frac{\partial \tilde{L}}{\partial \omega_x} \\ \frac{\partial \tilde{L}}{\partial \omega_y} \\ \frac{\partial \tilde{L}}{\partial \omega_z} \end{Bmatrix} - [\beta]^T \begin{Bmatrix} \frac{\partial \tilde{L}}{\partial q_4} \\ \frac{\partial \tilde{L}}{\partial q_5} \\ \frac{\partial \tilde{L}}{\partial q_6} \end{Bmatrix} + [\Omega]\begin{Bmatrix} \frac{\partial \tilde{L}}{\partial \omega_x} \\ \frac{\partial \tilde{L}}{\partial \omega_y} \\ \frac{\partial \tilde{L}}{\partial \omega_z} \end{Bmatrix} = [\beta]^T \begin{Bmatrix} Q_4 \\ Q_5 \\ Q_6 \end{Bmatrix}}$$

Flexible DOFs remain the same (except that we must use the modified Lagrangian $\tilde{L}$)

$$\boxed{\frac{d}{dt}\frac{\partial \tilde{L}}{\partial \dot{q}_i} - \frac{\partial \tilde{L}}{\partial q_i} = Q_i \quad for\ i \geq 7}$$

where:

$$[\Omega] = \begin{bmatrix} 0 & -\omega_z & \omega_y \\ \omega_z & 0 & -\omega_x \\ -\omega_y & \omega_x & 0 \end{bmatrix}$$

These are the equations of motion in terms of quasi - coordinates. They are the fundamental advance which allows us to formulate a unified set of equations that can be used without simplification for the aerodynamics, structures and stability and control of flexible aircraft - they allow us to place the aeroelastic problem into a coordinate system and notation that is used in flight mechanics and stability and control.

5.4 Energies - Noninertial Body - Axis Coordinates

The kinetic energy in terms of the body - axis variables is:

$$\begin{aligned} KE = & \tfrac{1}{2} M\left(\dot{q}_x^2 + \dot{q}_y^2 + \dot{q}_z^2\right) \\ & + S_x\left(\dot{q}_y \omega_z - \dot{q}_z \omega_y\right) + S_y\left(\dot{q}_z \omega_x - \dot{q}_x \omega_z\right) + S_z\left(\dot{q}_x \omega_y - \dot{q}_y \omega_x\right) \\ & + \tfrac{1}{2} I_{xx}\left(\omega_y^2 + \omega_z^2\right) - I_{xy}\omega_x\omega_y - I_{xz}\omega_x\omega_z \\ & + \tfrac{1}{2} I_{yy}\left(\omega_x^2 + \omega_z^2\right) - I_{yz}\omega_y\omega_z + \tfrac{1}{2} I_{zz}\left(\omega_x^2 + \omega_y^2\right) \\ & + S_{\dot{x}}\dot{q}_x + S_{\dot{y}}\dot{q}_y + S_{\dot{z}}\dot{q}_z \\ & + \left(I_{x\dot{y}} - I_{\dot{x}y}\right)\omega_z + \left(I_{y\dot{z}} - I_{\dot{y}z}\right)\omega_x + \left(I_{z\dot{x}} - I_{\dot{z}x}\right)\omega_y \\ & + \tfrac{1}{2}\left(I_{\dot{x}\dot{x}} + I_{\dot{y}\dot{y}} + I_{\dot{z}\dot{z}}\right) \end{aligned}$$

where typical inertia integrals are:

$$M = \int_{body} dm$$

$$S_x = \int x dm = \sum_i \left(\int x_i dm\right) q_i = \sum_i S_{x_i} q_i$$

$$S_{\dot{x}} = \int \dot{x} dm = \sum_i \left(\int x_i dm\right) \dot{q}_i = \sum_i S_{x_i} \dot{q}_i$$

$$I_{xy} = \int_{body} xy dm = \sum_{i,j} \left(\int x_i y_j dm\right) q_i q_j = \sum_{i,j} I_{x_i y_j} q_i q_j$$

$$I_{\dot{x}y} = \int_{body} \dot{x} y dm = \sum_{i,j} \left(\int x_i y_j dm\right) \dot{q}_i q_j = \sum_{i,j} I_{x_i y_j} \dot{q}_i q_j$$

The potential energy due to gravity will come from our gravitational model. In the case of a "flat earth":

$$V_g = -g \int_{mass} \left(Z - Z_{ref}\right) dm$$

$$= -g\left(q_3 - Z_{ref}\right) m - g \begin{bmatrix} 0 & 0 & 1 \end{bmatrix} [\tau] \sum_{i=7}^{n} \begin{Bmatrix} S_{x_i} \\ S_{y_i} \\ S_{z_i} \end{Bmatrix} q_i$$

We expect the potential energy due to flexibility to be of the form

$$V_f = \frac{1}{2} \sum_{i=7}^{n} \sum_{j=7}^{n} V_{b_{ij}} q_i q_j$$

Or perhaps a more general expression for larger deflections

$$V_f = \frac{1}{2} \sum_{i=7}^{n} \sum_{j=7}^{n} V_{b_{ij}} q_i q_j + \frac{1}{2} \sum_{i=7}^{n} \sum_{j=7}^{n} \sum_{k=7}^{n} V_{b_{ijk}} q_i q_j q_k$$

The author has performed those operations, and the complete set of differential equations is available (but too lengthy to present here).

5.6 Simplification to the "Flat" Airplane

If we specialize the general body to consider an essentially "flat" surface in the xy plane (Right handed xyz coordinate system attached to the body), Figure 12, and make the usual definitions

$\dot{q}_x = U$ velocity along the x axis

$\dot{q}_x = V$ velocity along the y axis

$\dot{q}_x = W$ velocity along the z axis

$\omega_x = P$ angular velocity about the x axis

$\omega_y = Q$ angular velocity about the y axis

$\omega_z = R$ angular velocity about the z axis

$$z(x,y,t) = \sum_i z_i(x,y) q_i(t)$$

The equations of motion become

Translation

$$M \begin{Bmatrix} \dot{U} \\ \dot{V} \\ \dot{W} \end{Bmatrix} + \begin{bmatrix} 0 & 0 & -S_y \\ 0 & 0 & S_x \\ S_y & -S_x & 0 \end{bmatrix} \begin{Bmatrix} \dot{P} \\ \dot{Q} \\ \dot{R} \end{Bmatrix} + \begin{Bmatrix} WQ - VR \\ UR - WP \\ VP - UQ \end{Bmatrix} M + \begin{bmatrix} -\left(Q^2 + R^2\right) & PQ & \\ PQ & -\left(P^2 + R^2\right) & \\ PR & QR & \end{bmatrix} \begin{Bmatrix} S_x \\ S_y \end{Bmatrix}$$

$$+ g \begin{Bmatrix} s_5 \\ -c_5 s_6 \\ -c_5 c_6 \end{Bmatrix} M + \sum_i \left(\begin{Bmatrix} 0 \\ 0 \\ 1 \end{Bmatrix} \ddot{q}_i + 2 \begin{Bmatrix} Q \\ -P \\ 0 \end{Bmatrix} \dot{q}_i + q_i \begin{Bmatrix} \left(\dot{Q} + PR\right) \\ \left(-\dot{P} - QR\right) \\ -\left(P^2 + Q^2\right) \end{Bmatrix} \right) S_{z_i} = \begin{Bmatrix} F_x \\ F_y \\ F_z \end{Bmatrix}$$

Rotation

$$\begin{bmatrix} I_{xx} & -I_{xy} & 0 \\ -I_{xy} & I_{yy} & 0 \\ 0 & 0 & I_{zz} + I_{yy} \end{bmatrix} \begin{Bmatrix} \dot{P} \\ \dot{Q} \\ \dot{R} \end{Bmatrix} + \begin{bmatrix} VQ + WR & -UQ & \\ VP & UP + WR & \\ -WP & -WQ & \end{bmatrix} \begin{Bmatrix} I_{xx} \\ I_{yy} \end{Bmatrix} + \begin{bmatrix} 0 & -c_5 c_6 & \\ c_5 c_6 & 0 & \\ -c_5 s_6 & -s_5 & \end{bmatrix} \begin{Bmatrix} S_x \\ S_y \end{Bmatrix}$$

$$+ \sum_i \left(\begin{bmatrix} 0 & 0 & 1 \\ 0 & -1 & 0 \\ 0 & 0 & 0 \end{bmatrix} \ddot{q}_i + \begin{bmatrix} -V & 0 & 0 \\ U & 0 & 0 \\ 0 & -2P & -2Q \end{bmatrix} \dot{q}_i + \begin{bmatrix} -\left(V + UR\right) & -\left(R + PQ\right) & \left(R^2 - Q^2\right) \\ \left(U - VR\right) & \left(P^2 - R^2\right) & -\left(R - PQ\right) \\ \left(UP + VQ\right) & -\left(P - QR\right) & -\left(Q + PR\right) \end{bmatrix} q_i \right) \begin{Bmatrix} S_x \\ S_z \\ S_y \end{Bmatrix}$$

$$+ g \begin{bmatrix} c_5 c_6 & 0 & 0 \\ s_5 & 0 & 0 \\ 0 & 0 & 0 \end{bmatrix} \sum_i \begin{Bmatrix} S_x \\ S_z \\ S_y \end{Bmatrix} q_i + \sum_{i,j} \begin{Bmatrix} 2\dot{q}_j P + q_j \left(\dot{P} - QR\right) \\ 2\dot{q}_j Q + q_j \left(\dot{Q} + PR\right) \\ 0 \end{Bmatrix} I_{z_i z_j} = \begin{Bmatrix} M_x \\ M_y \\ M_z \end{Bmatrix}$$

Flexible

$$\left(\dot{W} + VP - UQ\right) S_{z_i} - \left(\dot{Q} - PR\right) S_{xz_i} + \left(\dot{P} + QR\right) S_{y_i}$$

$$+ \sum_j \left[\ddot{q}_j - \left(P^2 + Q^2\right) q_j \right] I_{z_i z_j} + \frac{\partial V_e}{\partial q_i} - g c_5 c_6 S_{z_i} = Q_i$$

The equations above are the equations to solve for the static and dynamic response and stability of a flexible, "flat" aircraft under steady state flight or in accelerations and maneuvers. They are nonlinear and mutually couple the overall rigid body motions with the flexible deflections. They can be used for analyses of aircraft performance, stability and control, flight loads, control effectiveness and aeroelastic divergence and flutter. Of course they are more complicated than the conventional nonlinear equations for rigid body motions or the linear equations for aeroelastic response (which are coupled to the rigid body equations only through the aerodynamics).

5.7 Perfect Masses and Modes

In the special case of

a. Mass symmetry about the y axis

b. Origin at the center of mass
c. Perfectly orthogonal free - free modes

the equations of motion simplify further to the usual rigid body equations and the modified flexible equations:

Translation

$$\begin{Bmatrix} \dot{U} \\ \dot{V} \\ \dot{W} \end{Bmatrix} + \begin{Bmatrix} WQ - VR \\ UR - WP \\ VP - UQ \end{Bmatrix} + g \begin{Bmatrix} s_5 \\ -c_5 s_6 \\ -c_5 c_6 \end{Bmatrix} = \frac{1}{M} \begin{Bmatrix} F_x \\ F_y \\ F_z \end{Bmatrix}$$

Rotation

$$\begin{Bmatrix} \dot{P} \\ \dot{Q} \\ \dot{R} \end{Bmatrix} + \begin{Bmatrix} QR \\ -PR \\ \frac{I_{xx} - I_{yy}}{I_{xx} + I_{yy}} PQ \end{Bmatrix} = \begin{Bmatrix} M_x / I_{yy} \\ M_y / I_{xx} \\ M_z / (I_{xx} + I_{yy}) \end{Bmatrix}$$

Flexible

$$\left\{ \ddot{q}_i + \left[\omega_i^2 - \left(P^2 + Q^2 \right) \right] q_i \right\} I_{z_i z_i} = Q_i$$

where

ω_i = natural frequency of the perfect ith mode

If we assume, for the moment, that the angular velocities **P** and **Q** are constant, then one approximation would be to treat the flexible equations as if the effective structural frequency for any mode is just replaced by

$$\omega_i^2 \rightarrow \omega_i^2 - \left(P^2 + Q^2 \right)$$

On the other hand, since **P** and **Q** will be functions of time, the actual behavior will be more like the behavior of solutions to Mathieu's equations.

Many recent developments numerically integrate the linearized equations of motion with nonlinear aerodynamics on the RHS. It seems that, once the analyst has committed to numerical integration of the equations of motion, there is very little additional labor (or computational time) to use the more comprehensive equations of motion above.

6. Summary, Conclusions

1. Whittaker's and Olsen's expressions can be useful to formulate the equations of motion for complicated geometries with many degrees of freedom.

2. The "sprung pendulum" shows that a rigid body motion with constant angular velocity can reduce the "effective" natural frequencies. Using the resemblance to Mathieu's equation, we have seen that there is a coupling mechanism between the rigid body and flexible motions, even in the absence of aerodynamics. It appears that if a flexible frequency is up to 1.3 - 1.5 times a rigid body frequency, then those coupling effects should be considered. In some cases ("slender" aircraft) the natural frequencies may already be in those ranges. In other cases (the X - 29) the aerodynamic forces drive some of the flexible frequencies down toward the rigid body frequencies.

3. The airfoil on an accelerating/rotating fuselage shows that the effective bending stiffness is reduced by a constant pitch rate. It also shows that torsional stiffness is increased or decreased by constant acceleration/deceleration, depending on the sign of the unbalance. The results modify the divergence and flutter speeds. If we impose the rigid body motions as forced, sinusoidal, damped motions - then terms appear in the differential equations which can produce additional instabilities, such as in Mathieu's equation.

4. In the case of general motion of a flexible body, the combination of energy methods and quasi - coordinates can produce a practical set of equations that govern the aerodynamics, flight mechanics and structures problems of flexible aircraft. They allow the determination of the effects of structural flexibility on aircraft performance, stability and air loads and the effects of the "rigid body" motions on aeroelastic control - effectiveness, divergence and flutter.

5. For the special case of the "flat airplane" with perfect mass distribution and perfect modes, a simple preliminary estimate of the effects of rigid body motions on flexible motions would be to replace all of the structural frequencies by:

$$\omega_i^2 \rightarrow \omega_i^2 - \left(P^2 + Q^2 \right)$$

7. References

1. A. R. Dusto, et al; "A Method for Predicting the Stability Characteristics of Control Configured Figures"; AFFDL TR 74 - 91; 1974.

2. E. C. Bekir, et al; "Modeling Flexible Aircraft for Flight Control Design"; AFWAL TR 88 - 3089; 1989.

3. M. R Waszak and D. K. Schmidt; "Flight Dynamics of Aeroelastic Vehicles", AIAA Journal of Aircraft, Volume 25, Number 6, June 1988.

4. R. L. Bisplinghoff, H. Ashley and R. L. Halfman; Aeroelasticity; Addison - Wesley; Reading, Mass; 1955; (Section 3 - 8. Energy Methods).

5. E. T. Whittaker; A Treatise on the Analytical Dynamics of Particles and Rigid Bodies; Dover Publications; New York; 1944; (Section 28. The

Explicit Form of Lagrange's equations; Section 30. The Lagrange's equations for Quasi - Coordinates).

6. J. J. Olsen; "Coupled Flight Mechanics and Aeroelasticity - Some Effects of Aircraft Maneuvers on Aeroelastic Divergence and Flutter"; 19th ICAS Congress; Los Angeles; 1994.

7. N. W. McLachlan; Theory and Application of Mathieu Functions; Oxford Press; London; 1947.

8. H. Ashley and G. Zartarian; "Piston Theory, A New Aerofynamic Tool for the Aeroelastician"; J. Aero. Sc.; Vol 23; No. 6; June 1958.

9. B. Etkin; Dynamics of Flight, Stability and Control; Wiley; New York; 1959 (Section 4.5. Orientation and Position of the Airplane).

10. A. Hamel; Zeitschrift fur Mathematiks und Physiks; 1904.

11. R. Boltzmann; Sitzungsberichte; Wien; 1902

12. L. Meirovitch; Methods of Analytical Dynamics; McGraw - Hill; New York; 1970; (Section 4.12. The Lagrange's equations for Quasi - Coordinates).

13. A. H. Nayfeh and D. T. Mook; Nonlinear Oscillations; Wiley; New York; 1979; (Section 6.1.3. A Restricted Ship Motion).

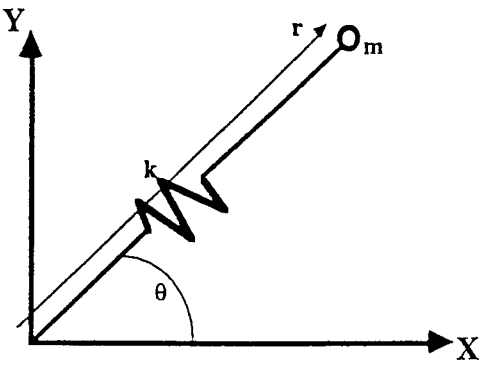

Figure 1. The Sprung Pendulum

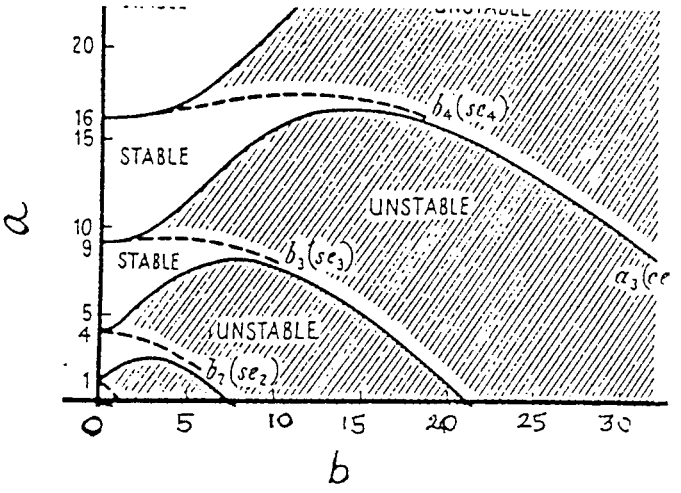

Figure 2. Regions of Stability/Instability for Periodic Solutions of Mathieu's Equation

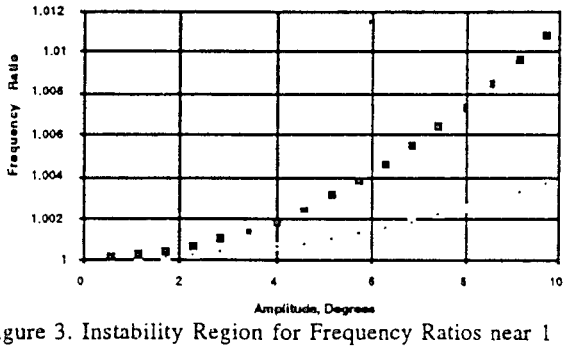

Figure 3. Instability Region for Frequency Ratios near 1

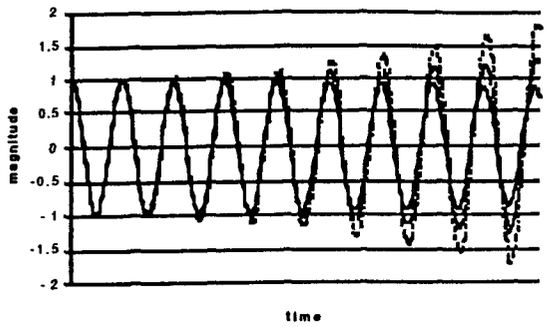

Figure 4. Time Histories for Frequency ratio 1.1

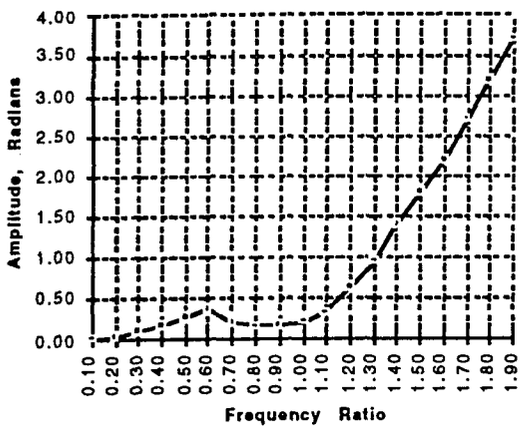

Figure 5. Smallest value of Amplitude to Become Unstable

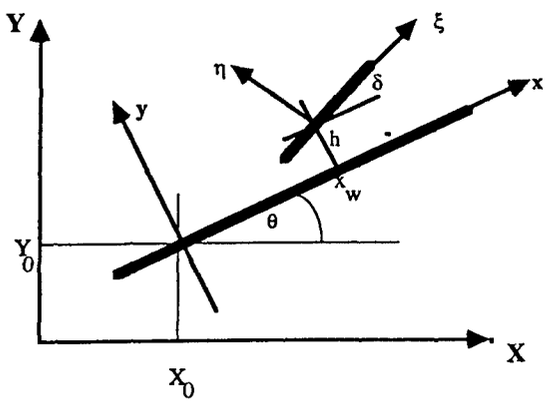

Figure 6. Airfoil on an Accelerating, Rotating Fuselage

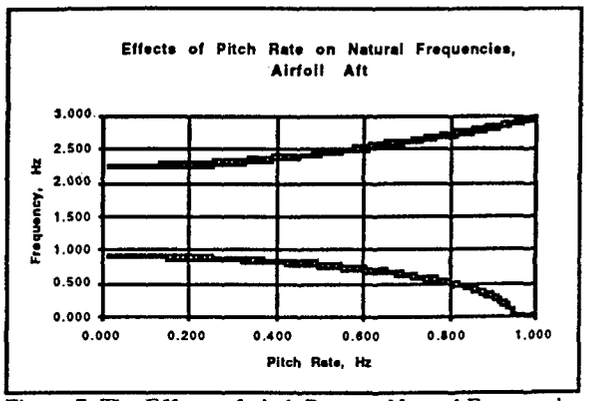

Figure 7. The Effects of pitch Rate on Natural Frequencies, $x_w^* = -1.0$

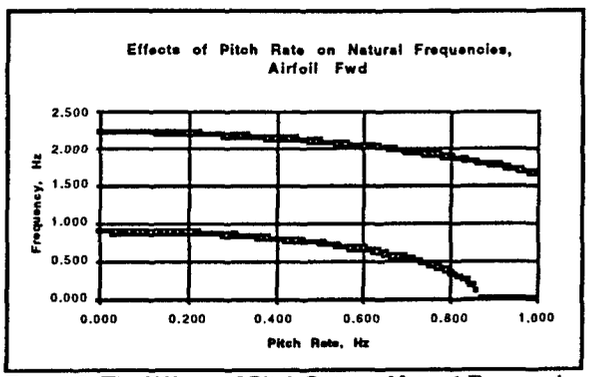

Figure 8. The Effects of Pitch Rate on Natural Frequencies,

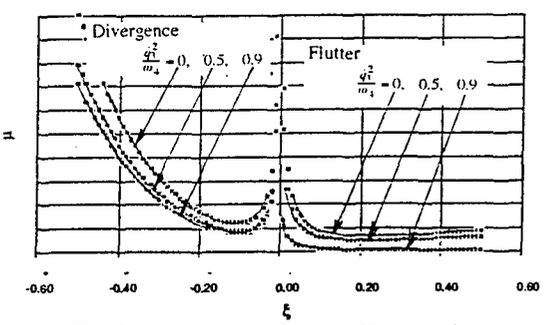

Figure 9. The Effects of Pitch Rate on Hypersonic Divergence and Flutter

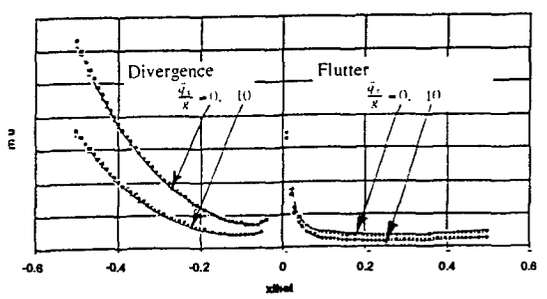

Figure 10. The Effects of Acceleration on Hypersonic Divergence and Flutter

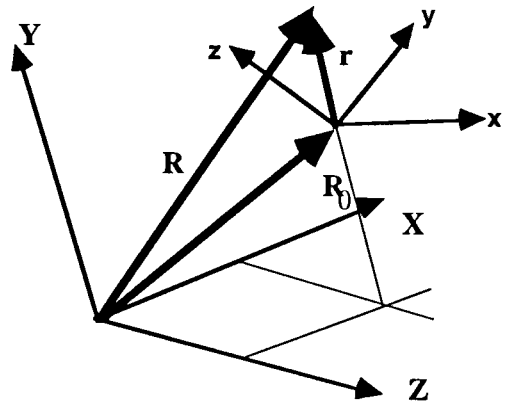

Figure 11. General Motion of a Flexible Vehicle

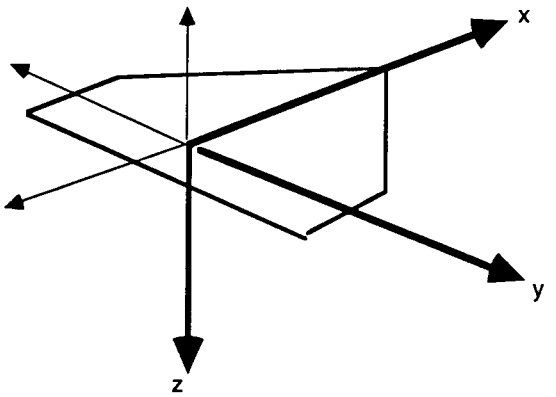

Figure 12. The "Flat"Airplane

An Integrated Design Procedure for Aircraft Structure Including the Influence of Flight Control System on Aircraft Flutter

W. Luber, J. Becker

Daimler Benz Aerospace AG
Military Aircraft MT24
D-81663 Munich, Germany
Tel.: +49-89-607-26996
Fax: +49-89-607-28707
email: Wolfgang.Luber@m.dasa.de

Abstract

Modern fighter aircraft are using high sophisticated power control and automatic flight control systems, which basically are designed to maneuver the airplane and to provide sufficient damping for the rigid body modes. Since the sensors are attached to the flexible structure, motions of the elastic aircraft will be measured and may influence the control system. In order to avoid instabilities it is necessary to predict the response of the aircraft with the control system and to correlate with flight test data. An analytical approach for the complete system including flight mechanics and unsteady aerodynamic forces is presented. The elastic structure is described by a set of normal modes which have been updated by results of ground resonance survey tests. Flutter calculations in open and closed loop on different flight conditions as well as incidence variations are demonstrated as common flutter plots. For the flutter analysis a set of notch filter is required, which should be determined in an integrated design step.

1. Introduction

The Eurofighter EF2000 will be developed and produced within a four national cooperation. Such a multi national cooperation requires special agreements of system design responsibilities (SDR). The design and development of a component is done by the partner company (PC) who manufactures this component. The overall design activities are shared between partners with SDR for e.g. flutter with and without FCS and with and without carrying stores.

The structural design of an aircraft evolves through several stages where the conflicting requirements of weight, stiffness, flight control system, flutter, cost, serviceability, etc. are matched to the required degree.

During this period a number of structural models might be created to assist in the design and development process. Each model would use the best available information on structural configuration and sizes, aerodynamic loads, the distribution of mass, flight parameters etc.

Once the design has stabilized a final model of the complete aircraft structure is created to verify structural integrity and the flexural characteristics.

The final model for the development phase the checkstress model was to embody the 'best possible representation of the actual aircraft'. The procedure of assembling the components to the dynamic model will be described.

Figure 1 shows the two side view of the aircraft.

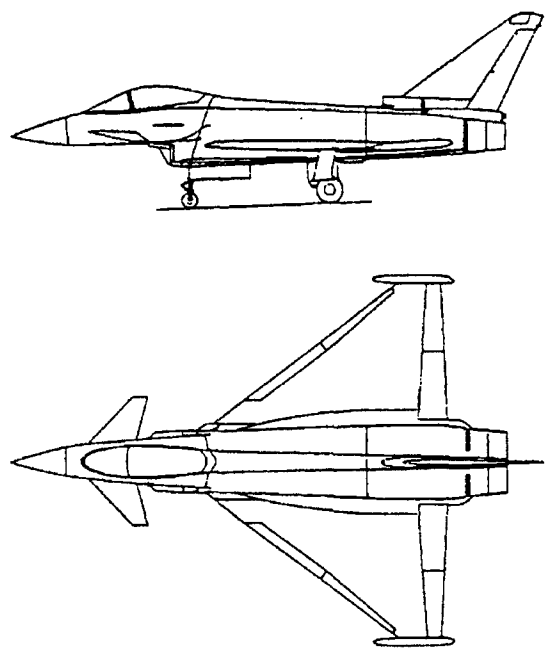

Figure 1: Two side view of the Aircraft

Paper presented at the RTO AVT Specialists' Meeting on "Structural Aspects of Flexible Aircraft Control", held in Ottawa, Canada, 18-20 October 1999, and published in RTO MP-36.

Due to the fly by wire system the advanced digital flight control system for a modern military aircraft is strongly influenced by aeroservoelastic effects. The flexible aircraft behavior especially for artificial unstable aircraft configurations with outer wing missiles, tip pods and heavy under wing stores and tanks has significant effects on the flight control system. The signals of the Aircraft Motion Sensor Unit (AMSU) - the gyro platform - contain besides the necessary information of rigid aircraft rates and accelerations also flexible aircraft rates and accelerations in the frequencies of the aircraft elastic modes. The 'flexible' aircraft rates and accelerations measured by the inertia measuring unit (IMU) are passed through the flight control system control paths, they are multiplied by the FCS gains and FCS filters and inserted in the control surface actuator input which then drives the controls in the frequencies of the elastic modes of the aircraft. The flexible aircraft is excited by the high frequency control deflections and might also experience aeroservoelastic instabilities i.e. flutter or limit cycle oscillations may occur, and dynamic load and fatigue load problems can arise. The FCS design therefore has to minimize all structural coupling effects through the available means like optimum sensor positioning, notch filtering and additional active control. This paper describes the aeroservoelastic work and problem areas which must be considered during the clearance work for an artificial unstable aircraft. Many of the design and clearance aspects have been published in previous papers, Ref.'s [1,4,8-11,15,16]. For integrated design of notch and phase advanced filters see Ref.[2] ,for unsteady aerodynamic see Ref. [8,12-14] and for testing and qualification Ref.[3,5-7]

2. Aeroservoelastic design requirements, Philosophy to get certification

2.1 Design Requirements

2.1.1 Flutter Requirements

Analyses, wind tunnel tests, and airplane ground and flight tests up to design limit speeds shall demonstrate that flutter, buzz, divergence and other related aeroelastic or aeroservoelastic instability boundaries occur outside the 1.15 times design limit speed envelope.
Figure 2 summarizes the requirements and evidence required for qualification and certification of a typical military aircraft.

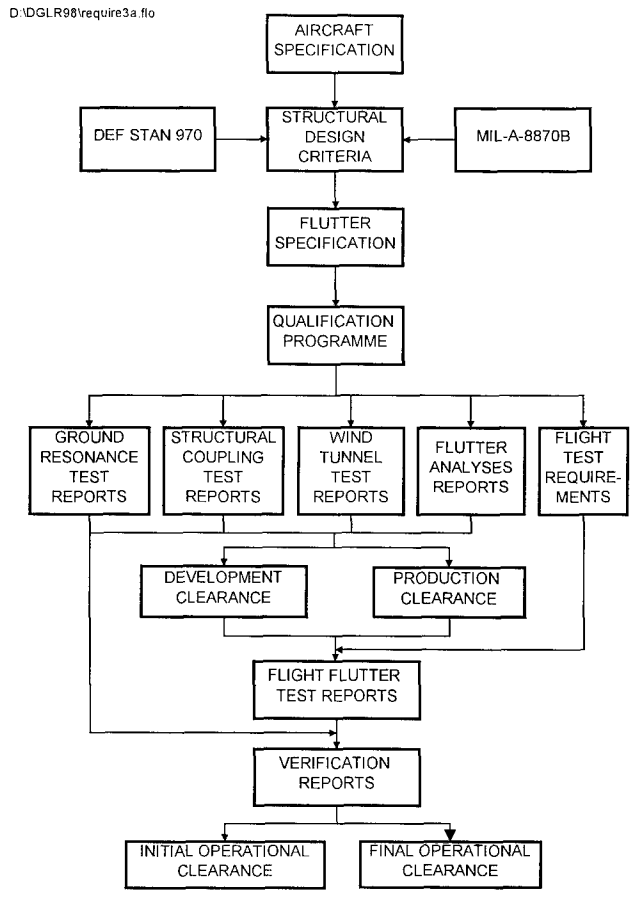

Figure 2: Requirement for Qualification

The flutter requirements are mainly derived from the U.S.–MIL-SPEC and the British DEF-STAN documents.
From these documents specific requirements for airspeed margins, aeroelastic and aeroservoelastic stability requirements can be derived.

Therefore the aircraft shall meet the following stability design requirements for both normal and emergency conditions.

- Margin:
  Fifteen percent equivalent airspeed margin on the applicable design limit speed envelope, both at constant altitude and constant Mach number.

- Clean Aircraft Damping:
  The damping coefficient g (structural damping) for any critical flutter mode or for any significant dynamic response mode shall be at least three percent for all altitudes on flight speeds up to design limit speed.

- Aircraft with Stores Damping:
  Critical flutter modes whose zero airspeed damping is less than 3% 'g', the damping coefficient 'g' need only be greater than the zero airspeed damping coefficient in that mode.

The full requirements of the specification are subjected to the MIL-A-8870B, Airplane Strength and Rigidity Vibration, Flutter, and Divergence.

For the first flight standard the DEF-STAN was adapted:
The clean aircraft shall be allowed to fly up to half calculated flutter speed for any critical flutter mode.
The aircraft with stores shall be allowed to fly up to the minimum of half calculated flutter airspeed and half required airspeed.
It should be mentioned that the calculated flutter airspeed includes validation of the theoretical model by ground testing. After first flight the expansion of the flight envelope is based on theoretical analysis with flight test results.

2.1.2 Aeroservoelastic Stability Requirements

Interaction of the control system with aircraft elastic modes shall be controlled to preclude any structural coupling. Structural coupling is a phenomenon associated with the introduction of the closed loop control system into flexible aircraft structure.
The equivalent airspeed margin and damping requirements shall be met with the FCS open and closed loop. In addition, the stability margin of the flutter system shall respect the structural frequency stability margins in the flight control system requirements.

The aeroservoelastic design requirements are primarily stability requirements for all flight control rigid/flexible aircraft modes. The stability is achieved by the introduction of notch filters. The open loop frequency response requirements are demonstrated in Figure 3, which describes gain and phase margins for production aircraft for configurations which are flight tested on prototypes including structural coupling flight tests. In contrary to the production criteria a more conservative clearance requirement was established for the prototype aircraft, Figure 4. For the initial phases of the prototype program the decision was made to a 9 dB stability margin requirement for all structural mode frequencies. The first frequency of the low flexible modes are phase stabilized and higher frequency flexible modes are gain stabilized.

The Military Specification MIL-F-9490 D for FCS requirements shall be meet, the design boundaries, which include rigid aircraft motion, structural elastic modes and system modes.

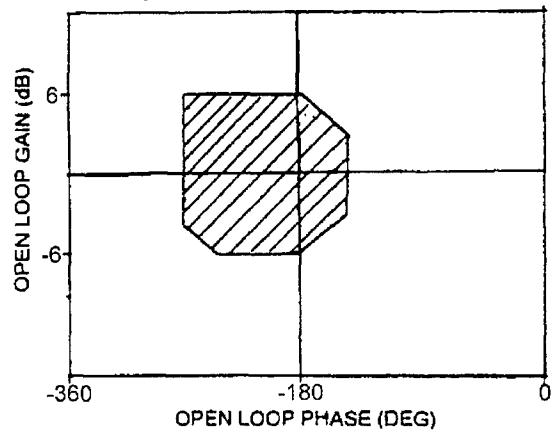

Figure 3: Production Stability Margin Criteria for Open Loop Frequency Response Function

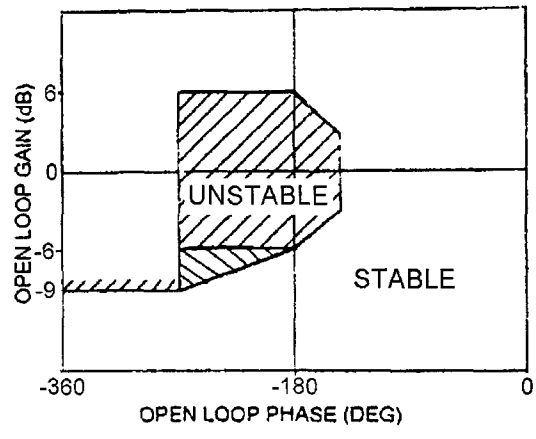

Figure 4: Prototype Stability Margin Criteria for Open Loop Frequency Response Function

2.1.3 Vibration/Dynamic Loads Requirements

In addition to the stability requirements for the structural coupling unacceptable vibration levels must be avoided including noise levels. The vibration levels induced by structural coupling might create high fatigue loads to actuators and to aircraft structure. The notch filters together with noise filters have to be designed to meet the specific vibration requirements.

2.1.4 Backlash Requirements

Aircraft backlash ground tests are required on all control surfaces to meet the flutter MIL-SPEC Requirements:

Flaperons:	Outboard	0.0022 Radians (pitch)
	Inboard	0.0200 Radians (pitch)
Foreplane:	0.0006 Radians (Pitch)	
Rudder:	0.0022 Radians (yaw)	

For normal operation and during steady flight, the flight control system induced aircraft residual oscillations at the crew station shall not exceed 0.04 g's vertical acceleration. For a typical unstable aircraft configuration the FCS backlash requirement for the flaperon and foreplane is 0.0006 Radians.

2.2 Design philosophy for aeroservoelasticity

Aeroservoelasticity or also called FCS-structural coupling is a phenomenon associated with the introduction of a closed loop flight control system into a flexible airframe. The system might be provided to enhance the natural stability of the aircraft, or, to provide artificial stability to a configuration which has been designed to be unstable to achieve the aerodynamic system specification.
For solution of the structural coupling problem, attenuation of the high frequency oscillatory signal introduced into the flight control system by the flexible aircraft motion should be provided and notched, such that the closed loop is stable and degradation of the performance of the flight control system, or damage of the aircraft structure, is avoided.
Therefore an integrated design shall include the derivation of FCS gains, phase advance filters and notch filters to minimize structural coupling in one combined optimization process. The FCS shall be designed to cover the full rigid, flexible aircraft frequency range with respect to aircraft rigid mode and structural mode coupling stability requirements for each control system individual loop for on ground and in flight. The structural coupling influences shall be minimized by FCS notch filters. The FCS shall be designed to be as robust as possible with respect to all possible aircraft configurations and configuration changes, (missiles on, off, tanks on and off etc.). That includes that all structural coupling changes with configuration should be covered by a constant set of notch filters to avoid system complexity due to configuration switches for different sets of notch filters. In addition any scheduling of notch filters with flight conditions should be avoided in a wide range of the flight envelope but not excluded for critical structural coupling areas. In order to avoid problems in the notch filter design due to non-linear unsteady elastic mode and control surface aerodynamics and non-linear actuator dynamics the elastic mode stability requirements should mainly be based on gain stabilization of the flexible modes. Phase stabilization shall only be applied to low frequency elastic modes in order not to create too complex design and clearance procedures. Phase stabilization of low frequency elastic modes might not be avoided, it is used as tool to meet handling requirements.

The notch filter design can be based upon an analytical model of the aircraft structure including a linear FCS model. The analytical model must however be verified through ground test results both from ground resonance and structural coupling testing and from in flight flutter and structural coupling testing. The model should be updated by the test results for different configurations. Due to restrictions in the accuracy of the analytical model predictions on ground and in flight mainly at high frequency elastic modes where the prediction becomes more and more unrealistic the analytical model data with respect to inertia shall be replaced by on ground measured data. In order to cover all possible sets of aircraft store configurations a selection of critical configuration has to be established by analytical model investigation in advance.

The most critical selected configurations have to be introduced into the design of the structural filters.

The integrated FCS gain, phase advance filter and notch filter design shall cover the full range of stores and fuel states for the absolute worst case of FCS gain for trimmed aircraft conditions and shall also take into account worst gain situations in out of trim conditions.

2.3 Qualification and Certification

For flutter and structural modes coupling stability it is required to provide evidence of Qualification to prove that the aircraft is free from structural instabilities and to ensure safe flight, necessary for the flight testing task and verification against the specification.
As mentioned before, qualification is to demonstrate that the aircraft shall be free from flutter and aeroservoelastic instabilities at speed up to 1.15 times the maximum airspeed and the maximum Machnumber for all flight conditions.

Flutter and Aeroservoelastic qualification is achieved by:

- Theoretical calculations:
  Including the characteristics of the Flight Control System for all possible configurations (clean and with external stores) as well as failure cases.

Supported by:

- Ground Tests:
  Ground vibration and resonance tests on components and completed aircraft, structural mode coupling tests, actuator impedance tests, static stiffness tests and backlash tests.

- Wind tunnel Tests:
  Flexible and rigid model testing, with dynamic similar models

- Flight Tests:
  Vibration and flutter flight tests and inflight structural mode coupling tests.

Figure 5 shows in principle the aeroelastic stability qualification route to flight clearance.

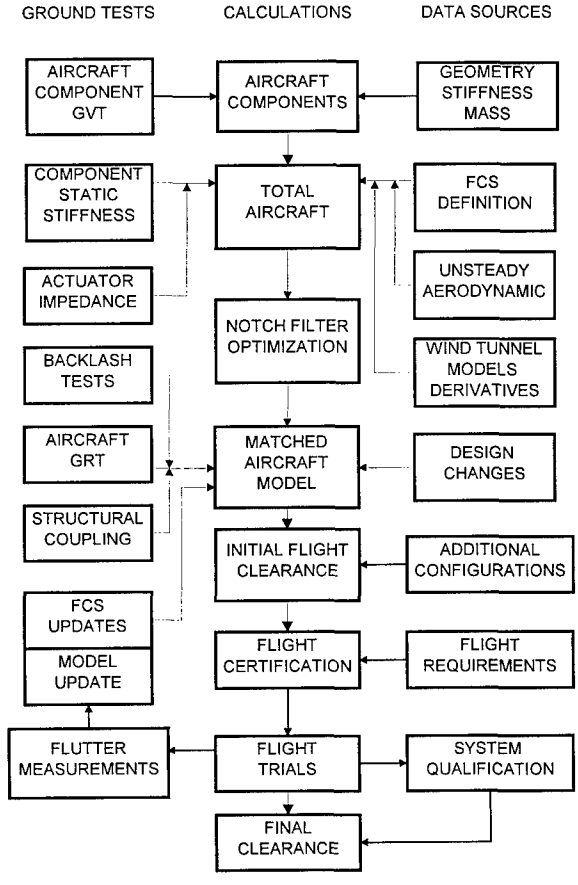

Figure 5: Flight Certification Route

Theoretical Models

The aeroelastic and aeroservoelastc models are base on a theoretical finite element model representative of the stiffness and mass characteristics of the actual aircraft, by means of dynamic assembly. The complete flutter model is assembled using the dynamic model by components and includes unsteady aerodynamic forces to analyze the aeroelastic stability characteristics of the aircraft. Sensitivity studies are performed to investigate parameter and failure variations (e.g. store and fuel mass, attachment stiffness and FCS configurations).

Validation of Models by Ground Testing

Stiffness and mass data of the theoretical aircraft model will be validate by component and total aircraft ground vibration tests. Ground vibration testing is performed on components, like wing, fin, foreplane, pylons and on fully assembled aircraft a ground resonance test (including hydraulic system) is performed.

Static stiffness testing is performed on selected combinations of pylon and store configurations and impedance actuator testing covering single and dual hydraulic system working as well as failure cases. Where any definite difference exist between the tests and predictions derived from the theoretical models, the models are updated to account for the results of the ground testing.

In general, the result of ground testing will be a validated aeroelastic model which is the basis for predicting flutter characteristics for selected key configurations.

Validation of Models by Flight Testing

The main validation of the flutter model is made with flight flutter testing, and this model is used to derive clearances up to the required 115% of the design speed envelope. The flight flutter tested key configurations establish measured data, which are compared with the theoretical results. Where any differences reveal, the models will be adjusted to account for the results of the measurements. The flight envelope expansion is done by a Machnumber/airspeed survey. In the beginning phase of flight flutter testing, the test will be concentrated on areas with high flutter stability. When the measurement of frequency and damping shows a more conservative flutter onset or confirms the predicted flutter point, the test in of more critical points will be performed. In case of fundamental differences to the predictions, the test will be interrupted and the differences are investigated and the models are updated.

2.4 Aeroservoelastic Design Tools

The integrated FCS design for the flexible aircraft is possible with the assumption that the aircraft characteristics are predictable to the necessary accuracy to optimize notch filters which meet the requirements. The characteristics of the controlled flexible aircraft shall be described in the form of open loop frequency transfer functions of the FCS control path feedback loops to a sufficient high frequency, see block diagram in Figure 9 for longitudinal and Figure 10 for lateral control. In detail for the longitudinal control system the pitch rate, the normal acceleration and the flow sensor α open loop signal at the control opening point has to be known. For the lateral control the roll rate -, yaw rate-, lateral acceleration - and flow sensor signal β open loop signal has to be described. The open loop signal consists of the transfer function of the aircraft due to control surface input sensed at the inertia measuring unit (rates and accelerations) and at the flow sensors, and the transferfunction of the FCS from the sensor to the opening point and from the opening point to the actuators.

The individual transfer function can be derived from two different methods the first using the analytical dynamic model calculation, the second using on ground measured sensor to actuator input transfer functions from the structural coupling test superimposed with calculated magnitudes of unsteady aerodynamic transfer functions. The applicability of the analytical dynamic model calculation depends on the accuracy of the modeling and its verification. Both methods depend on the accuracy of the unsteady aerodynamic transfer functions which are in both methods derived from theoretical predictions of unsteady aerodynamics for elastic modes and control surface deflection.

3. Analytical Model of the Flexible Aircraft with Flight Control System

The analytical model of the flexible aircraft with FCS consists of the linear dynamic description of the flight mechanic equations of motion, the description of the flexible aircraft through modal description using generalized coordinates, generalized masses, stiffness and model structural damping and generalized aerodynamic forces of the flexible modes and generalized control surface inertia and unsteady aerodynamic terms, the FCS is described through linear differential equations. In addition hardware and software, i.e. all sensors, actuators, computer characteristics are described by differential equations. The flexible aircraft with FCS can be demonstrated in a matrix form.

Assuming linear behavior of the structure the flutter equations of an non-augmented aeroelastic system can be written in matrix differential equation form:

$$m_r b_r^2 \begin{bmatrix} M_{qq} & M_{q\delta} \\ M_{\delta q} & M_{\delta\delta} \end{bmatrix} \begin{Bmatrix} \ddot{q} \\ \ddot{\delta} \end{Bmatrix} +$$

$$+\frac{s_R}{kV}\left\{\omega_r^2 m_r b_r^2 \begin{bmatrix} gK_{qq} & 0 \\ 0 & K''_{\delta\delta} \end{bmatrix} + \frac{\rho}{2} V^2 F s_R \frac{b_r}{S_R} \begin{bmatrix} C''_{qq} & C''_{q\delta} \\ C''_{\delta q} & C''_{\delta\delta} \end{bmatrix}\right\} \begin{Bmatrix} \dot{q} \\ \dot{\delta} \end{Bmatrix} +$$

$$+\left\{\omega^2 m_r b_r^2 \begin{bmatrix} K_{qq} & 0 \\ 0 & K'_{\delta\delta} \end{bmatrix} + \frac{\rho}{2} V^2 F s_R \frac{b_r}{s_R} \begin{bmatrix} C'_{qq} & C'_{q\delta} \\ C'_{\delta q} & C'_{\delta\delta} \end{bmatrix}\right\} \begin{Bmatrix} q \\ \delta \end{Bmatrix} = \{Q(t)\} \quad [1]$$

where m_r b_r and ω_r are the reference mass, length and frequency and M, K and C are referred to as the generalized mass, stiffness and aerodynamic matrices which are nondimensional. The generalized mass and stiffness matrices are calculated using a finite element mode (FEM) of the total aircraft. For dynamic response calculation the FEM is reduced to representative generalized dynamic DOF`s. The true airspeed V and semispan s_R of the reference plane are used to form the reduced frequency $k = (\omega s_R)/V$. F is the area of reference plane and g is the structural damping of the elastic modes. The generalized forces $Q(t)$ are equal to zero for the conventional flutter problem. The generalized coordinate q describes the amplitude of the elastic airplane modes including elastic control surface modes for a system with actuators whereas δ_0 denotes the rotation of the rigid control surface according to the complex actuator stiffness represented by the impedance function of equation (2).

$$K_{\delta_0\delta_0} = K'_{\delta_0\delta_0} + iK''_{\delta_0\delta_0} \quad [2]$$

For the controlled aircraft the servo-induced control deflection $\Delta\delta$ has to be introduced as an additional degree of freedom for each control surface. The generalized forces generated by the servo induced control deflections $\Delta\delta$ can be described as the right-hand term of equation (1) by

$$\{Q(t)\} = -m_b b_r^2 \begin{Bmatrix} M_{q\Delta\delta} \\ M_{\delta_0\Delta\delta} \end{Bmatrix} \Delta\ddot{\delta} - \frac{\rho}{2} V^2 F s_R \frac{b_r^2}{s_R^2} \frac{s_R}{k \cdot V} \begin{Bmatrix} C''_{q\Delta\delta} \\ C''_{\delta_0\Delta\delta} \end{Bmatrix} \Delta\dot{\delta}$$

$$-\frac{\rho}{2} V^2 F s_R \frac{b_r^2}{s_R^2} \begin{Bmatrix} C'_{q\Delta\delta} \\ C'_{\delta_0\Delta\delta} \end{Bmatrix} \Delta\delta \quad [3]$$

Assuming normalized rigid control surface modes δ_0 and $\Delta\delta$, the rotation of each control surface can be superimposed by

$$\delta = \delta_0 + \Delta\delta \qquad [4]$$

δ is used here as abbreviation of foreplane, inboard and outboard flap or for rudder, and differential inboard and outboard flap.

Closed loop analysis:
For each control loop the motion of the structure picked up by the sensor can be expressed in terms of the gyro station and the generalized coordinates.

$$x_s = \Phi_{xs} \cdot \dot{q} \qquad [5]$$

The relation between the servo induced control surface deflections and the structural displacements sensed by the IMU are descried as:

$$\Delta\delta = F_{Servo} \cdot F_{FCS} \cdot F_{Servo} \cdot x_s \qquad [6]$$

where the transferfunction of the FCS also includes existing interfaces between the individual control loops. Combination of the above equations, the control surface deflection $\Delta\delta$ can be expressed by a transfer matrix which contains the properties of the interconnected control loops and the modal velocities, or displacements or accelerations at the sensor station.
With the assumptions

$$q(t) = \hat{q} \cdot e^{pt} \qquad [7]$$

the equation can be transformed into frequency domain.

Open loop analysis:
In case of open loop analysis the signal is cut off behind the sensor. This means for the flutter analysis no feedback of the control surface motion and the classical solution can be applied, and for the structural coupling analysis a harmonic oscillating electrical input signal with constant amplitude for different frequencies. The deflection of the single input can then calculated.

With the inclusion of the flight control system into the flutter stability calculation, analysis methods and aspects of control engineering have to introduced. These methods are considerably different from the classical aeroelastic methods.

The state-space-description of the dynamic equation describing the aeroservoelatic behavior is as follows:

$$\{\dot{X}\} = [A]\{X\} + [B]\{x_i\} \qquad [8]$$

where:

A	Dynamic matrices
B	Input matrices
u	Input quantities
X	State Vector

The matrix in equation (1) describing the flexible aircraft with FCS is enlarged by linearized rigid flight mechanic equations. For example the state vector for longitudinal control includes then rigid aircraft state variables

$$X = \left\lfloor \Delta V/V; \Delta\alpha; \Delta\omega; \Delta\theta; \dot{q}; \dot{\delta}_0; \Delta\dot{\delta}; q; \delta_0; \Delta\delta \right\rfloor \qquad [9]$$

The flight mechanic equations may in a first approximation contain elastified aerodynamic derivatives as function of incidence, Mach number and they are for low frequency assumed to be decoupled from the flexible aircraft equations. In another approximation the flight mechanic equations are fully rigid and theoretical inertia and unsteady aerodynamic coefficients are introduced.
The flight mechanic equations for longitudinal control are described below:

Rigid aircraft equation with flexible coupling terms Normal Force equation

$$\begin{aligned}\sum Z = &-\frac{\rho}{2}V^2F\left[C'_{z\alpha}(\omega)\cdot\alpha + C''_{z\alpha}(\omega)/\omega\cdot\dot{\alpha}\right]\\ &-mV\cos(\alpha\omega_y) - \frac{\rho}{2}V^2F\cdot\bar{c}\left[C'_{zq}(\omega)\cdot\omega_y + C''_{zq}(\omega)\cdot\dot{\omega}_y\right]\\ &-mg\sin(\alpha\theta)\\ &-\frac{\rho}{2}V^2F\left[C'_{z\delta}(\omega)\cdot\delta + C''_{z\delta}(\omega)/\omega\cdot\dot{\delta}\right] - Z_{m\delta}\cdot\ddot{\delta}\\ &-\frac{\rho}{2}V^2F\left[\sum_j C'_{zqj}(\omega)q_j + \sum_j C''_{zqj}(\omega)q_j\right] = 0\end{aligned} \qquad [10]$$

Elastified normal force 'rigid' aircraft equation

$$\begin{aligned}\sum Z = &-\frac{\rho}{2}V^2F\cdot C_{zq}(\alpha)\alpha - mV\cos(\alpha\omega_y) \qquad [11]\\ &-\frac{\rho}{2}V^2F\cdot\bar{c}C_{zq}\omega_y - mg\sin(\alpha\theta) - \frac{\rho}{2}V^2F\cdot C_{z\delta}(\alpha)\delta = 0\end{aligned}$$

Pitch Moment equation with flexible coupling terms

$$\sum M = -\frac{\rho}{2}V^2 F\cdot\bar{c}\left[C'_{m\alpha}(\omega)\alpha + C''_{m\alpha}(\omega)\dot{\alpha}\right]$$
$$-I_y\dot{\omega}_y - \frac{\rho}{2}V^2 F\cdot\bar{c}^2\left[C'_{mq}(\omega)\omega_y + C''_{m}(\omega)\dot{\omega}_y\right]$$
$$-\frac{\rho}{2}V^2 F\cdot\bar{c}\left[C'_{m\delta}(\omega)\delta + C''_{m\delta}(\omega)/\omega\cdot\dot{\delta}\right] - M_{m\ddot{\delta}}\ddot{\delta}$$
$$-qFs\left[\sum_j C'_{mqj}(\omega)q_j + C''_{mqj}(\omega)/\omega\cdot q_j\right] = 0 \qquad [12]$$

Elastified Pitch Moment 'rigid' aircraft equation

$$\sum M = -\frac{\rho}{2}V^2 F\cdot\bar{c}C_{m\alpha} + \alpha + I_y\dot{\omega}_y - \frac{\rho}{2}V^2 F\cdot\bar{c}C''_{m\delta}(\alpha)\delta$$
$$-\frac{\rho}{2}V^2 F\cdot\bar{c}^2 C_{mq}\omega_y - \frac{\rho}{2}V^2 F\cdot\bar{c}^2 C_{m\dot{\alpha}}\cdot\dot{\alpha} = 0 \qquad [13]$$

C'	Real part of calc. aerodynamic coefficient
C''	Imag. part of calc. aerodynamic coefficient
$\rho/2 V^2$	dynamic pressure
F	Reference area
$\bar{c}, s$	Reference length
q_j	generalized coordinate

It should be mentioned that at DASA structural dynamics in principle the same software for structural coupling and flutter is applied. Input datasets for both programs are common. Different solutions are used, because the flutter problem will be solved as a linear algebraic eigenvalue, whereas the structural coupling will be solved as a response problem with right hand side by inversion of the matrix. Therefore some general remarks for both solutions are summarized:

Structural Modeling

The assumptions to be made for dynamic modeling including hardware have to be conservative in order to cover any system failure.

Consideration of the full travel of the flexible mode frequencies with flight condition, fuel contents and actuator failure cases is necessary. The minimum experienced structural damping shall be applied. In order to be accurate, the analytical model has to be updated from ground resonance test results mainly with respect to mode frequencies.

In addition the aircraft identification test results from structural coupling test shall be adopted. Flexible mode frequency shifts with actuator demand amplitude shall be adopted to the modeling to represent minimum and maximum possible mode frequency.

The transfer function of the actuators shall meet the upper gain boundary. The actuator phase characteristic shall include both extremes for minimum and worst phase boundaries. Non-linear actuator characteristics with amplitude reduce structural coupling.
The actuator phase characteristic is important for the phase stabilization concept.

The transfer function of the sensor platform IMU (Inertial Measuring Unit) has to describe the upper gain boundary and the minimum and maximum phase boundary. Only the upper linear boundary is necessary to be represented.

Approximated measured flow sensor transfer functions shall be used.

Unsteady Aerodynamic Modeling

The unsteady forces used in the dynamic model calculation shall be represented in a conservative manner.
The magnitude (modulus) of the unsteady forces of the flexible modes and of the control surface defection shall be predicted to represent a realistic high value for all Mach numbers and incidences. Since flow separation at higher incidences is leading to alleviation in the motion induced pressure distributions of the flexible modes and of the control surface deflections the introduction of unsteady aerodynamic forces from pure linear theory is regarded to be conservative. Special attention has to be put to transonic effects on the unsteady aerodynamic forces. Since, however, the structural coupling critical conditions which are related to the worst gain condition of the FCS are high incidence conditions, because the FCS gains result from low control surface efficiencies at high incidence, the assumption of linear unsteady subsonic and supersonic aerodynamics derived by linear theory or numerical Euler code calculations Ref [10] in the linear range is believed to be conservative throughout the full flight envelope.

The magnitude for the unsteady aerodynamic forces is sufficient for the design of high frequency elastic mode notch filters, because only a gain margin requirement is requested.

It shall be stated that the unsteady forces must be calculated for a number of reduced frequencies to cover the full frequency range.

For the phase stabilization of low frequency flexible modes like the first wing/fin bending the unsteady

aerodynamic phase shall be represented in a conservative manner. A reasonable approach for the phase of the first elastic mode is again the application of linear theory. The augmentation is that at high incidence and combined high FCS gains the aerodynamic damping is increased compared to low incidence from experience found for different wing configurations. In terms of phase stability margin Ref. [8] explains the difference in a Nichols diagram, where linear theory shows the more critical condition.

FCS Model

In order to design in a robust manner the calculation of open loop transfer functions shall consider the worst FCS gain conditions. The worst trimmed end to end gain conditions have to be included into the model calculations. Special consideration shall be also put to the maximum out of trim gain conditions with respect to structural coupling criticality.

4. Theoretical Modeling of the Structure

Figure 6 depicts the general layout of the EF2000. The aircraft was dynamically modeled by a 6 degree of freedom finite element model which fully representative of the total aircraft stiffness and mass.

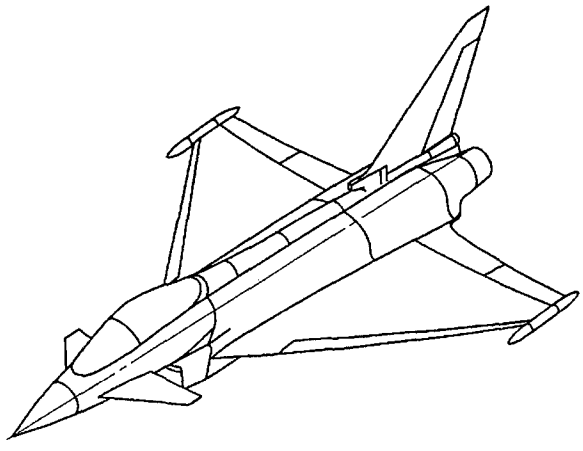

Figure 6: EF2000 General Layout

The clean aircraft was split up into different substructures, namely, foreplane, wing with flaps and slats, fuselage, fin and rudder. All substructures stiffness matrices were calculated with MSC NASTRAN, starting with a very fine static finite element model Figure 7 by applying a dynamic condensation to a coarse dynamic model, see Figure 8. For the fuselage generalized and equipment points were generated.

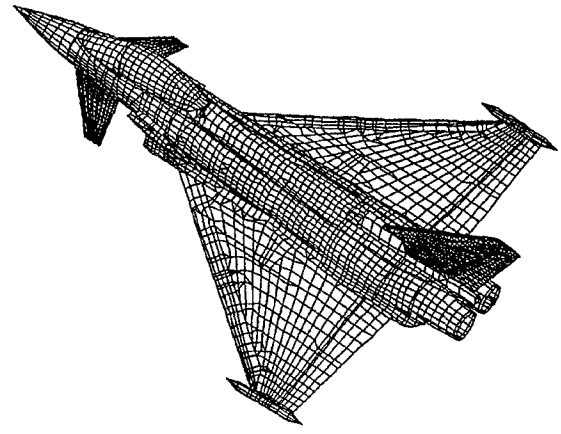

Figure 7: Finite Element Model Aircraft, static fine mesh

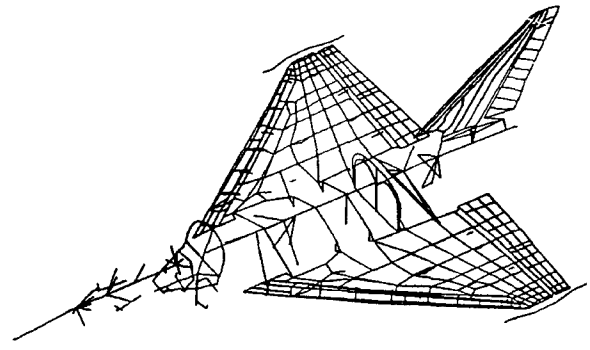

Figure 8: Finite Element Model Aircraft, dynamic coarse mesh

Definition of a fuselage Generalized Point

For each chosen fuselage section, a point was required, such that its motion would be representative of the section as a whole. Thus for a series of such points distributed along the length of the fuselage, the reduced stiffness and mass matrices could be obtained and hence the mode shapes and frequencies. The generalized point for the section was located at the center of gravity of the set of grid points to which it was connected. This generalized point was then connected, using an NASTRAN RBE3 element, to this set of points, each of which was a local hard point and had stiffness in X, Y and Z directions at least. The RBE3 element defines the motion as the weighted average of this set of points on the section. This method eliminates the local eigenmodes which are inside the fine gird system.

Fuselage Equipment points

Special grid points were created at the center of gravity of large items (greater than 30 kg) of non-structural mass, such as engines, undercarriage, gun, or avionics etc. where inertia loads were applied or

mass and inertia properties allocated. Each equipment point was connected back to the structure, using either elastic or rigid elements, in a manner representative of the actual installation.

Vibration normal modes of each substructure were produced and compared with and adjusted to available component tests.

In order to check the flutter mechanisms sensitivity to changes in structural stiffness and mass, actuator impedance etc. on investigated components and total aircraft using the branch mode model method. Using this method it is possible to identify flutter parameter which are sensitive to components (e.g. wing, foreplane) and control surfaces or store attachments.
The branch mode model is based on separate component stiffness and concentrated masses for the wing box, slats, flaps, fuselage, foreplane and fin and rudder. Basis for the calculation of the branch mode model is the NASTRAN component analysis. Additional coupling, junction and direct loads data are required to assemble the complete aircraft model. The coupling data for instants are actuator impedance, foreplane spigot bearing and back up stiffness, wing to fuselage attachment stiffness, fin to fuselage attachment stiffness, flap, slat, rudder attachment stiffness, pylon and pylon to wing attachment stiffness.
The branch mode method allow very easy the selection of symmetric and antisymmetric calculations.
The vibration modes of all substructures were used as branch modes and dynamically coupled together with rigid body modes to produce free-free total airplane vibration modes. Starting with 283 branch modes for the complete clean aircraft for the symmetric calculation 42 normal modes were used together with the rigid body modes for and aft, heave and pitch and rigid surface mode for inboard, outboard and foreplane rotation. For the antisymmetric calculation also 42 normal modes were used together with rigid body modes of side translation, roll and yaw and the surface rigid rotation of inboard, outboard and rudder.

Vibration Modes – modal analysis
As mentioned before for the flutter analysis the model was divided into a symmetric and antisymmetric dynamic half model. The fundamental normal modes at zero airspeed are described in Table 1.

Description of symmetric Modes	Frequency [Hz]
1st sym. wing bending	6.53
1st vertical fuselage bending	12.35
radome vertical mode	16.42
engine pitch symmetric	19.63
2nd sym. wing bending	20.33
tip pod pitch symmetric	21.54
1st wing torsion	23.88
engine lateral	25.04
chordwise wing bending sym.	29.97
1st sym. foreplane bending	32.80

Description of antisymmetric Modes	Frequency [Hz]
1st antisym. wing bending	7.27
1st fin bending	10.61
1st lateral fuselage bending	13.33
engine pitch antisymmetric	17.35
engine fore and aft	19.42
flap rotation	21.10
tip pod pitch antisymmetric	22.61
1st foreplane bending	23.42
1st wing torsion antisym.	26.81
foreplane bending	27.09

Table 1: Symmetric and Antisymmetric Mode Shapes of the clean Aircraft.

This modeshapes were use for calculating the unsteady aerodynamic forces for flutter analysis.

5. Flutter Calculations

The flutter calculations are produced using a modified in-house p-k method. The results are performed for different mission configurations, Mach number, altitudes and the corresponding flight control laws, by interpolation of frequency, flutter speed and unsteady aerodynamics. No interpolation was made between the investigated Mach number and the flight control data, because the change in flutter speed should be shown as functions of different gains. 2.5% structural damping (g) was introduced into the calculation.
In general, we have to look for three flutter modes:

- wing bending mode on antisymmetric / symmetric calculation. The flutter onset is very high and above the flight envelope at sub and supersonic speed
- foreplane torsion in the symmetric flutter calculation
- flap mode in the antisymmetric calculation

Figures 11-14 depicts v-g plots for sub and supersonic analysis for longitudinal investigation. The flutter onset is nearly unchanged for the wing bending mode at subsonic speed. Whereas the flutter point of the foreplane mode decreases about 50 Kts in closed loop at supersonic analysis. At high α (α=15' or -3') an additional decrease of about 50 kts were calculated showing the same flutter behaviour.
Some practical remarks about the flutter calculation including FCS. The analysis is divided into an open loop and a closed loop analysis. Zero speed eigenfrequencies were used as a starting point for the closed loop analysis because the calculation should show the influence of FCS on elastic modes. Later, all modes (elastic and system) were calculated to understand more the behaviour of the elastic modes. In the longitudinal analysis the notch filters were phase stabilized which includes some active control parts into the elastic system area. The result of phase stabilization is an increase of damping for the wing bending mode at unchanged flutter point.
The antisymmetric calculations are not shown in this paper, because the flutter mechanism and the flutter point is almost the same with and without FCS.

6. Flight Flutter Testing

For flutter it is necessary to provide evidence of qualification or verification of fitness of purpose to ensure safe flight, adequacy for the flight test' g task and verification against the specification.
Flight flutter test were performed applying a FBI (Frequency Bias Injection) signal input by the flight test group of British Aircraft Corporation. Fist data evaluations show that differences in frequency and damping of the conditions are within the measuring accuracy, Ref. 3.

7. Conclusion

This paper describes briefly the flutter experience gained on a modem fighter project including the Flight Control System. The theoretical work which describes the expansion of the dynamic equation with the control equation of the classical flutter solution is shown. The following points should be highlighted:

- It is absolutely necessary to have a reliable dynamic model of the elastic aircraft which must be verified by ground vibration tests.
- Ground tests to check structural mode coupling interaction must be performed to assure stability and to compare with analytical predictions. If correlation is achieved variation of parameters such as external stores, fuel content can be investigated pure analytically
- Open and closed loop flutter calculations have to be done to cover the full flight envelope. Calculations have shown negligible influence of FCS on flutter at lg flight, but an decrease of flutter onset at high a conditions.
- Using phase stabilized notch filter, the damping of the first wing bending mode increases substantially by nearly unchanged flutter point.

8. References

[1] Lotze A., Sensburg O., and Kühn M.
Flutter Investigations on a Combat Aircraft with a Command and Stability Augmentation System
AIAA Paper No. 75-1025, AIAA 1975 Aircraft Systems and Technology Meeting, Los Angeles

[2] Becker J., Luber W.
Flight Control Design Optimization with Respect to Flight and Structural Dynamics Requirements
AIAA 96-4047, 6th AIAA/NASA Symposium on Multidisciplinary Analysis and Optimization, MDO
Bellevue, WA, USA, Sept. 1996

[3] Ramsay R. B.
Flight Flutter Testing of Combat Aircraft
AGARD Structure and Material Panel Meeting, Rotterdam, The Netherlands, 8-10 May 1995, AGARD CP-566

[4] Luber W.
Flutter Investigation of a Fighter Aircraft Including Flight Control System
International Forum on Aeroelastic and Structural Dynamics, Rome, Italy June 1997

[5] Ramsay R. B.
Flutter Certification and Qualification of Combat Aircraft
International Forum on Aeroelastic and Structural Dynamics, Manchester, UK, June 1995

[6] Ramsay R. B.
In-Flight Structural Mode Excitation System for Flutter Testing
AGARD Conference Proceedings 519
Chania, Crete, Greece, 11th-14th May 1992

[7] Vaccaro V., Becker J.
Ground Structural Coupling Testing and Model Updating in the Aeroservoelastic Qualification of a Combat Aircraft.
AGARD, Meeting on Advanced Aeroservoelastic Testing and Data Analysis,
Rotterdam, The Netherlands, 8-10 May 1995.

[8] Becker J., Luber W.
Unsteady Aerodynamic Forces at High Incidence and their Application in Structural- and Flight Control Design.
International Forum on Aeroelasticity and Structural Dynamics; Manchester, UK; 26-28 June 1995

[9] Becker J., Vaccaro V.
Aeroservoelastic Design, Test Verification and Clearance of an Advanced Flight Control System.
AGARD Meeting on Advanced Aeroservoelastic Testing and Data Analysis,
Rotterdam, The Netherlands, 8-10 May 1995

[10] Hönlinger H., Zimmermann H., Sensburg O., Becker J.
Structural Aspects of Active Control Technology
AGARD Conference Proceedings on Active Control Technology, FMP Symposium held at Turin, Italy, May 1994

[11] Caldwell B.D.
The FCS-Structural Coupling Problem and its Solution.
AGARD Conference Proceedings on Active Control Technology, FMP Symposium held at Turin, Italy, May 1994

[12] Heller G., Kreiselmeier E.
Eulerluftkräfte für Klappenschwingungen
TUM-FLM-96/05; Lehrstuhl für Fluidmechanik, Technische Universität München

[13] Bennekers B.
Description of the computer programs for the calculation of aerodynamic loads on oscillating wing-body configuration in subsonic flow (NLRI-Method)
NLR-TR-76120 C

[14] Roos F., Bennekers B., Zwaan T.
Calculation on unsteady subsonic flow about harmonically oscillating wing/ body configurations
Journal of Aircraft Vol. 14. No. 5. May 1977

[15] Becker J., Weiss F., Sensburg O.
Compatibility of active control technologies with aircraft structure design.
International Symposium on Structural Control
University of Waterloo/Ontario (Canada), July 1985

[16] Försching H.
Introductory survey of aeroelastic problems in separated and transonic flow
Von Karman Institute for Fluid Dynamics Lecture Series 1981-4

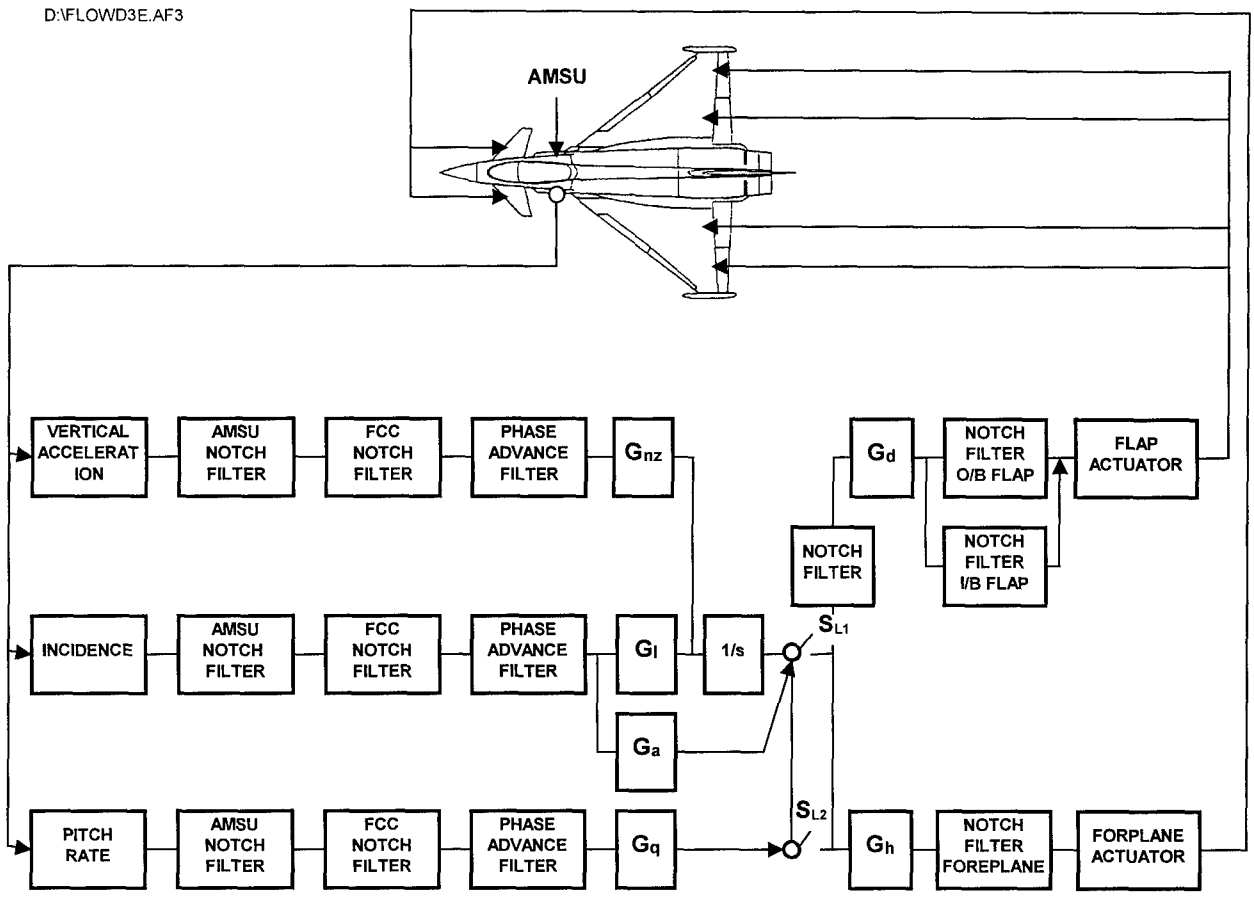

Figure 9: Flow chart of longitudinal control

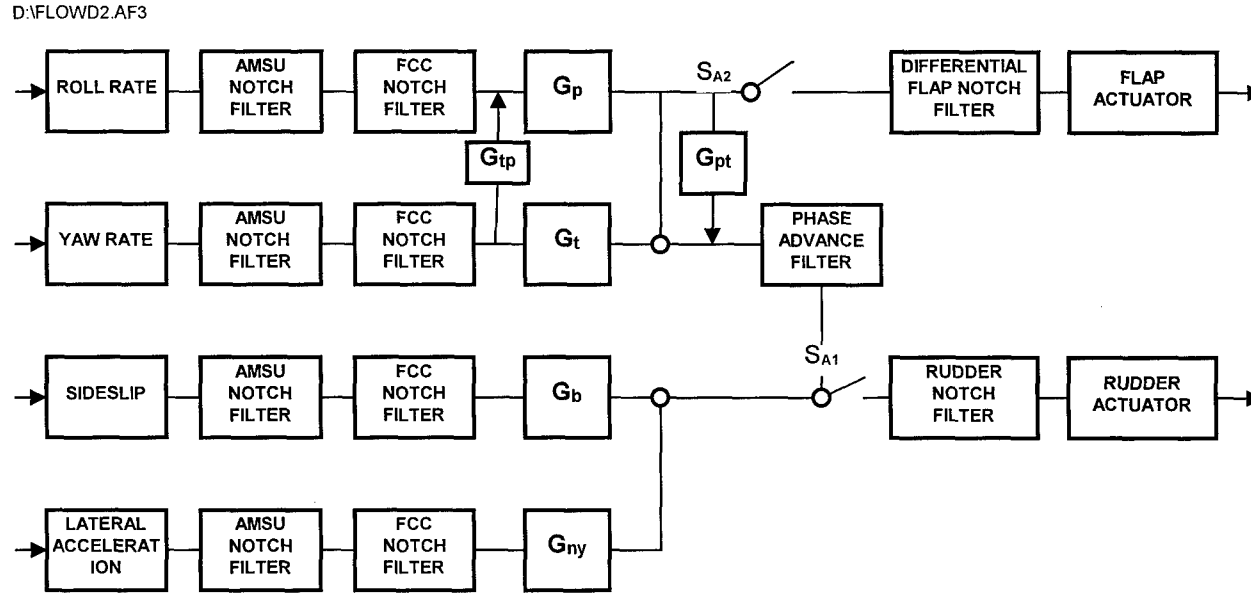

Figure 10: Flow chart of lateral control

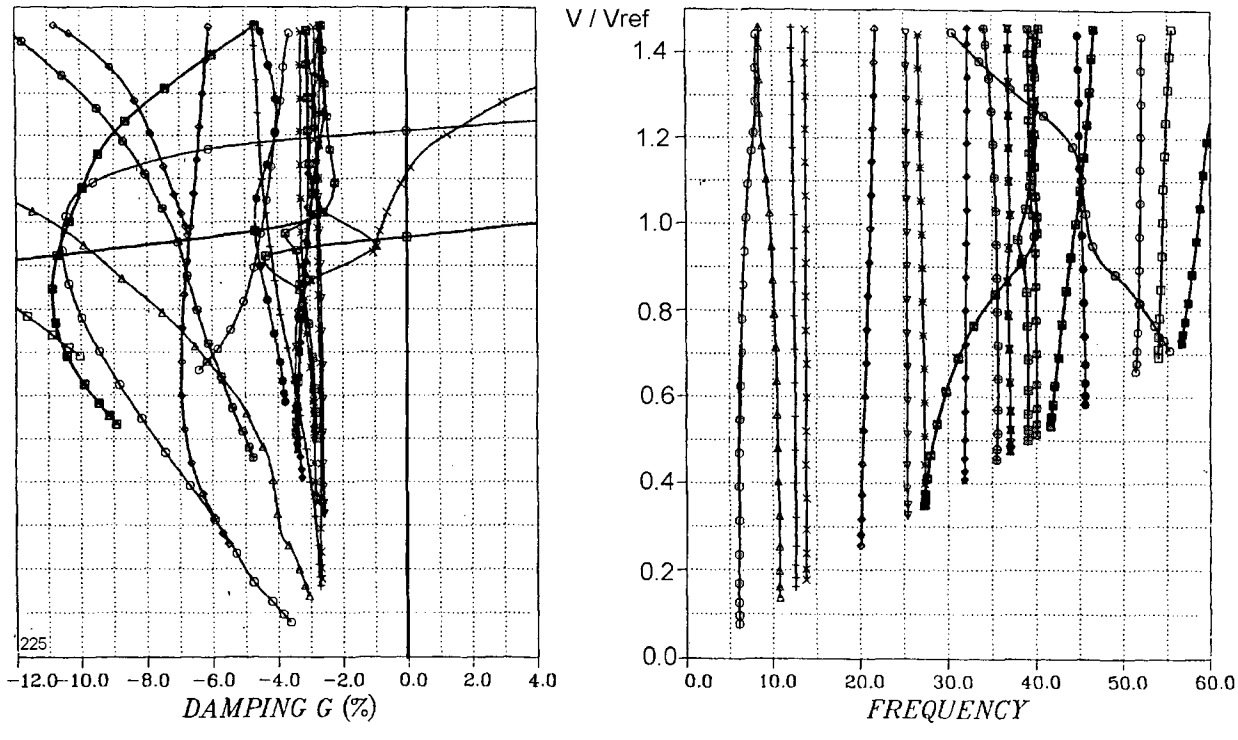

Figure 11: Damping and Frequency versus Flutterspeed, Mach=0.9, Symmetric, sea level, open loop

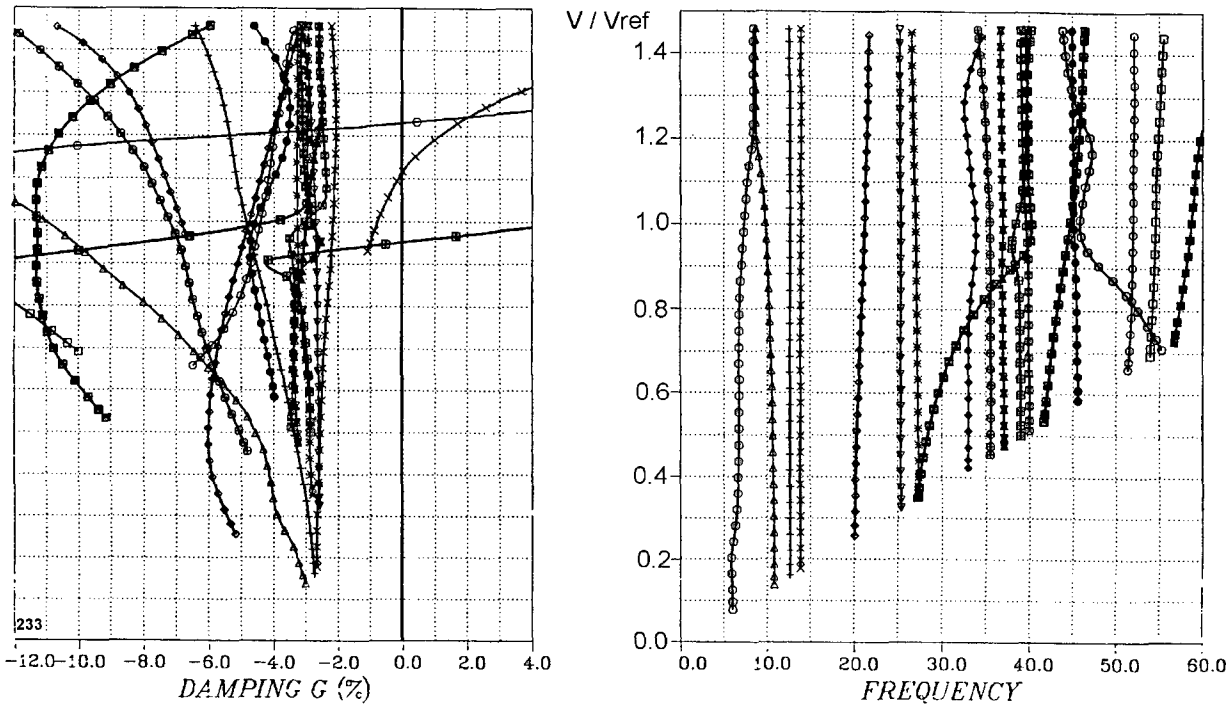

Figure 12: : Damping and Frequency versus Flutterspeed, Mach=0.9, Symmetric, sea level, closed loop

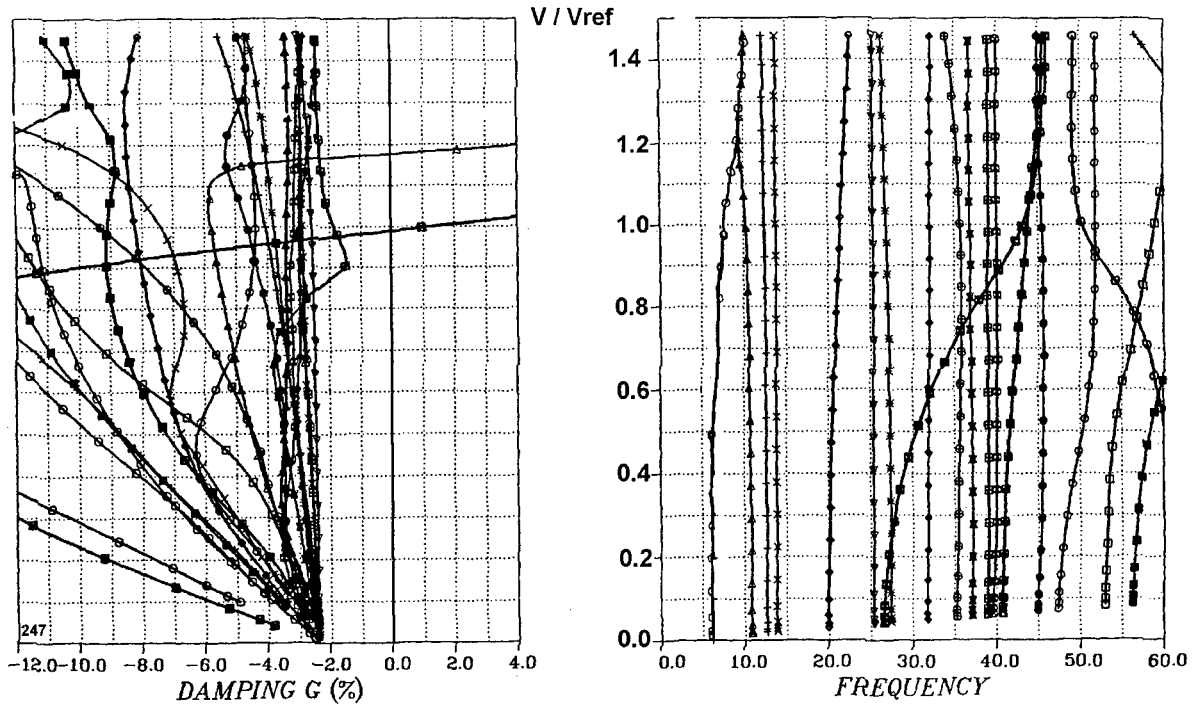

Figure 13: : Damping and Frequency versus Flutterspeed, Mach=1.2, Symmetric, sea level, open loop

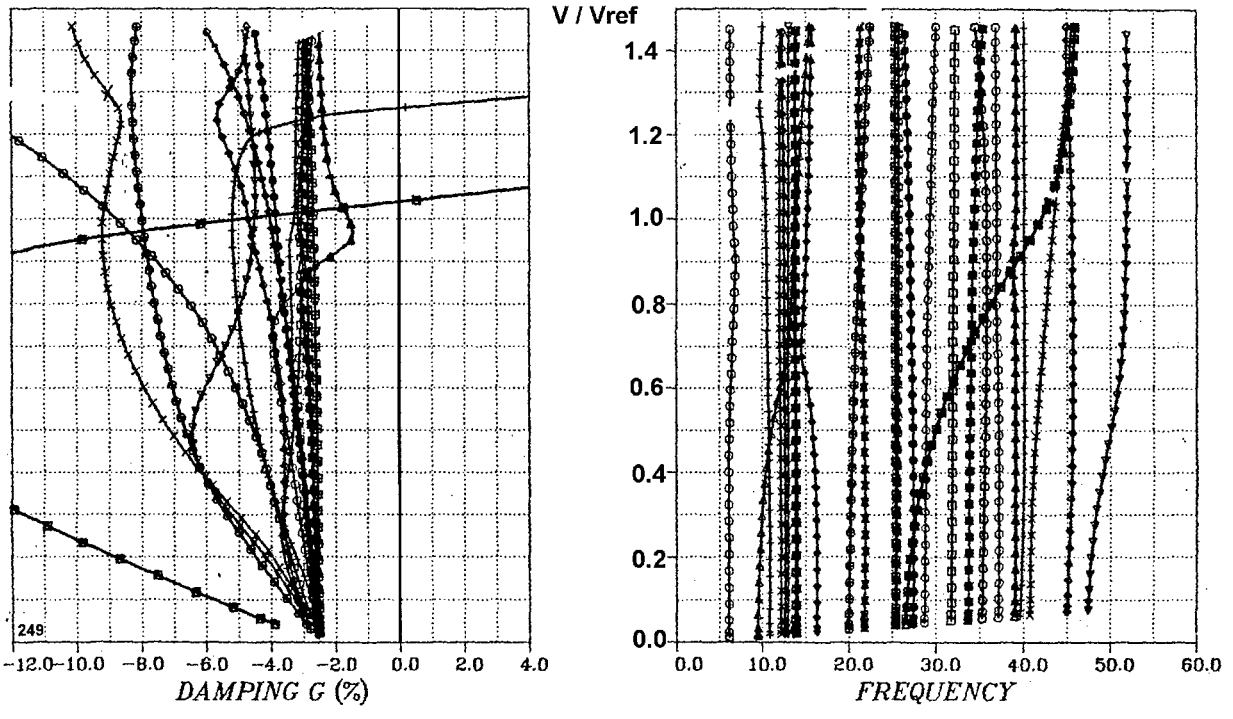

Figure 14: : Damping and Frequency versus Flutterspeed, Mach=1.2, Symmetric, sea level, closed loop

Characterisation of nonlinear aeroservoelastic behaviour

G. Dimitriadis & J. E. Cooper
School of Engineering
University of Manchester
Oxford Road, Manchester M13 9PL
United Kingdom
mbgssgd2@fs1.eng.man.ac.uk
jecooper@man.ac.uk

Abstract

The characterisation of the behaviour of nonlinear aeroelastic systems has become a very important research topic. Nevertheless, most of the work carried out to date concerns the development of unsteady CFD solutions in the transonic region. Important though this work is, there is also a need for research which aims at understanding the behaviour of nonlinear systems, particularly the occurance of Limit Cycle Oscillations (*LCOs*). The purpose of this paper is to study the stability of a simple aeroservoelastic system with nonlinearities in the control system. The work considers both structural and control law nonlinearities and assesses the stability of the system response by use of bifurcation diagrams. It is shown that simple feedback systems designed to increase the stability of the linearised system also stabilise the nonlinear system, although their effects can be less pronounced. Additionally, a nonlinear control law designed to limit the control surface pitch response was found to increase the flutter speed considerably by forcing the system to undergo limit cycle oscillations instead of fluttering. Finally, friction was found to affect the damping of the system but not its stability, as long as the amplitude of the frictional force is low enough not to cause stoppages in the motion.

1 Introduction

Over the past two decades there has been a pronounced increase in research into nonlinear aeroelasticity. It has been known for quite some time that aircraft contain a number of nonlinearities which can significantly affect vibratory characteristics. These nonlinearities give rise to phenomena (e.g. Limit Cycle Oscillations (LCO)) that cannot occur if the system is linear. Consequently, it is impossible to model and predict such behaviour using a linear analysis. This limitation is becoming of increasing importance with the latest generations of aircraft.

Some early work on nonlinear aeroelasticity [1] showed that limited amplitude oscillations in aircraft are nonlinear phenomena. Breitbach [2] identified a number of sources of nonlinearity in aircraft such as kinematic deflections of control surfaces, solid friction in hinge bearings as well as distributed nonlinearities due to elastic deformations in riveted, screwed and bolted connections. Since then, several investigations of nonlinear aeroelastic behaviour have been conducted, most of which concentrated on structural and aerodynamic nonlinearities. The whole area of prediction and characterisation of LCO has been defined as being an area of critical research interest [3]. However, most work has concentrated upon the development of unsteady CFD solutions [4] primarily in the transonic region. Some recent notable exceptions are the experimental work carried out by Holden et al [5] and Conner et al [6] as well as various numerical studies such as [7].

The increasing power of modern computers allowed the use of increasingly computationally intensive mathematical tools for the characterisation of nonlinear behaviour, such as bifurcation plots [8] and parameter-space sections [9]. Limit Cycle Oscillations (*LCOs*) have been observed and explained in terms of Hopf bifurcations [10] and the possibility of LCO control and suppression has been investigated [11], [12]. However, the main subject of all this research has been structural nonlinearities and, to a lesser extent, aerodynamic nonlinearities [13]. Little research has been conducted into the effects of nonlinearities in the control system even though, with the advent of Active Control Technology (*ACT*), control systems are becoming increasingly nonlinear. Aeroservoelasticity [14] is a relatively recent research topic which is generally dominated by case studies such as [15].

Stability is of paramount importance in the design of all control systems whether they be linear or nonlinear. However, the performance of nonlinear aeroservoelastic systems throughout the desired flight envelope as well as their interaction with non-designed nonlinearities, such as backlash in the linkage elements of the control system, has not been thoroughly investigated.

In this paper, the aeroservoelastic behaviour of a number of simulated systems is investigated and characterised. The purpose of the work is to give an overview of possible nonlinear behaviour that may occur either near flutter, or as a result of the interaction of the control system with structural nonlinearities. Partricular emphasis is given to assessing whether control laws designed to improve the stability of linear systems also have a stabilising influence on nonlinear systems. The simulated systems

Paper presented at the RTO AVT Specialists' Meeting on "Structural Aspects of Flexible Aircraft Control", held in Ottawa, Canada, 18-20 October 1999, and published in RTO MP-36.

considered contain a variety of nonlinearities that can occur in the control system, ranging from nonlinear springs in the control actuator to nonlinear control laws.

2 Simulated aeroservoelastic systems

The basis of all the systems investigated in this work is an extension of the Hancock aeroelastic model [16]. The basic Hancock model is a rigid wing with two springs at the wing root, giving the system two degrees of freedom, heave and pitch. The aerodynamics is modelled using quasi-steady strip theory with approximate unsteady aerodynamic derivatives. The model used here also includes a control surface [12], i.e. it incorporates an additional degree of freedom. The control surface is driven by a Power Control Unit (*PCU*) or Power Actuator. The PCU provides both stiffness and structural damping. The basic simulated system, which is shown in figure 1, was modified by the addition of a number of nonlinearities giving rise to four different systems, with two possible control laws.

2.1 Bilinear PCU spring

The Power Control Unit contains a pressure feedback spring, as shown in figure 2. The first system examined in this paper has a bilinear pressure feedback spring. Bilinear stiffness is a piecewise linear function shown in figure 3. The stiffness, K_1, in the inner region (delimited by $\pm\delta$ in figure 3) is lower than the stiffness in the outer region, K_2.

This is not a straightforward case of bilinear stiffness in the control surface since, because the bilinear spring is in the PCU, it affects the control surface velocity as well as displacement. The PCU equation is

$$\frac{VK_F}{4N}\dot{P}_J + K_V A_F \sqrt{P_s/2} P_J = dK_F A_P \dot{\beta} + \mu d K_F K_V \sqrt{P_s/2}\beta - \mu d K_F K_V \sqrt{P_s/2}\beta_i \quad (1)$$

where V is the volume of the PCU, N is the bulk modulus of oil, P_J is the difference of pressures in the two PCU compartments P_1 and P_2 (see figure 2), K_V is a valve flow constant, A_F is the effective area of the pressure sensing chamber, P_s is the supply pressure, K_F is the stiffness of the pressure feedback spring, μ is the lever arm ratio, d is the distance between the PCU axis and the wing chord, β is the control surface deflection and β_i is the demand angle. It can be seen that K_F multiplies both the $\dot{\beta}$ and β terms. Hence, a nonlinear pressure feedback spring affects both control surface velocity and displacement.

2.2 Freeplay in PCU spring

In this case, the pressure feedback spring contains freeplay. Freeplay stiffness is also a piecewise linear function, depicted in figure 4. In this case, the stiffness in the inner region is zero. Again, the freeplay affects both control surface velocity and displacement.

2.3 Backlash in PCU spring

Backlash is a piecewise linear hysteretic nonlinearity. Figure 5 shows the variation of the force in the PCU with control surface deflection during a Limit Cycle Oscillation, in the presence of backlash in the pressure feedback spring. Whenever the control surface pitch changes direction, the force in the PCU jumps from one of the sloped lines to the other. The horizontal distance between the two branches is called the backlash distance. Such behaviour can be observed for example in the bearings of all-movable control surfaces of military aircraft [17]. In the american literature backlash is sometimes referred to as freeplay however, in this paper, the terms backlash and freeplay denote two distinct types of nonlinearity.

As with bilinear stiffness and freeplay, backlash affects both the velocity and displacement of the control surface of the system investigated here.

2.4 Friction in PCU

This case models friction between the piston seals and the chamber. The friction depends on the piston velocity, hence the force, F, in the piston is given by

$$F = A_p P_J + F_R \mathrm{sgn}(\dot{\beta}) \quad (2)$$

where F_R is the magnitude of the friction force. Generally, it was assumed that F_R was low enough to allow movement of the piston without stoppages.

2.5 Delayed Feedback

A displacement feedback loop was added to the linear system, in order to increase the separation of the natural frequencies. The feedback gains were calculated such that the separation of the two closest natural frequencies was increased by 20%. The changes in the natural frequencies at a speed of 40m/s are tabulated in table 1

Open Loop	Closed Loop
37.2441 Hz	46.3668 Hz
14.3522 Hz	15.2619 Hz
8.7812 Hz	8.4752 Hz

Table 1: Open and closed-loop natural frequencies of linear system at V=40m/s

A further consequence of the displacement feedback was that the flutter speed of the linear system was increased by 1.9%. Figures 6 and 7 show the open and closed loop natural frequencies and dampings respectively for a range of airspeeds. The open loop eigenvalues were obtained by direct solution of the system equations of motion while the eigenvalues of the closed loop system were calculated by curve-fitting the impulse response, hence

they look less smooth. The figures show that all the natural frequencies of the closed-loop system are more separated than those of the open loop system and that, even though the damping of the critical degree of freedom in the closed loop system is lower, the closed loop flutter speed is higher than that of the open loop system.

To simulate the fact that real control systems do not act spontaneously, the feedback signal was delayed by $n\Delta t$ seconds, where n can be varied. The delayed feedback control system was also used in conjunction with the freeplay, bilinear, backlash and friction nonlinearities mentioned above.

2.6 Control Surface pitch limit

An active control system was devised to limit the control surface pitch. Initially, it was assumed that the control system knows at all times the exact value of the control surface pitch. The pitch, β, at time t is used in conjunction with the value of the pitch at time $t - \Delta t$ to predict $\beta(t + \Delta t)$ using linear curve-fitting, i.e.

$$\beta(t + \Delta t) = 2\beta(t) - \beta(t - \Delta t)$$

If $\beta(t + \Delta t)$ exceeds a given limit, β_{lim}, then the control system feeds back $-K\beta$ through the actuator, where K is some constant. Since a real control system would not be able to instantaneously complete all the calculations, acquire the current value of β and feed it to the actuator, the feedback in the simulated system is delayed by Δt.

3 Limit Cycle Oscillations and bifurcation diagrams

For a single degree-of-freedom system, a Limit Cycle Oscillation (*LCO*) is a limited amplitude oscillation occurring around a line singularity in the phase-plane called a limit cycle. Such a limit cycle can be seen in figure 8. The figure plots velocity ($\dot{\beta}$) against displacement (β) for a system undergoing LCO. The resulting curve is the limit cycle. Limit cycles are singularities since they can either attract the phase trajectories (stable limit cycle) or repel them (unstable limit cycle). In the case of figure 8, where a stable limit cycle is shown, the system response will always wind onto the limit cycle both from the inside and from the outside. In turn, this signifies that the limit cycle cannot be crossed. A limit cycle can be classed as period-1, period-2, etc depending on its complexity. Figure 8 shows a limit cycle with only one loop, i.e. period-1. A period-3 limit cycle, with three loops, can be seen in figure 9.

For a multiple degree-of-freedom system, a limit cycle is a multi-dimensional singularity, its dimensions being equal to the number of states in the system. However, limit cycles can still be visualised using phase-plane plots of the type shown in figures 8 and 9, provided the velocity and displacement for the same degree-of-freedom (or mode) is plotted. In the case of aeroelastic systems, whose behaviour changes with airspeed, phase-plane plots are not sufficient to determine their stability. To this purpose it is necessary to use bifurcation plots, which can track the stability of a system over any range of airspeeds. Bifurcation plots can be constructed by obtaining the impulse response of a system and then calculating the displacement of one of the degrees of freedom when the velocity of the same degree of freedom is zero. If the system is undergoing a limit cycle at a particular velocity, then the values of the displacement will be repeated. For example, in the case of figure 8, when, the displacement takes two values at zero velocity. In figure 9, there are six possible values of the displacement at zero velocity. A bifurcation plot is obtained when all the values of the displacement when the velocity of that DOF is zero are plotted against airspeed.

Figure 10 shows a bifurcation plot for the system with bilinear pressure feedback spring described earlier. For airspeeds where the system is stable (up to 45 m/s), only zeros are plotted. Between 45 m/s and just over 52 m/s, the system undergoes LCOs. The limit cycles are period-1, hence there are only two points plotted at each airspeed. The amplitudes of the limit cycles increase almost linearly up to approximately 51 m/s. Between 51 and 52 m/s, the amplitudes increase exponentially, which is a sign that the system is close to instability. At speeds above 52 m/s, the system becomes completely unstable and flutters.

4 Stability of the Aeroservoelastic Systems

The impulse response of the non-linear systems described in section 2 were calculated for a range of different airspeeds. Bifurcation plots were then generated in order to characterise the Limit Cycle behaviour.

4.1 Stability of Bilinear System

As mentioned already, figure 10 is the bifurcation plot for the system with bilinear pressure feedback spring. There are three distinct regions of stability, tabulated in table 2.

Airspeed (m/s)	Stability
< 45.2	Stable
45.2-52.2	Period-1 Limit Cycle
> 52.2	Unstable (flutter)

Table 2: Stability of bilinear system

Systems with bilinear systems have already been extensively analysed in previous work such as reference [18]. The purpose of this section is to investigate the effects of bilinearity in conjunction with control action to the stability of an aeroservoelastic system. Hence, results are presented from the coupling of the bilinear system with the displacement feedback of section 2.5. It has already been

mentioned that the displacement feedback system was designed to stabilise the linear aeroservoelastic system. The two main considerations in this section are whether the feedback system can also stabilise the bilinear system and also what are the effects of delaying the feedback. It is of interest to note that the system with bilinear stiffness undergoes LCOs at airspeeds above the flutter speed of the linear system with stiffness K_1 and below the flutter speed of the linear system with stiffness K_2.

Figure 11 shows the bifurcation diagram for the bilinear system with feedback (not delayed). It can be seen that LCOs only begin to occur at airspeeds higher than 49 m/s. Additionally, up to approximately 51.5 m/s the amplitudes of the limit cycles are very low. Flutter occurs at 54 m/s. The stability of the system is summarised in table 3

Airspeed (m/s)	Stability
< 49	Stable
49-54	Period-1 Limit Cycle
> 54	Unstable (flutter)

Table 3: Stability of bilinear system with undelayed feedback

Consequently, the effect of the feedback was to stabilise the system, despite the bilinear actuator spring. Limit cycles appear later than in the open loop system and they are of lower amplitude. Additionally, flutter is delayed by approximately 3%.

Delaying the feedback signal by one simulation timestep has an adverse effect on the stability of the closed-loop system. Figure 12 shows the bifurcation diagram for the bilinear system with delayed feedback. Limit cycles (period-1) first appear at 46 m/s but their amplitudes remain low up to an airspeed of just over 48 m/s. At 51 m/s, the limit cycles change to period-3. Finally, at 52.5 m/s the system starts to flutter. Table 4 summarises the information from figure 12.

Airspeed (m/s)	Stability
< 46	Stable
46-51	Period-1 Limit Cycle
51-52.5	Period-3 Limit Cycle
> 52.5	Unstable (flutter)

Table 4: Stability of bilinear system with delayed feedback

Nevertheless, the system with delayed feedback is more stable than the open-loop system since limit cycles appear later and are initially of much smaller amplitude.

4.2 Stability of freeplay system

As with bilinear stiffness, freeplay has been already thoroughly investigated, most recently in [7] and [6]. Here, the effect of freeplay in conjunction with displacement feedback is of interest. Firstly, it should be mentioned that freeplay is a much more nonlinear function than bilinear stiffness and that its effects are more pronounced. With the reference to the system investigated here, it should be noted that, since the stiffness is zero inside the freeplay region, the only source of stiffness in the control surface pitch direction is aerodynamic stiffness. This in turn signifies that LCOs are expected to be encountered at lower airspeeds than in the bilinear system.

Figure 13 is the bifurcation plot for the system with freeplay in the pressure feedback spring but no feedback. The first limit cycles appear at 19m/s and they are period-2. At approximately 33m/s the limit cycles change to period-1. Finally, the system flutters at 52m/s (see table 5).

Airspeed (m/s)	Stability
< 19	Stable
19-33	Period-2 Limit Cycle
33-52	Period-1 Limit Cycle
> 52	Unstable (flutter)

Table 5: Stability of freeplay system without feedback

Figure 14 shows the bifurcation diagram for the freeplay system with undelayed feedback. The system is stable up to an airspeed of 20m/s when period-3 limit cycles appear. The amplitude of the limit cycles increase slowly until 53m/s when the system begins to undergo period-4 LCOs. Finally, flutter occurs at 55 m/s. The stability summary in table 6 shows that the feedback has stabilised the system by delaying the appearance of LCOs by 1m/s and delaying flutter by 3m/s. Additionally, the amplitudes of all limit cycles are lower than in the open loop system. However, the stabilisation is not as radical as it was with the bilinear system.

Airspeed (m/s)	Stability
< 20	Stable
20-53	Period-3 Limit Cycle
53-55	Period-4 Limit Cycle
> 55	Unstable (flutter)

Table 6: Stability of freeplay system with undelayed feedback

Finally, figure 15 shows the bifurcation diagram for the freeplay system with delayed feedback. Limit cycles first appear at 20m/s and are period-3, as with the undelayed feedback however, in this case there are no period-4 LCOS. Flutter occurs at 53m/s.

Airspeed (m/s)	Stability
< 20	Stable
20-53	Period-3 Limit Cycle
> 53	Unstable (flutter)

Table 7: Stability of freeplay system with delayed feedback

Figure 15, as well as table 7, show that the main effect

of the delay is to decrease the flutter airspeed. Nevertheless, as with the bilinear case, the delayed feedback system is more stable than the open loop system since flutter occurs 1m/s later and the limit cycles have smaller amplitudes.

4.3 Stability of system with backlash

Figure 16 is the bifurcation plot for the open-loop system with backlash in the pressure feedback spring. The system is stable up to an airspeed of 44m/s when very low amplitude period-1 limit cycles appear. At approximately 51.5m/s the system flutters (see table 8). Hence, backlash decreases the flutter velocity of a system and introduces small amplitude limit-cycles at the high subcritical airspeed range.

Airspeed (m/s)	Stability
< 44	Stable
44-51.5	Period-1 Limit Cycle
> 51.5	Unstable (flutter)

Table 8: Stability of backlash system without feedback

Figure 17 displays the bifurcation diagram for the system with backlash in the pressure feedback spring and undelayed feedback. Again, the first limit cycles appear at 44m/s and are low amplitude period-1. However, flutter is delayed beyond the flutter airspeed of the linear system by high amplitude period-1 LCOs in the range 52.5-53.5m/s. After 53.5m/s continuous bifurcations to higher period limit cycles occur. Such behaviour is termed period-doubling [12] and is an indication of imminent instability either to flutter or to chaotic behaviour. In this case period-doubling leads to flutter at 53.8m/s.

Airspeed (m/s)	Stability
< 44	Stable
44-52.5	Low amplitude Period-1 Limit Cycle
52.5-53.5	High amplitude Period-1 Limit Cycle
53.5-53.8	Period doubling
> 53.8	Unstable (flutter)

Table 9: Stability of backlash system with feedback, no delay

Finally, figure 18 shows the bifurcation diagram for the backlash system with delayed feedback. The behaviour of the system is identical to that of the undelayed system up to an airspeed of 53.5m/s. In this case however, period doubling-behaviour does not take place. Instead, the high amplitude period-1 limit cycle behaviour continues up to an airspeed of just over 54 m/s when the system begins to flutter.

Consequently, unlike the bilinear and freeplay cases, delayed feedback increases the stability of the backlash system by delaying flutter. This phenomenon is due to the nature of the backlash function itself. When the control surface pitch displacement changes direction, the direction of the delayed displacement feedback is still unchanged and therefore the backlash region of figure 5 is shrunk, thus diminishing the effect of the nonlinearity.

Airspeed (m/s)	Stability
< 44	Stable
44-52.5	Low amplitude Period-1 Limit Cycle
> 54.3	Unstable (flutter)

Table 10: Stability of freeplay system with delayed feedback

4.4 Stability of system with control surface pitch limit

The nonlinear function described by the control scheme presented in section 2.6 is shown in figure 19. The feedback signal is zero unless the linear extrapolation of β, the control surface pitch degree of freedom, suggests that the value of β in the next step will be higher than the defined pitch limit, in which case the feedback signal is equal to $-a\beta$ where a is a gain coefficient. Consequently, it is obvious that, if the pitch limit were equal to zero, then the control law would be a linear proportional feedback. For the purposes of this work, the limit was set to $\pm 10^{\circ}$.

The effectiveness of the control scheme is demonstrated in figure 20 where the control surface pitch is plotted against time. The dashed line is the demand signal fed to the control surface through the power control unit. It can be seen that pitch rarely exceeds the limit of 10°, even though the demand angle is 12°.

Since the control system only engages when the control surface pitch lies near the limit, it does not affect the decaying impulse response of the system. Hence, self-excited oscillations are only possible when the linear system flutters. In other words, the control system contains flutter by constraining the system response onto a limit cycle. This can be seen in figure 21 where the bifurcation diagram for the pitch limited system is shown. Up to 52.7m/s, the flutter speed of the linear system, the response is decaying. Limit cycles exist at airspeeds between 52.7m/s and 57.7m/s. Beyond this range, the closed-loop system flutters.

Airspeed (m/s)	Stability
< 52.7	Stable
52.7-57.7	Period-3 Limit Cycle
> 57.7	Unstable (flutter)

Table 11: Stability of system with control surface pitch limit

It can be seen from the figure that the limit cycles are very complex since many points appear at each airspeed, in fact so many that it is impossible to classify the limit cycles in terms of period. A phase-space plot of a limit cycle at an airspeed of 55m/s is shown in figure 22. The complicated shape of the limit cycles is due to the simplistic manner in which the value of the control surface pitch

at the next time step is calculated. A more detailed prediction algorithm would give rise to better behaved limit cycles but would be less realistic.

4.5 Stability of system with friction in the PCU

Friction is a mechanism that removes energy from the motion of a system. Given that the amplitude of the frictional force, F_R, is low enough not to cause stoppages, its main effect is to increase the damping present in the motion. A frictional force of varying amplitude was added to the open-loop linear, freeplay and bilinear systems. As was expected, the main consequence for all the systems was an increase in damping. This effect can be observed in figures 23 and 24 where the control surface pitch impulse response of the frictionless linear system is plotted on the same axes as that of the system with friction. In figure 23, showing impulse responses at a subcritical airspeed (V=30m/s), the response of the frictional system dies away 0.35 seconds after the application of the impulse while the frictionless system still oscillates visibly after one second. Figure 24 shows impulse responses at an airspeed very close to the flutter speed of the linear system. In this case, the response of the system with friction takes a little longer to die away but its motion looks still far more damped than that of the frictionless system.

Nevertheless, friction does not alter the stability of any of the systems investigated in this work. The flutter speeds of the linear, bilinear and freeplay systems are not affected by the introduction of friction when F_R is low enough not to cause stoppages. Additionally, the limit cycle amplitudes of the bilinear and freeplay system also remain unaffected. However, when F_R exceeds a certain level, stoppages in the motion occur and the stability of all the systems is affected dramatically. Figure 25 shows the variation of flutter airspeed for the freeplay and bilinear systems with friction of increasing amplitude. In both cases, the flutter speeds remain at their respective frictionless values until $F_R = 1.4$N. At that particular value, the friction starts to cause stoppages and the LCOs that would have occurred in the absence of friction are inhibited. Additionally, the flutter speed is increased and keeps increasing at even higher values of F_R. The response of the bilinear system with friction of amplitude $F_R = 2$N is compared to that of the frictionless bilinear system in figure 26. It can be seen that, in the absence of friction, the system undergoes limit cycle oscillations. Friction suppresses the LCO by inhibiting the motion to such an extent that only irregular, low-amplitude oscillations are possible.

5 Conclusions

A simple aeroservoelastic system has been used to explore the effect of nonlinearities on the aeroservoelastic behaviour. It was found that it is possible for Limit Cycle Oscillations to occur, which may be of high period. The linear feedback that was applied still helped to stabilise the system, even with the presence of nonlinearities. Delays in the feedback signals reduced the effectiveness of the control in all systems apart from the system with backlash. If this delay was too great, then instability occurred almost immediately. A nonlinear control law designed to limit the control surface pitch response was found to increase the flutter speed considerably by forcing the system to undergo limit cycle oscillations instead. Friction was not found to alter the stability of any of the systems investigated here as long as its amplitude was low enough not to cause stoppages in the motion.

References

[1] D. S. Woolston, H. L. Runyan, and T. A. Byrdsong. Some effects of system nonlinearities in the problem of aircraft flutter. Technical Note TN 3539, NASA, October 1955.

[2] E. Breitbach. Effects of structural nonlinearities on aircraft vibration and testing. Technical Report AGARD-R-665, AGARD, January 1978.

[3] J. E. Cooper and T. T. Noll. Technical evaluation report on the 1995 specialists' meeting on advanced aeroservoelastic testing and data analysis. In *AGARD-CP-566*, May 1995.

[4] AGARD report 822. Numerical unsteady aerodynamic and aeroelastic simulation, May 1998.

[5] M. Holden, R. E. J. Brazier, and A. A. Cal. Effects of structural non-linearities on a tailplane flutter model. In *International Forum on Aeroelasticity and Structural Dynamics*, Manchester, UK, 1995.

[6] M. D. Conner, D. M. Tang, E. H. Dowell, and L.N. Virgin. Nonlinear behaviour of a typical airfoil section with control surface freeplay: a numerical and experimental study. *Journal of Fluids and Structures*, 11:89–109, 1997.

[7] S. H. Kim and I. Lee. Aeroelastic analysis of a flexible airfoil with a freeplay non-linearity. *Journal of Sound and Vibration*, 193(4):823–846, 1996.

[8] I. Lee and S. H. Kim. Aeroelastic analysis of a flexible control surface with structural nonlinearity. *Journal of Aircraft*, 32(4):869–874, 1995.

[9] S. J. Price, B. H. K. Lee, and H. Alighanbari. Postinstability behaviour of a two-dimensional airfoil with a structural nonlinearity. *Journal of Aircraft*, 31(6):1395–1401, 1994.

[10] S. J. Price, H. Alighanbari, and B. H. K. Lee. The aeroelastic behaviour of a two-dimensional airfoil with bilinear and cubic structural nonlinearities. *Journal of Fluids and Structures*, 9:175–193, 1995.

[11] F. Mastroddi and L. Morino. Limit-cycle taming by nonlinear control with applications to flutter. *Aeronautical Journal*, pages 389–396, November 1996.

[12] G. Dimitriadis and J. E. Cooper. Limit cycle oscillation control and suppression. *Aeronautical Journal*, pages 257–263, May 1999.

[13] S. A. Morton and P. S. Beran. Hopf bifurcation analysis of airfoil flutter at transonic speeds. *Journal of Aircraft*, 36(2):421–429, 1999.

[14] H. Zimmermann. Aeroservoelasticity. *Computer Methods in Applied Mechanics and Engineering*, 90:719–735, 1991.

[15] J. Becker and V. Vaccaro. Aeroservoelastic design, test verification and clearance of an advanced flight control system. In *AGARD-CP-566*, May 1995.

[16] G. J. Hancock, J. R. Wright, and A. Simpson. On the teaching of the principles of wing flexure-torsion flutter. *Aeronautical Journal*, pages 285–305, October 1985.

[17] W. G. Luber. Flutter prediction on a combat aircraft involving backlash and actuator failures on control surfaces. In *Proceedings of the International Forum on Aeroelasticity and structural dynamics*, Manchester, UK, May 1995.

[18] Z. C. Yang and L. C. Zhao. Analysis of limit cycle flutter of an airfoil in incompressible flow. *Journal of Sound and Vibration*, 123(1):1–13, 1988.

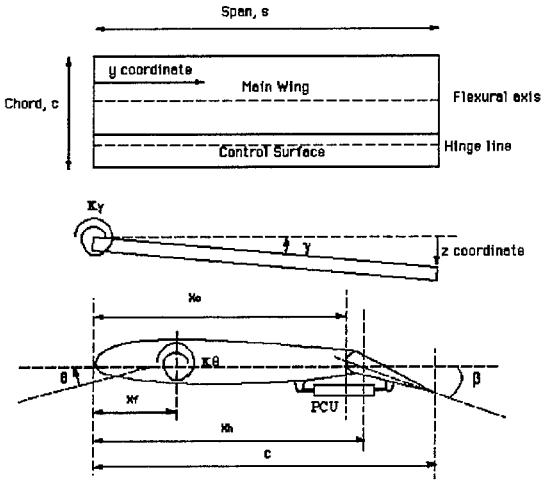

Figure 1: Basic Hancock model with control surface and PCU

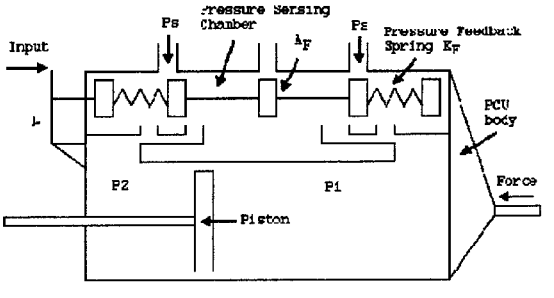

Figure 2: Power Control Unit

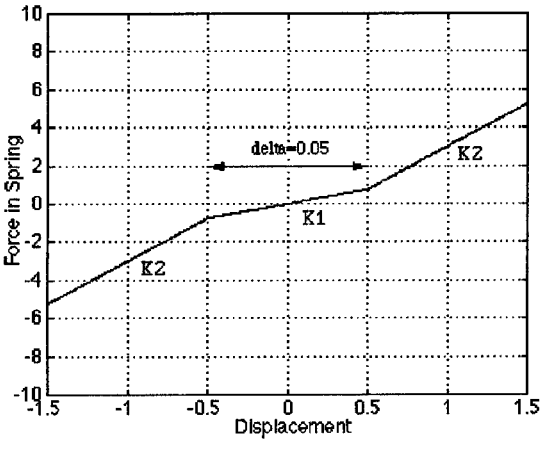

Figure 3: Bilinear stiffness vs displacement

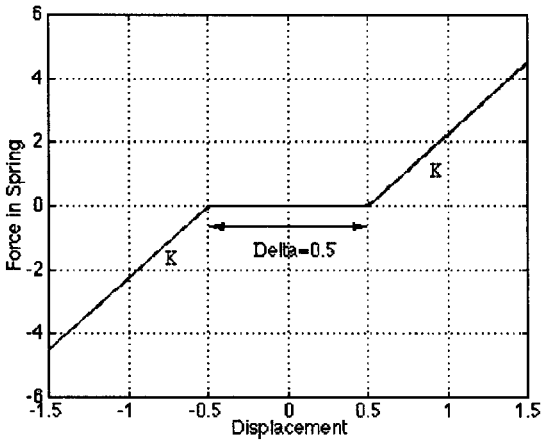

Figure 4: Freeplay stiffness vs displacement

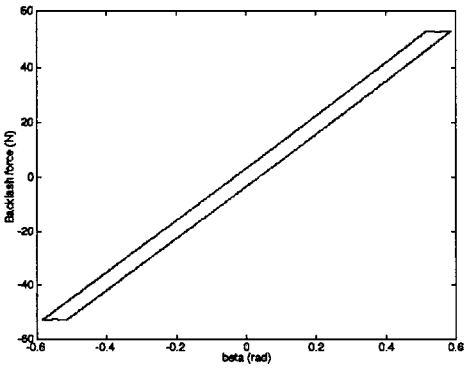

Figure 5: Backlash stiffness vs displacement

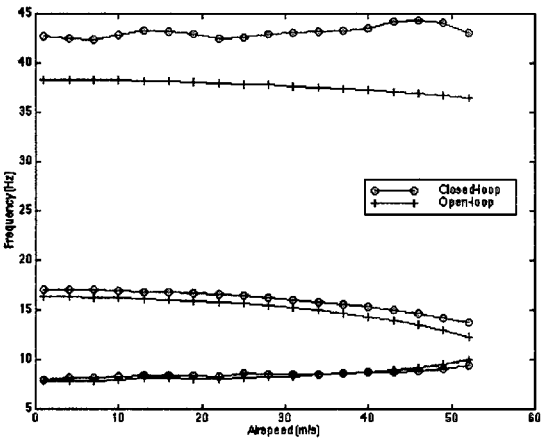

Figure 6: Open and closed loop natural frequencies of linear system

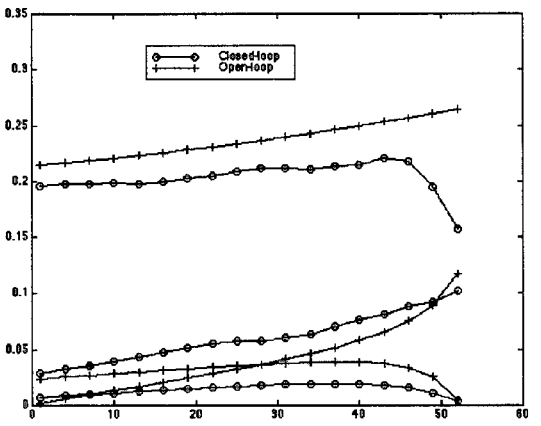

Figure 7: Open and closed loop damping ratios of linear system

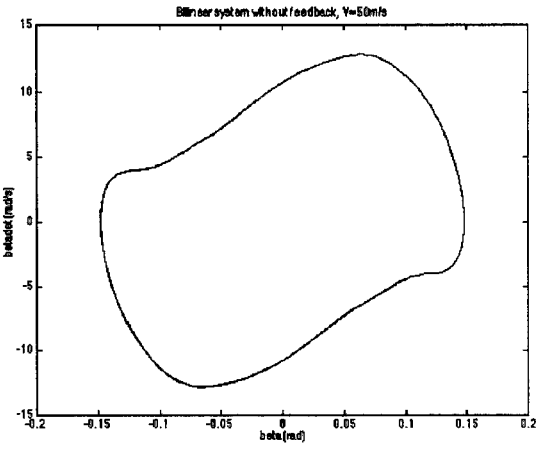

Figure 8: Phase-space diagram of period-1 limit cycle

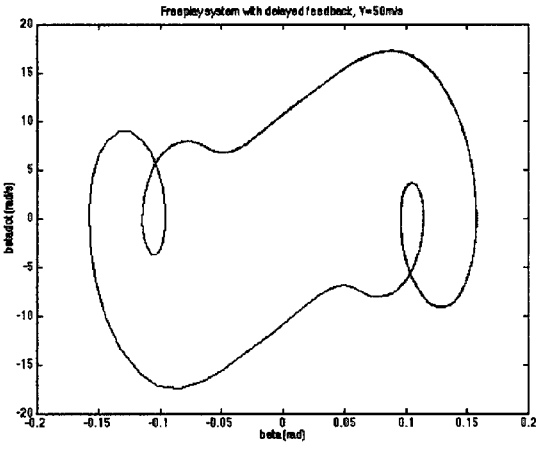

Figure 9: Phase-space diagram of period-3 limit cycle

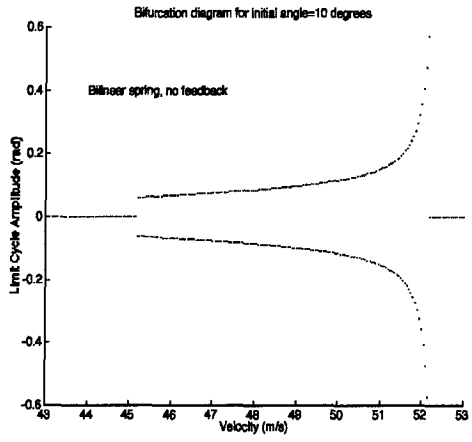

Figure 10: Bifurcation diagram of system with bilinear spring, no feedback

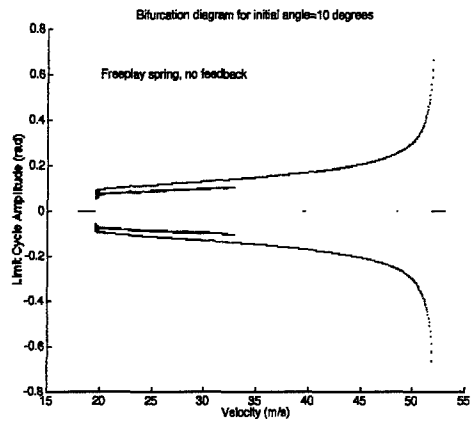

Figure 13: Bifurcation diagram of system with freeplay spring, no feedback

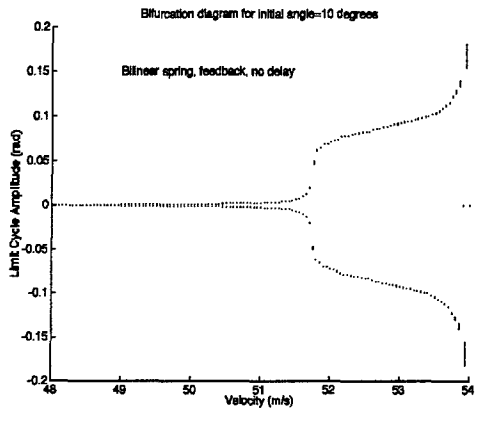

Figure 11: Bifurcation diagram of system with bilinear spring and feedback, no delay

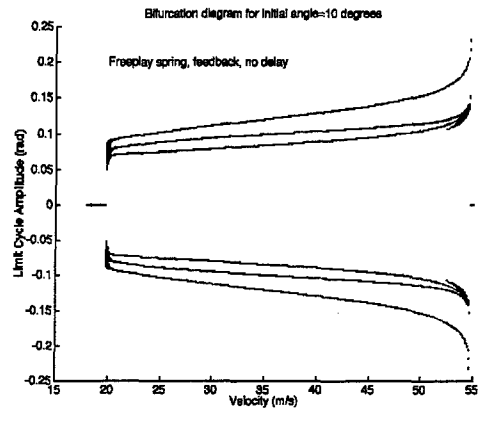

Figure 14: Bifurcation diagram of system with freeplay spring and feedback, no delay

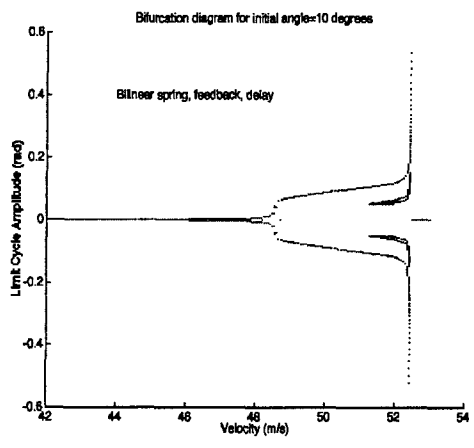

Figure 12: Bifurcation diagram of system with bilinear spring, feedback and delay

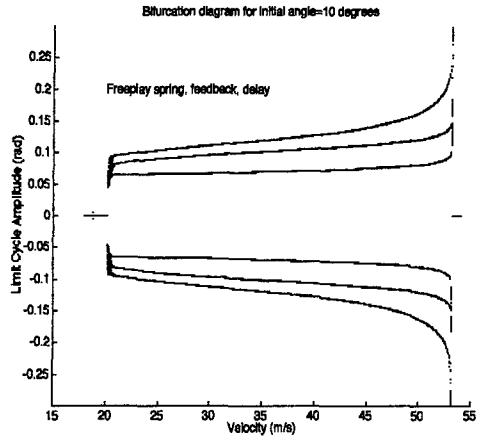

Figure 15: Bifurcation diagram of system with freeplay spring, feedback and delay

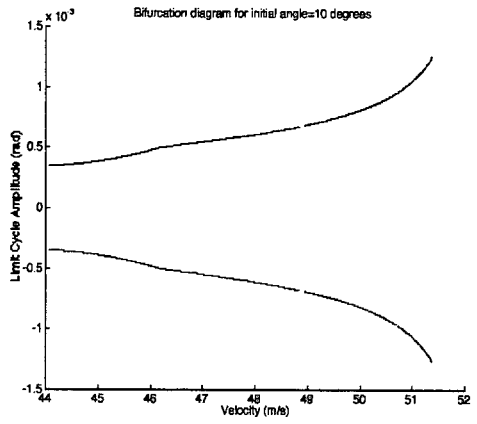

Figure 16: Bifurcation diagram of system with backlash, no feedback

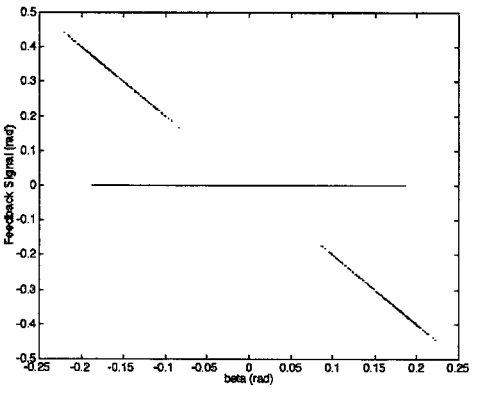

Figure 19: Nonlinear function of control surface pitch limiting control scheme

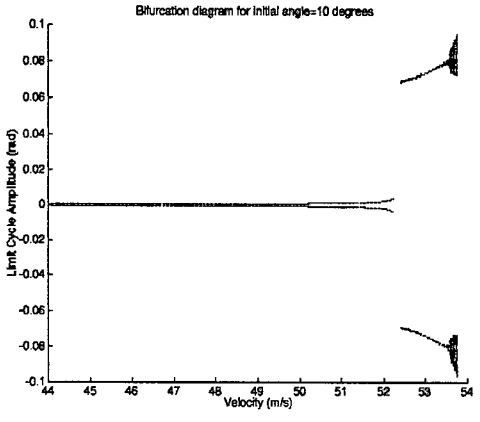

Figure 17: Bifurcation diagram of system with backlash and feedback, no delay

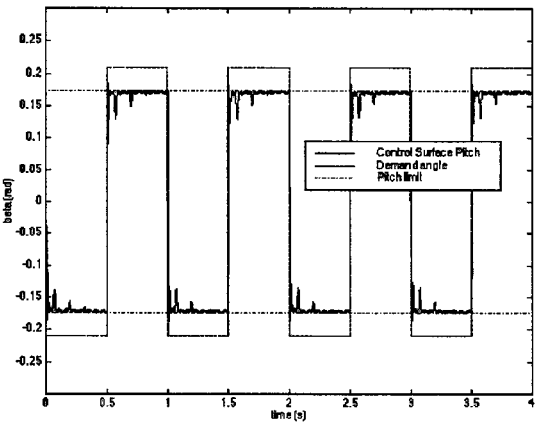

Figure 20: Performance of control surface pitch limiting control scheme

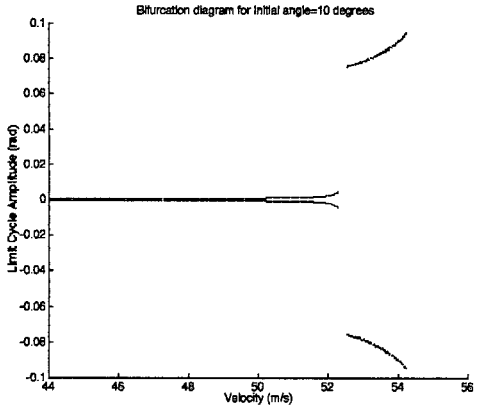

Figure 18: Bifurcation diagram of system with backlash, feedback and delay

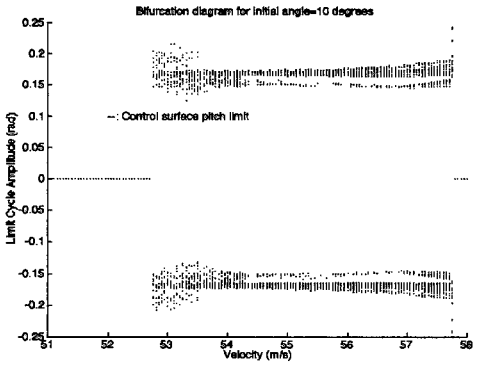

Figure 21: Bifurcation diagram of system with control surface pitch limit

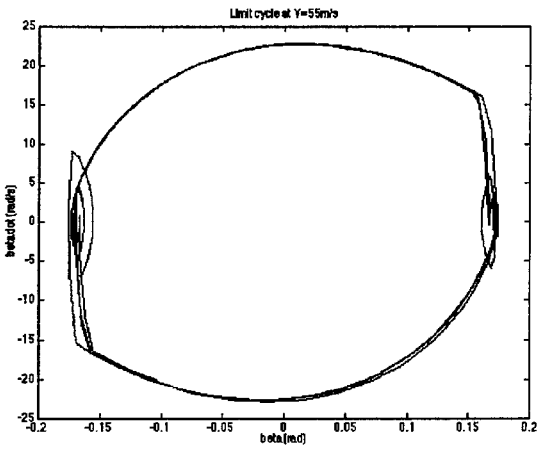

Figure 22: Limit cycle of system with control surface pitch limit at V=55m/s

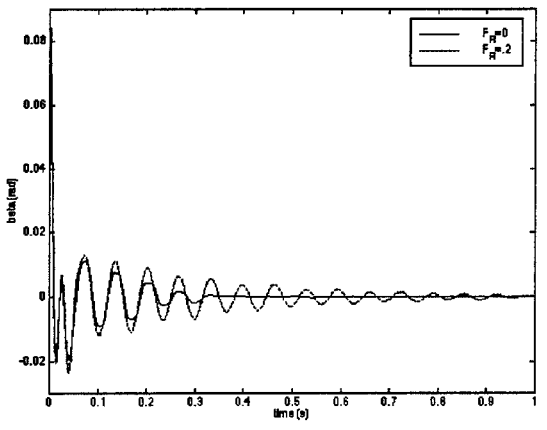

Figure 23: Comparison of responses of frictionless system and system with friction at V=30m/s

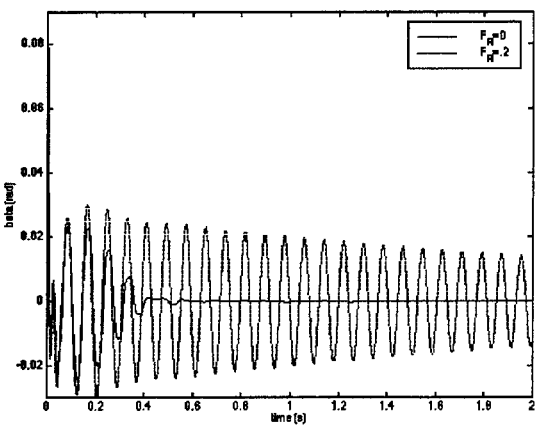

Figure 24: Comparison of responses of frictionless system and system with friction at V=52m/s

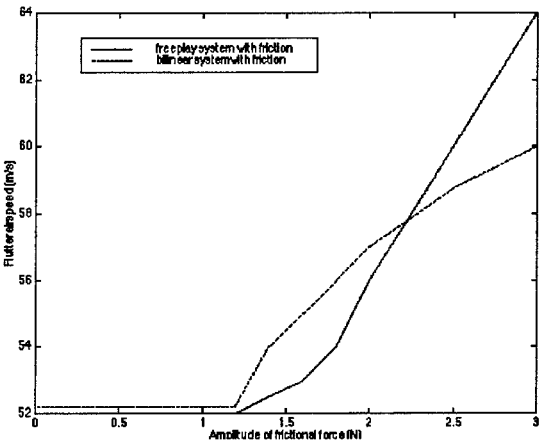

Figure 25: Variation of flutter speed of bilinear and freeplay systems with increasing frictional amplitude

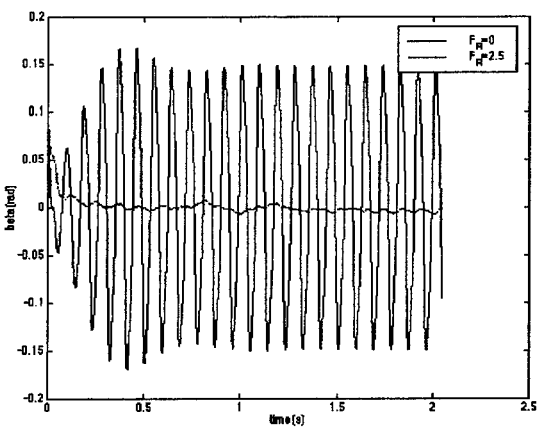

Figure 26: Comparison of responses of bilinear system with and without friction at V=50m/s

METHODE DE CALCUL DU FLUTTER EN PRESENCE DE JEU MECANIQUE ET VERIFICATION EXPERIMENTALE

(FLUTTER ANALYSIS METHOD IN PRESENCE OF MECHANICAL PLAY AND EXPERIMENTAL VERIFICATION)

par
C. PETIAU, B. JOURNEE, E. GARRIGUES
Aviation Marcel Dassault
78, Quai Marcel Dassault
Cedex 300
92552 St Cloud Cedex
France

RESUME

Le calcul de flutter en présence de jeu mécanique intervient pour la certification des timoneries fail-safe des empennages des Falcon.

Une méthode de calcul appropriée a été développée dans notre logiciel ELFINI ; elle est fondée sur :

- une modélisation structurale dynamique Eléments Finis,
- la représentation des forces aérodynamiques instationnaires dans le domaine temps par modèle type Karpel,
- une intégration implicite dans le temps,
- la résolution des jeux et contacts par un algorithme dérivé des techniques d'optimisation quadratique.

Nous exposons la méthodologie de validation expérimentale sur maquette dynamique en soufflerie, en 3 étapes :

- définition, calcul préliminaire, dimensionnement de l'expérience pour vérifier l'observabilité des phénomènes recherchés,
- vérification, calibration du modèle structural par essais statique et de vibration, du modèle aérodynamique à partir de mesures de pressions stationnaires et instationnaires et confrontation des vitesses critiques de flutter calculées/mesurées contact bloqué,
- confrontations calculs/essais de flutter en présence de jeux/contacts.

En procédant à partir des modèles structuraux et aérodynamiques recalés classiquement, la simulation restitue les résultats d'essais à la fois qualitativement (comportement amorti, cycles limites, divergences et quantitativement (niveaux d'accélération).

ABSTRACT

Flutter analysis in presence of mechanical play occurs in the certification of fail-safe linkage of Falcon horizontal stabilizer.

The corresponding calculation method has been developed in our ELFINI software, it is based on :

- a Finite Element structural dynamics model,
- a time domain model of unsteady aerodynamics (Karpel type),
- an implicit time integration,
- the resolution of play/contact by an algorithm derived from quadratic optimization techniques

We expose the experimental verification methodology with dynamic model in wind tunnel, in 3 steps :

- definition, preliminary calculations, sizing of experience for checking observability of studied phenomena,
- verification, calibration of structural F.E. model with static and vibration tests, of aerodynamic model with steady and unsteady pressure measurements, comparison of calculated / measured critical flutter speeds with fixed contact,
- flutter calculation/test comparison in the presence of plays/contacts.

From classically calibrated structural and aerodynamic models, the simulation reproduces test results both qualitatively (damped behaviour, limit cycles, divergence) and quantitatively (acceleration levels).

Paper presented at the RTO AVT Specialists' Meeting on "Structural Aspects of Flexible Aircraft Control", held in Ottawa, Canada, 18-20 October 1999, and published in RTO MP-36.

INTRODUCTION

Le problème de l'analyse du flutter en présence de jeu mécanique se pose régulièrement pour la certification des avions civils. Dans le cas des avions DASSAULT (Mercure, Falcon), il résulte du montage "fail-safe" de la timonerie de calage de l'empennage horizontal ; un élément de secours est monté avec jeux pour ne transmettre les charges qu'en cas de défaillance de l'élément principal (voir planche 1).

Pour traiter ce cas, nous avons développé dès la fin des années 70, et perfectionné depuis, un module d'analyse spécifique dans le cadre de notre système d'analyse structurale et aéroélastique ELFINI. Ce module couple l'analyse dynamique Eléments Finis avec non linéarité de contact avec un calcul d'aérodynamique instationnaire domaine temps ; nous en présentons les grandes lignes au § 2.

La certification d'un avion fondé sur un tel outil a posé dès le départ le problème de sa validation.

On a commencé par des vérifications partielles, en s'assurant :

- de la convergence et de la stabilité des solutions avec les hypothèses de modélisation (variantes/finesse du modèle E.F., nombre et type des degrés de liberté dynamiques, raffinement du modèle aérodynamique),
- du comportement aux limites (contact permanent, jamais de contact) qui doit être recoupé par les calculs classiques,
- de la validité des composants de la méthode de calcul, qui, étant employés dans d'autres problèmes, ont fait par ailleurs l'objet de vérifications expérimentales (exemple contact statique, impact de projectile, interaction avion atterrisseurs, flutter de panneau avec non linéarité de membrane des tuiles de la navette Hermès, ...).

Pour une vérification expérimentale "complète", les essais en vol étant à l'évidence trop risqués, il a été décidé de lancer la campagne de validation par essais sur une maquette aéroélastique dynamique en soufflerie dont nous présentons la démarche et quelques résultats significatifs (§ 3).

Du fait de son coût important, cette opération, supportée par les Services Officiels Français (SPAé), a été menée conjointement entre DASSAULT, AEROSPATIALE et l'ONERA.

2. PRINCIPES DE LA METHODE DE CALCUL DE FLUTTER AVEC JEU

La méthode a plusieurs variantes dont les points communs sont :

- **une modélisation élastique dynamique Elément Fini classique (voir maillage type planche 2)**
- **une réduction de base** (facultative, voir plus loin) pour limiter le nombre de degrés de liberté, variantes base "modale" ou base de "charge" (principe spécifique à ELFINI, voir référence 1), dans tous les cas la base doit être enrichie des déformées statiques pour des charges unitaires aux points de contact.

  Hors modélisation jeux/contact, l'équation de la dynamique, dans la base de calcul, s'écrit :

$$\text{①}\quad [m]\ddot{x}+[C]\dot{x}+[k]x = f.aero + f.autres$$

- **Représentation rationnelle des forces aérodynamiques instationnaires** (approche type Karpel, réf. 2)

  Les forces aérodynamiques instationnaires, calculées normalement par ELFINI dans le domaine fréquence sont approximées (lissage au moindre carré) par une fonction de transfert de la forme :

$$f.aero=[\frac{1}{2}\rho V^2A_o+\frac{1}{2}\rho VsA_1+\frac{1}{2}\rho s^2A_2+\frac{1}{2}\rho VsD(\frac{s}{V}I-R)^{-1}E]x$$

  correspondant à une représentation par équations différentielles :

$$\text{②}\quad f.aero=\frac{1}{2}\rho V^2A_o x+\frac{1}{2}\rho VA_1\dot{x}+\frac{1}{2}\rho A^2\ddot{x}+\frac{1}{2}\rho VDy$$

$$\frac{\dot{y}}{V}-Ry = E\,x$$

  Les matrices A_i représentent des termes de rigidité, amortissement et masse ajoutée, les termes en y (éventuellement négligeables) correspondent à l'effet des degrés de libertés "internes" du fluide, pour la suite nous convenons de rassembler dans x tous les degrés de liberté, ce qui aboutit en réunissant ① et ②à la modélisation du mouvement par un système

d'équations différentielles ordinaires du 2ème ordre du type :

$$③ \quad [M]x'' + [B]\,x' + [K]\,x = f\,autres$$

- **Schéma d'intégration implicite** de l'équation précédente (Newmark, Humbolt, etc ...).

  Les termes en dérivées sont exprimés comme combinaison linéaire de l'état **x(t)** inconnu et des états précédents x_t - $n\Delta t$, l'équation différentielle (3) devient un système d'équations linéaires ordinaires.

$$④ \quad [H]\,x_{(t)} = f\,autres + \sum_{1}^{3ou4} Bn\; x(t - n\Delta t)$$

- **La résolution des jeux et contacts** est traitée comme solution d'un système d'équations et d'inéquations de la forme :

$$[H]\,x = f + [N]\,\alpha$$
Equations d'équilibre aéroélastique

$$[N]_t\,X - r \geq 0$$
Inéquations des jeux

$$\alpha \leq 0$$
Compression aux points de contacts

Elle est menée par une extension de l'algorithme dit de "gradient sphérique" utilisé dans ELFINI pour la résolution des contacts en élasticité linéaire.

La solution est recherchée comme combinaison linéaire de la solution sans contact

$$[H]^{-1}\,f$$

et des déformées pour des réactions de contact unitaire

$$[H]^{-1}\;[Nc]$$

soit

$$x = [H]^{-1}\;[f + [Nc]\,\alpha]$$

Les termes α, réactions de contact (ou multiplicateurs de Lagrange), correspondent aux réactions de contact, ils doivent être négatifs (compression) ou nuls.

Ils sont obtenus par la relation de jeu nul au contact

$$[Nc]t\,X - rc = 0 \quad soit$$

$$\alpha = [\,[Nc]t\,[H]^{-1}\,[Nc]\,]^{-1}\;[\,[Nc]t\,[H]^{-1}\,f - rc\,]$$

Il est à noter que la non symétrie de [H] ne remet pas en cause la validité de l'algorithme du "gradient sphérique" bien que ce dernier soit présenté habituellement (d'où son nom) comme correspondant à une minimisation sous contrainte de forme quadratique (rendue "sphérique" par changement de repère).

Autour des principes de base qui ont été présentés, la méthode a plusieurs variantes :

- sur la modélisation structurale E.F., qui peut être menée sans réduction de base, en particulier quand on est en présence de non linéarités structurales type grand déplacement ou plasticité (voir calcul des tuiles de la Navette Hermès réf. 3).
- sur la modélisation aérodynamique et ses possibilités de recalage expérimental (voir réf. 4), par le couplage direct avec calculs C.F.D. (non linéaires ou linéarisées, voir réf. 5).

3. VALIDATION DE LA METHODE, CONFRONTATION EXPERIMENTALE

L'organisation de cette étude a suivi une trame semblable à celle de l'enchainement conception/calculs/essais d'un projet d'avion, voir planche 3.

- **<u>1ère étape</u> : définition de l'expérience et de la maquette aéroélastique, calculs préliminaires supportant le dimensionnement et la vérification de l'observabilité des phénomènes recherchés.**
  Après avoir envisagé initialement de tester un empennage entier (dérive + P.H.) de Falcon 10 dans la soufflerie S1 de l'ONERA de Modane, on s'est limité à une maquette dynamique générique, de la forme d'un empennage horizontal d'avion type Airbus doté d'une gouverne de bord de fuite, testée dans la soufflerie transsonique S2 de l'ONERA (voir planche 2).
  Le caisson du plan fixe est fixé à la paroi par l'intermédiaire d'un talon situé à l'emplanture du caisson. La gouverne est guidée en rotation par quatre charnières fixées sur le caisson du plan fixe. Le blocage de la gouverne en rotation est assuré par l'intermédiaire d'une lame fixée en extrémité de l'axe d'articulation. Cette lame est bloquée en rotation par un dispositif réglable à butée que l'on peut déplacer le long de la lame. Ce dispositif associé à des lames d'épaisseurs différentes facilement interchangeables permet de régler la fréquence de rotation gouverne sur une valeur choisie. On a adjoint à cette maquette une palette sur le saumon du caisson afin de pouvoir introduire une excitation forcée. Cette palette est commandée par un vérin hydraulique situé dans le caisson du plan fixe.

L'instrumentation d'essai est constituée par un ensemble de 17 ponts de jauge, de 20 accéléromètres, de 5 fibres optiques, de 84 capteurs de pression, ainsi que de deux potentiomètres pour mesurer la rotation de la gouverne.
Cette maquette possède plusieurs degrés de liberté au niveau du blocage de la lame en rotation. Ce blocage est réalisé au niveau de la lame par un dispositif mobile le long de la lame qui permet de modifier la longueur d'encastrement de la lame. Il existe plusieurs lames d'épaisseurs différentes. Ces deux possibilités donnent une grande latitude pour le réglage de la fréquence de rotation gouverne qui pilote le mécanisme de flottement ainsi que la Pi critique.
A ce dispositif de réglage, on a ajouté un dispositif permettant d'introduire un jeu au niveau de l'encastrement de la lame pour étudier les comportements non linéaires en présence de jeu en soufflerie. Un schéma de ce dispositif est présenté planche 2.

Le prédimensionnement de l'expérience a été mené avec le modèle Eléments Finis présenté planche 4.

- <u>2ème étape</u> : **calibration des modèles élastique et aérodynamique classiques, hors effet de jeux,** menée en sous-étapes.

  - **Validation du modèle Elements Finis statique** avec les corrélations calcul-essais des réponses de jauges de contraintes à 12 chargements statiques. Cette corrélation est relativement satisfaisante en dehors de tout recalage (voir planche 5).

  - **Validation du modèle dynamique** (modes propres). Nous n'avons eu à procéder qu'à la seule calibration du coefficient d'encastrement de la lame sur l'axe (indépendante de l'épaisseur et la longueur de la lame) pour obtenir une confrontation calcul essais satisfaisante (voir planche 6).

  - **Validation du modèle aérodynamique** (à Mach 0.6). Elle a été fondée sur la confrontation du calcul aux mesures de pression pour des excitations par braquage de la gouverne en stationnaire et instationnaire (planche 7). Le résultat est conforme à notre expérience habituelle de la méthode des doublets :
    . le calcul prévoit correctement les pressions sur le caisson
    . les pressions de bord d'attaque sont surestimées
    . les pressions sur la gouverne et le moment de charnière sont surestimés d'un facteur 2

  Cette confrontation a confirmé le facteur de correction de 0.5 des pressions gouvernes qui avait déjà été introduit "par expérience" dans les calculs de prédimensionnement. Cette correction a été reconduite pour la suite des calculs.

  - **Validation du modèle de calcul du flutter hors effets de jeux/contacts.**

  Des résultats types de la confrontation calcul essais sont présentés planche 8. Les comparaisons de pressions dynamiques (Pi) critiques et des évolutions des fréquences/amortissements sont satisfaisantes.

  Nous avons aussi mené une vérification par expérience numérique du modèle de rationalisation des forces aérodynamiques instationnaires, le modèle semble quasi exact tant pour la reconstitution des forces généralisée que pour la vitesse de flutter (voir planche 9).

- <u>3ème étape</u> : **confrontation des résultats de flottement non linéaire.**

  Nous en présentons des extraits, planches 10 et 11, concernant un jeu "centré" de 0.1 mm (épaisseur lame 4,5 et 1,5 mm longueur 130 mm).
  Le calcul, comme les essais, permettent d'identifier 3 régimes de fonctionnement : stabilité, cycles limites, divergences. Dans le cas des cycles limites les niveaux d'accélération calculés/mesurés se comparent bien.
  A noter que le domaine de pression génératrice des cycles limites ne coïncide pas avec l'intervalle des pressions critiques gouverne libre - gouverne bloquée ; on peut rencontrer des cycles limites en dessous de la Pi critique gouverne libre et des cycles limites "conditionnels" au-delà de la pression critique gouverne bloquée, en fonction de l'énergie initiale donnée au système.

4. CONCLUSIONS, LECONS A TIRER

La chaine de calculs de modélisation du flutter en présence de jeu mécanique est déjà convenablement validée avec cette première confrontation expérimentale.
Les causes d'imprécision potentielle des calculs n'apparaissent pas devoir venir des parties les plus originales de l'algorithme comme la modélisation dynamique des contacts ou l'aérodynamique instationnaire domaine temps, mais plutôt des

parties "classiques" du modèle intervenant déjà dans le calcul du flutter linéaire, en particulier :

- le modèle Eléments Finis dynamique qui doit être vérifié/recalé sur les essais de vibrations au sol

- le modèle des forces aérodynamiques stationnaires et instationnaires qui doit être recalé, si on le peut sur des essais en soufflerie et surtout sur les essais en vol (voir réf. 4).

C'est d'ailleurs sur l'aérodynamique que nous attendons les principaux progrès des calculs de flutter linéaire ou non linéaire comme ici ; nous remplaçons progressivement les modèles classiques de potentiel aérodynamique traités par singularité par des méthodes Eléments Finis "Euler" nonlinéaires ou "linéarisées" (voir réf. 5). Nous envisageons ainsi une prochaine étape de confrontation calcul-essai dans la zone du transsonique avec la même maquette, cela pour des configurations sans et avec jeu mécanique.

REFERENCES

1 C. PETIAU, S. BRUN
Tendances Actuelles de l'Analyse Aéroélastique des Avions Militaires
AGARD, Conference Proceedings n° 403, Athènes 1986

2 M. KARPEL
Time-Domain Aeroservoelastic Modeling Using Weighted Unsteady Aerodynamic Forces
J. GUIDANCE, Vol 13, N° 1, Jan-Feb 1990, p. 30-37

3 C. PETIAU, A. PARET
Dimensionnement et Qualification Aéroacoustique des Tuiles Hermès
AGARD, Conference Proceedings N° 549, Lillehamer 1994

4 C. PETIAU, E. GARRIGUES, Ph. NICOT
Méthode d'Identification Mathématique des Modèles de Forces Aérodynamiques Instationnaires sur les Essais en Vol, Validation Expérimentale
R.T.O. Specialists' Meeting on Structural Aspects of Flexible Aircraft Control, Ottawa 1999.

5. C. PETIAU, B. STOUFFLET, Ph. NICOT
Aéroélasticité et C.F.D.
AGARD-R-822, Aalborg 1997

PLANCHE 1

ORIGINE DE L'ETUDE

problème de certification de l'empennage

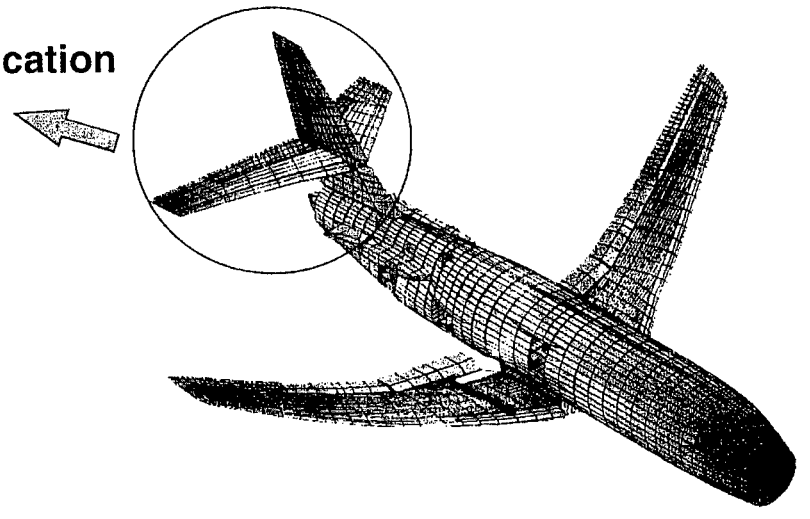

- **Mercure**
- **Falcon 900**
- **Falcon 2000**

- **conception fail-safe de la bielle d'attaque de l'empennage**
- **solution technique comportant un jeu**
- **comportement dynamique non-linéaire**

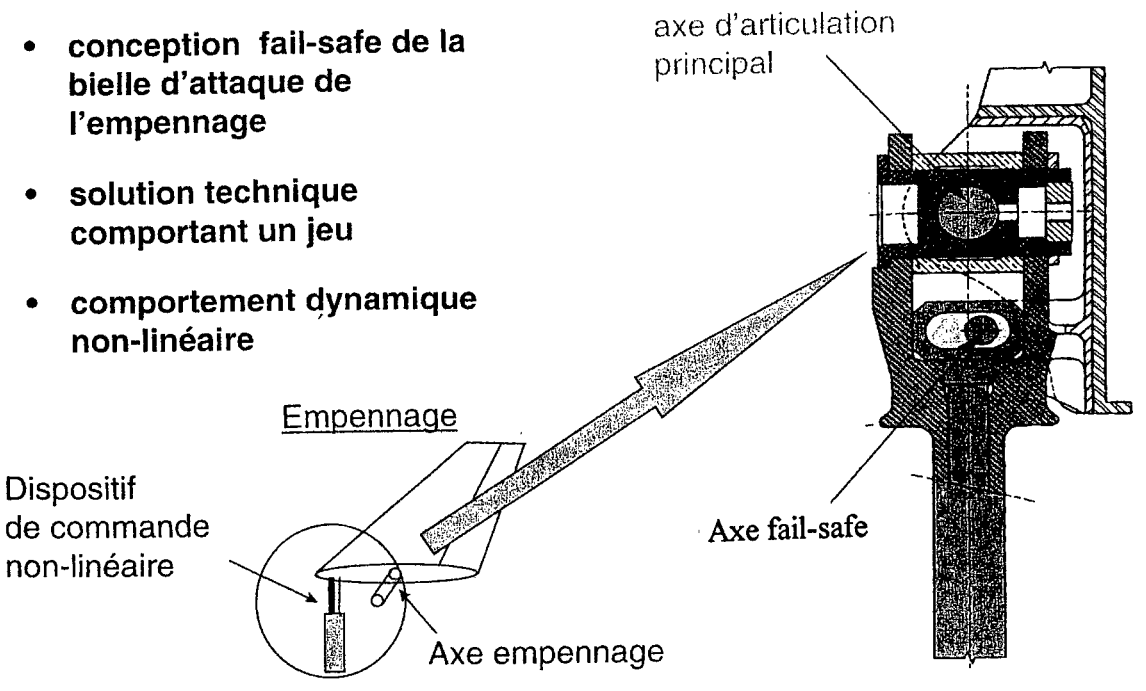

PLANCHE 2

MAQUETTE AEROELASTIQUE D'EMPENNAGE TYPE "AIRBUS" ESSAYE A LA SOUFFLERIE S2 DE L'ONERA

- **Structure de type aéronautique**
- **dispositif de réglage de la fréquence de rotation gouverne**
- **palette d'excitation**
- **encastrement au mur**
- **250 capteurs (pression, jauge, accéléromètre, fibre optique)**

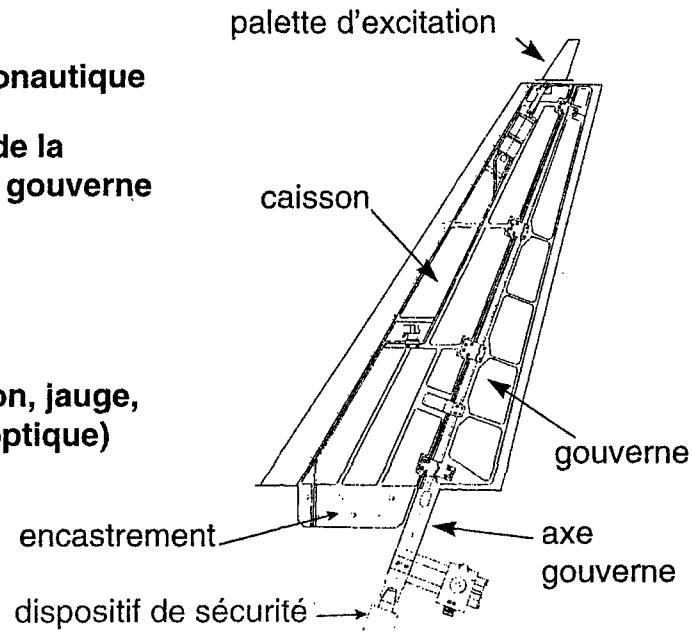

BUTEE A JEU

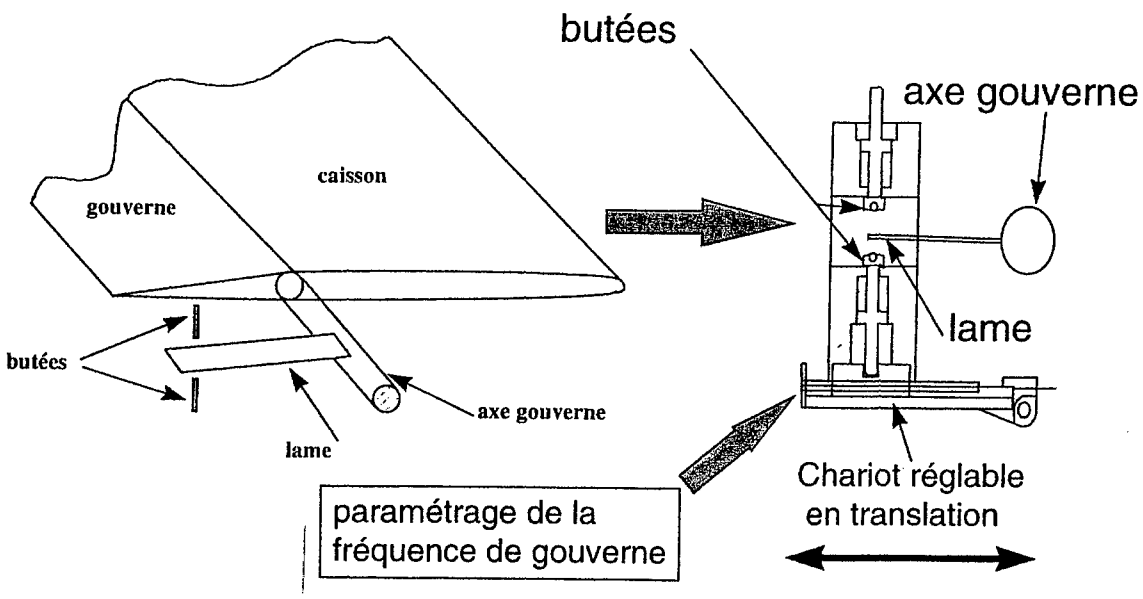

PLANCHE 3

ORGANISATION DE L'ETUDE
SEMBLABLE AU PROCESSUS CONCEPTION / CALCUL / ESSAIS D'UN AVION

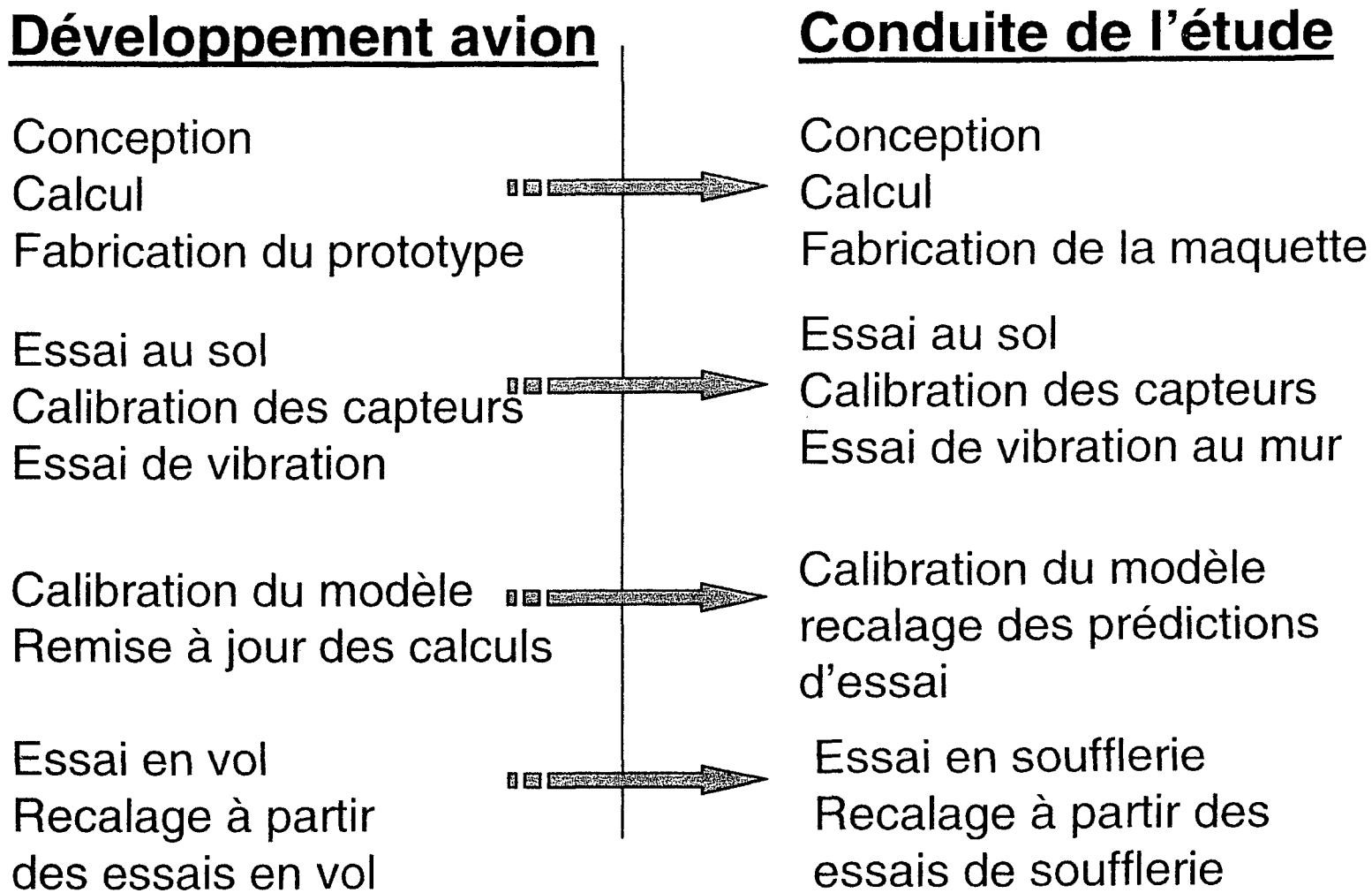

PLANCHE 4

MODELE STRUCTURAL
ELEMENTS FINIS

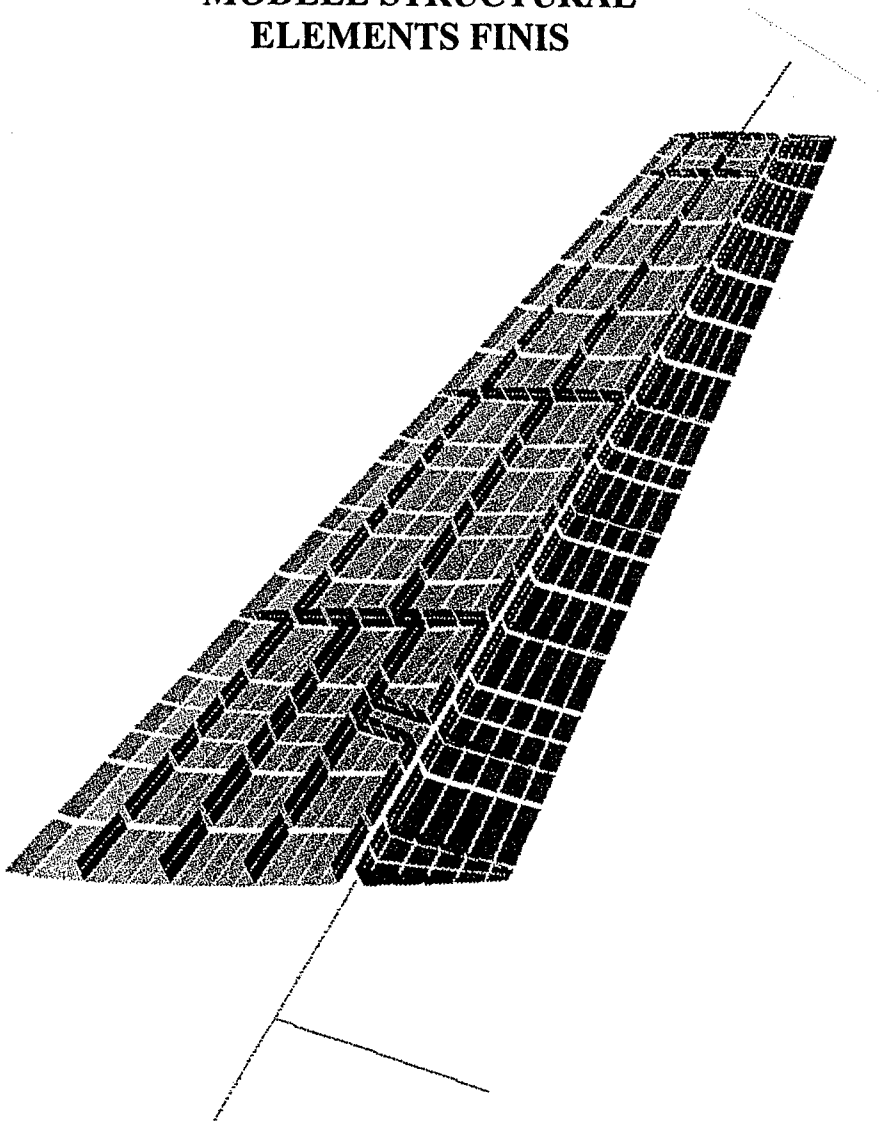

MODELE AERODYNAMIQUE
("DOUBLETS")

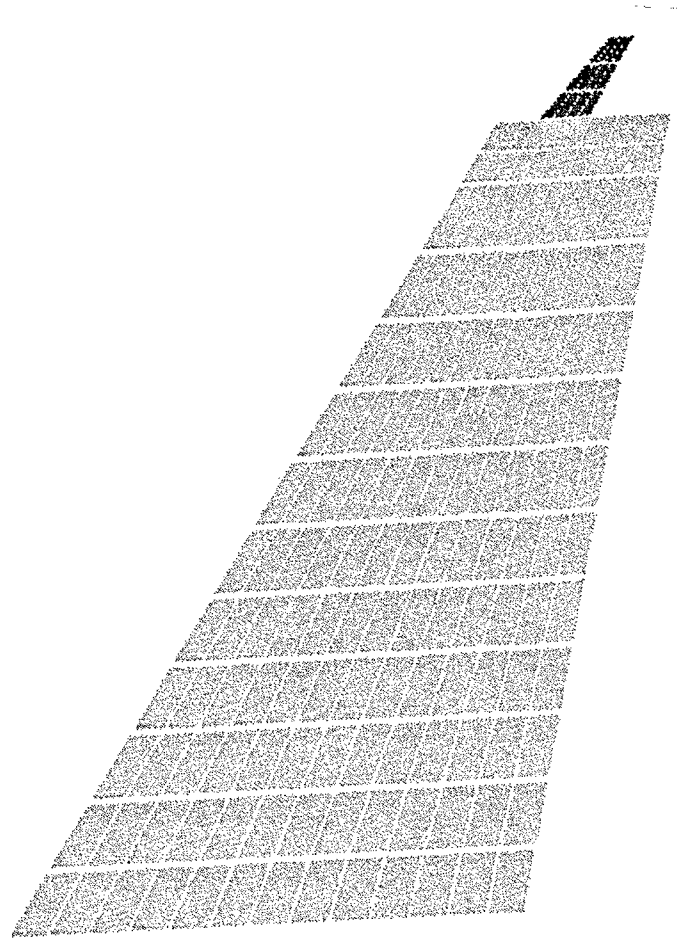

PLANCHE 5

VALIDATION DU MODELE STATIQUE
(MODELE PRELIMINAIRE, MODELE FINAL)

CORRELATION MESURES JAUGES DE CONTRAINTE - CALCUL

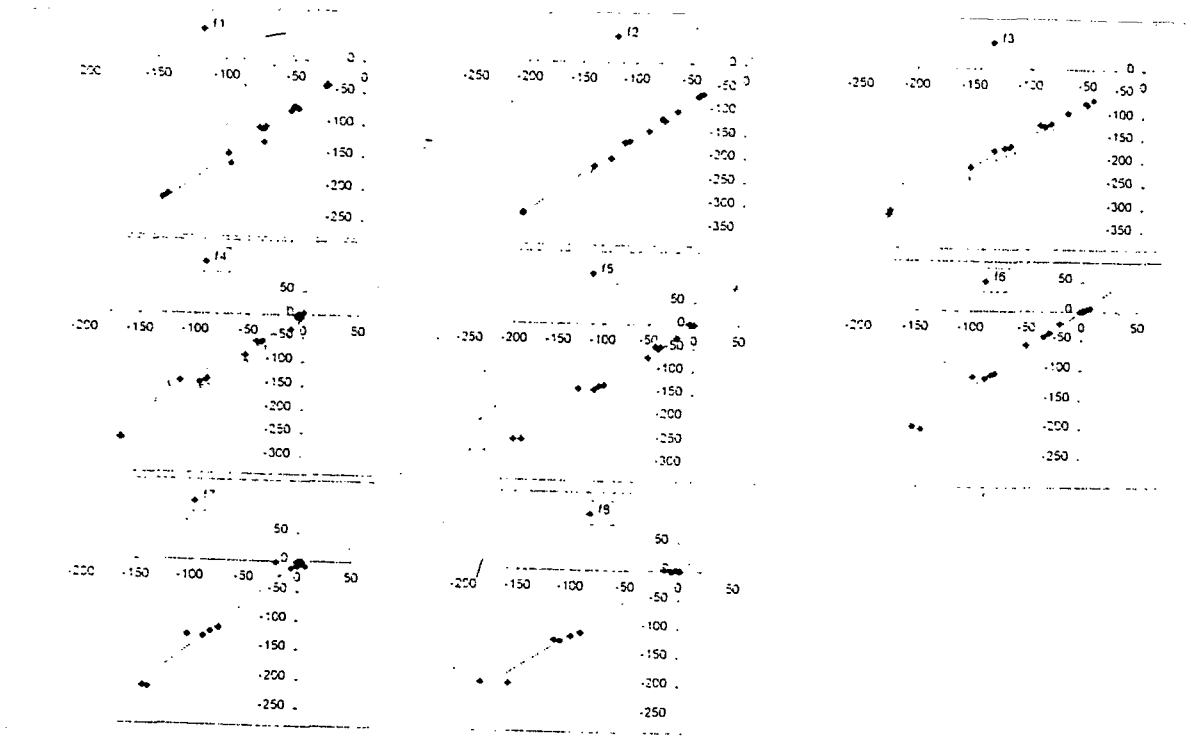

nom et nature de la jauge	r sur modèle initial	r sur nouveau modèle
flexion 1	0.930	0.985
flexion 2	0.995	0.998
flexion 3	0.995	0.998
flexion 4	0.983	0.989
flexion 5	0.990	0.993
flexion 6	0.990	0.993
flexion 7	0.972	0.981
flexion 8	0.985	0.989
torsion 1	0.962	0.976
torsion 2	0.985	0.989
torsion 3	0.939	0.923
torsion 4	0.840	0.865
torsion 5	0.918	0.947
torsion 6	0.676	0.719

PLANCHE 6

VALIDATION / RECALAGE DU MODELE DYNAMIQUE (RECALAGE DU SEUL COEFFICIENT D'ENCASTREMENT DE LA LAME)

Valeurs des fréquences de flexion empennage **mesurées** pour des longueurs de lame variables.

Epaisseur \ longueur de lame	l = 30 mm	l = 55 mm	l = 80 mm	l = 105 mm	l = 130 mm
1.5			31.4	31.1	30.9
4		28.9	29.0	29.0	29.1
4.5	28.1	28.9	29.2	29.3	29.3

Valeurs de fréquence de flexion empennage **calculées** sur **modèle théorique recalé** les mêmes longueurs de lame que le tableau 3.

Epaisseur \ longueur de lame	l = 30 mm	l = 55 mm	l = 80 mm	l = 105 mm	l = 130 mm
1.5	32.4	31.8	31.4	31.2	31.1
3	27.0	27.9	28.1	28.0	27.7
4	28.1	28.9	29.2	29.3	29.4
4.5	28.3	29.1	29.4	29.5	29.6

PLANCHE 7

MODELE AERODYNAMIQUE INSTATIONNAIRE
COMPARAISON ESSAIS - CALCULS DES PRESSIONS
(Calcul intégrant les effets d'aéroélasticité dynamique)

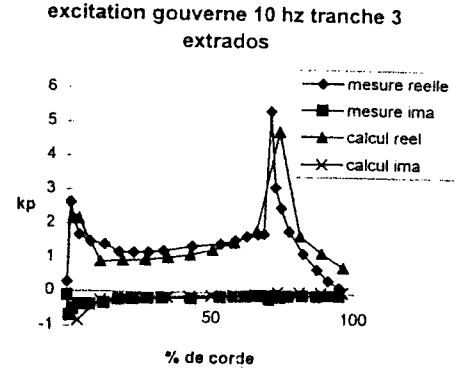

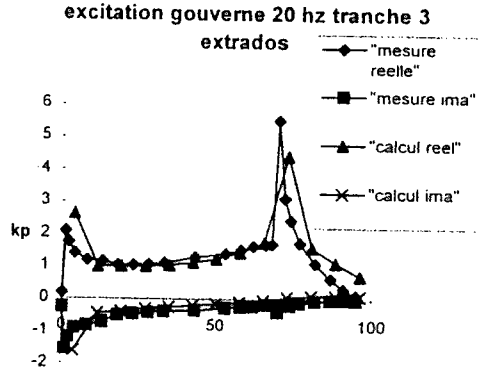

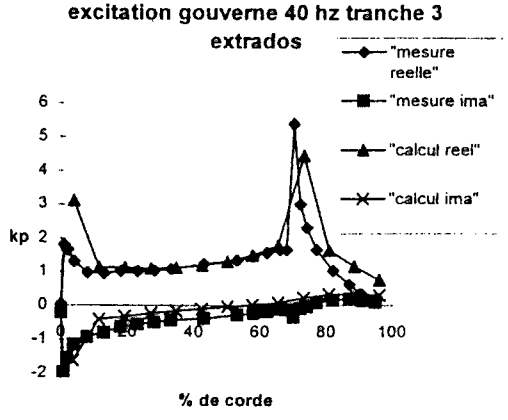

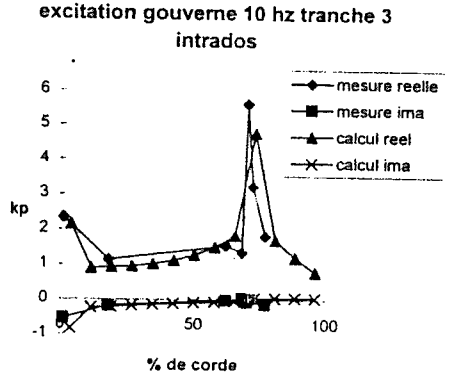

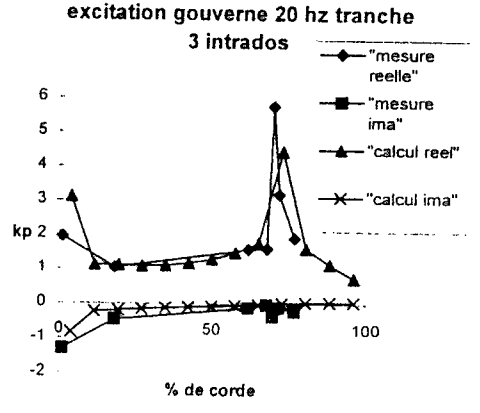

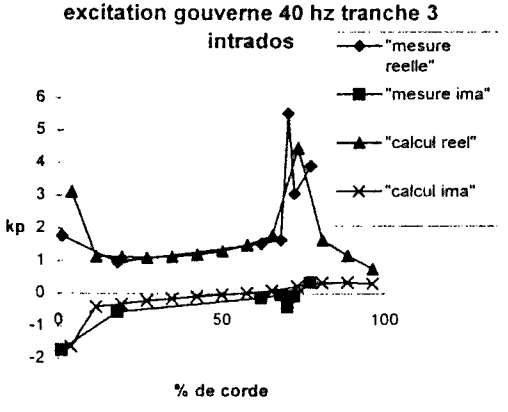

⇒ CORRECTION FACTEUR 0.5 SUR LES PRESSIONS GOUVERNE

PLANCHE 8

PREVISION DE FLUTTER SANS EFFETS DE JEU / CONTACT
COMPARAISON CALCUL - ESSAIS
(Modèles structural et aérodynamique recalés)

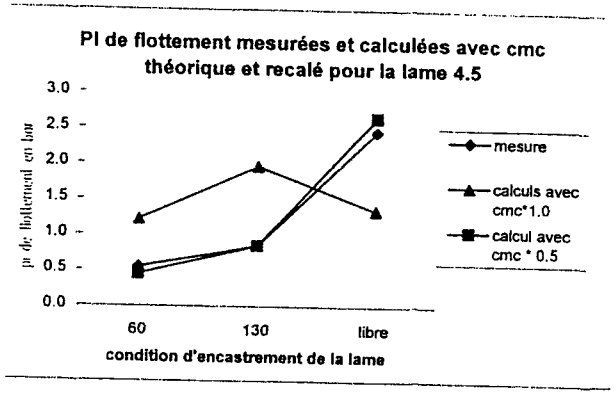

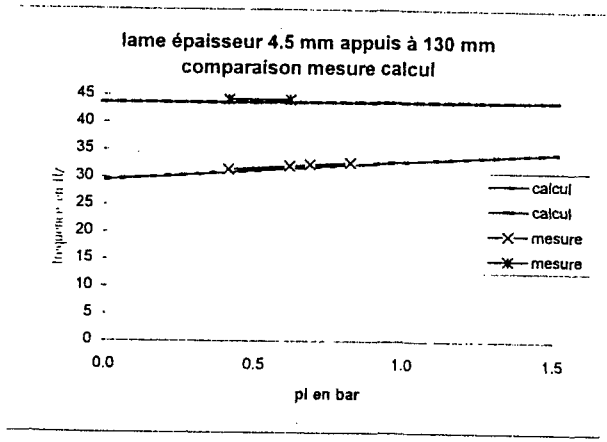

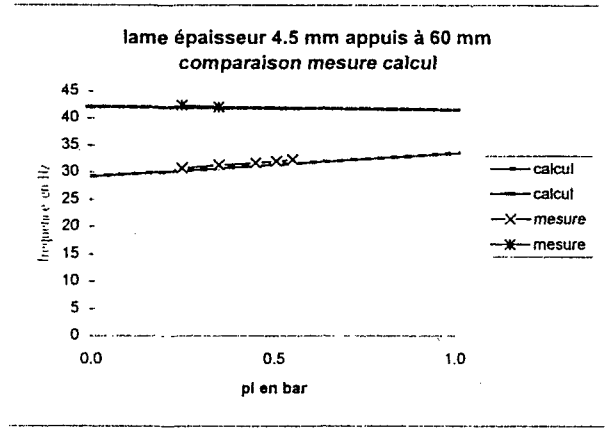

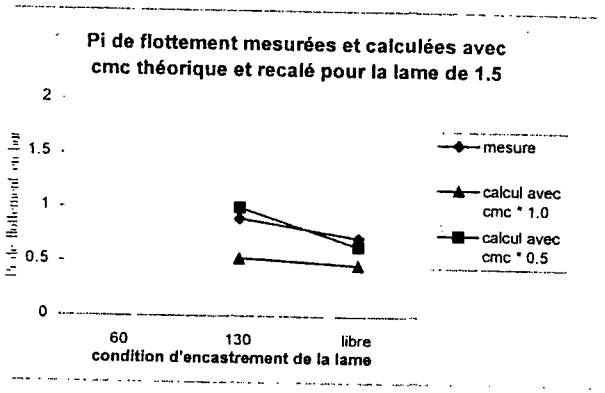

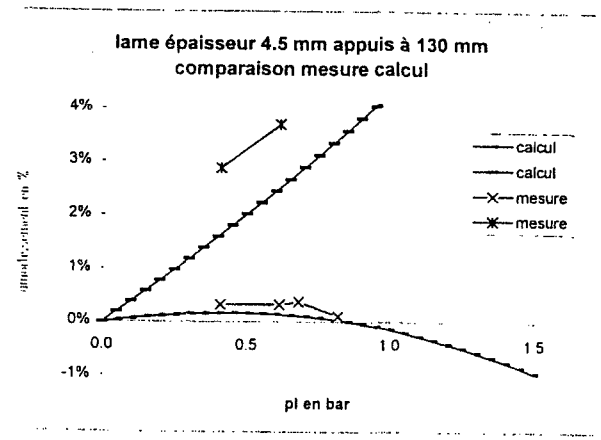

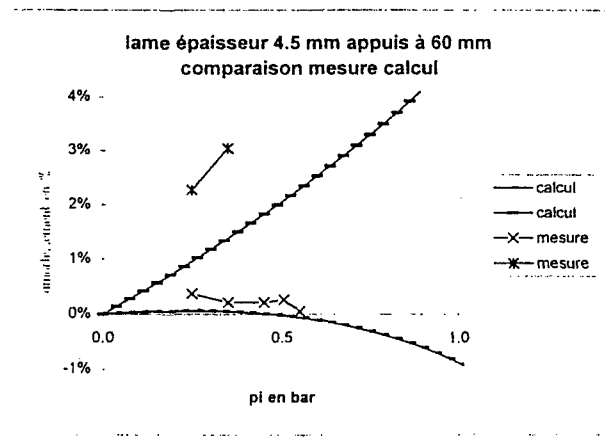

PLANCHE 9

LA RATIONALISATION DES FORCES AERODYNAMIQUES INSTATIONNAIRES EST EXACTE

FREQUENCES

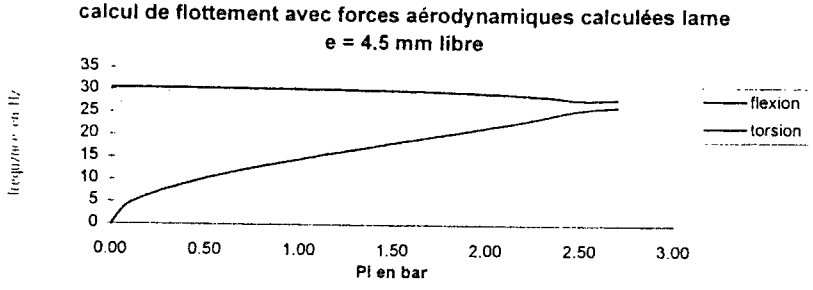

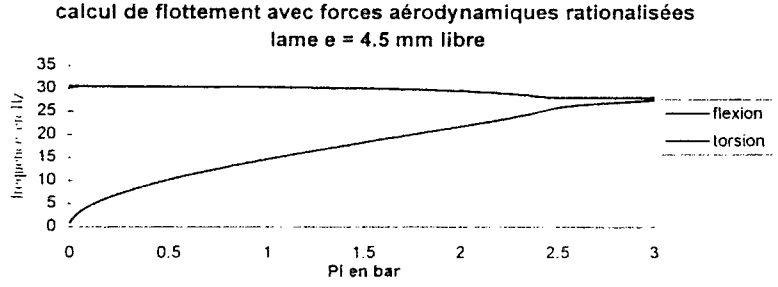

AMORTISSEMENT

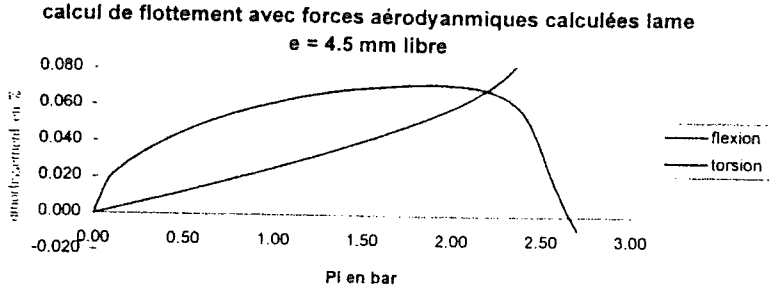

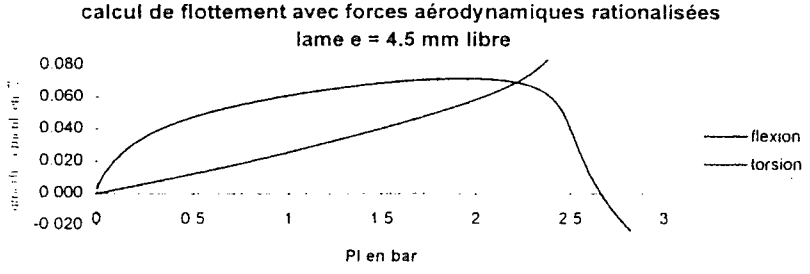

PLANCHE 10

SYNTHESE ETUDE DE FLUTTER AVEC JEUX

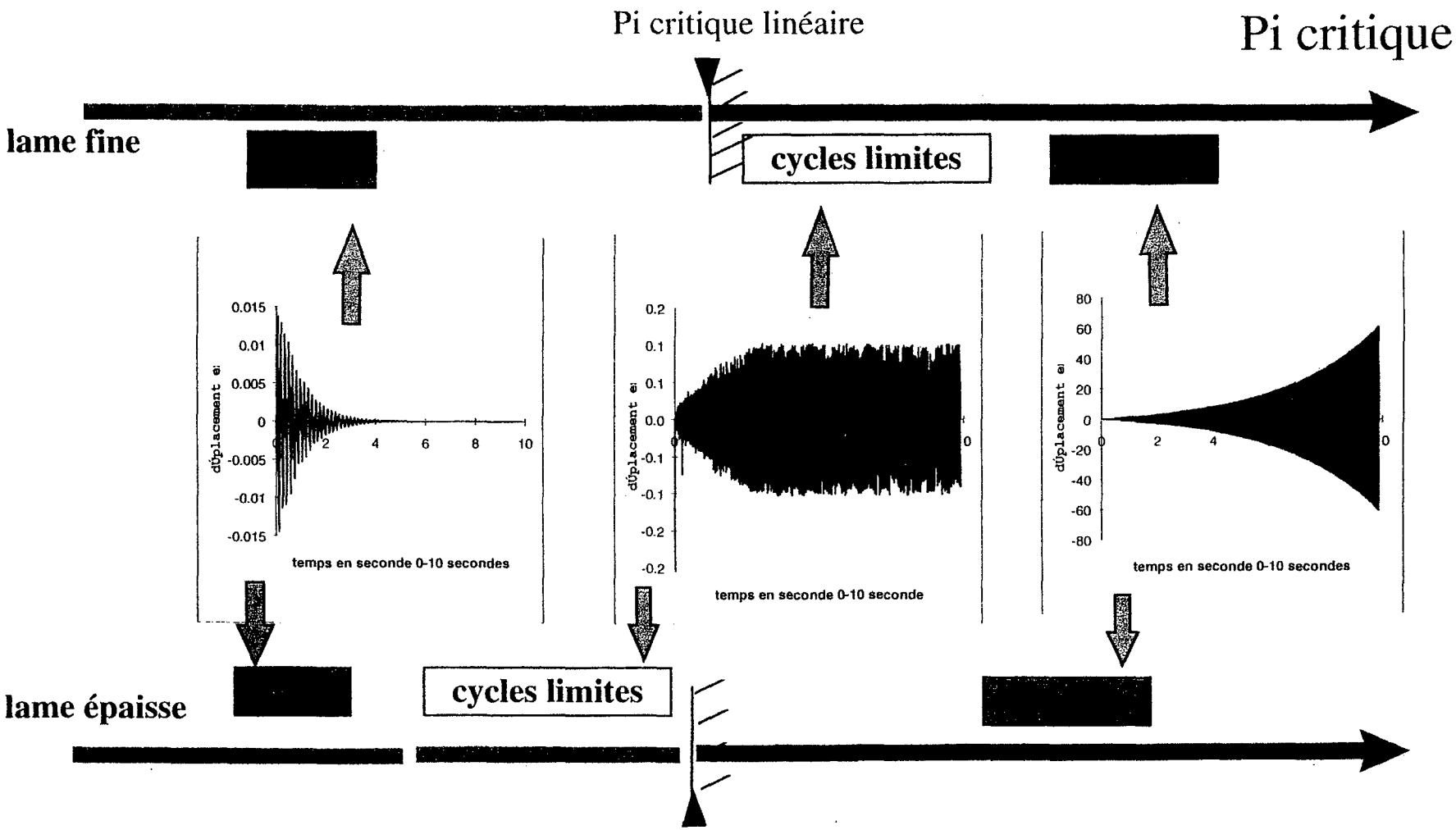

Amplitude des cycles limites : comparaison calculs-mesures

- **bonne prise en compte des variations liées à la pression génératrice**

- **bonne prise en compte des variations liées aux mécanismes de flottement**

évolution de l'amplitude accélérométrique du capteur d'emplanture gouverne

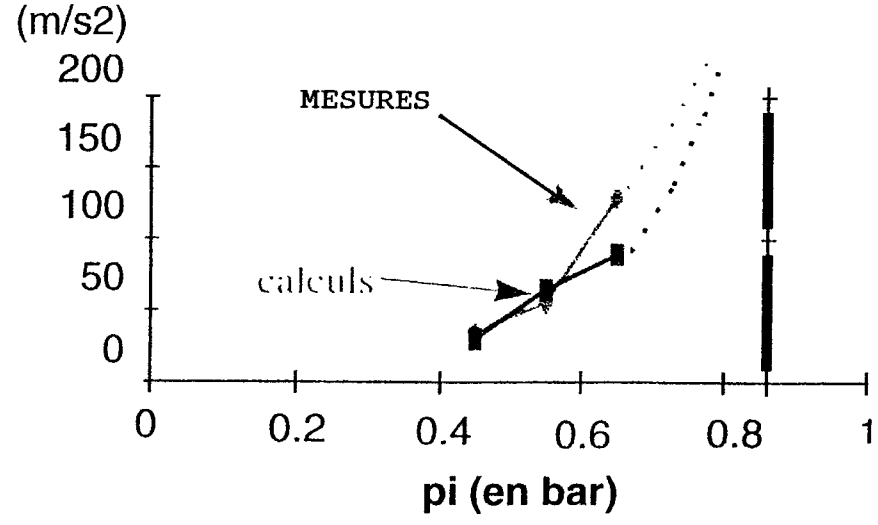

(jeu 0.1 mm appui à 130 mm)

AN INTEGRATED PROCESS FOR DESIGN AND VALIDATION OF FLIGHT CONTROL LAWS OF FLEXIBLE AIRCRAFT STRUCTURE

Michel Lacabanne, Marc Humbert

Aerospatiale Matra Airbus
316 route de Bayonne, 31060 Toulouse, France

Abstract

This paper recalls some problems which need to be carefully studied in relation with flexibility of large transport aircraft and control laws design. The evolution of flexible aircraft models is described, and it is shown that the evolution of the FCS design process is coming along with more interdisciplinary models. The FCS validation process is supported by models, and by flight tests. The need to perform an in flight identification of structural modes is explained, as well as the methodology which could be used for future very large transport aircraft.

Introduction

Electronic Flight Control Systems (EFCS) have been implemented on AIRBUS subsonic civil aircraft since A320. The Airbus family has grown, mainly with derivatives of A320, and also with long range twin and four engine aircraft. From this date, EFCS have been embodied on all Airbus types civil transport aircraft. The increasing size of aircraft has emphasized the effects of structural flexibility on general aircraft performance. The evolution of aircraft features in combination with the implementation of EFCS is leading to promote interdisciplinary ways of working and to develop new tools, wherever necessary, in order to better predict the overall aircraft performance and to obtain the best achievable design.

This paper shows that the evolution of the FCS design and validation process strongly depends on the progress made with the flexible aircraft models. The flexible aircraft models upgrade the flight mechanics models, and, according the assumptions made, they can be used for FCS design or validation. The use of such models helped FCS designers to implement active control of flexible modes. For this reason, if high performance of the controller is looked for, progress will have to be made in order to achieve an in flight identification of structural and flight mechanics modes consistent with the performance level which is aimed.

List of notations

$[M]$ $[B]$ $[K]$ Mass, damping and stiffness matrices
$[\mu]$ $[\beta]$ $[\gamma]$ Generalized Mass, damping and stiffness matrices
$[\phi]$ modal displacement matrix
$\{X\}$ structure displacement vector, or state vector
$\{q\}$ generalized coordinated vector
$[GAF]$ Generalized aerodynamic forces matrix
$[GAF_\delta]$ Generalized aerodynamic forces matrix associated with control surface rotation
δ control surface rotation
$\{U\}$ input vector (control surface rotation...)
$\{Y\}$ output vector (sensor accelerations, speed...)
$[A]$, $[B]$, $[C]$, $[D]$ state space model matrices

Typical FCS design problems in relation with structural flexibility

A large number of problems need to be solved during FCS design. Some of them are directly linked with the aircraft structural flexibility. Three typical FCS design problems are briefly reminded below:

- **Interaction of Control, with Aerodynamic and Structure (ICAS)**

The FCS designers must be careful in order to avoid the Interaction of Control, with Aerodynamic and Structure in the whole flight domain, for all mass configurations, slats and flaps configurations.

Paper presented at the RTO AVT Specialists' Meeting on "Structural Aspects of Flexible Aircraft Control", held in Ottawa, Canada, 18-20 October 1999, and published in RTO MP-36.

Indeed, the direct consequence of ICAS is the modification of "in flight" structural modes damping. A damping decrease of some structural modes can be observed.
ICAS should not give zero damping for any of the structural mode and a sufficient stability margin should exist. While flutter of modern civil transport aircraft, which is due to Interaction of Aerodynamic and Structure is likely to happen at high speeds in the transonic regime, on contrary ICAS, can occur at low speeds and Mach numbers according to the FCS tuning (gain and phase values).

- **Oscillatory Failure Loads (OFL)**

The oscillatory failures on control surfaces are another important concern. In some failure cases (for example, actuator bad functioning or control laws failure), the FCS do not operate properly.

The Control surfaces can oscillate at a fixed frequency and produce high structural loads, except if special care is taken during structural and FCS design (for example, monitoring the oscillations which would impair structural integrity, then switch FCS to a safe configuration).

- **Aircraft Pilot Coupling (APC)**

The Aircraft Pilot Coupling, which is the coupling of the pilot with Aircraft structural modes through the FCS, is not acceptable for handling.
APC can generally be prevented thanks to appropriate filtering in the feed forward path.

Evolution of Flexible aircraft modelizations: from the flutter equations to the integral model

The history of aeronautical progress demonstrated that new technologies have always pushed the need for new models; the aeroelasticity field is a clear example of this link. Aeroelastic models have deeply evolved recently to handle the new issues raised by very flexible, new large transport aircraft, and the integration of digital technology into the flight control system. This kind of evolution of the aeroelastic models developed by AM-Airbus for Airbus programs development and certification is described below.

- **The flutter equation in the frequency domain and its improvement to cope with the electronic flight control system apparition**

The first historical model of the flexible aircraft consists in the flutter equations expressed in the frequency domain. This model is built from a structural model and an aerodynamic model linked together to describe coupling between structural and aerodynamic forces. It is commonly written in the normal modal basis, driving the following well-known equation:

$$-\varpi^2 [\mu]\{q\} + (j\varpi)[\beta]\{\dot{q}\} + [\gamma]\{q\} = \bar{q}.[GAF]\{q\} \quad (1)$$

The fact that this equation is named "the flutter equation" may lead to think that all of the aeroelastic science lies in this single equation. One has to admit that this statement is not so false. This model is dedicated to analysis of the stability of the structural forces – aerodynamic forces coupling that is still the first concern of aeroelasticians, and is therefore still widely used today. Moreover, this historical model is still living, and has known many evolutions to integrate the best structural and aerodynamic data available, from the first finite element models in structure and aerodynamics, to today's last unsteady aerodynamic transonic codes.
However, today's flexible aircraft challenges can not be addressed using this only model.
The first evolution of it was driven by the EFCS integration that requires pushing forward this stability model into an input – output model. A flexible aircraft model describing the dynamics between control surfaces movements to control law sensors was required and derived by adding few terms to model (1):

$$\left.\begin{array}{l} -\varpi^2 [\mu]\{q\} + (j\varpi)[\beta]\{\dot{q}\} + [\gamma]\{q\} = \\ \ldots \bar{q}.[GAF]\{q\} + \bar{q}.[GAF_\delta].\ \{\delta\} \\ \{Y\} = [\phi].\{q\}\ or\ (j\varpi).\ [\phi].\ \{q\}\ or\ -\varpi^2.[\phi]\{q\} \end{array}\right\} \quad (2)$$

The aeroelasticians were then able to analyse EFCS effects on flexible mode stability by introducing a control law model in a linearized form, in the frequency domain, into the model (2):

$$\{\delta\} = H(j\varpi).[Y]$$

- **The time domain approximation of unsteady aerodynamic forces; the aeroelastic model in the state space form and its derivatives**

Because the unsteady aerodynamic forces are easily computed in the frequency domain only, the previous models are limited to the frequency domain only. This barrier was broken in the 70's by the proposal of a time domain approximation of the unsteady aerodynamic forces:

$$[GAF(M, \varpi/V)] \approx [gaf(M, p)] \quad p = j.\varpi$$

Where

$[\mathrm{GAF}(\mathrm{M}, \varpi/\mathrm{V})]$, *p rational approximation of the GAF matrix*

Two methods are offered to carry this approximation; the Roger's approximation or the minimum state method (Ref 1 and 2). Using one of these, the model (2) can be turned into a time domain model. These approximations open the aeroelasticians to some of the special features of the time domain simulations: comparisons between flight test and model time histories, analyses of some non-linearities (structure, control system...).
Moreover, the time domain aeroelastic model can then be easily expressed in the state space form:

$$\left.\begin{aligned}\{\dot{X}\}&=[A]\{X\}+[B]\{U\}\\ \{Y\}&=[C]\{X\}+[D]\{U\}\end{aligned}\right\} \quad (3)$$

The state space form may be regarded as a standard of dynamic system modelization, around which a large number tools have been developed by the automaticians community for analyses, simulation, reduction, and control.

The state space formulation was a really strong evolution in flexible aircraft modelization. Thanks to its well known form, it created the basis for an interdisciplinary modelization of the flexible aircraft, and an efficient communication tool between aeroelasticians and specialists from other fields (flight mechanics, control law design, simulation...), who became involved in the structural dynamics issues.

The first example of interdisciplinary modelization around the flexible aircraft was the introduction of some flight mechanics behaviour informations into the state space aeroelastic model (3). This was achieved and used in AM-Airbus following two axes: The first one consists in taking into the normal modal basis of (3) the rigid body modes. This approach is commonly used for dynamic loads computation. Using the same formulation of (3), the model is now extended by some flight mechanics representation; when doing so, care must be taken to insure community with already existing flight mechanics models. A second approach consists in putting the aeroelastic model (3) together with a flight mechanics model also derived in the state space form, by simply adding the outputs of both models.

$$\left.\begin{aligned}&\text{Approach 1:}\\ &\text{Model (3) with } [\phi]=\left[\phi_{rigid}\ \ \phi_{flexible}\right] \Rightarrow \{X\}=\begin{Bmatrix}X_{rigid}\\ X_{flexible}\end{Bmatrix}\\ &\text{Approach 2:}\\ &\text{Model (3) together wit flight mechanics state space model}\end{aligned}\right\} (4)$$

- **Coming to an interdisciplinary flexible aircraft model: the integral model**

With the development of new very flexible aircraft, together with the introduction of active flexible mode control into the flight control system of Airbus aircraft, AM-Airbus felt the need for pushing further the development of a new multidisciplinary modelization of the flexible aircraft.
Models (4) present a first level modelization of the flight mechanics; however this representation is not suitable for a complete simulation in the whole flight envelope, as it is only a simplified, linearized model. Moreover, the approach (2) assumes no dynamic couplings between flight mechanics and structural dynamics modes, an hypothesis that is endangered with new very large aircraft that exhibits a reduced frequency separation between flight mechanics and first with flexible modes, whereas approach (1) raises the community problems mentioned above.
To pass through these limitations Aérospatiale developed an integrated model that joined together the best representative models in aeroelasticity and flight mechanics. This model is also upgraded by a load model, as the load analysis process showed a strong dependency with flight mechanics, flight control system, and structural dynamics fields. The flight mechanics model is identical to the ones used in flight simulators, and is therefore valid for simulations in the whole flight envelope. The structural dynamics model is derived from the state space aeroelastic model (3); a specific Mach number and speed interpolation procedure has been incorporated to match its behaviour with the actual flight condition. Coupling equations between flight mechanics and structural dynamics are added for a proper description of the first flexible mode responses. The load model runs a monitoring of about fifteen loads of special interest, during all of the simulation:

$$\left.\begin{aligned}&\{\dot{X}\}=f(X,U,\ flexible\ behaviour)\\ &\text{Flight mechanics model}\\ &\{\dot{X}_{flexible}\}=\begin{matrix}[A\ (Mach,\ speed)]\ .\ \{X_{flexible}\}\\ +\ [B\ (Mach,\ speed)]\ .\ \{U,\ rigid\ behaviour\}\end{matrix}\\ &\text{Aeroelastic model}\\ &\{loads\}=f'\ (X,U)\quad \text{Loads model}\end{aligned}\right\} \begin{matrix}(5)\\ \text{intégral}\\ \text{model}\end{matrix}$$

This interdisciplinary model is named "the integral model", and is dedicated to the flight control system validation. It can be run in differed time on a desk simulator, as well as on real time on a development simulator, with a realistic cockpit environment.

- **The other way in aeroelastic modelling : CFD / FEM time domain coupling**

The evolutions of flexible aircraft modelizations described above were mostly required by the implementation of the EFCS. Aside from these motivations is now growing the simulation in the time domain of a CFD code together with the dynamic finite element model of the structure. The objective of such procedures is to make aeroelastic analyses inherit the progress of last transonic, unsteady aerodynamic codes.

$$\left.\begin{aligned}&[M]\{\ddot{X}\}+[B]\{\dot{X}\}+[K]\{X\}=Faero\\ &Faero=fn(X)\end{aligned}\right\} \quad (6)$$

These new modelizations offer promising progresses in the flutter analyses of large transport aircraft flying in the transonic regime. However, such modelizations require high computationnal capabilities and are today only dedicated to some flutter analyses at high mach number. However, some results of these time domain analyses are incoporated in a linearized form in the aeroelastic models already mentioned.

Summary of flexible aircraft modelizations Capabilities

Model / Analysis	(1) Flutter equations in the frequency domain	(2) Flutter equations with input / output definitions	(3) Structural dynamics in the State Space form
Aeroelastic Stability	X	X	X
Aeroservoelastic stability		X	X
Active mode Control law design			X
Integrated control law design			
Flight control system validation			
Flight test comparison capabilities	F / α	F / α ,TF	F / α , TF, f(t)

Model / Analysis	(4) Structural dynamics +Flight mechanics State Space form	(5) Integral model Non linear flight mechanics + structural dynamics	(6) CFD / FEM Time domain coupling
Aeroelastic Stability	X		X (with non linear aero)
Aeroservoelastic stability	X		
Active mode Control law design	X		
Integrated control law design	X		
Flight control system validation		X	
Flight test comparison capabilities	F / α , TF, f(t)	f(t), whole flight envelope	f(t) (including unsteady aero measurements)

F / α frequency/damping
TF Transfer functions
f(t) accelerometers time domain response

Evolution of FCS design and validation process

The evolution of the process has been pushed by two major reasons :

- the need to reduce the FCS design and validation cycles,
- the need to have an early and right assessment of adverse risks due to flexibility (ICAS, APC, OFL...).

We show below that AM-Airbus has prepared this evolution of FCS design and validation process simultaneously with the development, the issue of new flexible aircraft models and the merge of skills.
As long as the FCS design problems related to flexibility were not crucial, the FCS specialists used a linearized flight mechanics model in order to design flight control laws. The control laws were defined on the basis of classical or optimal control techniques.
The state space form of the flight mechanics model being easy to derive from the full non linear flight mechanics model, it was quite natural for FCS specialists to use the optimal control techniques.
Even if the problems described above were not a major concern on Airbus A320, it was necessary to check the absence of ICAS, to compute the OFL and to assess the effect of GLA (Gust Load Alleviation embedded in the FCS) on gust dynamic loads. For A320, most of the FCS validation work induced by the interacting systems and structure problems was made a posteriori after the FCS was defined. This a posteriori analysis was sufficient, because many problems had been anticipated and solved thanks to simple design precautions (e. g., low pass filtering of structural modes). At this time, the inhibition of structural modes responses was the policy of FCS designers.
But, when the aircraft become more and more flexible-it was the case of Airbus A330 and A340 - the classical process becomes too risky and too long.

A right in time and satisfactory design is very difficult to obtain if FCS is designed only on the basis of the flight mechanics model.

The evolution of the process comes along with the state space form of the aeroelastic model.and with the need to anticipate design problems coming from the presence of structural modes close the flight mechanics modes.
In the research field, this formulation has been widely used since the late seventies.
At AM-AIRBUS, these models were used later, typically in the mid eighties, but, first limited to aeroelasticity applications.
The development of Airbus A340 family gave the opportunity to distribute the aeroelastic model to FCS designers and to share more and more the skills involved in FCS design and validation (FCS, loads and aeroelasticity specialists). The model (4) approach 2 is now used for FCS design.

To distribute this model is preferred to the exchange of transfer functions often used for military aircraft FCS design, because the model (4) is adequate for a direct application of all recent optimal control techniques.

Other advantages in using model (4) for FCS design are listed below :

- the possibility to combine several design criteria, not limited to handling, but including structural loads and dynamics criteria,
- ICAS and APC can be monitored,
- optimisation of sensors position is easily achievable.

It means that handling objectives of the control can be worked out with structural dynamics objectives, including an active control of flexible structural modes (Ref 6). These objectives can be met while reducing the number of iterations between FCS, loads and aeroelasticity specialists.
However, because of some simplifications which were made to build model (4) approach 2, - e.g., no dynamic coupling between flight mechanics and structural dynamics modes, use of a limited number of modes -, it remains necessary to perform validation of the FCS design with more complete models and with tests.

Before the flight test, the current practice is the validation of the FCS design with the complete flight mechanics, complete loads and aeroelastic models. Typically, model (2) is used for aeroelasticity, model (4) approach 1 for loads analysis and the complete non linear mechanics model for handling qualities analysis.
The validation process with the complete models is long. If some problems are found with the complete models- for example, loads increase which cannot be sustained by the structure- , it can be too late to find a solution which would avoid structural reinforcements. Therefore, it is necessary to improve the validation process in order to anticipate and find, earlier than before, solutions to problems which can happen in relation with structural flexibility and FCS design (Ref. 5).
A way to anticipate better such problems is to extensively use the integral model (5). Even if the integral model cannot replace the individual specialized models, it is the best model for flight mechanics simulation of a flexible aircraft and for quick design validation purpose. With the possibility to survey structural dynamic responses as well as loads, the integral model offers capabilities for FCS design analysis in relation with questions raised by structural flexibility (including loads).

Finally, flight test results are used to consolidate theoretical analysis and validation activities. We show below how the flight tests can support FCS design and validation process.

Flight test identification of the structural dynamics and its use for EFCS design and validation

Previous paragraphs have presented the increasing use of models for control law design of today's high flexible transport aircraft. The complexity of the modelizations have grown up to respond to the new issues raised by integrated flight mechanics – flexible mode control systems.
These new flight control systems push the flight tests in a similar way. The main objectives of flight testing are more or less unchanged from the early years of first flight control system development : aircraft security demonstration, analyses of control system performances, data recording for model validation and adjustement. However, these three activities have known recently many evolutions linked to the specific flexible aircraft flight control laws.

With the Airbus A320 was first introduced EFCS in a civil aircraft. Even if the flight control law of this aircraft is not dedicated to flexible mode control, the in-flight flutter clearance demonstration had to take into account the new specificities of the "aeroservoelasticity". The influences of the flight control law on the dampings of the flexible modes had to be measured during the flight tests. Another consequence is that the transfer functions characteristics (aircraft response / control surface order) of the aircraft became of first interest for flutter clearance, and a major point for aeroservoelastic model validation, in addition to the usual frequency / damping characteristics (Ref. 3).

Introduction of an active flexible mode control function, (passenger comfort improvement on Airbus A340-A330) brought a second evolution in flight testing. Flutter flight tests results took place not only in the control law validation process, but were used for control law adjustement. Aircraft transfer functions of interest for control law tuning were measured, using control surface sine sweep excitations usuallly used for flutter flights. Although the aeroelastic model behaviour was very close to the aircraft , some refinements of the flexible mode control law were performed using these transfer functions. Later flights were then dedicated to comfort law performance and stability margins demonstration (Ref 4).

All of these new flight tests driven by new flight control systems should not hide the older in-flight identification of the flight mechanics that was still an important feature for these aircraft. These tests followed classic procedures : calibrated inputs on the control surfaces are applied to induce a proper excitation of the flight mechanic modes ; aircraft responses are recorded, and used in an identification procedure of the flight mechanics derivatives. The process is repeated for many flight conditions and excitation levels, providing an identification of the aerodynamic gradients, including

their non linearities, in the whole flight domain. From this data package a model of the aircraft flight mechanics is built that produces responses nearly identical to the one of the real aircraft. This model is the basis of the design of an efficient control of the rigid-body modes.

For the development of a streched version of the A340-300 (the A340-600/500) the flight test activities is going to evolve once again. The integration process between flight mechanics and structural dynamics discussed in the previous paragraphs in the modelization and control law synthesis fields will reach the flight testing . As a model of the flexible modes behaviour is necessary for the integrated control system design, the identification of this model during flight test will be performed and used for control law adjustement, as it is today's usual pratice for the rigid body mode. Moreover, this identification will be linked with the classic flight mechanics identification, to provide "integral identified models", describing both rigid-body and structural dynamics responses.

The identification of this model will be based on both usual rigid body excitations and sine-sweep excitations for flexible modes . The beginning frequency will be lower than the one used for flutter sweeps to provide information about the aircraft response in the overlap aera of flight mechanics and structural dynamics bandwith. The identification methodology used the output-error approach. Initialization of the flight mechanics parameters is taken from the theoretical model, weheras the flexible aircraft model is initialized by a combination of a least–square estimation of the impulse response, transformed into the state space form with the ERA procedure (Eigenspace Realization Algorithm). The output-error minimization process can then be carried out on a model of both rigid and flexible modes; influences of rigid-body modes at the structural modes frequency is therefore taken into account properly.

This identification provides the control law designers with the model required by the integrated flight mechanics and flexible modes control law approach selected by AM-Airbus for future large civil aircraft.

Conclusions

With the development of large transport aircraft, the structural dynamics issue is no more the field of dynamics loads and flutter specialists only. Control law design, flight control system validation, flight test identification are now activities where strong capabilities around the flexible aircraft questions are needed. Exchanges of modelizations, flight test results, and knowledge between the specialists of these different areas is a key point for the realization of the best flight control system on these aircraft.

References

(1) Roger, K.L, "*Airplane Math Modeling Methods for Active Control Design*", Structural Aspects of Active Control Design, AGARD-CP-228, Aug. 1977, pp. 4-1 to 4-11.

(2) Karpel, M., "*Physically weighted approximations of unsteady aerodynamic forces using the minimum – state method*", NASA TP3025, March 1991.

(3) Lacabanne M., Esquerre JP., "Correlation between Theoretical Flutter Models and Tests for Civil Aircraft", International Forum on Aeroelasticity and Structural Dynamics, June 1991, 91-133, pp. 594 to 602.

(4) Seyffarth K, , Lacabanne M., Koenig K., Cassan H., "*Comfort In Turbulence for a Large Civil Transport Aircraft*", International forum on aeroelasticity and structural dynamics, Strasbourg 1993.

(5) Besch, H.M., Giesseler, H.G., Schuller, J., "*Impact of Electronic Flight Control System Failure Cases on Structural Design Loads*", AGARD Report 815, Sept. 1996, pp. 14-1 to 14-10.

(6) Kubica, F, "*New flight control laws for large capacity aircraft experimentation on Airbus A340*", ICAS 1998.

The Impact of Active Aeroelastic Wing Technology on Conceptual Aircraft Design

Peter M. Flick
U.S. Air Force Research Laboratory, AFRL/VASD, Bldg 45, 2130 8th Street
Wright-Patterson AFB, Ohio 45433-7542, USA

Michael H. Love
Lockheed Martin Tactical Aircraft Systems, Fort Worth, Texas

P. Scott Zink
Georgia Institute of Technology, Atlanta, Georgia

Abstract

Active Aeroelastic Wing (AAW) Technology represents a new design approach for aircraft wing structures. The technology uses static aeroelastic deformations as a net benefit during maneuvering. AAW is currently being matured through a flight research program[1]; however, transition of the technology to future systems will require educating designers in multiple disciplines of this new design approach. In order to realize the full benefits of AAW, aeroelastic effects will need to be accounted for from the beginning of the design process. Conceptual design decisions regarding parameters such as wing aspect ratio, wing thickness-to-chord ratio (t/c), and wing torque box geometry may be influenced, if designers choose to utilize AAW.

This paper presents recent efforts in developing conceptual aircraft design guidance for AAW technology and identifies improvements to the design process that could facilitate future AAW design applications. This process involves using results from aeroelastic design methods, typically used in preliminary design, with conventional conceptual design methods. This approach will allow aeroelastic effects to be considered in making conceptual design decisions.

Introduction

Conventional aircraft design philosophy views the aeroelastic deformation of an aircraft wing as having a negative impact on aerodynamic and control performance. The twisting of a wing due to aileron deflection during a roll maneuver can produce the phenomena of aileron reversal. Aileron reversal is the point where the deflection of the aileron produces no rolling moment. That is, the rolling moment produced by the change in camber due to aileron deflection is offset by the effective reduction in wing angle of attack due to the aeroelastic wing twist. Aircraft designers have generally tried to limit the effects of aeroelastic deformation by designing geometrically stiff planforms (low aspect ratio, high t/c), increasing structural weight to provide additional stiffness, and/or using horizontal tails to provide supplemental roll moment. A conventional wing design presents a severe compromise between aerodynamic, control, and structural performance.

Active Aeroelastic Wing (AAW) technology is a new wing structural design approach that integrates flight control design to enhance aerodynamic, control, and structural performance.[2] AAW exploits inherent structural flexibility as a control advantage, utilizing both leading and trailing edge control surfaces to aeroelastically shape the wing. The entire wing acts as a control surface, with the leading and trailing edge surfaces acting as tabs. The power of the air stream is used to twist the wing into a favorable shape. The degree of deformation is not necessarily any more than for a conventional wing; however, the deformation is advantageous instead of adverse to the maneuver (See Figure 1). AAW can be used to generate large roll control authority at higher dynamic pressures, and enables maneuver load control for both symmetric and asymmetric maneuvers. AAW does not require "smart structures", advanced actuation concepts, or adaptive control law techniques; however, AAW may complement these other advanced technologies. The key difference between AAW and the conventional approach is the exploitation of aeroelastic methods throughout the design process.

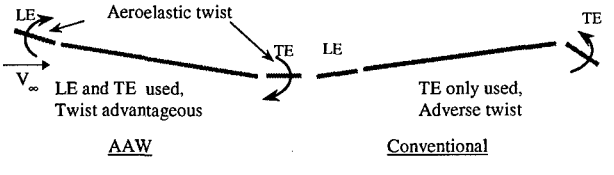

Figure 1. AAW vs. Conventional Roll Maneuver

The AAW approach removes static aeroelastic constraints in the wing design. Previous studies have

Paper presented at the RTO AVT Specialists' Meeting on "Structural Aspects of Flexible Aircraft Control", held in Ottawa, Canada, 18-20 October 1999, and published in RTO MP-36.

shown that an AAW can generate sufficient roll moment without the need for a horizontal tail to provide supplemental roll moment.[2,3,4] AAW expands the design space for a design team by enabling thinner, higher aspect ratio wings to be weight competitive with geometrically stiffer planforms. AAW technology is currently being matured through a full-scale flight research program.[1] While this full-scale demonstration and characterization of AAW is absolutely necessary to validate the technology, transition to future air vehicles will ultimately depend on educating aircraft designers on the AAW design approach. The objective of this paper is to present findings of a lightweight fighter design study to aid future conceptual design teams in the application of AAW technology.

Impact of AAW on Conceptual Design Decisions

Conceptual aircraft design results in the specification of the vehicle geometry that will best meet the mission and design requirements. Conceptual designers quantify a number of conceptual design parameters such as wing area, aspect ratio, thickness-to-chord ratio (t/c), taper ratio, sweep angle, etc. The AAW design approach enables designers to consider configurations outside the conventional design space. Because the AAW approach enables designers to use static aeroelastic deformation as a net advantage, thinner and/or higher aspect ratio wings can be effectively employed. Previous AAW design feasibility studies have demonstrated the benefits of AAW by expanding this design space.[2,3,4,12] In addition, these studies indicate that AAW may enable configurations with dramatically reduced horizontal tail area. Based on current design methods, conceptual designers would find it difficult to choose the best configuration for an AAW design, because AAW represents a dramatic change in the design paradigm. Designers trying to employ AAW would likely have many questions and few answers. How high of an aspect ratio is feasible? How low of a wing t/c is feasible? Where should the leading and trailing edge spars be located? How should the control surfaces be sized and located? In order to effectively exploit AAW technology, designers will need benchmark design studies to reference and a design process that enables the quantification of flexibility effects on aerodynamics, control performance, loads, and structural weight.

Limitations in the Conventional Design Process

Conceptual designers typically use a combination of empirical and relatively low fidelity analytical methods, and simplify the design problem by making assumptions such as a rigid structure for the purposes of estimating aerodynamic and control performance. Designers will, in large part, quantify design parameters based on experience and a historical database of existing aircraft. The methods are generally an effective approach early in design, but their effectiveness can be limited when designing for many new technologies, such as AAW. These empirical methods were developed from a database that does not include AAW designs, and AAW represents a revolutionary shift in the design paradigm. Likewise, the analytical methods typically employed during conceptual design are not likely to be multidisciplinary and, therefore, do not account for interactions such as flexibility effects on aerodynamics, control performance, loads, and structural weight. The current approach to a conceptual aircraft design would be to constrain the design space early in the design to avoid "problems", like static aeroelastic effects, as the design progresses. These constraints would be based on the designers' experience.

In designing with the AAW philosophy, quantifying the effects of airframe flexibility is an absolute necessity. In order to account for flexibility, it is necessary to employ methods such as TSO [5] or higher fidelity finite element based methods such as ASTROS[13] or NASTRAN[14]. The problem with using such methods to influence conceptual design decisions is the time required to build the models and perform the analyses and/or design optimizations. Typically a conceptual design will undergo many changes very rapidly, and it is difficult to build the models and perform the higher fidelity analyses quickly enough to influence the conceptual design decisions. A design environment that includes parameterization of design and analysis models and associativity between the models and conceptual design parameters would enable higher fidelity models to be updated as the conceptual design parameters are changed. With this capability, higher fidelity methods could be employed to make better decisions during conceptual design.

Process and Methods Used in this Study

A lightweight-fighter mission was chosen for this design study because of the familiarity of designers with the conventional design space for this type of aircraft, and the availability of design and analysis models. Choosing this design space will provide an excellent point of comparison for designers to reference. A design process was established with methods and models available to the Air Vehicles Directorate of AFRL. Figure 2 shows the design process used in this study.

Algorithms were developed to generate wing geometry based on wing area, aspect ratio, t/c, taper ratio, and the

sweep angle of a user-specified constant chord line. The algorithms also allowed for the definition of torque box geometry and a spanwise control surface break location. The algorithms assume a trapezoidal wing planform, constant t/c along the span, and four control surfaces (2 leading edge and 2 trailing edge). The entire input for all of the design and analysis models was associated with these design parameters using a Microsoft EXCEL spreadsheet environment.

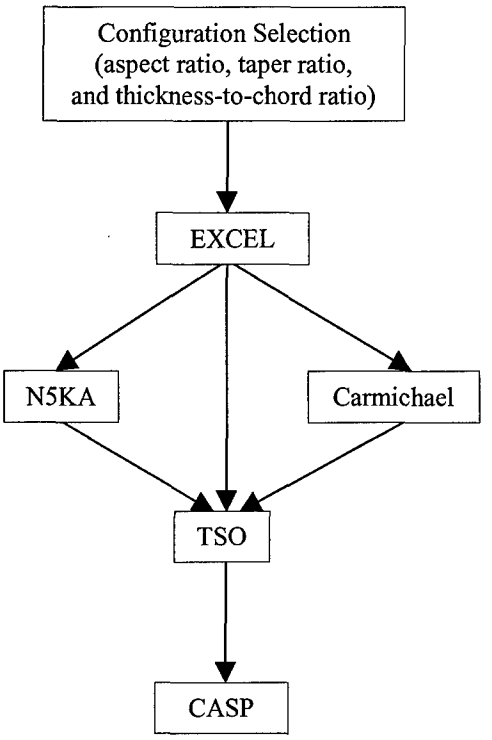

Figure 2. Design Process

For this study, the torque box and control surfaces were held constant in terms of percent chord and percent span of the wing. Also, in an attempt to isolate the effects of aspect ratio and t/c from sweep effects, the wing 40% chord was held constant at 24 degrees. This assumption was made because the 40% chord represents the maximum thickness of the airfoil, which influences structural stiffness and critical Mach number. The ¼ chord point of the mean aerodynamic chord was also held at a constant fuselage station.

TSO[5] (Wing Aeroelastic Synthesis Procedure) was chosen to conduct aeroelastic analysis and structural sizing. TSO is a multidisciplinary method that combines aerodynamic, static aeroelastic, and flutter analyses with structural optimization. It was developed by General Dynamics under an Air Force contract in the early 1970s to enable the consideration of composite structure impact on configuration selection during the early stages of the aircraft design process. TSO does not require the high degree of modeling detail that is needed by finite element methods such as ASTROS or NASTRAN, making it an ideal method for considering aeroelasticity impacts on conceptual design decisions. TSO utilizes a Rayleigh-Ritz equivalent plate technique for the wing structural model.[8,9] TSO provides the designer with a first-order estimate of structural material weight and its distribution (including composite ply orientation) required to meet strength and aeroelastic requirements. TSO's simplicity does bring with it additional limitations. TSO sizes

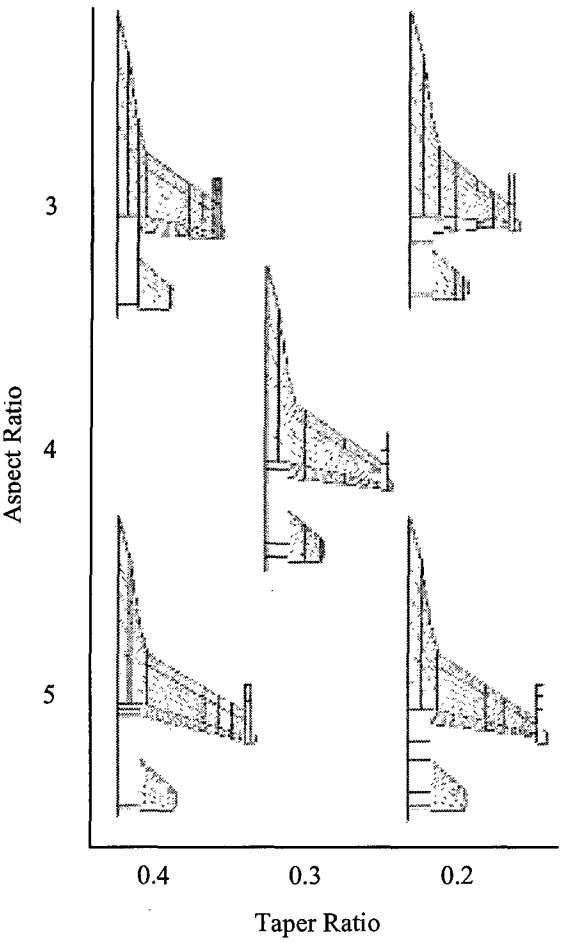

Figure 3. Range of Configurations Investigated

only the wing skins, and the upper and lower wing skins are constrained to be the same thickness. The wing substructure weight is calculated using a density factor and internal wing box volume. There are no

buckling constraints. The load conditions are limited to two symmetric conditions and one asymmetric condition. A 9 g symmetric pull-up at Mach 0.9 and 10000 ft, a 7.2 g symmetric pull-up at Mach 1.2 and 10000 ft, and a 7.2 g, 100 degree/sec rolling pull-out at Mach 1.2 and 10000 ft were used in this study. The Carmichael linear aerodynamic method[15] was used for steady aerodynamic loads, and the N5KA doublet lattice method[5] was used for unsteady aerodynamics. The steady aerodynamic model, shown in Figure 4, used 398 panels for the semispan configuration. The unsteady aerodynamic model was a wing only model, extending to the side of body. The flutter analyses were based on Mach 0.9, sea level conditions. The optimization approach in TSO is a Davidon-Fletcher-Powell unconstrained minimization with a penalty function to account for constraints.

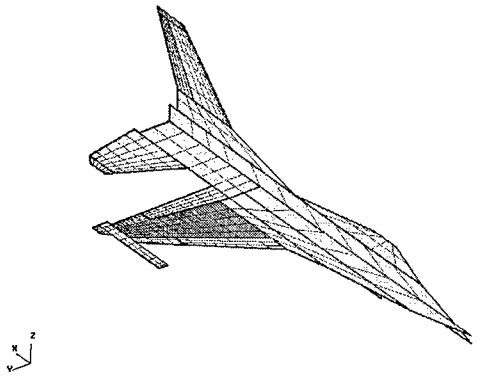

Figure 4. Steady Aerodynamic Model (wing control surfaces and structural box highlighted)

For each configuration, N5KA and Carmichael [5] were executed to provide the aerodynamic data needed for TSO. A TSO structural optimization was completed for both the conventional philosophy and the AAW philosophy. The wing box skin thickness was represented by a quadratic polynomial in both the chordwise and spanwise directions. The coefficients of this polynomial and the orientation of the composite laminate were chosen as the structural design variables. The TSO model also accounted for the flexibility of the control surfaces; however, the fuselage and empennage were considered to be rigid. Both the conventional and the AAW models utilized strength constraints on the wing using strain allowables (.003 in/in tension and compression and .01 in/in shear at limit load) consistent with damage tolerance requirements. Additional constraints included a minimum allowable flutter speed of 780 knots at sea level, a minimum gage of .005" per ply (0, +/-45, 90 laminate), and a maximum thickness per ply of 70% total skin thickness. The structural constraints were evaluated at 24 points distributed over the wing box. The experience of the authors is that the TSO design will typically be somewhat lighter than a finite element model prediction due, in part, to the limited number of evaluation points; however, the trends over the design space should be consistent with the finite element designs.

In design optimization using the conventional philosophy, aircraft trim was satisfied using angle-of-attack and horizontal tail deflection for the symmetric maneuvers. For the antisymmetric portion of the asymmetric maneuver, the aileron and horizontal tail were used to generate rolling moment with a horizontal tail-to-aileron blend ratio of 0.33. In addition to the constraints mentioned above, the conventional cases were also designed to meet a roll effectiveness constraint. This constraint was defined such that the minimum roll moment flexible-to-rigid ratio of the aileron was 0.62 at the Mach 0.9, 10,000 ft. condition. This value was chosen based on the authors' experience to maintain some contribution from the wing to maneuvering forces. For the supersonic asymmetric design condition, the horizontal tail could provide sufficient rolling moment; however, this would induce large weight penalties in the aft fuselage and empennage, and large yaw moments during the roll maneuver. These are both undesirable from a vehicle design standpoint, and could not be accounted for in the models used for this study.

The AAW design philosophy incorporated a gearing of the four wing control surfaces along with the angle-of-attack and horizontal tail deflection to trim for each symmetric condition. An antisymmetric component gearing of the four wing control surfaces was added to the symmetric gearing ratio for the asymmetric condition. The horizontal tail was not deflected to generate rolling moment. The gearing ratios were determined through a separate trim optimization model described in References 10 and 11. The authors also tried other gearing ratios, based on their experience, for the antisymmetric portion. Both the symmetric and antisymmetric gearing ratios allowed maneuver load control to be employed. The maximum deflections allowed for symmetric maneuvers were $\pm$30 deg. on the wing trailing edge surfaces, and +30/0 deg. on the leading edge surfaces (all surface deflections are positive down). The antisymmetric deflections were limited to $\pm$5 deg. for all wing control surfaces in the AAW models.

Based on the optimized structural designs for the AAW and conventional approaches, a ratio of the TSO wing weight predictions for each approach was then determined. This ratio was then used as a technology

factor to be applied to the wing box structural weight equation in a vehicle synthesis procedure to represent the wing structural weight advantage of the AAW design philosophy. This technology factor was assumed to be constant for a configuration over a range of vehicle design weights.

CASP (Combat Aircraft Synthesis Program)[6] was the method chosen to conduct vehicle sizing. It is typical of many vehicle synthesis procedures in that it utilizes statistically based methods for weight estimation. The aerodynamics and control analyses are based on Digital Datcom[7] empirical methodology. CASP has several sizing options available, but the program was only executed in a single point design mode and was used to minimize take-off gross weight (TOGW) for a typical lightweight fighter air-to-air mission. Vehicle sizing is driven by range requirements, and point performance metrics do not drive sizing in CASP. To ensure comparable maneuverability levels between configurations, wing loading (83 psf), vehicle thrust-to-weight ratio (0.8), and static margin (0.01) were held constant for all configurations for both the conventional and AAW design approaches.

Design Study Results

Table 1 shows the configurations that were investigated. This matrix was chosen to facilitate a Design of Experiments and statistical multivariate regression analysis as described in Reference 10. Least squares fits of a second order polynomial were used to generate approximate models of the design space with respect to wing box skin weight and TOGW. These approximate models were then used to provide the graphical representation of the design space in Figures 5 through 8. Table 1 also shows the technology factor used to account for AAW structural wing box weight savings for each configuration. The aspect ratio 5, t/c 0.03 configurations did not meet all of the design requirements for the conventional design philosophy. The taper ratio 0.2 configuration could only achieve a roll effectiveness value of 0.56, while the taper ratio 0.4 configuration could only achieve a roll effectiveness value of 0.34 and a roll rate of 50 deg/sec. The other conventionally designed configurations met all of the design requirements. All of the configurations using the AAW approach met the design requirements. Despite the inability of two of the conventionally designed configurations to meet the requirements, the authors chose to use these values in order to enable the regression analysis and graphical representation of the design space. However, it is likely that the technology factor for these two configurations would be lower than the values used. Table 1 also shows that the roll effectiveness constraint was active for each configuration using the conventional design approach.

aspect ratio	t/c	taper ratio	tech factor	conv active constraints	AAW active Constraints	conv TOGW	AAW TOGW
3	0.030	0.2	0.87	1,5	2,3,4	1.053	1.021
3	0.060	0.2	0.84	1,2,3	2,3	1.084	1.040
3	0.030	0.4	0.91	1,2,3	2,3,4	1.195	1.149
3	0.060	0.4	0.82	1,2,3	2	1.395	1.294
5	0.030	0.2	0.46*	1,2,3	2,3,4	1.219	0.871
5	0.060	0.2	0.66	1,2,5	2,3,5	1.159	1.009
5	0.030	0.4	0.62*	1,2,3	2,3,4	1.832	1.247
5	0.060	0.4	0.48	1,5	2,3,4	1.688	1.374
3	0.045	0.3	0.74	1,2,5	4	1.115	1.045
5	0.045	0.3	0.53	1	2,3,4	1.336	1.041
4	0.045	0.2	0.63	1,3	3,4	1.052	0.935
4	0.045	0.4	0.63	1,5	2,3,4	1.408	1.219
4	0.030	0.3	0.52	1,2,3	2,3,4	1.261	0.984
4	0.060	0.3	0.73	1,2	2,3,5	1.283	1.176
4	0.045	0.3	0.57	1,2,3,5	3,4	1.210	1.029

Constraint Key
1- Roll effectiveness
2- Minimum gage
3- Strength
4- Flutter
5- Ply thickness %

* Conventional design did not meet all design requirements

Table 1. TSO Design Results Summary

Other than for the highest t/c configurations, flutter became an active constraint for the AAW designs. The final two columns of the table show the results from the vehicle synthesis for each configuration. The TOGW values for the conventional and AAW designs are normalized by the lowest conventional design TOGW. Based on the approximate model derived from the regression analysis, the lowest TOGW for the conventional approach was found to be an aspect ratio 3, taper ratio 0.2, and t/c 0.04 configuration. The table shows that the best configuration for the AAW design approach was an aspect ratio 5, taper ratio 0.2, and t/c 0.03 configuration. The data indicates that the TOGW savings due to AAW is approximately 13% for this lightweight fighter mission. The reader should note that the technology factor used for this configuration was likely not as low as it would have been had the conventional design met all of the design requirements.

Conventional design wisdom indicates that wing box structural weight increases directly with aspect ratio and taper ratio, and inversely with t/c over the range of the variables in this study. Figure 5 clearly shows these trends. In these figures, the wing box structural weight has been normalized to that of the lowest conventional TOGW configuration (aspect ratio 3, taper ratio 0.2, and t/c 0.04). Figure 6 presents the wing skin weight vs. aspect ratio for a t/c of 0.03 and 0.045. The figures also show that the sensitivity of wing box structural weight with respect to aspect ratio and t/c is less for an AAW approach than a conventional approach especially as aspect ratio increases and t/c decreases beyond the conventional design space. AAW philosophy should enable an expansion of the design space for a lightweight fighter design. Figure 7 shows the impact of the

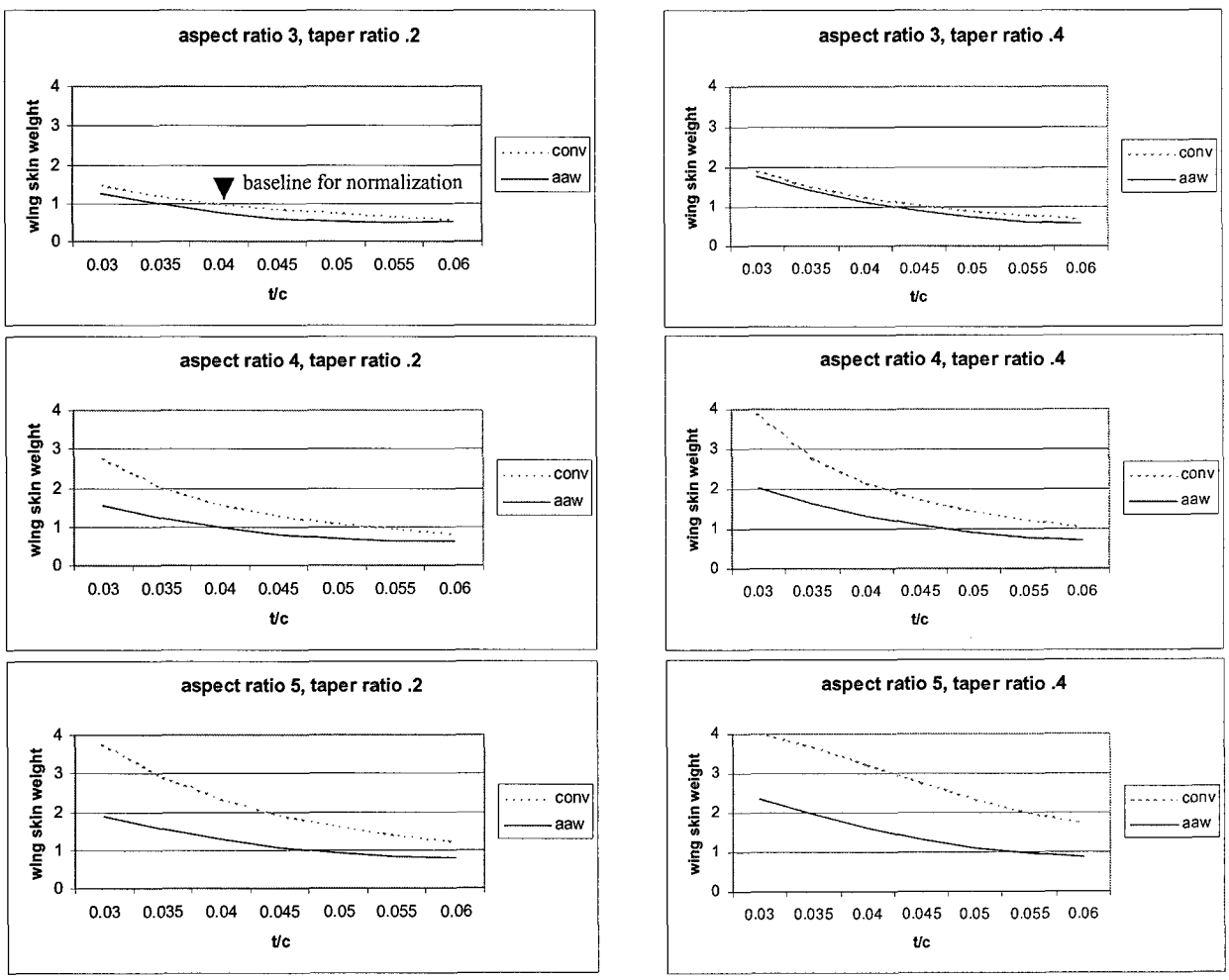

Figure 5. Summary of wing box skin weight vs t/c

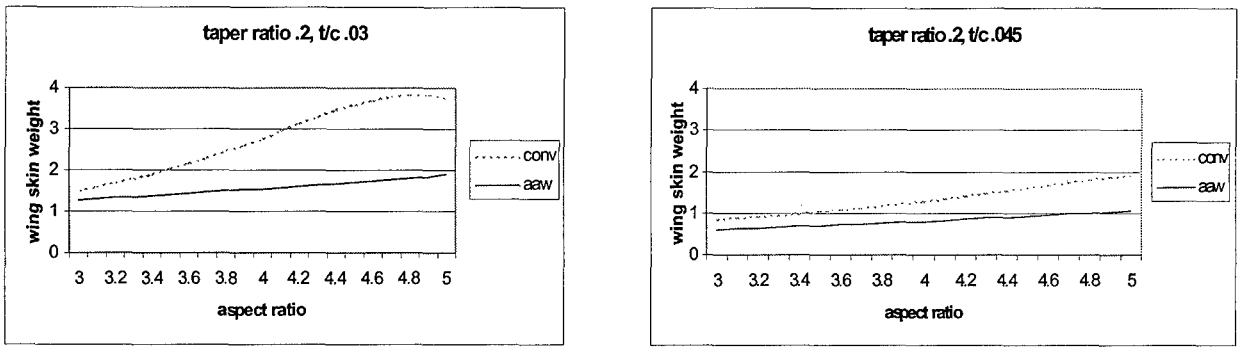

Figure 6. Summary of wing box skin weight vs aspect ratio

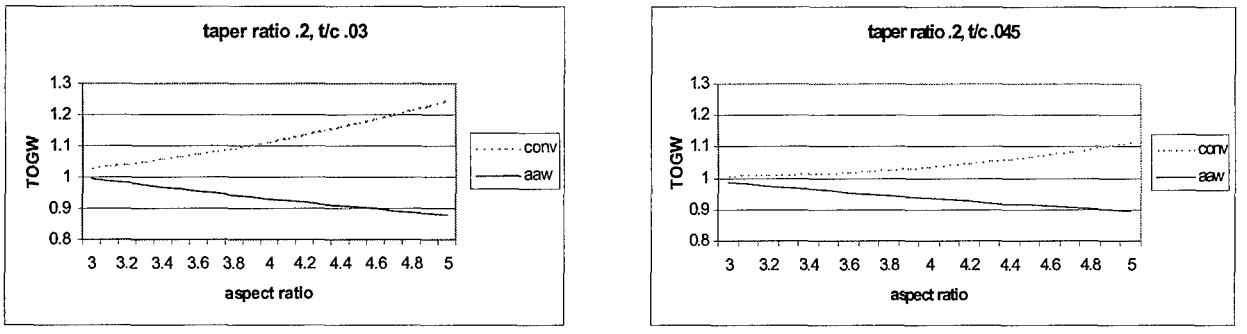

Figure 7. Summary of TOGW vs aspect ratio for taper ratio 0.2

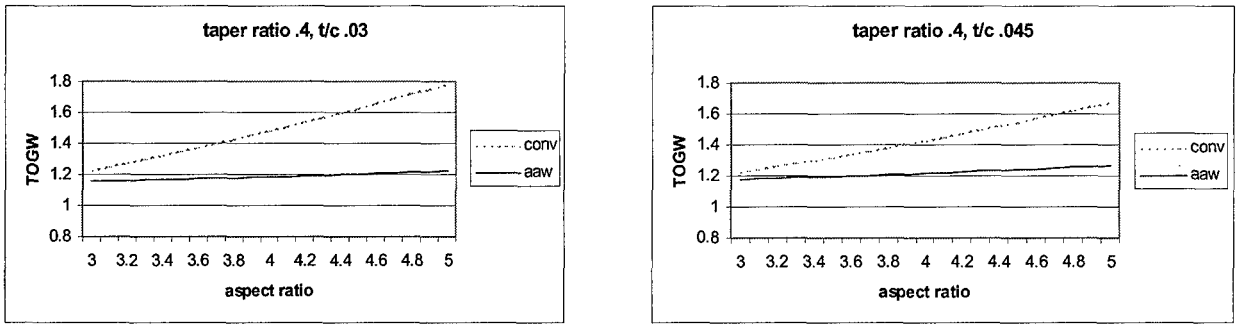

Figure 8. Summary of TOGW vs aspect ratio for taper ratio 0.4

AAW approach on TOGW for the same range of variables shown in Figure 6. Figure 8 shows the impact on TOGW for taper ratio 0.4. It is interesting that the sensitivity of TOGW with respect to aspect ratio is highly dependent on taper ratio, and results in a change of sign in the AAW design space. The reader should notice a slight downward turn of the curves representing the conventional approach at the highest aspect ratios. This is due to the inclusion in the approximate models of the two conventional cases mentioned above that did not meet all of the design requirements.

Conclusions

This study demonstrated that AAW technology can have a significant effect on conceptual aircraft design decisions, and enable expansion of the feasible design space for a lightweight fighter aircraft. In order to implement the AAW design approach, design teams must account for structural flexibility throughout the design process. This study demonstrated the importance of accounting for structural flexibility at the earliest stage of the design process, if a configuration is to be selected that takes maximum advantage of the technology.

The parameterization of the design and analysis models used in this study facilitated its completion in a timely manner. This study utilized approximate methods typically not used in the conceptual design phase. The TSO method provided timely results, however, its approximations necessitate user expertise to acquire meaningful information. Higher fidelity design and analysis methods and more complete aircraft models are required to refine the data and better quantify savings. The authors realize that extrapolation of the empirical structural box weight equation in the vehicle synthesis tool may result in inaccuracies. While this study demonstrates that benefits due to the AAW design approach exist, the extent of the benefits may be difficult to completely assess with these methods. The reader should note several issues that could affect the results of this study; 1) the AAW designs may incur a relatively small weight penalty for leading edge surface actuation hardware, 2) it is likely that better gearing ratios for the AAW designs could be found with an improved design method, 3) the AAW designs would likely benefit from other configuration changes such as a reduction in horizontal tail area, and 4) additional load conditions and design requirements could affect structural sizing.

Related/Future Work

Reference 10 documents a similar study using an ASTROS finite element design model. The authors compared the designs from both studies and found similar trends in the predicted weight benefits.

The authors recognize many opportunities for extending this effort. It would be interesting to investigate the effect of other design parameters such as wing box geometry, control surface sizing, maneuver requirements, wing area, and vehicle design weight on the benefits of the AAW approach. Improvement in the optimization methodology to enable more optimal gearing ratios, simultaneous structure and controls optimization, and possible configuration optimization will be considered for further investigation. Additional AAW design guidance will be developed through the correlation of full scale flight test data with higher fidelity analytical predictions and scaled experimental predictions.

Acknowledgement

The authors would like to acknowledge the support of Mr David Adamczak of AFRL for his help in using CASP.

References

1) Pendleton, E., Bessette, D., Field, P., Miller, G., and Griffin, K., "The Active Aeroelastic Wing Flight Research Program," 39th AIAA/ASME/ASCE/AHS/ASC Structures, Structural Dynamics, and Materials Conference, April 1998.

2) Miller, G.D., "Active Flexible Wing (AFW) Technology," Air Force Wright Aeronautical Laboratories, TR-87-3096, February 1988.

3) Miller, G.D., "AFW Design Methodology Study", Rockwell-Aerospace Report No. NA 94-1731, December 1994.

4) Norris, M., and Miller, G.D., "AFW Technology Assessment", Lockheed Aeronautical Systems Company and Rockwell-Aerospace Report No. NA 94-1740, December 1994.

5) Lynch, R.W., Rogers, W.A., Braymen, W.W., and Hertz, T.J., "Aeroelastic Tailoring of Advanced Composite Structures for Military Aircraft" (AFFDL-TR-76-100 Volume III, February 1978).

6) Adamczak, D., "Combat Aircraft Synthesis Program", Internal AFRL User's Manual February 1994.

7) Williams, J.E., and Vukelich, S.R., "The USAF Stability and Control Digital Datcom: Volume 1, User's Manual", AFFDL-TR-79-3032, April 1979. Williams, J.E., and Vukelich, S.R., "The USAF Stability and Control Digital Datcom: Volume 1, User's Manual", AFFDL-TR-79-3032, April 1979.

8) Love, M., and Bohlman, J., "Aeroelastic Tailoring and Integrated Wing Design", Second NASA/Air Force Symposium on Recent Advances in Multidisciplinary Analysis and Optimization, September, 1988.

9) Love, M., and Bohlman, J., "Aeroelastic Tailoring in Vehicle Design Synthesis", AIAA SDM, April 1991.

10) Zink, P.S., Mavris, D.N., Flick, P.M., Love, M.H., "Impact of Active Aeroelastic Wing Technology on Wing Geometry Using Response Surface Methodology", International Forum on Aeroelasticity and Structural Dynamics, June 1999.

11) Zink, P.S., Mavris, D.N., Flick, P.M., and Love, M.H., "Development of Wing Structural Weight Equation for Active Aeroelastic Wing Technology," SAE/AIAA World Aviation Congress and Exposition, San Francisco, CA, October 19-21, 1999. SAE-1999-01-5640.

12) Yurkovich, R., "Optimum Wing Shape for an Active Flexible Wing," 36th AIAA/ASME/ASCE/AHS/ASC Structures, Structural Dynamics, and Materials Conference, April 1995, AIAA-95-1220.

13) Neill, D.J., Johnson, E.H., and Canfield, R., "ASTROS – A Multidisciplinary Automated Design Tool," Journal of Aircraft, Vol. 27, No. 12, 1990, pp. 1021-1027.

14) MacNeal, R.H., The NASTRAN Theoretical Manual, NASA SP-221(01), April 1971.

15) Carmichael, R.L., Castellano, C.R., and Chen, C.F., The Use of Finite Element Methods for Predicting the Aerodynamics of Wing-Body Combinations, NASA SP-228, October 1969.

ACTIVE AEROELASTIC AIRCRAFT AND ITS IMPACT ON STRUCTURE AND FLIGHT CONTROL SYSTEMS DESIGN

Johannes Schweiger, Johann Krammer
DaimlerChrysler Aerospace AG
Military Aircraft
P. O. Box 801160
D-81663 Muenchen
Germany

Abstract

Active aeroelastic concepts have been proposed for several years now. Their common incentive are improvements of aircraft performance and stability by the intentional use of aeroelastic effects. This means that the basic flexibility characteristics of a new aircraft project must be included in the early conceptual design process, and the structural and flight control system design must be coupled very closely.

The knowledge about the magnitude of aeroelastic impacts on aerodynamic forces and aircraft stability is still very limited within the community of people involved in aeronautical engineering - even among the specialists in aeroelasticity. For a successful application of active aeroelastic concepts, their proper identification is therefore the first step. It will be shown for some selected examples, which static aeroelastic effects are usually very important for conventional designs, and how they can be made even more effective in a positive sense for future designs.

The accuracy and proper use of aeroelastic prediction methods and analysis models is addressed briefly in the context of interactions with other disciplines, and ideas are developed for the multi-disciplinary design process of active aeroelastic aircraft concepts.

Whereas static aeroelastic effects usually only become important with increasing airspeed, a concept will be demonstrated for aeroelastic improvements, which also works at low speeds.

1. Introduction

Traditionally, aircraft structure and flight control design could be handled as quite independent processes. The flight control concept was defined as a part of the conceptual design process. After this, the structural design concept was defined, taking into account that the structure had to be strong enough to bear the loads for all desired maneuvers, including the forces from the predefined control surfaces. The detailed dimensions of the individual structural components could then be determined by a refined assessment and distribution of aerodynamic and inertia loads. For each of the following design loops, these loads were considered invariable from changes of the local mass distributions, from resulting changes of the control forces, or from aeroelastic effects on the aerodynamic loads. These changes could only be analyzed after each major design loop, and then be used as an update for the next loop.

This hierarchical approach allowed no feed-back from the structural design to the flight control system design. In the past, flexibility or structural dynamic effects could only be identified and quantified very late in the design process. This resulted in additional weight, degraded performance, or costly redesigns. On the flight control side, adjustments to optimize the handling qualities could be made quite easily during the flight test program, as long as the flight control system was manually actuated. This was also possible, if servo actuators were used. Even an analog electrical flight control system with feed-back loops allowed quick fixes or adjustments by trial and error methods.

For a modern airplane the development of the digital flight control system is a time consuming and costly process. Therefore, it is today much more important, to know the aeroelastic characteristics of the airplane as good and as early as possible during the design process.

This fact becomes even more important, when active aeroelastic concepts are considered for a design. They will either have their own control system, which may create strong interactions with the aircraft's main flight control system, or they are directly controlled by this one. In this case, it means direct impacts on the flight control system's authority and stability.

2. Historic developments

Although aeroelasticity was still completely unknown to the pioneers of aviation, the success of the first powered flight may be contributed to a great extend to a sophisticated active aeroelastic concept for directional control. In his book "How we invented the airplane"[1], Orville Wright describes this system of cables, connecting the sliding cradle, which could be moved by the pilot, to the wing tips, which were twisted by the pilot' motion in opposite directions. This provided roll control without ailerons.
On the other hand, the Wright brothers' main competitor, Samuel P. Langley, was very likely less fortunate with his Aerodrome designs because of insufficient aeroelastic stability[2].
An other example demonstrates how strongly interdisciplinary the design of airplanes already was in those early years. During the First World War, designers and government authorities began to fear the loss of structural integrity from battle damage and looked for redundancy of major load-carrying parts. In the case of the monoplane Fokker D.VIII, shown in Figure 1, a superior design with cantilevered wings, where the box structure provided excellent redundancy, the rigid certification rules caused a series of fatal accidents,

Paper presented at the RTO AVT Specialists' Meeting on "Structural Aspects of Flexible Aircraft Control", held in Ottawa, Canada, 18-20 October 1999, and published in RTO MP-36.

which were caused by aeroelastic divergence. As Anthony Fokker describes in his book[3], sufficient strength of the design had already been demonstrated by proof load and flight tests, when regulations called for a reinforced rear spar with proportional strength capacity to the front spar. This redistribution of stiffness caused torsional divergence under flight loads.

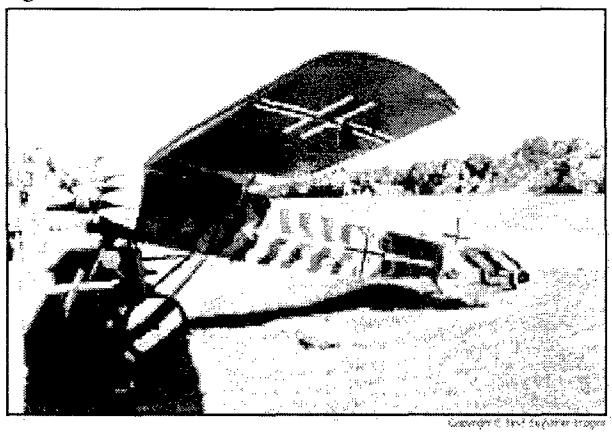

Figure 1: Fokker monoplane D-8

In the following years, designers began to fear the flexibility of the structure, as quoted from a review paper on Aeroelastic Tailoring by T. A. Weisshaar[4] *"As a result, aeroelasticity helped the phrase "stiffness penalty" to enter into the design engineer's language. Aeroelasticity became, in a manner of speaking, a four-letter-word. ...it deserves substantial credit for the widespread belief that the only good structure is a rigid structure."*

Only recently the authors could listen to this demand again, when a colleague from flight control systems design asked to build future airplanes as rigid as possible.

Today, the high performance of fighter aircraft, and the increasing size of transport aircraft, together with modern light weight structures, have enlarged the flexibility effects on the aerodynamic characteristics of airplanes. Modern airplanes are also operating more often near and closer to the high speed edge of the flight envelope. In the past, it was for example sufficient to ensure the avoidance of aileron reversal at limit speed, a speed where the aircraft would usually not operate.

In the past, the structural dynamic characteristics of an airplane had only rarely to do with the flight control system. Flutter as the classical aeroelastic instability could be treated independently from the flight control system by proper adjustments to the stiffness and mass distributions. The frequency band of the aircraft's rigid body Eigenmodes and the dynamic characteristics of the control surface actuators were usually well below those of the flexible aircraft. Today's actuators however as well as the speed of the flight control computers are causing overlaps which require careful aeroservoelastic analysis. Stability deficiencies are usually treated by implementing notch filters for the structural dynamic Eigenfrequencies into the flight control laws. For a fighter airplane which is usually flying in many different configurations and at different flight conditions, a multitude of these filters may be required to provide sufficient stability. This usually results in a considerable degradation of the aircraft's agility.
This implies that a different approach will be required in the future for the treatment of flight control system and structure in the design process, with or without active aeroelastic concepts.

3. Active aeroelastic concepts

3.1. Definitions for active aeroelastic concepts

In a more traditional sense, active aeroelastic concepts can be defined as active control concepts for the cure of static or dynamic aeroelastic deficiencies with respect to stability, maneuverability, loads, or aerodynamic performance. In this case, the aeroelastic impacts are considered to be bad in general.

Examples are gust load alleviation or active flutter suppression concepts, where control surfaces are actively deflected to counteract loads or create unsteady aerodynamic damping forces. One reason why these systems did not become common practice, is the insufficient static aeroelastic effectiveness of typical control surfaces like ailerons.

Since several years, the expression "active aeroelastic" is more used for concepts, where aeroelastic effects are exploited in a beneficial way to improve aircraft performance, handling, or directional stability compared to a rigid aircraft. Using this definition, only static aeroelastic concepts are addressed.

Possible benefits from aeroelasticity were already addressed in the seventies and eighties, when advanced composite materials together with formal structural optimization methods offered the possibility of Aeroelastic Tailoring an aircraft structure[5]. One of the first demonstrations was the Active Flexible Wing wind tunnel test program[6]. On this model, Figure 2, two leading and two trailing edge surfaces are adaptively deflected at different aerodynamic conditions to achieve optimum roll control power. This multiple surface control concept allows to use the trailing edge surfaces beyond their reversal speed.

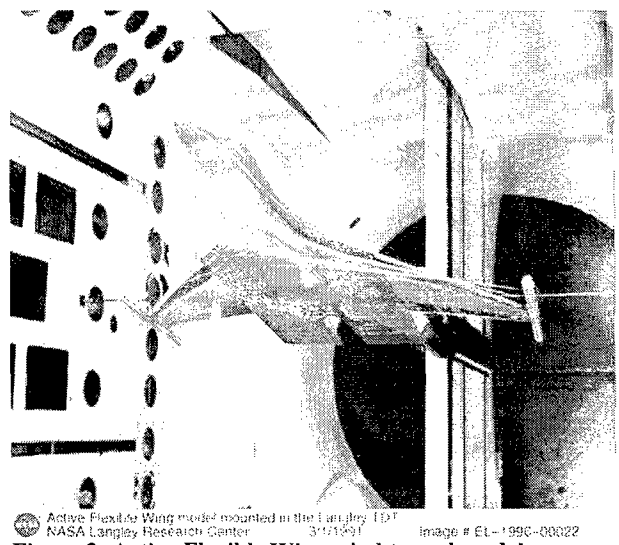

Figure 2: Active Flexible Wing wind tunnel model

To demonstrate this concept in flight, an F-18 is currently modified with a more flexible wing, other control surfaces, and the appropriate flight control laws[7] .A more flexible wing means in this case, that an original F-18 wing torque box will be used. This structure had to be reinforced after initial tests because it did not provide the desired roll control power.
The expression "Active Flexible Wing" may have mislead to the believe that an airframe structure must now be made as flexible as possible to improve an airplane's performance.

This is as wrong as the above quoted "as rigid as possible", because excessive weight penalties would be created in both cases. The objective must be a minimum weight design, where the external geometry, the arrangement and shape of control surfaces, are optimized together with the flight control law to achieve aeroelastic tuning or amplification of aerodynamic forces at all flight conditions.

Additional interest in active aeroelastic concepts arose in recent years with the development of active materials, where the stiffness can actively be adjusted. Active structures concepts, where the stiffness of individual components is actively modified, also belong to this category.

The overview paper from McGowan et al.[8] gives an excellent overview on recent activities for static and dynamic aeroelastic applications.

3.2. Classification of active aeroelastic concepts

3.2.1. Classification by aeroelastic phenomena

If the definition of active aeroelastic concepts is expanded to all active concepts, where structural dynamics or aeroelasticity are involved, the elastic mode control system ILAF (Identically Located Acceleration and Force)[9] of the XB-70 must be considered as one of the first applications. A similar system is installed today on the B-1B to counter turbulence.

In the seventies, active flutter suppression systems by means of activated control surfaces were developed and flight tested[10]. Besides the criticality aspect of a potential system failure, an other reason, why they are not yet in use, may be their limited static aeroelastic effectiveness, as already mentioned above.

In recent years, active concepts for the alleviation of dynamic loads from buffeting conditions of vertical tails were designed and tested in wind tunnels and on full scale ground tests with simulated loads[11,12].

The first demonstration of active materials concepts for the reduction of dynamic loads in a flight test was a smaller structural component. Piezo-active elements were used to reduce the vibration loads on a skin panel of the B-1B rear fuselage section[13].

The group of concepts, where aeroelastic phenomena can be used in a beneficial way, can be subdivided for the following applications.

Improvements of directional control forces by using classical aerodynamic control surfaces as tabs to initiate the main control force by an aeroelastic deformation of the fixed surface. Theoretically, the same effect could be achieved by an active deformation of the fixed surface directly. Several studies[14,15,16,17,18] demonstrate the principle of these concepts and explain the required design approach. Mainly roll control is addressed by these concepts, because the outboard ailerons on wings usually show the highest aeroelastic sensitivity.

A second application of static aeroelastic concepts is the reduction of gust or maneuver loads. Active load alleviation concepts in the past suffered from a lack of aeroelastic effectiveness of the control surfaces – usually the outboard ailerons.

Mainly for transport aircraft wings, active aeroelastic concepts offer an attractive opportunity to adjust the shape of the flexible wing for minimum drag under varying flight and internal loading conditions.

So far, mainly wings have been addressed by active aeroelastic concepts. But horizontal and vertical tails could be at least as attractive. Whereas wings have to meet a multitude of design objectives and requirements, which somehow limit the design space for active aeroelastic tailoring, the only purpose of empannage surfaces is the provision of directional stability and directional control about the pitch and yaw axis. This means, that they offer a larger design space. One such concept for a vertical tail is described below.

3.2.2. Classification by active devices

There are two major groups of active devices: aerodynamic control surfaces and structural devices. The first one creates external aerodynamic forces to stimulate deformations of the flexible fixed surface, while the other one is based on interactions between the active elements and the passive structure by internal forces.

The effectiveness of aerodynamic actuators relies upon the aerodynamic flow conditions. Their power increases linear with the dynamic pressure at smooth flow conditions. For turbulent flow, for example at high angles of attack, or for large deflections, they can completely lose their effectiveness. This makes them very efficient for applications at high speeds, where only small deflections are required. But this also requires, that their natural static aeroelastic effectiveness is high. Natural means that it already comes from the wing or stabilizer planform geometry and location of the control surfaces, with no additional investment of stiffness and weight.

Aerodynamic control surfaces are limited for dynamic applications by the frequency range of their hydraulic actuator. The active control system has to be integrated into the main flight control system, and depending on the required control surface authority, they will limit the basic aircraft performance.

The effectiveness of the achievable actuation from active structures and materials concepts is independent from the external flow conditions. The achievable stimulation of aeroelastic servo-effects however also here depends on the basic geometry and structural arrangement.

Their effectiveness relies upon the optimum placement within the passive structure to achieve the best possible deformation of the flexible structure. Active materials can be embedded within the passive structure or attached to, distributed over larger areas, or concentrated active elements are acting between a few selected points for high authority.

It is sometimes said that these concepts could completely replace conventional control surfaces. But this looks very unrealistic at the moment. The major difficulties for a successful application are here the limited deformation capacity of active materials, as well as their strain allowables, which are usually below those of the passive structure. However, this can be resolved by a proper design of the interface between passive and active structure. But the essential difficulties are the stiffness and strain limitations of the passive structure itself. It can not be expected that the material of the passive structure just needs to be replaced by more flexible materials without an excessive weight penalty. It

is also not correct to believe that an active aeroelastic concept will become more effective, if the flexibility of the structure is increased. The aeroelastic effectiveness depends on proper aeroelastic design, which needs a certain rigidity of the structure to produce the desired loads. A very flexible structure would also not be desirable from the standpoints of aerodynamic shape, stability of the flight control system, and transmission of static loads.

Because large control surface deflections are required at low speeds, where aeroelastic effects on a fixed surface are small, it is more realistic to use conventional control surfaces for this part of the flight envelope, and make use of active aeroelastic deformations only at higher speeds. This would still save weight on the control surfaces and their actuation system due to the reduced loads and actuation power requirements.

4. Optimization methods in aircraft design

Any improvement of a technical system is often referred to as an optimization. In structural design, this expression is today mainly used for formal analytical and numerical methods. Some years after the introduction of finite element methods (FEM) for the analysis of aircraft structures, the first attempts were made to use these tools in an automated design process. Although the structural weight is usually used as the objective function for the optimization, the major advantage of these tools is not the weight saving, but the fulfillment of aeroelastic constraints. Other than static strength requirements, which can be met by adjusting the individual finite elements' dimensions, the sensitivities for the elements with respect to aeroelastic constraints can not be expressed so easily.

In the world of aerodynamics, the design of the required twist and camber distribution for a desired lift at minimum drag is also an optimization task. Assuming that minimum drag is achieved by an elliptical lift distribution along the wing span, this task can be solved by a closed formal solution and potential flow theory. More sophisticated numerical methods are required for the 2D-airfoil design or for Euler and Navier-Stokes CFD methods, which are now maturing for practical use in aircraft design.

For the conceptual aircraft design, formal optimization methods are used since many years. Here, quantities like direct operating costs (DOC) can be expressed by rather simple equations, and the structural weight can be derived from empirical data. Formal methods like optimum control theory are also available for the design of the flight control system.

So one might think that these individual optimization tasks could easily be coupled for one global aircraft optimization process. The reasons why this task is not so simple are the different nature of the individual disciplines' design variables, and their cross sensitivities with other disciplines. The expression Multi-Disciplinary Optimization (MDO) summarizes all activities in this area, which have been intensified in recent years. It must be admitted that today most existing tools and methods in this area are still single discipline optimization tasks with multi-disciplinary constraints.

In order to design and analyze active aeroelastic aircraft concepts, especially when they are based on active materials or other active structural members, new quantities are required to describe their interaction with the structure, the flight control system, and the resulting aeroelastic effects.

Besides formal methods, an efficient MDO approach also requires experienced engineers with a broad knowledge in all involves disciplines and their interactions. It is also essential, that the proper levels of single-discipline analysis models and methods are used for the integrated design process.

5. Approach for the aeroelastic analysis of an active structure

For the static aeroelastic analysis of the achievable rolling moment, induced by active structural elements, the optimization program LAGRANGE[19] was modified. For the static aeroelastic analysis of a conventional passive structure, the analysis process is initialized by defining the aerodynamic deflections of control surfaces. The resulting "rigid" aerodynamic load is then used as a starting point to obtain the aeroelastically balanced equilibrium condition, as depicted in Figure 3.

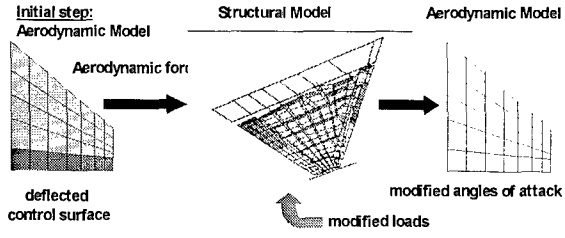

Figure 3: Process for static the aeroelastic analysis with control surfaces

For an active structure, the chosen new approach first simulates the deformation of the structure under the loads of the activated elements. This static solution delivers the initial angle-of-attack distribution for the aeroelastic analysis, as shown in Figure 4.

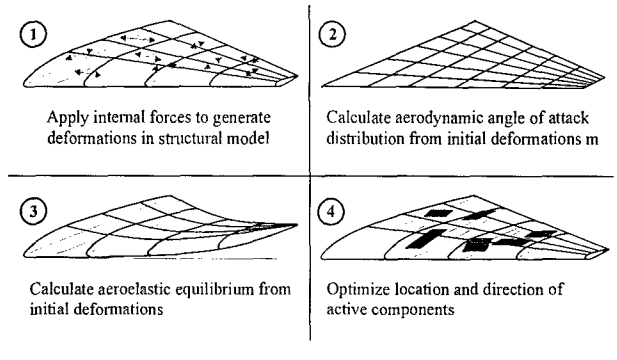

Figure 4: Static aeroelastic analysis steps for an active structure

To verify the approach, three different cases were analyzed, using the wing model from the example below: one for a conventional control surface deflection by specifying its initial aerodynamic deflection, one with the equivalent deflection from static loads applied to the element that represents the actuator, and one, where in-plane loads are applied to the skins of the control surface. The results are shown in Figure 5.

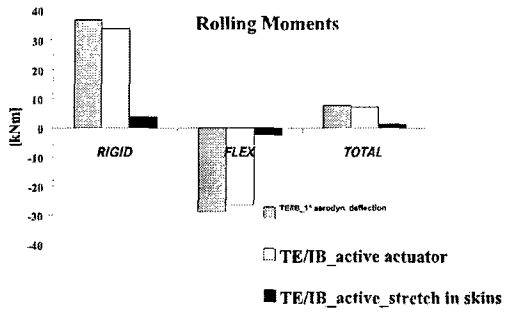

Figure 5: Results for test cases

6. Examples for active aeroelastic concepts

6.1. Active aeroelastic wing

To demonstrate the principle of active aeroelastic concepts for improved roll performance, a low aspect ratio fighter aircraft wing was chosen., because here one would not expect considerable aeroelastic improvements. The Finite Element model for this generic wing is shown in Figure 6.

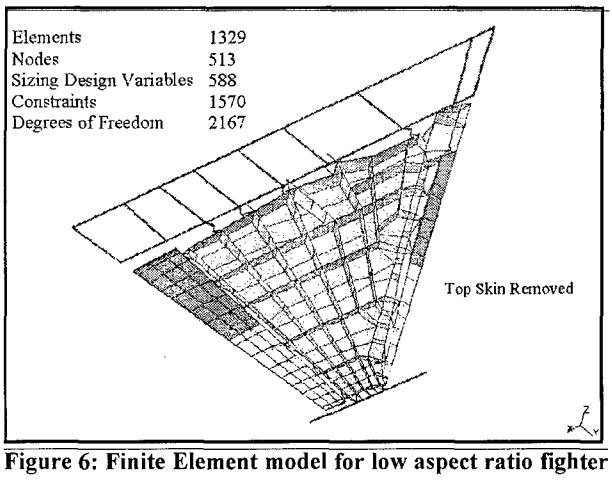

Figure 6: Finite Element model for low aspect ratio fighter wing

The original model, which had only two trailing edge flaperons for roll control, was modified by two addition leading edge surfaces for roll control. The had to be rather small to avoid modifications of the torque box structure. Figure 7 shows their representation in the aerodynamic analysis model. The basic design conditions for the optimization are summarized in table 1.

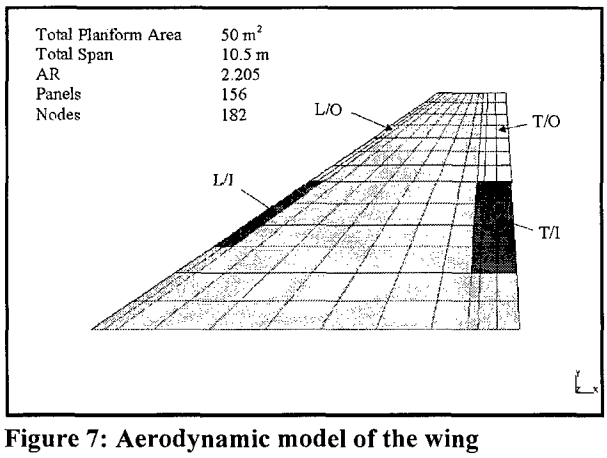

Figure 7: Aerodynamic model of the wing

Static load cases	+ 9g , - 4g
Roll rate at Ma 1.2, S/L	120 °/s
Max. hinge moment per surface	15 kNm
Max. control surface deflection	15 °

Table 1: Basic wing design conditions

Figure 8 depicts the achievable rolling moment with increasing airspeed for rigid conditions. These two graphs clarify, why usually only trailing edge surfaces are considered for roll control. Besides their different size, main reasons for better aerodynamic performance are the different sweep angles, and mainly the camber effect, which supports the trailing edge surfaces and counteracts at trailing edge deflections.

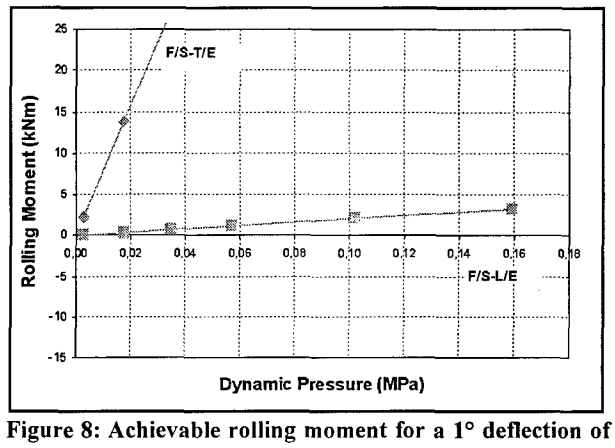

Figure 8: Achievable rolling moment for a 1° deflection of leading and trailing edge surfaces without structural flexibility

But things look quite different, as soon as the aeroelastic effects on the flexible structure are taken into account. For the initial structure, which had already been optimized for increased rolling moment effectiveness of the trailing edge surfaces, the achievable rolling moments are compared in Figure 9.

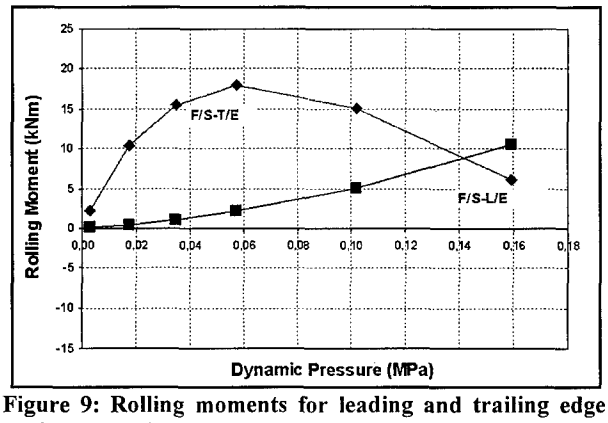

Figure 9: Rolling moments for leading and trailing edge surfaces with flexibilities of the initial design

Traditionally, if only the trailing edge surfaces are used for roll control, the achievable roll rates for a design with fixed planform and control surface geometry can only be improved by additional structural weight. For this example, the structural optimization of the wing box skins with different constraints for the rolling moment effectiveness results in the graph of Figure 10 for skin weight and effectiveness. If the leading edge surfaces are used in addition, the results in table 2 can be achieved for the basic static design. If buckling

stability is not considered for the wing skin design, which could be possible by additional spars, the rolling moments vs. dynamic pressure for the individual control surfaces in Figure 11 are obtained. In this case, the leading edge surfaces get more effective, and the trailing edge surface could be used beyond the reversal speed. More details about this study are reported in refs.[16,17].

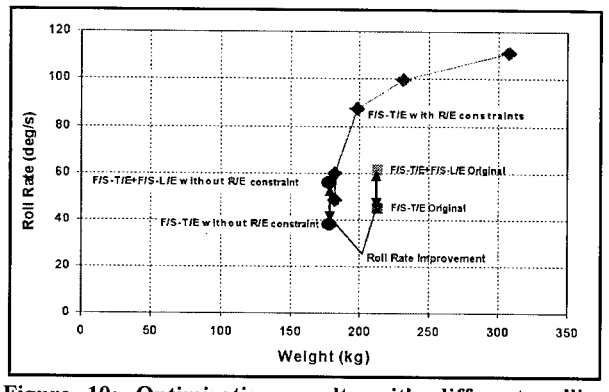

Figure 10: Optimization results with different rolling moment effectiveness constraints

	Conventionally optimized design	Static design with additional roll control from L/E surfaces		
		Without L/E	With L/E, basic configuration	With L/E, 50 % larger differential deflections
Skin weight per side [kg]	307	178	178	178
Total rolling moment for 1 °				
T/E – I/B	32.0	9.00	9.00	9.00
T/E – O/B		2.94	2.94	2.94
L/E – I/B			2.39	2.59
L/E – O/B			3.01	4.52
Total hinge moment for 1 °				
T/E – I/B	3.07	2.86	2.86	2.86
T/E – O/B	1.79	1.53	1.53	1.53
L/E – I/B			0.34	0.51
L/E – O/B			0.20	0.30
Required hinge moment for 120 ° /s and flap deflection [kNm]				
T/E – I/B	16.1. 5°	47.0. 16.5°	32.1. 11.4°	14.3. 5.0°
T/E – O/B	9.4. 5°	27.7. 16.5°	18.7. 11.4°	15.3. 5.0°
L/E – I/B			3.8. 11.4°	7.7. 15.0°
L/E – O/B			2.2. 11.4°	4.5. 15.0°

Table 2: Optimization results for the wing

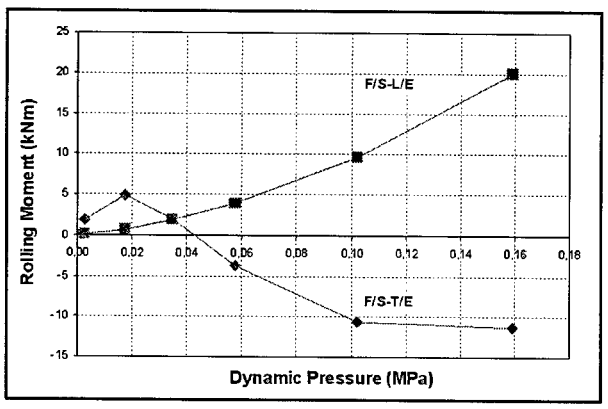

Figure 11: Rolling moments for the static design without buckling stability

6.2. Active aeroelastic vertical tail

The structural design of the vertical tail for a fighter aircraft usually requires additional stiffness for the static aeroelastic effectiveness of the lateral stability and for the rudder yawing moment. A typical effectiveness-vs.-weight trend is depicted in Figure 12. To improve this situation, the concept of a Diverging Tail was developed by Sensburg et al.[20].In a first step, the effectiveness is increased by means of aeroelastically tailored skins.

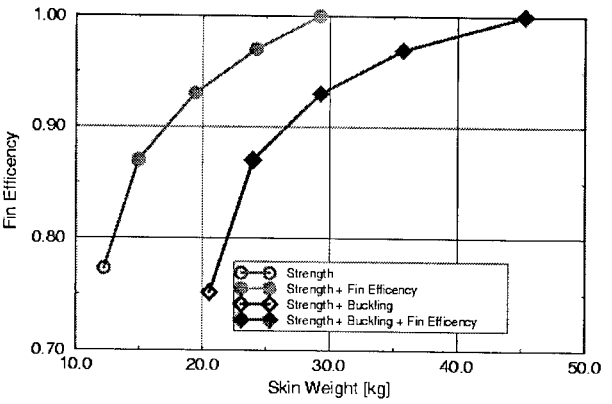

Figure 12: Static aeroelastic effectiveness vs. structural weight for a typical vertical tail

Although this means a weight increase for the cover skins, the total structural weight can be decreased by reducing the size of the tail proportional to the increase in effectiveness. Additional increases are then obtained by relaxing the stiffness of the forward root attachment and modifying the rear attachment in such a way that the aerodynamic surface can be deformed in a more favorable way.

For further improvements, the concept of an Active Vertical Tail was developed. The principle is depicted in Figure 13. It is an all-movable tail, where the attachment is positioned in such a way, that the aeroelastic effectiveness is above 1.0 for all aerodynamic flow conditions. The amount of effectiveness can be adjusted by a variable torsional stiffness element. This can for example be achieved by a mechanical, hydraulic, electric, or active materials system. The actuation of the tail for yaw control can be integrated into the same system, or it can be designed as a separate system. A separate actuation system by a conventional actuator with constant stiffness would be less complex for the flight control system.

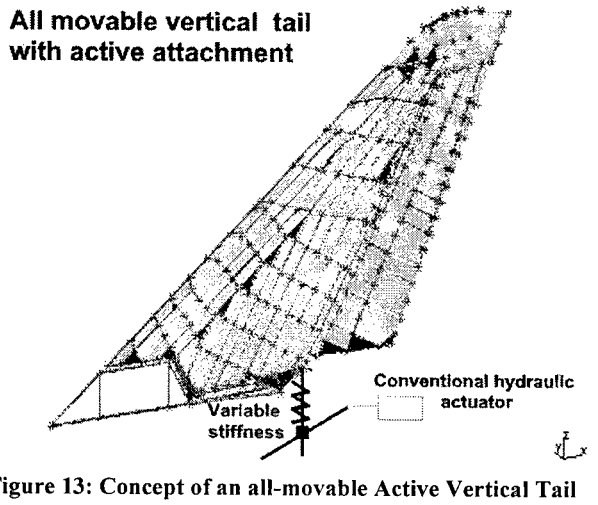

Figure 13: Concept of an all-movable Active Vertical Tail

This vertical tail needs no additional weight for aeroelastic effectiveness. Its size can be reduced to the value, where sufficient directional stability and yaw control are provided by the proper amount of effectiveness from the variable attachment stiffness. The lower boundaries for the stiffness are defined by sufficient flutter stability. This means, that flutter stability and aeroelastic effectiveness have the same stiffness demands: low at low speeds, and high at high speeds.

This concept reverses the traditional design approach for improved aeroelastic effectiveness, where an increase is

achieved by additional stiffness. Whereas the minimum size of the passive design for the diverging tail is limited by stability and control requirements at low speeds, where no aeroelastic effectiveness improvements are possible, the Active Vertical Tail also provides increased effectiveness at low speeds.

A different concept for a variable stiffness actuation system is already used for the new F/A-18E/F[21]. Here the hydraulic pressure switches from 207 bar to 345 bar (3000 to 5000 PSI) at high dynamic pressures to compensate aeroelastic losses.

7. Impacts from active aeroelastic concepts on the FCS design

The design of the flight control system should not become more complex because of an active aeroelastic concept. But the impacts from this active concept on the aircraft's parameters, which are implemented in the flight control laws, must be known and respected.

The performance of the flight control system should not be degraded in the presence of an active aeroelastic system. If designed properly, there should even be improvements, like reduced power and stiffness demands for the flight control actuation system.

As an example, the simplified schedule in the flight control laws for the leading and trailing edge surfaces for roll control of the wing above could look like in Figure 14.

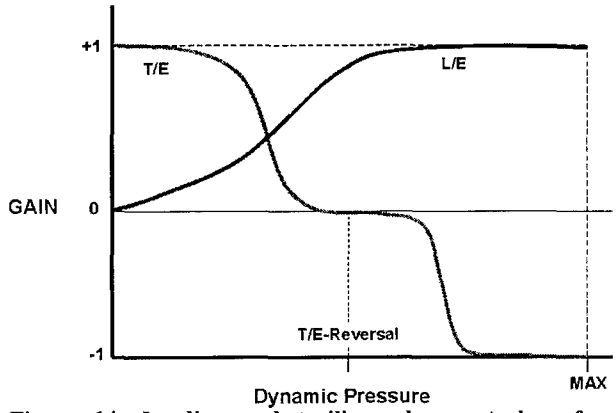

Figure 14: Leading and trailing edge control surface authority for roll control

The variable stiffness for the attachment of the vertical tail might look like in Figure 15. Here, the optimum stiffness for aeroelastic effectiveness must be tuned together with the flight control laws for handling and stability requirements.

8. Impacts from active aeroelastic concepts on the structural design

In order to incorporate active aeroelastic concepts into the structural design, it is no longer sufficient to specify aeroelastic constraints like for flutter or control surface effectiveness, and apply it to the structural optimization process for a predefined structural concept.

The design space for aeroelastic effects must be as wide as possible in the beginning. That means, the sensitivities of basic geometry parameters for wings and control surfaces, the positions of control surfaces, and their functions must be considered as design variables in the beginning.

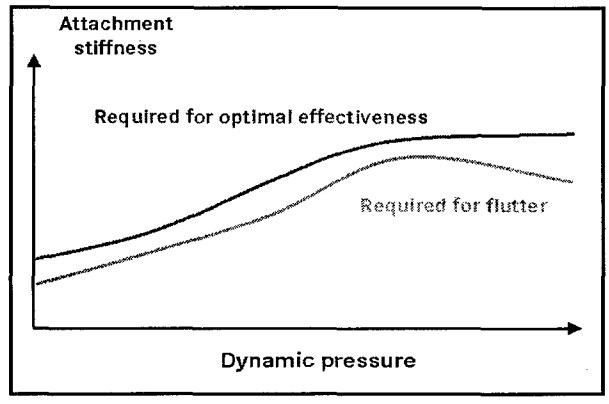

Figure 15: Attachment stiffness requirements for Active Vertical Tail

The design space for aeroelastic effects must be as wide as possible in the beginning. That means, the sensitivities of basic geometry parameters for wings and control surfaces, the positions of control surfaces, and their functions must be considered as design variables in the beginning.

The analytical description of active aeroelastic concepts must directly be included in the structural analysis model because of the impacts from the passive structure's design constraints on the effectiveness of active aeroelastic systems. In order to make them efficient, it is required to understand, design and simulate the interfaces between components and the passive, load-carrying structure.

9. Needs for the integrated design of airplanes with active aeroelastic concepts

It is obvious that integrated design and multi-disciplinary optimization processes are an absolute must for active aeroelastic concepts.

MDO does not mean to combine single discipline analysis tools by formal computing processes. It means first a good understanding of what is going on. This is already essential for a conventional design. Only after this understanding the creative design of an active concept can start.

It is then very important to choose the proper analysis methods for the individual disciplines. Usually, not the highest level of accuracy is suitable for the simulation of important effects for other disciplines. This also refers to refinement of the analysis models, where local details are not interesting for interactions. It is more important to keep the models a versatile as possible for changes of the design concepts to allow the simulation as many variants as possible. This also means an efficient process for the generation of models, including the knowledge of the user for this process. Fully automated model generators can create terrible results, if the user can not interpret or understand the modeling process.
Also the quality and completeness of analysis models is essential, as far as impacts on neighbor disciplines are concerned. Especially for formal optimization processes, model errors will create foolish results. To achieve good results, a careful selection and combination of the design variables and the completeness of the design requirements are important.

10. Conclusions

The qualities and quantities of impacts from aeroelasticity on structural loads, aerodynamic performance, maneuverability,

stability and agility of the flight control system of an airplane became more and more important in recent years. This fact is now more and more often also recognized outside the aeroelastic community.

Especially the complexity of a modern digital flight control system requires a careful identification of aeroelastic impacts to avoid degradations or costly redesigns. If an efficient MDO process can be set up early enough for a new design, aeroelastic impacts can be minimized or can even be used in a positive sense.

While this is slowly being accepted for a conventional design, concerns are already expressed, that active aeroelastic concepts may not be desirable because of possible negative interferences with the flight control system, which is already complex enough.

The development of active aeroelastic concepts should therefore not merely be seen as a task in acroelasticity. It must be a creative part of the overall flight control system design, together with the aerodynamic and structural design. This process must include experts from all involved disciplines (flight control laws, actuation systems, including those for active structures, aerodynamics, structure, and aeroelasticity) with a good understanding of the other disciplines.

If this is possible, great achievements from active aeroelastic concepts can be expected for future designs of airplanes and all kinds of flying vehicles.

References

[1] Wright, O.: How we Invented the Airplane. Dover Publications, Mineola, NY, 1988

[2] Flomenhoft, H. I.: The Revolution in Structural Dynamics. Dynaflow Press, Palm Beach Gardens, FL, U.S.A..1997

[3] Fokker, A. H. G.; Gould, B.: Flying Dutchman. The Life of Anthony Fokker. Henry Holt and Company, New York, U.S:A., year unknown

[4] Weisshaar, T. A.: Aeroelastic Tailoring – Creative Use of Unusual Materials. AIAA-87-0976-CP

[5] Shirk, M. H.; Hertz, T. J.; Weisshaar, T. A.: A Survey of Aeroelastic Tailoring – Theory, Practice, Promise. AIAA-84-0982-CP

[6] Journal of Aircraft, Vol. 32, No.1, Special Section: Active Flexible Wing, 1995

[7] Pendleton, E.; Griffin, K.E.; Kehoe, M.W.; Perry, B.: A Flight Research Program for Active Aeroelastic Wing Technology. Conference Proceedings AIAA-96-1574-CP

[8] McGowan, A.-M. et al.: Aeroservoelastic and structural dynamic research on smart structures conducted at NASA Langley Research Center. SPIE Vol. 3326, 1998.

[9] Pace, S.: Valkyrie- North American XB-70A. Aero Series Vol. 30; Tab Books, Blue Ridge Summit, PA, U.S.A..1984

[10] Noll, T.; Hönlinger, H.; Sensburg, O.; Schmidt, K.: Active Flutter Suppression Design and Test, a Joint U:S.-F.R.G. Program. ICAS- CP 80-5.5. Munich, Germany, 1980.

[11] Hopkins, M.A.; Henderson, D.A.; Moses, R.W.: Active Vibration Suppression Systems Applied to Twin Tail Buffeting. SPIE's 5th Annual International Symposium „Smart Structures and Materials". San Diego, CA, 1998.

[12] Simpson, J.; Schweiger, J.: Industrial Approach to Piezo-electric Damping of Large Fighter Aircraft Components. SPIE's 5th Annual International Symposium "Smart Structures and Materials". San Diego, CA, 1998.

[13] Larson, C.R.; Falanges, E.; Dobbs, S.K.: Piezoceramic Active Vibration Suppression Control System Development for the B-1B Aircraft. SPIE's 5th Annual Interntional Symposium "Smart Structures and Materials". San Diego, CA, 1998.

[14] Crowe, C.R.; Sater, J.M.: Smart Aircraft Structures. AGARD Symposium on Future Aerospace Technology in the Services of the Alliance. CP-600, Vol. I. Paris, 1997

[15] Andersen, G.; Forster, E.; Kolonay, R.; Eastep, F.: A Study of Control Surface Blending for Active Aeroelastic Wing Technology. 37th AIAA-SDM Conference CP-96-1443

[16] Khot, N.; Eastep, F.; Kolonay, R.: A Method for Enhancement of the Rolling Maneuver of a Flexible Wing. AIAA-CP-96-1361.

[17] Schweiger, J.; Simpson, J.: Weiss, F.; Coetzee, E.; Boller, Ch.: Needs for the analysis and intedrated design optimization of active and passive structure for active aeroelastic wings. SPIE's 6th Annual International Symposium on "Smart Structures and Materials". Newport Beach, CA, 1999.

[18] Schweiger, J.; Krammer, J.; Coetzee, E.: MDO Application for Active Flexible Aircraft Design. 7th AIAA/NASA/ISSMO Symposium on Multidisciplinary Analysis and Optimization. CP-4169, St. Louis, MO, 1998.

[19] Schweiger, J.; Krammer, J.; Hörnlein, H.: Development and Application of the Integrated Structural Design Tool LAGRANGE. 6th AIAA/NASA/ISSMO Symposium on Multidisciplinary Analysis and Optimization. CP-4169, Seattle, WA, 1996

[20] Sensburg, O.; Schneider, G.; Tischler, V.; Venkayya, V.: A Unique Design for a Diverging Flexible Vertical Tail. Specialists' Meeting on Structural Aspects of Flexible Aircraft Control. RTA Meeting on Design Issues. Ottawa, Canada; October 1999.

[21] Balanced Upgrade. Flight International, January 20-26 1999.

Aeroservoelastic Characteristics of the B-2 Bomber and Implications for Future Large Aircraft

R. T. Britt*, J. A. Volk, D. R. Dreim, and K. A. Applewhite

*Northrop-Grumman Corporation
Military Aircraft Systems Division
8900 E. Washington Blvd 9K01/ub
Pico Rivera, CA 90660-3783
United States

Abstract. Design and development of the B-2 Bomber presented many challenges in flexible vehicle control, many related to the unique configuration and design requirements. The technical challenges posed by the aeroelastic characteristics of the all-wing aircraft were recognized at the outset of the development program and included the configuration's near-neutral pitch stability and light wing loading which made the aircraft highly responsive to atmospheric turbulence. This dictated the requirement for an active digital flight control system to provide both stability augmentation and gust load alleviation. The gust load alleviation flight control system was designed by a multidisciplinary team using a combination of optimal and classical control design techniques and a common analysis model database. Accurate representation of the vehicle aerodynamics characteristics, actuators, and sensors were key to successfully developing and testing the flight control system and verifying performance requirements. Flight test data analysis included the extraction of the vehicle open loop response which were utilized to adjust the analytical models and make final revisions to control law gains. The multidisciplinary design approach resulted in the successful development of a control augmentation system that provides the B-2 with superb handling characteristics, acceptable low altitude ride quality, and substantial alleviation of gust loads on the airframe. With this back drop, a technology assessment is performed which discusses potential technology improvements for application to future bomber and large transport aircraft.

Key words: Aeroservoelasticity, Gust Load Alleviation, Flight Test, Ride Quality, Structural Mode Control

1. Introduction

Design goals for the B-2 flight control system included aggressive gust load alleviation, good ride quality, and a stable platform for weapons deployment. The design effort required a multidisciplinary team approach involving structural dynamics, aeroelasticity, and flight control specialists. Design activities included refinement of the planform configuration, design and placement of control surfaces with the required control authority to meet flying qualities and gust load alleviation objectives, selection and placement of appropriate sensors, definition of actuator force, rate and bandwidth requirements, and synthesis of the control laws.

A common analysis database was utilized by all disciplines to ensure consistent, adequate performance with the final design. This database evolved from analytical models which were then revised as results of laboratory and flight test data became available. The flight test program showed the vehicle to possess more pitch stability than predicted by wind tunnel tests. This required adjustments to the analysis models and revision to flight control feedback gains. The flutter clearance wind tunnel test program was not designed to assess rigid body pitch/flex mode coupling at transonic speeds, and unpredicted response characteristics were later discovered during the flight test program.

This paper discusses elements of model development, methodologies used to design the gust load alleviation (GLA) control system, analyses to define gust design load requirements and verify aeroservoelastic stability, and the flight test program used for system verification. Recommendations will be discussed as appropriate, as well as a discussion of new innovative approaches to flexible vehicle control and analysis.

2. B-2 Configuration Overview

The B-2 is an all wing, high subsonic aircraft which utilizes three sets of elevons for combined pitch and roll control, a centerline gust load alleviation surface (GLAS) for pitch control, and upper and lower split drag rudders for yaw control. The planform and airfoil design are dictated from a combination of aerodynamic performance, control authority, and low observables requirements. At maximum fuel loading conditions the 1st flexible symmetric wing bending mode is less than 2 hz while for low altitude high speed conditions the short period mode can approach 1.5 hz.

The aircraft employs a full time active flight control stability augmentation system. Figure 1 shows a schematic of the quad redundant flight control architecture and major components. The feedback sensors used for active stability augmentation include the Air Data System (ADS) to measure the flight condition, aerodynamic angle of attack and angle of sideslip, and the Attitude Motion Sensor Set (AMSS) to provide inertial response data.

The Flight Control Computers (FCC's) functions include computing surface position commands in response to the feedback sensor inputs, pilot inputs, and guidance commands as well as redundancy management. The FCC's also interface with other elements of the avionics system.

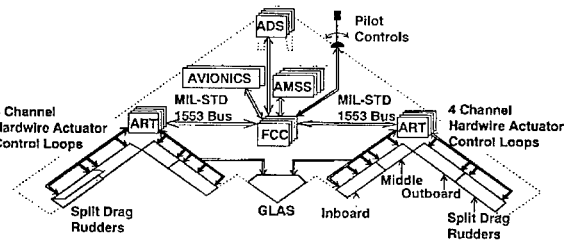

Figure 1 Flight Control Architecture

Paper presented at the RTO AVT Specialists' Meeting on "Structural Aspects of Flexible Aircraft Control", held in Ottawa, Canada, 18-20 October 1999, and published in RTO MP-36.

3. Analytical Models

Figure 2 shows the basic flow of modeling activities which supported the various analysis requirements. All models evolved from the appropriate databases. To support the many parametric analyses required to understand the vehicle response characteristics and to rapidly design effective realizable control laws, a low order structural model was desired. The aerodynamic formulation needed to reflect available wind tunnel test data, especially with respect to pitch stability, since a flying wing design is inherently marginally stable or unstable in pitch. The models also needed to be capable of including a representative model of the actuation system and sensors. MSC/NASTRAN was the primary tool for conducting the modeling activities and for performing the analyses for determining flutter speeds and gust loads. Elements of the NASTRAN solution were also used as input to a state space model formulation used for control law synthesis and analysis. Note that the flow of information through the system was driven by many different separate programs and analysis steps and was by no means automated.

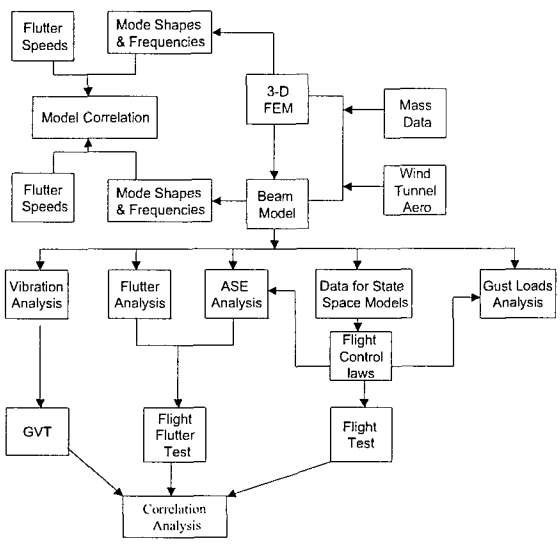

Figure 2 Model Synthesis

Structural Modeling

Basic structural and aerodynamic modeling was carried out in the MSC/NASTRAN[2] finite element modeling system. The majority of dynamic analyses utilized half-span models. Separate symmetric and antisymmetric response analyses being accomplished by inserting the appropriate centerline boundary conditions. A high order stress model was reduced for dynamic analyses and included over 10,000 elements, 3800 grid points and a reduced analysis set (A-set) of 631 degrees of freedom (Figure 3). A simpler 'beam' FEM was constructed for use in the many parametric analyses. The models were reviewed and modified as appropriate subsequent to the full scale vehicle ground vibration test.

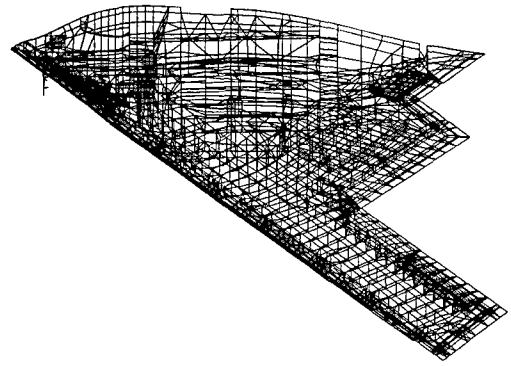

Figure 3 Half-Span Finite Element Model

Aerodynamic Modeling

The subsonic aerodynamic forces for both motion and gust induced angle of attack were generated from a half-span 384 box model (Figure 4) developed to satisfy reduced frequency requirements for both flutter and dynamic gust response analyses. The two dimensional Doublet Lattice Method (DLM) was selected to develop the unsteady forces.

Steady wind tunnel test data was available from testing performed on two models. The first model was 0.032 scale and the objective was obtaining an airloads database including the effects of controls and inlet mass flow. This model was tested in the Arvin-Calspan 8 ft by 8 ft transonic tunnel. A second model of the 0.06 scale was tested in the PWT 16 foot tunnel. Test objectives included obtaining data for basic stability, control effectiveness, Reynolds No., and airloads verification.

Comparisons were made between the low frequency prediction of the Doublet lattice model and certain parameters derived from measured data. Coefficients of particular concern were the spanwise distributions of lift curve slopes and aerodynamic centers, and the total pitching moments due to control surface deflection. These were developed from pressure distributions at angles of attack representative of trim. These are important parameters relative to the assessment of basic vehicle pitch stability and for developing active control schemes for ride quality and gust load alleviation. A correction factor program (reference 3) was utilized to develop weighting factors which when applied to the DLM aerodynamics insured that the spanwise distribution of lift curve slopes and aerodynamics centers matched wind tunnel test data. The weighting factors are applied directly to the box forces in NASTRAN (via DMAP Alter) and, therefore, apply to all modes. The correction factor methodology was unable to generate factors which would also satisfy the pitching moment due to control surface deflection constraint and therefore they were handled as part of the gain scheduling in the active system implementation. Figure 5 shows the aerodynamic model box layout with the values of the factors shown on the figure.

Since the correction factors were generated for steady flow conditions the application of them to all reduced frequencies was reviewed. Early flutter analysis comparisons with both low and high speed flutter model test results demonstrated

that the flutter phenomena could be successfully predicted without the aid of correction factors, and therefore it was decided to schedule these factors as a function of reduced frequency. A reduced frequency of 0.4 was chosen as the point at which all the correction factors would become unity. This value was recommended in reference 21. Therefore, the factors generated for each box force coefficient were linearly interpolated with reduced frequency so as to become unity at a reduced frequency of 0.4.

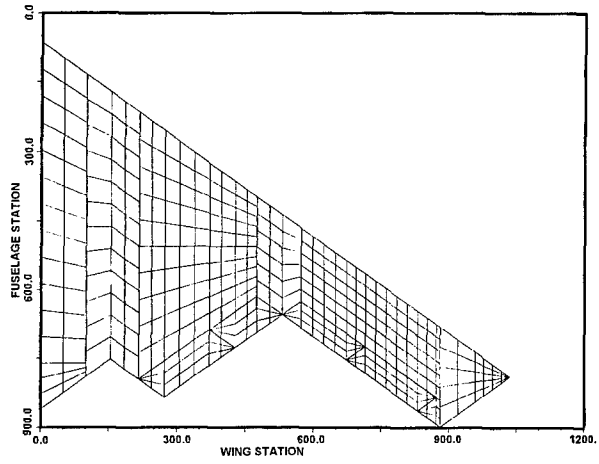

Figure 4 Doublet Lattice Model

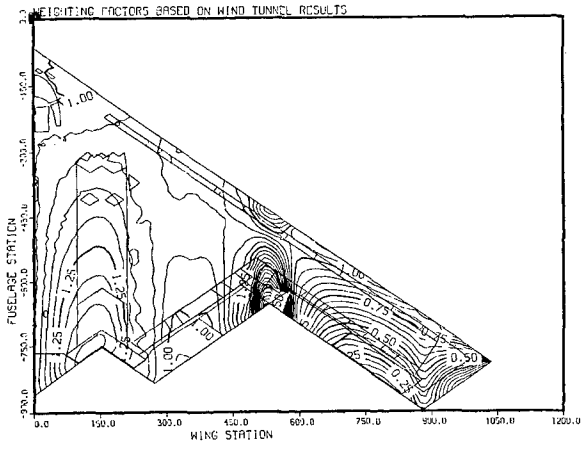

Figure 5 Weighting Factor Distribution

Frequency Domain - State Space Conversion

MSC/NASTRAN was utilized to generate the basic data necessary to transform the 2nd order frequency domain equations of motion into a state space formulation required for flight controls design tasks. Generalized mass, stiffness and aerodynamic matrices (both motion dependent and gust disturbance) were the starting point for this model. A subset of the physical degrees of freedom in the mode shapes were provided at locations of interest so that physical motions could be recovered to define sensor feedback outputs and forces developed by the actuation system. Bending moment modal coefficient data were also provided.

Conversion into a state space formulation[4,16] requires a frequency domain approximation of the doublet lattice aerodynamics. The method of reference 17 was used for this purpose. The resulting analog state space models retain 2 rigid body (pitch and plunge) modes, 16 flexible modes, four control surface inputs, and a gust disturbance input. The analog state space models generally have about 100 states. The large number of states utilized by the method of reference 17 limited the number of structural modes that could be retained. The use of alternate aerodynamic approximations, which feature a smaller number of states, has not been explored on the B-2 but would be recommended for future development work.

Excellent agreement between the NASTRAN frequency domain solution and the state space model was achieved as seen from the comparison of Figures 6. Close agreement is absolutely mandatory if control law performance is going to be consistent between the two models.

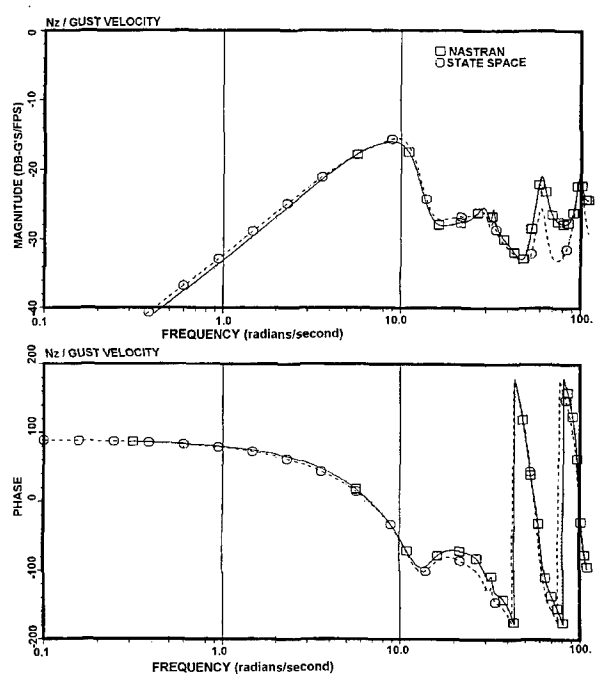

Figure 6 Response due to Gust

Actuator Modeling

A model of the actuation system was required in both the NASTRAN formulation and the state space model. The actuator was modeled as a force-producing element between the control surface and back-up structure rather than as an enforced deflection. This allows the dynamics of the combined actuator and control surface to be reflected in the analysis. In NASTRAN the multi-point constraint (MPC) feature is used to define relative motion using *scalar point* degrees of freedom. The block diagram in Figure 7 shows the general form of the model[1]. The actuator includes an outer position control loop and dynamic pressure feedback control loop to dampen the control surface resonance modes at low dynamic pressure (or low aerodynamic damping). *Extra point* degrees of freedoms are used to define other block diagram variables. The transfer function (TF) option is used to define the actuator model in NASTRAN. Figure 8 shows the actuator and surface response to command, illustrating the surface dynamics included in the model.

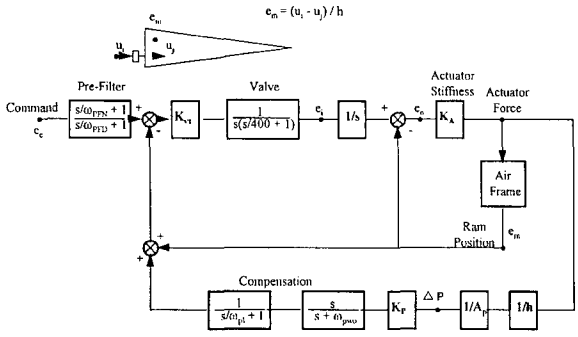

Figure 7 Actuator model

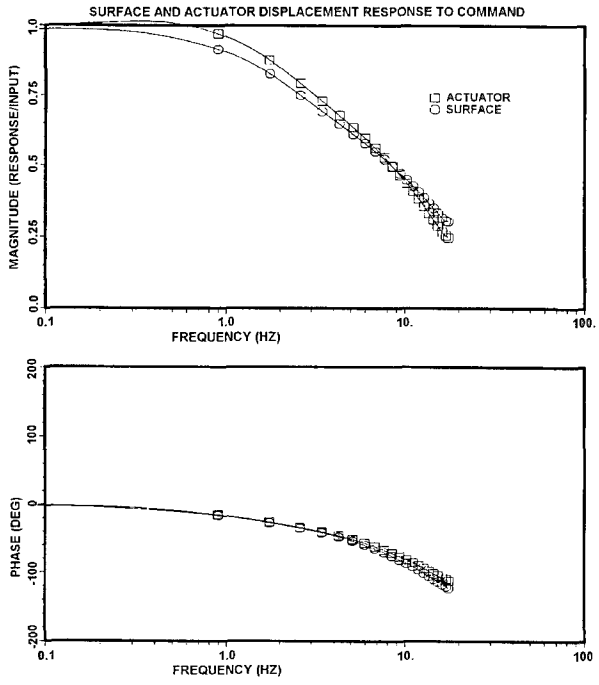

Figure 8 Surface Response to Command

Actuator dynamic stiffness and hinge line back-up stiffness can be included in the basic structural model which produces the vehicle modes. An alternative approach is to omit these springs in the modal analysis and add them back in at the modal level when the actuator equations are added to the equations of motion. The latter approach, using a truncated set of structural modes, leads to greater accuracy than the former. The actuator model shown in the block diagram of Figure 7 is for the zero frequency control surface mode formulation.

This model of the actuator allows the calculation of actuator rates which can then be used to determine practical gain scheduling based on realizable surface rates. The model is extendible to use in non-linear simulations where the effects of actuator rate and deflection limits, hinge moment limiting, and actuator hydraulic pressure limits could be assessed.

Digital Effects

Early flight control analysis showed the high bandwidth required for effective GLA performance was sensitive to the phase degradation of feedback signal data latency and digital implementation. To minimize these effects, a "bottom up" approach was taken to define performance and throughput requirements for the sensors, MIL-STD-1553 multiplex bus traffic and timing, FCC timing and throughput calculations, actuator bandwidths, and surface rates.

Feedback signal data latency was defined and included into the digitized models as partial and full frame delays. Feedback data latency is the finite time delay measured from the analog air vehicle motion or state feedback, through the Flight Control Computer (FCC) surface command calculations to the actuator command at the Actuator Remote Terminals ARTs. The digital response in Figure 9 shows the phase lag due to throughput and digitization effects compared to the analog response.

Analog filters were developed to approximate the ratio of the open loop digital and analog model frequency responses. These filters were then applied to the NASTRAN analog model to approximate the GLA performance with the digital and throughput delay effects. Figure 9 shows how these analog filters adequately approximate the digital model response up to 70 radians/second, which is well beyond the GLA controller frequency range of interest. Flutter analyses included additional filters to assess the impact of phase shifts beyond this frequency.

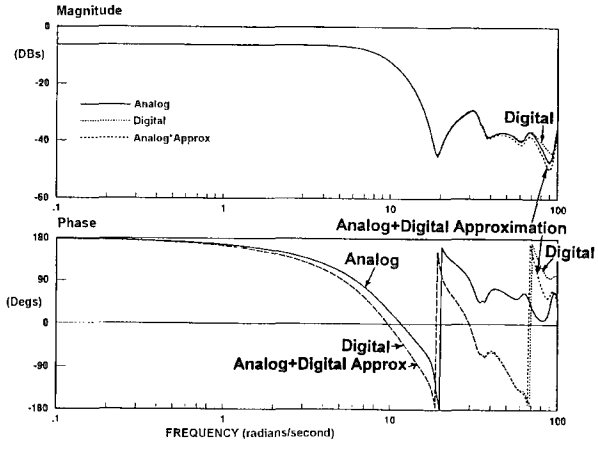

Figure 9 Open Loop Pitch Rate to Inboard Elevon

4. Gust Load Alleviation(GLA) Summary

Gust load alleviation control of the B-2 involves quickly pitching the aircraft into the gust to control the build up of gust angle of attack and thereby minimize normal acceleration and structural loads. Effective gust load alleviation performance requires a high bandwidth pitch control augmentation system with high control surface rates. Lateral gust load alleviation was not required due to the low projected side area.

Figure 10 shows an example of the centerline bending moment gust load alleviation performance achieved on the B-2. Generally, the GLA controller performance reduces incremental gust loads by up to 50% when compared to an

open loop (unaugmented) model, or a closed loop handling qualities controller design. Similar ride quality improvements are also attained.

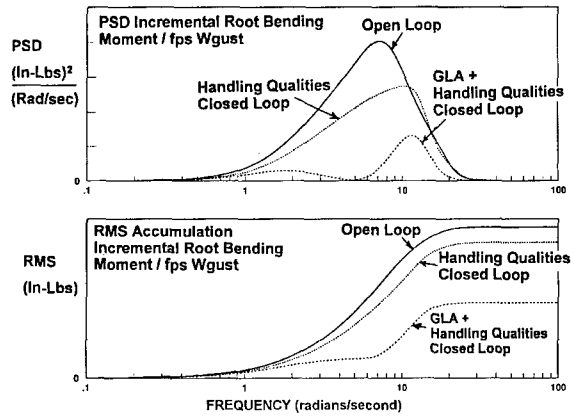

Figure 10 GLA Performance

Gust design load requirements were derived from continuous turbulence analysis criteria[8] and are greater than maneuver requirements over a significant portion of the inboard wing. Considerations related to development of phased load design conditions for structural analysis followed approaches similar to those in reference 9. Effects of control system nonlinearities at peak gust conditions were included, also in a manner similar to those in reference 9. Non-uniform spanwise gust effects have also been examined for the B-2[10].

Gust Load Alleviation Controller Development

The Pitch Control Augmentation System (PCAS) GLA synthesis utilized classical and modern control theory methods. Piloted simulation was used to verify and adjust, as required, the predicted handling qualities.

Optimal controller results were used to bound the achievable GLA performance and focus development of a classical multiple input multiple output (MIMO) design. Each feedback loop was confirmed by classical analyses and a solid physical understanding before implementation. This quickly eliminated many ineffective "optimal" gains, and retained the available elevon surface rates for the best control loop GLA performers.

The B-2 PCAS achieves consistent Level 1 handling qualities throughout the flight envelope using a load factor and pitch rate proportional plus integral (NZQPPI) design. GLA performance is achieved with a combination of NZQPPI low frequency control and a *gust sniffer* loop for mid and high frequency control. The *gust sniffer* loop senses the aerodynamic gust angle (Figure 11) of attack by subtracting the inertial angle of attack from the total (inertial + gust) aerodynamic angle of attack at the nose. Feedback gains, loop shaping compensation, and surface utilization mixing are scheduled with flight condition.

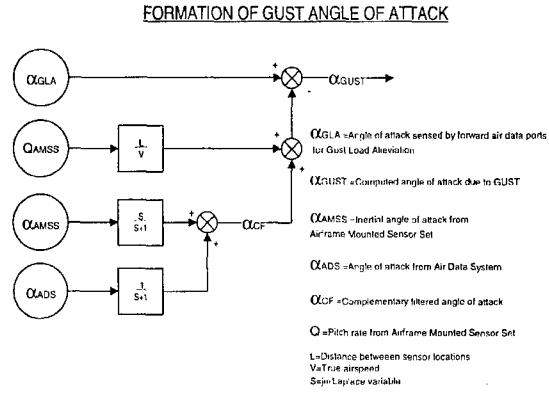

Figure 11 Gust Angle of Attack

Pitch Control Surface Utilization

Innovative pitch control surface mixing is used to provide active flexible mode damping at low and high altitudes. Figure 12 shows the node line of the first flexible symmetric mode. Aggressively pitching the B-2 into vertical gusts at low altitude using the GLAS and Inboard Elevons significantly reduces the low frequency rigid body gust response, but tends to excite the first flexible mode. Since the Outboard Elevon is outboard of the node line, commanding it out of phase with respect to the Inboard Elevon dampens the first flexible mode response. The Outboard Elevon also provides local high frequency direct lift control by decambering the local wing chord.

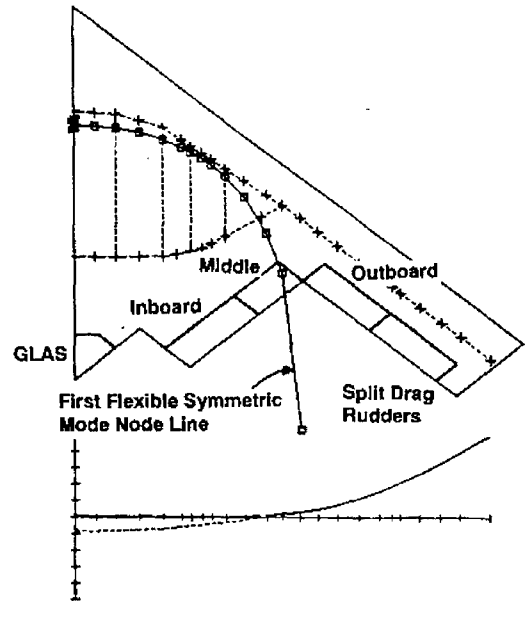

Figure 12 1st Flexible Symmetric mode

Figure 13 shows the effectiveness of utilizing the outboard elevon out of phase in reducing the center line bending moment.

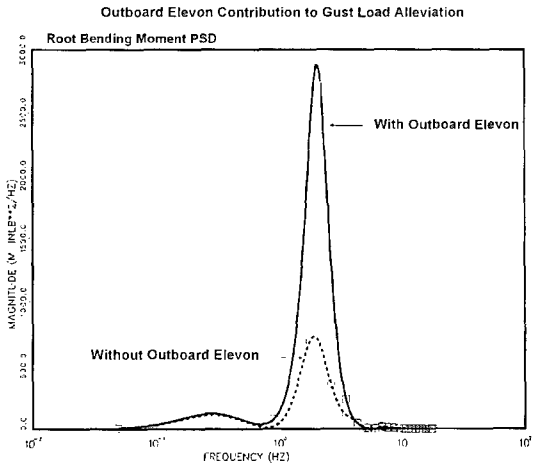

Figure 13 Effectiveness of Outboard Elevon

Reduced aerodynamic damping at high altitude produced a significant flexible mode contribution to the total pitch control loop for heavy outboard fuel conditions. An innovative control surface mixing concept, referred to as the *Inertial Damper*(reference 18*)*, was developed to minimize the excitation of and dampen the 1st flexible mode while still maintaining the required control loop bandwidth. Flight test data in Figure 14 shows how the *Inertial Damper* surface mixing achieves the desired flexible mode gain attenuation without incurring the additional phase lag from a classical notch filter implementation.

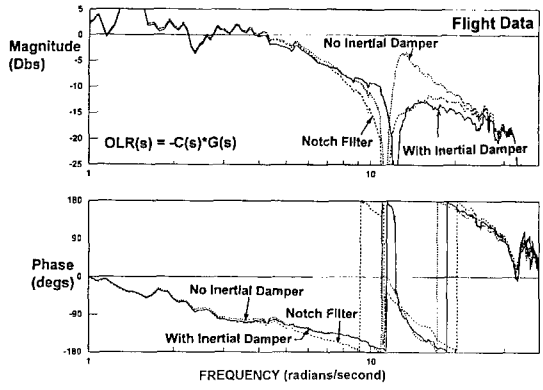

Figure 14 High Altitude Inertial Damper

5. Flutter Analysis

Matched point flutter analyses were performed using the PK solution in NASTRAN. Both symmetric and antisymmetric analyses were conducted. Matched point flutter analyses including the active flight control system were also performed. The spanwise stiffness distribution of the graphite composite wing box of the B-2 was tailored to achieve a wide separation between the fundamental bending and torsion frequencies. As a consequence the basic flutter speeds were predicted to be well outside of the required flutter boundary. The minimum flutter speed condition involved coupling between antisymmetric 1st and 2nd bending and 1st torsion modes. The flutter frequency was approximately 9 hz and the flutter speed was well outside the required envelope.

A series of wind tunnel tests, both high and low speed were performed during the development program. One low speed test featured a model which was cable mounted and included an active system for dynamic pitch control. Correlation of this test with analysis was excellent and provided confidence in the modeling analysis procedures.

There were a series of three transonic flutter model entries. Two entries were wall mounted semispan models of 3.5% scale. The third entry was of a full span model on a sting of 1.75% scale. A set of flutter speed correction factors was developed from the semispan models by comparing test results with corresponding analysis of the flutter model. The full span model was used primarily to verify that the antisymmetric flutter mechanism produced the lowest flutter speed. None of these tests were able to evaluate the interaction between the pitch mode and the flexible modes of the vehicle.

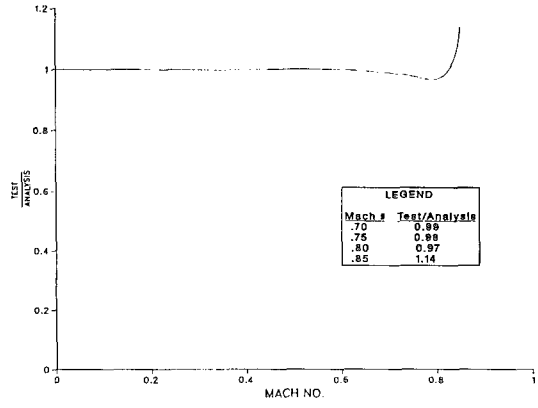

Figure 15 Transonic Flutter Speed Correction

6. Flight Testing

Flight testing (reference 12 and 18) was conducted to verify that flutter, flying qualities, and other dynamic response characteristics were satisfactory. Because of the highly augmented flight control design, integrated flight control and flutter flight tests were required during envelope expansion.

The vehicle was dynamically excited by oscillating the control surfaces. This was accomplished with pilot pitch and roll stick inputs or by special test hardware (Flight Control Test Panel (FCTP)), mounted in the cockpit. The bandwidth of the actuation system, together with the size of the B-2 control surfaces, was sufficient to provide effective excitation of the air vehicle. Frequency and damping could be readily determined from the recorded data.

The final test matrix for flutter clearance did not include the assessment of payload effects. Test schedule and asset availability required a continual review of test requirements. Low speed wind tunnel flutter model testing and extensive parametric analysis did not indicate flutter sensitivity to payload so these points were not flight tested.

Subsequent flight controls clearance testing with payload showed an apparent coupling between the rigid body pitch

and first wing bending mode at a Mach number just beyond the operational limit. This has been reported in references 19 and 20 and referred to as Residual Pitch Oscillation or RPO.

7. Flight Test Matching/Model Update

Full time active flight control augmentation requirements prohibited testing with the augmentation disengaged. Control surface effectiveness, surface mixing, and short period/flexible mode interaction are important to both the B-2's high altitude *Inertial Damper* and low altitude high speed GLA performance. Verification of the accuracy of the open loop aeroservoelastic model, therefore, was necessary.

B-2 flight test data parameter identification and model matching attempts using NASA's MMLE3 (Modified Maximum Likelihood Estimator[14]) program gave inconsistent results, with wide variations in model estimates between very close flight conditions, for all except the basic dominant derivatives. Parameter identification was further complicated by the sensitivity of closely coupled flying wing aircraft to differential motions between the structural(sensor) and mean inertial axes[15]. While early flight test results verified the basic aeroelastic stability and flying quality performance, detailed correlation with the analytical models indicated that some aerodynamic terms required adjustments.

The flight data verification bypassed the difficulties and limitations experienced in the past by directly developing open loop frequency domain "Flight Data Models", G(s), from the closed loop responses. The open loop "Flight Data Models" (FDMs) permitted direct frequency domain comparisons with the aeroservoelastic models, closed loop design performance verification, and flight test based analysis confirming proposed design adjustments. Quasi-steady low frequency (wind up turn) flight test results compared reasonable well with predicted wind tunnel data. The FDMs successfully captured the effects of the unsteady aerodynamics and flexible vehicle interaction for the mid frequency range near and around the short period and first symmetric flexible mode. The high altitude *Inertial Damper* was efficiently tuned using the open loop FDMs.

Figure 16 shows the open and closed loop MIMO FDM frequency response matrix format. Closed loop time response flight test data to individual pitch control surface random excitations were collected using the Flight Control Test Panel. High coherency frequency responses of the closed loop outputs to the known random surface excitations were then constructed during post flight analysis, and included in the appropriate column of the closed loop frequency response matrix Gcl(s). C(s) is the "constant" MIMO Controller for the tested condition. By keeping the vehicle configuration and flight condition constant, the only unknown in the closed loop equation is the open loop frequency response G(s), shown in Figure 16.

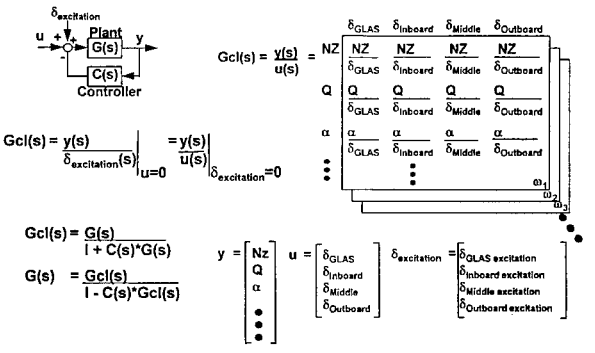

Figure 16 Open Loop Response Calculation

The vehicle configuration gross weight, center of gravity, and fuel distribution were kept approximately constant by collecting all the necessary individual surface excitations for a given flight condition in rapid succession. The flight condition was kept constant by using the autopilot to maintain pitch attitude and thereby trim altitude and angle of attack. The pilot's only task was to maintain the desired speed condition using slow smooth throttle movements. Keeping the pilot's hands off the stick eliminated any "disturbances" in the closed loop response due to unknown and adaptive human pilot control loop inputs.

The open loop MIMO FDM compared well with the open loop quasielastic (rigid + elastic corrections) and aeroservoelastic models. Increased pitch stability and variations in individual surface effectiveness were noted. Comparisons were also made of the total pitch control open loop return (OLR= -C(s) *G(s)) developed from a single pilot pitch frequency sweep and the open loop FDM. Figure 17 shows a good match between approximately 2 to 40 radians/second which was the frequency range of interest and where the individual surface excitation power was concentrated.

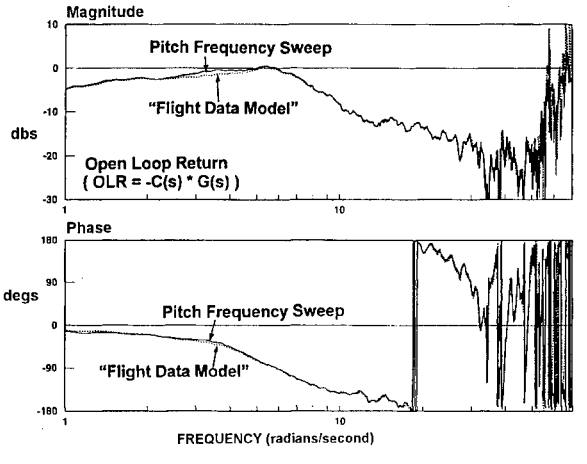

Figure 17 Flight Data Model

Post flight analysis compared the FDMs with the predictions of the NASTRAN model. Flight data analysis indicated that the vehicle had more static stability than predicted. A uniform adjustment (% MAC shift) in aerodynamic center was made across the span of the wing by modifying the aerodynamic weighting factors as shown in Figure 18. Figures 19 shows good agreement of the adjusted NASTRAN models and FDMs.

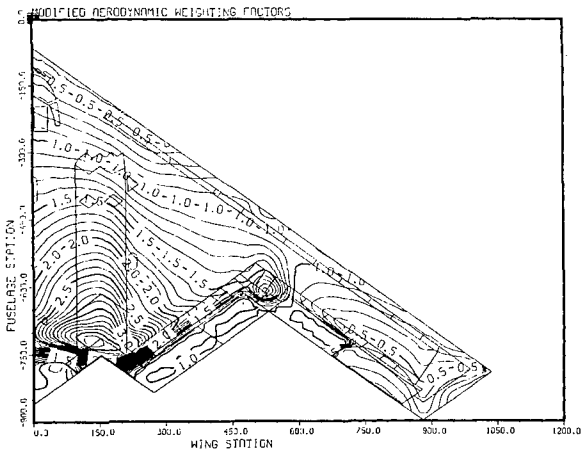

Figure 18 Flight Test Adjusted Weighting Factors

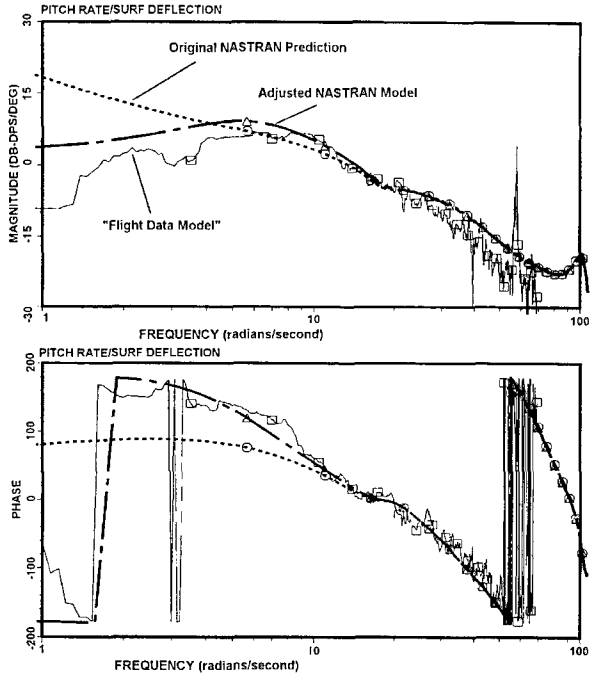

Figure 19 Open Loop Pitch Rate to Inboard Elevon

8. Residual Pitch Oscillation

The B-2 aircraft encountered a nonlinear aeroelastic Residual Pitch Oscillation (RPO) during low altitude high speed flight testing. The RPO response was observed after control surface pitch doublets were input at flight conditions outside the operational envelope. The initial air vehicle response decayed in amplitude but transitioned to a small, constant amplitude, residual pitch oscillation after several cycles (See Figure 20).

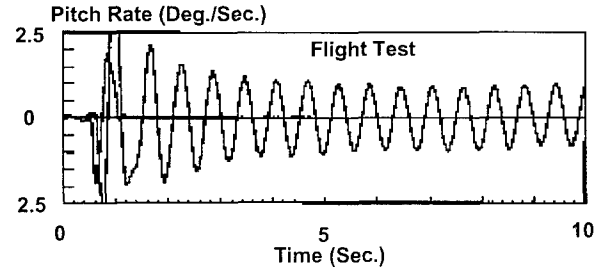

Figure 20 - Typical RPO Response To Pitch Doublet

The RPO phenomenon was not predicted by analytical methods to this point in the program, was not observed during low or high speed wind tunnel flutter testing, and was not observed during the previously completed flight flutter testing. Aeroelastic models using linear aerodynamic representations were incapable of capturing RPO. The low speed wind tunnel testing lacked the effects of transonic flow. When the high speed wind tunnel flutter model was designd it was decided to mount it rigid and avoid the complexity of making the model free flying since the flying wing was statically unstable for certain conditions. This prevented detection of RPO during the high speed wind tunnel programs. RPO was not observed during the flight flutter test program because the most RPO critical configuration of heavy payload and forward center of gravity condition had not been included in the final test matrix.

After the RPO was encountered, 11 dedicated flights were flown to collect data to better understand the phenomenon and to define the on-set boundaries. Figure 21 shows typical vertical load factor responses to pitch doublets as an RPO condition is approached by slowly increasing Mach number in level flight. The response transitions from being highly damped to being oscillatory with a relatively small increase in Mach number. During the flight program, conditions of zero damping were encountered on the critical heavy weight configuration.

Analysis of the RPO flight data did not show the characteristics normally expected of a classical flutter phenomenon. An oscillating shock was visible in the condensation cloud over the engine nacelles during some of the forced response tests. Flight test data indicated that the aircraft aerodynamic center moved aft by as much as 3 feet as the RPO Mach was approached.

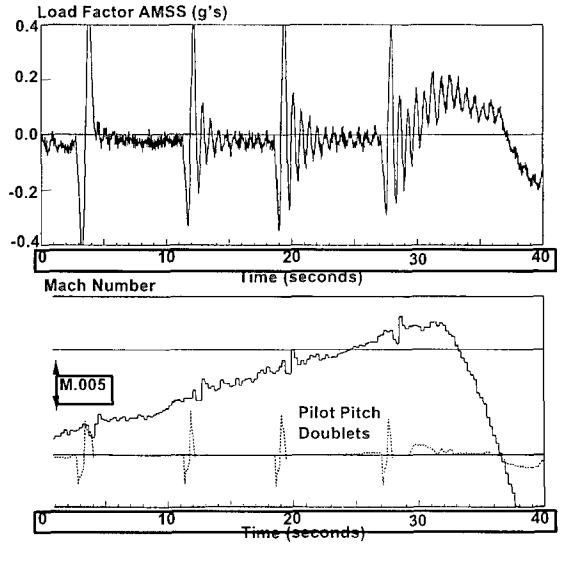

Figure 21 - Pitch Response Approaching RPO

Two analytical model development approaches were initiated to increase the understanding of the RPO phenomenon and investigate potential fixes. The first approach assumes that the unsteady air loads in the transonic regime can be represented as the superposition of linear theory and a supplemental linearized transonic shock force doublet. Model solutions are performed in the frequency domain with

conventional methods. The shock force doublet phase lag relative to angle of attack could be tuned to produce a zero damped condition. The second approach utilized the time marching computational aeroelastic method of NASA Langley's CAP-TSDv code. Good success was achieved with CAP-TSDv in simulation of RPO. Details from these studies have been reported in References 19 and 20.

These studies combined with the flight test results, provided insight into the RPO mechanism. As the vehicle airspeed is increased toward RPO, shock formation on both the upper and lower surfaces cause an aft shift in the aerodynamic center. This increases the static stability and increased the frequency of the rigid body short period motion. For low altitude high speed conditions, the increased short period frequency causes an interaction with the 1st symmetric wing bending mode (for certain configurations). As RPO oscillations ensue, the shock locations become oscillatory and participate in the aeroelastic phenomenon. The constant amplitude residual pitch oscillations (as shown in Figure 20) were determined to be caused by deadband in the control surface actuators and to occur at conditions where the critical mode damping was small.

A Mach number overspeed protection warning was developed to help the pilots avoid encountering an RPO outside the operational envelope. The primary concerns that required avoiding the RPO included undefined structural loads in an RPO with turbulence and reduced fatigue life considerations, flying qualities, and safety of flight considerations. This system includes an audio warning to the pilot which is a function of the configuration, current Mach number, and acceleration rate. Pilots are alerted to reduce thrust to slow the acceleration when approaching a potential RPO condition. Piloted simulator and flight test evaluations were performed to show that the Mach overspeed protection system provided good lead time indications so the pilots could avoid RPO.

10. Technology Assessment

This section of the paper, in light of the B-2 aeroelastic and aeroservoelastic design challenges presented, assesses technology needs for a future heavy bomber or transport of a similar configuration. Technologies assessed will include those to improve the design process, as well as consideration of emerging hardware concepts.

Design Methods

Areas of recent research activity relating to improved design tools for aeroelastic and aeroservoelastic design can be categorized into two areas, 1) High Fidelity Simulation and Test 2) Multidisicplinary Design Environment.

A recurring theme related to areas needing improvement is in the area of aerodynamic analysis and test, both steady and unsteady. For example, the RPO condition previously discussed was not predicted by either analysis or test, primarily due to the inability to capture transonic shock oscillations. The high speed flutter model used during B-2 design development was fixed on a sting, therefore the rigid body modes that are key ingredients of the phenomenon were not represented. A high speed flutter model to predict RPO would have required an unrestrained model with an active control system. This was not deemed practical, and it is unlikely that this is a viable avenue for future programs. Scaling issues in themselves are intractable, for example actuators do not scale down well and would likely impose mold line bumps which may significantly influence results.

A more affordable practice may be to perform unsteady (forced oscillation) wind tunnel tests where pressure data is captured, then imported into analytical models. It is possible that sufficient data would have been available to capture the B-2 phenomenon if such a test and analysis were performed, however boundary layer and shock scaling need to be considered carefully. Such tests with flexible models would be preferable, but not always necessary, and may not be practical with high Reynold's number loads.

The CAP-TSDv code was able to simulate the RPO condition *after the fact,* requiring a significant effort to extend the code's capability to include rigid body modes and an active control system. Even though chosen over other CFD based aeroelastic tools for computational efficiency , each time accurate RPO simulation takes approximately 8 hours of CPU on a high end multiprocessor workstation. Considering projected advances in computational performance it is still doubtful that the number of simulations required to capture like phenomenon could be accomplished in a manner consistent with vehicle program development schedules. Navier-Stokes based aeroelastic CFD approaches would take at least an order of magnitude more compute time than CAP-TSDv. For this reason research into Reduced Order Methods is of interest, such that results of high fidelity aerodynamics codes may be used in quick turnaround aeroservoelastic, flutter and static aeroelastic analysis. aeroelastic analysis. The duration of time required to assemble and execute a high fidelity analysis to simulate behavior such as the B-2 RPO
is of concern. The extensive, focused effort also resulted in a procedure with many elements specific to the B-2. Modifying the code for each new applications will require problem specific changes. The ability to quickly assemble and execute high fidelity aeroservoelastic systems is imperative to minimizing the likelihood of future problems such as RPO, as
well as addressing issues that do arise.

Regarding the multidisciplinary design environment, recent research emphasis has been on developing multidisciplinary frameworks for design and analysis. One representative system in development is the MultiDIsciplinary Computational Environment (MDICE)[22] activity funded by the Air Force Research laboratory (AFRL). The strategy of this design framework is that of the loosely coupled systems - a framework where user selected CAD and CAE tools may be 'mixed and matched' to perform model generation and multidisciplinary analysis. The MDICE software is a graphically driven, object oriented system providing dynamic data sharing, execution control and synchronization. A key element of the system are interdisciplinary interfaces - such as algorithms to connect fluid-structure boundaries. MDICE hosts a library of interface routines selectable by the user, as well as the ability for the user to attach routines of choice. Various aeroelastic applications have been demonstrated[23], with plans to extend demonstrations to aeroservoelasticity.

MDICE is just one of many frameworks being developed for engineering design environment automation. Maturation and implementation of systems to conveniently and robustly couple engineering design disciplines is imperative to cost effective future design and development programs. The ability to *selectively* incorporate high fidelity modules is a very attractive feature of loosely coupled systems.

Actuation and Sensor Technology

A problem area typically encountered to some levels in vehicle development is accurate determination of vehicle body axis rates. Flexible modes are typically filtered out by notch filters. Resulting phase lag reduces system stability margins, and sensor noise causes design and performance issues. To address this, under the AFRL AMICS[24] program, a Rigid Body Synthetic Sensor (RIBS) approach was designed and tested analytically. This approach proposed a distributed sensor network whose data was processed by neural network algorithms, providing spatial filtering. The test demonstrated the ability of the RIBS approach for control law state system feedbacks which could be used both in the design process, as well as real time on board sensing. Research and development is continuing in the microsensor area such that they could be affordably implemented into vehicle structure. Micro gyros are projected to have unit costs under $10. Figure 23 presents a high level schematic of the RIBS approach for lateral directional rate sensing.

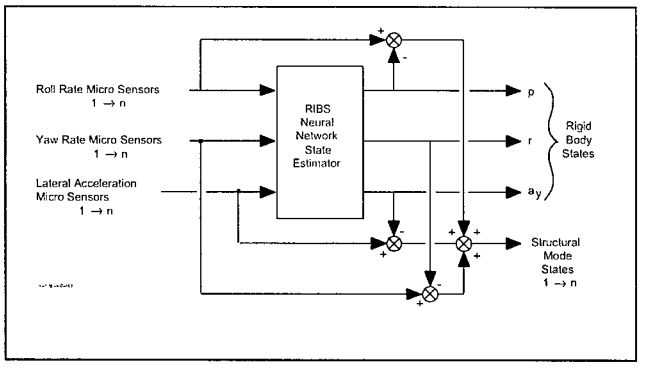

Figure 23 - RIBS Simplified Block Diagram for the Lateral-Directional Axis.

Much of the research in advanced actuation is in the area of electric actuators. The primary motivation is to reduce manufacturing costs and maintenance costs by replacing costly hydraulic systems with potentially lower cost electrical ones. Both electromechanical (EMA) and electrohydrostatic (EHA) actuators are being developed. The electrohydrostatic actuators are self contained units incorporating electrically driven 'local' hydraulic systems which power the individual actuator. The DARPA Fly-By-Light Advanced Systems Hardware (FLASH)[25] program is performing modeling, analysis, testing and system demonstration of EHAs.

The B-2 requires relatively high bandwidth control actuation due to the inherent instability of the system and the GLA system requirements. Slight lags are induced by the centralized hydraulic system, but somewhat larger lags are realized by the direct valving system. This valving system also resulted in some secondary ringing in conjunction with the RPO phenomenon, as reported in the previous section. In general the lags were manageable, the primarily impact being increased control system design costs to model and accommodate the lags to meet system requirements.

Electrohydrostatic actuation is a promising technology, however most of the gains are related to overall system level benefits (lower cost, improved reliability and maintainability) with goals to meet current conventional actuation performance. Lags due to valving may be addressed in a similar manner whether conventional or EHA, so this may not be a significant discriminator. Lags due to distance from the centralized unit of conventional systems are eliminated.

Electromechanical actuators also strive for similar system level benefits as the electrohydrostatic. A clear benefit would be the inherent near zero lag of electromechanical systems. However there is a tradeoff in bandwidth due to the large amount of gearing required. ElectroMagnetic Interference (EMI) of the actuator is an area that also needs to be addressed. In the cases of both the EHA and EMA, fiber optic control is proposed and has been demonstrated. Fiber optics provide data rates that easily meet specification, however both systems require power distribution by electrical cabling which is being evaluated for cost, reliability and maintainability vs. conventional hydraulics.

Adaptive Structures

Active Aeroelastic Wing (AAW)[26] is a technology about to go into the flight demonstration phase on a modified F/A-18. This technology is most applicable to designs requiring additional structural weight to prevent control surface aeroelastic degradation at high dynamic pressure. Instead of stiffening the structure, innovative control logic optimizes the surface usage for given flight conditions to both alleviate maneuver loads and provide control authority. It is not felt that the technology would be well aligned with a B-2 class vehicle, because wing stiffness design is dominated by strength considerations from a variety of sources not including static aeroelasticity as illustrated in figure 24.

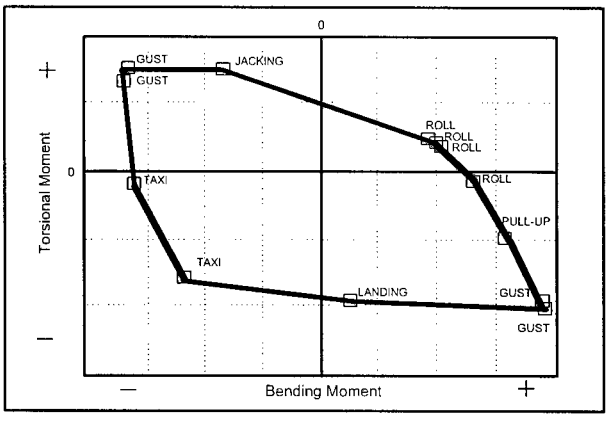

Figure 24 - This load diamond of a B-2 wing station illustrates the wide variety of loading conditions that define the wing stiffness (Roll refers to roll maneuver).

The AAW concept also leans towards larger numbers of control surfaces to provide more design variables to optimize

for various maneuver and dynamic pressure conditions. B-2 class vehicles strive for continuous structure and low control surface activity to minimize radar cross section and improve survivability. AAW was initially conceived for fighter aircraft weight reduction and performance enhancement. This technology may also be conducive to supersonic transports or bombers, where slenderness constraints impose intrinsic stiffness limits, however flutter suppression may be required.

The Twist Adaptive Wing System (TAWS)[27] and Continuous Aerodynamic Control Surface concepts strive for aerodynamic controls which are seamless for both improved aerodynamic performance and survivability. TAWS is geared towards medium to high aspect ratio wings. It incorporates an internal mechanism to twist the wing to provide incremental lift for maneuvering, load alleviation and performance optimization. The TAWS concept has also showed significant potential in reduced manufacturing costs by reduced part count and sealing the structure from environmental damage. Continuous aerodynamic control surfaces technologies can be generally describes as advanced seals which maintain structural continuity for relatively conventional aerodynamic control mechanisms.

Concepts in this class will be of continued interest for military bombers and transports due to multiple benefits provided, particularly survivability. In fact, deformable surfaces were considered in the early B-2 design stages, but were abandoned due to lack of technical readiness and inadequate control authority at low speed.

Summary

Future bomber and large transport designs can clearly benefit from emerging technologies in the following fields:

- Multidisciplinary Frameworks Which Manage and Couple Multidisciplanry Databases and Models in an Automated, Consistent and Robust Fashion
- Practical Methodologies for Incorporating Unsteady Wind Tunnel Pressures into Flutter and Aeroservoelastic Simulations
- Reduced Order Aerodynamic Methods for Aeroservoelastic Simulation
- Embedded Distributed Sensor Networks for Robust Real Time State Determination
- Improved Linearity and Frequency Response Actuation (eliminate deadband)
- Deformable/Adaptive Structures for Improved Aerodynamic Performance and More Affordable and Maintainable Survivability

11. Concluding Remarks

The B-2's unconventional configuration, low wing loading, broad operating envelope, and unique aeroelastic characteristics presented a number of design challenges. The design solution integrates three-axis stability augmentation and vertical gust load alleviation functions into a quad redundant digital flight control system which provide the vehicle outstanding handling and ride qualities throughout the flight envelope.

This paper outlines the multidisciplinary approach to developing the analytical models used in refining and validating the total system design. Some of the unique aeroelastic characteristics have also been discussed. Finally, a technology assessment is performed which discusses design methods and technology improvements in the areas of actuators, sensors, and adaptive structures that could benefit future bombers and large transport aircraft.

References

1. Schaefer, W. S. , Inderhees, L. J., and Moynes, J. F., "Flight Control Actuation System for the B-2 Advanced Technology Bomber," SAE Technical Paper #911112, October 1990.
2. "MSC/NASTRAN Aeroelastic Supplement," June 1980, by the MacNeal-Schwendler Corporation
3. Giesing, J. P., Kalman, T. P., and Rodden, W. P., "Correction Factor Techniques for Improving Aerodynamic Prediction Methods," NASA CR-144967, May 1976.
4. Stone, C.R., "Modelling For Control," Proceedings For The Aeroservoelastic Specialists Meeting, AFWAL-TR-84-3105, Vol II, October 1984.
5. Thompson, P. M., "Hybrid Statistics of Sampled-Data Systems with Delays", Systems Technology, Inc. Hawthorne CA., 18 October 1991.
6. Whitbeck, R. F., "Short Course on Hybrid Stats," Northrop Grumman Corporation., September 1990.
7. Jacobson, S. B. & Moynes, J. F., "Ride qualities Criteria for the B-2 Bomber," AIAA-90-3256, September 1990.
8. Military Specification, "Airplane Strength and Rigidity, Flight Loads," MIL-A-008861A(USAF), March 1971
9. Hoblit, F. M., *Gust Loads on Aircraft: Concepts and Applications*, AIAA Education Series, American Institute of Aeronautics and Astronautics, Inc., Washington D.C., 1988, pp.166.
10. Crimaldi, J. P., Britt, R. T., and Rodden, W. P., "Response of B-2 Aircraft to Nonuniform Spanwise Turbulence," Journal of aircraft, Vol 30, No. 5, 1993, pp. 652-659.
11. NASA TM X-62,282 CONMIN - A Fortran Program for Constrained Function Minimization
12. Britt, R. T. "Elements of the B-2 Flight Flutter Test Program," presented at the Structures and Materials Panel Specialists' Meeting on "Advanced Aeroservoelastic Testing and Data Analysis", held in Rotterdam, The Netherlands, May 1995.
13. Sanathanan, C. K., and Koerner, J., "Transfer Function Systhesis as a Ratio of Two Complex Polynomials," IEEE Transactions on Automatic Control, PP. 546-58, January 1963.
14. Maine, R.E. and Iliff, K.W., "User's Manual for MMLE3, a General FORTRAN Program for Maximum Likelihood Parameter Estimation", NASA Technical Paper 1563, Dryden Research Center, Edwards, California, 1980.
15. Winther, B. A., Hagemeyer, D. A., Britt, R. T., and Rodden W. P., "Aeroelastic Effects on the B-2 Maneuver Response," Journal of Aircraft, Vol 32, No. 4, 1995, pp. 862-867.

16. Honeywell Systems and Research Center(Internal Document), "Development of Linear Symmetric Model, Minneapolis, Minnesota
17. Roger, K.L., "Airplane Math Modeling Methods for Active Control Design", Structural Aspects of Active Controls, AGARD CP-228, August 1977
18. Britt, R. T., Jacobson, S. B., and Arthurs, T. D., "Aeroservoelastic Analysis of the B-2 Bomber", presented at the CEAS International forum on Aeroelasticity and Strucgtural Dynamics, Rome, Italy, June 17-20, 1997
19. Jacobson, S. B., Britt, R. T., Dreim, D. R. and Kelly, P. D., "Residual Pitch Oscillation (RPO) Flight Test and Analysis on the B-2 Bomber", AIAA 98-1805, 39th AIAA/ASME/ASCE/AHS/ASC Structures, Structural Dynamics, and materials Conference, April 20-23, 1998.
20. Dreim, D. R., Jacobson, S.B. and Britt, R. T., "Simulation of Non-Linear Transonic Aeroelastic Behavior on the B-2", Presented at the International Forum on Aeroelasticity and Structural Dynamics, Williamsburg, Va., June 22-25, 1999
21. Croxen, H. H., Giesing, J. P., Kalman, T. P., McGrew, J. A., and Rodden, W. P., "Nuclear Blast Response Computer Program," AFWL-TR-S1-32, August 1981.
22. Kingsley, Gerry, et. al. , "Development of a Multidisciplinary Computing Environment (MDICE)", AIAA-98-4738, April 1998.
23. Siegel, John M. Jr. "Application of a Multidisciplinary Computing Environment (MDICE) for Losely Coupled Fluid-Structural Analysis", AIAA-98-3865, Sept. 1998.
24. Adaptive Multi-Multimensional Integrated Control (AMICS) Final Report , WL-TR-96-3037, Wright Laboratory Flight Dynamics Directorate, January 1996.
25. Roach, Jeffery M., "FLASH Electrohydrostatic Actuation Modeling, Analysis and Test Results" SAE-97123, 1997.
26. Miller, G., "Active Flexible Wing (AFW) Technology," Air Force Wright Aeronautical Laboratories, TR-87-3096, Feb. 1988.
27. "Flight Demonstration Plan for the Twist Adaptive Wing System", Lt. D. Siler, J.A. Volk,. AIAA-97-1165, Presented at 38th AIAA/ASME/ASCE/AHS/ASC Structures, Structural Dynamics, and Materials Conference

Research Activities within NASA's Morphing Program

Anna-Maria R. McGowan*, Lucas G. Horta, Joycelyn S. Harrison, and David L. Raney

*NASA Langley Research Center
218 Dodd Blvd, Mail Stop 340
Hampton, VA 23681-2199, United States
Phone: 757-864-2846; Fax: 757-864-8678; e-mail: a.r.mcgowan@larc.nasa.gov

Abstract

In the last decade, smart technologies have become important enabling technologies that cut across traditional boundaries in science and engineering. Here smart is defined as the ability to respond to a stimulus in a predictable and reproducible manner. While multiple successes have been achieved in the laboratory, we have yet to see the general applicability of smart technologies to actual aircraft and spacecraft. The NASA Morphing program is an attempt to couple research across a wide range of disciplines to integrate smart technologies into high payoff applications on aircraft and spacecraft. The program bridges research in several technical disciplines and combines the effort into applications that include active aerodynamic control, active aeroelastic control, and vehicle performance improvement. System studies are used to assess the highest-payoff program objectives, and specific research activities are defined to address the technologies required for development of smart aircraft and spacecraft. This paper will discuss the overall goals of NASA's Morphing program, highlight some of the recent research efforts and discuss the multidisciplinary studies that support that research and some of the challenges associated with bringing the smart technologies to real applications on flight vehicles.

Introduction

The Aerospace Vehicle Systems Technology (AVST) Program office of the NASA Office of Aero-Space Technology has been developing coordinated research programs in which individual disciplines are supported in a collaborative environment to foster the development of breakthrough technologies. As part of AVST, the goals of the Morphing program at the NASA Langley Research Center (LaRC) are to develop and mature smart technologies and address the multidisciplinary issues associated with their efficient use to provide cost-effective system benefits to aircraft and spacecraft. The program seeks to conduct research that will enable self-adaptive flight for a revolutionary improvement in the efficiency and safety of flight vehicles.

The Morphing program is an inherently multidisciplinary program, and has been built around a core discipline-based structure to provide the fundamental technology base. This maximizes the leveraging of all technology developed in the program, and more fully integrates the output of each part of the program. The key disciplines in the program include materials, integration, structures, controls, flow physics, and multidisciplinary optimization. The discipline-based research activities are integrated to support the program application areas that include active aerodynamic control, active aeroelastic control, and other aerospace areas. Smart technologies are currently under development for each application area. In some cases, the smart technologies are consolidated into devices that have local sensing and feedback control. For many applications, these devices will modify local phenomena to support a macroscopic strategy, such as flow separation control for advanced high lift systems. Consequently, a combined approach to control systems and system identification is being used in the Morphing program to address the control laws and controller responses required for the individual devices, as well as addressing global requirements for distributed arrays of devices to achieve an overall system benefit. Furthermore, a research area in the Morphing program referred to as "integration" is targeted at developing smart devices via a mechatronics-based design approach and devising embedding strategies. At the system level, multidisciplinary design optimization will take advantage of the tools developed in the program to optimize the component technologies and provide a systems approach to component integration.

This paper highlights some of the research activities in the Morphing program beginning with the research on smart materials and fiber optics. Various application areas are also discussed herein including a summary of some of the issues associated with final application of smart technologies on aircraft and spacecraft. Although specific application areas are summarized in this paper, much of the research on the development of enabling technologies can be applied to a wide range of engineering applications.

Smart Materials Research

The foundation of the Morphing program at NASA is research on smart materials to develop actuators and sensors for aircraft and spacecraft applications. Three aspects of smart materials research at NASA are summarized herein: advanced piezoelectric materials, fiber optic sensors, and development of smart devices. Research in the area of advanced piezoelectric materials includes optimizing the efficiency, force output, use temperature, and energy transfer between the host structure and the piezoelectric material for both ceramic and polymeric materials. Fiber optics research is focused on non-destructive evaluation of the composite cure process and monitoring the health and configuration of aerospace structures. Device development research in the Morphing program integrates smart materials (actuators and sensors) into devices that are designed to address specific engineering applications.

Paper presented at the RTO AVT Specialists' Meeting on "Structural Aspects of Flexible Aircraft Control", held in Ottawa, Canada, 18-20 October 1999, and published in RTO MP-36.

Advanced Piezoelectric Materials

Piezoelectric materials have been identified as a promising actuator technology for numerous flight vehicle applications including active flow control, active noise control and active aeroelastic control. However, many potential applications require displacement performance larger than that currently achievable in conventional piezoelectric materials. Researchers at NASA LaRC have developed a high-displacement piezoelectric actuator technology, THUNDER (THin layer composite UNimorph ferroelectric DrivER and sensor) to meet these high displacement requirements. THUNDER actuators are unimorph-type actuators, which consist of a piezoelectric ceramic layer bonded to one or more non-piezoelectric secondary layers. Because of the use of elevated temperatures during consolidation, internal stresses are created in the layers of materials; these internal stresses significantly enhance displacement through the thickness of the actuators. Currently, the processing, characterization, and modeling of these high-displacement actuators are under investigation. References 1-3 contain more information on THUNDER devices and their application.

High performance piezoelectric polymers are also of interest to the aerospace community as they may be useful for a variety of sensor applications including acoustic, flow, and strain sensors. Over the past few years, research on piezoelectric polymers has led to the development of promising high temperature piezoelectric responses in some novel polyimides. The development of piezoelectric polyimides is discussed in references 4-6.

A comparison of the characteristics of two new polyimides, identified as P2 and P5, to the only commercially available piezoelectric polymer, polyvinylidene fluoride (PVDF), is shown in Figure 1. This figure shows the value of the piezoelectric constant, d_{31}, as a function of temperature for PVDF, P2 and P5. The polymer structures for P2 and P5 are shown in Figure 2. In general, loss of the piezoelectric effect occurs for both PVDF and the polyimides over time and temperature. However, for PVDF this loss occurs at lower temperatures (approximately 80°C) and is not recoverable due to a loss in the mechanical orientation of the material. Within the operating range of PVDF (approximately 25°C to 80°C) the piezoelectric constant of PVDF is two orders of magnitude higher than those for either polyimide, as shown in Figure 1. Typically, PVDF is not used above 80°C since at these temperatures the polymer begins to loose its mechanical orientation imparted during processing. The material also starts degrading chemically, and aging of the piezoelectric effect is precipitated at these high temperatures.

On the other hand, the new polyimides, P2 and P5 are resistant to temperature effects in this range. For the range of temperatures examined in Figure 1, the polyimides are in the glassy state; hence, they do not deform readily. As polymers approach their respective glass transition temperatures, d_{31} increases due to a decrease in the material modulus making the new polyimides useable in a higher temperature regime. Notice that at 150°C, the piezoelectric constant of P2 is only one order of magnitude lower than that of PVDF. Moreover, at two times the operating temperature of PVDF, the piezoelectric constant of P5 is the same order of magnitude as that of PVDF. Furthermore, any loss in piezoelectric effect in P2 and P5 is recoverable: as amorphous polyimides, P2 and P5 can be regenerated by repoling.

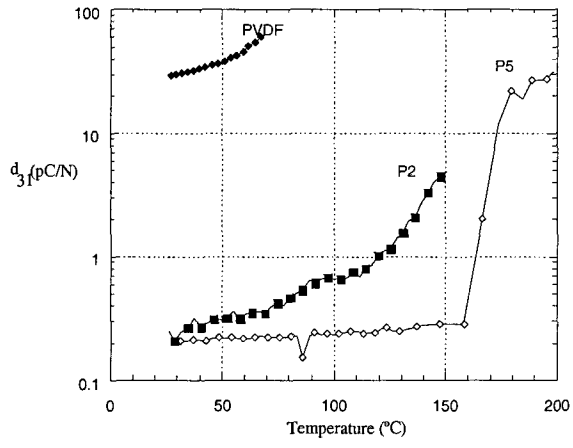

Figure 1 Piezoelectric constant as a function of temperature

Polymer Structure	ID
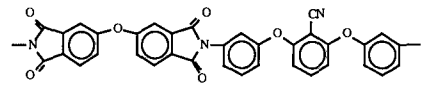	P2
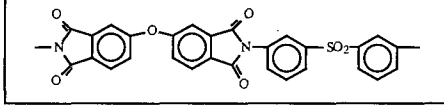	P5

Figure 2 Polymer structure for P2 and P5

Fiber Optic Sensors

Significant research is also being done in the development of fiber optic sensors for cure, health and configuration monitoring of aerospace structures.[7,8] Currently, techniques are being developed for using optical fibers to monitor composite cure in real time during manufacturing and to monitor in-service structural integrity of the composite structure. A fiber optic sensor is currently under development that is capable of measuring chemical composition, strain and temperature. Both single mode and multimode optical fibers with and without Bragg gratings have been investigated. Chemical spectra of a high performance epoxy resin were obtained using both types of fibers. Temperature and strain measurements were made using single mode fibers containing Bragg gratings and compared to data obtained using conventional techniques and the results showed excellent agreement.[8] Further work is being done on creating a more robust chemical sensing region in the fiber that will better withstand the harsh composite cure environment. A patent

application has been filed for the chemical/strain/temperature sensor.

Developing Smart Devices for Steering Optical Mirrors

Another aspect of smart technologies under study is the integration of smart materials into devices to address specific engineering problems. One example of integration for space application uses curved piezoelectric actuators for steering optical mirrors. A prototype system, initially discussed in reference 9, is shown in Figure 3. This mechanism consists of a curved piezoelectric actuator bonded to a polypropylene mount with a mirror attached to the center of the actuator. To get rotational motion of the mirror using the curved actuator, the piezoelectric actuator has individually electroded sections on each side. By applying opposite voltages to each side, one side expands while the other side contracts causing the actuator to flex into an 'S' shape making the mirror rotate.

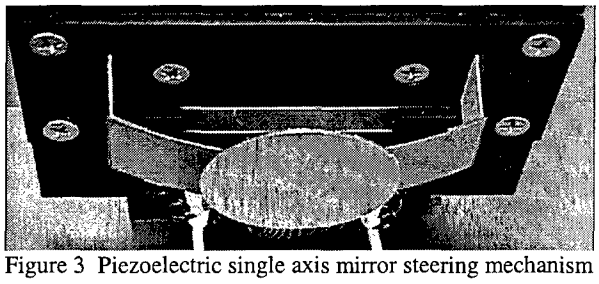

Figure 3 Piezoelectric single axis mirror steering mechanism

The photograph in Figure 4 shows a closer look at the actuator used in the mirror steering mechanism shown in Figure 3. Actuator characterization to predict shape after the consolidation process and performance when driven electrically is discussed in reference 10. Accurate and experimentally validated tools to predict the response of such systems will accelerate integration of these technologies into engineering applications.

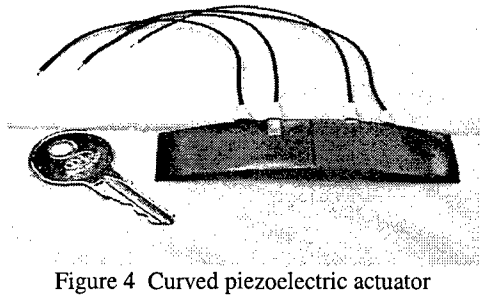

Figure 4 Curved piezoelectric actuator

Novel Actuator Arrays for Active Flow and Flight Control

Recent discoveries in material science and fluidics have been used to create a variety of aerodynamic control devices that have great potential to enable entirely new approaches to aerospace vehicle flight control. A number of flow control actuation concepts were considered including piezoelectric actuators and fluidic effectors which can produce forces and moments by creating small flow distortions over the surface of an airfoil as described in references 11-13. Here an effector is defined as the mechanism that has an effect on the airflow with the purpose of controlling the flow (e.g., a control surface or jet of air) and the actuator is defined as the mechanism that creates the movement of the effector (e.g. hydraulics or piezoelectrics). Fluidic effectors can also be used to alter the degree of separated flow over specifically-designed portions of an airfoil.[14,15] An advanced aerospace vehicle might use distributed arrays of hundreds of such effectors on its surface to generate forces and moments for stabilization and maneuver control, without the need for conventional, hydraulically-actuated ailerons, flaps or rudders as investigated in references 16 and 17.

Development of Actuators for Active Flow Control

An important element of creating a more optimized smart actuation device is using a mechatronics-based design approach. The term "mechatronics" implies the consideration of integrated mechanical and electrical properties, drive electronics, computational control algorithms and hardware, sensor and interface impedance for the purpose of tailoring and optimizing the device design to a specific application. Several smart actuation devices for active flow and flight control are being developed with a mechatronics-based design approach in the Morphing program including synthetic jet actuators and vorticity-on-demand actuators.[18] Coupling mechatronics-based design with more effective piezoelectric actuators, new structural embedding technologies, adaptive controls methods and a systems-based optimization scheme may result in revolutionary improvements in the efficiency and safety of flight vehicles.

Recently, a significant amount of research has been devoted to developing zero-mass synthetic jet actuators for control of flow separation over an airfoil. The actuator is a diaphragm that, when actuated, sucks and blows air through a small orifice. The amount of air sucked in and blown out are equal, hence the name "zero-mass". Figure 5 shows a photograph of one of the piezoelectrically-driven synthetic jet actuators under development and testing. The actuator in Figure 5 is being developed for application to cavity noise control. One of the many challenges with synthetic jets is to get the necessary flow momentum to affect flow over an airfoil at high Reynolds numbers, as discussed in reference 19.

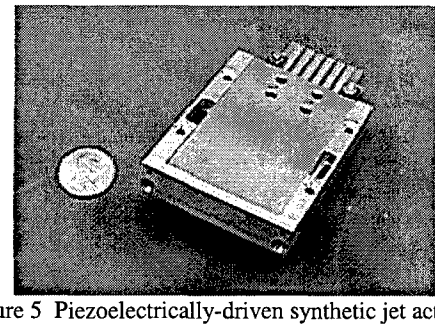

Figure 5 Piezoelectrically-driven synthetic jet actuator

Flight Control Using Fluidic Effectors

A portion of the research in the Morphing program seeks to address controls issues related to the goal of using smart actuators and fluidic effectors for localized flow control and global flight control. Some of the important issues are: how does one determine where to distribute fluidic effectors over the aircraft or spacecraft surface, and how does one use such radically new effectors in a control system to actually maneuver and fly the vehicle? The controls research in the program attempts to address such questions by applying arrays of a generic shape-change actuator to a conceptual aircraft configuration called ICE (Innovative Control Effectors)[20] in a dynamic simulation. NASA is using the ICE design, shown in Figure 6, as an example configuration under a cooperative agreement with Lockheed Martin.

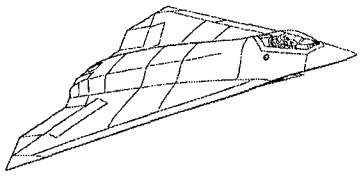

Wing Characteristics
Area .... 75.12 m^2 (808.6 $ft.^2$)
Span .... 11.43 m (37.5 ft.)
Aspect Ratio ... 1.74
Leading Edge Sweep ... 1.134 rad. (65 deg.)

Figure 6 Lockheed Martin Innovative Control Effector (ICE) configuration

An interactive Matlab-based design tool has been developed which allows quick build up and analysis of distributed arrays of small shape-change effectors on the surface of the ICE aircraft. The shape-change effectors in the design tool simulate the virtual shape change created by fluidic effectors (i.e., a small bump on the airfoil). This tool helps the designer to determine placement, size, and shape of the array so that the array can produce the desired forces and moments to maneuver the vehicle. Figure 7 illustrates the graphical user interface for the Matlab-based effector array design tool. The shaded regions in the figure (colored regions on the computer screen) present sensitivity data that indicate the best locations to place the shape-change effectors. The sensitivity data is obtained by differentiating a computational fluid dynamics panel code (PMARC, a Panel Method from the Ames Research Center)[21] using the ADIFOR tool (Automatic Differentiation of Fortran)[22] applied to the ICE configuration model. The sensitivity data consists of the partial derivative of the forces and moments on the aircraft with respect to displacement along the surface normal to every grid point on the aircraft or spacecraft geometry model as described in reference 23.

Using this tool, the designer can quickly build up and analyze an array of shape-change effectors by designating geometry grid points at which he or she wishes to place each element of the array. Once a grouping of shape-change effectors has been defined, the designer can obtain a preliminary prediction of its effectiveness and generate a perturbed geometry grid, which includes the deployed effector array. This geometry file can then be used with aerodynamic analysis programs to further assess the effectiveness of the effector.

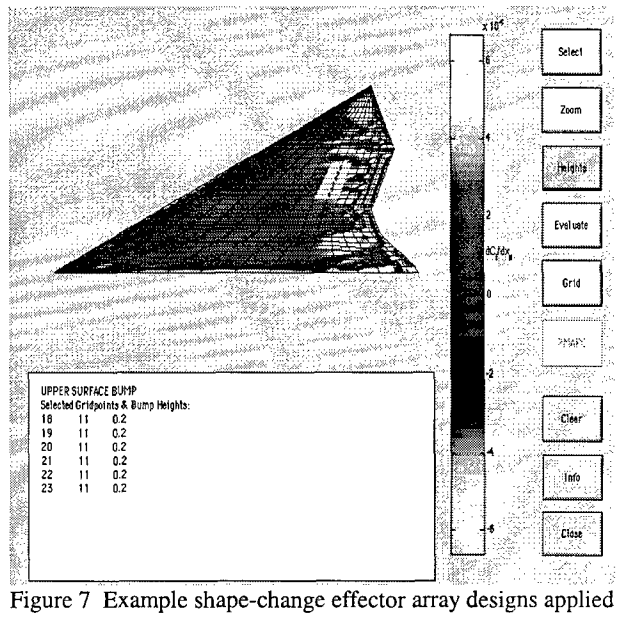

Figure 7 Example shape-change effector array designs applied to the ICE configuration

Four such distributed shape-change effector arrays that were designed using this tool are shown in Figure 8. This figure shows the ICE configuration at a positive pitch and a negative pitch orientation, with the shaded regions indicating the shape change effectors used. These effectors were applied to the ICE vehicle in a simulation and used in a stability augmentation and control system design. The control system deploys the effector arrays in a "quantized" fashion. That is to say that each shape change (modeled as a small bump) in an array is either completely on or off, and more of them are turned on to produce larger forces as needed. Using these effector arrays, the control system is able to stabilize and maneuver the vehicle without conventional moving surfaces such as ailerons or a rudder. The predicted authority of these effectors is still rather low when compared to a rudder or aileron, so the control system generates relatively low-rate maneuvers (roll rates of 5 degrees per second). Future research will focus on experimental validation of the predicted authority of various flow control effectors and on flight control using large arrays of interacting effectors.

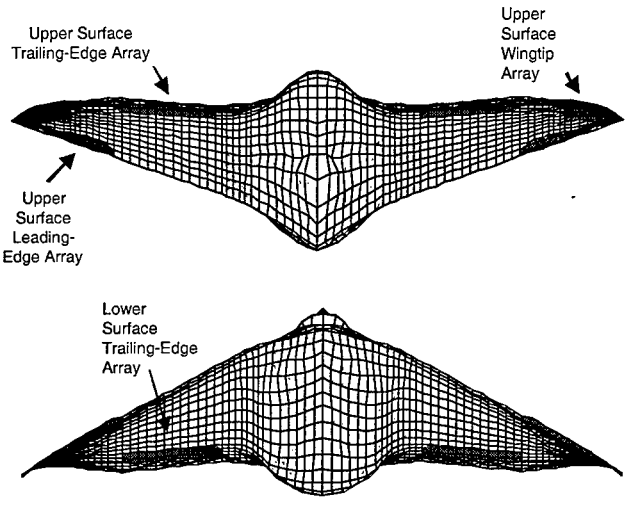

Figure 8 Example shape-change effector arrays design applied to ICE configuration

Integrating Smart Actuators into Structures for Enhanced Performance

Shape memory alloys, piezoelectrics (including piezo fiber composites and single crystals), and magnetostrictive materials have been successfully demonstrated as strain actuators for controlling structural response. At NASA, research on integrating smart actuators and sensors into structures has focused primarily on integrating piezoelectric materials and shape memory alloys. The goal of this research is to advance the technology of embedded strain actuation to a level such that system designers may employ the use of active strain actuation for revolutionary advances in aerospace vehicles. These advances may include significant reductions in structural weight, dramatically increased fatigue life and improved ride comfort. Active strain actuation typically refers to dynamically or statically straining (bending or twisting) a structure to achieve control.

There are numerous challenges in embedding smart materials into composite structures including: electric circuit failures due to dielectric breakdown and arcing, breaking of ceramic wafers and electric leads (particularly in curved surfaces), low performance due to temperature changes or impedance mismatches, and compromised structural integrity due to microcracking and macrocracking in the host composite structure.[24] These complications are even more problematic when high strain, high stress applications are pursued; which is typical of aerospace applications.

Fabrication of Composites with SMAs for Noise and Panel Flutter Suppression

Two aerospace applications being studied at NASA LaRC are noise suppression and panel flutter suppression using embedded SMA wires. Interior noise, sonic fatigue, and panel flutter are important issues in the development and design of advanced subsonic, supersonic, and hypersonic aircraft. Conventional air vehicles typically employ passive treatments, such as constrained-layer damping and acoustic absorption material to reduce the structural response and resulting acoustic levels in the aircraft interior. To prevent the potential destruction of panels that may result from panel flutter, conventional air vehicles employ thickened panels and added stiffeners. These conventional techniques require significant addition of mass and only attenuate relatively high frequency noise transmitted through the fuselage. Adaptive and/or active methods of controlling the structural acoustic response and flutter of panels to reduce the transmitted noise and avoid panel destruction may be accomplished with the use of SMA hybrid composite panels. These panels have the potential to offer improved thermal buckling/post buckling behavior, dynamic response, fatigue life, and structural acoustic response.[25-26]

Initial work at NASA LaRC in the fabrication of active composites has focused on the manufacture of E-glass/ Fiberite 934 epoxy panels with embedded shape memory alloys. Quasi-isotropic panels with unstrained SMAs embedded in the zero degree direction have been successfully fabricated. Test specimens machined from a cured hybrid panel are shown in Figure 9. Future panels will be fabricated with prestrained SMA strips. These panels will require tooling which will restrain the SMA strips from contracting during the thermal cure. Panels with bi-directional (0°/90°) SMAs as well as hybrid built-up structures will also be fabricated. All panels will be subjected to various tests to assess their noise, buckling, and fatigue characteristics as compared to baseline panels without embedded SMAs.

Figure 9 SMA wires in composites

Fabrication, Modeling and Validation of Structures with Piezoelectric Materials

Due to their 20 KHz bandwidth and effectiveness in strain actuation, piezoelectric materials used as actuators have been the smart material of choice for numerous control applications were high bandwidth is required. One fabrication issue that became apparent after experimenting with integrating several piezoelectric actuators into curved structures (which is common in aerospace structures) was the compliance and

flexibility of piezoelectric actuators. Figure 10 shows a newly developed encapsulated piezoelectric actuator being flexed without damaging the actuator. This flexibility allows shape forming of the actuator to different contoured surfaces. Another actuator that can be easily integrated into curved surfaces is a fiber-based piezoelectric actuator,[27] where interdigitated electrodes are used to actuate the piezoelectric fibers (see Figure 11). Once integrated into composite structures, these actuators are very effective in controlling structural response as has been demonstrated in laboratory experiments.

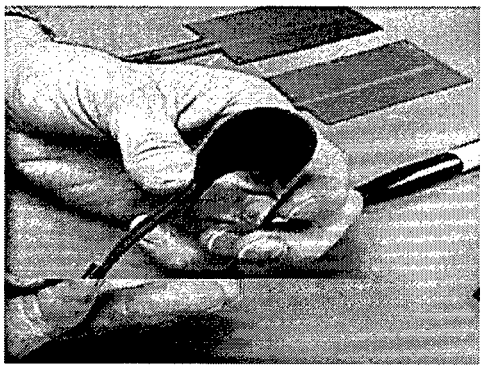

Figure 10 Flexible piezoelectric patch

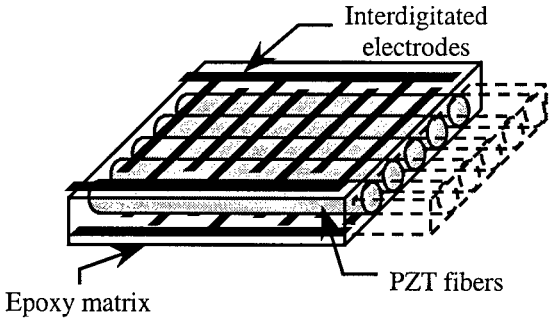

Figure 11 Fiber-based piezoelectric actuator

Fundamental understanding of the behavior of in situ piezoelectric actuators including the development of high fidelity analytical models is extremely important to help bridge the gap between isolated laboratory demonstrations and practical implementation. Towards this end, a number of simple structures are being fabricated at NASA for the purpose of creating a database with test data for model validation. Figure 12 shows a photograph of an aluminum beam with a newly developed piezoelectric actuator bonded to the surface.

Although this particular test-bed is extremely simple, the idea is to investigate modeling of such a system using commercially available analysis tools and to provide a benchmark problem for individuals developing new analysis tools. A second-generation test-bed is shown in Figure 13, constructed with a hollow box cross-sectional area (to mimic more realistic wing-box structures) using composite materials. Localized behavior of actuators and strain transfer efficiencies are being measured to better understand the modeling problems associated with this type of structure. This class of structure presents a different set of modeling and fabrication problems, particularly with strain transfer of piezoelectric actuators when bonded or embedded into composite structures.

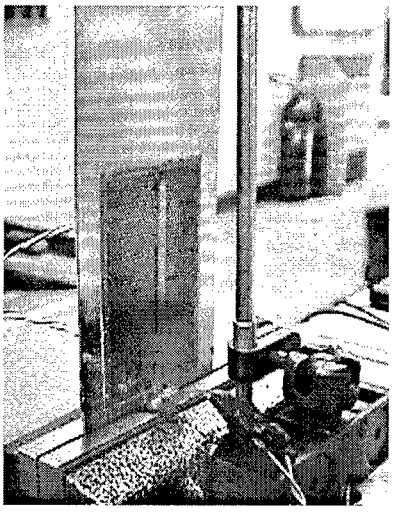

Figure 12 Aluminum beam with surface-bonded piezoelectric actuator

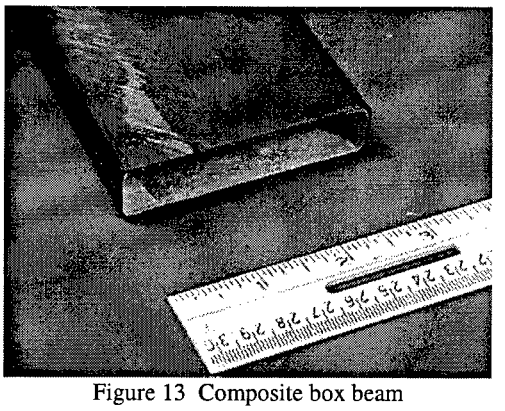

Figure 13 Composite box beam

Using Smart Materials to Control Structural and Aeroelastic Response

The goals of applying smart devices to aeroelastic problems are to control the aerodynamic and/or structural characteristics of air vehicles to improve flutter, gust, buffet and maneuver load behavior of fixed-wing vehicles and reduce dynamics and loads on rotorcraft. In many cases, applications of smart devices will take advantage of the inherent flexibility in air vehicles; using flexibility to create more efficient structural designs. Several analytical and experimental studies clearly demonstrate that piezoelectric materials (piezoelectrics) can be used as actuators to actively control vibratory response, including aeroelastic response.[28] One important study has successfully demonstrated using piezoelectric actuators to control buffeting on the vertical tails of twin-tail, high-performance military aircraft. This international effort includes wind-tunnel testing of a 1/6 scale F/A-18 model experiencing aerodynamic buffet29 and ground-testing of a full-scale F/A-18 airplane using simulated buffet input.[30] Previous studies have also demonstrated active flutter suppression and gust load alleviation using piezoelectric actuators.[31] Piezoelectric actuators have also shown to be effective in active noise suppression.[32]

Depending on the application, there are some important issues in using piezoelectrics as actuators for active control: 1) the potentially large amount of power required to operate the actuators, and 2) the complexities involved with active control (added hardware, control law design, and implementation). Active or passive damping augmentation using shunted piezoelectrics may provide a viable alternative. This approach requires only simple electrical circuitry and very little or no electrical power. A recent NASA analytical study examined the feasibility of using shunted piezoelectrics to reduce aeroelastic response using a typical-section representation of a wing and piezoelectrics shunted with a parallel resistor and inductor.[33] Using Theodorsen aerodynamics, the bending (plunge) response of two aeroelastic models to sinusoidal forcing functions was examined to study the effectiveness of using shunted piezoelectrics to reduce aeroelastic response. These results demonstrate that shunted piezoelectrics can significantly reduce aeroelastic response; for example, reductions of up to 70% in plunging response were realized. Figure 14 shows an example of the results obtained (discussed in reference 33) for the reductions in peak plunging response achieved using the shunted piezoelectrics at several airspeeds. The effectiveness of the shunted piezoelectrics was found to be a strong function of the inherent structural and aerodynamic damping. Thus, this application may not be effective for highly damped structures. However, for lightly damped structures, shunted piezoelectrics provide a simple, low-power, fail-safe vibration suppression mechanism. Follow-on studies are planned to explore developing higher fidelity models and to validate the results via wind-tunnel testing.

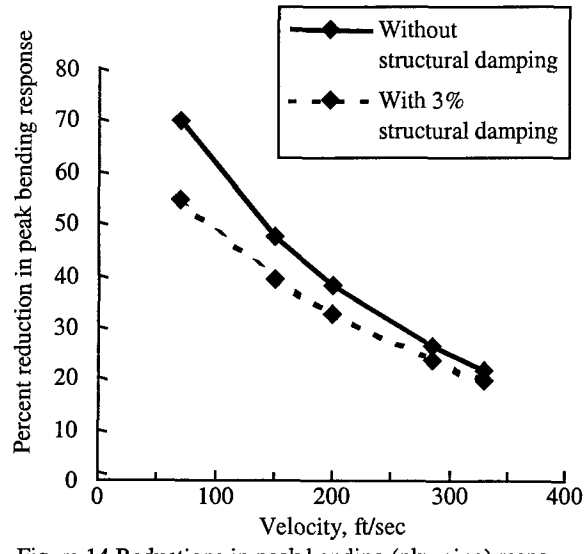

Figure 14 Reductions in peak bending (plunging) response using shunted piezoelectrics

Using Smart Materials to Improve Vehicle Performance

Also within the Morphing Program, NASA has collaborated with DARPA, the Air Force and the Navy in two unique programs investigating using smart materials to improve the performance of military vehicles. The DARPA/AFRL/NASA Smart Wing program, conducted by a team led by the Northrop Grumman Corporation (NGC), addresses the development of smart technologies and demonstration of relevant concepts to improve the aerodynamic performance of military aircraft. Reference 34 provides on overview of the DARPA/AFRL/NASA Smart Wing program. During Phase I of this program, a 16% scale, semi-span wind-tunnel model, representative of an advanced military aircraft wing, was designed and fabricated by NGC and wind-tunnel tested at NASA LaRC's Transonic Dynamics Tunnel (TDT) in May 1996 and June-July 1998. The "smart wing" model incorporated contoured, hingeless flap and aileron designs actuated using built-in SMA tendons. Control surface deflections of up to 10° were obtained. Variable spanwise twist of the smart wing was achieved using mechanically simple SMA torque tubes that employed novel connection mechanisms to effect a high degree of torque transfer to the structure; 3200 in-lbs. of torque was generated by the SMA tubes. Up to 5° of spanwise twist at the wing tip was demonstrated. Under steady-state conditions, 8% to 12% improvements in lift, pitching and rolling moments were achieved over a broad range of wind tunnel and model configurations, in comparison to a conventional design incorporating hinged control surfaces. During Phase II of the Smart Wing program, research and development are focused on the application of smart technologies to uninhabited air vehicles and further raising the technology readiness level of these technologies for future applications.

In the Smart Aircraft and Marine Propulsion System Demonstration (SAMPSON) program, NASA LaRC is

collaborating with DARPA and the Navy's Office of Naval Research (ONR) on a team led by the Boeing Company to demonstrate the application of smart materials and structures to large-scale aircraft and marine propulsion systems.[35] This program seeks to show that smart materials can be used to significantly enhance vehicle performance, thereby enabling new missions and/or expanding current missions. Currently, a demonstration of a full-scale adaptive fighter engine inlet is planned for testing in the NASA Langley 16-foot Transonic Tunnel in the Spring of 1999. Smart technologies will be utilized to actively deform the inlet into predetermined configurations to improve the performance at all flight conditions. The inlet configurations to be investigated consist of capture area control, compression ramp generation, leading edge blunting, and porosity control. The wind-tunnel demonstrations will serve to directly address questions of scalability and technology readiness, thereby improving the opportunities and reducing the risk for transitioning the technology into applications. The analytical and experimental expertise gained from the wind-tunnel tests conducted in the Smart Wing and SAMPSON programs are an important part of the technology development process in the Morphing program and provide an excellent opportunity for collaborative research.

Concluding Remarks

The integration of smart technologies into aircraft and spacecraft structures shows the promise of high benefits if the appropriate technological issues are addressed. To effectively approach the long-term technology issues, the Morphing program at NASA Langley Research Center integrates smart material and structures research efforts across many disciplines. For example, coupling mechatronics-based design of smart devices with new embedding technologies, more effective piezoelectric materials, adaptive controls methods and a systems-based optimization scheme may result in revolutionary improvements in the efficiency and safety of flight vehicles. These improvements are not limited to, but may include a significant increase in the fatigue life of structures undergoing high-cycle response (such as buffeting, gust, or acoustic response), a significant reduction in the structural weight of load-carrying components such as wing boxes, and dramatic improvements in high lift systems. Ground and wind-tunnel tests are currently underway in the Morphing program to bring these technologies to fruition. The Morphing program strives to assure the ultimate usability of the technological product of this work and, potentially, have a major impact on air and space travel and the way in which aircraft and spacecraft are manufactured and flown.

Acknowledgements

The authors wish to acknowledge the invaluable assistance of the rest of the Morphing Integrated Project Team: Jean-Francois Barthelemy (Project Manager), Ronald Joslin, Sharon Padula, and Gary Fleming. In addition, the following colleagues provided crucial assistance: Robert Rogowski, Roberto Cano, Karen Wood, Richard Silcox, Mercedes Reaves, Garnett Horner, Barmac Taleghani, and Keats Wilkie.

References

1 Bryant, R., Fox, R., Lachowicz, J., Chen, F., Proceedings of Society for Photo-Optical Instrumentation Engineers, Vol 3674, 220-227 (1999).

2 Mossi, K., Selby, F., and Bryant, R.: Materials Letters, 35,29 (1998).

3 Bryant, R.G. "Thunder Actuators", 5th Annual Workshop: Enabling Technologies for Smart Aircraft Systems, NASA Langley Research Center, May 14-16, 1996.

4 Ounaies, Z., Park, C., Harrison, J.S., Smith, J.G., and Hinkley, J.A., Structure-Property Study of Piezoelectricity in Polyimides, Proceedings of Society for Photo-Optical Instrumentation Engineers, Ed. Y. Bar-Cohen, Vol 3669, 171-178 (1999).

5 Ounaies, Z., Young, J.A., and Harrison, J.S., An Overview of Piezoelectric Phenomenon in Amorphous Polymers in Field Responsive Polymers: Electroresponsive, Photoresponsive, and Responsive Polymers in Chemistry and Biology, Ed. Khan, I. and Harrison, J.S., ACS Symposium Series 726, Washington, DC, (1999).

6 Ounaies, Z., Young, J.A., Simpson, J.O., Farmer, B., Dielectric Properties Of Piezoelectric Polyimides, Materials Research Society Proceedings: Materials for Smart Systems II, Ed. E.P. George, R. Gotthardt, K. Otsuka, S. Trottier-McKinstry, and M. Wun-Fogle, Vol. 459, 59(1997).

7 M. Froggatt and J. Moore, "Distributed measurement of static strain in an optical fiber with multiple Bragg gratings at nominally equal wavelengths," Applied Optics, 37, pp. 1741-1746 (1998).

8 Brown, T., Wood, K., Childers, B., Cano, B., Jensen, B., Rogowski, R., Fiber Optic Sensors for Health Monitoring of Morphing Aircraft, Proceedings of Society for Photo-Optical Instrumentation Engineers, Vol 3674, 60-71 (1999).

9 Horner, G.C., Taleghani, B.K, "Single Axis Piezoceramic Gimbal," Proceeding of the SPIE International Symposium on Smart Structures and Materials, Newport Beach, CA, 1999.

10 Taleghani B.K, and Campbell, J.F., "Non-linear Finite Element Modleing of THUNDER Piezoelectric Actuators," Proceedings of the 6th Annual International Symposium on Smart Structures and Materials, Newport Beach, CA, 1999.

11 Donovan, J.F., L.D. Kral, and A.W. Cary, 1998. "Active Flow Control Applied to an Airfoil," 36th AIAA Aerospace Sciences Meeting, paper AIAA 98-0210, Jan. 1998.

12 Kral, L., Dononvan, J. Cain, B, Cary, A.: "Numerical Simulation of Synthetic Jet Actuators", AIAA paper 97-1824.

13 Nae, C., "Synthetic Jet Influence on NACA 0012 Airfoil at High Angles of Attack," AIAA Paper 98-4523.

14 Seifert, A., Darabi, A., Wygnanski, I., "Delay of Airfoil Stall by Periodic Excitation," Journal of Aircraft, Vol. 32, No. 4, July-August, 1996.

15 Seifert, A., Pack, L., "Oscillatory Control of Separation at high Reynolds Numbers," AIAA Paper 98-0214, Aerospace Sciences Meeting and Exhibit, 1998.

16 Scott, M., Montgomery, R., and Weston, R.: "Subsonic Maneuvering Effectiveness of High Performance Aircraft Which Employ Quasi-Static Shape Change Devices," SPIE 1998 International Symposium on Smart Structures and Materials, paper 3326-24.

17 Allan, B., Holt, M., Packard, A.: "Simulation of a Controlled Airfoil with Jets," NASA CR-201750; ICASE Report No. 97-55, October 1997.

18 Pack, L.G., Joslin, R.D., "Overview of Active Flow Control at NASA Langley Research Center", SPIE 1998 International Symposium on Smart Structures and Materials, paper 3326-22.

19 Joslin, R.D., Horta, L.G., Chen, F-J., " Transitioning Active Flow Control to Applications," Proceedings of the 30th AIAA Fluid Dynamics Conference, AIAA 99-3575, Norfolk, VA, 1999.

20 Dorsett, K. M. and D.R. Mehl, 1996. "Innovative Control Effectors (ICE)," Wright Laboratory Report, WL-TR-96-3043, January 1996.

21 Ashby, D., Dudley, M., Iguchi, S., Browne, L., and Katz, J.: "Potential Flow Theory and Operation Guide for the Panel Code PMARC_12", NASA Ames Research Center, Moffett Field, CA, Dec. 1992.

22 Carle, A., Fagan, M., and Green, L., "Preliminary Results from the Application of Automated Adjoint Code Generation to CFL3D," AIAA Paper 98-48078, Sept. 1998.

23 Park, M., Green, L., Montgomery, R., Raney, D., "Determination of Stability and Control Derivatives using Computational Fluid Dynamics and Automatic Differentiation," AIAA Paper 99-3136, June 1999.

24 Belvin, W.K., Horner, G.C., Hardy, R.C., Armstrong, D., and Rosenbaum, D.M., "Integration Issues for High-Strain Actuation Applications", SPIE 1998 International Symposium on Smart Structures and Materials, paper 3326-25.

25 Turner, T. L.; Zhong, Z. W.; and Mei, C., "Finite Element Analysis of the Random Response Suppression of Composite Panels at Elevated Temperatures using Shape Memory Alloy Fibers," AIAA-94-1324-CP, Proceedings of the 35th Structures, Structural Dynamics, and Materials Conference, Hilton Head, SC, April 18-21, 1994, pp. 136-146.

26 Mei, C.; Zhong, Z. W.; and Turner, T. L., "Control of Sonic Fatigue for High Speed Flight Vehicles Using Shape Memory Alloy," Proceedings of the SPIE 5th Annual International Symposium on Smart Structures and Materials, San Diego, CA, March 1-5, 1998.

27 Wilkie, W.K., Park, K.C., Belvin, W.K., "Helicopter Dynamic Stall Suppression Using Piezoelectric Active Fiber Composite Rotor Blades," AIAA Paper No. 98-2002, Proceedings of the 39th AIAA/ASME/ASCE/AHS/ASC Structures, Structural Dynamics, and Materials Conference, Long Beach, CA, April 20-23, 1998.

28 McGowan, A. R., Wilkie, W. K., Moses, R. W., Lake, R. C., Florance, J. P., Wieseman, C. D., Reaves, M. C., Taleghani, B. K., Mirick, P. H., and Wilbur; M. L., "Aeroservoelastic and Structural Dynamics Research on Smart Structures Conducted at NASA Langley Research Center"; SPIE's 5th Annual International Symposium on Smart Structures and Materials; Industrial and Commercial Applications Conference; Paper 3326-21; San Diego, CA; March 1998.

29 Moses, R. W., "Contributions to Active Buffeting Alleviation Programs by the NASA Langley Research Center", Proceedings of the Proceedings of the 40th AIAA/ASME/ASCE/AHS/ASC Structures, Structural Dynamics and Materials Conference, AIAA 99-1318, St. Louis, MO, April 1999.

30 Hopkins, M.A., Henderson, D.A., Moses, R.W., Findlay, D., Voracek, D.F., Spangler, R.L., Ryall, T., and Zimcik, D., "Active Vibration Suppression Systems Applied to Twin Tail Buffeting," Proceedings of SPIEís 5th Annual Symposium on Smart Structures and Materials, Paper No. 3326-05, San Diego, CA, March 1-5, 1998.

31 McGowan, A. R., Heeg, J., and Lake, R.C., "Results of Wind-Tunnel Testing From the Piezoelectric Aeroelastic Response Tailoring Investigation," Proceedings of the 37th AIAA/ASME/ASCE/AHS/ASC Structures, Structural Dynamics and Materials Conference, Salt Lake City, UT, April 1996.

32 Gibbs, G.P, Eure, K.W., and Lloyd, J.W., "Active Control of Turbulent Boundary Layer Induced Sound Radiation from Aircraft Style Panels," Proceedings of Active99, Ft. Lauderdale, FL, December 2-4, 1999.

33 McGowan, A. R., "A Feasibility Study of Using Shunted Piezoelectric Piezoelectrics to Reduce Aeroelastic," SPIE's 6th Annual Symposium on Smart Structures and Materials, Industrial and Commercial Applications Conference, Newport Beach, CA Paper number 3674-20, March 1999.

34 Kudva, J.N, Martin, C.A., Scherer, L.B., Jardine, A.P., McGowan, A.R., Lake, R.C., Sendeckyj, G.P., and Sanders, B.P., "Overview of the DARPA/AFRL/NASA Smart Wing Program", SPIE's 6th Annual Symposium on Smart Structures and Materials, Industrial and Commercial Applications Conference, Newport Beach, CA Paper number 3674-26, March 1999.

35 Dunne, J.P., Hopkins, M.A., Baumann, Pitt, D.M., and White, E.V., "Overview of the SAMPSON smart inlet", SPIE's 6th Annual Symposium on Smart Structures and Materials, Industrial and Commercial Applications Conference, Newport Beach, CA Paper number 3674-43, March 1999.

Design Aspects of the Elastic Trailing Edge for an Adaptive Wing

H. P. Monner*, D. Sachau*, E. Breitbach*
*German Aerospace Center (DLR)
Institute of Structural Mechanics
Lilienthalplatz 7
38108 Braunschweig, Germany

ABSTRACT

According to predictions of market researchers a large growth in numbers of passengers as well as of airfreight volume can be expected for the civil transport aircraft industry. This will lead to an increased competition between the aircraft manufacturers. To stay competitive it will be essential to improve the efficiency of the new aircraft generation. Especially the transonic wings of civil aircraft with their fixed geometry offer a large potential for improvement. Such fixed geometry wings are optimized for only one design point characterized by the parameters altitude, mach number and aircraft weight. Since these vary permanently during the mission of the aircraft the wing geometry is only seldom optimal. As aerodynamic investigations have shown one possibility to compensate for this major disadvantage lies in the chordwise and spanwise differential variation of the wing camber for mission duration. This paper describes the design of a flexible flap system for an adaptive wing to be used in civil transport aircraft that allows both a chordwise as well as a spanwise differential camber variation during flight. Since both lower and upper skins are flexed by active ribs, the camber variation is achieved with a smooth contour and without any additional gaps. This approach for varying the wing's camber is designed to be used for replacement and enhancement of a given flap system. In addition the kinematics of the rib structure allows for adaptation of the profile contour to different types of aerodynamic and geometric requirements.

1. INTRODUCTION

Already Otto Lilienthal who is also called the "Father of Modern Aviation", recognized through extensive observations of bird's flight that camber is essential for generating lift. With this knowledge he managed to perform the first successful glide of a human being in 1891. Many others followed. The wings of these first aircraft where of fixed geometry where the flight control was realized by weight transfer and a nearly artistic body control of the pilot. It was soon discovered that a variation of the camber enabled improved maneuverability. In 1903 this was the case with the first motorized flight of the Wright brothers, where lateral control was realized by twisting the wings in opposite direction to each other. But a twisting of the wings for lateral control did not remain practicable very long because structural stiffness of the airplanes increased with the need for more performance. Thus, in 1910 Henry Farman introduced the first ailerons. Due to continuously increasing weight and size of the airplanes high lift flaps soon became necessary in order to increase the camber and therefore the lift during the start and landing phase. Since 1919 these are in use [1].

Basically, this principle application of flaps has not changed to date, also not in modern transonic civil transport aircraft. With the exception of the starting and landing phase, no considerable use of flaps and therefore change of camber is being performed. During most of the flight the wing is of fixed geometry and therefore of constant camber. The major disadvantage of fixed geometry wings is that they can only be optimized for one design point characterized by the parameters altitude, mach number and aircraft weight. Since these vary continuously during the mission of the aircraft the wing geometry is only seldom optimal. The development of wings with fixed geometry is therefore always the best compromise between design and off-design point where a better performance at the design point leads to a worse off design performance. E.g., for a civil aircraft it may be necessary to fly fast and at low altitude with light weight over a short stretch one day. The next day it may be beneficial to fly at high altitude with maximum load, and at an economical velocity for a much longer range. In the first case the lift coefficient could be only 0.08 whereas in the second case it might be as large as 0.4. Thus, values of the maximum cruise lift coefficient can be as much as five times the minimum for most airliners [2]. In addition, the airplane weight drops up to 30% during a long range mission due to fuel consumption [3]. Such significant changes in flight conditions can be compensated sufficiently by varying the wing camber for mission duration to obtain near optimum geometry for the flight conditions to be encountered. This approach has the potential to lead to a considerable improvement of the aerodynamic and structural efficiency of an aircraft.

The introduction of new technologies such as camber variation to improve aircraft efficiency is essential for the future success of the airplane manufacturers. Especially since market research predicts a very positive development for the aircraft industry an increasing competition is to be expected: The civil aircraft industry, has shown strong economic growth during the past decades with an average increase of 6% per year. For the next 20 years the large airplane manufacturers Airbus Industry and Boing expect growth rates of around 4.5% per year [4]. This means that over the next 15 years the number of passengers is expected to double, the amount of airfreight probably will increase even more. The expectation of a steady growth in aircraft industry over the next 20 - 25 years is justified when taking into consideration that only a very small part of the world population is responsible for a great deal of the world wide air traffic today: e.g., US-citizens make up only 4.6% of the world population but hold 41% of the worldwide km flown per passenger. In contrast, China and India together represent 37% of the world population but hold only 3.4% of the worldwide km flown per passenger. If in the future the worldwide population flies as much as US-citizens today, and taking into consideration the predicted world population growth from 5.6 billion to 8.3 billion by the year 2025, then the km flown per passenger would rise by a factor of 13. At a growth rate of 4.5% per year this factor would first be reached in 60 years. Assuming a healthy worldwide economic development there is no danger of market saturation in the near future [5, 6].

2. VARIABLE CAMBER PRINCIPLE

It is of special interest to achieve a chordwise and spanwise differential camber variation with one structural system providing a smooth contour having no additional gaps. The camber variation concentrates on the trailing edge since under aerodynamic as well as structural aspects this region has the highest efficiency [7]. On civil transport aircraft the

Paper presented at the RTO AVT Specialists' Meeting on "Structural Aspects of Flexible Aircraft Control", held in Ottawa, Canada, 18-20 October 1999, and published in RTO MP-36.

Fowler flaps and ailerons are positioned in this region (see Fig. 1).

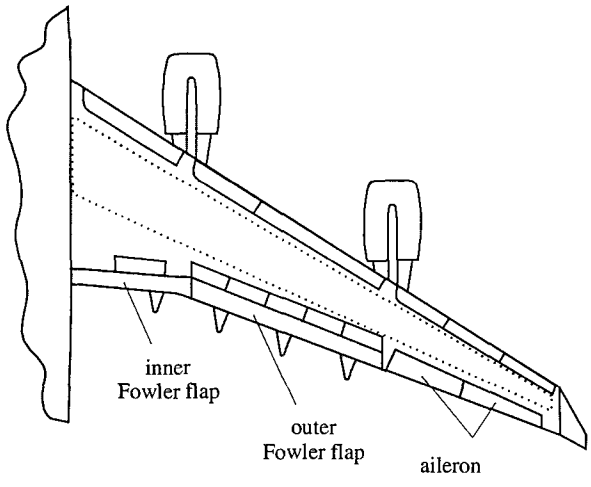

Fig. 1: Flaps of a civil transport aircraft

Therefore it is important to develop a cambering system that on the one hand can be used to enhance the Fowler flaps by an additional cambering function and on the other hand enables a complete substitution of an aileron. Fig. 2 shows this principle for a Fowler flap with enhanced cambering.

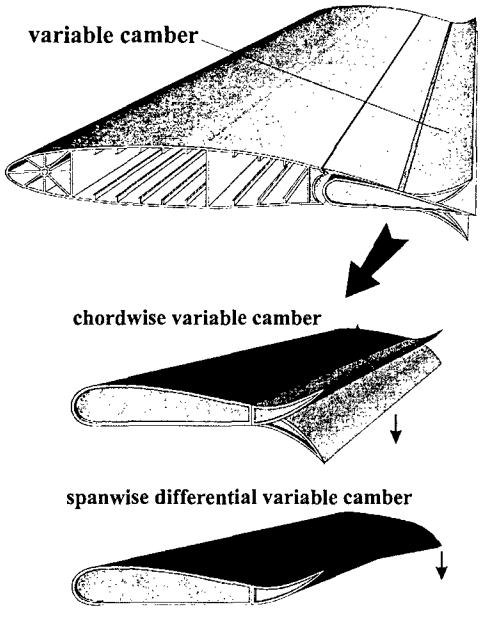

Fig. 2: Chordwise and spanwise differential camber variation of Fowler flaps with an enhanced cambering function

The cambering system should also be constructed such that during its actuation the structural stiffness does not change. This ensures that sudden changes in loading caused by gust for example, lead to failure. When the Fowler flaps are enhanced by an additional cambering function they should still retain their primary function as a high-lift device. If the ailerons are replaced with such a cambering system the actuators have to be positioned inside the structure. In addition it is important to be able to adapt the profile contour to different types of aerodynamic and geometric requirements for the median line. Considering the remarks made above, the following basic requirements can be defined:

- the structural system has to be suitable for replacement and enhancement of a given flap system
- a chordwise and spanwise differential camber variation has to be achieved with one structural system
- a smooth contour having no additional gaps has to be provided
- the actuators have to be integrated into the flap structure
- the profile contour has to be able to be adapted to different types of aerodynamic and geometric requirements
- the structural stiffness is not allowed to change during actuation

Both chordwise and spanwise differential camber variation are expected to have various effects on aerodynamic and structural efficiency. The following improvements over fixed geometry wings are expected:

- higher aerodynamic efficiency due to optimized lift/drag (L/D) ratio leads to an extended cruise range and reduction in fuel consumption
- improved operational flexibility by shifting the maximum L/D ratio to higher values
- extended buffet boundary enlarges the operative range and reduces structural weight
- reduction of wing root bending moment leads to a reduction of structural weight
- increased stretch potential leads to a significant reduction of development costs

A general description of the effects of these two types of camber adjustments for a typical civil transport aircraft of the early 90's is given in the next two sections.

2.1 Chordwise camber variation

The chordwise camber variation is mainly responsible for the improvement of the aerodynamic efficiency by optimizing the L/D ratio for present flight situation. This directly leads to a reduction in fuel consumption. The L/D ratio results from the wing data, altitude, mach number, and aircraft weight. Special emphasis is given to the weight loss due to fuel consumption (>30% during a long distance flight) which has considerable negative influence on the L/D ratio of the aircraft that can be compensated by a camber variation. Thus, at the beginning of the flight the camber has to be large, to decrease later with the reduction in weight. As shown in Fig. 3, the chordwise camber variation leads to an optimization of the L/D ratio according to the present flight situation between 3% to 10%. The dashed curve indicating the variable camber presents the envelope of a number of optimal camber positions. This results in an extended cruise-range in comparison to a fixed wing (solid line) by shifting the maximum L/D to up to 12% higher C_L-values. Another advantage of a wing with variable camber consists in the improved buffet boundaries. This is equivalent to an enlarged speed range meaning that, for instance, during the landing phase a larger time range is available so that unnecessary holding patterns can be avoided [7, 8].

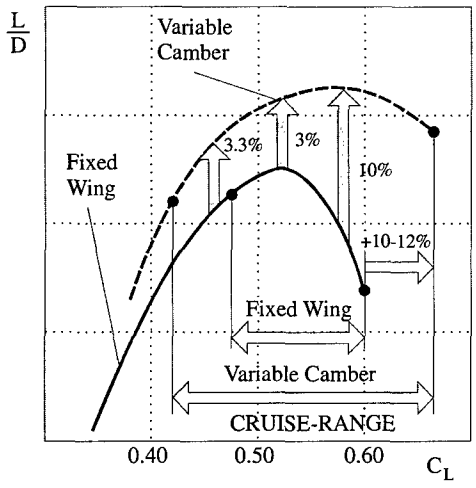

Fig. 3: Variable camber effect on L/D [7, 8]

2.2 Spanwise differential camber variation

Besides L/D optimization, this system can be used to gain control over dimensioning load cases such as the maneuver situation where the pilot has to execute a 2.5g maneuver load. In Fig. 4 the potential of spanwise camber control is demonstrated. Compared with the typical lift distribution for optimal performance (solid line) the differential deflection leads to a significant reduction of the root bending moments (RBM) through redistribution of the spanwise lift distribution (dashed line). This is achieved by cambering the inboard and de-cambering the outboard wing. In all a 12 - 15% reduction of the RBM is achieved leading to an increase of the payload/structural weight ratio. When combined with a chordwise camber variation a wing with a high adaptability towards different types of requirements can be provided [3, 9].

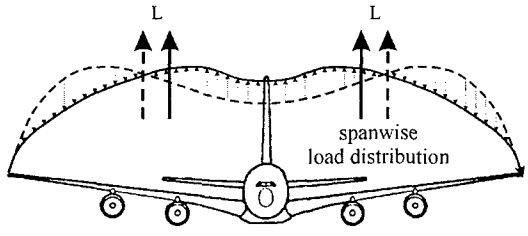

Fig. 4: Load control by means of variable camber [3]

3. STRUCTURAL CONCEPT

As mentioned the cambering system has to be suitable for replacement of an aileron as well as enhancement of a Fowler flap. Under structural mechanical aspects it is more demanding to enhance a given flap structure with a cambering system since there is less space available and also the stiffness of the flap is much more critical. This means that when a solution can be found that can enhance a single flap it is all the more usable to substitute a total flap. Therefore the approach demonstrated in this paper is presented for a Fowler flap with an enhanced cambering system. As shown in Fig. 5, the basic concept for the design of the flexible Fowler flaps consists of replacing the stiff inflexible rib elements reaching into the flexible section (dark gray) by active deformable elements with high stiffness. This means the skin fields must then be able to glide on the flexible ribs. The basic design of the front fixed part (light gray) is changed as little as possible to avoid a totally new design concept for the fixed flap section [10, 11, 12].

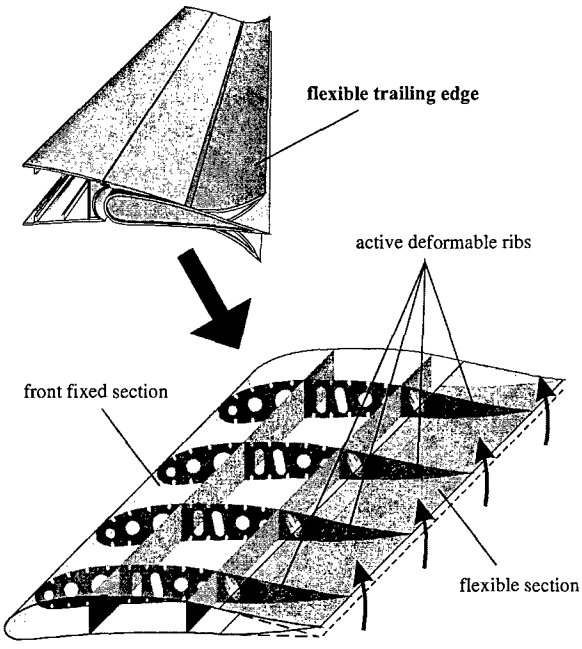

Fig. 5: Position and distribution of active deformable ribs in the Fowler flaps

The flexible ribs were realized by combining separate plate like elements with revolute joints having the kinematics described in Fig. 6a. Fig. 6b represents one rib of the flexible section. Each rib only has to be actuated at one single point. The rotation of the driven element is transferred gradually from element to element by the kinematics and this way provides the wanted rib contour.

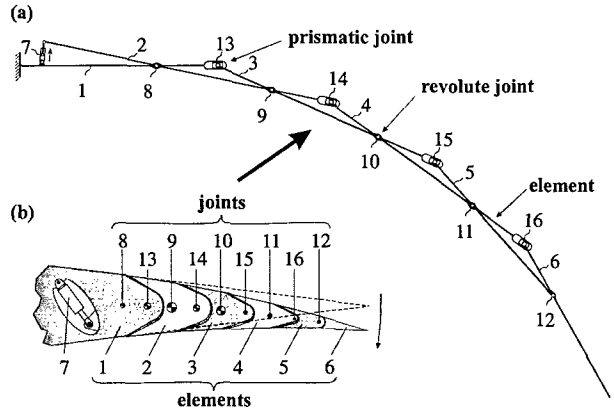

Fig. 6: Kinematics of active deformable rib

The kinematics will be described by referring to the first three elements (1 to 3): An actuator (7) is supported by the fixed first element (1) which represents the continuation of the rib in the front fixed section (Fig. 5). The actuator (7) drives a second element (2) which is attached to the first element (1) by a revolute joint (8). The second element (2), too, is connected to the third element (3) by a revolute joint (9). In addition the third element (3) is connected to the first one (1) by a prismatic joint (13). By putting the actuator (7) into motion the second element (2) rotates about revolute joint (8). Due to revolute joint (9) the third element (3) rotates about revolute joint (8), too, and is supported by the first element (1) in prismatic joint (13). This way the third element (3) is bent towards the second one (2) about revolute joint (9). These kinematics can be applied to an unlimited number of elements. To provide functionality at least three elements must be used. A variation of the individual length between the joints (e.g. the

region between the joints (8) and (9), (8) and (13) as well as (9) and (13)) allows a precise adjustment of the rib contour.

Fig. 7. shows a modification of the active deformable rib in Fig. 6 with an additional lever (17) in order to reduce structural loads and the driving force. The kinematics of the active deformable rib remains the same with the exception that the actuator (7) is attached to lever (17) and not to element (2). The lever is connected to the first element (1) by revolute joint (8) and with element (4) by a prismatic joint (18). To provide functionality at least four elements must be used.

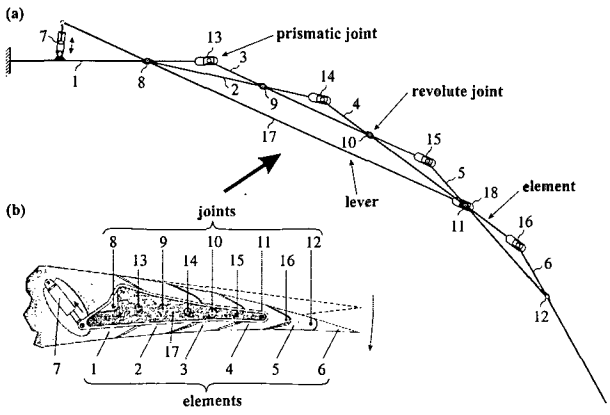

Fig. 7: Kinematics of flexible rib with additional lever

Fig. 8 shows how the elements are configured using the third element (3) as an example. For the purpose of good load transmission a symmetrical design was developed. In the horizontal projection the elements have the shape of a tuning fork. The element itself consists of one inner and two outer parts which are attached to each other with an adhesive. Every element is provided with two bore holes for the prismatic and revolute joints.

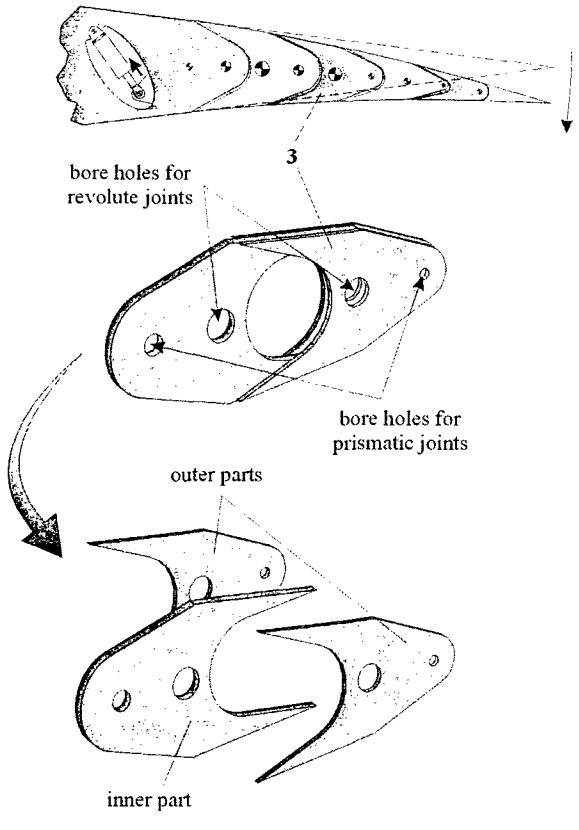

Fig. 8: Geometry of an element

An aluminum model of the flexible rib is demonstrated in Fig. 9. It shows the rib in its neutral position as well as at maximum upper and lower deflection. A carbon fiber composite rib has also been constructed. It has stiffness similar to the aluminum version with about 40% reduction in weight. For this rib a spindle drive is used as actuator.

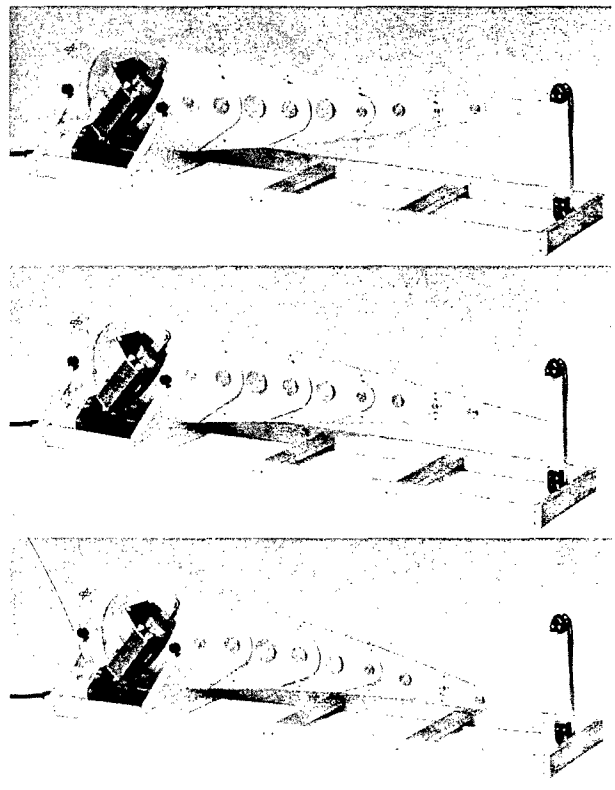

Fig. 9: Active adjustable rib in neutral position and total upper and lower deflection

The design of the upper and lower skin is presented in Fig. 10. As shown in section A-A the stringers are interrupted by a linear slide bearing. At the upper and lower part of the rib elements counterparts are attached which make up the inside part of the linear slide bearing. These bearings allow a chordwise displacement between the rib and the upper and lower skin. Simultaneously a lift-off of the upper and lower skin due to aerodynamic loads is prevented. At the trailing edge the upper and lower skins are combined by a linear slide bearing allowing a chordwise translation here, too. In addition the trailing edge can easily be replaced if damaged.

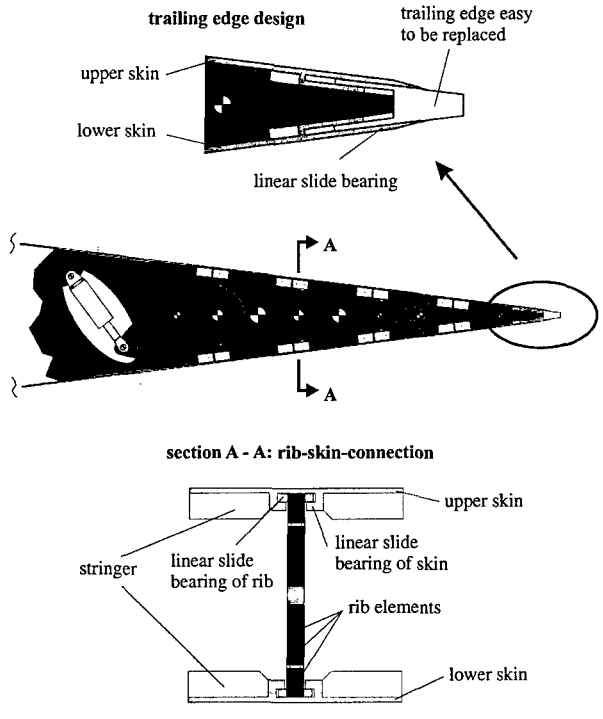

Fig. 10: Design of upper and lower skin

As described every rib element is connected to the upper and lower skin by linear slide bearings. These are individually dimensioned and positioned on the skin according to the loading that appears. Fig. 11 shows that in the front region where the second elements are located the linear slide bearings are shorter than towards the end. This is due to the larger displacement between rib and skin at the trailing edge.

In order to achieve a high stiffness of the linear slide bearings on the skin it is important to position the stringer in their middle. Depending on the available space the stringer have to be varied in their height according to the maximum needed and maximum possible values [13].

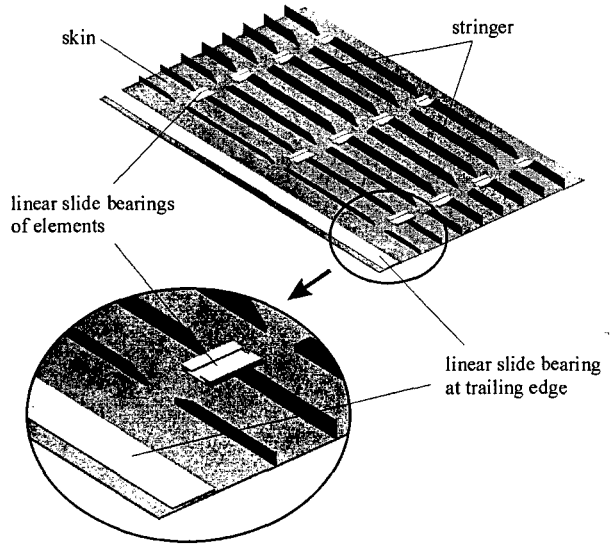

Fig. 11: Skin with linear slide bearings

For reasons of a better description of the kinematics the ribs in Fig. 6 and Fig. 7 are driven by a linear actuator. Since with this type of activation every rib has to be driven by an individual actuator, the number of them is quite high. Moreover the total loading is introduced directly into the actuator requiring a powerful drive. By using a transmission beam together with a wedge system the amount as well as the loading of the actuator can be reduced.

In Fig. 12 this drive system is presented with five ribs coupled to each other. The first rib element is provided with an opening where the transmission beam and the wedges are positioned. Since the beam is driven altogether by two actuators, less drives than ribs are needed. The actuators are mounted on the rear spar. When they are activated, the transmission beam to which the wedges are attached moves horizontally. This way the horizontal movement is transferred into a vertical one, pushing the slide block upward or downward. To these slide blocks the second elements or the levers are attached (see Fig. 6 and Fig. 7) leading to the wanted deflection. Due to the small gradient of the wedge most of the loading is directly transferred into the structure of the first element leading to a reduced actuator force. When the actuators are retracted the flexible region is de-cambered, an extension results in added camber. When actuated in the opposite direction a spanwise differential cambering is provided [14].

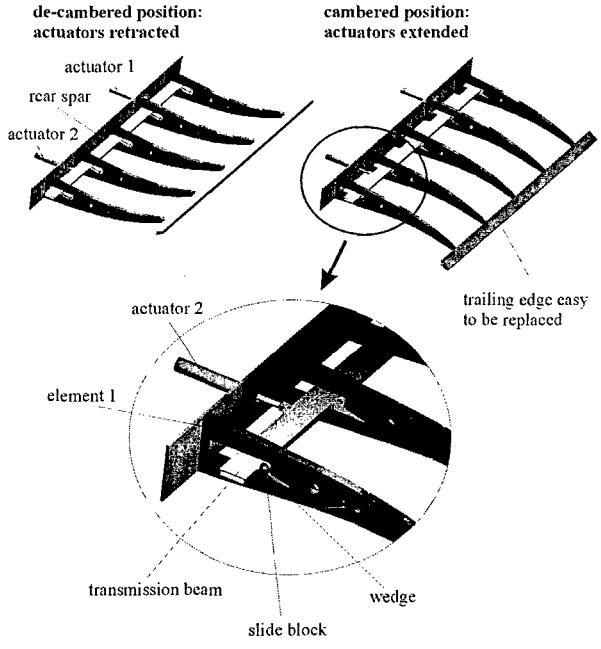

Fig. 12: Drive system

4. CALCULATION OF RESULTS

Since a sufficient amount of data is now available the following calculations have been made for an A340-300. For this airplane the aerodynamic investigations show that the camber variation is supposed to start from the spoiler trailing edge, which is also called the shroudline and corresponds to about 90% of the wing chord. In order to show some results a representative section was chosen (see Fig. 13) with defined geometry and aerodynamic loading. This section goes through the inner part of the outer Fowler flap. Here the flexible region makes up 50% of the Fowler flap chord leading to a cambering length of 840mm. The maximum camber variation shall be ±15°, which results in a deflection of ±185mm of the trailing edge. As maximum aerodynamic loading the maneuver load case is relevant. Moreover it has to be considered that this load is divided up over 21 active deformable ribs at a Fowler flap length of 10210mm

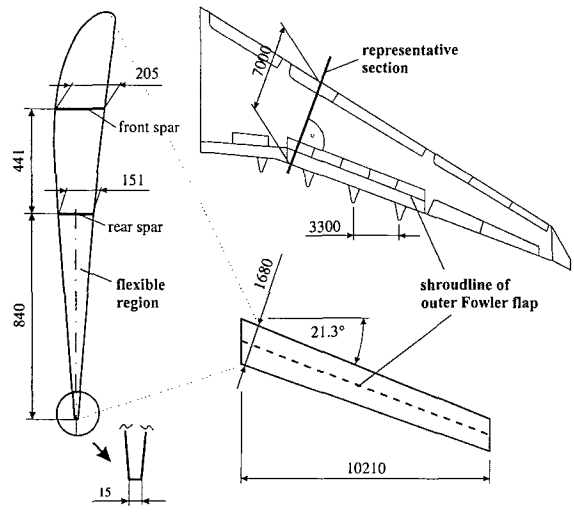

Fig. 13: Geometrical requirements

In this paper the calculation and presentation of results will concentrate on the rib structure. Therefore in Fig. 14 the following designations for the rib are chosen. The segment length indicated as l_i (i = 1, 2, ..., n) is defined describing the distance between the revolute joints (see Fig. 6 and Fig. 7, No. 8-12) whereas n indicates the number of segments. The revolute joints are now described by G_{i1} (i = 1, 2, ..., n), the prismatic joints by G_{i2} (i = 1, 2, ..., n-1). In addition the function $f_S(x)$ for the median line is introduced.

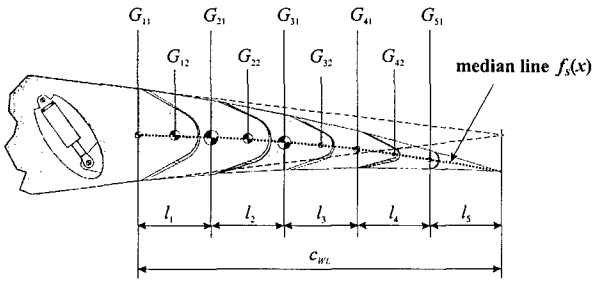

Fig. 14: Designations of rib structure

According to the defined basic requirements it is important to provide the possibility to adapt the contour towards different median lines occurring due to different aerodynamic and geometrical demands. Therefore the kinematics of the rib is investigated for three different types of functions $f_S(x)$ for the median lines which are shown in Fig. 15.

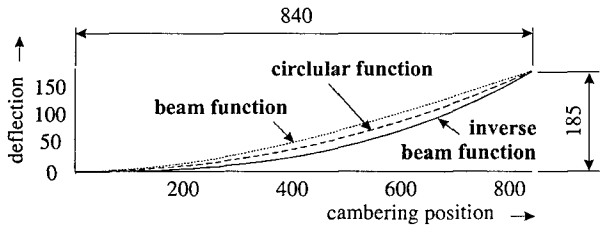

Fig. 15: Three different types of median lines

The first function is for the median line equivalent to elastic line according to Bernoulli's beam theory for a one sided rigidly clamped beam with a displacement applied to the free end.

$$f_S(x) = \frac{\Delta z}{2}\left(3\frac{x^2}{c_{WL}^2} - \frac{x^3}{c_{WL}^3}\right) \qquad (1)$$

By the second function a bending line is used, too. The difference is that it is inverted meaning that the free end of equation (1) is now rigidly clamped with an angle $f_s'(x) = 0$.

$$f_S(x) = \frac{\Delta z}{3}\left(\frac{x^2}{c_{WL}^2} + 2\frac{x^3}{c_{WL}^3}\right) \qquad (2)$$

For the third median line the circular function is being used. An arc of a circle is totally defined when it runs through two defined points where from one of the points the gradient is known. In this case the position of the rigidly clamped and the free displaced end is known. At the rigidly clamped end the angle is $f_s'(x) = 0$.

$$f_S(x) = \frac{1}{2}\left(\Delta z + \frac{c_{WL}^2}{\Delta z}\right) - \sqrt{\frac{1}{4}\left(\Delta z + \frac{c_{WL}^2}{\Delta z}\right)^2 - x^2} \qquad (3)$$

For rib structure general formulations have been established allowing calculation of the rib geometry and the joint loading according to any given aerodynamic and geometric requirement. Parameter variations have shown that the most useful configurations occur by an amount of segments n = 4 and n = 5 which is why the following presentation of results concentrates on these two cases.

The results for the joint loading of the rib without lever (see Fig. 6) for the three median lines are shown in Fig. 16. It can be seen that independent of the number of segments and the type of median line the maximum loading appears in the front two joints G_{11} and G_{21}. Moreover, in all joints the global loading is higher at n = 5 than at n = 4. It is also obvious that the maximum loading clearly appears for the beam function, the lowest for the inverse beam function. The circular function leads to slightly higher values than the latter.

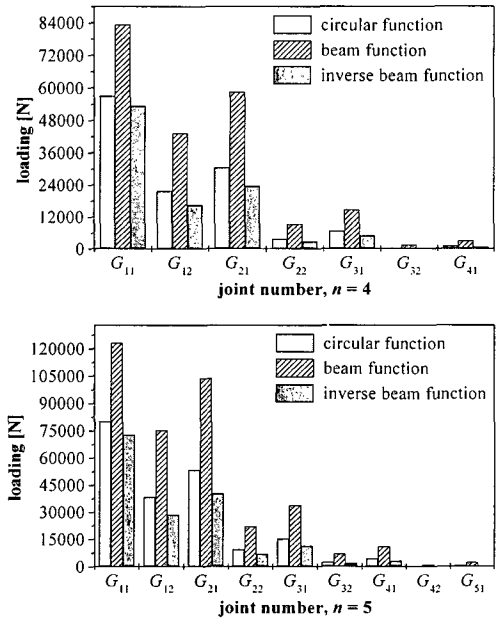

Fig. 16: Joint loading for rib without lever

The joint loading for the rib without lever is quite high, especially for the beam function. An additional lever allows a significant reduction of this loading. In this case the lever was attached to the joints G_{11} and G_{31}. As can be seen in Fig. 17 the lever relieves the front joints from the high loads. Similar to the rib without lever the beam function causes the highest loads, too. Also a higher number of segments results in higher joint loading.

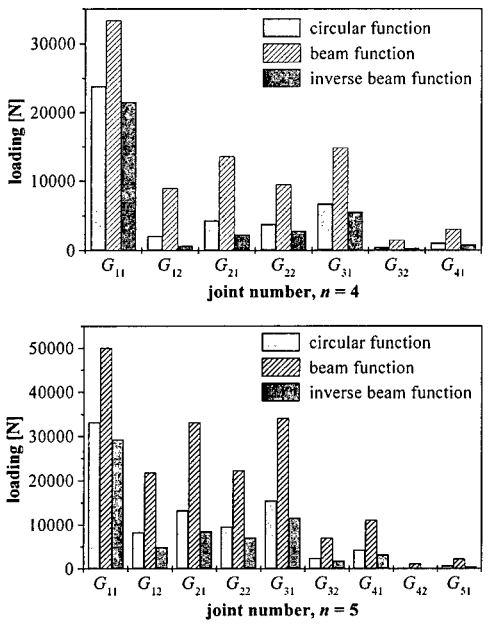

Fig. 17: Joint loading for rib with lever

A comparison of the joint loading for the rib with and without lever shows a significant reduction by the active deformable rib with lever (see Fig. 18). For joint G_{11} loading decreases by 60% and is nearly independent of the number of segments and the function for the median line. For the joints G_{12} and G_{21} improvements between 70% - 95% can be achieved. All other joint loadings stay unchanged.

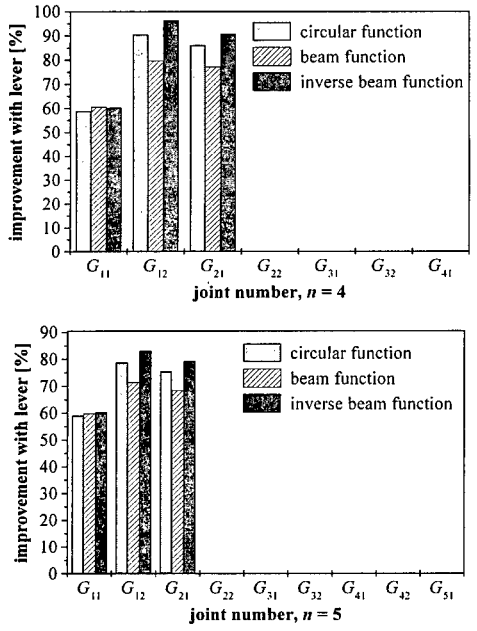

Fig. 18: Comparison of joint loading for rib with and without lever

Since the rib with an additional lever shows a significantly reduced joint loading compared to the version without (see Fig. 18) it is advantageous to use the former for the given maneuver load case. Therefore the complete rib geometry in Fig. 19 has been calculated for the preferred configuration with a lever. Since the formulations have been made in a general form it is easily possible to perform these calculations for the given median line and the calculated joint loading. In order to get a better overview the lever is not included in the illustrations of Fig. 19.

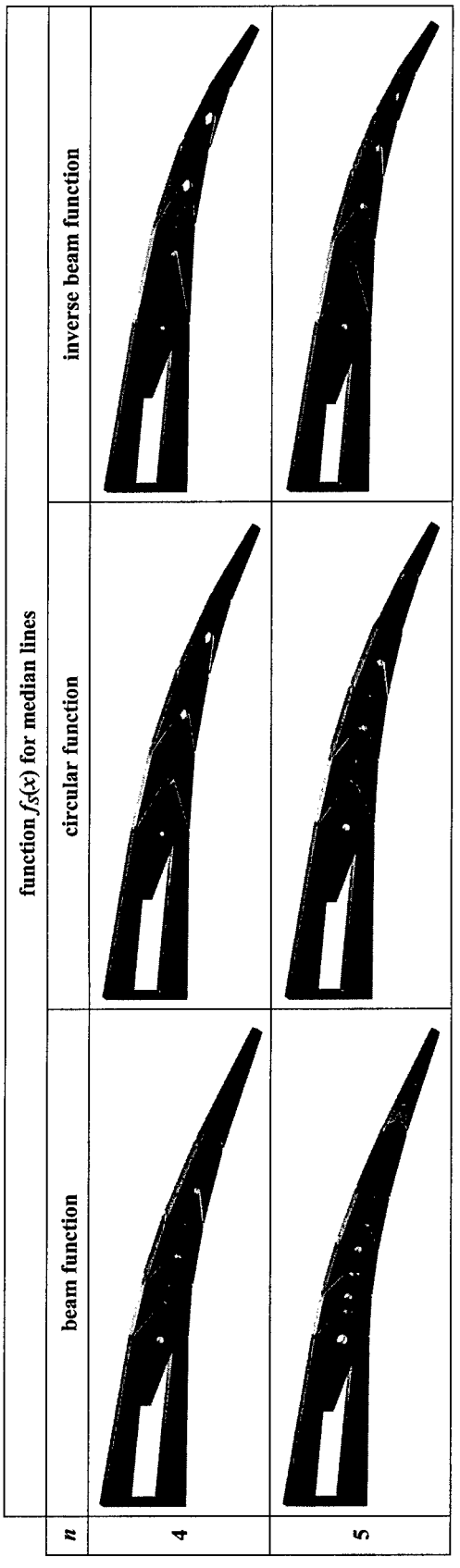

Fig. 19: Rib geometry for different types of median functions and number of segments

The first rib element is already provided with the necessary opening for the transmission beam and the wedge system of the drive system. Investigations with the finite element method (FEM) have shown that no critical deformation or strain appears. Moreover it can be seen that

depending on the median line the length of the segments varies. The stronger the curvature is the shorter the segments have to get in order to reproduce the median line in a sufficient way. Therefore, by the circular function all segments are of equal length due to the constant curvature. By the beam function the shortest segments are close to the fixed region and get longer towards the trailing edge. As to be expected by the inverse beam function, the shortest segments are at the trailing edge with increasing length towards the fixed section. The overall length of the segments gets shorter when the number of segments increases. For the rest of the elements FEM calculations have also been performed showing that here, too, no critical deformation or strain occurs.

5. CONCLUSIONS

The present paper describes an approach to achieve a chordwise as well as spanwise differential camber variation in the wings of civil transport aircraft by designing a flexible flap system for the trailing edge. According to the aerodynamic investigations the camber variation should start after 90% of the wing chord which corresponds to the shroudline. On civil transprt aircraft the ailerons and Fowler flaps are positioned in this region. Therefore the demonstrated cambering system can both be used as total replacement of an aileron and as enhancement of a Fowler flap. Because of less space being available and structural stiffness being critical it is much more demanding to enhance a given flap structure which is why the variable camber concept was presented for the enhancement of a Fowler flap. This means the trailing 50% of the Fowler flap had to be modified. As a design approach active deformable ribs were introduced into this flexible flap section. These active ribs consist of separate plate-like elements connected by revolute joints that can be driven from one single point. The rotation of the driven element is transferred gradually from element to element by these kinematics. Two variations of these kinematics were developed and different configurations were compared with each other for different types of profile contours. One system consists of the basic kinematics, the other one was enhanced by an additional lever. It was shown that the large joint loading of the solution without lever can be reduced by up to 90% using the solution with an additional lever. This makes the approach with lever advantageous for this given maneuver load case. In addition the kinematics has the advantage that by varying the distances between the revolute and prismatic joints the rib can be adjusted to nearly any desired median line. Moreover, the formulations for calculating the rib have been made in a general form and allow an easy adaptation of the rib design for different geometrical and aerodynamical requirements. Taken together the results of the investigations made this far are very promising for the continuing work on this concept.

6. ACKNOWLEDGEMENTS

The present investigation was carried out by the department Adaptive Structural Systems of the DLR Institute of Structural Mechanics in collaboration with the partners DaimlerChrysler Aerospace Airbus and DaimlerChrysler Research and Technology department of the major project ADIF (Adaptiver Flügel - Adaptive Wing).

7. REFERENCES

[1] L. Bölkow. "Ein Jahrhundert Flugzeuge", Düsseldorf: VDI Verlag, ISBN 3-18-400816-9, 1990

[2] J. J. Spillman, "The use of variable camber to reduce drag, weight and costs of transport aircraft", Aeronautical Journal, Vol. 96, No. 951, pp. 1-9, 1992

[3] H. Ahrend, D. Heyland, W. Martin, "Das Leitkonzept 'Adaptiver Flügel' (ADIF)", DGLR-Jahrestagung, DGLR-JT97-147, München 1997

[4] Airbus Industry, "Global Market Forecast 1997 - 2016", March 1997

[5] R. Kelm, B. Kiebebusch, H. G. Klug, H.-H. Thiele, K.-H. Vahle, "Grenzen Flugtechnischer Entwicklung: Überlegungen zum mittel / langfristigen Potential der Treibstoffeinsparungen und Emissionsreduzierung im zivilen Luftverkehr", DGLR-Jahrestagung, DGLR-JT97-106, München, August 1997

[6] Statistisches Bundesamt, "Statistical Yearbook 1996 for Foreign Countries", Metzler-Poeschel, Stuttgard 1996

[7] H. Hilbig, H. Wagner, "Variable wing camber control for civil transport aircraft", *ICAS Procedings*, ICAS-84-5.2.1, pp. 107-112, Toulouse 1984

[8] J. Szodruch, "The Influence of camber variation on the aerodynamics of civil transport aircraft", AIAA-Paper 85-0353, Reno, November 1985

[9] E. Greff, "The development and design integration of a variable camber wing for long/medium range aircraft", Aeronautical Journal, pp. 301-310, November 1990

[10] H. P. Monner, "Anströmprofil mit variabler Profiladaption", German Patent Application 197 41 326.9-22, 1997

[11] H. P. Monner, H. Hanselka, E. Breitbach, "Development and design of flexible Fowler flaps for an adaptive wing", SPIE's 5th Annual International Symposium on Smart Structures and Materials, Paper No. 3326-08, San Diego, CA 1-5 March, 1998

[12] A. Klose, H. P. Monner, "Konstruktion eines Funktionsdemonstrators der flexiblen Rippenstruktur einer adaptiven Fowlerklappe", IB 131-98/1, Braunschweig 1998

[13] V. Kilimann, H. P. Monner, "Finite-Elemente-Berechnung der flexiblen Hautstruktur einer adaptiven Fowlerklappe", IB 131-98/20, Braunschweig 1998

[14] C. Anhalt, H. P. Monner, "Entwicklung und Konstruktion von Antriebskonzepten für die formvariablen Fowlerklappen des adaptiven Flügels", IB-131-98/44, Braunschweig 1998

NASA LANGLEY RESEARCH CENTER'S CONTRIBUTIONS TO INTERNATIONAL ACTIVE BUFFETING ALLEVIATION PROGRAMS

Robert W. Moses
Aeroelasticity Branch
NASA Langley Research Center
Mail Stop 340
Hampton, VA 23681-2199, USA

Abstract

Buffeting is an aeroelastic phenomenon which plagues high performance aircraft, especially those with twin vertical tails like the F/A-18, at high angles of attack. This buffeting is a concern from fatigue and inspection points of view. By means of wind-tunnel and flight tests, this phenomenon is well studied to the point that buffet loads can be estimated and fatigue life can be increased by structural enhancements to the airframe. In more recent years, buffeting alleviation through active control of smart materials has been highly researched in wind-tunnel proof-of-concept demonstrations and full-scale ground tests using the F/A-18 as a test bed. Because the F/A-18 resides in fleets outside as well as inside the United States, these tests have evolved into international collaborative research activities with Australia and Canada, coordinated by the Air Force Research Laboratory (AFRL) and conducted under the auspices of The Technical Cooperation Program (TTCP). With the recent successes and advances in smart materials, the main focus of these buffeting alleviation tests has also evolved to a new level: utilize the F/A-18 as a prototype to mature smart materials for suppressing vibrations of aerospace structures. The role of the NASA Langley Research Center (LaRC) in these programs is presented.

Introduction

The Problem

For high performance aircraft, such as the F/A-18, at high angles of attack, vortices emanating from wing leading edge extensions (LEX) often burst, immersing the vertical tails in their wake (Figure 1). Although these vortices increase lift, the resulting buffet loads on the vertical tails are a concern from airframe fatigue and maintenance points of view.

Previous Investigations

Previous wind-tunnel and flight tests have been conducted to quantify the buffet loads on the vertical tails of the F/A-18. These tests were designed to characterize the flow mechanism and to quantify the unsteady differential pressures acting on the vertical tails during high-angle-of-attack maneuvers[1-7]. The major findings of these tests were: 1) that the buffet pressures vary with flight conditions; 2) that the buffeting (response of the tail) varies with flight conditions; and 3) that the frequency spectra scale with Strouhal number. Later comparisons among pressure data from reduced-scale wind-tunnel, full-scale wind-tunnel, and flight tests revealed that the (spatial) correlation time delays as well as the frequency spectra scale with Strouhal number[6-7].

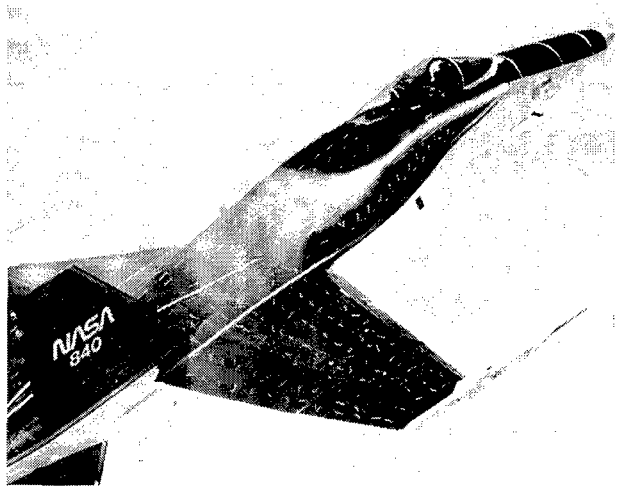

Figure 1. Flow Visualization of Vortex from the LEX Bursting ahead of the Vertical Tail
(Photograph Courtesy of the
NASA Dryden Flight Research Center)

Past Alleviation Techniques

Historically, solutions to these fatigue problems have involved controlling the vortex or altering the structural properties of the vertical tail[8]. Vortex control has included blowing and sucking flow from various ports on the aircraft and at various rates[9-11], attaching different size and shape leading edge extensions (LEX)[12], and attaching fences[3,4] to these LEX. These changes have had limited success since they are

Paper presented at the RTO AVT Specialists' Meeting on "Structural Aspects of Flexible Aircraft Control", held in Ottawa, Canada, 18-20 October 1999, and published in RTO MP-36.

effective only at specific flight conditions. Modification of structural properties has included increasing the damping and stiffness of the vertical tail. Structural damping has been increased by applying various concepts such as constrained-layer damping, damped-link, tuned-mass damper, interface damping, and solid-spacer damping[13,14]. Each of these treatments has demonstrated the ability to effect the dynamic response of the structure, but is limited to specific locations, modes, or within specific operating environments.

Stiffness increases have been implemented by means of increasing skin or spar thickness or applying reinforcing members such as brackets, cleats, or doublers. An example of a structural stiffness modification is the composite skin doubler, or "Exoskin," devised by McDonnell Douglas Corporation for a specific series of fighter aircraft[15]. The doubler is bonded to the outboard skin of the vertical tail's main torque box and effectively increases the tail's stiffness. The doubler decreases the load on the internal structure under the patch thus reducing the fatiguing strain in that area. This doubler has effectively eliminated a buffet induced fatigue damage site within those vertical tails with a minimal increase in overall vehicle weight (16 pounds). Often, changes such as these yield the undesirable result of increasing the overall vehicle weight and transfer the load and damage to other structural members. To date, however, the modifications to the set of vertical tails with the doubler attached have not shown counterproductive effects. Ferman et al.[15] point out that selective stiffening such as this is "especially applicable when a single mode produces a highly concentrated area of strain energy density." However, when the modal strain energy is evenly distributed throughout a structure, alternate means must be sought.

Since passive methods did not fully solve the buffeting problem on the F/A-18, active buffeting alleviation control schemes were investigated. Rock et al.[16] analyzed active buffeting alleviation systems for the F-15 and F/A-18 that employed the rudder as the primary actuator. For the F/A-18, their analyses showed that if the rudder actuation frequency bandwidth could be increased to include that of the first two structural modes, then the root mean square (rms) of the root bending moment could be reduced by as much as 33 percent using 3.2 degrees rms rudder deflection. Furthermore, their analyses showed that the fatigue life might be increased by a factor as high as 25. Lazarus, Saarmaa, and Agnes[17] developed an analytical model of an active buffeting alleviation system utilizing linear control algorithms and distributed, layered, piezoelectric strain actuators that were bonded to the surface of the vertical tail. Their analysis indicated that more than a 50 percent reduction in the root mean square (rms) strain at the root of the tail could be achieved at selected flight conditions with a smart material system. Moses[18,19] and Hauch et al.[20] separately investigated active buffeting alleviation control systems utilizing piezoelectric strain actuators (among other strategies) on sub-scale, twin-tail, fighter-like aircraft models. Both researchers found that active control systems can significantly reduce buffeting. As indicated in Figure 2, Moses' effort also showed that rudder and piezoelectric actuation are similarly effective up to the worst case buffeting conditions. At angles of attack above the worst case condition, the rudder becomes less effective because of separated flow over the aircraft. However, the piezoelectric actuators, that are not dependent upon the flow characteristics, continue to perform well beyond this point.

Recent Research

Several international programs are performing buffeting alleviation research by means of wind-tunnel, ground, and flight test demonstrations of advanced concepts. The Aeroelasticity Branch at the NASA LaRC is contributing to these ongoing programs by testing scaled F/A-18 models in the Transonic Dynamics Tunnel (TDT) and by participating in conducting full-scale ground tests and in planning flight demonstration tests.

During the ACROBAT (Actively Controlled Response Of Buffet-Affected Tails) program at the LaRC, feedback control to the rudder on the starboard fin and to piezoelectric patches on the port fin were implemented to reduce fin buffeting on a 1/6-scale full-span F/A-18 model[18,19]. The rms value of the root bending moment was reduced by as much as 20% using magnitudes well below the physical limits of the actuators. These experimental results agree well with the analysis results of Reference 16. Other important findings were that the rudder's effectiveness was limited by degrading flow field conditions due to separated flow at high angles of attack. However, the piezoelectric actuators maintained their effectiveness regardless of flight condition. In addition, not only did the modal response in the first three modes (first bending, first torsion, and second bending) of the tail change with angle of attack, but also the frequency of the first bending mode changed with angle of attack while maintaining a constant tunnel speed. As a result,

the control laws developed had to be sufficiently robust to account for these changes in the "plant". Similar plant sensitivities were later corroborated in a separate wind-tunnel investigation[21]. To demonstrate active buffeting alleviation during the ACROBAT test, one time-invariant, fixed-parameter, single-input-single-output control law worked well to alleviate the buffeting for all flight conditions. This control law was not optimized for any particular flight condition, and it is thought that its performance would be improved considerably using optimal controller design techniques with "plant" information from all possible flight conditions.

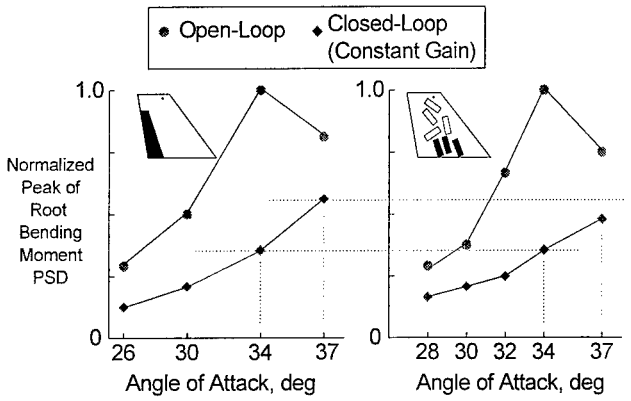

(a) Rudder Results (b) Piezo Results

Figure 2. Comparisons of the Normalized Peak Values of the PSD of the Root Bending Moment at the Frequency of the First Bending Mode, Open-Loop and Closed-Loop Conditions, Various Angles of Attack, 14 psf

The lessons learned during the ACROBAT program were incorporated into a full-scale ground test of a buffeting alleviation system on an F/A-18 at the AMRL in early 1998. During this AFRL program, conducted under the auspices of TTCP, researchers from the United States, Australia, and Canada used feedback control of piezoelectric patches to reduce the response of the starboard fin to simulated buffet loads. For this test, the International Follow-On Structural Testing Project (IFOSTP)[22] rig at AMRL (Figure 3) was used. This buffeting alleviation system used off-the-shelf piezoelectric actuators[23], shown in Figure 4. Researchers from Active Control eXperts (ACX), NASA LaRC, AMRL, and the National Research Institute (NRC) - Canada designed and tested control laws to alleviate buffeting resulting from four different simulated flight conditions[24]. Unfortunately, the nonlinear effects of the load shaker on the modal response of the tail were not considered in the mathematical models of the "plant"; consequently, the actuators did not provide the same level of effectiveness that was predicted using these mathematical models. As a result, the alleviation targets were not quite reached, as shown in Figure 5. Additionally, to maximize control authority for each simulated flight condition, a separate optimal controller was designed and tested by ACX for each of the four flight conditions illustrated in Figure 5. During the worst case flight condition, only one control law lasted the entire duration of the load cycle without overdriving the amplifiers and thus triggering a shut-down switch inside the amplifiers for protecting the system from harmful electrical inputs. This control law was designed for controlling responses in the first bending mode of the tail only and commanded only one of the two amplifier channels driving the piezoelectric actuators. Further details and results may be found in Reference 24.

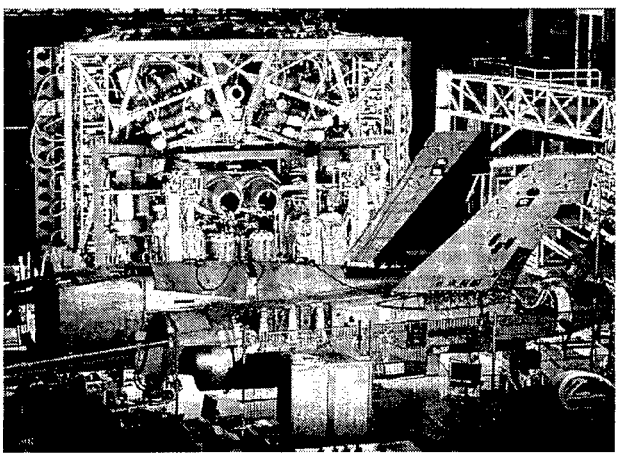

Figure 3. IFOSTP Facility with the F/A-18 Test Article

Although this test was highly successful, recent improvements in amplifiers and piezoelectric patches promise superior capabilities to the system tested at the AMRL. Ongoing programs at AFRL, NASA, and AMRL address the transition of these newly improved components to vibration suppression of aerospace structures through wind-tunnel demonstration tests at LaRC, future full-scale ground tests at AMRL, and planned flight demonstration tests at the NASA Dryden Flight Research Center (DFRC).

In a parallel effort at LaRC called SIDEKIC (Scaling Influences Derived from Experimentally-Known Impact of Controls), scaling relationships of piezoelectric actuators are being derived and verified using results from the full-scale ground test at the

AMRL and data acquired in the fall of 1998 on a 1/6-scaled F/A-18 model tested in the TDT. During this test, additional concepts and configurations were tested as proof-of-concept for buffeting alleviation systems. Additional concepts are planned to be tested in the TDT during 1999. LaRC plans for contributing to these programs are presented next.

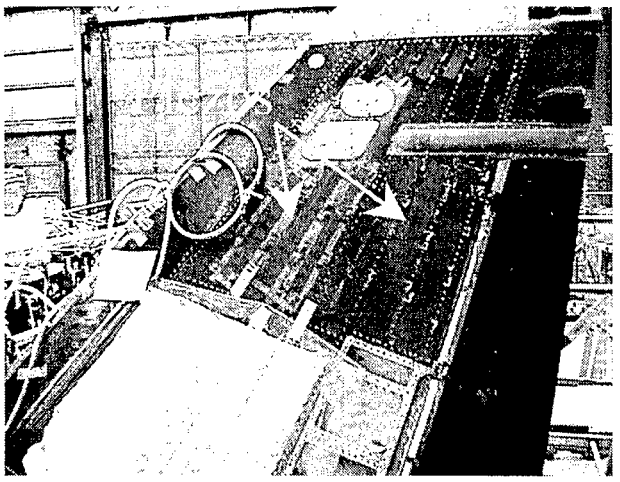

Figure 4. Piezoelectric Actuators Being Bonded to Inboard Surface of the F/A-18 Vertical Tail

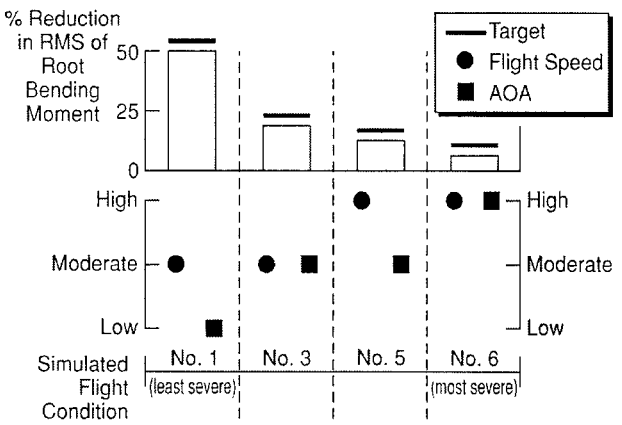

Figure 5. Summary of Alleviation Results for Four Simulated Flight Conditions in the IFOSTP

Current Programs and Plans at LaRC

SIDEKIC

The SIDEKIC model shown in Figure 6 differs from the ACROBAT model in three ways: 1) continuous skin construction was used for the tails; 2) the layout of the piezoelectric actuators; and 3) the type of amplifiers used in the buffeting alleviation system. The port fin, shown in Figure 7, is a scaled version of the buffeting alleviation system tested at the AMRL. After the establishment of target tip deflections and the estimation of force output of the actuators from their specifications, frequency response methods were employed for determining actuator layout and sizes. Results of the ACROBAT and F/A-18 ground test programs were used to guide the establishment of target tip deflections in two ways: 1) the tip deflections caused by the buffeting at various flight conditions were known; and 2) the tip deflections achievable by shaking the tail using just the piezoelectric actuators were known.

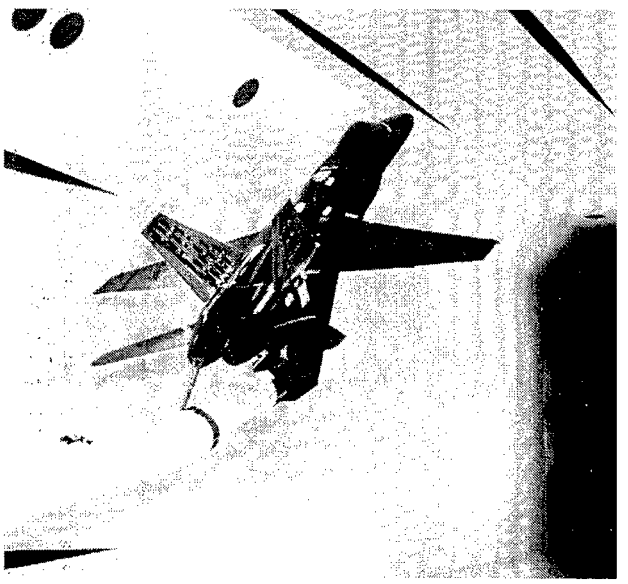

Figure 6. 1/6-scale F/A-18 SIDEKIC Model Mounted in the TDT

For SIDEKIC, a higher tip deflection ratio of item 2 with respect to item 1 was selected as the target because the manufacturer specifications tend to overstate the authority of the actuators that is achievable when bonded to host structure. The resulting additional actuators did not pose a problem for the amplifiers since they could easily handle the additional capacitance load posed by the piezoelectric actuators. Switching amplifiers were selected for the SIDEKIC test because they are better suited for driving capacitance loads more efficiently than the linear amplifiers that were used in the ground test. Because

the voltage levels required for SIDEKIC were below 200 volts (400 volts peak-to-peak), suitable amplifiers could be obtained from commercial sources.

The starboard fin, shown in Figure 8, employs an active rudder for controlling responses in the first bending mode, around 16 Hz, and active piezoelectric actuators for controlling responses in the first torsion mode, around 50 Hz. The rudder is activated using a hydraulic actuator and a servo valve. The piezoelectric actuators are the same type used on the port fin. This configuration of control effectors, referred to as a blended system because two actuator technologies were blended, provides a compromise between using an existing control surface and a reduced number (relative to port fin) of additional devices (piezoelectric actuators) that would require integration into an already tightly-packed aircraft.

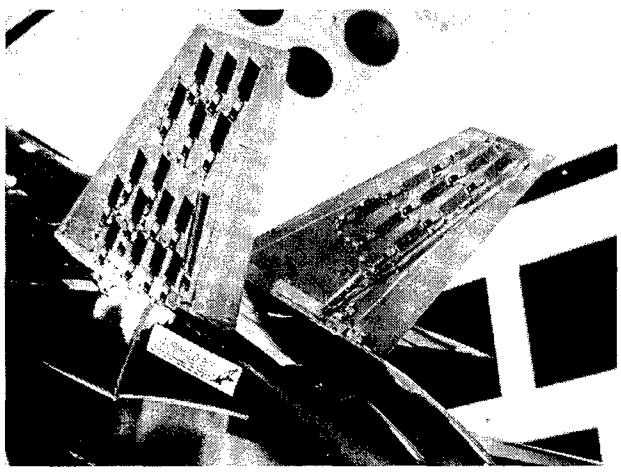

Figure 7. Details of Port Vertical Tail, 1/6-scale F/A-18 SIDEKIC Model Mounted in the TDT

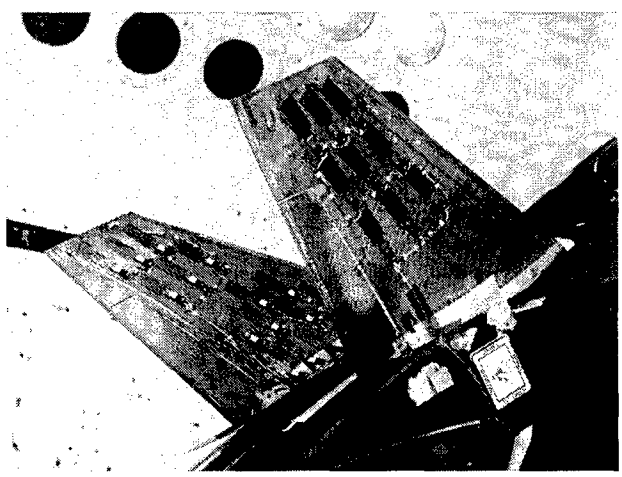

Figure 8. Details of Starboard Vertical Tail, 1/6-scale F/A-18 SIDEKIC Model Mounted in the TDT

A variety of control schemes were investigated for alleviating the tail buffeting. Boeing, who participated in the SIDEKIC tests through a Memorandum of Agreement (MOA), designed and tested a variety of shunt circuits and neural predictive controllers. A variety of modern state-space controllers were designed by LaRC and tested for reducing tail buffeting in the first two modes mentioned previously. For example, shown in Figure 9, simultaneous feedback control of the rudder (top graph) and of the piezoelectric actuators (bottom graph) caused a pronounced difference in the root bending moment (RBM, second graph) and the tip accelerations (third graph) compared to the open-loop case (when the values of the rudder and piezo commands in top and bottom graphs are zero). For a better comparison, power spectral densities of tip accelerations and root bending moment are computed for open-loop and closed-loop conditions. In Figure 10, significant reductions in the first bending mode (around 17 Hz) and the first torsion mode (around 58 Hz) were accomplished when feedback to the rudder and piezoelectric actuators are turned on.

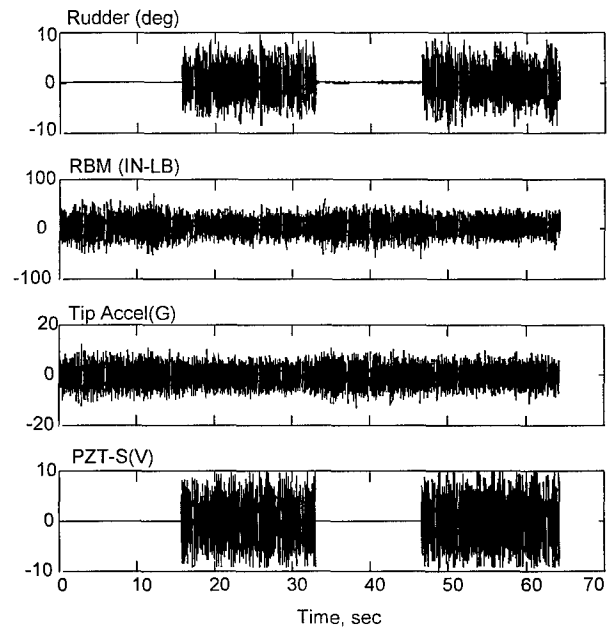

Figure 9. Time Histories of Actuator and Sensors During Feedback Off and On, Blended Buffeting Alleviation System, Starboard Vertical Tail, 1/6-scale F/A-18 SIDEKIC Model

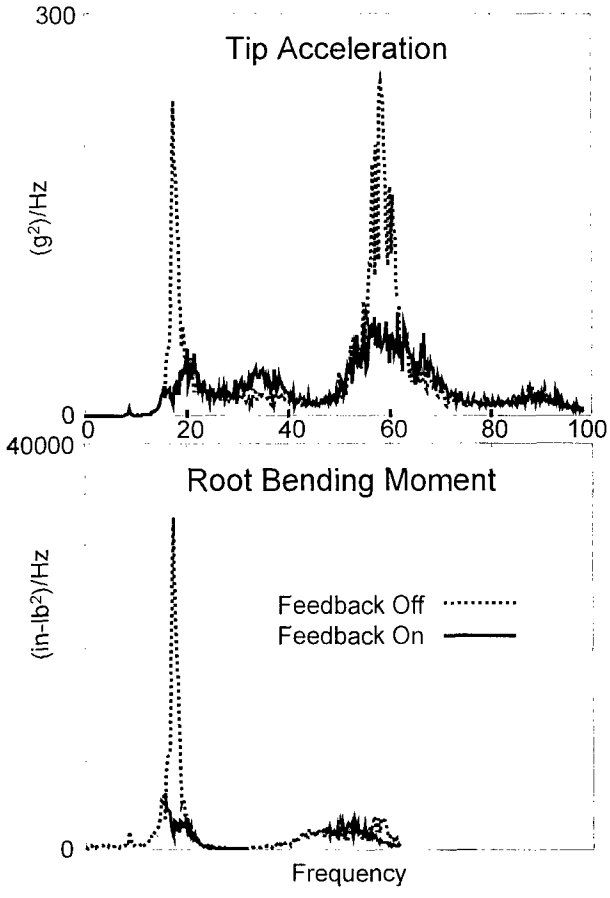

Figure 10. Power Spectral Densities of Buffeting During Feedback Off and On Conditions, Blended Buffeting Alleviation System, Starboard Vertical Tail, 1/6-scale F/A-18 (SIDEKIC) Model

F-22 Buffet Tests

In collaboration with the F-22 System Program Office (SPO) and the AFRL at Wright-Patterson Air Force Base, a 13.5% F-22 model (an aerodynamics model designated D6), shown in Figure 11, was refurbished with a new, starboard-side, flexible vertical tail and mounted in the TDT. The purpose of this test was to determine if the F-22 configuration would experience buffeting of the vertical tails similar to that encountered on the F/A-18 at high angles of attack, and to measure the F-22 rudder's effectiveness at the buffeting conditions if encountered. Because of restrictions placed on dissemination of test results by the F-22 SPO, only a description of the test is provided herein.

The flexible tail shown in Figure 12 had a rudder surface driven by a hydraulic actuator for potential buffeting alleviation investigations, and strain gages and accelerometers were bonded to the tail surface for measuring modal response if buffeting was encountered. The rigid, port-side, vertical tail shown in Figure 13 was instrumented with pressure transducers bonded to both surfaces for measuring unsteady pressures. In addition, tests were performed to measure the rudder's effectiveness at high angles of attack. This was accomplished by implementing a closed-loop control system that moved the rudder in response to any buffeting. The control system was designed so that the rudder could reduce buffeting if it occurred. The model was tested at angles of attacks between 7 degrees and 40 degrees and at Mach number between 0.03 and 0.11.

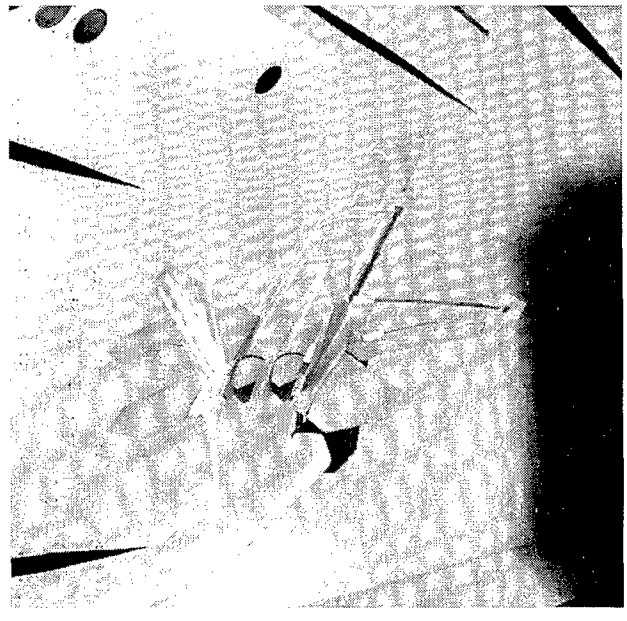

Figure 11. 0.135 Scale F-22 Model Mounted in the TDT

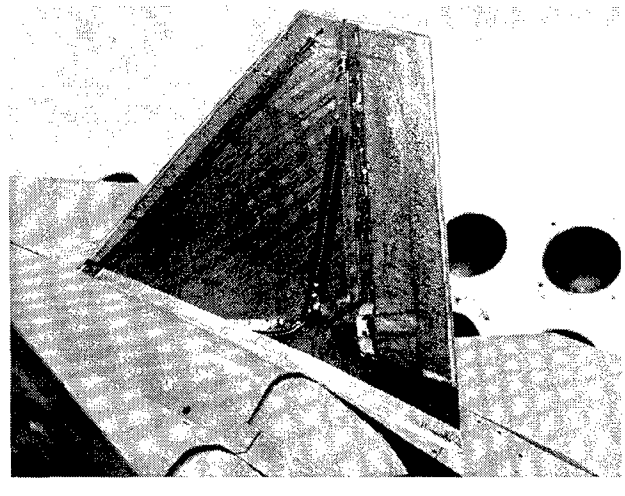

Figure 12. Details of the Flexible Starboard Vertical Tail, 0.135 Scale F-22 Model Mounted in the TDT

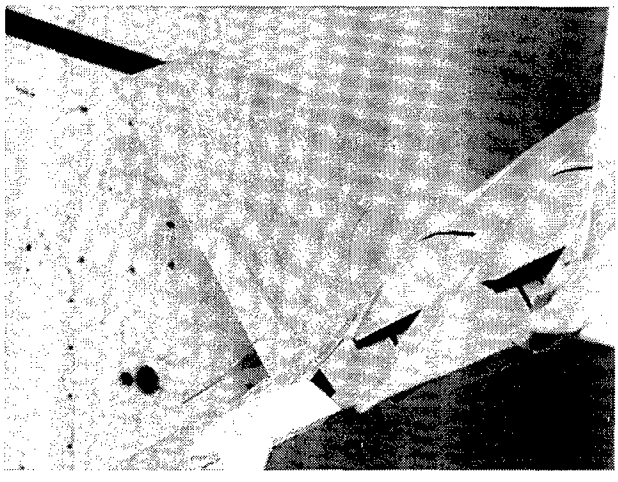

Figure 13. Details of the Rigid Port Vertical Tail, 0.135 Scale F-22 Model Mounted in the TDT

Future Efforts and Their Planned Support by LaRC

Planned Ground Test Follow-On Activity

Because of the recent significant strides made in piezoelectric actuator and amplifier technologies, the AFRL is planning with the AMRL, NASA (LaRC and DFRC), and the NRC to ground test these new technologies in the IFOSTP rig using the F/A-18 aircraft. The primary actuator candidates are some new interdigitated piezoelectric actuators being developed at LaRC. A program at LaRC is underway to mature these new actuator concepts for ground test program at the AMRL. Within the scope of this program is a planned TDT test of these actuators embedded in the skins of a vertical tail of the 1/6-scale F/A-18 model. This wind-tunnel test will be conducted under the Evaluation of New Actuators in a Buffet Loads Environment (ENABLE) program at LaRC[25]. Following this test, additional lab tests will be conducted for estimating the fatigue life of these actuators when subjected to a high strain environment. Any required enhancements to the actuators will be accomplished prior to the ground test at the AMRL.

Planned Flight Tests at NASA DFRC

Under its Active Buffeting Alleviation of vertical Tails Experiment (ABATE) program, the AFRL plans to flight test a buffeting alleviation system on an F/A-18 at the NASA DFRC. The objective of this program is not only to alleviate buffeting on the F/A-18, but also to demonstrate that the technology has matured sufficiently for vibration suppression of general aerospace structures. In support of this program, LaRC plans to design and test control laws for the rudder and for the piezoelectric actuators, as well as to provide technical oversight as needed. Separate, and as a precursor to the ABATE program, DFRC plans to assess the effectiveness of the rudder on the F/A-18 at high angles of attack for confirming some of the results of the ACROBAT program. LaRC plans to assist DFRC with test planning, some data analysis, and control law design as needed.

Conclusions

The NASA LaRC is playing a vital role in maturing smart materials for vibration suppression on aerospace structures. Specifically, LaRC is conducting wind-tunnel tests of new devices to demonstrate their effectiveness under specific load conditions. From these tests, LaRC will continue to extend any lessons learned directly to other national and international buffeting alleviation programs. In conjunction with plans at the AFRL to mature smart material technologies for general aerospace use by means of full-scale ground and flight tests, LaRC plans to continue the development of new interdigitated piezoelectric actuators and to use these new devices during future buffeting alleviation demonstrations.

Acknowledgments

The author would like to express his gratitude to the AFRL for its support of the collaborative programs at LaRC in the field of buffeting alleviation. Its support has been critical to the success of the wind-tunnel tests at LaRC. Appreciation is extended to the F-22 System Program Office at Wright-Patterson Air Force Base for loaning the F-22 model for this research. In addition, researchers from ACX, CSA Engineering, the AFRL, the AMRL, and the NRC are acknowledged for their excellent work during the TTCP ground test at the AMRL. It was truly an international collaborative activity that increased the awareness of the then-current capabilities of piezoelectric actuators to resolve problems on aerospace structures. The participation of Boeing enhanced the SIDEKIC program significantly. Last, and far from least, sincere gratitude is extended to the LaRC wind-tunnel test teams, and especially the technicians who refurbished many elements of the ACROBAT, SIDEKIC, and F-22 models. The TDT

tests could not have been performed without their devotion to this research activity.

References

1 Zimmerman, N. H., and Ferman, M. A., "Prediction of Tail Buffet Loads for Design Application," Vols. I and II, Rept. No. NADC-88043-60, July 1987.

2 Lee, B. H. K., Brown, D., Zgela, M., and Poirel, D., "Wind Tunnel Investigation and Flight Tests of Tail Buffet on the CF-18 Aircraft", AGARD-CP-483, Advisory Group for Aerospace Research and Development Specialist's Meeting, Sorrento, Italy, April 1990.

3 Pettit, C. L., Banford, M., Brown, D., and Pendleton, E., "Full-Scale Wind-Tunnel Pressure Measurements on an F/A-18 Tail During Buffet," Journal of Aircraft, Vol. 33, No. 6, November-December 1996, pp. 1148-1156.

4 Meyn, L. A. and James, K. D., "Full-Scale Wind-Tunnel Studies of F/A-18 Tail Buffet," Journal of Aircraft, Vol. 33, No. 3, May-June 1996, pp. 589-595.

5 Moses, R.W. and Ashley, H., "Spatial Characteristics of the Unsteady Differential Pressures on 16% F/A-18 Vertical Tails," AIAA-98-0519, 36th AIAA Aerospace Sciences Meeting and Exhibit, Reno, Nevada, January 12-15, 1998.

6 Moses, R. W. and Shah, G. H., "Spatial Characteristics of F/A-18 Vertical Tail Buffet Pressures Measured in Flight," AIAA-98-1956, 39th AIAA/ASME/ASCE/AHS/ASC Structures, Structural Dynamics, and Materials Conference and Exhibit, Long Beach, CA, April 20-23, 1998.

7 Moses, R. W. and Pendleton, E., "A Comparison of Pressure Measurements Between a Full-Scale and a 1/6-Scale F/A-18 Twin Tail During Buffet," 83rd Structures and Materials Panel Meeting of the Advisory Group for Aerospace Research and Development (AGARD), 2-6 September 1996, Florence, Italy.

8 Calarese, W. and Turner, E. W., "Progress and New Techniques in Buffet Alleviation," USAF Wright Laboratory Technical Memorandum 97-3084, September 1997.

9 Bean, D. E., Greenwell, D. I., and Wood, N. J., "Vortex Control Technique for the Attenuation of Fin Buffet," *Journal of Aircraft*, Volume 30, Number 6, November-December 1993.

10 Mabey, D. G. and Pyne, C. R., "Tangential leading-edge blowing on a combat aircraft configuration," Defence Research Agency Report, 1994.

11 Huttsell, L. J., Tinapple, J. A., and Weyer, R. M., "Investigation of Buffet Load Alleviation on a Scaled F-15 Twin Tail Model," AGARD SMP Panel Meeting, Aalborg, Denmark, October 1997.

12 Shah, G. H., "Wind-Tunnel Investigation of Aerodynamic and Tail Buffet Characteristics of Leading-Edge Extension Modifications to the F/A-18," AIAA Atmospheric Flight Mechanics Conference, AIAA 91-2889, New Orleans, LA, August 12-14, 1991.

13 Gibson, W. C., Maly, J. R., and Austin, E. M., "Conceptual Design of Damping Treatments for the F/A-18 Vertical Tail," CSA Engineering Report No. 88-11-02, November 1988.

14 Liguore, S., Ferman, M., and Yurkovich, R., "Integral Damping Treatment for Primary Aircraft Structures," Damping '91 Conference, San Diego, CA, 13-15 February 1991.

15 Ferman, M. A., Liguore, S. L., Colvin, B. J., and Smith, C. M., "Composite 'Exoskin' Doubler Extends F-15 Vertical Tail Fatigue Life," 34th AIAA Structures, Structural Dynamics, and Materials Conference, La Jolla, CA, 19-22 April 1993.

16 Rock, S. M., Ashley, H., Digumarthi, R., and Chaney, K., "Active Control for Fin Buffet Alleviation," Proceedings from AIAA Guidance, Navigation and Control Conference, 1993, pp. 1051-1056.

17 Lazarus, K. B., Saarmaa, E., and Agnes, G. S., "An Active Smart Material System for Buffet Load Alleviation," Proceedings from SPIE's 2nd Annual International Symposium on Smart Structures and Materials, Volume 2447, 1995, pp. 179-192.

18 Moses, R. W., "Vertical Tail Buffeting Alleviation Using Piezoelectric Actuators – Some Results of the Actively Controlled Response of Buffet-Affected Tails (ACROBAT) Program," SPIE's 4th Annual International Symposium on Smart Structures and Materials, San Diego, CA, 4-6 March 1997.

19 Moses, R. W., "Active Vertical Tail Buffeting Alleviation on a Twin-Tail Fighter Configuration in a Wind Tunnel," CEAS International Forum on Aeroelasticity and Structural Dynamics, Rome, Italy, 17-20 June 1997.

20 Hauch, R. M., Jacobs, J. H., Dima, C., and Ravindra, K., "Reduction of Vertical Tail Buffet Response Using Active Control," *Journal of Aircraft*, Volume 33, Number 3, May-June 1996.

21 Beier, T., Lichtenwalner, P., and Findlay, D., "Active Load Alleviation Technology," Presentation at the First Annual Joint

DoD/NASA/FAA Conference on Aging Aircraft, Ogden, Utah, 10 July 1997.

22 Conser, D. P., Graham, A. D., Smith, C. J., and Yule, C. L., "The Application of Dynamic Loads to a Full-Scale F/A-18 Fatigue Test Article," 20th Congress of the International Council of the Aeronautical Sciences (ICAS), Sorrento, Napoli, Italy, 8-13 September 1996, ICAS-96-5.10.5, Volume 2, pp. 2465-2480.

23 Moore, J. W., Spangler, R. L., Lazarus, K. B., and Henderson, D. A., "Buffet Load Alleviation Using Distributed Piezoelectric Actuators," Symposium on Adaptive Structures, ASME International Mechanical Engineering Congress and Exposition, Atlanta, GA, November 1996.

24 Hopkins, M., Henderson, D., Moses, R., Ryall, T., Zimcik, D., and Spangler, R., "Active Vibration Suppression Systems Applied to Twin Tail Buffeting," SPIE 5th Annual International Symposium on Smart Structures and Materials, San Diego, CA, 1-5 March 1998.

25 Moses, R. W., "Contributions to Active Buffeting Alleviation Programs by the NASA Langley Research Center," AIAA-99-1318, 40th AIAA/ASME/ASCE/AHS/ASC Structures, Structural Dynamics, and Materials Conference and Exhibit, St. Louis, Missouri, 12-15 April 1999.

METHODE D'IDENTIFICATION DES FORCES AERODYNAMIQUES INSTATIONNAIRES SUR LES ESSAIS EN VOL, VALIDATION EXPERIMENTALE

(METHOD OF MATHEMATICAL IDENTIFICATION OF UNSTEADY AIRLOADS FROM FLIGHT MEASUREMENTS, EXPERIMENTAL VALIDATION)

by
C. PETIAU, E. GARRIGUES, Ph. NICOT
Aviation Marcel Dassault
78, Quai Marcel Dassault
Cedex 300
92552 St Cloud Cedex
France

RESUME

Nous avons développé dès la fin des années 70 dans notre logiciel ELFINI des techniques mathématiques originales d'identification de modèles, en particulier pour les modèles dynamiques Eléments Finis et pour le recalage des modèles de charges aéroélastiques stationnaires sur les essais en vol.

Nous nous sommes maintenant attaqués au recalage des charges aérodynamiques instationnaires sur les essais de vibration en vol.

Sur le plan mathématique nous utilisons toujours la même approche, qui diffère notablement des méthodes classiques de moindres carrés (minimisation d'une "distance" calcul-mesure en fonction des paramètres d'ajustement). Nous préférons utiliser une approche type optimisation quadratique en minimisant une "distance" entre les paramètres d'ajustement et leurs valeurs théoriques ou présumées, en forçant la solution à satisfaire les inéquations de reconstitution des mesures par le modèle à une précision donnée.
Parmi tous les avantages de cette technique le principal est de s'affranchir du problème des paramètres mal observables.

Nous montrons 2 applications en aéroélasticité :

- Le recalage des champs de pression aérodynamiques stationnaires par les mesures en vol de réponses de jauges de contraintes en manoeuvre, illustré par un exemple issu de la mise au point des charges du RAFALE.

- Le recalage des forces aérodynamiques instationnaires sur la mesure en soufflerie, mais transposable en vol, des fréquences et amortissements d'une maquette aéroélastique d'empennage type Airbus. Nous montrons que le calcul de la vitesse critique de Flutter est recalé à partir d'essais à vitesse bien inférieure.

Nous concluons en présentant les perspectives de développement de la méthode.

ABSTRACT

Since the end of the 70ies we have developed, within the frame of our ELFINI software, original techniques for mathematical model identification, in particular for calibration of dynamic Finite Element models from ground vibration tests and of steady aeroelastic loads from flight tests.

Now we have tackled calibration of unsteady airloads from flight vibration tests.

Mathematically speaking, we keep the same approach, which differs notably from classical least square methods (minimization of a calculation - measurement "distance" in function of calibration parameters). We prefer to use a quadratic optimization type approach with the minimization of a "distance" between calibration parameters and their theoretical or presumed values, constraining the solution to satisfy measurement reconstitution by the model at a given accuracy.

Among advantages of this technique, the principal is to get rid of ill-observable parameters.

We describe two applications :

- Calibration of steady aerodynamic pressure fields from flight measurements of strain-gage responses in maneuver, illustrated by an example coming from the calibration of Rafale airloads,

- Calibration of unsteady airloads from wind tunnel measurements, transposable to flight measurements, of frequencies and dampings of an aeroelastic dynamic model of an Airbus type stabilizer. We show that critical flutter speed is identified from tests at much lower speed.

As a conclusion we present the future prospects of the method.

Paper presented at the RTO AVT Specialists' Meeting on "Structural Aspects of Flexible Aircraft Control", held in Ottawa, Canada, 18-20 October 1999, and published in RTO MP-36.

1 INTRODUCTION

Par définition l'analyse aéroélastique couple 2 types de modèle qui au départ sont issus de calculs sur plan :

- modèle structural dynamique Eléments Finis de l'avion (déformations "souples" de l'avion en fonction charges ; voir planche 1),

- modèle aérodynamique théorique "linéarisé" par méthode de singularité et/ou Eléments Finis Euler, ..., stationnaire et instationnaire (charges aérodynamiques en fonctions des mouvements "rigides" et "souples"),

qu'elle réunit (voir planche 2) en des modèles de mécanique du vol "avion souple" et de vibrations aéroélastiques, eux-mêmes support des calculs de stabilité (divergence, Flutter) et de réponse structurale en manoeuvre, turbulence, etc ...

Une des complexités de l'analyse aéroélastique est de rendre ces modèles théoriques cohérents avec les résultats expérimentaux issus :

- des essais statiques et de vibration au sol,
- des essais en soufflerie,
- des essais en vol, de réponse en manoeuvre et d'excitations vibratoires.

En réponse à ce besoin, nous avons développé progressivement, depuis la fin des années 70, une panoplie d'outils de **recalage du modèle structural dynamique et de la partie stationnaire des charges aérodynamiques** sur les résultats expérimentaux.

Ces outils sont fondés sur une technique mathématique originale d'identification de modèle (voir référence 2 et 3) ; ils sont intégrés dans notre logiciel général d'analyse aéroélastique ELFINI (voir référence 1). Cette approche est exposée dans les § 2 et 3.

Nous pressentions que la même technique pouvait s'appliquer à l'identification des forces aérodynamiques instationnaires et permettre le recalage du calcul des vitesses critiques de Flutter par des essais en vol à des vitesses bien inférieures (voir référence 3).

La démonstration de validité de cette approche par essais en vol étant évidemment trop risquée, nous montrons ici (§ 4) comment nous avons profité pour la tester de la campagne de validation des modèles de flutter en présence de jeux mécaniques par des essais d'une maquette aéroélastique d'empennage "type Airbus" dans la soufflerie S2 de l'ONERA (voir notre présentation sur ce sujet dans ce meeting, référence 4).

2 PRINCIPES GENERAUX DES TECHNIQUES MATHEMATIQUES D'IDENTIFI-CATION DE MODELE

Nous nous plaçons dans le cas général ou nous disposons des résultats de mesures expérimentales rassemblés dans un vecteur σ**mes**, et des mêmes quantités $\sigma(\lambda)$, calculées par un modèle numérique dépendant de paramètres d'ajustement λ.

L'approche habituelle en identification de modèle, dont nous allons montrer les inconvénients en particulier pour l'aéroélasticité, est la méthode des moindres carrés, avec le principe de minimisation d'une fonction d'erreur $E(\lambda)$ de la forme :

$$E(\lambda) = \sum \Pi i \, (\sigma_i(\lambda) - \sigma_i \mathbf{mes})^2$$

(Π**i** = facteur de pondération des différentes mesures)

Cette minimisation est traitée par une méthode type Newton, ou la matrice Hessienne de E est approximée par :

$$[H] = \sum \Pi i \, (\partial \sigma i / \partial \lambda j)t \, ((\partial \sigma i / \partial \lambda j)$$

dite matrice de Fisher (voir référence 4).

La méthode ne fait intervenir comme calculs lourds que ceux des $\sigma(\lambda)$ et des gradients $\partial\sigma / \partial\lambda$ qui sont calculés de façon standard par ELFINI (voir référence 1) :

Le choix des facteurs de pondération Π**i** pouvant poser problème, est souvent résolu avec la variante dite "maximum de vraisemblance" (voir référence 5 et 6) ou on itère la méthode des moindres carrés en prenant comme facteur de pondération à chaque itération l'inverse du carré de l'erreur de reconstitution de l'itération précédente.

La difficulté de ces techniques de moindres carrés est leur impossibilité de traiter des paramètres ou combinaison de paramètres d'ajustement mal observables par les mesures (entraînant la singularité de la matrice de Fisher), ce qui est le cas presque général avec les paramètres d'ajustement "naturels" des modèles aérodynamiques (voir § 3 et 4). La solution, souvent préconisée, de réduire l'espace des paramètres d'ajustement (sous espace des vecteurs propres à vàleurs propres non nulles de la matrice de Fisher), n'est pas "physique" car elle fait

dépendre l'espace des paramètres d'ajustement des points de mesures choisies.

Cet inconvénient nous a amené à reformuler complètement le problème d'identification sous la forme :

- **minimiser** $Z = \sum (\lambda_j - \lambda_j \text{ th})^2$

  Z représente une distance entre les valeurs recherchées λ_j des paramètres d'ajustement et leurs valeur λ_j **th**, théoriques si elles sont issues de calculs ou présumées s'il s'agit de données physiques.

- En satisfaisant les inéquations :

$$\sigma_i \text{ mes} - \varepsilon i \leq \sigma_i(\lambda) \leq \sigma_i \text{ mes} + \varepsilon i$$

  restitution des mesures par le modèle à une précision donnée εi.

  Cette minimisation sous-contraintes de **Z** est traitée par une technique d'optimisation quadratique, où comme pour les moindres carrés les seuls calculs "lourds" sont ceux de $\sigma(\lambda)$ et $\partial\sigma / \partial\lambda$.

Les principaux avantages comparés aux moindres carrés sont :

- pas de difficulté avec les paramètres mal observables, ils sont automatiquement laissés à leur valeur théorique ; on n'est donc pas limité par le nombre des paramètres d'ajustements,

- les facteurs de pondération des mesures, Πi plus ou moins subjectifs, sont remplacés par une précision de reconstitution des mesures εi, qui peut être estimée objectivement à partir de la précision des mesures et de celle du modèle,

- si le biais du modèle est trop grand, l'algorithme donne un diagnostique clair des mesures que le modèle n'arrive pas à reconstituer.

3 APPLICATION A L'IDENTIFICATION DES CHARGES AERODYNAMIQUES STATIONNAIRES A PARTIR DES MESURES EN VOL

La méthode a été appliquée dès la fin des années 70 pour le MIRAGE 2000 (voir référence 2) elle a été perfectionnée et utilisée systématiquement pour le programme RAFALE :

- **Les paramètres d'ajustement sont là directement** les composantes des champs de pression discrétisées dans la base de charges ELFINI (plusieurs centaines de composantes pour un champ), pour les effets de chaque degré de liberté de mouvement rigide (incidence, dérapage, ..., braquages gouvernes, ...).

- **Les mesures sont directement les réponses de jauges de contraintes** réparties sur l'avion (quelques centaines), mesurées pendant un ensemble de **manoeuvres d'oscillation de tangage, roulis, dérapage à fréquences variables, dites "stimuli"** (exemple planche 2), qui rendent observables les effets de chaque degré de liberté du mouvement. Pour observer les effets non linéaires de grandes incidences on complète par des montées lentes en facteur de charge.

  Le modèle aéroélastique ELFINI (voir planche 1) fournit directement la reconstitution théorique de ces mesures $\sigma(\lambda)$ en fonction des paramètres d'ajustement λ des champs de pression (qui coïncident directement avec les composantes du champ de pression discrétisé), ainsi que leurs gradients $\partial\sigma / \partial\lambda$.

  Ces opérateurs sont non linéaires par l'effet "aéroélastique" des modes souples (ces effets aérodynamiques des modes souples ne sont pas ajustés du fait de leur faible observabilité dans les manoeuvres considérées).

  Nous montrons des exemples extraits des travaux de calibration des charges du RAFALE.

- Un exemple de manoeuvre de stimulus par excitation du canard avec, planche 3, la réponse ou incidence de l'avion, la réponse de la jauge d'emplanture du canard avant et après recalage, le recalage est là presque parfait puisque cet essai a servi de base au recalage.

- La comparaison essais-calculs avant et après recalage, avec des manoeuvres contrées de roulis complexes, n'ayant pas servi au recalage, pour des jauges de dérive et d'élevon externe, planche 4, le résultat est très satisfaisant.

Un point important à signaler pour l'application de la méthode est la nécessité absolue de recalage préalable du modèle Eléments Finis statique de l'avion (voir planche 1) pour garantir la validité de l'opérateur donnant les contraintes élastiques en fonction des charges appliquées, au travers duquel sont observés les charges aérodynamiques. Cette calibration, ou souvent simple validation, se fait à partir des corrélations calcul/mesures des réponses des jauges de contrainte sous quelques dizaines de changements d'étalonnage au sol (voir références 2 et 3).

4 IDENTIFICATION FORCES AERODYNAMIQUES INSTATIONNAIRES

Pour évaluer la capacité des techniques précédentes à calibrer les modèles de calcul des vitesses critiques de Flutter, nous avons profité de la disponibilité du jeu complet de calculs et de mesures expérimentales réalisé avec la campagne d'essais dans la soufflerie S2 de l'ONERA d'une maquette dynamique d'empennage type Airbus, destiné initialement à la validation des calculs de Flutter en présence de jeux mécaniques (voir planche 5).

- **Paramètres d'ajustement**

  En considérant l'équation du Flutter exprimée dans la base des modes propres :

  $$[(K) - \omega^2 (M) - \tfrac{1}{2} \rho V^2 [A(\omega/V)] \, x = f$$

  et sachant que nous ne sommes pas contraints par leur observabilité, nous avons pris directement comme paramètres d'ajustement tous les termes des matrices complexes $[A(\omega/V)]$ sous la forme rationalisée de Karpel (voir références 6 et 7).

  Les matrices (K) et (M) sont considérées là comme constantes (modes propres recalés avec les essais de vibration sans vent).

- **Mesures**

  Le recalage se fait directement à partir de la "mesure" en soufflerie des fréquences et amortissements des seuls 2 modes intervenant dans le Flutter (flexion, empennage, rotation gouverne), à quelques points de pressions dynamiques (1 et 2 dans l'exemple que nous présentons).

  A noter que la "mesure" de ces fréquences/amortissement résulte de l'identification par la méthode de Prony des pôles des fonctions de transferts entre l'effort de la palette d'excitation et les mesures accélérométriques (voir conclusion, développement).

  Nous présentons des résultats caractéristiques menés à partir du modèle aérodynamique par méthode de doublets (maillage planche 5) n'ayant pas subit de recalage en particulier sans le recalage par les mesures de pressions instationnaires présenté dans la référence 7).

Sont présentés planche 6 :

- **Comparaison calcul-essais sans recalage,** pression critique calculée 128000 Pa contre 85000 Pa mesurée.

- **Comparaison avec 1 seul point en Pi** de recalage à 38700 Pa, la pression critique calculée devient 73000 Pa.

- **Comparaison avec 2 points en Pi** de recalage (37800 Pa et 60000 Pa), la pression critique calculée est de 84500 Pa.

  A noter cependant que pour que l'algorithme trouve ces solutions nous avons été conduits à relâcher la précision de reconstitution de l'amortissement du mode très amorti de torsion voir axe de développement (§5).

  D'autres tests menés à partir de calculs aérodynamiques volontairement erronés (défaut sur la forme géométrique) donnent des résultats semblables, ce qui montrerait une certaine robustesse de la méthode.

5 CONCLUSION, AXES DE DEVELOPPEMENT

On imagine sans peine l'intérêt potentiel de la méthode de recalage des forces aérodynamiques instationnaires présentées, en particulier pour assurer la sécurité de l'ouverture des domaines de vol, cela d'autant plus que la mise en oeuvre est relativement simple et peut coûteuse (le calcul des gradients des fréquences/amortissement est insignifiant quand on travaille en base réduite, voir référence 1).

On peut cependant se poser la question de la validité et la cohérence physique et mathématique de tels recalages "brutaux" sur les forces aérodynamiques instationnaires généralisées. Ce qui nous mène à étudier des sophistications notables de la méthode, principalement :

- Prendre les paramètres d'ajustement du modèle aérodynamique instationnaire directement "à la source", en se rapprochant des coefficients de la matrice d'influence aérodynamique

  $$[\partial Cp / \partial \alpha \, (\omega/V)]$$

  reliant les coefficients de pression **Cp** sur la surface avion aux incidences locales α de cette surface.

  Un des avantages est de forcer la cohérence entre les effets aérodynamiques non indépendants (exemple : incidence et vitesse de pompage avion).

- Prendre aussi les mesures plus "à la source", avec les fonctions de transfert mouvements-gouvernes-réponses accélérométriques voir jauges de contrainte, ce qui a l'avantage de s'affranchir de l'imprécision éventuelle de l'identification des fréquences amortissement par la méthode de Prony, et surtout des difficultés possibles d'appariage modes calculés - modes mesurés dans les situations complexes. On pourrait, à la limite, exploiter directement les mesures en temps.

- Intégrer en une seule approche l'identification des charges stationnaires présentées §3 et celle des charges instationnaires.

- A la limite intégrer aussi la calibration du modèle structural dynamique, à partir de stimuli à basse vitesse. L'intérêt serait de simplifier la procédure, le recalage du modèle dynamique se faisant souvent* par des essais d'excitation par les gouvernes l'avion reposant sur son train, ce qui peut nécessiter des corrections de modèle.

* Sur les MIRAGE 2000 et RAFALE qui disposent d'une puissance et d'une bande passante de servo-commande importante.

REFERENCES

1. C. PETIAU, S. BRUN
   Tendances Actuelles de l'Analyse Aéroélastique des Avions Militaires. AGARD Conférence proceedings n° 403 - Athènes 1986

2. C. PETIAU & M. DE LAVIGNE
   Analyse Aéroélastique et Identification des Charges de Vol. AGARD Conferences proceeding n° 375 - "Operational Loads Data" - Sienne 1984

3. C. PETIAU, Ph NICOT
   A General Method for Mathematical Model Identification in Aeroelasticity. International Forum on Aeroelasticity and Structural Dynamics, Royal Aeronautical Society - Manchester 1995

4. E. WALTER, L. PRONZATO
   Identification de modèles paramétriques à partir de données expérimentales - MASSON 1994

5. STEPNER D.E. & MEHRA R.K.
   Maximum Likelihood Identification and Optimal input design for identifying aircraft stability & control derivatives.
   NASA CR 2200 - MARCH 1983

6. M. KARPEL
   Time domain Aeroservoelastic Modeling Using Weighted Unsteady Aerodynamic Forces
   J. GUIDANCE, Vol 13, N° 1, Jan-Feb 1990, p. 30-37

7. C. PETIAU, B. JOURNEE, E. GARRIGUES
   Méthode de Calcul du Flutter en Présence de Jeu Mécanique et Vérification expérimentale
   R.T.O. Specialist Meeting ou Structural Aspects of Flexible Aircraft, OTTAWA 1999

PLANCHE 1

MODELE ELEMENTS FINIS POUR CALCULS AEROELASTIQUES

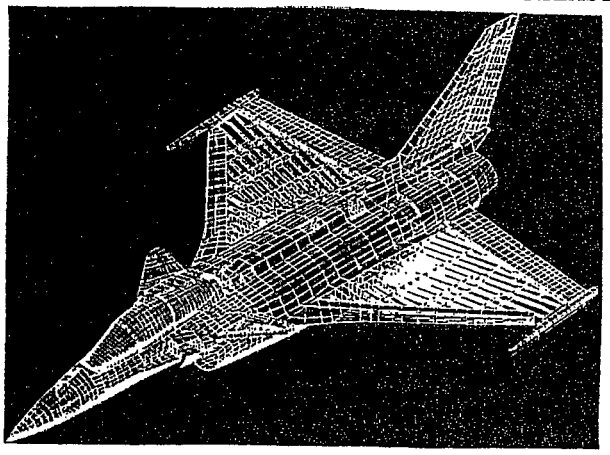

FACTEUR DE CHARGE 9g
x 5

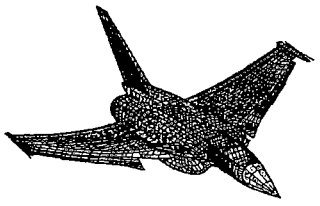

ROULIS STABILISE 260°/s
x 8

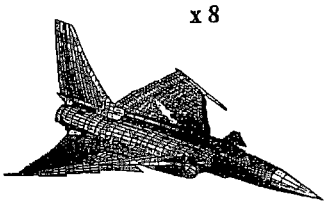

DEFORMEES AEROELASTIQUES

PLANCHE 2

ELFINI - AEROELASTICITY

ENSEMBLE DES MODELES

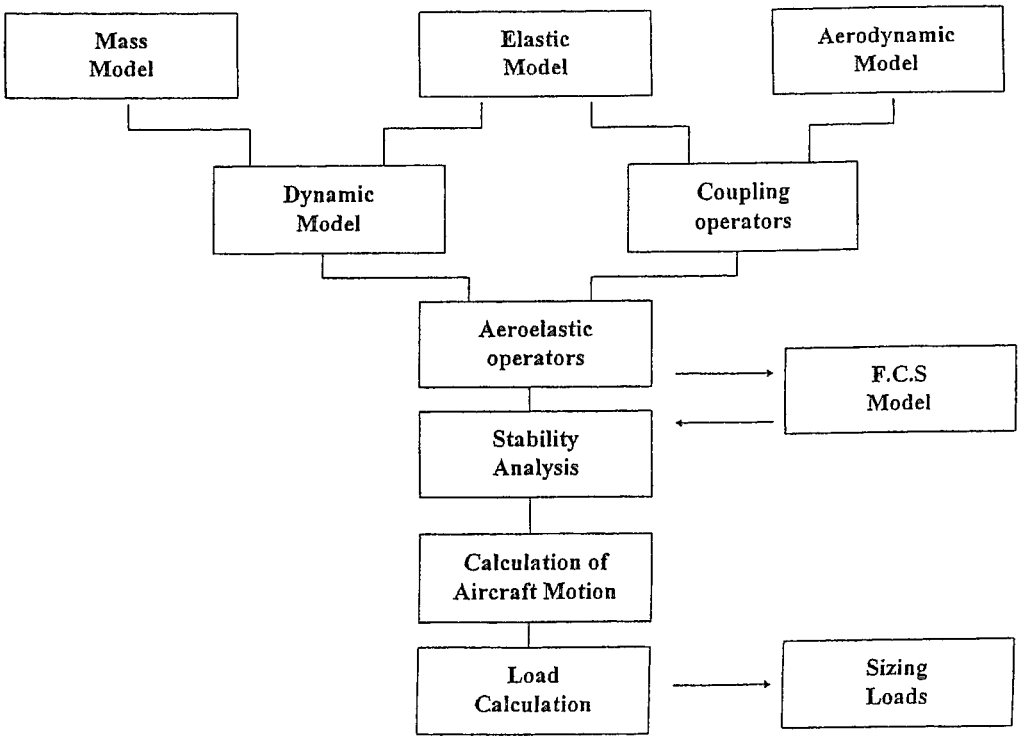

PLANCHE 3

STIMULUS PAR EXCITATION CANARD

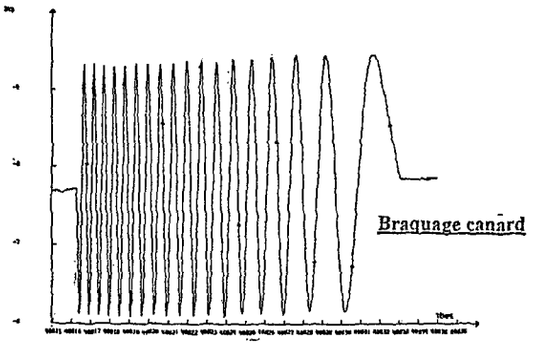

Braquage canard

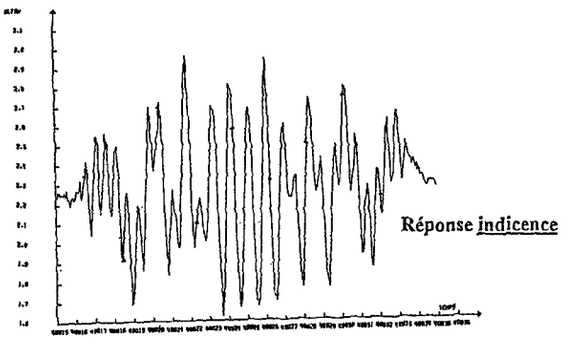

Réponse indicence

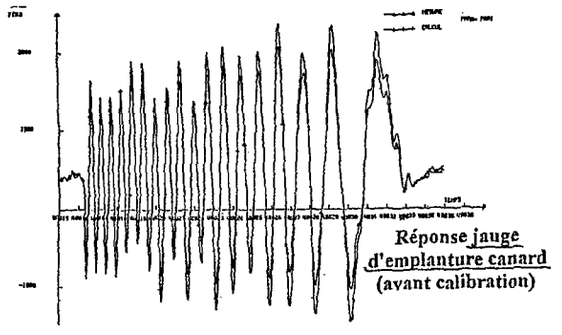

Réponse jauge d'emplanture canard (avant calibration)

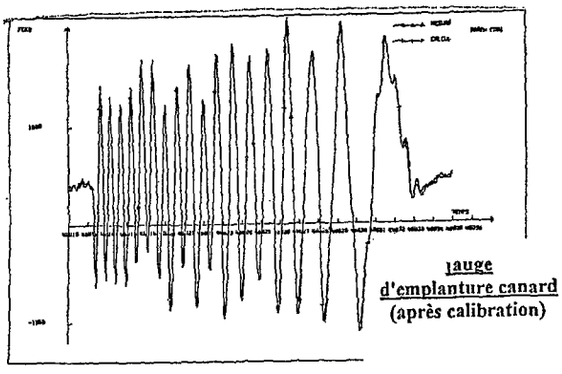

jauge d'emplanture canard (après calibration)

PLANCHE 4

MANOEUVRE CONTREE DE ROULIS*

Comparaison modèle - mesure avant / après recalage

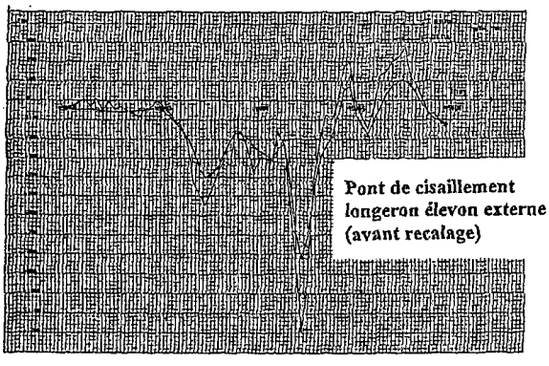

Pont de cisaillement longeron élevon externe (avant recalage)

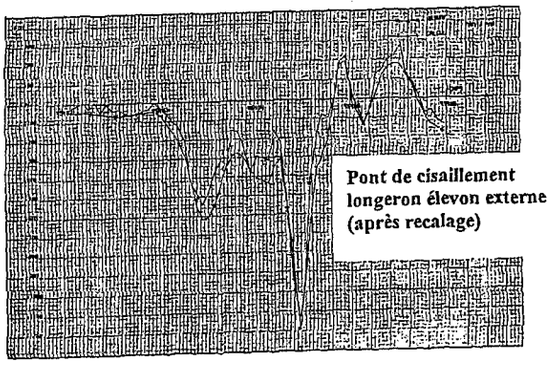

Pont de cisaillement longeron élevon externe (après recalage)

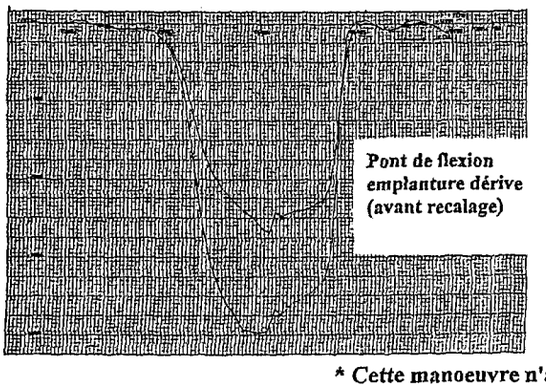

Pont de flexion emplanture dérive (avant recalage)

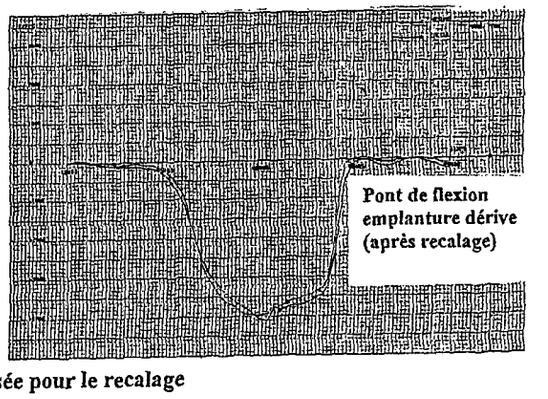

Pont de flexion emplanture dérive (après recalage)

* Cette manoeuvre n'a pas été utilisée pour le recalage

PLANCHE 5

MAQUETTE AEROELASTIQUE D'EMPENNAGE TYPE "AIRBUS"
ESSAYEE DANS LA SOUFFLERIE S2 DE L'ONERA

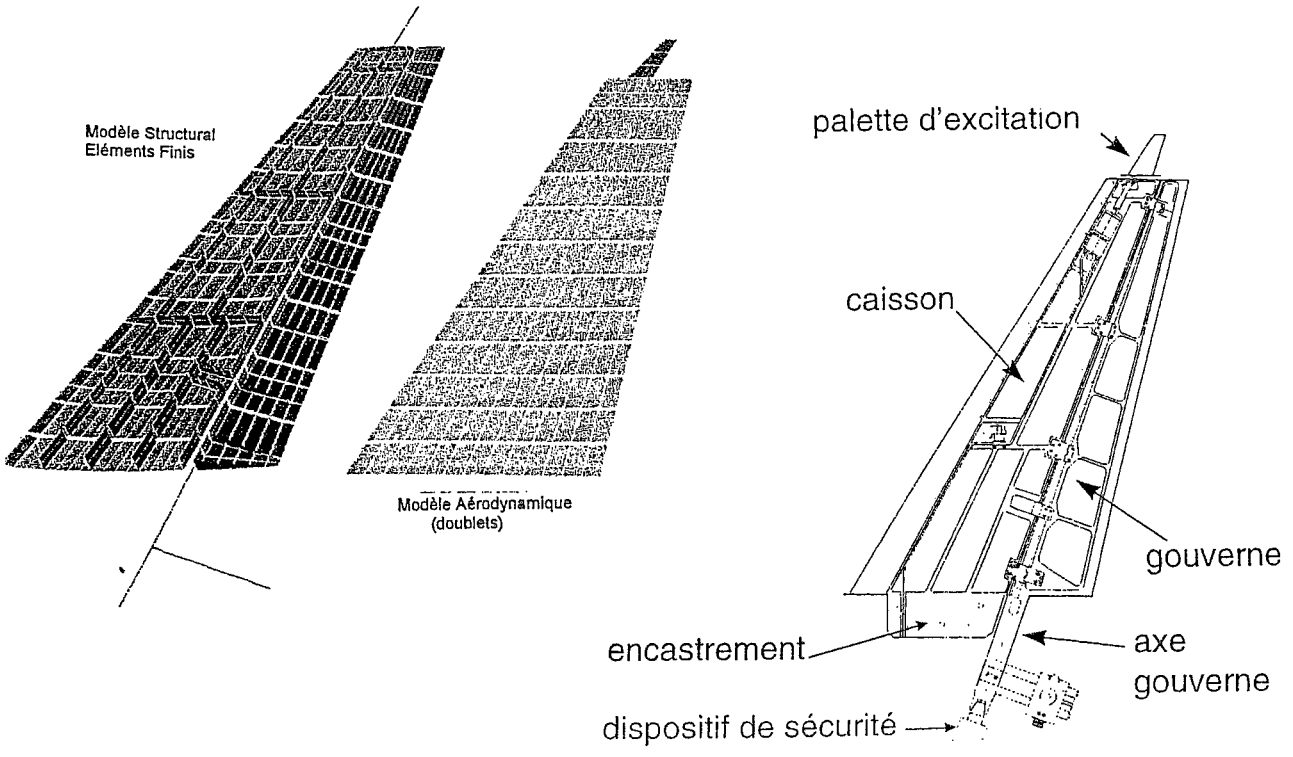

PLANCHE 6

CONFRONTATION CALCUL - ESSAIS - RECALAGE
(Fréquences - Amortissement)

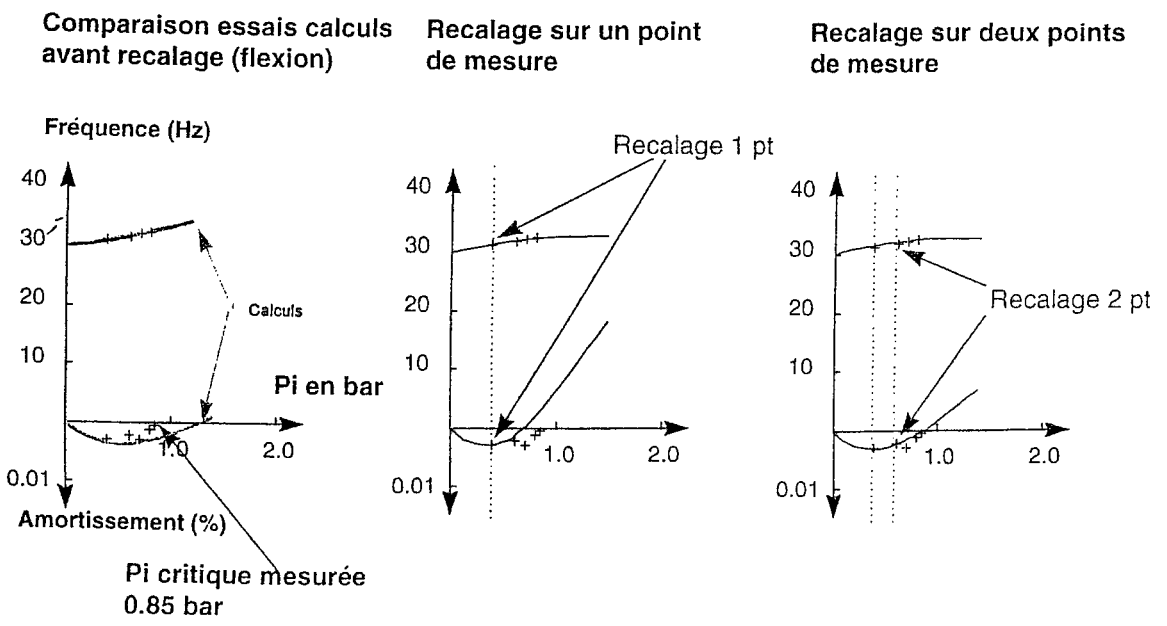

PASSENGER COMFORT IMPROVEMENT BY INTEGRATED CONTROL LAW DESIGN

François Kubica, Béatrice Madelaine

Aerospatiale Matra Airbus
316 route de Bayonne, 31060 Toulouse, France

Abstract

This paper presents comfort criteria based on ISO 2631-1 standard, and shows how these criteria can be applied to a large capacity civil aircraft for passenger comfort evaluation.

The results obtained show that fly-by-wire allows to improve comfort with respect to the natural aircraft. More over an active control of the first flexible modes allows not only to improve 'low frequency' comfort (vibrating comfort), but also 'very low frequency' comfort (motion sickness phenomenon).

This study defines tools for comfort analysis and control law design, which could be used for future large civil aircraft, like the A340-500/600 and the A3XX.

Introduction

Today, air transport growth is making the aeronautical industry become aware of the necessity of developing high capacity long-range aircraft. These large aircraft are characterized by flexible structures which lead to new technological challenges. As regards the flight control system, this flexibility increases the interaction between control laws and structural dynamics modes, the frequency of which becomes lower.

In order to cope with this problem, two ways can be considered:

- A passive approach which consists in filtering the flexible modes in order to avoid coupling with the control laws,
- An active philosophy which consists in controlling the first flexible modes.

It was shown that the second approach seems to be more convenient from the handling qualities point of view [1].

As regards comfort, it seems more difficult to make comparisons because comfort evaluation is a complicated problem.

The first objective of this paper is to define the more convenient comfort criteria for aeronautics field. These criteria must take into account both rigid-body and elastic dynamic aircraft responses. In a second step, these criteria will be used in order to choose the best methodology for control laws design.

Definition of comfort criteria

Comfort evaluation is a difficult challenge, because a lot of elements can influence it (sound, temperature, smells, passenger activity, ...). In this paper, we will focus on vibrational comfort, which is recognized to be preponderant for passenger comfort.

Numerous studies have been conducted to examine the effects of aircraft vibrations on passenger comfort. Generally, the effects of vibration on passenger comfort are considered in the frequency range [1 Hz-80 Hz].

Our experience in the design of flight control system (Concorde, A320 family, A330/A340) shows that some particular attention must be focused on frequencies below 1 Hz. Indeed, flight mechanics modes are located in this frequency band and can influence passenger comfort.

A recent international standard [2] gives some criteria for the complete frequency range. In fact comfort evaluation is split into two frequency bands:

- 'Very low frequency' range (frequency below 1 Hz),
- 'Low frequency' range (frequency above 1 Hz).

For these two bands, specific criteria are defined in order to evaluate comfort sensitivity.

Paper presented at the RTO AVT Specialists' Meeting on "Structural Aspects of Flexible Aircraft Control", held in Ottawa, Canada, 18-20 October 1999, and published in RTO MP-36.

Concerning 'very low frequency' comfort, the standard is based on vertical acceleration felt by human passenger. A frequential weighting is introduced in order to represent sensitivity to motion sickness. This filtering is presented in Figure 1.

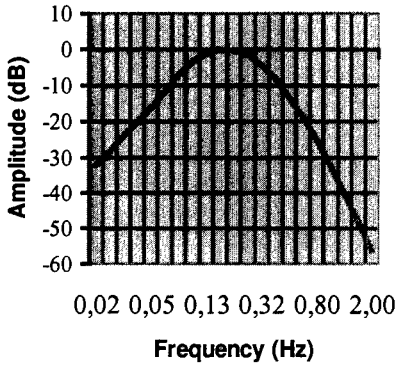

Figure 1: Motion sickness sensitivity

It consists in a band-pass filtering centered at 0.16 Hz which is considered as the critical frequency for motion sickness phenomenon.

The ISO 2631-1 standard proposes to compute a motion sickness index representative of the Percentage of Ill Passengers (PIP). PIP is defined as:

$$PIP = 1/3 * \left[\int_0^T a_w^2(t)dt \right]^{1/2}$$

where a_w is the measured vertical acceleration (m/s^2) during T seconds weighted by the motion sickness filtering.

We have to underline that this standard contains some limitations for aeronautics applications. It was derived from seaboard studies, and the specifications are only given for vertical axis. In this paper, we will consider that the specifications are also applicable to lateral axis.

Concerning 'low frequency' comfort, the standard is based on measurement or calculation of the acceleration felt by a human passenger at one point and in one direction.

As for motion sickness, frequency weighting functions are introduced in order to represent the physiological response of human body. For a seated person, two frequency weightings are used, for vertical (z axis) and lateral (x and y axis) accelerations; these filters, presented in Figure 2, emphasize the frequency range between 4 to 8 Hz for vertical acceleration and 1 Hz for the lateral ones.

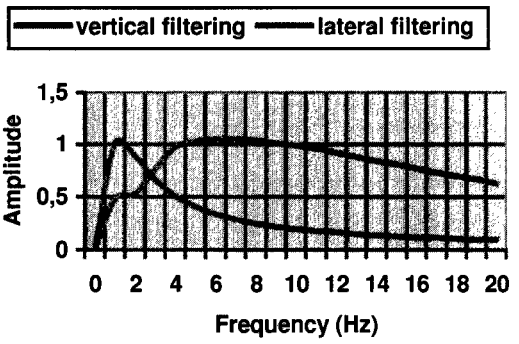

Figure 2: Frequency weighting for comfort

The standard proposes to compute the root mean square (r.m.s.) value of the weighted acceleration a_w (m/s^2) during T seconds:

$$a_{rms} = \frac{1}{T}\left[\int_0^T a_w^2(t)dt \right]^{1/2}$$

At a measurement point *p*, a global comfort criterion can be computed from r.m.s. values of weighted accelerations in each direction:

$$a_p = (k_x^2 a_{px}^2 + k_y^2 a_{py}^2 + k_z^2 a_{pz}^2)^{\frac{1}{2}}$$

where :

a_{px}, a_{py}, a_{pz} are r.m.s. values of weighted accelerations respectively on x, y and z axes ;

k_x, k_y, k_z are weighting factors ; for a seated person the standard proposes the following factors :

- at the supporting seat surface : k_x=1, k_y=1, k_z=1;
- at the feet : k_x=0.25, k_y=0.25, k_z=0.4.

In order to evaluate the discomfort level felt by a person, the above procedure has to be applied to each movement transmitted to the human body by supporting surfaces. Then for a seated person, vibrations at the supporting seat surface, at the feet and at the back of the seat have to be taken into account (comfort of a seated person may also be affected by rotational vibrations on the seat; the standard proposes specific frequency weightings for these ones).

When comfort is affected by vibrations at several points, the overall vibration can be computed from the r.m.s. value of global vibrations at each point:

$$a_{tot} = (a_{p1}^2 + a_{p2}^2 + a_{p3}^2)^{\frac{1}{2}}$$

For civil aircraft applications, rotational vibrations as well as the ones transmitted by the back of the seat may be neglected. Then only vertical (z axis) and lateral (y axis) accelerations at the supporting seat surface and at the feet are taken into account. Accelerations at the

supporting seat surface are obtained by filtering accelerations at the feet with an experimentally determined filter, representative of the mean response of a seat with a person.

The standard gives approximate indications of the likely reactions to various magnitudes of frequency-weighted r.m.s. accelerations:

< 0.315 m/s^2	not uncomfortable
$0.315 - 0.63$ m/s^2	a little uncomfortable
$0.5 - 1$ m/s^2	fairly uncomfortable
$0.8 - 1.6$ m/s^2	uncomfortable
$1.25 - 2.5$ m/s^2	very uncomfortable
> 2 m/s^2	extremely uncomfortable

Large capacity aircraft application

For 'very low frequency comfort', we applied this standard to a large capacity aircraft in order to evaluate passenger comfort in different airplane locations (forward fuselage, center fuselage, aft fuselage). Standard missions were simulated including manœuvres (heading change, level change, ...) and turbulence for different configurations:

- natural aircraft without high level control law (yaw damper only),
- passive control law (filtering of flexible modes),
- active control law (control of flexible modes).

PIP in manaoeuvres were found negligible for any type of control laws and passenger locations (less than 0.1%). Concerning turbulence, some differences can be noticed and the results are shown in Figures 3 and 4 (simulations of 3 minutes in strong turbulence).

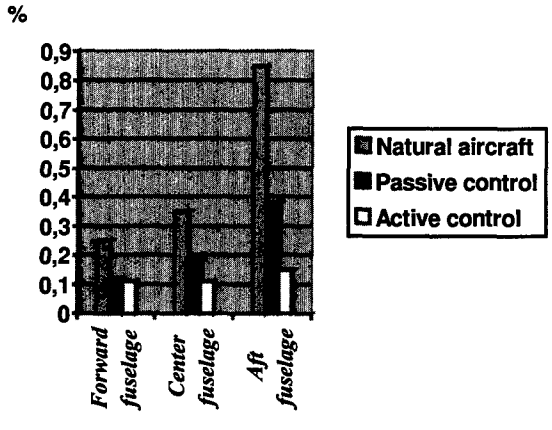

Figure 3: PIP in turbulence (lateral axis)

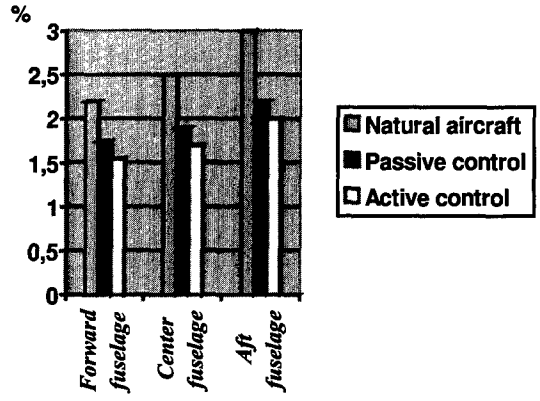

Figure 4: PIP in turbulence (vertical axis)

At first, we can notice that the PIP is small whatever the configuration (<0.9% for lateral axis and <3% for vertical axis). This means that aircraft is a comfortable way of transport. We can remark that the level of comfort depends on location in the aircraft, and that the PIP progressively increases with respect to the distance from aircraft nose (whatever the type of control law).

Control laws allow to improve comfort for all locations, and the active control seems to be the more efficient. We can explain it by the fact that the active control allows to increase control law bandwidth, and thus to accelerate flight mechanics modes (short period, dutch roll, ...). It means that the global aircraft dynamics will be faster than the motion sickness critical frequencies (about 0.16 Hz). With a passive control, which means low frequency filtering, it is not possible to significantly increase the aircraft dynamics, which can remain in the motion sickness frequencies.

These results are coherent with our experience in the field of flight control system development (sensitivity around 0.16 Hz, control law tuning, ...). The ISO2631-1 seems to be a useful tool for comfort evaluation.

Concerning 'low frequency' comfort, the standard was applied to evaluate passenger comfort in different locations all along the fuselage. Realistic turbulence during a cruise configuration was simulated for two configurations:

- natural aircraft,
- active control law (control of flexible modes).

The case of passive control law is not mentioned here since the passively controlled aircraft has the same behavior as the natural one, from a low frequency comfort point of view.

Figure 5 presents the results for a vertical turbulence, rather than the ones for a lateral one, since acceleration level due to a lateral turbulence is far less critical.

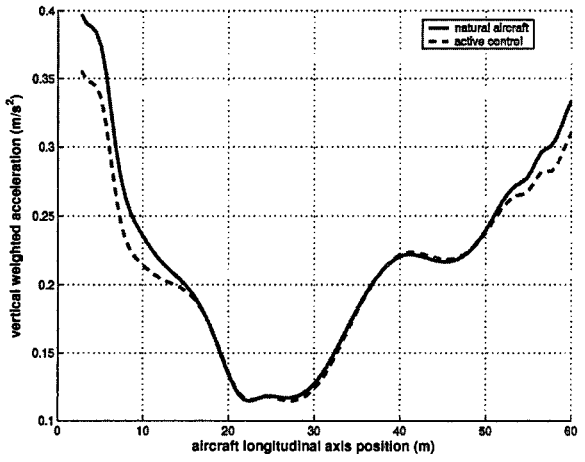

Figure 5: Comfort in turbulence (vertical axis)

Note first that computed acceleration levels are rather small. According to indications given by the standard, the aircraft is considered not uncomfortable nearly all along the fuselage; only the pilot location (at the very front of the fuselage) and the very rear of the fuselage may be felt a little uncomfortable.

The active control law improves comfort particularly at the front of the fuselage, also at the rear of the fuselage, but not at other locations. This is due to the active control of the "2 nodes fuselage bending" mode at 2.5 Hz, which appears particularly at the front and at the rear of the fuselage.

The maximum improvement of the comfort criterion due to the active control law is 10%. The significance of this improvement was successfully checked, since it was indeed noticed by passengers during laboratory tests with a vibrated seat.

Conclusion

This paper shows how comfort criteria based on ISO 2631-1 standard can be applied to a large capacity civil aircraft for passenger comfort evaluation.

The results obtained show that control laws allows to improve comfort with respect to the natural aircraft. More over an active control of the first flexible modes allows not only to improve 'low frequency' comfort (vibrating comfort), but also 'very low frequency' comfort (motion sickness phenomenon). It means that an integrated design, which actively controls both rigid and flexible modes, seems preferable for comfort improvement.

This study defines tools for comfort analysis and control law design, which could be used for future large civil aircraft, like the A340-500/600 and the A3XX.

References

[1] "New flight control laws for large capacity aircraft. Experimentation on Airbus A340", F. Kubica, in proceedings ICAS, 1998.

[2] "Mechanical vibration and shock - Evaluation of human exposure to whole body vibration", ISO2631-1, 1997.

INTEGRATED FLIGHT MECHANIC AND AEROELASTIC MODELLING AND CONTROL OF A FLEXIBLE AIRCRAFT CONSIDERING MULTIDIMENSIONAL GUST INPUT

Patrick Teufel, Martin Hanel, Klaus H. Well
Institute of Flight Mechanics and Control
Stuttgart University
Pfaffenwaldring 7a
70550 Stuttgart, Germany

Abstract

In this paper, the influence of gusts on the dynamics of a large flexible aircraft is analyzed, and an integrated flight and aeroelastic control law that reduces gust sensitivity is presented. The calculations are based on an integrated model that includes all 1st order couplings between flight mechanic and structural degrees of freedom. Uniform, 1-dimensional and multidimensional gust models are implemented and used for gust sensitivity analysis. For the example aircraft, the differences in gust sensitivity calculated with the 1-dimensional and multi-dimensional gust models are significant. Integrated attitude, stability augmentation, and aeroelastic control laws for longitudinal and lateral motion are designed using μ - synthesis. With the control laws, flight maneuvers do not excite elastic reactions, and the sensitivity to gusts is considerably reduced.

Nomenclature

B_{hh}	= modal damping matrix
k	= reduced frequency
K_{hh}	= modal stiffness matrix
L	= characteristic wave length for gust (2500 ft)
M_{hh}	= modal mass matrix
P_h	= modal applied aerodynamic forces (gust)
$Q(ik)$	= modal aerodynamic force coefficient matrix tabulated for reduced frequencies k
q	= state vector in generalized coordinates
x_j	= x location of aerodynamic panel
x_0	= reference value for aerodynamic coordinate system
u,v,w	= longitudinal, lateral and vertical velocity
p,q,r	= roll, pitch and yaw rate
w	= aerodynamic downwash
α,β,γ	= angle of attack, sideslip angle and flight path angle
γ	= dihedral angle
Φ	= mode shape matrix
ϕ,θ,ψ	= roll attitude, pitch attitude and heading
φ	= phase angle
Φ	= matrix of one dimensional spectrum function
Ψ	= matrix of two dimensional spectrum function
ξ_{si}, ξ_{so}	= symmetric and antimetric deflection of
ξ_{ai}, ξ_{ao}	inner and outer ailerons
ξ,η,ζ	= aileron, elevator and rudder deflection
ω	= frequency
Ω	= ω/V wave number

1 Introduction

Today's airlines are requesting bigger and more fuel efficient aircraft to reduce their operation costs. Consequently, fuselages and spans of new aircraft designs are getting longer, and the need to reduce structural weight reduces structural stiffness. Both effects lead to more flexible aircraft structures with significant aeroelastic coupling between flight mechanics and structural dynamics, especially at high speed, high altitude cruise. To counteract gust and maneuver induced aeroelastic vibrations, which impair ride comfort and structural loads, active aeroelastic control strategies are investigated.

Using separate models for flight mechanics and aeroelastics (sufficient for the smaller and more rigid aircraft in service today) aeroelastic coupling cannot be described. Further, it is doubtful whether simple uniform or 1D gust models are still adequate for large aircraft. To address the former deficiency, integrated models describing both the flight mechanic and the aeroelastic behavior of flexible aircraft have been developed recently[1]. The issues of gust modelling and active aeroelastic control are addressed here.

Calculations of gust loads are of major importance for the structural and aerodynamic layout of an airplane. Certification requirements due to discrete gusts as well as continuous gust loads have been developed. FAR 25[2] describes one dimensional (1D) 1-cos shape gust requirements. The FAA-ADS 53[2] report describes 1D continuous gust requirements, which are based on power spectral density PSD methods.

There always have been efforts to extend existing gust formulations to a more realistic modelling as the most widely used 1D gusts are the most abstract realization of real gusts, which will be random not only in one direction but in each direction. The energy distribution within gusts has already been described in the early 60s by Dryden and von Kármán. These gust spectra have been developed in 3D space, but in the later years only the 1D spectra have been used. Nevertheless, research on multidimensional formulations of gusts and the modelling of the induced aerodynamic forces is continuing. On the evaluation of multidimensional gust fields and the resulting airplane responses, most authors rely on cross-spectral formulations. Crimaldi[3] describes a method for 2D gust modelling which is based on calculations of the cross-spectrum of a gust acting on single aerodynamic strips of panels along the longitudinal axis of the airplane. These gust cross-spectra depending on the lateral separation distance have been developed by Eichenbaum[4] and are described by Bessel functions of the third kind.

The gust models described in this paper avoid the evaluation of cross-spectral density functions by applying directly 1D and 2D PSD functions to vertical and lateral gusts as in Etkin[5]. Starting from a very basic formulation gust models are step by step developed towards a fully multidimensional gust description, so that effects caused by the increase in accuracy of the models can be identified.

Conventional flight control systems are designed to assure good handling qualities and to eliminate the influence of elasticity, treating the aircraft as a rigid body. For ride comfort improvement, separate aeroelastic control loops have been implemented on some modern aircraft[6]. The flight control and

Paper presented at the RTO AVT Specialists' Meeting on "Structural Aspects of Flexible Aircraft Control", held in Ottawa, Canada, 18-20 October 1999, and published in RTO MP-36.

the aeroelastic control loops are then separated by dynamic filters. As rigid body dynamics and low frequency elastic modes get closer with increasing structural flexibility, separate design of stability augmentation systems and aeroelastic control loops becomes more difficult. Therefore, several recent studies[1,7,8,9,10] have investigated integrated flight mechanic and aeroelastic control design. In this study, an integrated flight and aeroelastic control law for a heavy study four-engine civil transport aircraft at high-speed, high-altitude cruise is presented, and the influence of the integrated control law on gust sensitivity is analyzed.

2 Integrated aircraft model

Linearized integrated flight mechanic and aeroelastic models for different flight (20000ft to 30000ft altitude and Ma=0.4 to Ma=0.86) and load (full and empty wing and trim tank) conditions are derived for the example aircraft. The modelling follows the procedure described by Schuler[1].

Structural Dynamics

The structural dynamics of the aircraft structure are analyzed using a detailed full-span FEM-model. A normal mode analysis is performed and the low-frequency elastic modes up to a frequency of about 20Hz are retained. Additional mode shapes for rigid body motion and control surface deflections are generated. Modal coordinates q (q_r for rigid body motion and q_e for elastic modes) are introduced and used to describe rigid body and structural dynamics:

$$\begin{aligned} \ddot{q}_r &= f(\dot{q}_r) + F_r^F + F_r^G + F_r^A \\ \ddot{q}_e &= -2\zeta_m \Lambda \dot{q}_e - \Lambda^2 q_e + F_e^F + F_e^A \end{aligned} \tag{1}$$

with $\Lambda = \mathrm{diag}(\omega_i)$, modal damping coefficient ζ_m, (here $\zeta_m = 0.01$), aerodynamic forces F^A, thrust forces F^F and gravitational forces F^G. Displacement, velocity and acceleration of the structure in physical degrees of freedom (z, $\dot{z}$, $\ddot{z}$) are expressed in terms of modal coordinates by

$$z = \Phi q\,,\ \dot{z} = \Phi \dot{q}\,,\ \ddot{z} = \Phi \ddot{q}\,, \tag{2}$$

where Φ is the mode shape matrix.

Aerodynamics

Steady and unsteady aerodynamic forces are calculated using the Doublet-Lattice method[11], as implemented in NASTRAN. The location of the 1570 boxes (each representing a doublet-singularity) is shown in Fig. 1. Aerodynamic force coefficients are calculated for 18 discrete reduced frequencies and tabulated in matrices $Q(ik)$. Linearized aerodynamic forces can then be written as

$$\begin{bmatrix} F_r^A \\ F_e^A \end{bmatrix} = \begin{bmatrix} Q_{rr}(ik) & Q_{re}(ik) \\ Q_{er}(ik) & Q_{ee}(ik) \end{bmatrix} \begin{bmatrix} q_r \\ q_e \end{bmatrix} + \begin{bmatrix} Q_{rg}(ik) \\ Q_{eg}(ik) \end{bmatrix} w_g \tag{3}$$

with Q_{re} and Q_{er} representing the cross-coupling between rigid-body and structural modes and Q_{rg} and Q_{eg} the forces due to gust vector inputs w_g. In the form of Eq. 3, aerodynamic forces can only be evaluated for harmonic oscillations at given discrete frequencies. For simulation purposes and control law design, the aerodynamic force description is therefore extended to the Laplace domain, approximated by a rational transfer function matrix and then transformed to the time domain. For this study, the Minimum State Method of Karpel[14] has been used to perform the approximation.

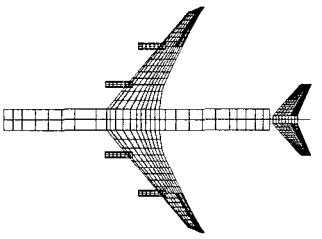

Fig. 1: Aerodynamic model (NASTRAN) - the lifting surface is discretized using 1570 doublet elements (boxes)

For the time-domain model, gusts are modelled as acting uniformly on the aircraft structure and separately on longitudinal and lateral motion. Then a (linear, time-invariant) state-space description of the (linearized) aircraft dynamics

$$\begin{aligned} \dot{x} &= Ax + Bu + Ew \\ z &= Cx + Du + Fw \end{aligned} \tag{4}$$

with control inputs u and (uniform) gust inputs w is derived[12,13,1]. The uniform gust model however is too inaccurate an approximation for gust analysis. Therefore, in the sequence, more realistic gust models are discussed (sections 4 and 5). Finally it is analyzed how the controllers designed with the uniform gust model perform with respect to more realistic gust models (section 9).

3 Random turbulence models

For most evaluations turbulence is regarded as a random phenomenon. Its energy distribution has to be described in the 3D space.

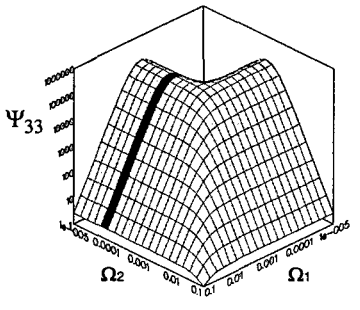

Fig. 2: 2D spectrum Ψ_{33} of vertical von Kármán turbulence

Considering vertical gusts for airplane, it is apparent that only variations in longitudinal and lateral direction will be significant and variations of gust velocity in vertical direction can be neglected as the airplane height is small in comparison to span and length. 2D spectra will therefore be appropriate. In this study, the von Kármán Spectrum[15] is used to describe the energy distribution versus frequency. For vertical turbulence it is given by

$$\Psi_{33}(\Omega_1, \Omega_2) = \frac{16\sigma^2(\alpha L)^4}{9\pi} \cdot \frac{(\Omega_1^2 + \Omega_2^2)}{(1 + \alpha^2 L^2 (\Omega_1^2 + \Omega_2^2))^{7/3}}. \tag{5}$$

Results presented in this paper will be calculated with the appropriate 1D and 2D von Kármán spectra. Fig. 2 shows the 2D von Kármán spectrum. 1D spectra are obtained by integrating Eq. 5 with respect to Ω_2. Wavenumber Ω_2 and Ω_1 will be discussed in section 5.

4 Standard 1D continuous gusts response

For 1D gust loads only changes of gust velocity in flight direction are considered, for vertical as well as for lateral gusts. One way to compute these gust forces is to assume a uniform gust velocity over the airplane. Gust forces are obtained that are equal to the generalized aerodynamic forces of the translational vertical and lateral rigid body modes. Standard gust calculations (NASTRAN) consider phase delay effects along the flight path. The gust field is assumed to be frozen (Taylor's hypothesis). Gust forces are related to a normal downwash at a specific aerodynamic box j by

$$P_h(\omega) = Q_{hj}(Ma, k)w_j(\omega), \tag{6}$$

where Q_{hj} relates downwash and modal aerodynamics forces and is available through NASTRAN. The downwash of a vertical gust which actually describes the phase delay is given by[16]

$$w_j(\omega) = \cos\gamma_j e^{-i\omega\frac{(x_j - x_0)}{V}}, \tag{7}$$

where the normal downwash on a aerodynamic box is proportianal to the dihedral angle γ_j. For lateral gusts $cos\gamma_j$ has to be replaced by $sin\gamma_j$. .

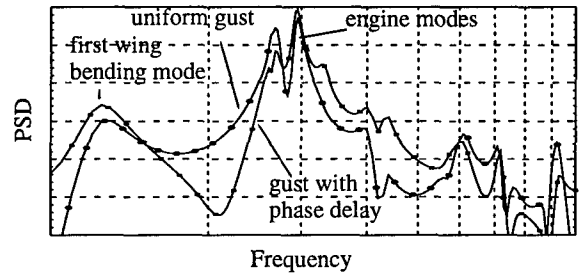

Fig. 3: PSD of acceleration of outer wing due to uniform vertical gust and gust with phase delay effects in flight path direction

The flutter equation in generalized coordinates is used for open loop simulations with applied forces:

$$\left[-M_{hh}\omega^2 + iB_{hh}\omega + K_{hh} - \left(\frac{1}{2}\rho V^2\right)Q_{hh}(Ma, k)\right]q = P_h(\omega) \tag{8}$$

In this equation modal masses M_{hh}, damping B_{hh} and stiffness B_{hh} are real matrices, the matrix of modal aerodynamic forces Q_{hh} coefficients is complex. The result is obtained in modal coordinates. Displacement, velocity and acceleration of the structure in physical degrees of freedom can be computed with Eq. 2..

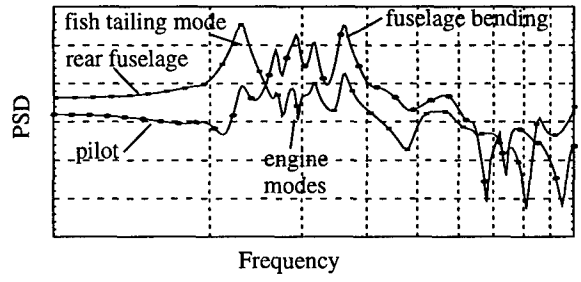

Fig. 4: PSD of acceleration of fuselage close to pilot and rear fuselage due to 1D lateral gust with phase delay

The RMS values of the response in physical coordinates are obtained by applying 1D gust spectra. Considering the phase delay along the flight path is the first step towards a 2D gust model. The effect on the acceleration of the wing can be seen in Fig. 3. The evaluation of the response of the wing bending is used in most studies for the evaluation of the critical loads of an airplane. This might be in general true for smaller aircraft, but from Fig. 3 two important things can be seen: Phase delay changes the aircraft response, and there are modes beside symmetric wing bending at higher frequencies that will be considerably excited independent of gust model.

As to the response of an airplane to lateral gusts, it is obvious that the so called "fish tailing" mode and "fuselage bending" mode at higher frequency should be considered. The "fish tailing" mode results in high accelerations in the rear fuselage of the airplane and small loads at the front fuselage, see Fig. 4. For clarity: response of uniform gust is not depicted.

5 Multidimensional continuous gust response

Gust calculations for multidimensional continuous gusts are based on the method described by Etkin[5]. It differs from the 1D continuous gust in that there is an additional variation along the span. The gust velocity is varying along the flight direction as before and is "wavy" over the airplane.

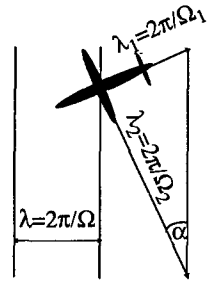

Fig. 5: Aircraft flying through a 2D vertical gust field

For the vertical gust case a 2D gust field is obtained, where the downwash is dependent on wave numbers $\Omega_1=\omega/V$ and Ω_2. Eq. 7 is modified:

$$w_j = \cos\gamma_j e^{i(\Omega_1(x_j - x_0) + \Omega_2 y_j)} \tag{9}$$

It can be seen that the second wave number Ω_2 results in a different phase of the downwash compared to the 1D gust assumption. Assuming a fixed proportion of Ω_2 and Ω_1 the situation can also be described by the airplane flying over a 1D gust field with an angle α, see Fig. 5. Lateral gusts are implemented similar to vertical gusts. By implementing the dependence on Ω_2 Eq. 8 is extended to a 2D transfer function. As an example the acceleration of the wing for different values of Ω_2 is presented. It can be shown that dependent on each characteristic mode, the second wave number Ω_2 yields higher or lower accelerations. Additionally, it has to be mentioned that because of the phase delay the response of the left and right side of the airplane will be different. Similar to the 1D-case the response has been multiplied with the 2D-spectrum. Neglecting longitudinal gusts it has been shown[5] that the total RMS response for isotropic turbulence is given by the uncorrelated response of vertical and lateral gust. Therefore the spectra for lateral and vertical motion can be computed separately and added :

$$\Psi_{x_i x_i}(\Omega_1, \Omega_2) = |X_{iv}|^2 \Psi_{vv}(\Omega_1, \Omega_2) + |X_{iw}|^2 \Psi_{ww}(\Omega_1, \Omega_2) \tag{10}$$

In this equation Ψ_{xx} is the 2D spectrum response of a selected physical degree of freedom x_i. X_{iv} is the response due to unit gust input.

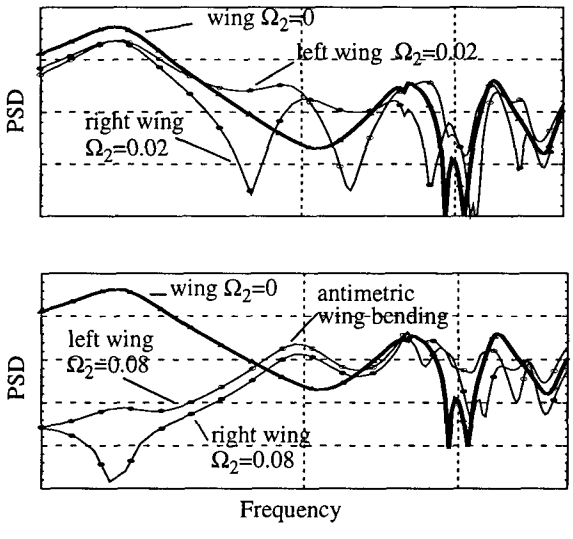

Fig. 6: PSD of acceleration of outer wing due to 2D vertical gust for Ω_2=0.02 and Ω_2=0.08

To compare these results with the 1D case we need

$$\Phi(\Omega_1) = \int_{-\infty}^{\infty} \Psi_{x_i x_i}(\Omega_1, \Omega_2) d\Omega_2. \qquad (11)$$

With this equation the acceleration of the wing and of the outer engine due to 1D and 2D gust input is compared and presented in Fig. 7.

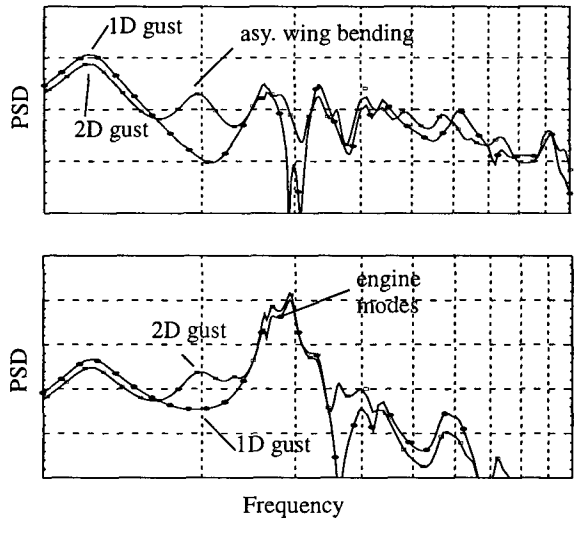

Fig. 7: PSD of vertical wing and lateral outer engine acceleration for 1D and 2D gust input

It can be seen that the 2D formulation leads to lower accelerations for the first wing bending mode. Due to the antimetric phase delay antimetric modes are excited, which can clearly be seen for the first antimetric wing bending mode . This antimetric response of the first wing bending explains the reduction in the symmetric wing bending, as the 1D spectrum with Ω_2=0 puts too much emphasis on the first wing bending mode. In contrast to the first wing bending mode, there are modes whose response can increase for the 2D gust formulation. The reason is that based on the phase delay there are situations when the gust shape over the wing is equal to a characteristic wing bending form and will therefore amplify the response at this frequency. As at higher frequencies gust spectra become very small, only the first number of elastic modes will lead to PSD values that are used for evaluation.

Adding lateral gusts to the response according to Eq. 10 causes a slight increase of loads on surfaces that are mainly affected by vertical gusts (see Fig. 8). For antimetric modes ("fish tailing") the situation will be vice versa.

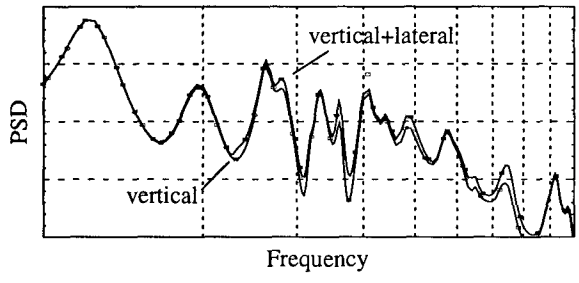

Fig. 8: PSD of vertical acceleration of outer wing due to vertical 2D gusts alone and a combination of vertical and lateral 2D gusts

6 Open loop system analysis

With all models based on NASTRAN frequency domain aerodynamics, frequency responses are the natural choice for aircraft dynamics analysis and offer the most accurate results. Further advantages are the possibility to clearly identify the influence of individual elastic modes, to assess the influence of random disturbances (such as gusts) and to readily draw conclusions for control design (stability margins etc.). While frequency responses could also be obtained from the linear state-space models (Eq. 4), those shown below have been calculated by directly solving the flutter equation (see Eq. 8), thus avoiding errors resulting from the transformation to the time-domain.

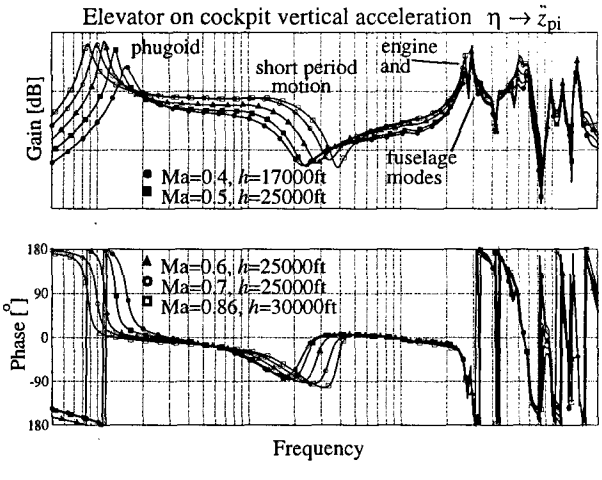

Fig. 9: Cockpit vertical acceleration frequency response to elevator input for different flight conditions

Fig. 9 shows the transfer function from elevator to cockpit vertical acceleration for different flight conditions. As expected from rigid-body flight mechanics, the gain amplitude increases with dynamic pressure, the phugoid frequency decreases, and the frequency of the short period motion increases with air speed. In the aeroelastic frequency range, the gain response shows the influence of dynamic pressure on amplitude, while phase response is not much affected by changes in flight condition. For changes in load condition, however, the situation is different. The load distribution (fuel and payload) strongly

influences the dynamic behaviour of the elastic structure and consequently aeroelastic coupling. Fig. 10 shows the frequency response for three different load conditions at constant flight condition. While changes in elastic mode shapes and frequencies are not unexpected (wing bending frequency should increase with fuel consumption), strong changes in damping (maximum amplitudes) and phase response are also observed.

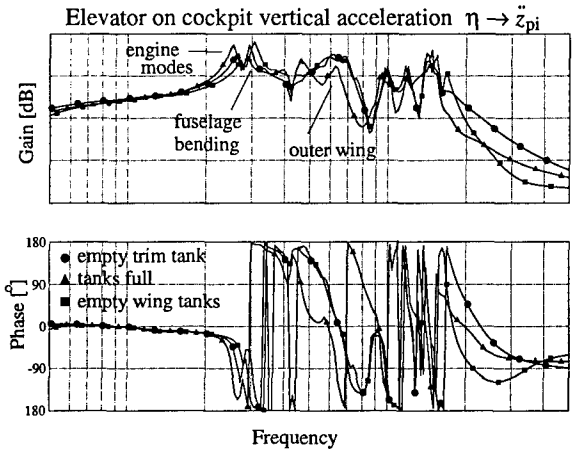

Fig. 10: Cockpit vertical acceleration frequency response to elevator input for different load conditions

A fixed gain control design therefore faces a robustness challenge in both the low-frequency range (rigid body dynamics changing mainly with flight condition) and the high-frequency range (aeroelastics changing mainly with load condition). With the low-frequency elastic modes being close to the short period mode, (the 1st wing bending mode is not visible in Figs. 9 and 10) strong coupling between rigid body and structural dynamics is observed.

Under these premises, the aforementioned difficulties associated with separate flight and aeroelastic control and the advantages offered by integrated control are evident.

7 Control design for integrated flight and aeroelastic control

Actuators

The integrated control law commands the conventional control surfaces for primary flight control, i.e. elevator, rudder, and inner and outer ailerons. While Schuler[1] assumes symmetrically deflected inner ailerons to be available in the longitudinal motion, in this study symmetric inner and outer aileron deflection is made available, however restricted to low authority aeroelastic control purposes.

Sensors

As all physically realizable sensor signals contain both rigid body and elastic motion, sensor number and position is an important consideration. Kubica and Livet[8] and Ward and Ly[7] use the signals of the conventional aircraft sensor platform. In this study, roll attitude ϕ and pitch attitude θ, roll, pitch and yaw rate (p,q,r), vertical and lateral acceleration are assumed to be measured by a sensor platform in the forward fuselage section. As in Schuler[1], additional accelerometers at different points of the aircraft structure are assumed to be available. They are placed at positions where low-frequency signals are dominant (providing for a physical low-pass filter) using a sensor placement strategy[17]. Vertical acceleration at a mid-wing position and lateral acceleration at inner and outer engines are retained for both longitudinal and lateral control. Lateral acceleration at a rear fuselage position is added for lateral control.

Model reduction

As the linearized integrated model (see section 2) features a high number of states (e.g. 103 states for the longitudinal motion) an order reduction is required to derive a control design model. A 30-state reduced order model is obtained by applying a combination of balanced truncation and balanced condensation model reduction techniques[18].

Choice of the Design Method

μ-synthesis[19,20] has been chosen for control design for several reasons. Since the aircraft model is based on frequency-domain aerodynamics, frequency domain control design is advantageous, as important time-domain model characteristics, such as pole positions do not directly relate to the physical modelling process but result from the transformation of the frequency domain model to the time domain. The interpretation of short period frequency and damping for example is not possible in terms of short-period-pole-position alone, because the influence of aerodynamic lag-states has to be considered.

A MIMO control design method has been selected, as combined control surface actuation is much more effective for aeroelastic control than separate control loops for each control input, given the position of elevator and ailerons on the aircraft structure. With 30-state control design models, the availability of numerically reliable algorithms for H_∞ - optimization / μ-synthesis is another important consideration. Closed loop shaping[21,22] has been chosen for setting up the H_∞ - optimization problem for its flexibility in translating design specifications into weighting functions.

The design process follows the procedure outlined in Ref. 10. The C^* combination of pitch rate and vertical acceleration ($C^* = q - \dot{z}/V$) is chosen as control variable for the longitudinal motion. A proportional-integral control characteristic is achieved by adding the integral of C^*, C_i^* as an additional measurement. Accordingly, in the lateral motion, roll rate p is the control variable and roll angle ϕ is added for PI-control.

Command tracking, vibration reduction, aeroelastic damping increase, control effort, disturbance attenuation, and gust sensitivity are considered for nominal performance in the design by including and weighting the corresponding transfer functions in the performance index for H_∞ - control. As the more sophisticated gust models described in this article are not available for (state-space-model-based) control design, the gust sensitivity objectives are formulated using the uniform gust approach. In a robust performance formulation, robustness is demanded against changes in the aeroelastic frequency and damping parameters and strengthened in several μ-synthesis design iterations. The μ -synthesis design is executed using the *Xmath*-Software package.

The resulting 40th-order longitudinal controller features relatively high low-frequency gains for pitch rate and C^* feedback to elevator, nearly no low-frequency aileron activity and a rapidly decreasing control effort in the frequency range of the elastic modes. Acceleration measurements are mainly used for aeroelastic control purposes in the lower frequency range. Using Hankel norm optimal model reduction[23], a controller order reduction to 26 states can be performed without significant performance losses. High-frequency control gain attenua-

tion however is lowered. If the controller order is further reduced, performance rapidly deteriorates. In the lateral motion, roll rate and roll angle feedback on ailerons and yaw rate and sideslip (estimated from lateral acceleration) feedback on rudder dominate the integrated control law as expected. Again, the feedback of the acceleration measurements is principally used for aeroelastic control in the low aeroelastic frequency range. Model reduction techniques are applied to reduce the controller order (to 26 states).

8 Closed loop system analysis

In this section, an analysis of the closed loop aircraft dynamics is presented. The discussion is intended to give an overview over the different performance objectives considered for μ-synthesis. For the sake of brevity, it is restricted to the longitudinal motion. The results achieved with the lateral control law are similar to previous results[10]. Robustness to system changes, however, has been increased considerably by using μ-synthesis instead of standard H_∞ control.

The robust integrated flight and aeroelastic controller considerably increases the damping of the low-frequency elastic modes as shown by the comparison of open and closed loop pole locations in Fig. 11. Damping increase is 40 to 400% for the first 6 elastic modes.

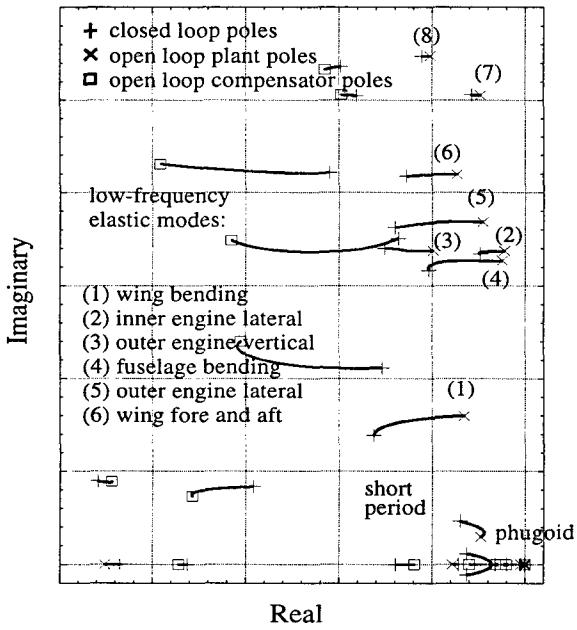

Fig. 11: Pole shifting - longitudinal control; final μ - controller on linearized plant model, Mach=0.86, h=30000ft; plant pole damping is increased, while compensator (observer) poles are shifted to the right

For geometric reasons it could be expected that the damping of wing and engine modes is mainly due to the availability of symmetric aileron control input, whereas the damping of fuselage bending modes is achieved by elevator activity. While this was generally confirmed in the design process, coordinated control surface deflection enhances performance. For flight and load conditions beyond the design case, the damping increase achieved with the robust fixed gain controller in the loop and control performance in general decreases. Although, in the present case, a damping increase can be achieved for all flight and load conditions, the limits of robust fixed gain control for changing flight conditions are evident.

The closed loop time response to a 1s - pulse command $\dot{\gamma}$=0.02°/s and a 3.5° symmetric aileron disturbance inpulse at t=6s is shown in Fig. 12 (empty symbols). .

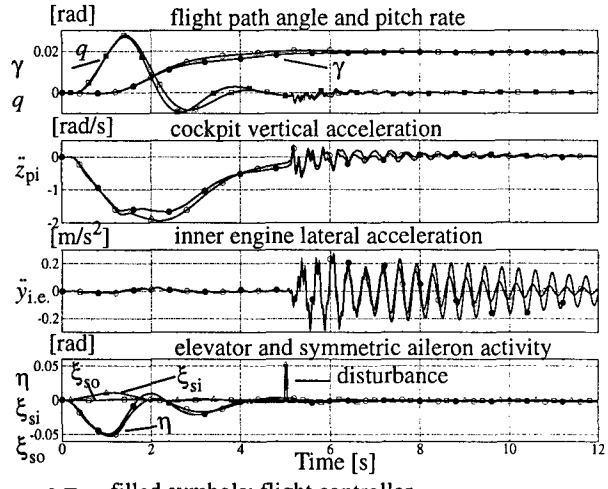

Fig. 12: Closed loop response comparison of a flight controller and the integrated flight and aeroelastic controller

For an assessment of the robust integrated controller, the time response of a simple C^* -flight controller is shown in comparison (filled symbols). Command tracking is equally fast for both controllers, with a somewhat lower short period frequency for the integrated controller.

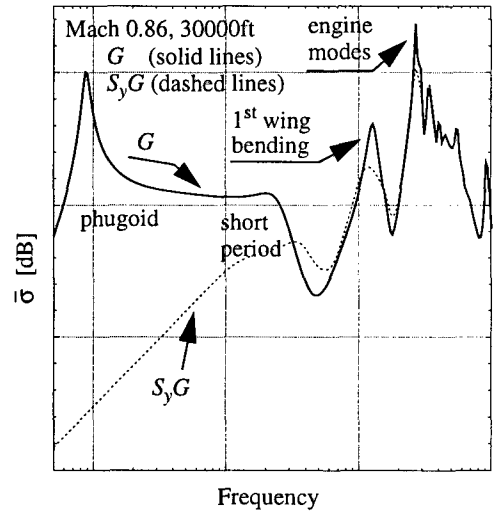

Fig. 13: Open and closed loop sensitivity to input perturbations - μ-controller longitudinal motion; Singular values of G and SyG; Sensitivity to input disturbances is reduced in the frequency range of controller operation;

The control effort of the integrated control law is based mainly on elevator. Low amplitude inner and outer aileron deflections are used for aeroelastic damping (but not for direct lift control).

While command tracking excites practically no elastic vibrations, the disturbance impulse causes aeroelastic vibrations. It can be seen that the integrated controller rapidly damps theses vibrations, especially in the fuselage, but also at the inner engine. The handling qualities achieved with this controller are significantly improved over previous results[10].

Input sensitivity

The singular values of the transfer matrix from the control (internal) inputs to the measurement (internal) outputs are calculated for both the open loop (G) and the closed loop system (S_yG) to analyze the sensitivity to input perturbations.

Fig. 13 shows the singular value diagram for the design flight and load condition for rigid body and elastic mode frequencies. It can be seen that the input disturbance sensitivity is considerably reduced in the frequency range of the phugoid and short-period motion, the lightly damped engine modes, and the fuselage bending mode. The input sensitivity in the range of higher frequency elastic modes is not affected by the control law. This observation confirms the conclusions drawn from the pole-shifting analysis.

9 Closed loop gust sensitivity

In this section, a detailed analysis of closed loop performance with respect to gusts is presented. In the first run, the uniform gust models used for control design and the NASTRAN 1D gust model (standard for smaller aircraft) are employed. In a second analysis run, the 2D gust model of section 5 is employed.

Gust sensitivity analysis using 1D gust models

For the gust sensitivity analyses of the first run, a 1D von Kármán gust spectrum[15] is used.

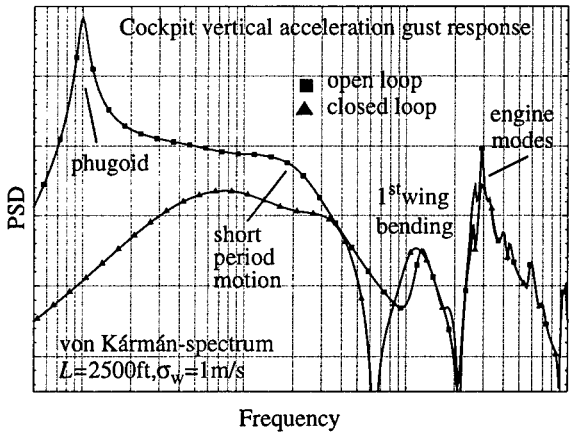

Fig. 14: 1D vertical gust response - vertical acceleration in the cockpit; open and closed loop sensitivity, Mach 0.7, h=25000ft, μ-controller; the gust sensitivity in the frequency range of the rigid body motion is reduced

Fig. 14 and 15 compare the open and the closed-loop cockpit vertical acceleration gust responses. As expected, a sensitivity reduction can be observed in the frequency range of the rigid body motion. Further, the integrated flight and aeroelastic controller achieves a significant reduction of the acceleration associated with engine and fuselage modes over the entire aircraft structure. The vertical gust-induced acceleration associated with e.g. the 1st wing bending mode is significantly reduced on the wing of the aircraft while no improvement (or even a deterioration) can be detected in the cockpit.

The influence of the controller on gust sensitivity is essentially similar for both the uniform gust model used for design and the 1D standard gust model, although the quantitative results differ.

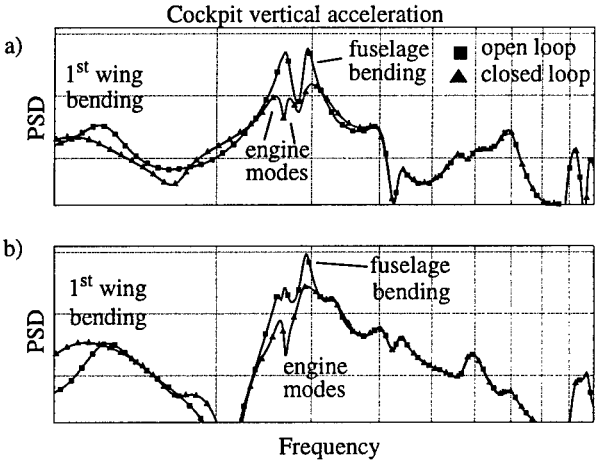

Fig. 15: Open and closed loop sensitivity to vertical gusts; a) uniform gust model; b) 1D gust model; von Kármán spectrum; μ-controller longitudinal motion, Ma=0.7, h=25000ft; the gust sensitivity reduction in the range of engine and fuselage modes is significant, independently of the gust model employed

The same analysis is performed for the lateral control law. Fig. 16 shows the cockpit lateral acceleration response to a von Kármán spectrum - based 1D lateral gust input for the open and the closed-loop system. Here the reduction in gust sensitivity achieved by the controller does not fulfill the expectations.

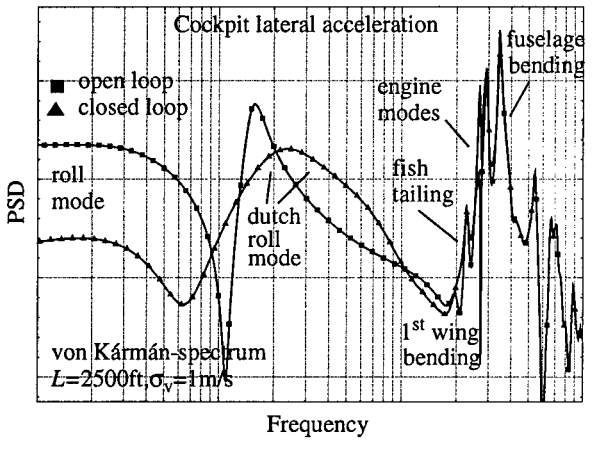

Fig. 16: 1D lateral gust response - lateral acceleration in the cockpit; open and closed loop sensitivity, Ma=0.7, h=25000ft, μ-controller; the gust sensitivity in the rigid-body mode frequency range is reduced;

While the gust sensitivity in the frequency range associated with the dutch roll mode is somewhat reduced and shifted to higher frequencies (as dutch roll frequency is increased), the sensitivity in the aeroelastic range is reduced only for some modes.

Fig. 17 shows the detailed results for both the uniform and the 1D gust models. It can be noted, that the significant reduction of the sensitivity peak associated with the fuselage bending mode in the case of uniform gusts is not achieved for 1D gusts. As the difference in phase between uniform and 1D lateral gusts unfolds over the length of the fuselage, it is not surprising that the fuselage bending mode is the most affected. Regarding the engine modes, the larger sensitivity reduction can be observed for the 1D gust model. For the fish-tailing mode, the

controller produces no improvement for uniform and even a deterioration for 1D gusts.

Therefore further research should concentrate on improving the performance with respect to fish-tailing. Further, it is expected that using the 1D gust model for control design will improve the achievable sensitivity reduction, especially with respect to fuselage bending.

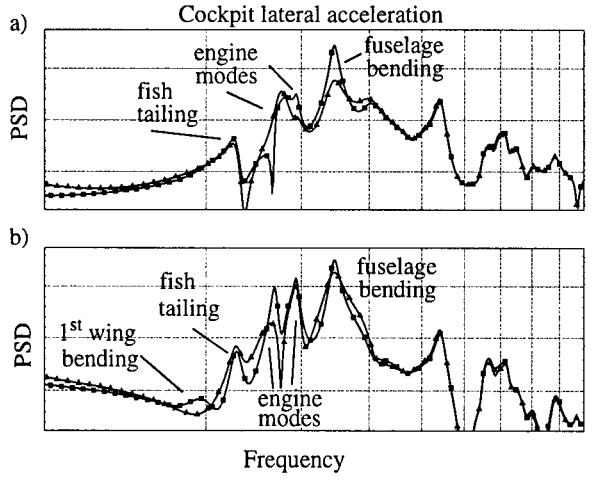

Fig. 17: Open and closed loop sensitivity to lateral gusts; a) uniform gust model; b) 1D gust model; μ-controller lateral motion, Ma=0.7, h=25000ft; sensitivity reduction depends strongly on the gust model

Gust sensitivity analysis using the 2D gust model

In the analysis run, the 2D gust model described in section 5 is employed to compare the open and closed loop gust sensitivity. Only the longitudinal controller is implemented.

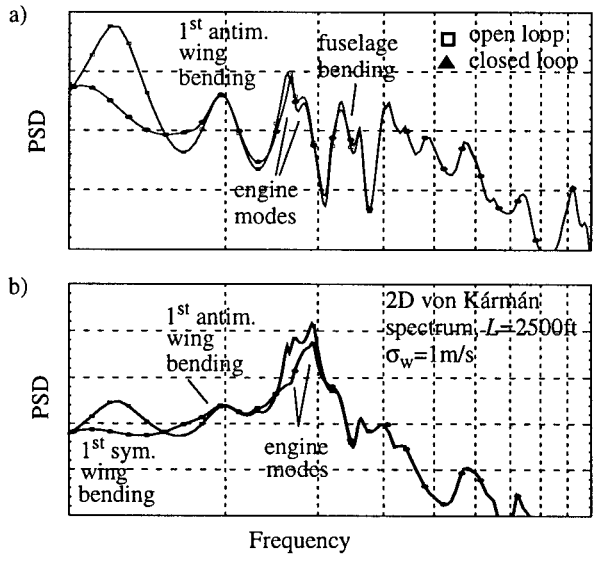

Fig. 18: Open and closed loop gust sensitivity to vertical gusts; 2D gust model; longitudinal μ-controller; a) PSD for outer wing vertical acceleration; b) PSD for outer engine lateral acceleration;

Fig. 18a shows the open and closed loop outer wing vertical acceleration PSDs. The outer engine lateral acceleration PSDs are given in Fig. 18b. The reduction of the sensitivity peaks associated with the symmetric modeshapes corresponds to the reduction observed for the 1D gust model. The increased damping of the wing bending and engine modes entails a gust sensitivity reduction.

Naturally, the longitudinal controller cannot reduce the excitation of antimetric modeshapes. Clearly, for the example aircraft, lateral aeroelastic control action is required for vertical gust sensitivity reduction. It should be noted however, that by considering (uniform) roll gusts for lateral control design, the influence of vertical gusts on the lateral motion has already been partly accounted for.

10 Conclusion

In this paper the response of a large aircraft to gust input has been evaluated. For the analysis, a high fidelity structural and aerodynamic model that also represents aerodynamic coupling between rigid body and structural modes is employed. Using gust models of different accuracy and complexity (uniform, 1D, 2D, vertical and lateral), it is shown that aircraft reaction can diverge significantly for large aircraft.

Aeroelastic vibrations of the aircraft are considerably excited by vertical and lateral gusts. Therefore, realistic gust models that describe the distribution of the gust over the aircraft structure are required. From the comparison of uniform and 1D gust responses in the aeroelastic frequency range (e.g. fuselage bending), it can be concluded that uniform gust approximations are inadequate for sensitivity analysis. This is especially true for large airplanes, where the delays between the gust effect at the front and the rear of the aircraft are more important.

Investigations often neglect the response of aircraft due to lateral gusts, which also lead to a considerable excitation of the airplane. In particular, the bending modes of the fuselage and the wing versus fuselage "fish tailing" mode have to be studied, as they cause high loads at the rear fuselage.

The implementation of 2D gust models adds new aspects to the problem, especially the response of the wing is further modified. Vertical gusts excite antimetric modes and the energy of the gust is distributed on more modes. This explains the PSD-reduction associated with the first wing bending mode. On the other hand there are modes whose response is amplified by a 2D gust. In particular, if the gust velocity distribution has the same form as certain mode shapes (e.g. higher order wing bending or engine modes), an amplification of the corresponding PSD results.

The closed loop system analysis (section 8) demonstrates that the integrated controller meets the formulated performance requirements. The comparison of open loop and closed loop gust induced acceleration PSD curves shows that aeroelastic control achieves a significant reduction. The use of uniform gust approximations for control design is not satisfactory, as the sensitivity reduction results are different for the uniform and the 1D gust models. In particular, 1D gust sensitivity peaks associated with fuselage bending modes cannot be reduced by the controller. This is not unexpected as the phase difference between uniform and 1D gust excitations is strongest over the length of the fuselage.

Therefore, future research should concentrate on developing a realistic time-domain gust formulation that can be employed for state-space-model-based control design. It is expected that this step will entail a significant improvement in the controller performance, especially with respect to the fuselage bending modes and the fish-tailing mode.

Parts of this study have been funded within the research project "Dynamik des flexiblen Flugzeugs" by the German Ministry of Reasearch and Technology (FKZ 20A9503G).

References

[1] Schuler, J., *Flugregelung und aktive Schwingungsdämpfung für flexible Großraumflugzeuge*, Dissertation Universität Stuttgart, 1997

[2] Hoblit, F.M., *Gust Loads on Aircraft: Concepts and Applications*, AIAA Education Series, Washington, 1988, ISBN 0-930403-45-2

[3] Crimaldi, J.P., Britt, R.T., Rodden W.P., *Response of B-2 Aircraft to Nonuniform Spanwise Turbulence*, Journal of Aircraft, Vol. 30, No. 5, Sept.-Oct. 1993

[4] Eichenbaum F.D., *Evaluation of 3D-Turbulence Techniques for Designing Aircraft*, Air Force Flight Dynamics Lab. TR-74-151, Wright-Patterson AFB, OH, Oct. 1972

[5] Etkin, B., *The Turbulent Wind and its Effect on Flight*, The AIAA Wright Brothers Lecture, 1980, UTIAS Review No. 44

[6] Seyffarth, K. et al., *Comfort in Turbulence for a Large Civil Transport Aircraft*, Proceedings of the International Forum on Aeroelasticity and Structural Dynamics, Strasbourg, May 1993

[7] Ward, G., Ly, U., *Stability Augmentation Design of a Large Flexible Transport Using Nonlinear Parameter Optimization*, Journal of Guidance, Control and Dynamics, Vol. 19, No. 2, March-April 1996, pp. 469-474

[8] Kubica, F., Livet, T., *Flight Control Law Synthesis for a Flexible Aircraft*, Proceedings of the AIAA Guidance, Navigation and Control Conference 1994, Scottsdale, AIAA-94-3630-CP, pp. 775-783

[9] Gregory, I.M., *Dynamic inversion to control large flexible transport aircraft*, AIAA GNC Conference, Boston, 1998, AIAA-98-4323

[10]Hanel, M., *Integrated Flight and Aeroelastic Control of a Flexible Transport Aircraft,* AIAA GNC Conference, Boston, 1998, AIAA-98-4297

[11]Rodden, W.P. , Albano E., *A Doublet-Lattice-Method for Calculating Lift Distributions on Oscillating Surfaces in Subsonic Flows*, AIAA Journal, Vol.7, No.2, Feb. 1969, pp.. 279-285.

[12]Rodden, W., Giesing, J., *Application of Oscillatory Aerodynamic Theory to Estimation of Dynamic Stability Derivatives*, Journal of Aircraft, Vol. 7, No. 3, June 1970, pp. 272 - 275

[13]Rodden, W. et al., Errata and Addenda to *Application of Oscillatory Aerodynamic Theory to Estimation of Dynamic Stability Derivatives*, Journal of Aircraft, Vol. 21, No.1, January 1984, pp. 93 - 96

[14]Karpel, M., *Minimum-State Unsteady Aerodynamic Approximations with Flexible Contraints,* Journal of Aircraft, Vol. 33, No.6, Nov.-Dec. 1996, pp. 1190-1196

[15]Sawdy, D.T., *On the Two-Dimensional Atmospheric Turbulence Response of an Airplane*, Dissertation, University of Kansas, 1966

[16]MSC NASTRAN, *Aeroelastic Analysis,* Manual, 1994

[17]Hanel, M., Well, K.H., *Optimierte Sensorpositionierung zur Regelung elastischer Strukturen*, DGLR Jahrestagung, München, October 1997

[18]Moore, B., *Principal Component Analysis in Linear Systems: Controllability, Observability and Model Reduction*, IEEE Transactions on Automatic Control, Vol. AC-26, No. 1, Feb. 1981, pp. 17-32

[19]Packard, A., Doyle, J., *The Complex Structured Singular Value*, Automatica, Vol. 29, No.1, pp. 71-109, 1993

[20]Balas, G. J., Doyle, J. C., Glover, K., Packard, A., Smith, R., *μ-Analysis and Synthesis Toolbox*, MUSYN Inc., and The MathWorks Inc., 1991.

[21]Doyle, J., Glover, K., Khargonekar, P., Francis, B., *State-Space Solutions to Standard H_2 and H_∞ Control Problems*, IEEE Transactions on Automatic Control, Vol. 34, No. 8, August 1989, pp. 831-847

[22]Glover, K., Doyle, J., *State-Space Formulae for all Stabilizing Controllers that Satisfy an H_∞ -Norm Bound and Relations to Risk Sensitivity*, System & Control Letters 11, 1988, pp. 167-172

[23]K. Glover *All Optimal Hankel-Norm Approximations of Linear Multivariable Systems and their L^∞ -Error Bounds*, International Journal of Control, 1984, Vol.39, No.6, pp. 1115-1193

Integral Control of Large Flexible Aircraft

Klaus König
Jörg Schuler
DaimlerChrysler Aerospace Airbus GmbH
Hünefeldstraße 1–5
28183 Bremen
Germany

SUMMARY
In a flexible aircraft flight control, load control and structural mode control interfere with each other. Therefore, an integral design of controller(s) is necessary. This paper describes how an integral aircraft model covering the requirements of all three disciplines can be derived and how an integral controller can be designed by multiobjective parameter optimization. General design criteria for mode control are proposed.

1. INTRODUCTION

Flight control and aeroelastics are two disciplines for aircraft (a/c) design which have worked more or less independently from each other in the past. Flight control deals with the nonlinear rigid–body motion of the a/c and aeroelastics deals with linear vibrations of the a/c structure.
This was possible as long as the eigenfrequencies of rigid–body motion and structural vibrations were clearly separated from each other and slow movements of control surfaces were sufficient. But with modern large and flexible a/c there are interferences of both types of motion.
There are three reasons for this.
First the eigenfrequencies of rigid–body motion and structural vibrations come close together causing stronger cross coupling.
Second the measured input signals of the electronic flight control system (EFCS) might contain signal parts of structural vibrations. Feeding back these signals could therefore lead to instability of flutter.
Third there may be the phenomenon of aircraft pilot coupling (APC) where vibrations of the cockpit floor structure may lead to movements of the side stick via pilot seat and pilot body/pilot arm, thereby causing control surface movements with eigenfrequencies of the rigid–body and the a/c structure.
With modern a/c it is therefore no longer possible to neglect the coupling between rigid–body motions and deflections of the structure. Interdisciplinary cooperation of flight control, aeroelastics and of the discipline loads prediction is therefore required. An integral a/c model and an integral controller covering the requirements of all these disciplines are necessary for a successful a/c design.
In the following some details of integral model derivation and some remarks on the design of integral controllers are given. Emphasis is put on the structural vibrations part of this controller.

2. THE INTEGRAL MODEL

The integral mathematical model of the a/c must include rigid–body movements and structural vibrations. This causes problems.
In the past rigid–body movements studied by flight mechanics covered large movements such as large angles of attack, and this required nonlinear aerodynamics and nonlinear Euler–Newton equations. Elasticity or structure deformation was only introduced via "elastified" aerodynamic coefficients taking into consideration steady state deflections of the a/c structure.
On the contrary, structural vibrations studied by aeroelastics were described by linear equations paying attention to the first harmonics of unsteady aerodynamics with small amplitudes of angle of attack and neglecting completely aerodynamic forces in fore and aft direction. Therefore, rigid–body motion is included – if at all – in these linear equations only in a rather rough manner.
An integral model covering the requirements of both disciplines may therefore be rather complicated. It should superimpose small deflections of the grid point masses of a huge FE–model with large three-dimensional movements in space. It should take into account aerodynamic loads due to large angles of attack and large amplitudes of the phygoid for 100000 degrees of freedom. In addition, Navier–Stokes CFD codes and nonlinear Euler–Newton inertias should be implemented. But for the time being, another approach is necessary.
One of the most obvious models is therefore a linear model valid for a working point under steady state flight conditions. This allows the study of movements around this point, and flights within the whole envelope are possible by interpolation between different working points.
The model presented here is based on the traditional aeroelastics model in frequency domain. But it has been improved so that its rigid–body modes should approach the modes of the linearized flight mechanics model. The improved model includes the following:

- –1 *stiffness matrix of structure*
- –2 *inertia matrix including all grid points*
- –3 *aerodynamic panels, also for the fuselage*
- –4 *steady state air loads at the working point*
- –5 *steady state elastic deformations of the structure*
- –6 *corrections of the stiffness matrix due to steady state deformations*
- –7 *corrections of the inertia matrix due to steady state deformations*
- –8 *eigenvalue analysis of the structure (without aerodynamics)*
- –9 *mode reduction by truncation*
- –10 *addition of control modes for compensation of truncation effects*
- –11 *transformation of rigid–body modes from main inertia axes to geodetic aircraft reference axes*
- –12 *traditional unsteady air loads*
- –13 *addition of missing elements to traditional unsteady air loads*
- –14 *inclusion of gust loads*
- –15 *smoothing of rigid–body air loads at zero frequency*
- –16 *engine loads*
- –17 *weight force*
- –18 *structural damping*
- –19 *linearization and transformation into time domain*
- –20 *eigenvalue analysis at working point*
- –21 *introduction of nonlinear rigid–body motion*
- –22 *installation of actuators*
- –23 *if wanted, transformation of rigid–body modes into completely moving coordinates of flight mechanics*
- –24 *if wanted, further mode reduction for use in flight simulators*
- –25 *addition of aircraft pilot coupling (APC) transfer functions*
- –26 *addition of electronic flight control system (EFCS)*

Items – 1, 2, 3 (partially), 8, 9, 12, 18, 20 are already covered by classical aeroelastic analyses. Items –10, 22, 26 are to be added at least for the analysis of "structural coupling of EFCS". The others are recommended for integral control design and analysis.
In the following some of these items are discussed in more detail.

2.1 Aerodynamic Panels (–3)

Classical aeroelastics most often neglects the air loads of the fuselage. This is not sufficient for an integral model. The inclusion of a panel cross (s. Fig. 2.1–1) with vertical and horizontal panels may be the most simple approach if loads caused by roll movements are excluded and if all loads are scaled (from panel to cylinder loads). A scaling factor of 0.5 was sometimes found by experience.

2.2 Stiffness and Inertia Corrections (–6, –7)

They are second order effects, but their realization is rather simple. It simply requires the multiplication of the original stiffness and inertia matrices from the right and the left side by a transposition matrix resulting from steady state structure deformations.

Paper presented at the RTO AVT Specialists' Meeting on "Structural Aspects of Flexible Aircraft Control", held in Ottawa, Canada, 18-20 October 1999, and published in RTO MP-36.

2.3 Control Modes (–10)

A classical flutter analysis includes about 100 modes with the lower frequencies of a system of about 100000 degrees of freedom. Due to this truncation, local stiffnesses may be lost. But just such local connection stiffnesses may be important if control surfaces are to be moved via EFCS by actuator loads. Therefore, assumed modes according to Rayleigh–Ritz are added. These modes are defined by a unit deflection of the actuator and the resulting deflections of the other grid points of the structure. These modes are called control modes and are to be introduced in addition to the classical rotation modes of the control surfaces. With rigid aircraft both modes would be identical.
More details about the influence of control modes are given in ref. 1.

2.4 Unsteady Air Loads (–13)

Until now traditional unsteady air loads are e.g. NASTRAN doublet lattice air loads. These are the first harmonics for a panel oscillating in an air stream. The initial angle of attack is zero and the Mach number (Ma) is constant. Therefore, the following loads are not covered:

- *in plane loads (mainly fore and aft drag and side loads)*
- *unsteady loads due to*
  - *in plane movements (mainly fore and aft)*
  - *air density ϱ varying with altitude*
  - *Mach number varying with altitude and velocity.*

For an integral model this approximation is not sufficient. If better air loads (e.g. from CFD codes) are not available, some corrections are necessary. Details for this are given in ref. 2.
Here it can be stated that steady state air loads p0 – also computed by the doublet lattice method in NASTRAN for each aerodynamic panel – can be used to establish the missing elements. This results in the following:

For lift forces resulting from steady state drag loads

$$\Delta pz = - p0x \cdot \Delta\dot{z}/\dot{x}0 \qquad 2.4\text{–}1$$

For negative drag loads (induced drag, neglecting friction)

$$\Delta px \approx (\Delta pz) \cdot \alpha 0 - p0z \cdot \Delta\dot{z}/\dot{x}0 \qquad 2.4\text{–}2$$

For side loads

$$\Delta py \approx -p0z \cdot \Delta\varphi + p0x \cdot \Delta\dot{y}/\dot{x}0 \qquad 2.4\text{–}3$$

For in plane movements

$$\Delta p(\dot{x}) \approx \frac{p0}{\dot{x}0^2} \cdot 2 \cdot \dot{x}0 \cdot \Delta\dot{x} \qquad 2.4\text{–}4$$

For dependencies from ϱ and Ma

$$\Delta p(\varrho) \approx \frac{p0(\varrho_2(z_2)) - p0(\varrho_1(z_1))}{z_2 - z_1} \cdot \Delta z \qquad 2.4\text{–}5$$

$$\Delta p(Ma) \approx \frac{p0(Ma2) - p0(Ma1)}{Ma2 - Ma1} \cdot \left(\frac{\Delta\dot{x}}{a0} - \frac{Ma0}{a0} \cdot \frac{a(z_2) - a(z_1)}{z_2 - z_1} \cdot \Delta z \right) \qquad 2.4\text{–}6$$

Another deficit to be mentioned here are the doublet lattice air loads of control surfaces. Usually, they are too large and should be corrected to wind tunnel results of hinge moments. But the corrections must also include the airfoil in front of the control surface. Correction factors of up to 0.6 are possible.

2.5 Smoothing of Rigid–Body Air Loads at Zero Frequency (–15)

If steady state air loads from wind tunnel measurements are available, it should be possible to improve the doublet lattice air loads of rigid–body modes at zero frequency. This can be done by separating these loads by an eigenvalue analysis. After transformation of the separated doublet lattice air loads into the coordinate system of the measurement, these loads can be substituted by Fourier – transformed air loads measured for zero frequency and the smallest non–zero frequency.

For the other frequencies a smoothed change to doublet lattice air loads can be chosen. For a linear smoothing this yields:

$p = p_{measured}(\omega)$ if $\omega < \omega_1$

$p = p_{measured}(\omega) \cdot (\omega_r - \omega) / (\omega_r - \omega_1) + p_{doublet\ lattice}(\omega) \cdot (\omega - \omega_1) / (\omega_r - \omega_1)$ if $\omega_1 \le \omega \le \omega_r$

$p = p_{doublet\ lattice}(\omega)$ if $\omega > \omega_r$

2.6 Engine Loads and Weight Forces (–16, –17)

Loads such as gross thrust, ram drag and gravity weight are not included in aeroelastic analyses, but they are of influence for flight mechanics. Therefore, they must be introduced.
As to the engines, their unsteady load portion is due to three different reasons:
First from the unsteady movement of the engine position and its steady state loads, i.e. due to the change of direction (T'_{ePo}) and due to transposition (V'_{Ea0})

$$p0 + \Delta p = V'_{Eo0} \cdot T'_{eEo} \cdot p0_{eE}$$

resulting in

$$\Delta p = - FP(p0_{eE}) \cdot \Delta r_{oE} \qquad 2.6\text{–}1$$

with

$$FP(p0_{eE}) = \begin{bmatrix} 0 & 0 & 0 & 0 & -p0z & p0y \\ 0 & 0 & 0 & p0z & 0 & -p0x \\ 0 & 0 & 0 & -p0y & p0x & 0 \\ 0 & -p0z & p0y & 0 & 0 & 0 \\ p0z & 0 & -p0x & 0 & 0 & 0 \\ -p0y & p0x & 0 & 0 & 0 & 0 \end{bmatrix}; \quad \Delta r_{oE} = \begin{bmatrix} \Delta x \\ \Delta y \\ \Delta z \\ \Delta\varphi \\ \Delta\vartheta \\ \Delta\psi \end{bmatrix}$$

Second from their derivatives due to velocity and altitude changes as the air loads (2.4–5, –6)

$$\Delta p = \frac{p0(Ma2) - p0(Ma1)}{Ma2 - Ma1} \cdot \left(\frac{\Delta\dot{x}}{a0} - \frac{Ma0}{a0} \cdot \frac{a(z_2) - a(z_1)}{z_2 - z_1} \cdot \Delta z \right) + \frac{p0(\varrho_2(z_2)) - p0(\varrho_1(z_1))}{z_2 - z_1} \cdot \Delta z \qquad 2.6\text{–}2$$

Third from their derivatives due to control inputs

$$\Delta p = \frac{p0(n_2) - p0(n_1)}{n_2 - n_1} \cdot \Delta n \qquad 2.6\text{–}3$$

The weight must be introduced if the final equations are transformed from the geodetic (g) to the moving coordinate system (f)

$$\Delta g_f = g_g \cdot \begin{bmatrix} -\Delta\vartheta \cdot \cos\varphi 0 \cdot \cos\vartheta 0 + \Delta\psi \cdot \sin\varphi 0 \cdot \cos\vartheta 0 \\ \Delta\psi \cdot \cos\varphi 0 \cdot \cos\vartheta 0 - \Delta\psi \cdot \sin\vartheta 0 \\ -\Delta\varphi \cdot \sin\varphi 0 \cdot \cos\vartheta 0 + \Delta\vartheta \cdot \sin\vartheta 0 \end{bmatrix} \qquad 2.6\text{–}4$$

2.7 Linearization and Transformation into Time Domain (–19)

For the purpose of controller design, the subsequent inclusion of nonlinearities or the use in flight simulators, the integral model is required in time domain. When starting with the aeroelastics model in frequency domain, a linearization of air loads and a transformation are necessary. Methods for this were proposed by Vepa (s. ref. 3), Roger (s. ref. 4) or Karpel (s. ref. 5). Especially the minimum state method of Karpel was successfully used, though it requires a larger amount of computing. Fig. 2.7–1 shows an example of good approximation.

2.8 Introduction of Nonlinear Rigid–Body Motion (–21)

All the improvements mentioned above may not be sufficient for a precise rigid–body movement as required by flight mechanics. Therefore, a substitution of the improved "aeroelastic" rigid–body motion by the "flight mechanics" motion is recommended. In this process a nonlinear rigid–body movement can also be introduced.
Of course this substitution must only be done for the decoupled orthogonal modes followed by a modal retransformation to the original coordinates.

By starting from the aeroelastics equation

$$\dot{x}A = AA \cdot xA + BA \cdot u \qquad 2.8\text{–}1$$

with

$$xA = \begin{bmatrix} xAr \\ xAe \end{bmatrix} = \phi A \cdot \begin{bmatrix} qAr \\ qAe \end{bmatrix}$$

$$\psi A = \phi A^{-1}$$

resulting in the orthogonal coordinates

$$\begin{bmatrix} \dot{q}Ar \\ \dot{q}Ae \end{bmatrix} = \begin{bmatrix} \lambda Ar & 0 \\ 0 & \lambda Ae \end{bmatrix} \cdot \begin{bmatrix} qAr \\ qAe \end{bmatrix} + + \begin{bmatrix} \psi Arr \cdot BAr + \psi Are \cdot BAe \\ \psi Aer \cdot BAr + \psi Aee \cdot BAe \end{bmatrix} \cdot u \qquad 2.8\text{–}2$$

with the eigenvalues

λAr (rigid) and λAe (elastic)

and defining

$$xFr = \phi Arr \cdot qAr \qquad 2.8\text{–}3$$

as intended by traditional flight mechanics,

one obtains with equation 2.8–2

$$\dot{x}Fr = \phi Arr \cdot \lambda Ar \cdot \phi Arr^{-1} \cdot xFr + + \phi Arr \cdot (\psi Arr \cdot BAr + \psi Are \cdot BAe) \cdot u \qquad 2.8\text{–}4$$

Further on it results after some rearrangements:

$$\begin{bmatrix} \dot{x}Ar \\ \dot{x}Ae \end{bmatrix} = \begin{bmatrix} 1 \\ \phi Aer \cdot \phi Arr^{-1} \end{bmatrix} \cdot \dot{x}Fr + + \begin{bmatrix} \phi Are \cdot \lambda Ae \cdot \psi Aer & \phi Are \cdot \lambda Ae \cdot \psi Aee \\ \phi Aee \cdot \lambda Ae \cdot \psi Aer & \phi Aee \cdot \lambda Ae \cdot \psi Aee \end{bmatrix} \cdot \begin{bmatrix} xAr \\ xAe \end{bmatrix} + \begin{bmatrix} \phi Are \cdot (\psi Aer \cdot BAr + \psi Aee \cdot BAe) \\ \phi Aee \cdot (\psi Aer \cdot BAr + \psi Aee \cdot BAe) \end{bmatrix} \cdot u \qquad 2.8\text{–}5$$

Briefly, equation 2.8–4 and –5 can be written as follows:

$$\begin{bmatrix} \dot{x}Fr \\ \dot{x}Ar \\ \dot{x}Ae \end{bmatrix} = \begin{bmatrix} AFrr & 0 & 0 \\ AFrr & ALrr & ALre \\ \phi Ler \cdot AFrr & ALer & ALee \end{bmatrix} \cdot \begin{bmatrix} xFr \\ xAr \\ xAe \end{bmatrix} + + \begin{bmatrix} BFr \\ BFr + BLr \\ \phi Ler \cdot BFr + BLe \end{bmatrix} \cdot u$$

or

$$\dot{x}I = AI \cdot xI + BI \cdot u \qquad 2.8\text{–}6$$

That is the integral equation of aeroelastics and flight mechanics. If required, AFrr and BFr (implying ϕFrr and λFr) may be taken from flight mechanics or the nonlinear $\dot{x}Fr = f(xFr, u)$ of flight mechanics may be introduced. In any case, it is the most reasonable compromise. It keeps the eigenvalues of the rigid a/c λr of the discipline defining xFr and keeps the eigenvalues of the elastic structure λe of aeroelastics unchanged as can easily be proven. Even simulations in a moving simulator with elasticity included can be performed. The eigenvector matrix of AI reads:

$$\begin{bmatrix} (\phi Frr \text{ or } \phi Arr) & 0 & 0 \\ (\phi Frr \text{ or } \psi Arr) & -1 & \phi Are \\ \phi Aee \cdot \phi Are^{-1} \cdot (\phi Frr \text{ or } \psi Arr) & -\phi Aer \cdot \phi Arr & \phi Aee \end{bmatrix}$$

and their eigenvalue matrix:

$$\begin{bmatrix} (\lambda Fr \text{ or } \lambda Ar) & & \\ & 0 & \\ & & \lambda Ae \end{bmatrix} \qquad 2.8\text{–}7$$

2.9 Installation of Actuators (–22)

Actuators are highly nonlinear elements, mainly due to the viscous damping effect of the oil flow, the overlapping of the throttle orifices and the quantization effects of the digital servo control loop. Therefore, actuators have to be substituted by their frequency response functions (in the following called transfer functions), if linear systems are to be used. This includes the first harmonic but neglects all higher orders or subharmonic responses. Then a decision has to be taken on the actuator model. There are two possibilities for actuators with closed control loop.

The stroke model:

$$zA = H_{zA,u} \cdot u \qquad 2.9\text{–}1$$

and the load model:

$$zA = H_{zA,u} \cdot u + H_{zA,pA} \cdot pA \qquad 2.9\text{–}2$$

where zA = realized actuator stroke
u = commanded actuator stroke
pA = actuator action load
$H_{.,.}$ = transfer function
($H_{zA,u}$ may be called "frequency response function of control" and $H_{zA,pA}$ "frequency response function of disturbance")

and after some rearrangements of equation 2.9–2 for the loads model:

$$pA = pH - k_A \cdot z_A \qquad 2.9\text{–}3$$

with

$$pH = H_{pH,u} \cdot u + H_{pH,zA} \cdot z_A$$

$$H_{pH,u} = -H^{-1}_{zA,pA} \cdot H_{zA,u}$$

$$H_{pH,zA} = H^{-1}_{zA,pA} + k_A$$

kA = chosen more or less arbitrarily

Both models have their advantages and disadvantages.

2.9–1 The stroke model

This is the simpler model and the one most often used. It requires the elimination of z_A, the actuator stroke or deflection, from aircraft structure equations and its transfer to the right side of these equations to make it available as excitation.

The remaining homogenous equations of structure on the left side do no longer include actuators. They are only valid for rigid actuators or rigid connections between control surface and aircraft. Therefore, two eigenvibration calculations are required. The usual one for classical flutter analyses without electronic control but with flexible actuators and the other one for flutter analyses with electronic control and with rigid actuators. Most probably, the eigenfrequencies and mode shapes of these two models will vary to a greater extend.

The models represent two different working points. The one with rigid actuator may be too far away from the conditions needed later when the actuator is flexible and moved by electronic control.

Besides, it should also be mentioned that in case of polynomial approximations of the transfer function of the stroke model, the order of the denominator polynom must be two orders higher than the nominator polynom to get accelerations of actuator stroke from commanded stroke.

2.9–2 The loads model

This model is the more complicated one. Its advantage is that it allows the inclusion of actuator flexibility existing under dynamic conditions. The model operates as a real linear spring and a disturbance load p_H in parallel. If the spring term $-k_A \cdot z_A$ of equation 2.9–3 is brought to the left side of aircraft structure equations, a classical eigenvibration calculation with flexible actuators can be performed and one set of modes can be used for flutter analyses with and without electronic control. This is a second advantage of the loads model. The stiffness k_A (and perhaps even an additional damping term) can be taken from ground vibration tests. A third advantage could be the fact that the introduction of $H_{pH,zA}$ in principle allows a stiffness correction even after modal truncation, as explained already in ref. 1.

The control term $H_{pH,u} \cdot u$ and the difference between complex and real negative actuator spring $(H^{-1}_{zA,pA} + k_A) \cdot z_A$ remain on the right side of aircraft equations. An example of the negative complex spring "stiffness" $H_{pA,zA}$ is given in Fig. 2.9–1, together with a chosen real substitute $-k_A$. The differences are not negligible.

Fig. 2.9–2 gives some information about the influence of different terms of the actuator transfer function. It shows a vertical wing tip

acceleration response due to elevator movement in flight. Three cases are shown. The first one for the complete actuator model with

$$H_{pH,u} = -H^{-1}_{zA,pA} \cdot H_{zA,u}$$
$$H_{pH,zA} = H^{-1}_{zA,pA} + k_A$$

the second one arbitrarily with

$$H_{pH,u} = -H^{-1}_{zA,pA} \cdot H_{zA,u}$$
$$H_{pH,zA} = 0$$

the third simplified one with

$$H_{pH,u} = k_A \cdot H_{ZA,u}$$
$$H_{pH,zA} = 0$$

In the figure the peaks of structural response are clearly visible. The second case shows large deviations at about 17 Hz, while for the third case, only small deviations at about 8 Hz are visible. So it can be concluded that the complex frequency response function of disturbance $H_{zA,pA}$ has a larger influence and should be precise enough, if used.

2.9–3 Scatter

Another important factor of actuator models is the large number of influence parameters, such as

- ☐ temperature, environment
- ☐ backlash, wearing
- ☐ supply and return pressure
- ☐ servo control law (gain, sample rate)
- ☐ activated mode
- ☐ amount of mass to be moved
- ☐ static load in working point
- ☐ static position in working point
- ☐ amplitude and frequency of command
- ☐ amplitude and frequency of external load
- ☐ failure conditions
  - • supply pressure decrease
  - • leakage
  - • wrong activation status
  - • desynchronization of multiple actuators
  - • mechanical blocking or fracture
  - • air in hydraulic oil

Therefore, a broad scatter band of transfer functions is to be expected. The influence of this scatter is shown in Fig. 2.9–3. The same transfer function as the one shown in Fig. 2.9–2 is given for the complete actuator model, together with its upper and lower tolerance (mainly due to oil temperatures of 90°, 35° and –15°). The differences are dramatic. As a consequence, stability and response analyses must include a reasonable amount of scatter.

2.10 Transformation into Completely Moving Coordinates (–23)

Flight mechanics use a coordinate system which moves completely with deflection. Aeroelastics use an inertial geodetic coordinate system. The integral model derived from aeroelastics starts with the inertial system. Therefore, a transformation may sometimes be necessary. For the sake of completeness, it should be mentioned here that any transformation into the flight mechanics system adds so–called Euler terms to the equations. They can simply be derived as follows:

If

$$\dot{s}_{ft} = T_{fAg} \cdot \dot{s}_{gt} \qquad 2.10\text{–}1$$

with

$\dot{s}_{gt}$ velocity with components measured in the inertial coordinate system g

$\dot{s}_{ft}$ same velocity, but its components are now measured in the completely moving coordinate system f.

T_{fAg} matrix of coordinate transformation from g to f with Euler angles

the following results:

$$\ddot{s}_{ft} = \dot{T}_{fAg} \cdot \dot{s}_{gt} + T_{fAg} \cdot \ddot{s}_{gt} \qquad 2.10\text{–}2$$

with the first term being the Euler term (derivated without cross products or special derivation symbols for derivation in moving coordinate systems!). The Euler term is not negligible since $\dot{s}_{gt}$ includes the velocities of the aircraft. All the other terms contain small variables.

2.11 Addition of Aircraft Pilot Coupling (APC), (–25)

In classical aeroelastics the movement of an aircraft is determined exclusively by the aircraft structure and the air. But with highly flexible a/c, a pilot in the loop must also be investigated.

If e.g. the floor of the aircraft cabin is vibrating, this vibration is transferred via seat, pilot body and arm to the side stick. The side stick is unintentionally moved and introduces signals to the actuators deflecting the control surfaces which excite the aircraft via air loads and closes the loop of vibration (s. Fig. 2.11–1).

This is not only of theoretical interest, critical cases – called PIO cases before – are known from several aircraft.

Therefore, the complete integral model should include this biomechanical closed loop circuit of APC.

This can be done if a transfer function from aircraft cabin floor vibration to stick input is available. Such functions were recently measured and some are published in ref. 6. Fig. 2.11–2 shows an example.

If everything mentioned up to now is introduced, the integral model is ready for design and application of integral control.

2.12 Results from an Integral Model

An aircraft model including most of the effects mentioned above was established and its characteristics were studied.

Based on flight mechanics, three different sets of linearized rigid–body models were available. An early one F1Lr, an improved one with "rigid" aerodynamic coefficients F2Lr and one with "elastified" aerodynamic coefficients F2Le.

Based on aeroelastics, three different sets of models are available. The first one A(qr) includes only rigid–body modes, the second one A(qs) includes the first six symmetric and six antisymmetric elastic modes, and the third one A(qc) includes two times 27 instead of 12 elastic modes.

2.12–1 Eigenvalues

Table 2.12–1 gives a survey of the eigenvalues (frequency fn and damping ξn) of the most important rigid–body modes.

For the "short period" the frequencies of flight mechanics are in general smaller than the frequencies of aeroelastics, while the dampings show opposite tendencies. Elastic a/c show smaller frequencies and larger dampings for both disciplines. The influence of elasticity is not negligible.

For the "dutch roll" the frequencies are in better agreement, where as the dampings of flight mechanics show larger scatter. The influence of elasticity is smaller.

The "phygoid" is rather sensitive and a larger scatter is visible for the values of flight mechanics. Nevertheless, the frequencies of aeroelastics do not differ so much. The influence of elasticity is visible.

The other aperiodic rigid–body modes show relatively good approximation. The increase of the number of elastic modes to 54 has minor influences on the frequencies and dampings of the first 12 elastic modes.

2.12–2 Response to Control Inputs

Figures 2.12–1 to –4 show examples of time response of rigid–body states

- • pitch acceleration due to elevator "step" (+1 degree)
- • roll acceleration due to aileron "stair" (+1°, 0°, –1°, 0°)
- • yaw acceleration due to rudder step (+1°)

Figure 2.12–1 compares the different models of flight mechanics with the reference model of aeroelastics A(qs). The differences, mainly in yaw damping, and the influence of elasticity are clearly visible.

Fig. 2.12–2 compares the influence of a different number of elastic modes. It shows the influence of elasticity more clearly. Especially with pitch and roll acceleration, it is visible that with elastic modes the vibrations move around their own average curve but not around the curve of the simple rigid model. This proves again the influence of elasticity on rigid–body movement.

Fig. 2.12–3 compares the results of the integral model I(A(qs)), i.e. (s. § 2.8) rigid–body behavior determined by aeroelastics, xFr = xAr(A(qs)) with I(F2Lr), i.e. rigid–body behavior determined by flight mechanics, xFr = xF(F2Lr).

The differences are rather small. They result from the different rigid–body models.

In addition, one can see clearly that the same elastic vibration is superimposed to the applied rigid–body movement. This proves

again that elasticity can be superimposed by applying equation 2.8–5 if a good rigid–body model is available.
Finally Fig. 2.12–4 shows the measurable acceleration at the pilot seat (model (A(qs)) due to control commands. Here the influence of elasticity is rather large as already shown. The response amplitudes due to rudder step are nearly twice as large as those of rigid a/c, the same applies to the elevator step which introduces a strong response peak right at the beginning.
Naturally, such a large elastic a/c response would be reduced in reality by electronic filtering or by mechanical reduction due to slow actuators. In this simulation no reduction was introduced. The transfer functions of actuators were set to 1=constant with the intention to show the potential of the aircraft.

3. THE INTEGRAL CONTROLLER

3.1 Objectives

There are three different tasks of the integral controller to be distinguished: flight control, load control and mode control. Their objectives are rather different.
In general one can name:

flight control:
- flight stability
- aircraft protection
- maneuverability
- defined flight path following
- reduction of workload of pilot

load control:
- reduction of limit loads
- reduction of fatigue loads
- avoidance of critical failure conditions

mode (or structural vibrations) control
- aeroelastic stability
- minimization of structural vibrations
- improvement of passenger comfort

All these objectives interfere with each other, some are even contradictory to each other, and most of them can be subdivided into a larger number of subobjectives.
Nevertheless, they can be detailed and – with some exceptions – given as criteria in a mathematical formulation. So an integral controller can be designed in a multicriteria optimization process, with targets and constraints.
For the purpose of mode control, which is of main interest in this context, one can distinguish three different types of controller objectives: flutter suppression, flutter margin augmentation and reduction of vibration level for comfort. Flutter suppression would cure a flutter case within the flight envelope. Flutter margin augmentation would cure a flutter case in an area for which the aircraft is not designed but which must be covered as required by law.
Comfort control would reduce the natural structural vibrations caused by air turbulence down to a comfortable level on a naturally stable aircraft.
All mode controllers aim at an increase of the damping of structure modes. Their main difference is the required level of safety.

3.2 Requirements and Restrictions for Mode Control

3.2–1 Airworthiness Requirements

For mode controllers the main safety requirements are also airworthiness requirements. For civil aircraft and structural aspects, these are the FAR or JAR 25 requirements, here § 25.629 "Flutter, Deformation and Fail Safe Criteria" and § 25.302 "Interaction at Systems and Structure". If one looks at the flutter speed to be reached a literal interpretation of the requirements leads to Fig. 3.2–1 for its definition. The required speed depends on the system's probability of being in failure. So one can read in Fig. 3.2–1 that:

- ❑ flutter suppression controllers need a probability of being in failure state of $<10^{-9}$, since they have to shift the flutter speed from below VD up to 1.15 VD
- ❑ flutter margin augmentation controllers need $<10^{-5}$, since they have to shift from above VD up to 1.15 VD
- ❑ comfort controllers need <1, since here the natural a/c reaches already 1.15 VD. If the system fails, there is no safety problem but only a comfort problem which is not the subject of these paragraphs.

A special situation arises if a high speed protection (HSP) system and a mode control (MC) system are used in combination to keep $V \le V_C$ and to avoid flutter within $V_C<V_F<V_D$. If both systems have an independent probability of being in failure state of $<10^{-5}$, in combination they can reach a value of $< 10^{-9}$, as required. But nevertheless, $V_F<V_D$ if the MC system fails, although VF cannot be reached due to the HSP system.

3.2–2 Mode Control Design Criteria

Any controller should be safe, efficient, robust and should not disturb other positive features of the controlled system.
For safety reasons, the a.m. JAR requirements defined by the flutter speed to be reached must be fulfilled. But there are other safety criteria too.
First the amount of modal damping which indicates a certain stability robustness against scatter, ageing or disturbances.
Second the phase and gain margins (well known for single input/ single output (SISO) – systems) which show the robustness against deviations from nominal conditions or against minor failures not especially mentioned.
The efficiency or performance of the controller can very simply be defined in most cases by the flutter velocity or the modal damping to be reached.
The robustness is a more complex issue. One aspect, the "safety robustness" was already mentioned before. Another aspect is "performance robustness" against disturbances or against operation conditions. The number of the latter one is huge. It includes, among others, a/c velocity, altitude, flap/slat setting, payload, fuel and their distributions. Each combination of these conditions defines a load case to be included in the controller design.
Finally it must be shown by the evaluation of time response due to step input or frequency response due to random excitation that the controller neither introduces unwanted features nor reduces wanted features, such as good a/c maneuverability.
In the following some requirements are detailed as a first proposal for a multi–input / multi–output (MIMO) controller.

- ❑ Flutter control:
  For modal damping "ξn" of each of n eigenvalues shall be $\xi n \ge 0.5\%$ (% of critical) and
  $$\frac{d\xi n}{dv} > -0.01 \text{ [\% / kts CAS]}$$
  This guarantees stability.

- ❑ Comfort control:
  The maximal singular value "$\bar{\sigma}$" of a number m of pick–up signals "ym" due to gusts "w" in frequency range "f_1" to "f_2" shall be minimal and at least smaller than a limit value $G_{Hym,w}$ i.e.
  $$\max (\bar{\sigma} (Hym,w (i\omega))) \rightarrow \min$$
  $$f_1 \div f_2$$
  $$\max (\bar{\sigma} (Hym,w (i\omega))) < G_{Hym,w}$$
  $$0 \div \infty$$
  where Hym,w (iω) is the transfer function from gust w to the pick–up signal ym.
  This should reduce the response to turbulence.

- ❑ Robustness of control (based on ref. 7):
  The phase margin of the open loop transfer function Hu,u (iω) of all actuator signals u shall be
  $$\frac{30^\circ \cdot \pi}{180} \le | 2 \cdot \arcsin (\min (\underline{\sigma} (1 + Hu,u (i\omega))) /2) |$$
  the gain margin of the open loop transfer function Hu,u (s) of all actuator signals u shall be
  $$1 / (1 - \min (\underline{\sigma} (1 + Hu,u (i\omega)))) > 2$$
  and
  $$1 / (1 + \min (\underline{\sigma} (1 + Hu,u (i\omega)))) \le 0.66$$
  where $\underline{\sigma}$ is the minimum singular value.
  This should ensure safety robustness.

If these criteria were really met in the whole envelope of velocity and altitude as well as in all loading conditions of fuel and payload, a good controller should be reached.
But these requirements are probably too stringent and some monitored exceptions are therefore necessary. At the moment, there is insufficient experience available to present more details on this issue. But one thing is beyond question: some requirements of this type are necessary.
The mere definition of the required flutter speed, as given in FAR 25.302, is not sufficient. At least a certain amount of robustness is necessary for safety to cover smaller scatter or deviations from

nominal conditions which are not defined as separate failure states.

3.2–3 Reliability / Failure Probability
A good reliability or low failure probability can be reached by different methods. For example, redundancy of hardware installations and signal monitoring are well known. For MIMO controllers studied here, special attention should also be paid to the minimization of interactions between the different signal lanes of the controller.

3.2–4 Safety Restrictions for Mode Control
This could include:

- Low pass filter for the flight control signal part and band pass filter for the signal part of mode control. This prevents a failure in the more complicated flight controller part from causing flutter problems and a failure in the mode controller part from influencing the flight path.

- Decoupling network with diagonal structure of the controller transfer matrix of MIMO systems. This could e.g. be done by superposition of different effective SISO systems which do not interfere with each other.
  If all SISO systems are stable and effective for themselves, a failure and a switch–off of one of these lanes will not lead to a complete loss of the controller.

Admittedly, such measures cannot always be taken. Especially a separation by filter does not work if rigid–body frequencies and elastic mode frequencies are close together. But if it works, these filters should be used under all circumstances. Missing filters present an unnecessary risk.

3.3 Design

The design of the integral controller is a multidisciplinary process of multicriteria optimization. Fig. 3.3–1 may give a survey of its principle structure.
First an integral model of the a/c must be established and made available in linear and nonlinear form for all loading and flight conditions to be covered.
Second a complete list of criteria is to be established, including all objectives of the different disciplines.
Then the question arises how the controller should be structured. In most cases experience answers this question, otherwise, theoretical methods of robust optimal control law design as e.g. the H_∞ method are available to find a good structure.
If the structure is known its parameters can be optimized by a multiobjective optimization strategy.
Finally the resulting controller must undergo a special assessment by the different disciplines, including simulations with pilot in the loop.
Of course, one has to keep in mind that by increasing the number of aims the efficiency of the controller will be reduced.
It is still impossible to get everything simultaneously!
Modifications of controller structure, of criteria or even of control surfaces or systems may be necessary.
The first three iteration steps of an example of such a multicriteria optimization is shown in Fig. 3.3–2 (s. ref. 8) where a limited number of criteria was studied. One can see that finally all criteria are met. The program stops when "pareto optimal" results are reached, i.e. when a value of one criteria can only be improved by impairing another one.

4. CONCLUSION

- Increasing a/c flexibility requires integral controllers for flight, load and mode control.
- The controller design must be based on an integral a/c model which covers the requirements of flight mechanics, loads and aeroelastics.
- The integral model can be based on a classical aeroelastics model if several improvements are introduced.
- Linear or nonlinear rigid–body motion of traditional flight mechanics can be coupled with structural vibrations of traditional aeroelastics without restrictions.
- APC can be included.
- Controller design should be performed by a multiobjective parameter optimization to reach an optimum for all criteria.
- Safety and design criteria for mode control need further discussion.

Aknowledgement:
This work was partialy sponsored by the german BMBF.

REFERENCES

1. K. König "On the New Quality of the Flutter Problem Due to Coupling of Structure and Electronic Flight Controls in Modern Large and Flexible Civil Aircraft" International Forum on Aeroelasticity and Structural Dynamics, Straßbourg, May 24 – 26, 1993

2. J. Schuler "Flugregelung und aktive Schwingungsdämpfung für flexible Großraumflugzeuge" VDI Fortschrittsbericht Reihe 8 Nr. 688 Düsseldorf: VDI Verlag 1998

3. R. Vepa "On the Use of Padé Approximants to Represent Unsteady Aerodynamic Loads for Arbitrarily Small Motions of Wings", Proceedings of the AIAA 14th Aerospace Sciences Meeting, AIAA Paper No. 76–17, Washington, D.C., January 26–28, 1976.

4. K.L. Roger "Airplane Math Modeling Methods for Active Control Design, AGARD–CP–228, pp. 4.1–4.11., August, 1977

5. M. Karpel and E. Strul "Minimum – State Unsteady Aerodynamic Approximations with Flexible Constraints, Proceedings of the International Forum on Aeroelasticity and Structural Dynamics, pp. 66.1–66.8, Manchester, June 26 – 28, 1995

6. L. Böger et. allied "Experimentelle Ermittlung der kinematischen Rückkopplung des Piloten aufgrund von Cockpit Beschleunigungen", DGLR – JT 98–008 p.753–762, Bremen, October 6th, 1998

7. N.A. Lektomaki, N.R. Sandell Jr., M. Athans "Robustness Results in Linear–Quadratic Gaussion Based Multivariable Control Design", IEEE Transactions on Automatic Control, vol. AC–26 No. 1 , p. 75–93, February, 1981

8. G. Grübel et. allied "ANDECS / MOPS 3.0 Tutorials" DLR Oberpfaffenhofen, July 1995

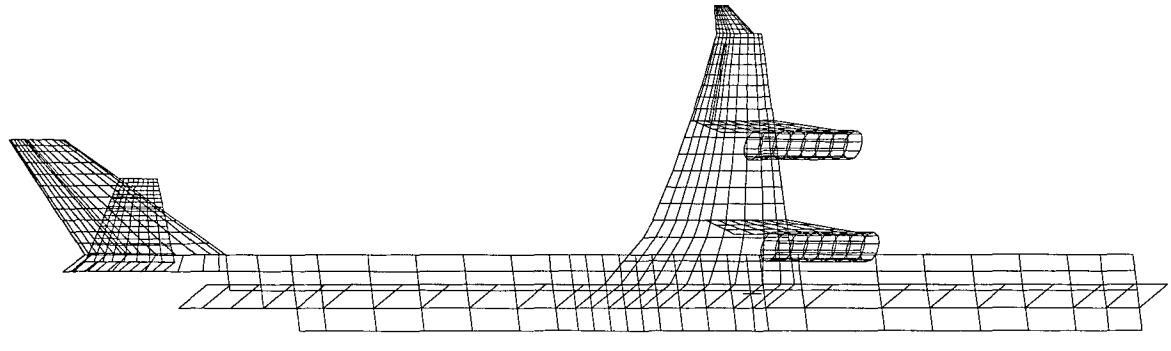

FIG. 2.1–1: MODELING OF FUSELAGE FOR AIR LOADS

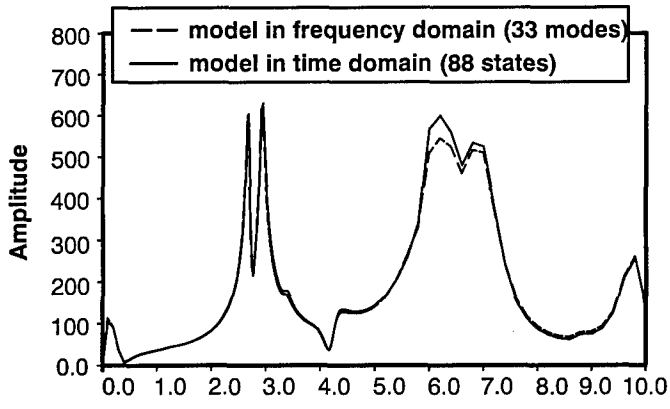

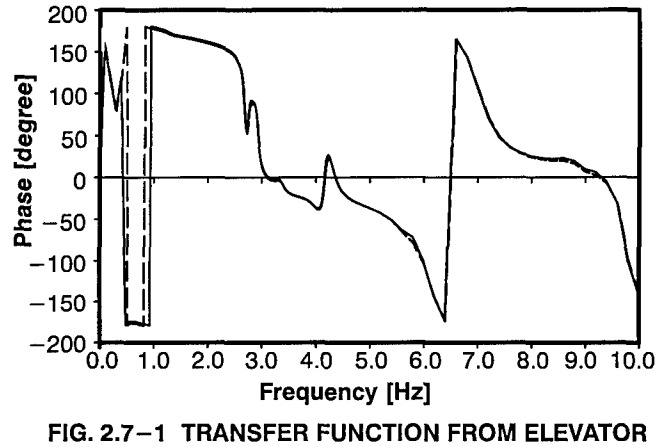

FIG. 2.7−1 TRANSFER FUNCTION FROM ELEVATOR TO FRONT FUSELAGE ACCELERATION

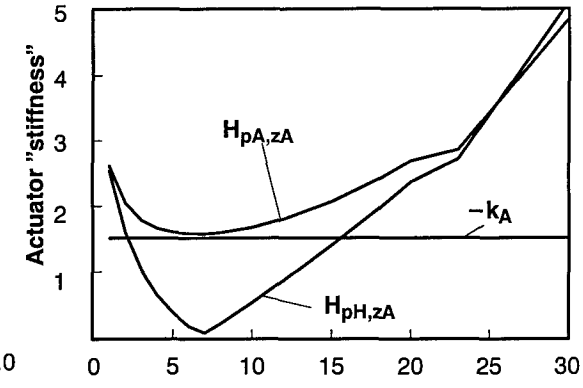

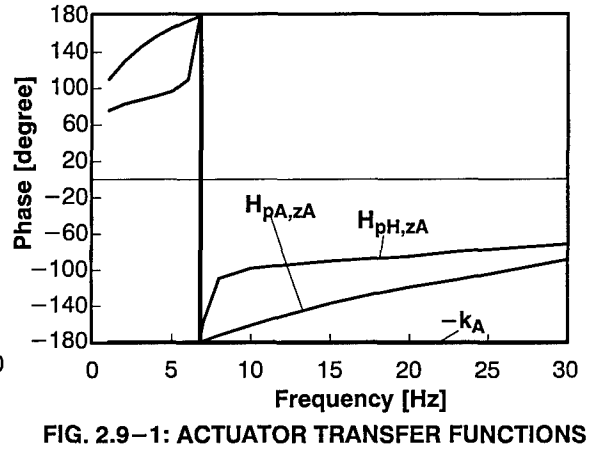

FIG. 2.9−1: ACTUATOR TRANSFER FUNCTIONS OF DISTURBANCE OR FLEXIBILITY

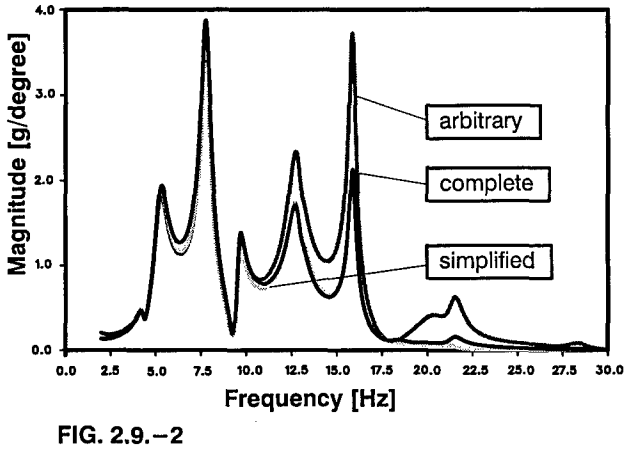

FIG. 2.9.−2
Hż,u TRANSFER FUNCTION FROM ELEVATOR TO WING TIP
INFLUENCE OF ACTUATOR MODEL

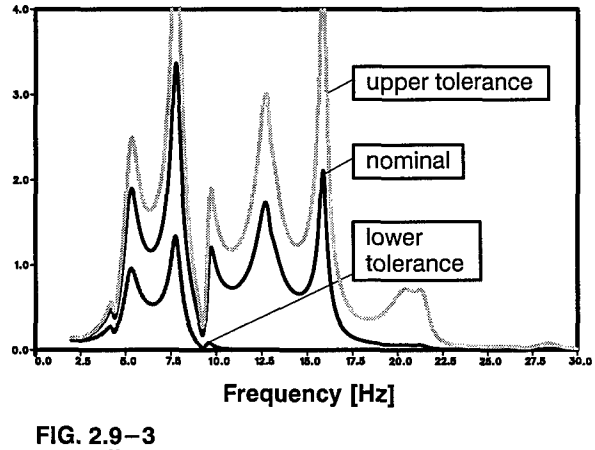

FIG. 2.9−3
Hż,u TRANSFER FUNCTION FROM ELEVATOR TO WING TIP
INFLUENCE OF ACTUATOR SCATTER

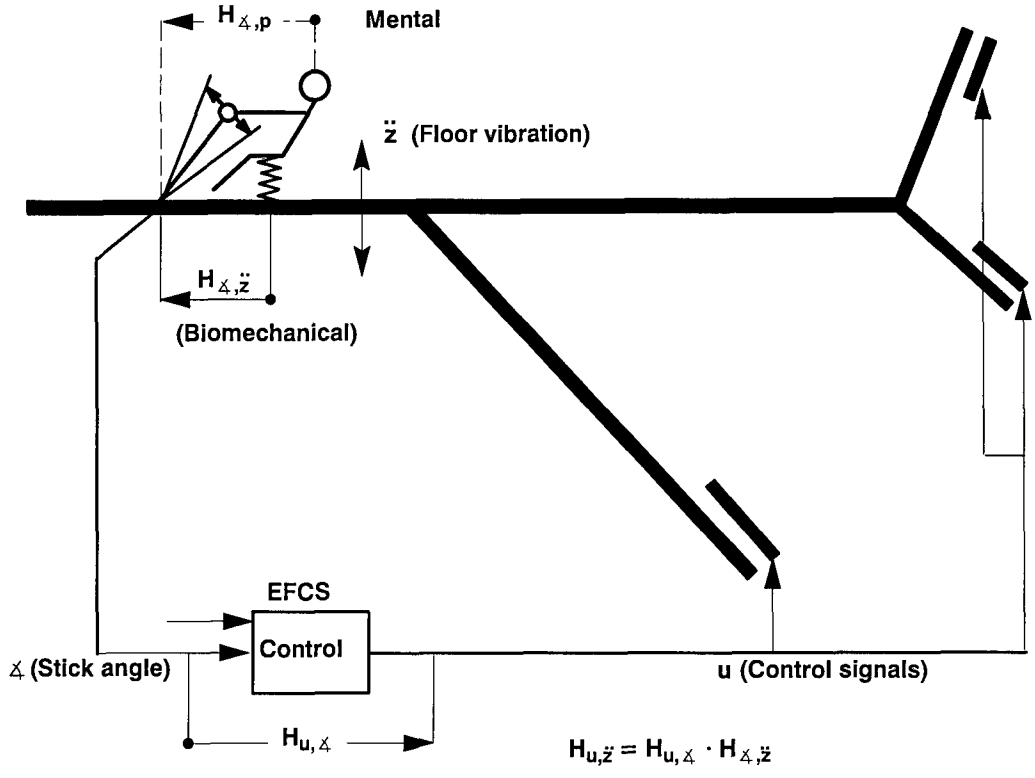

FIG. 2.11−1: AIRCRAFT PILOT COUPLING MECHANISM

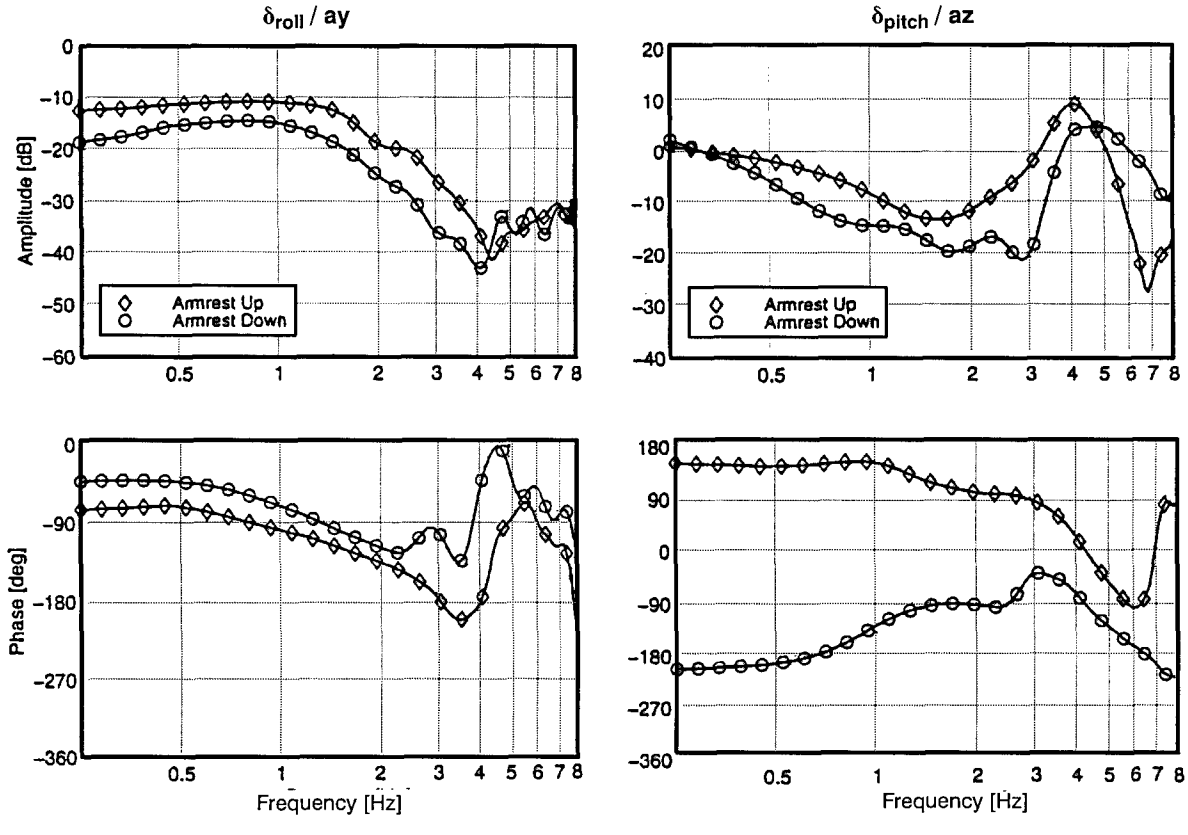

FIG. 2.11−2: TRANSFER FUNCTION FROM A/C FLOOR VIBRATION TO SIDE STICK MOVEMENT

		phygoid	dutch roll	short period
A(qr)	fn [Hz] ξn [%]	0.01076 5.22	0.1596 10.70	0.2442 48.76
A(qs)	fn [Hz] ξn [%]	0.01160 7.30	0.1551 10.87	0.2202 48.96
A(qc)	fn [Hz] ξn [%]	0.01232 8.14	0.1480 10.01	0.1876 51.87
F1Lr	fn [Hz] ξn [%]	0.007706 −8.05	0.1640 11.20	0.1694 55.08
F2Lr	fn [Hz] ξn [%]	0.009915 2.65	0.1685 6.83	0.2105 52.72
F2Le	fn [Hz] ξn [%]	0.01140 2.01	0.1630 2.17	0.1391 68.26

TABLE 2.12−1: EIGENVALUES OF INTEGRAL MODELS

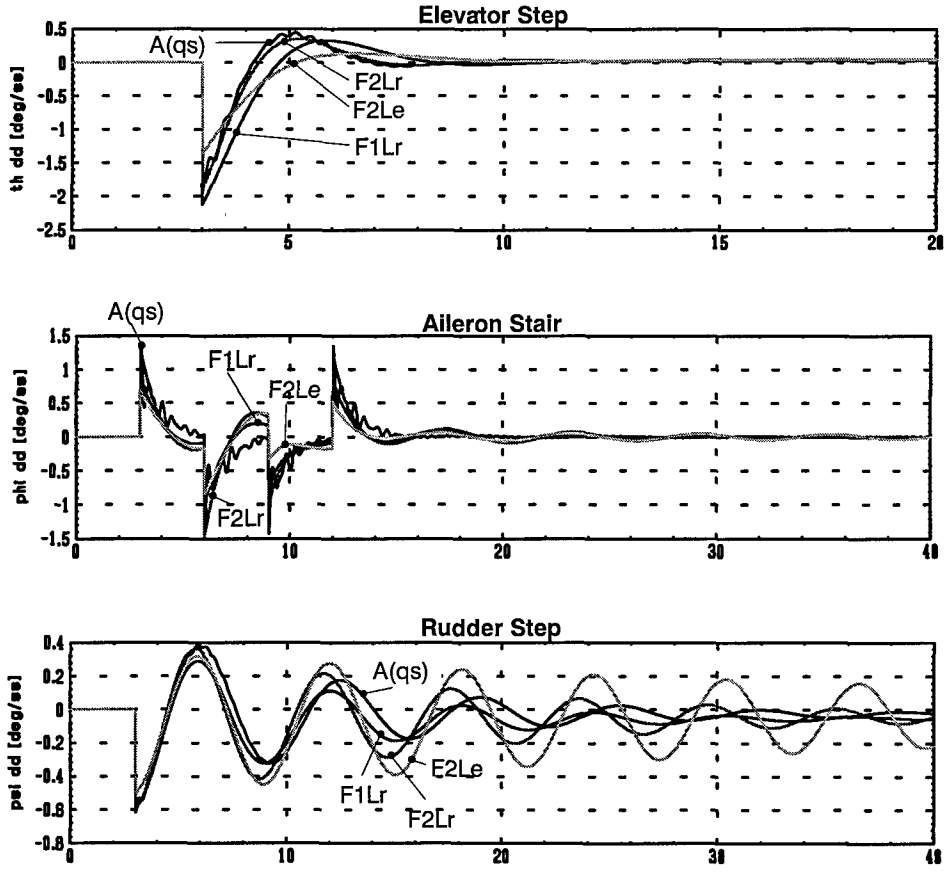

FIG. 2.12−1: ACCELERATION RESPONSE TO CONTROL COMMAND (Comparison of Data)

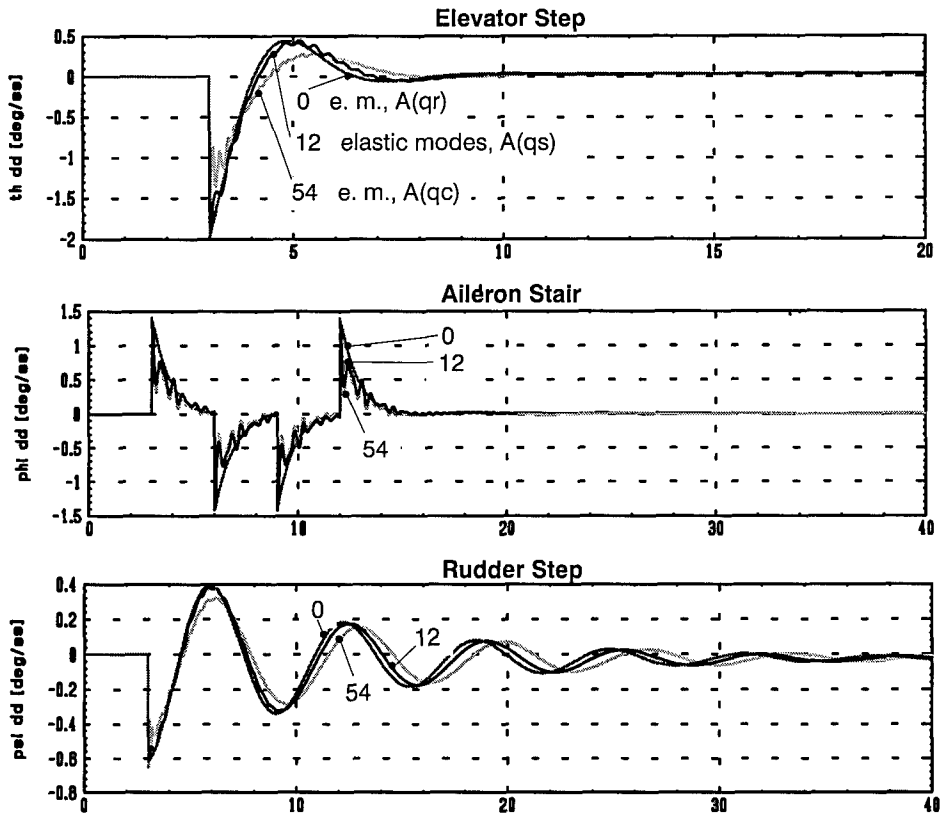

FIG. 2.12–2: ACCELERATION RESPONSE TO CONTROL COMMAND (Influence of Number of Elastic Modes on Rigid–Body State Response)

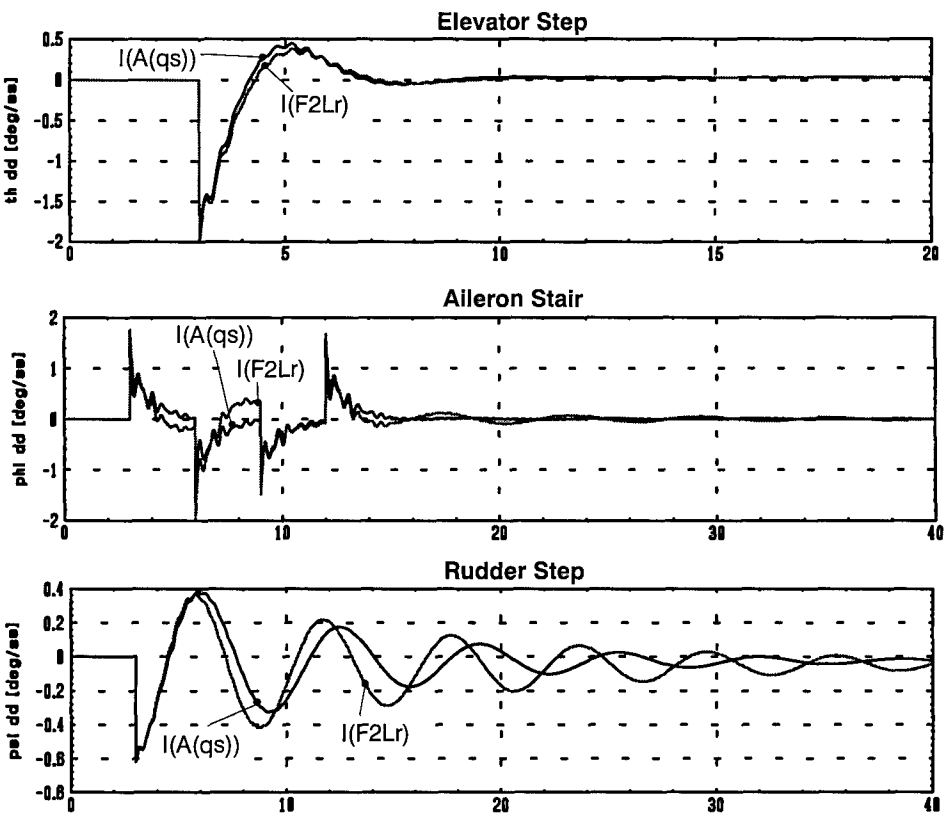

FIG. 2.12–3: ACCELERATION RESPONSE TO CONTROL COMMAND (Comparison of Integral Models Based on Aeroelastics A(qs) and on Flight Mechanics F2Lr)

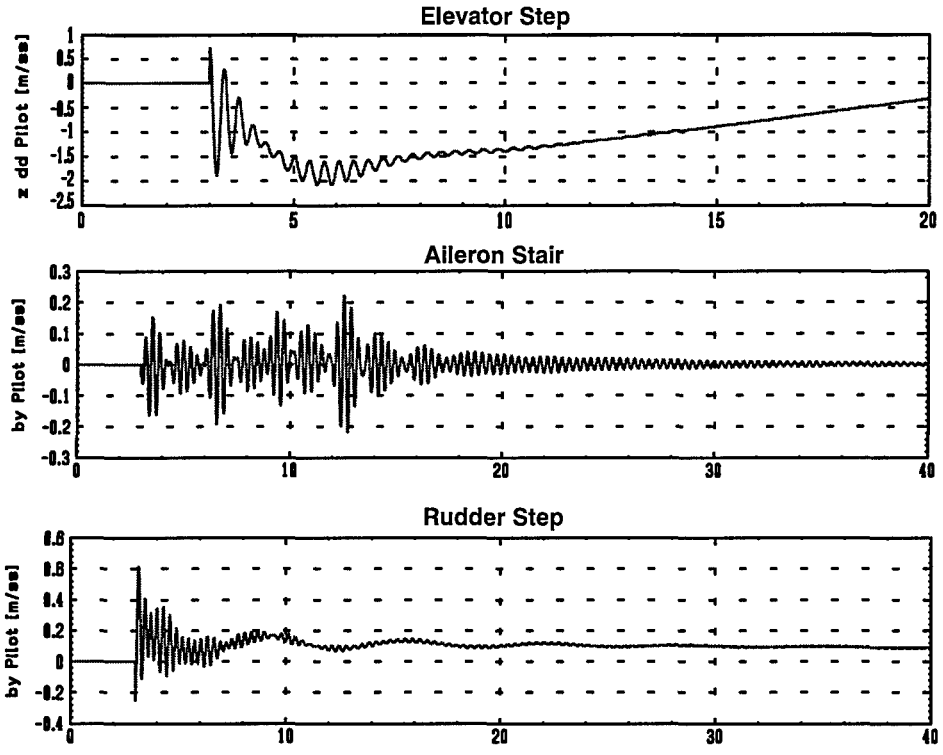

FIG. 2.12–4: PILOT ACCELERATION IN ELASTIC A/C

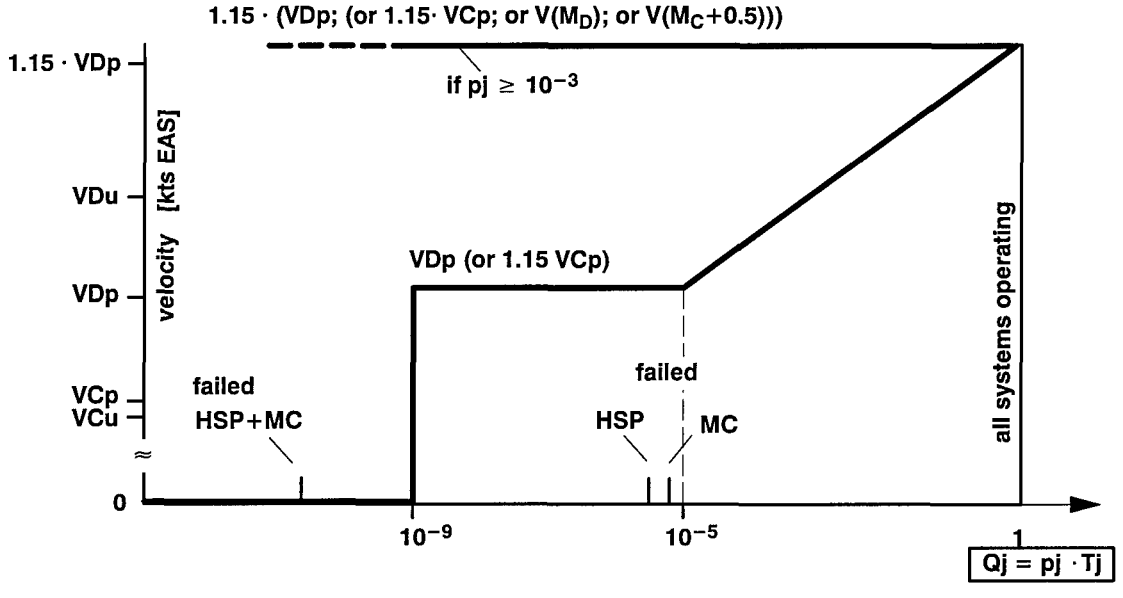

Probability of being in failure state Qj = pj · Tj with average time Tj spent in failure condition and pj probability of occurrance of failure mode per flight hour.

e.g.:

VDu – VCu ≈ 60 kCAS unprotected
VDp – VCp ≈ 35 kCAS protected

FIG: 3.2–1: REQUIRED FLUTTER SPEED (NPA 25C–199/ACI 25.302 § 4.1.2.2)

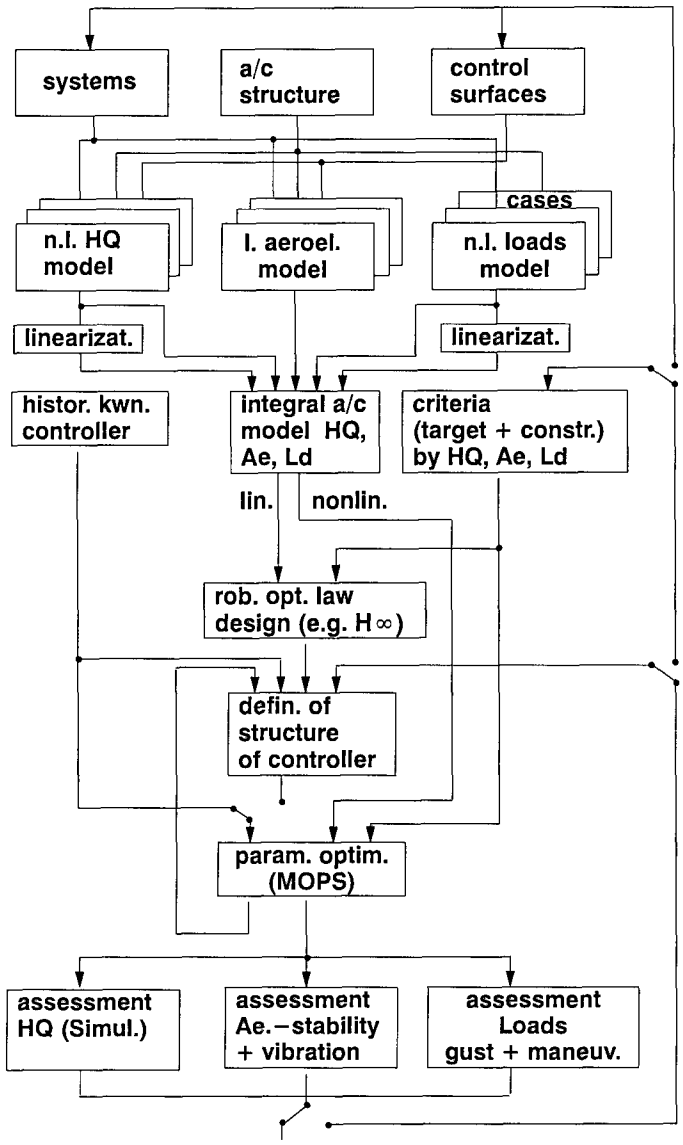

FIG. 3.3–1: INTEGRAL CONTROL LAW DESIGN

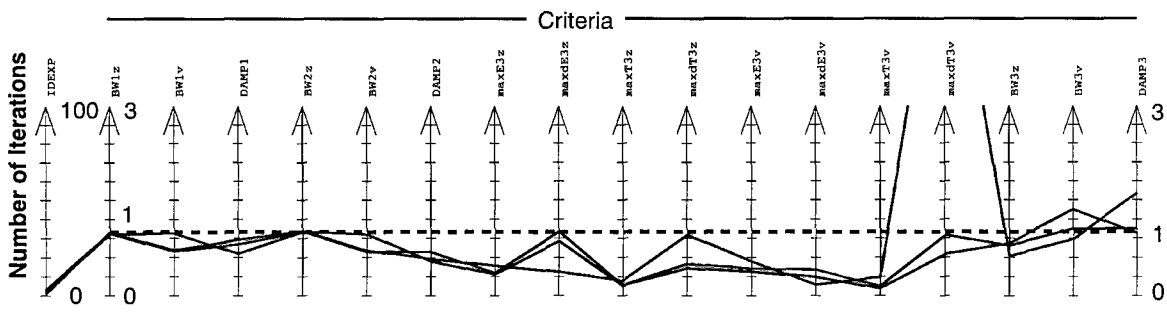

Development of Design Criteria per Iteration

FIG. 3.3–2: MULTIOBJECTIVE PARAMETER OPTIMIZATION

DESIGN OF CONTROL LAWS FOR ALLEVIATION OF GROUND - INDUCED VIBRATIONS

W.R. Krüger,* W. Kortüm
DLR - Institute for Robotics
& System Dynamics, AE-OP
Münchner Strasse, 20
D - 82234 Wessling

1 Summary

An aircraft is subject to a great number of different loads during one operational cycle. For the aircraft, not only the flight loads but also the ground loads are of importance. A crucial point is therefore the development of airframe and landing gears in an integrated design process.
Semi-active landing gears are able to effectively suppress fuselage vibrations which have been excited by an uneven runway. During the design process of such control structures the dynamics of landing gear and airframe have to be known.
At the example of the control design for a semi-active damper it will be shown how existing design tools can be used for the integrated design process. The design process will be described and simulation results for aircraft with semi-active landing gears controlled by a skyhook controller and a state feedback controller.

2 Introduction, Problem

2.1 Landing Gears as a Source of Resonance Problems for Elastic Aircraft

An aircraft is subject to a large number of different loads in its lifetime. During an operational cycle, not only flight maneuvers and gusts but also the ground operations add their share to the loads acting on the aircraft. Obviously, ground loads are design factors for the landing gears, but, less evident, also for large parts of the airframe. Next to the loads of the touch-down further load peaks result from the accelerations induced by single obstacles (e.g. repaired patches of runway or thresholds) or rough runways. These accelerations might well be of higher amplitude than those resulting from the landing impact.
For operation on an aircraft the landing gears have to comply with the certification requirements, which deal mainly with landing gear strength by rather rough estimations of ground loads acting on the aircraft, but the resulting dynamics of the aircraft on the landing gears is also of great importance and not addressed in those requirements. If the design has weaknesses in the interaction of the components, runway undulations can induce vibrations into the fuselage which can become so large, especially if a resonance frequency of fuselage or wings is excited, these vibrations are not only bothersome but can become a serious danger for a safe aircraft operation.
The lighter and the longer a transport aircraft becomes, the greater is the danger that it will encounter such a resonance problem. One reason for the large number of slender aircraft today is the airframers' standard procedure of stretching existing aircraft by introducing fuselage sections while retaining as many components of the original type as possible to reduce development time, costs and certification effort. However, a combination of system parameters that performed well for the original design might perform unsatisfactorily for a derivative type.

2.2 The Conventional and the Integrated Design Process

Airframers very often assign the design and manufacturing of landing gears to specialized companies. As a rule, the basic aircraft configuration will be determined at a very early stage in the development process. With these basic data, the specialist develops a landing gear. In parallel, the airframer develops the airframe structure which is in part - e.g. around the landing gear attachments and at the rear fuselage - itself dependent on the layout of the landing gear.
However, the optimization of single system components does not guarantee the optimal layout of the integrated system. The later problems of dynamic interaction between airframe and landing gears are discovered, the more difficult and expensive an alternative solution will become, if a completely satisfactory solution can be obtained at all.
It is clear that the consideration of the influence of components on each other has a significant impact on the design process. Neither the airframer nor the landing gear manufacturer can expect the design data to remain constant over the design time. Significant factors, as e.g. aircraft weight and airframe natural frequencies, are subject to constant changes. The design strategy has to be do flexible that model changes can be quickly intro-

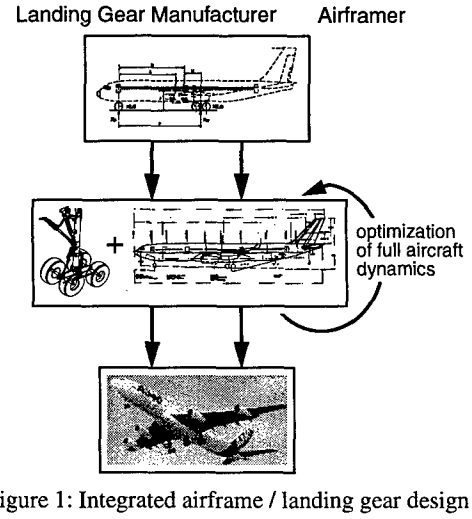

Figure 1: Integrated airframe / landing gear design [1]

Paper presented at the RTO AVT Specialists' Meeting on "Structural Aspects of Flexible Aircraft Control", held in Ottawa, Canada, 18-20 October 1999, and published in RTO MP-36.

duced. The management of data of decentralized origin is essential, and the modifications in calculation methods must be included into the design process immediately. The "integrated design" requires a close coordination of all companies and engineering disciplines involved.
Numerical simulation is an invaluable tool for the integration of system components. It allows the user to analyze his system up to any chosen degree of complexity, to determine physical variables (e.g. forces, acceleration) at any given point of the system, to change design parameters and perform numerical optimizations, and, by doing so, to keep the costs of the aircraft design down.
The importance of this topic has led to a project in the course of the German aerospace research program, "Flexible Aircraft: Integrated Airframe / Landing Gear Development". An overview over the project and its results has been given in [1].

2.3 Landing Gear Control

Suspensions, not only of aircraft, but also of other ground transport vehicles, are subject to a so-called "design conflict". Many requirements which have to be fulfilled are partially contradictory. In the case of the aircraft, the requirements for the landing impact (a landing with high sink speed; to keep the structural weight as low as possible, the shock absorber will be designed such that the loads for the certification case are minimized) lead to a relatively soft damping factor allowing the use of the full shock absorber stroke. For taxiing, however, a high damping factor is desirable to reduce aircraft pitch and heave motions. Obviously, only one of these conditions can be fully met with a fixed-orifice shock absorber. To satisfy both requirements, modifications at the shock absorber can be made. Possible alternatives to the fixed-orifice shock absorber are systems with stroke-dependent damping (the so-called "metering pin", which is also used to optimize the shock absorber performance at touch-down) [2] or a double-stage shock absorber which varies either the air spring stiffness or the damping factor as a function of the load. A variable damping system (the so-called "taxi-valve") is used in the main landing gears of large aircraft. While taxiing, a high damping factor is used, at high loads (e.g. at the landing) a spring-supported valve is opened to obtain a small damping coefficient. Such a taxi-valve has been investigated in the course of the above-mentioned "Flexible Aircraft" project.
One way to avoid such a design conflict is the use of a semi-active damper. As a conventional oleo, this damper is set up of a gas spring and, in parallel, an oil damper. However, the damper makes use of a variable valve which can be controlled to allow arbitrary damping factors (figure 2). Such a semi-active damper cannot introduce energy into the system aircraft / landing gear. Only for the valve motion a small amount of external energy is needed. It is possible to use such systems for an optimization of the landing impact [3], the study presented here, however, only deals with the rolling case. Semi-active shock absorbers are state-of-the-art in automotive, truck and railway applications [4]. For aerospace applications, though, no system is, to our knowledge, commercially available. In the EU-project ELGAR, the landing gear manufacturer Liebherr Aerospace Lindenberg has built a test-rig with a modified production landing gear which was able to demonstrate the feasibility of the technology [5].

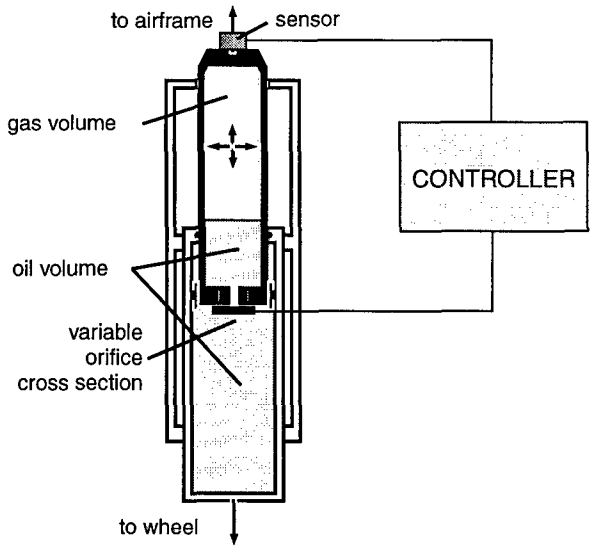

Figure 2: Semi-active oleo [1]

3 System Analysis Tools

3.1 Multibody Systems

For a thorough analysis of a technical system the results of a number of engineering disciplines from the areas of computer aided manufacturing (CAE) have to be introduced into the simulation. A powerful tool for the development of dynamic systems is the method called multibody simulation (MBS). In the DLR, the multidisciplinary simulation program SIMPACK has been developed which allows the integration of models from different CAE products as CAD (Computer Aided Design), FEA (Finite Element Analysis) and CACE (Computer Aided Control Engineering). Specialized programs of other disciplines, e.g. hydraulics or CFD (Computational Fluid Dynamics) can be connected by co-simulation. Thus, the calculation and evaluation of a complex system can be achieved with the desired precision and high calculation speeds. The multibody simulation forms the core of such a multidisciplinary design environment.

3.2 SIMPACK

The MBS tools SIMPACK, [6], has been developed at the DLR as a tool for the analysis of dynamic structures for aerospace applications as well as for ground transport vehicles and robotics. By continuous development the program has evolved into a mechatronic simulation and design tool. The basis of SIMPACK is formed by efficient algorithms for the generation of equations of motion of the model [7], which can be set up by using a graphical interface. The equations of motion can be or-

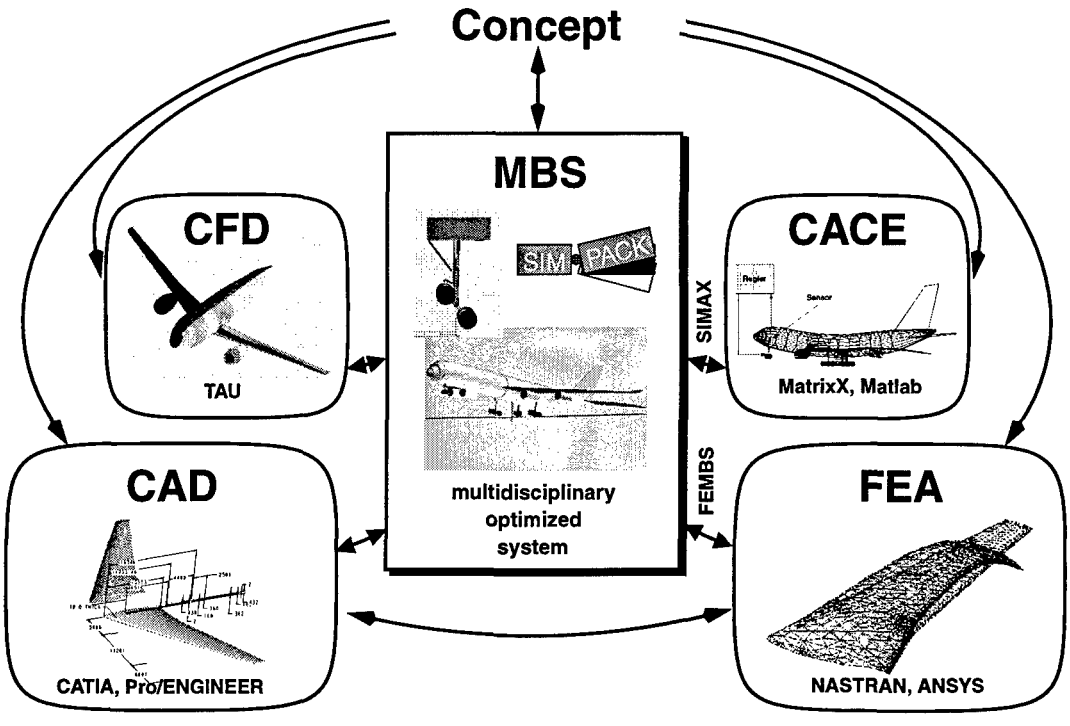

Figure 3: Tools for the integrated design

dinary differential equations of differential-algebraic equations (e.g. for closed kinematic loops). Several fast and specialized integrators for the solution of those (nonlinear) equations are available, [8], as well as all the "classical" methods for linear system analysis, e.g. linearization, eigenvalues, frequency response, stochastic analysis in the time and frequency domain. Methods of parameter variation and a multi-objective parameter optimization [9] have become an invaluable tool for many research and industrial applications.

SIMPACK has bi-directional interfaces to many CAE tools, cf. figure 3. For this work, the three interfaces that are most important are the integration of elastic bodies from FEA models, the controller definition in MATLAB or MATRIXx, and the connection to the multi-objective parameter optimization. As an example, the following paragraph will present those interfaces to MATRIXx that have been used in the control design and optimization for the semi-active damper.

3.3 MATRIXx

MATRIXx by ISI (Integrated Systems) is a tool for control design and system analysis which comes with a block-oriented simulation environment ("SystemBuild"). The package is similar in structure and complexity to MATLAB / Simulink by MathWorks, which is no coincidence, since both programs evolved from the same roots, the original Matlab by Little and Moler (cf. [10]).

MATRIXx / SystemBuild has different interfaces for model import and export which have been connected to SIMPACK via the interface package "SIMAX".

3.4 SIMAX

Using SIMAX, models can be set up in SIMPACK, and made available to MATRIXx for control design and simulation.

The Linear System Interface

SIMPACK models can be linearized and exported in the form of linear system matrices in a MATRIXx-readable format. Inside SystemBuild, the model can be used directly in a state-space block. This interface allows a very fast model export, a restriction is that it is, as the name says, limited to linearized models and a re-transfer of the results is not possible.

Symbolic Code Interface

Models with non-negligible nonlinear effects can be exported in a platform independent way in the form of so-called *Symbolic Code*. Here, SIMPACK generates model dependent, portable FORTRAN code which can be connected to the SystemBuild UserCode Block interface. The symbolic code can also be converted into C to be used in a Hardware-in-the-Loop environment.

Function Call Interface

The most comfortable interface is the Function Call Interface which allows to include SIMPACK in its full functionality. It also works using the UserCode Block. The numerical integration is performed in MATRIXx which calls SIMPACK for the right-hand-side for the equations of motion, the results can afterwards be plotted and animated in SIMPACK. Models with closed kinematic loops can also be integrated separately in the respective packages, using discrete co-simulation, with all SIMPACK post-processing capabilities available. Using inter-process-communication (IPC), MATRIXx and SIMPACK can also run on different platforms.

SIMAX[1]: "AutoCode" - Import

After a control design concept is set up in SystemBuild, any chosen parameters can be defined as free and the control structure can be exported. For this kind of model export, MATRIXx offers the - separately licensed - module "AutoCode" which generates C code from SystemBuild models. This code can be used as a user-defined controller and connected to the multibody simulation via the SIMPACK programmable interface. All these functionalities allow the model setup inside SIMPACK, a model export to MATRIXx in a way adjusted to the desired complexity, a control design inside MATRIXx/SystemBuild, and a re-import of the control structure after the control design for a fast parameter optimization or verification and evaluation simulations in SIMPACK.

4 Control Concepts for a Semi-Active Damper

4.1 Landing Gears of Variable Characteristics

Conventional landing gears are suspensions with fixed spring/damper characteristics. Those passive systems are restricted to generating forces in response to *local relative* motion. To obtain an improved performance with respect to comfort and loads the suspension characteristics can be made adaptable to aircraft parameters, as well as to environment conditions, e.g. the quality of the runway. Active systems may generate forces which are a *function of many variables*, some of which may be remotely measured, e.g. aircraft weight and forward speed. Adaptive suspensions are already state-of-the-art in automotive and railway applications.

Basically, two different adaptive suspension strategies exist. A first step is a non-feedback setting of spring or damper characteristics according to the expected runway quality and aircraft weight prior to touch-down, and keeping those suspension characteristics constant during roll. This variant has been examined by Somm, Straub, Kilner in 1978 [11] who used a gas spring with an adaptive pressure which was used for military aircraft landing on unpaved runways. Another variant of this suspension type are those suspensions of luxury cars which can be switched between sportive and comfortable operating modes.

A further step is the feedback of vehicle motion and, consequently, a suspension control. The basic sensor and control layout is similar for most systems and has already been described in the seventies and eighties by Corsetti/Dillow [12] for aircraft and Karnopp [13] for ground vehicles: a sensor at the vehicle measures acceleration and velocity of the sprung mass and suspension deflections and, via a control law, results in a change of suspension characteristics.

In 1984 an AGARD conference was dedicated to the state-of-the-art of active suspensions [14]. Freymann proposed a fully active nose landing gear for the reduction of ground loads [15]. Most investigations, however, were dedicated to the reduction of peak loads at landing impact. One example was the study of active landing gears for an F-106 fighter [16].

4.2 Semi-Active Control

The idea of a semi-active damper for use in suspension systems has already been introduced in the early seventies by Karnopp [17]. Catt/Cowling/Sheppard performed simulation studies on semi-active aircraft suspensions [18]. Wentscher [2] investigated the use of a semi-active Skyhook-controller for an A300 model. Duffek [19] developed a semi-active control concept for landing which could be combined with a control concept for ground ride.

The concept of semi-active control is to use a variable damper to produce suspension forces that can be influenced by a feedback controller. Thus, the force input was is achieved using a servomechanic device requiring an external power supply as in [15] and [16] but rather with a controllable dissipative device (hence, semi-active control is sometimes also known as *active damping*, [18]).

In a semi-active damper the applicable force depends on the sign of the stroke velocity across the damper, see figure 4. Since the damper can only dissipate energy, forces can only be produced in the first and third quadrant of the force / stroke velocity plane, i.e. a positive force F_d in the sense of figure 4 can only be fulfilled while the oleo is compressing, a negative force can be fulfilled by an expanding oleo. If the controller commands a negative force during oleo compression, the best that can be done is to generate only a compression force as small as possible, in other words, to open the orifice as far as possible. Keeping this in mind the semi-active damper is an inherently highly non-linear device which has to be able to switch from force generation to near zero force in a very short time.

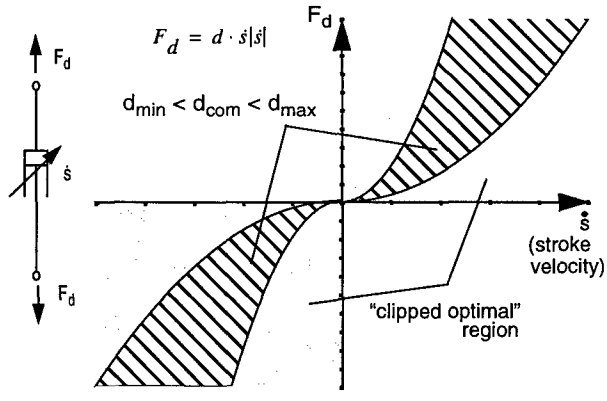

Figure 4: Semi-active control

A controller with a semi-active control scheme is often designed as if it was a fully active system. Control commands that lie in quadrant 2 and 4 of figure 4 are then set to zero. This is known as a "clipped optimal" approach.

A technical semi-active damper, on the other hand, has a minimum and a maximum orifice size for the oil flow, resulting in a respective minimum and maximum con-

trollable damping coefficient. Therefore, a clipped optimal scheme has to be replaced by a realistic, limited system, setting boundaries for the commands for technical realization.

In this work the control has been designed using fully active approaches. The control parameters have then been optimized on the semi-active model with control command boundaries.

It should be noted that the control input for the system by both skyhook (section 4.3) and state feedback (section 4.4) control is a force which is a direct function of the system output, be it measurements or the state vector, and can be positive or negative. The oleo, however, works with an (always positive) orifice cross-section as control input. This requires first a check of the applicability of the control force. The commanded force can only be applied if it acts in the same direction as the current stroke velocity. Second, the force has to be transformed into a damping factor, taking into consideration minimum and maximum damping factor if the control law is not considered to be "clipped optimal":

$$d = \begin{cases} F/\dot{s}|\dot{s}| & \text{if} \quad \operatorname{sgn}(F) = \operatorname{sgn}(\dot{s}) \\ d_{min} & \text{if} \quad \operatorname{sgn}(F) \neq \operatorname{sgn}(\dot{s}) \end{cases}$$

$d_{min} = 0$ for clipped optimum

$d_{min} < d < d_{max}$ for non-clipped optimum

Finally, the commanded damping factor can be converted into a commanded orifice cross section.

4.3 Skyhook-Controller

In the literature several algorithms for active suspension control are proposed. One of the most simple, yet effective approaches is the "Skyhook" controller by Karnopp [13]. At this control scheme the actuator generates a control force which is proportional to the sprung mass vertical velocity. The skyhook principle can be shown on a simple, yet representative example ([20], see figure 5).

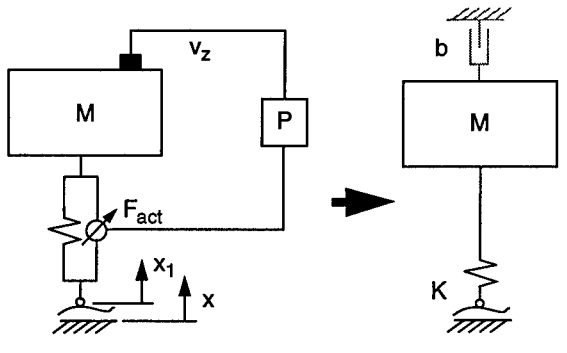

Figure 5: Skyhook control principle

The equation of motion of the one-degree-of freedom model is as follows:

$$m\ddot{x} = F$$

Now, the vertical acceleration of the mass $\ddot{x}$ as well as the suspension stroke shall be minimized. This leads to a classical optimization problem, the solution of which is shown in detail in [21] and [22]. Here, only the solution will be given - the optimal actuator force F_{act} will be

$$F_{act} = K(x - x_1) - b\dot{x}$$

This force law could be realized with a passive system if the mass was connected to the excitation by a spring with stiffness K, carrying the static weight, and to the inertial frame by a damper with damping factor b - the name "Sky-Hook" has been derived from this result. However, for obvious reason this passive solution is not feasible for aircraft. The answer to the problem is to place an actuator parallel to the spring and feed back the vertical velocity of the mass to simulate a fictitious damper to the inertial system.

Even though the derivation of the control law has been done for a single mass system, the same conclusions are true for a two-mass model (in automotive applications also known as the "quarter car model"), the "classic" dynamic model for suspension layout (see figure 7). The limitation applies hat not all control commands can be completely fulfilled by a semi-active controller, however, the commands can be realized in good approximation.

The main advantages of the skyhook damper are its simple implementation and relatively small size which often make the skyhook approach the reference control law which has been implemented in automotive applications a number of times (see [4], [23]).

The proportional gain of the Skyhook controller can be complemented by dynamic control elements. Wentscher, e.g, optimized a lead-lag controller for an A300 model [2].

In this study, the use of a PD-controller has proven to be useful.

4.4 State Feedback Controller

State feedback is a means to control the motion of a system by feeding back the state vector x via a control matrix K into a control signal u

$$u = K \cdot x \,.$$

The system performance can be modified this way since x contains all information about the process. The desired dynamic properties of the controlled system are obtained by the choice of the matrix K. The performance limits of the actuator concerning maximum frequency and maximum force level have to taken into consideration.

As a rule, in a complex system not all states are directly accessible. Thus, either a limited state feedback control is used or a state observer has to be designed. State observer and state controller can be designed independently.

Taking into consideration the stochastic excitation (e.g. runway unevenness) and measurement noise, the observer used has the form of a Kalman-Bucy filter [10]. A time-invariant (stationary) filter is sufficient for this application. Prerequisite are good estimations about measurement noise and the spectral density of the exci-

tation. For an implementation it is important to remember that the Kalman-filter has the same number of additional states as the model to be observed [10].
If the state vector is known, the state feedback controller can be designed. For this purpose there exist a number of methods, some of the most well-known the Pole Placement and the LQR (linear quadratic regulator) - method which have been used in suspension layout [23]. In this study, from the state vector x a number of states and measurements have been selected via a measurement matrix H which were then multiplied with a weighting vector $q = q_1, q_2, ..., q_n$. The actuation effort was introduced by a criterion r. The cost function which shall be minimized as follows:

$$J = \int_0^\infty (x^T H^T q H x + u^T r u) dt$$

Starting values for the parameters q_i and r for a subsequent numerical optimization were chosen according to Bryson and Ho [22].
The design of Kalman-filter and state controller are supported by standard MATRIXx functions, so observer and controller design took place completely in MATRIXx.

5 Control Design

5.1 The Model

The model used for the control design has been derived from the model described in [1]. The aircraft configuration is that of a large civil transport aircraft with a maximum landing weight of 250 tons, a two-wheel nose landing gear, two main landing gears (four wheels, bogie) and a two-wheel center landing gear.

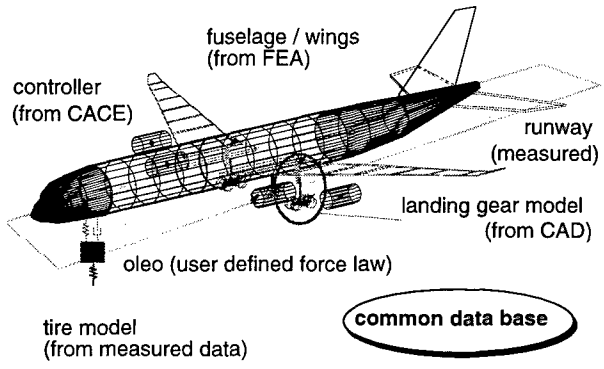

Figure 6: Aircraft model

Airframe
The airframe is described by a single MBS body. The structure has been derived from a NASTRAN finite element model of the complete structure which had been set up for loads and deformation analysis. Inside NASTRAN, a modal analysis was performed and the data transferred into SIMPACK via the pre-processor FEMBS in which the modes of interest for the simulation were selected [24].
Natural frequencies up to 15 Hz were included in the model. By doing that, 14 to 16 equations (16 when using static modes) were added to the equations of motion. A frequency dependent modal damping was introduced for all structural modes.
Landing Gear
The landing gear was modeled as a "classical" rigid body MBS system. The elasticity of the landing gear has been introduced as spring elements in the joints. The effects that were taken into consideration were horizontal motion ("gear walk" induced by spin-up of the wheel or braking) and the attachment stiffness between landing gear and airframe. The wheel has a rotational degree of freedom, the tire is modeled as a point follower with a vertical spring and horizontal slip.
The oleo consists of an air spring and a damping element in parallel. The passive damper corresponds to the one optimized in [1] (taxi-valve type). The semi-active damping has been described above in section 3.1 and 3.2.
Two-Mass-Model
For basic considerations and first realization studies the model of a "two-mass landing gear" was used, consisting of the complete landing gear, but replacing the elastic aircraft structure with an equivalent substitution mass (see figure 7). This model also plays a role in the certification rules according to (FAR 25).

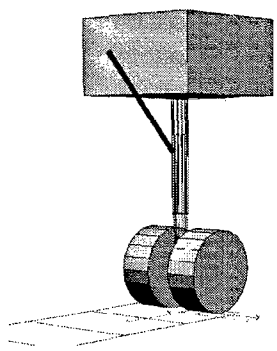

Figure 7: Conventional two-mass model

5.2 Controller Design

The controller design was performed in three steps. In the first step, the control concept was developed and set up in MATRIXx/SystemBuild. The controller was designed using a model exported from SIMPACK. The simulation used for design was based on a stochastic runway. Figure 8 a shows the skyhook controller as a SystemBuild block diagram. The inputs and outputs defined in the block correspond to the inputs and outputs of the SIMPACK programming interface.
Figure 8 b demonstrates the state controller in a SystemBuild simulation environment in a direct comparison to a passive model. In both cases the MBS model was first a two-mass model which was later replaced by a full aircraft model without a change in the control structure.
In a second step, the structure of the controllers was exported from MATRIXx by producing C-code with the help of MATRIXx "AutoCode" which was then implemented as a SIMPACK user force element. The parameters of the controller were subsequently optimized with MOPS, the Multi-Objective Parameter Synthesis tool. The model used was a more complex optimization

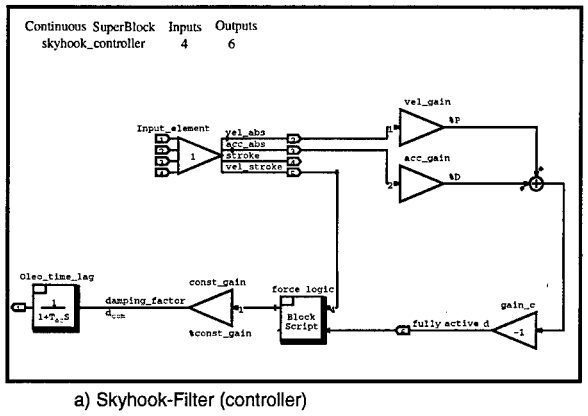

a) Skyhook-Filter (controller)

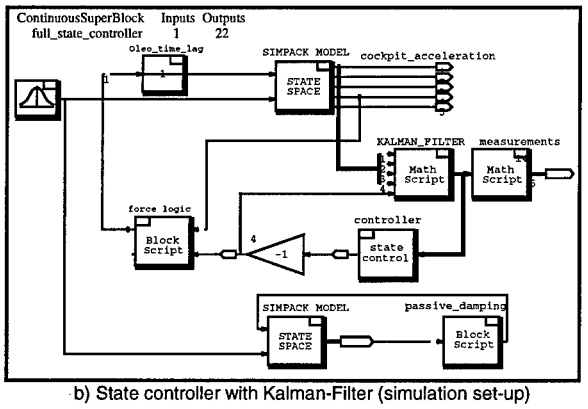

b) State controller with Kalman-Filter (simulation set-up)

Figure 8: Implementation of control laws in SystemBuild

model, the excitation used was a measured runway profile. The free parameters were, in the case of the skyhook controller, the gains P and D, in the case of the state controller the weighting factors r and $q_1 ... q_n$.
In the last step, a large number of comparison runs were undertaken for an evaluation of the semi-active model vs. a passive one using a full evaluation model, different load cases and different speeds.

6 Results

The evaluation was performed on the basis of the vertical cockpit accelerations. Here, the amplitude of the aircraft time response was one of the main criteria. Furthermore, the frequency response was of special interest, since comfort as well as load criteria are frequency dependent. For all cases, the results obtained with the semi-active landing gear were compared with those obtained for the passive reference suspension.
Figure 9 shows a comparison of the time response plots for an excitation by a measured runway. It is interesting to note that both controlled systems remain well below the level of the passive aircraft, however, no great difference can be seen between the skyhook and the state feedback controller. Both systems achieve approximately the same reduction of peak response.
The situation is somewhat different when the accelerations are analyzed in the frequency response (figure 10). Here it can clearly be seen that the skyhook controller can effectively damp the aircraft response in the low frequency range (rigid body pitch and heave motion up

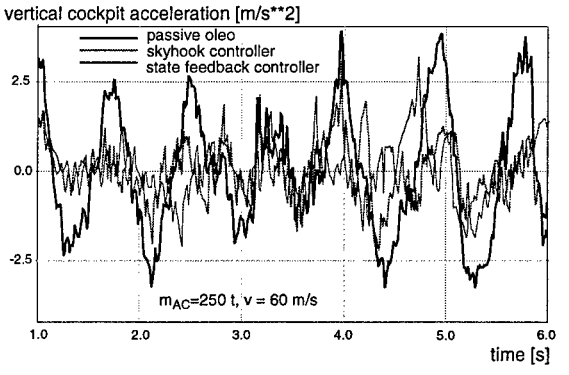

Figure 9: Comparison of simulations, time response

to a factor of 10) but can lead to a response above the passive system for the natural frequencies of wings and fuselage (see figure 10, ca. 3.5 Hz and above). The state feedback controller, on the other hand, can be tuned by the correct choice of the weighting factors such that arbitrary natural frequencies can be damped.

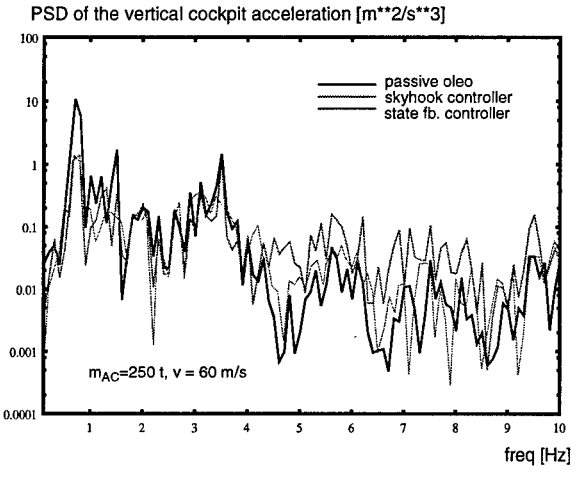

Figure 10: Comparison of simulations, frequency response

Physical limits are set by the performance of the actuator, the maximum size limiting the oil flow and the fact mentioned above that a semi-active controller cannot introduce energy into the system and is thus not able to execute all control commands.

7 Summary and Outlook

The integrated design process of modern transport aircraft includes interdisciplinary simulation and optimization methods as well as data exchange over company and country borders. In the development of landing gears there is still potential for improvement.
It could be shown at the example of a suspension layout how an integrated airframe / landing gear design can be performed using a design environment centered around the dynamic multibody simulation. The key elements are interfaces between the common tools of aircraft and landing gear design, i.e. CAD, FEA, and control design. These interfaces have to be bi-directional to allow not only a fast transfer of models but also a quick re-transfer of the results obtained in the simulation and optimiza-

tion to all involved disciplines.
With the methodology presented alternative suspension concepts as semi-active suspensions can be studied in parallel to conventional designs, and their improvement potential can be assessed. Semi-active systems allow the adaptation of the damper characteristics as a function of aircraft motion and can be used to effectively suppress resonance oscillations of fuselage and wings.
In the course of the study a skyhook and a state feedback controller were designed and were subject to a performance comparison. Furthermore it was tested how the used design software is capable to support the design of different control concepts.

8 Bibliography

[1] Krüger, W.R., Spieck, M.: "Interdisciplinary Landing Gear Lay-Out for Large Transport Aircraft", Proceedings of the AIAA/USAF/NASA/ ISSMO Symposium on Multidisciplinary Analysis and Optimization (AIAA-98-4964), St. Louis, 1998

[2] Wentscher, H.: "Design and Analysis of Semi-Active Landing Gears for Transportation Aircraft", DLR-Forschungsbericht 96-11, Oberpfaffenhofen, 1996.

[3] X. Wang, U. Carl: "Fuzzy Control of Aircraft Semi-active Landing Gear System", AIAA 99-0265, 37th AIAA Aerospace Sciences Meeting and Exhibit, Reno, NV, Jan. 1999

[4] O.
ß, M. Valasek: "COPERNICUS, Semi-Active Damping of Truck Suspensions and their Influence on Driver and Road Loads", Final Technical Report. SADTS, CIPA-CT-94-0130, DLR (Project Coordinator), Weßling 1998

[5] European Union (publ.): ELGAR - European Landing Gear Advanced Research, Project Summary, to be published in 1999.

[6] Kortüm, W., Rulka, W., Spieck, M.: "Simulation of Mechatronic Vehicles with SIMPACK", MOSIS 1997, Ostrava, Czech Republik 1997.

[7] Eichberger, A.: "Simulation von Mehrkörpersystemen auf parallelen Rechnerstrukturen", Fortschrittsberichte VDI, Reihe 8, Nr. 332, 1993.

[8] Eich, E., Führer, C.: "Numerische Methoden in der Mehrkörperdynamik", in: Bachem, A., Juenger, M., Schrader, J. (editors): "Mathematik in der Praxis - Fallstudien aus Industrie, Wirtschaft, Naturwissenschaften und Medizin", Springer Verlag Heidelberg, 1995.

[9] Grübel, G., Joos, H.-D.: "Multi-Objective Parameter Synthesis (MOPS)", in: Magni, J.-F., Bennani, S., Terlouw, J. (editors): "Robust Flight Control - A Design Challenge", Lecture Notes in Control and Information Sciences 224, Springer Verlag London Limited, 1997.

[10] Kortüm W., Lugner P.: Systemdynamik und Regelung von Fahrzeugen. Springer Verlag Berlin, Heidelberg, New-York 1994

[11] P. T. Somm, H. H. Straub and J. R. Kilner: Adaptive landing gear for improved taxi performance. Boeing Aerospace Company,1977, AFFDL-TR-77-119

[12] C.D. Corsetti, J. D. Dillow: A Study of the Practicability of Active Vibration Isolation Applied to Aircraft During the Taxi Condition, Technical Report AFFDL-TR-71-159, Air Force Flight Dynamics Laboratory, Wright-Patterson Air Force Base, Ohio, 1972

[13] D. Karnopp: "Active Damping in Road Vehicle Suspension Systems". in: Vehicle System Dynamics, 12(6), Swets & Zeitlinger, Lisse, 1983

[14] Landing Gear Design Loads (CP 484), AGARD,1990

[15] R. Freymann: An active control landing gear for the alleviation of aircraft taxi ground loads. Zeitschrift für Flugwissenschaft und Weltraumforschung, 1987

[16] W.E. Howell, J.R. McGehee, R.H. Daugherty, W.A. Vogler: F-106 airplane active control landing gear drop test performance. in: Landing Gear Design Loads (CP 484), AGARD,1990

[17] D. Karnopp, M. Crosby, R.A. Harwood: Vibration control using semi-active force generators. Journal of Engineering for Industry, No 96, pages 619-626, 1974

[18] Tyrone Catt, David Cowling and Alan Shepherd: Active landing gear control for improved ride quality during ground roll. Smart Structures for Aircraft and Spacecraft (AGARD CP 531), Stirling Dynamics Ltd, Bristol, 1993

[19] W. Duffek: Active Shock Absorber Control During Landing Impact. Final Report BriteEuram Research Project 2014 (LAGER 1, Task 5), IB 515/95-19, DLR, Oberpfaffenhofen 1995.

[20] J.K. Hedrick: "Railway Vehicle Active Suspensions". In Vehicle System Dynamics, 10, pp. 267-283. Swets & Zeitlinger, 1981

[21] D.A. Hullender, D.N. Wormley, H.H. Richardson: "Active Control of Vehicle Air Cushion Systems". In ASME Journal of Dynamical Systems, Measurements and Control, Vol. 93, No. 1, 1972

[22] A.E. Bryson, Y.C. Ho: Applied Optimal Control, Blaisdell, 1969

[23] E.M. Elbeheiry, D.C. Karnopp, M.E.Elaraby, A.M. Abdelraaouf: "Advanced Ground Vehicle Suspension Systems - A Classified Bibliography". In Vehicle System Dynamics, 24, pp. 231-258. Swets & Zeitlinger, 1995

[24] Wallrapp, O., Sachau, D.: "Space Flight Dynamic Simulations Using Finite Element Analysis Results in Multibody System Codes", Proceedings of 2nd Int. Conference on Computational Structures Technology, Athens, Greece, 1994.

NON LINEAR EFFECTS OF APPLIED LOADS AND LARGE DEFORMATIONS ON AIRCRAFT NORMAL MODES

M. Oliver
H. Climent
F. Rosich
Structural Dynamics and Aeroelasticity Department
CONSTRUCCIONES AERONÁUTICAS S.A.
Avda John Lennon
Getafe, 28906 Madrid, Spain

Summary

Ground Vibration Test (GVT) is the typical way to verify structural dynamic models. The conditions in which the GVT is performed –the aircraft subjected and deformed under gravity loads– are different from the conditions in which the Finite Element Method (FEM) model is usually elaborated (jig shape without loads). They are also different from the in-flight conditions (the aircraft subjected and deformed under inertia and aerodynamic forces). Although in most cases those differences can be negligible, it is not the case of a very large airplane in which the size and flexibility effects are of such nature that updating a FEM model to match GVT results could go in the opposite direction to the actual airplane in-flight. This paper analyses the influence of aircraft deformation (down bending for GVT, jig shape for FEM model, up bending for flight), shape (control surfaces deflections...), and loads (gravity on ground, inertial and aerodynamic forces in flight) on normal modes to have a better insight in GVT and flight test measurements interpretation of a very large airplane. Those effects are significant especially where large concentrated masses (engine-pylon) are present.

Nomenclature

E	Young´s modulus
f	frequency
FEM	Finite Element Method
g	gravity acceleration
GVT	Ground Vibration Test
HTP	Horizontal Tail Plane
I	polar inertia moment of cross section
L	length
m	distributed mass
MTOW	Maximum Take-Off Weight
N	axial force
N_{cr}	Euler buckling load
Ω	natural frequency
p	distributed axial force
q	distributed transversal force
t	time
v	transversal displacement
x	axial co-ordenate

Nomenclature for modal identification

nWB	nth order wing bending mode
nWT	nth order wing torsion mode
nWTX	nth order wing chordwise mode
WTT	wing tip torsion mode
IPP	inboard pylon pitch mode
IPY	inboard pylon yaw
IEY	inboard engine yaw
OPP	outboard pylon pitch
OPY	outboard pylon yaw
OEY	outboard engine yaw
ETL	engine truss lateral
ETZ	engine truss vertical
EYaw	engine yaw
ERoll	engine roll
HB	horizontal tail plane bending
HT	HTP torsion
HTX	HTP chordwise
ERP	elevator rotation in-phase
ERO	elevator rotation out of phase
IEB	inboard elevator bending
OEB	outboard elevator bending
IET	inboard elevator torsion
OET	outboard elevator torsion
EL	elevator lateral

1 Introduction

From the structural dynamics standpoint, a slender arrestor hook during the engagement phase, a rotating helicopter blade or a large flexible solar array of a spacecraft have something peculiar in common. Their dynamic behaviour can only be adequately known if the loads and/or large displacements that are acting on them are also considered.

In a simple structural element like a beam, the presence of large axial loads introduces a new term in the transversal equilibrium equation, thus modifying its solution. One of the most typical example happens when this axial load is constant: under tensile loads the natural frequency of the fundamental transverse bending modes increases while for compression loads diminishes, being zero when the compression load reaches the Euler buckling load.

New terms also appear in the beam equations when very large displacements are involved. Something similar

Paper presented at the RTO AVT Specialists' Meeting on "Structural Aspects of Flexible Aircraft Control", held in Ottawa, Canada, 18-20 October 1999, and published in RTO MP-36.

happens for other structural elements (shells, plates...) and in turn to the complex structures obtained by assembling these simple elements.

The dynamic solutions of the linear equations are no longer valid and some degree of non-linearity is introduced due to the new terms in the equations. Even in the simplest cases –beams, plates– a general solution of the equation can not be found. Approximate methods or an iterative process using the finite element technique should be used to obtain the correct solution.

This paper is devoted to analyse the effect of the applied loads and large deformations on the modes of a very large –and flexible– airliner. This topic is considered of relevance because the modes of an aircraft constitute the base for the solution of many structural dynamics and aeroelastic problems (flutter, response to gust and continuous turbulence, dynamic landing, etc.) that are necessary to consider in the certification process of an aircraft.

In the aeronautical industry, aircraft modes are computed using the finite element method (FEM). The modal base is typically defined in the jig shape in the assumption that it will span to the in-service modes. The dynamic model is validated through the modes obtained in a full-scale ground vibration test (GVT). If discrepancies arise between model and test, the model is updated to match GVT results.

This paper will show that due to the effect of large loads and displacements, some modes obtained simulating the GVT conditions (1g loads) can exhibit differences with respect to jig shape modes and also with respect to in-service modes. This effect should be taken into account during the model updating process.

Next section will be devoted to a literature survey and a brief description of theoretical background. In subsequent sections, the effect of large applied loads and deformations in the modes will be considered in a set of increasingly complex tasks (clamped wing without pylons, clamped isolated engine-pylon, clamped wing with two engine pylons fully representative of a megaliner wing). Gravity forces will be varied from –1g to 2.5g (the regular load factor envelope in the certification of an aircraft). Aerodynamic loads that equilibrate the aircraft are added to the wing in a second step to have a better insight in these two effects separately.

Large displacements can also be due to regular control surface movements or rotations. This effect is already routinely covered in the case of wing flaps –and will not be repeated herein-. Within the Airbus consortium, CASA has been responsible of the design, analysis, manufacturing and certification of the Horizontal Tailplanes (HTP). In the case of a megaliner, the horizontal tailplane area is well above 200 square meters. The effect of the deflections of the large split elevators on the HTP modes is a new problem that will be briefly described in the last part of the paper.

The paper ends with the conclusions and guidelines learned during this work.

2 Literature survey and theoretical background.

2.1 Introduction

This section is devoted to show a literature survey and a brief theoretical background of the effect of loads and large displacements on normal modes. The section is structured as follows:

- Beams under axial loads.
- Beams subjected to large applied loads and large static deformations.
- Plates under in-plane loading.
- Complex structures.

Although some of these cases are very academic, they will give a good insight into the basic principles underlying the most realistic cases that will be shown in subsequent sections.

2.2 Effect of axial loads on transverse vibration of beams

If the beam is subjected to a time invariant axial loading in the horizontal direction as shown in figure 1, in addition to the lateral loading, the local equilibrium of forces is altered because the internal axial force, N(x) interacts with the lateral displacements to produce an additional term in the moment equilibrium equation.

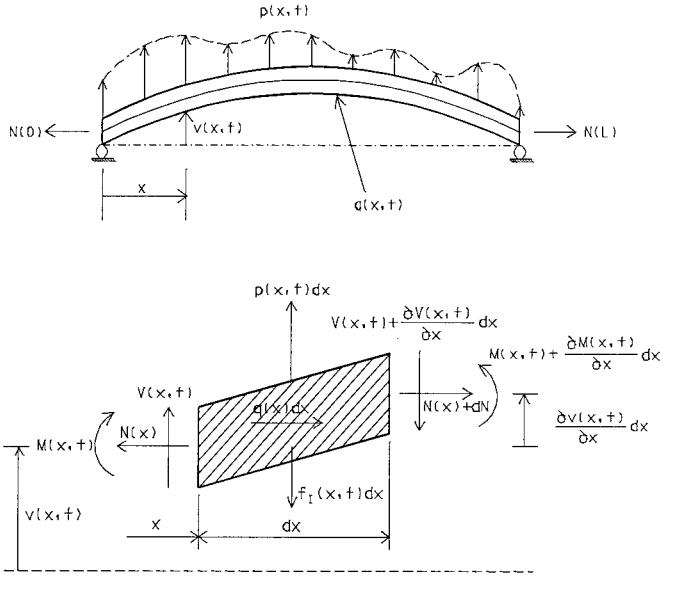

Figure 1. Beam with static axial load and dynamic transverse vibration. Upper: beam deflected. Lower: forces on a differential element.

After some manipulation, the transverse displacement of the beam is stated as:

$$\frac{\partial^2}{\partial x^2}(EI(x)\frac{\partial^2 v(x,t)}{\partial x^2}) - \frac{\partial}{\partial x}(N(x)\frac{\partial v(x,t)}{\partial x}) + \frac{\partial}{\partial t}(m(x)\frac{\partial v(x,t)}{\partial t}) = p(x,t)$$

This equation differs from the traditional one in the second term of the left hand side. As Nihous stated [1], the two last terms of the left-hand side correspond to the vibrating string, i.e. EI=0. Hence, limits of this equation for N>>EI and N=0 must reproduce the results of the vibrating string and a linear Euler beam respectively.

In most of the cases, an exact solution for the modes and frequencies of the system is difficult to obtain. The recourse would be made to one of the approximate solutions such as the Rayleigh-Ritz method, Galerkin's technique or the finite element method.

For uniform beams, the problem becomes simpler when constant axial loads are applied with various types of simple end conditions.

Galef [2] is likely the first to publish a practical formula for the natural frequencies of uniform single-span beams under a constant compressive axial force:

$$\frac{\Omega^2_{compressed}}{\Omega^2_{uncompressed}} = 1 - \frac{N}{N_{cr}}$$

where Ω stands for the natural frequencies, N is the compressive load, and N_{cr} is the Euler buckling load. The work of Shaker [3] is the first systematic approach to investigate three common problems in aerospace structures: a vibrating beam with arbitrary boundary conditions, a cantilever beam with tip mass under constant axial loads and a cantilever beam with tip mass under axial loads applied on the tip directed to the root. Another value added of the Shaker work is that it extends the analysis also to tension loads.

Continuing the Galef's work, Bokaian [4] establishes the set of boundary condition for which his approximation is correct, and studies the influence of a compressive load on natural frequencies and mode shapes in ten different combinations of boundary conditions. It is interesting to quote the final conclusions of Bokaian: " it is seen that Galef's approximate relationship is valid not only for clamped-clamped, clamped-pinned, pinned-pinned and clamped-free beams upon which this equation is based, but also for sliding-free, clamped-sliding, sliding-pinned and sliding-sliding beams. This is probably because, for this beams, the vibration mode with no axial force and the buckling mode are similar. Galef's expression is not, however valid for pinned-free and free-free beams. " [4].

In a subsequent work, Bokaian [5] extends his study to tension loads.

The arrestor hook behaviour during the engagement phase is one aeronautical problem in which this mentioned effect is present.

CASA is the company responsible of the arrestor hook system within the Eurofighter consortium. In the EF-2000 Typhoon, the arrestor hook is an emergency device which means that it is not regularly used in a normal landing. Therefore, the arrestor hook arm is slender and optimised for a reduced number of engagements. (This is completely different from a naval aircraft in which the arrestor hook is regularly used).

During engagement, the arrestor hook head captures the runway cable. The sudden application of force produces large displacements and deformation on the slender arrestor hook arm. There is an increase in the frequency in the transverse bending mode that is evident in both, the numerical non-linear simulation [6,7] and also in the test-measured results. Figure 2 shows the EF-2000 arrestor hook system and the responses in the engagement phase. A 30 Hz response in the bending moment is evident and it corresponds roughly with the frequency of the arrestor hook under the applied tensile load. This frequency without applied load is in the neighbourhood of 20 Hz.

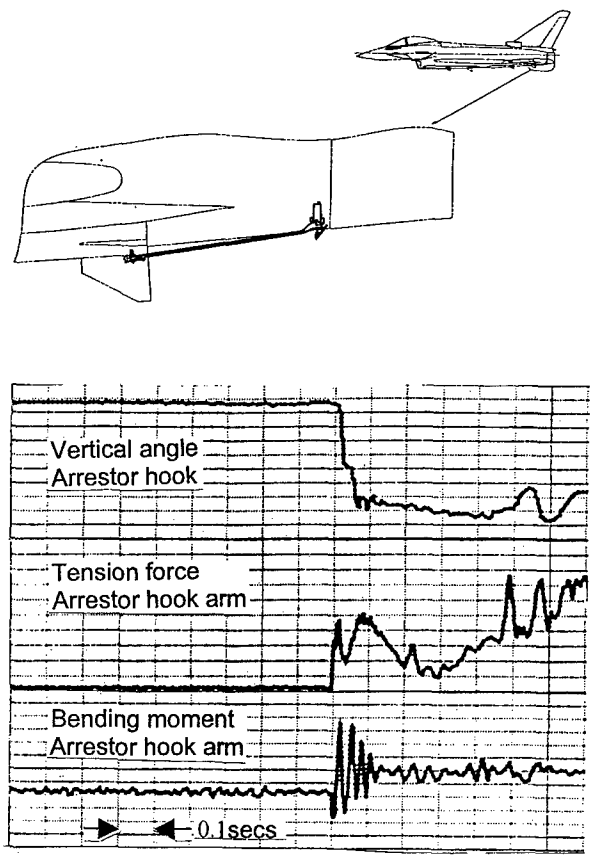

Figure 2. EF-2000 Arrestor hook system. Flight test measured response during engagement showing the increase in bending frequency due to the applied tensile load

2.3 Beams subjected to large applied loads and large static deformations.

Most of the studies in this subject have been promoted by the aeroelastic stability of helicopter rotor blades. Therefore, in many cases, external forces are due to centrifugal effects. The studies consider a beam rotating at constant angular speed about a fixed axis in space by determining first the steady equilibrium position due to centrifugal and gravitational or any other concentrated external load. Afterwards, using a small perturbation technique, the movement around the equilibrium position is studied. The small strain assumption is common in helicopter rotor blades analysis. The flap and lead-lag hinges allow large displacements without a large strain. This fact is used to simplify the stress tensor.

Papers devoted to this subject have been being published since early 40's (Southwell, 1941 [8], Love 1944 [9]) including important contributions like Rose and Friedman (1979, [10]) that analyse the non-linear behaviour of beams with bending-torsion coupling undergoing small strains with rotations.

The experimental studies include at least four references. Dowell, Traybar and Hodges (1977,[11]), Rosen (1983, [12]) Minguet and Dugundji (1990, [13],[14]) and Laulusa (1991, [15]). Natural frequencies of a cantilever beam are reported as function of tip deflection in Dowell & Minguet and the other works deal with static large deflected beams. Their results have been widely used in literature to determine the accuracy of theoretical methods.

The most recent papers that analyse the large loads and deflections on natural frequencies and mode shapes are the five shown in table 1 that shows a relative comparison of what are the contents of each paper.

Figure 3 shows one of the obtained results, quoted from Minguet [13]. This plot presents the changes in natural frequencies for beam with increasing tip deflections. These figures are relevant because they reflect some of the behaviours that have been found in actual airplane modes and will be presented in subsequent sections. Left figure shows the torsion and chordwise modes close coupled in the initial conditions. With increasing tip deflection, torsion mode (1T) changes its mode shape to become a chordwise mode (1F) and decreases significantly its frequency. On the other hand, the torsion mode changes its mode shape to become torsion and its frequency first increases and then decreases with tip deflection.

2.4 Plates under in-plane loading

ESDU 90016 [18] provides a mean of estimating the lower natural frequencies of isotropic or orthotropic, flat rectangular plates under static in-plane loading.

Natural frequencies are obtained by using beam characteristics orthogonal polynomials in the Rayleigh-Ritz method. The effect of in-plane loading is considered in two parts. First, effects of direct in-plane loading only and then the effects of shear loading only.

As in beams, tension in-plane loads will cause an increase of frequency. Compression will produce a decrease of frequency. But one of the differences of the plates subjected to direct in-plane compression loading with respect to beams is that the minimum frequency (reached at the buckling load) is not zero and that in the post-buckling region, the frequency increases with in-plane compression load.

This apparently anti-natural effect has been attributed to an increase of the stiffness of the plate due to curvature and effects associated with initial geometrical imperfections in the plate. The theoretical natural frequencies are evaluated assuming uniform in-plane stresses but in actual plates there is a redistribution of in-plane stress due to the growth of initial geometric imperfection with increasing compressive load.

Plates under shear loading show that natural frequencies are identical for equal positive or negative shear loads although nodal patterns for positive and negative shear loads are mirror images. Some modes can increase frequency with moderate shear loading. As shear loading is increased, the natural frequency of some modes decreases until shear buckling will occur at sufficiently high shear loading.

2.5 Complex structures

Complex structures can only be analysed by the Finite Element Method (FEM) technique.

Some commercial codes are essentially non-linear like the explicit codes used in the simulation of impacts and crashworthiness. Nevertheless, to assess the effect of loads and large displacements on normal modes, an implicit FEM code should be used. The non-linear solution 106 of MSC/NASTRAN in combination with several DMAP alters and in-house CASA software is the procedure adopted to compute the results that will be shown in next sections.

- Stiffness matrix updating.

It is performed using an iterative process. Starting from a converged solution, gradual incremental loads are applied. According to [19] the equilibrium equation in the g-set may be written as:

$$\{P_g\}+\{Q_g\}-\{F_g\}=\{0\}$$

where $\{P_g\}$, $\{Q_g\}$ and $\{F_g\}$ represent vectors of applied loads, constraint forces and element nodal forces, respectively. Since the equilibrium condition is not immediately attained, an iterative scheme such as the Newton-Raphson method is required.

Reference	Minguet,1990 [13][14]	Laulusa, 1991 [15]	Cveticanin 1994 [16]	Sälstrom 1996 [17]
Effects considered	Rotation, Ω. Torsion-bending-extension No shear deformation Translation inertia Small strain Large displacements Moderate rotations Linear material	Rotation, Ω. Torsion-bending (two planes) Warping Translation inertia General formulation Large displacements Large rotations Linear material	Axial-bending coupling No shear deformation Trans & rot. Inertia Small strains Small displacements Linear material	Torsion-bending coupling No shear deformation Translation inertia Small strains Large displacements Large rotations Linear material
Model	Equilibrium in section One dimensional Euler angle	Energetic approach Princ. Virtual Work Bidimensional	Equilibrium in section One dimensional	Equilibrium in section One dimensional Beam kinematics for large rotations
Solution scheme	Small perturbation Finite-difference	Small perturbation Finite elements	Small perturbation Modal expansion	Small perturbation Runge-Kutta integration scheme.
Application	Cantilever beam Composite beams with different lay-ups	Rotating simple-supported-free beam	Simple supported beam	Cantilevered beam
Results	Static deflection Mode shapes and frequencies Influence of tip deflection on frequencies and modes Effects of torsion coupling	Static deflection Influence of displacement and angular speed on natural frequencies.	Influence of load magnitude, rotary inertia and slenderness on the fundamental frequency.	Static deflection Poor dynamic result discussion

Table 1. Summary of recent works about non-linear effects on beam normal modes due to static initial effects

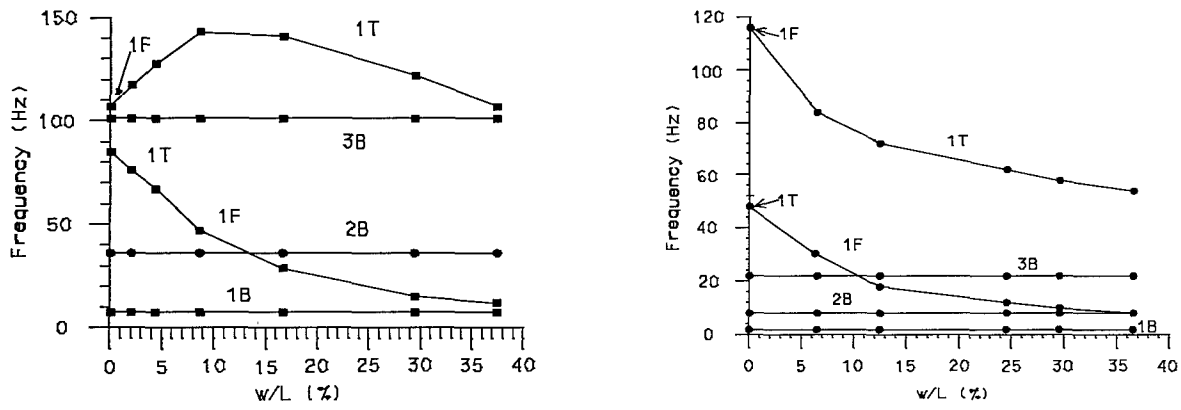

Figure 3 Changes in natural frequencies for beam with increasing tip deflections; a) composite beam, 560 mm in length, [0/90]3s lay-up; b) composite beam, 560 mm in length, [45/0]s lay-up. From Minguet [13], F stands for bending in the stiffest plane (chordwise), B represents modes oscillating in a vertical plane; T is a torsion mode.

Since the error vanishes at constraints points and the constraint forces vanishes at free points, the unbalanced forces acting at nodal points at any iteration step are conveniently defined as an error vector by (dropping the subscript):

$$\{R\} = \{P\} - \{F\}$$

Based on Newton's method, a linearised system of equations is solved for incremental displacements by Gaussian elimination in succession. The Jacobian of the error vector emerges as the tangential stiffness matrix.

New deformations are obtained, continuing the iteration until the residual error –unbalanced load– and the incremental displacements are negligible.

The tangential stiffness consists of the geometric stiffness in addition to the material stiffness.

$$[K_T] = [K^m] + [K^d]$$

$[K^m]$, the material stiffness represents the assembly of elements stiffness without geometric nonlinear effects

$[K^d]$ is the additional stiffness due to initial stresses that are included in the incremental process because the initial stresses exist from the second increment.

- Mass matrix updating.

The centres of gravity of the lumped masses have been moved to their corresponding deformed position.

The normal modes of the deformed/loaded structure are computed with the updated stiffness and mass matrices at the final load step.

3 Influence of loads and displacements in normal modes of an actual aircraft

3.1 Introduction

CASA is participating in the Airbus 3E flexible aircraft programme. This programme is dedicated to harmonise and coordinate the work of Airbus Industrie partners in technology acquisition of aeroelasticity with the aim to improve tools and methods, optimise resources and avoid duplication of work to face the development of a megaliner (A3XX) minimising the risk in this technical area. CASA has contributed in the Ground Vibration Test methods package by studying the influence of aircraft shape and loads in the measurements, which in turn can be applied to FEM updating procedures.

Aircraft normal modes are currently performed using a FEM model of the structure. In most of the cases, the FEM model geometry corresponds to the jig shape. Due to the wing size of the A3XX, a significant departure from jig shape can be anticipated for both ground shape and flight shape. This effect in combination with loads (gravity on ground and gravity + aerodynamics in flight) can modify the aircraft normal modes.

Therefore these effects should be analysed in order to have a better insight in GVT measurements and in the way to update FEM models to match test results. Figure 4 shows –at scale– the relative deformations that can be expected in the wing of a megaliner as function of the load factor. At in-flight 2.5g the tip deflection is 15% of the wing span. At in-flight 1g, it is 6%. In GVT conditions -3%.

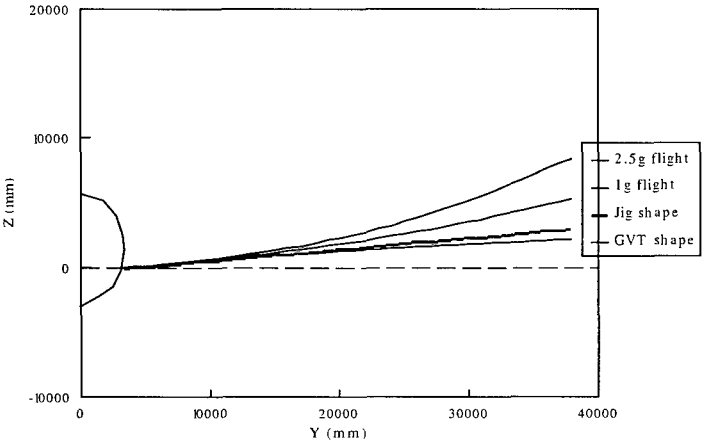

Figure 4.- Megaliner wing deformation in different conditions

In this paper the effect of large loads and displacements on normal modes have been considered in a set of increasingly complex tasks of an actual model of a megaliner structure:

- Wing without engine-pylons.
- Isolated Engine pylons.
- Wing with inboard and outboard engine pylons.

3.2 Analysis conditions

A structural model of the half-complete A3XX status 10c has been used (see figure 5). From this model, the wing and pylons have been extracted for normal modes calculations. Geometry, connectivity, properties, lumped masses, etc. are fully representative of the actual aircraft.

Inertia loads have been considered in the range –1g to 2.5 g (regular load factor envelope for certification). The case of 1g corresponds to GVT conditions. These loads have been applied to the structure in the centre of gravity of each lumped mass.

Aerodynamic loads have been obtained for trimmed flight using a linear method. For this task it has not been necessary to have an accurate information about aerodynamic loads, just a representative set of these loads.

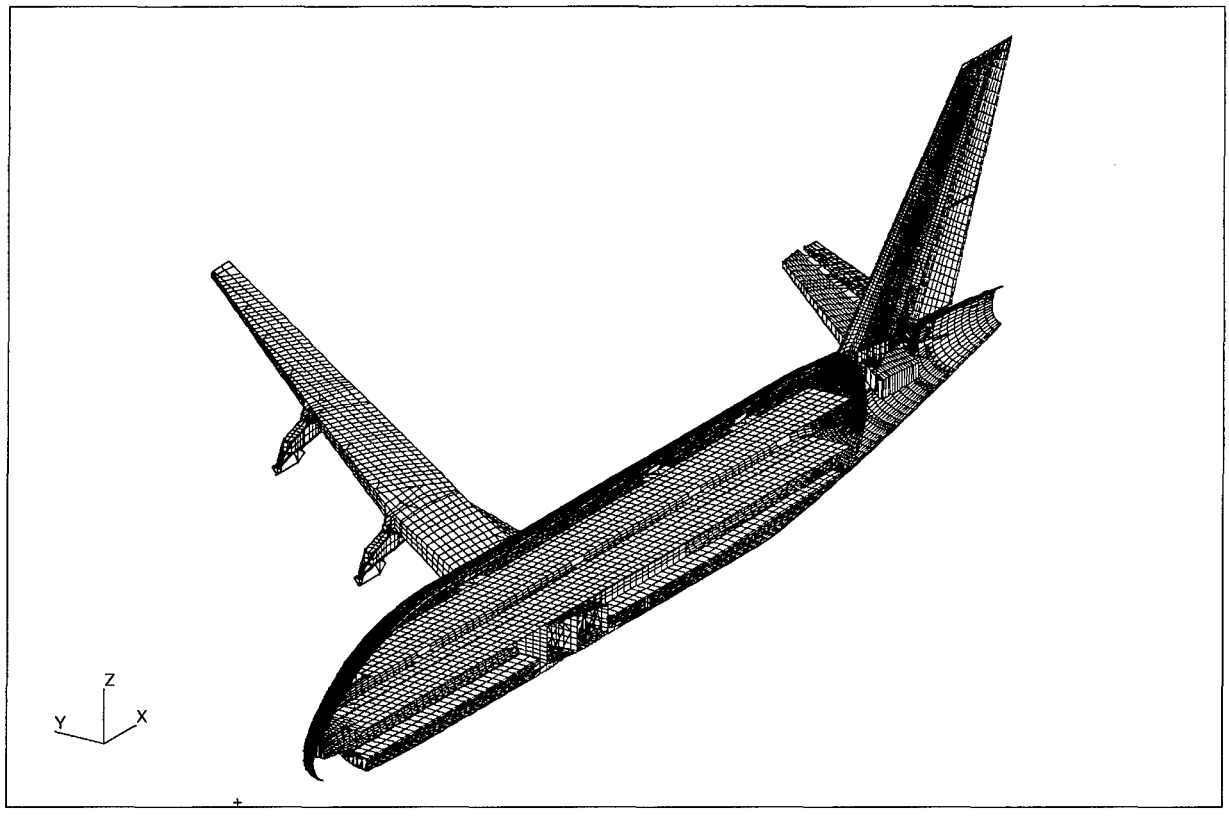

Figure 5.- Megaliner FEM model used to assess the effect of large loads and displacements.

3.3 Clamped wing normal modes results

Figure 6 shows the effect of the inertia loading in the range [-1g, 2.5g]. The case of 0g corresponds with the jig shape modes and has been obtained with the linear solution. The case of 1g corresponds with the GVT simulation.

The first non-linear analyses have been performed with a reduce level of loads (±0.1g) and therefore, they correspond to a reduced level of deformation. These first non-linear analyses have produced very similar results to the linear solution thus giving confidence on the results.

The evolution of modes is quite smooth although some crossings can already be detected, especially with the chordwise modes (WTX) which frequency decreases with increasing load factor and the corresponding increase in deformation. This effect is magnified if two modes of torsion and chordwise are close-coupled at 0g –like 3WT and 3WTX-. There is also a change in mode shape for these two modes: at large load factors the 3WT becomes 3WTX and vice-versa. This effect is very similar to the one reported by Minguet in his paper (see figure 3).

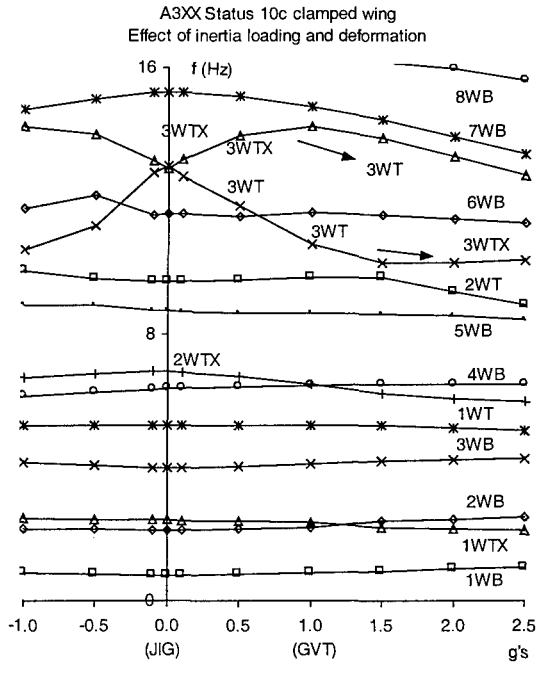

Figure 6.- Effect of inertia loading and deformation on clamped wing normal modes

Note that in the GVT simulation (1g) the 3WT mode is below the 6WB while in the jig-shape simulation (0g) this mode is above. In addition, the 3WT and 3WTX are well separated in GVT simulation while very close in jig-shape modal simulation.

Figure 7 shows the effect of inertia + aerodynamic loading. The modes show a similar pattern that in figure 6 although more pronounced.

Bending modes are not affected. The first torsion and chordwise modes decrease their frequency slightly with load factor. Large order torsion and chordwise modes change more its frequency with load factor.

Comparing figure 6 and 7 can conduct to an interesting remark. According with figure 6, GVT will require modifying the model to increase the frequency of the 3WTX mode with respect to the jig-shape solution. On the other hand, in the in flight condition at 1g, the frequency of this mode is **below** the jig-shape. The same happens with the torsion mode 3WT: the GVT will require modifying the model to decrease this mode from the jig shape solution although in flight at 1g the frequency of this mode is similar to jig-shape. In these two cases, correction of the model to match GVT will produce worse models for comparison with in-flight modes. It is believed that this behaviour happens particularly in these two modes because they are close coupled at 0g (linear solution).

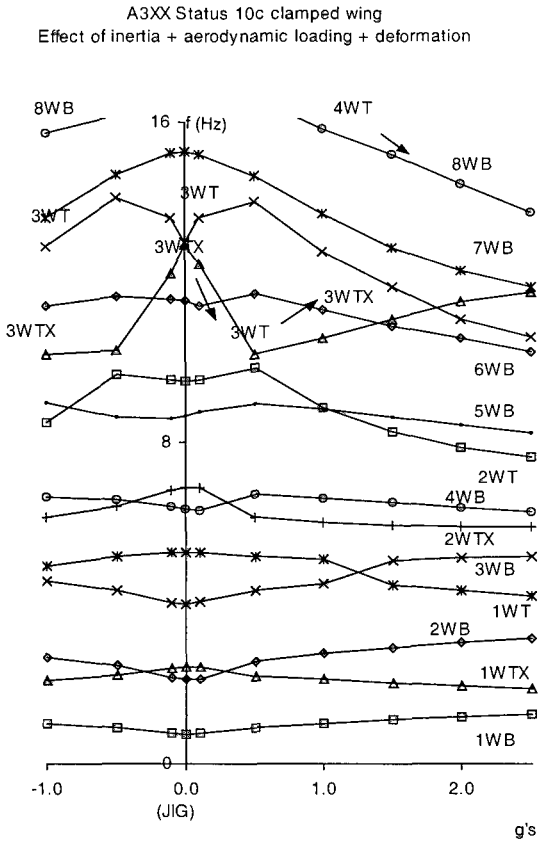

Figure 7.- Effect of inertia + aerodynamic loading + deformation on clamped wing normal modes

3.4 Inboard and outboard engine-pylon normal modes results

The isolated pylons have been also subjected to the inertia loading in the range [-1g, 2.5g].

Low frequency pylon modes found have been: lateral bending, pitch and yaw.

The evolution of frequency of these modes with the load factor has been completely flat in the studied range.

3.5 Clamped wing plus inboard and outboard engine pylons normal modes results.

Figure 8 shows the effect of the inertia loading in the range [-1g, 2.5g]. The case of 0g corresponds with the jig shape modes and has been obtained with the linear solution. The case of 1g corresponds with the GVT simulation.

The evolution of most of the modes is quite smooth. Due to the presence of the pylons, the crossings of modes are more pronounced that in the wing without pylons case. There is one eigenvalue that becomes negative at large load factors. It corresponds to the outboard pylon yaw mode.

Wing bending modes are not affected by load factor. Pylon yaws and wing chordwise modes (especially 3WTX) are the most affected modes. Wing torsion modes show slight variations.

Figure 9 shows the effect of inertia + aerodynamic loading on the clamped with pylons. The modes show a similar pattern that in figure 8 although a lot more pronounced. Even the bending modes change (very mild).

There are two eigenvalues that become negative at certain load factor. Both have in the end significant contribution of engine pylon yaw mode.

Again the modes more affected are the pylon yaw and the wing chordwise. Larger order wing torsion modes like (4WT) are also significantly affected

Due to the presence of pylons, the 3WTX and 3WT are not so coupled at 0g as in the wing without pylons case and their evolution with load factor is more similar between figure 8 and figure 9.

Comparing modes at 1g of figure 8 and figure 9 it can be seen that in two cases the tendency of a mode in GVT is different from in-flight: the O/B pylon yaw and the 2WT. Corrections of these two modes will produce a worse model for in-flight modal comparison.

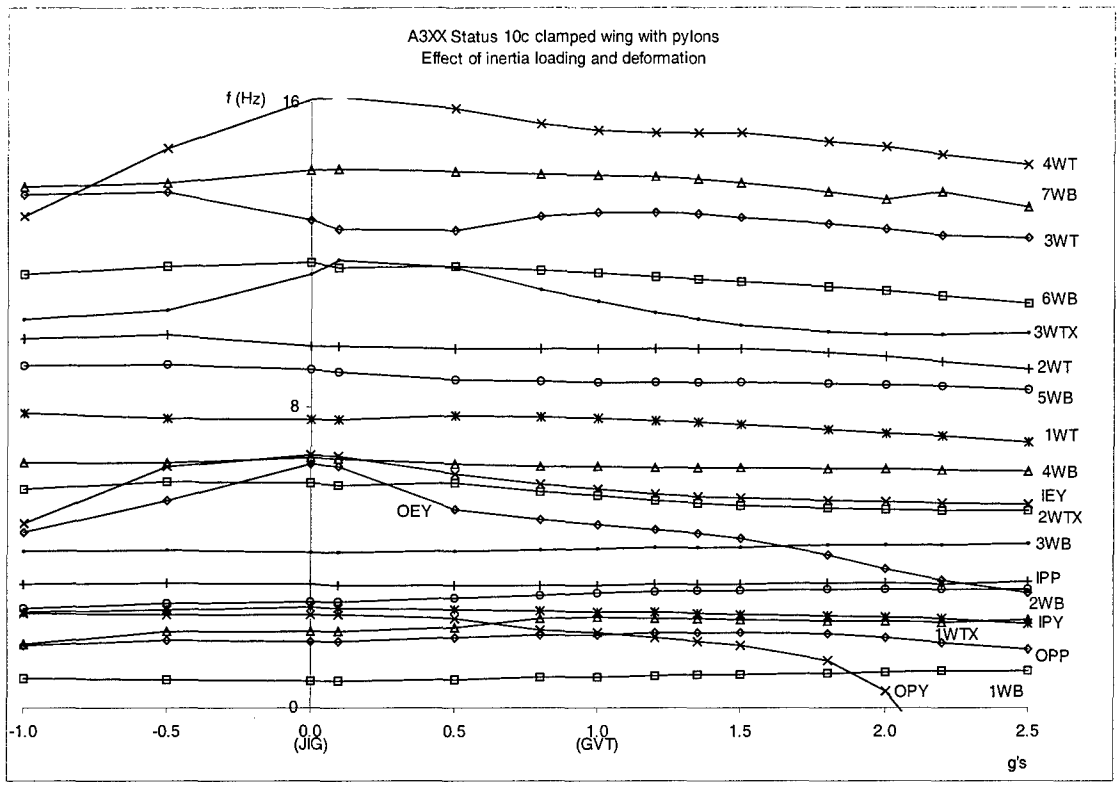

Figure 8.- Effect of inertia + deformation on clamped wing with engine pylons normal modes

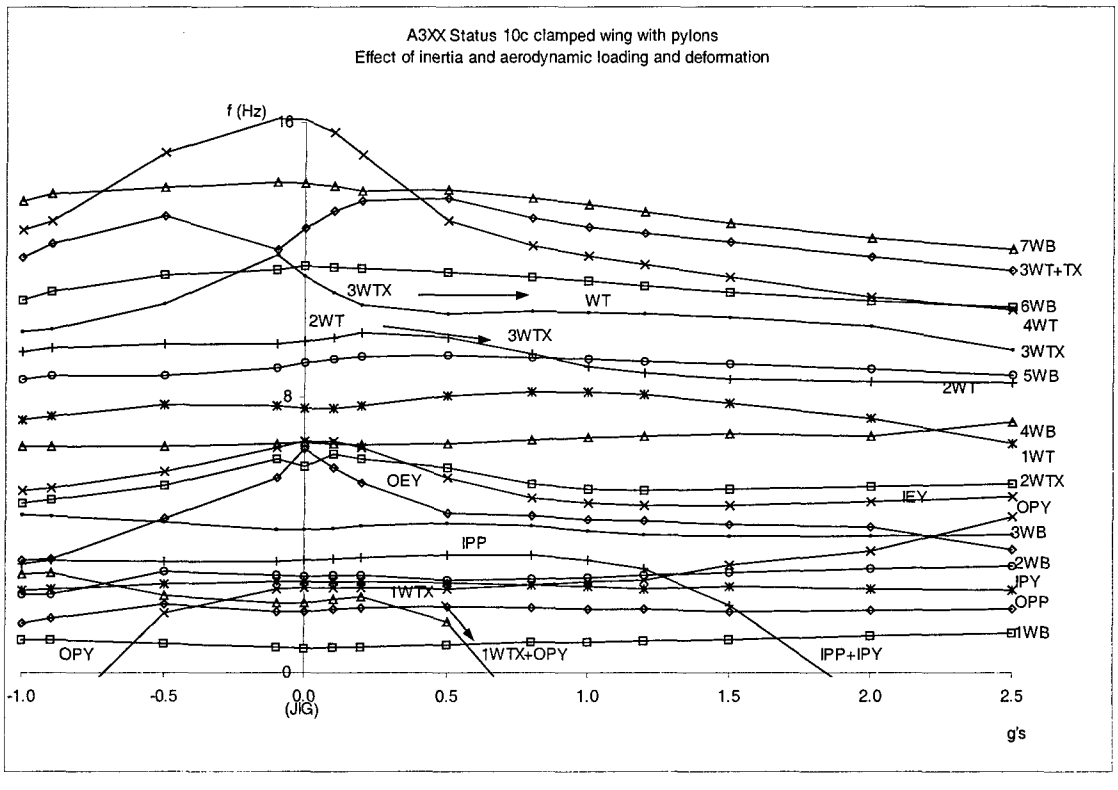

Figure 9.- Effect of inertia + aerodynamic loading + deformation on clamped wing with engine pylons normal modes

3.6 Effect of flexibility

To verify that the results found for a very flexible wing of a megaliner like the A3XX are indeed due to its large flexibility, a verification case has been run using a model of an aircraft significantly more rigid.

The CASA C-295 is a medium size military transport with 21000 kg of MTOW in civil operations and 23200 kg. of MTOW in military operations.

The frequency of the first symmetric wing bending of the C-295 is –roughly– between 4 and 5 times larger than that of the A3XX.

Figure 10 shows the effect of inertia, aerodynamic and displacement on the modes of the CASA C-295 wing at different load factors.

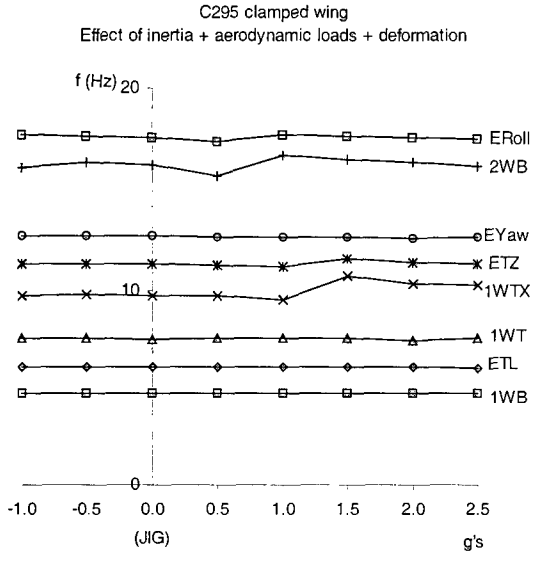

Figure 10.- Effect of large loads and deformations on a relatively rigid aircraft (CASA C-295)

Bending modes are un-affected as in the case of a more flexible wing. But, in addition, the torsion, chordwise modes, engine-truss etc are also basically un-affected showing that the non-linear effect in modes presented in previous sections is due to the large flexibility of the megaliner wing.

4 Effect on HTP modes of elevators deflection angle.

Within the Airbus consortium, CASA has been responsible of the design, analysis, manufacturing and certification of the Horizontal Tailplanes (HTP). In the case of a megaliner, the horizontal tailplane area is well above 200 square meters. The effect of the deflections of the large split elevators on the HTP modes is a new problem briefly described in this section.

The A3XX Horizontal Tailplane FEM model (status 10c) has been used to perform the analysis of the linear normal modes while changing the elevator angle.

Due to its size, the elevator of the A3XX will be split in two spanwise parts. In the present analysis both elevators have been deflected simultaneously from –25° to + 25°.

Figure 11 shows the effect of the elevator deflection in all clamped HTP modes up to 40. Hz

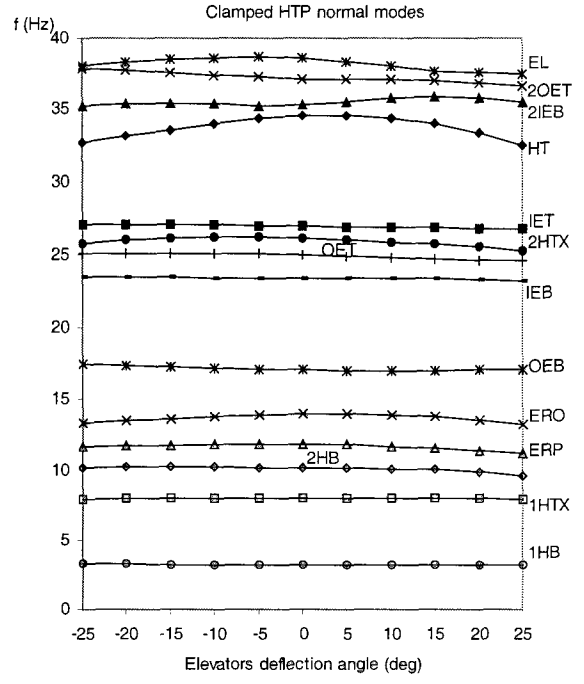

Figure 11.- Effect of elevator deflection angle on a megaliner HTP clamped modes.

Bending modes show no influence of the deflection angle. It means that the elevator chordwise bending contribution even at +25° or –25° is negligible. The most affected modes are:

- 2nd HTP chordwise (2HTX)
- Elevators rotation in-phase (ERP)
- Elevators rotation out of phase (ERO)
- HTP torsion (HT)
- 2nd Inboard elevator bending (2IEB)

The effect can be quantified in roughly 6 % in frequency at maximum deflection angle.

5 Conclusions

The effect of large applied loads and deformation in the normal modes of a very flexible megaliner wing has been presented.

These non-linear effects have been analysed using an iterative process with the finite element technique.

Confidence on the results has been achieved through several means:

- Non-linear solution with low level of loading (0.1g) has been very similar to the linear solution.
- Some modal tendencies found have been similar to the results published in academic papers.
- The larger the flexibility the larger the effect.

Nevertheless, a criticism can be done to the results presented herein. Is the FEM model suitable for the purposes shown? The most likely answer is that the model is not completely suitable especially in the neighbourhood of the large applied loads (engine-pylon fittings). It probably produces more pronounced tendencies that in the reality. For instance, the negative eigenvalues found are numerical results due to bad conditioning of the matrices that will not be present in reality and they will likely be solved using a finer mesh in those areas [19].

But basically the trends shown herein should be completely correct –although likely less pronounced–. Therefore the final message is that the effect of large applied loads and deformations in the normal modes of a very flexible structure –like the wing of a megaliner– must be taken into account.

Failing to do so could produce a misinterpretation of the GVT results and corrections in the FEM model that can go –in some cases– in the opposite sense of the desired one.

This effect should be taken into account. Dedicated FEM model for these purposes should be elaborated and validated. It is believed that the model will only require a finer mesh in certain areas –like the ones in the neighbourhood of large applied masses-.

Further work in this area will include the determination of a flexibility threshold beyond which it is mandatory to include the effect of large loads and displacements. Between the very flexible Airbus A3XX and the relatively rigid CASA C-295, other intermediate aircraft will be considered. Also the effect of the modelling will be studied with mesh size sensitivity analyses.

6 Acknowledgements

The present work has been carried out within the Airbus 3E flexible aircraft programme. Contributions of the rest of Airbus Industrie partners is gratefully acknowledged. Jesús López and Cristina Cuerno of the Universidad Politécnica de Madrid have contributed in the literature survey of the beam cases.

7 References

[1] G.C.Nihous. On the Continuity of the Boundary Value Problem for Vibrating Free-Free Straight Beams under Axial Loads. *Journal of Sound and Vibration* Vol. 200 No. 1 (1997) p. 110-119

[2] A. E. Galef. Bending frequencies of compressed beams. *Journal of the Acoustical Society of America* Vol. 44 No. 8 (1968) p. 643

[3] F.J. Shaker. Effect of Axial Load on Mode Shapes and Frequencies of Beams. NASA TN D-8109 1975

[4] A. Bokaian. Natural Frequencies of Beams under Compressive Axial Loads. *Journal of Sound and Vibration* Vol. 126 No. 1 (1988) p. 49-65

[5] A. Bokaian. Natural Frequencies of Beams under Tensile Axial Loads. *Journal of Sound and Vibration* Vol. 142 No. 3 (1990) p. 481-498

[6] H. Climent Análisis Dinámico Gancho de Frenado del EFA 1. CASA C/PD/88-083 (Jul 1988)

[7] J. Burgaz Análisis Dinámico Gancho de Frenado del EFA 2. CASA C/PD/88-113 (Dic 1988)

[8] R.V. Southwell. *An Introduction to the Theory of Elasticity*. Oxford University Press, Second Edition, London, 1941

[9] A.E.H. Love. *A Treatise on the Mathematical Theory of Elasticity*. Dover, Fourth Edition, New York, 1944

[10] A. Rosen, P. Friedmann. The Nonlinear Behavior of Elastic Slender Straight Beams Undergoing Small Strains and Moderate Rotations. *Journal of Applied Mechanics*, Vol. 46 (March 1979), p. 161-168

[11] E.H. Dowell, J. Traybar, D.H. Hodges. An Experimental-Theoretical Correlation Study of Non-Linear Bending and Torsion Deformations of a Cantilever Beam. *Journal of Sound and Vibration* Vol. 50 No.4 (1977) p. 533-544

[12] A. Rosen. Theoretical and Experimental Investigation of the Nonlinear Torsion and Extension of Initially Twisted Bars. *Journal of Applied Mechanics* Vol.50 (Jun 1983) p.321-326

[13] P. Minguet, J. Dugundji. Experiments and Analysis for Composite Blades under Large Deflections. Part I: Static Behavior. *AIAA Journal* Vol. 28 No. 9 (Sep 1990) p. 1573-

[14] P. Minguet, J. Dugundji. Experiments and Analysis for Composite Blades under Large Deflections.

Part II: Dinamic Behavior. *AIAA Journal* Vol. 28 No. 9 (Sep 1990) p. 1580-

[15] A. Laulusa. Theoretical and Experimental Investigation of the Large Deflections of Beams. ONERA TP 1991-35

[16] L.Cveticanin, T. Atanockvic. Non-Linear Vibration of an Extensible Elastic Beam. *Journal of Sound and Vibration* Vol.177 (1994) p.159-171

[17] J.H. Sällström, D.H.L. Poelaert, F.L. Janssens Small Displacements about Equilibrium of a Beam Subjected to Large Static Loads. *AIAA Journal* Vol. 34 No. 11 (Nov 1996) p. 2384-2391

[18] ESDU 90016 Natural Frequencies of Isotropic and Orthotropic Rectangular Plates under Static In-plane Loading (including shear loading) (1993)

[19] MSC/NASTRAN Handbook for Nonlinear Analysis. (Draft) Version 67. Sang H. Lee, Editor. March 31, 1992.

FLIGHT SIMULATION WITHIN THE FRAME OF MULTIDISCIPLINARY OPTIMIZATION OF LARGE FLEXIBLE AIRCRAFT

Armin Rommel*

DaimlerChrysler Aerospace Airbus GmbH
P.O. Box 95 01 09
D-21111 Hamburg

Abstract

The disciplines flight mechanics / flight control and structural dynamics have to work closely together when large flexible aircraft, such as A340-600 and A3XX, are designed. The flight-control system has to be designed under the constraint that structural oscillation resonances or unacceptable levels of structural loads have to be avoided. Especially the integration of flight control and structural control requires multidisciplinary cooperation. In the potential conflict between handling qualities and minimal structural loads requirements the flight-control law parameters have to be optimized. This paper describes enhancements of real-time flight simulation in order to integrate the pilot into the control loop especially with respect to the effects of cockpit accelerations. The enhancements cover the coupling of rigid body motion and flexible modes in order to analyze the effects of neighboring frequencies, as well as the inclusion of simplified loads computation within the real-time simulation environment. Moreover, a cost-effective way of simulation-model development is presented. This covers model development and testing/validation on a fixed-base engineering flight simulator followed by a proven model transfer onto a six degrees of freedom motion simulator where intensive pilot-in-the-loop investigations can be carried out.

Nomenclature

$\underline{\underline{A}}$	state matrix
$\underline{\underline{AL}}$	adapted state matrix
a/c	aircraft
APC	aircraft pilot coupling
AS	Aerospatiale
AST	automatic simulation test
$\underline{\underline{B}}$	control matrix
$\underline{\underline{BL}}$	adapted control matrix
$\underline{\underline{C}}$	output state matrix
$\underline{\underline{CL}}$	adapted output state matrix
c/g	center of gravity
CIFSI	cockpit interface simulation
$\underline{\underline{D}}$	output control matrix
$\underline{\underline{DL}}$	adapted output control matrix
DA	DaimlerChrysler Aerospace Airbus
FAR	federal aviation regulations
$\underline{F}_{aero}$	vector of aerodynamic forces and moments
$\underline{F}_{gear}$	vector of forces and moments due to l/g
$\underline{F}_{thrust}$	vector of engine forces and moments
$\underline{F}_{weight}$	vector of gravity forces
FBW	fly by wire
FCS	flight control system
fm	flight mechanical
$G_{nonlinear}$	function of forces and moments
H	altitude
$\underline{\underline{I}}$	moments of inertia
IRS	inertial reference system
JAR	joint aviation regulations
l/g	landing gear
Ma	mach number
n_y	lateral load factor
n_z	longitudinal load factor
p	pitch rate
q	roll rate
r	yaw rate
R/A	radio altitude
TUB	Technical University Berlin
$\underline{u}$	control vector
$\underline{x}_e$	vector of elasticity states
$\underline{x}_f$	vector of rigid a/c states (flight mechanics)
$\underline{x}_r$	vector of rigid a/c states (NASTRAN based)
$\underline{y}$	output vector
$\underline{\underline{\phi L}}$	interfacing matrix for $\underline{x}_f$
ϕ	roll angle
θ	pitch angle
ψ	yaw angle

Indices:

e	due to elasticity
ee	effect on elasticity due to elasticity
ef	effect on elasticity due to fm rigid a/c motion
er	effect on elasticity due to rigid a/c motion
f	due to fm rigid a/c motion
ff	effect on fm rigid a/c motion due to fm rigid a/c motion
f	body fixed axes
k	kinetic track fixed axes
r	due to rigid a/c motion
re	effect on rigid a/c motion due to elasticity
rr	effect on rigid a/c motion due to rigid a/c motion
yf	effect on output values due to fm rigid a/c motion

* Development Engineer Flight Mechanics, Flight Guidance and Control

Paper presented at the RTO AVT Specialists' Meeting on "Structural Aspects of Flexible Aircraft Control", held in Ottawa, Canada, 18-20 October 1999, and published in RTO MP-36.

1. Introduction

There is a correlation between aircraft size and the frequencies of the elastic modes i.e. the bigger an aircraft, the lower the frequencies. Large flexible aircraft have elastic modes in a frequency region which potentially overlaps with piloting activity. Therefore the flight control systems (FCS) of these aircraft have to be designed such that aircraft pilot coupling (APC) due to elasticity is impossible in every flight condition. Moreover with today's fly by wire (FBW) flight control technology there is potential for active control of the lower frequency elastic modes. Such active control is under development (see also /1/ and /2/) for large transport aircraft to be certified under JAR 25 / FAR 25. A major challenge of such active control development consists of the requirements being driven interdisciplinary by structural dynamics and handling qualities.

Traditionally, besides crew training, flight simulation is a tool in the discipline of flight mechanics which aims to achieve good handling qualities of new aircraft designs before first flight. This includes simulation usage for FCS development and testing. Flight simulators provide the possibility to bring the pilot into the control loop in real time. Embedded into the technology framework called 3E-Flexible-Aircraft, the Airbus partners are expanding flight simulation utilization into the aeroservoelastic design loop. The target is to identify and eliminate tendencies of APC due to a/c elasticity early in the development process. Inherent to the fact that frequencies of elastic modes are higher than frequencies of rigid a/c response, moving flight simulator utilization is a must. Development flight simulators with a motion system are very rare.

Located at Technical University Berlin there is a special A330/A340 training flight simulator featuring a doubled simulation computer which can be run alternatively instead of the certified, sealed training computer. Therefore the simulator is also accessible for scientific tasks. This accessibility to development engineers allows for varying a/c models as well as systems simulations to be implemented. Nevertheless, due to the limited, slotted access to this moving flight simulator, the main development work is better performed within a conventional fixed base flight simulation environment. Therefore a robust and efficient model transfer from the fixed base engineering onto the moving flight simulator is a major achievement.

The necessary interdisciplinary cooperation starts with the development of a mathematical model of large flexible aircraft. The modeling approach presented in this paper is distinguished by being generally exact in the core frequency regimes of the according disciplines. This means on the one hand that low frequency rigid body motion as well as higher frequency aircraft elasticity can be computed with the best algorithms available for the according physical problem. On the other hand the dynamic coupling between rigid body motion and elastic modes is fully included within the model. Such a solution can be achieved mathematically by elaboration of appropriate interfacing between the model contributions from the core activities of the concerned disciplines.

But this achievement is based strongly on good interdisciplinary cooperation of the relevant specialists, providing the proven and advanced know-how of their disciplines. The complexity of interdisciplinary rigid/elastic a/c modeling has been found mainly in the different specialized views between the handling quality and structural dynamics disciplines, due to the problems traditionally being addressed and the mathematical solving methods usually being applied. This situation is accompanied by the fact that, because already the complex core disciplines alone require specialist's know-how to cover the a/c behavior mathematically, it is nearly impossible for individuals to acquire sufficient knowledge and experience in each area, to achieve the mentioned model exactness in the lower, higher and in the intermediate frequency regime, where the disciplines and physical phenomena are overlapping.

Keeping the common goal of interdisciplinary harmonized modeling and control problem solving in mind, the specialists first need to exchange a sufficient, but limited knowledge of their traditional mathematical abstractions and solving methods. This includes usual methodological prerequisites, assumptions, approximations and limits. It is advantageous, when the participating specialists generally can remain within their traditional way of thinking. Then appropriate, harmonized interfacing and data exchange is the key, in order to achieve the interdisciplinary model architecture which allows flight mechanics as well as aeroelastics and loads disciplines to consider and implement the common model as an add-on to their traditional approaches, algorithms and software. Model application on each side leads consequently to comparing calculations and a fruitful, slightly iterative model fine tuning.

Specific adaptations and simplifications due to the needs of the varying model applications are jointly generated and cross checked between the disciplines. For example the real time calculation requirement for the flight simulator application leads to a limited number of elastic modes which can be taken into account. While the necessary selection and application of mode reduction methodology has been found best practicable by aeroelastics specialists, the real time specific coding as well as the integration method evaluation and selection profited by the flight mechanics' experience.

Concerning the interdisciplinary cooperation process which relies strongly on massive data exchange, automation has been found very important. Interdisciplinary model preparation and coding as well as model transfer between the flight simulators have been developed such that automatic software processes resulted immediately. This is already advantageous as long as the mentioned iterative fine tuning is performed.

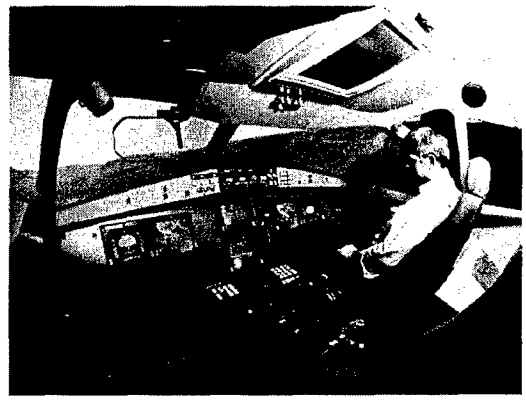

Figure 1: Development Flight Simulator Cockpit

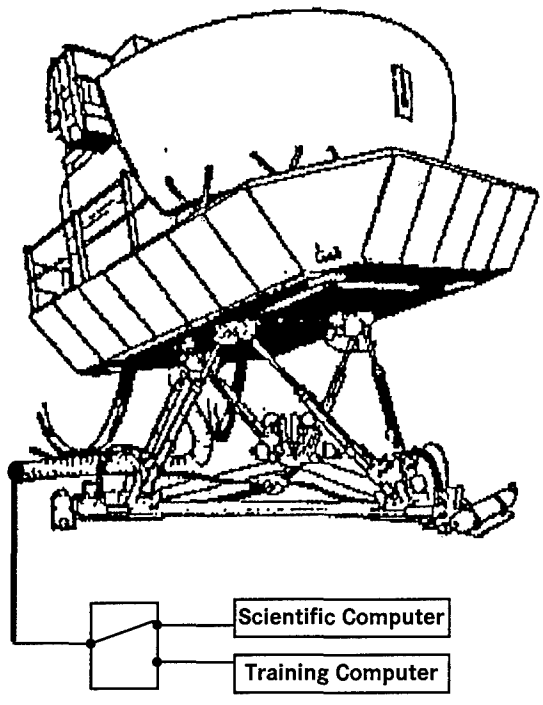

Figure 2: Motion Flight Simulator & Scientific Computer

2. Flight Simulation Activities

In order to ensure that aircraft elasticity does not lead to unfavorable coupling with pilot in the loop control, flight simulation can be an advantageous tool from early in the design process onwards. With respect to the efforts of supporting the aeroservoelastic design process introduced before, there are the following areas of flight simulation contributions:

2.1 Support for off-line Stability Calculations

The bio-mechanical coupling resulting from cockpit accelerations due to a/c elasticity has been addressed here. The outcome are transfer functions from cockpit accelerations to side-stick inputs, via seat and pilot. These transfer functions were included into aeroelastic stability calculations. In the past such specialized flutter calculations already considered the flight control system by inclusion of sensor feed-backs and flight control laws, but closing the loop via the pilot is new.

Flight simulation has played its role for the generation of the cockpit-to-stick transfer functions. In the moving flight simulator a series of tests with Airbus line and test-pilots was performed. Separated between low and high gain piloting tasks (attitude hold and landing approach respectively), there were artificial cockpit accelerations superimposed with the motions known from training simulators, especially without elastic modes in the a/c model. With the intention to have common excitations for all the tests, sweeps of known frequency behavior were imposed in z- as well as in y-direction. So here the flight simulator was used as a simple shaker, but with the real cockpit environment and pilots in real flying conditions.

Since the data acquisition, evaluation and interpretation was mainly performed by the cooperating partners from Technical University Berlin, and since the results can fill an extra paper at a later time, here only some general highlights shall be summarized:

- Obvious from the beginning was that significant coupling would occur only when the pilot has a tight grip on the side-stick. This was realized during the experiments by a mistrim (could be switched on/off) in pitch and roll axes within the a/c aerodynamic model, requiring to fly around a non-zero side-stick position. Since FBW control laws would compensate for that mistrim, flying in direct law was a must.

- The differentiation between lower and higher gain tasks was negligible in comparison to the differences between mentally lower and higher gain pilots. In order to investigate the worst case situation, the highest amplitude transfer functions should be considered in the off-line calculations.

- Understanding the seat as a damped spring-mass-system, typical eigenfrequencies around 4 Hz have been discovered.

- Interesting cross couplings between z-accelerations and roll-stick-inputs and (less severe) vice versa between y-accelerations and pitch-stick-inputs were observed, which should not be neglected in future aeroelastic stability calculations, since here a path to potential excitement of each (lateral and longitudinal) elastic mode is existent.

2.2 Inclusion of elastic Modes

In order to prepare piloted tests with respect to APC due to elasticity, flight simulators must include the effects resulting from elastic mode excitations. Two main kinds of additional signals have to be calculated:

- Cockpit accelerations being composed from rigid a/c movement and from elastic deformations, in order to be realized by the flight simulator's motion system.

- Sensor signals including elasticity contributions (mainly IRS signals) as load factors (n_y, n_z), rotational rates (p, q, r) as well as attitudes (ϕ, θ, ψ) to be interfaced with the flight control laws and for cockpit vision and indications.

Additionally the height of the landing gear above ground, including the variations due to the elastic a/c structure is valuable for improved touch down simulations. Once the calculation of the elastic modes and its coupling with the rigid a/c movement is included within the flight simulation software, all the above mentioned signals can be gained as output values. Up to now incorporation of the cockpit accelerations is completed.

It is evident that for utilization in flight simulators the a/c model has to be represented in time domain. The mathematical setup of the interdisciplinary model is described in chapter 3. The related software generation and transportation process follows in chapter 4.

Due to the fact that the flight simulator application requires real time calculation capability, the following aspects are of special importance:

- Computing power is a limiting factor. It has been a big step forward that both involved flight simulation environments (fixed base engineering as well as the moving-simulator) benefited from computer hardware upgrades during the elasticity inclusion phase up to the current status. The openness to such upgrades, following the still rapidly improving hardware development will once more be welcome when future simulation model enhancements (see chapter 5) will be incorporated.

- Special software coding, adapted to the real time requirement, is still favorable. Especially since the usage of intensive optimization during software compilation has once more been found being not adequately robust for flight simulation application, real time adaptations on source code level are valuable. Despite inline coding, with respect to larger matrix operations within the included elastic mode calculations, it has been achieved to save about 70% of computation time by automatic elimination of all permanent multiplication-by-zero-operations on source code level.

- Investigation for the most advantageous numerical integration method pays off. For the elasticity calculation part of the flight simulator application, the 2nd order Adam's Bashforth algorithm

$$y(t) = y(t-1) + \left(\frac{3 \cdot x(t) - x(t-1)}{2}\right) \cdot \Delta t \qquad (1)$$

  has been proven to be suited best. It offers a good compromise between numerical stability and total computation time. The according cycle time of 5.55 msec resulted from a general 60 Hz requirement due to the moving simulator environment and from a threefold computation of the elastic modes within this frame.

- Nevertheless, the number of calculated elastic modes has to be limited in comparison with usual off-line structural dynamics (loads and flutter) calculations. Mode reduction methods are a separate field of science. For the present implementation Karpel's method /4/ has been used by the structural dynamics specialists.

The realized inclusion of cockpit accelerations due to elasticity has been presented to pilots in the moving flight simulator. The feedback has been positive. Elastic vibrations have been found similar to the behavior known from slightly gusty conditions. Measured simulator cockpit accelerations show good coincidence with the commanded signals from the output of the included elastic mode calculations.

2.3 Inclusion of simplified Loads Computations

For the ability to investigate the influences of FCS designs on structural loads by piloted flight simulations, real time capable loads computations are also included into the flight simulation software. This is not intended for the reproduction of design loads, but for the judgment of future loads control functions and for the determination of the dependencies (sensitivities) of loads from critical, interdisciplinary relevant FCL parameters already in early design phases. The loads algorithms have been simplified by the contributing specialists, in order to meet the real time capability requirement.

At this stage the interfaced loads package is separate from the inclusion of the aeroelastic modes mentioned before. Explicit modes or loads computation can be switched on alternatively only. In the future both structural dynamics model contributions shall be merged. The reason for the current intermediate status is the already mentioned intention within the interdisciplinary cooperation that the participating specialists evolutionary contribute and enhance their proven methodologies while avoiding revolutionary forced changes of their proven ways of thinking.

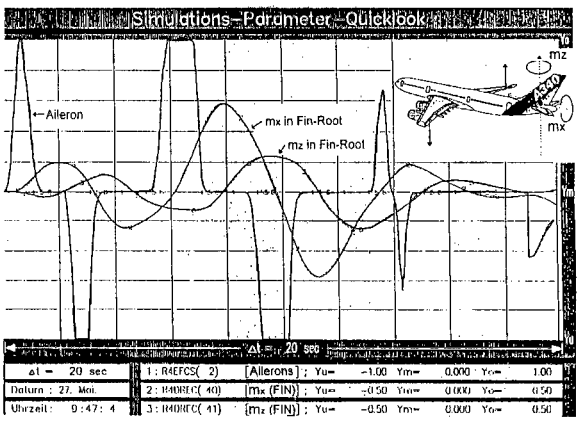

Figure 3: Quicklook on loads parameters during simulation

2.4 Simulator Motion System Validation

Before reliable predictions on APC tendencies with respect to new large flexible aircraft can be gained through piloted moving flight simulator investigations, it has been found favorable to validate the capability of the simulator's motion system being signaled by the enhanced a/c model. Besides data recordings of measured accelerations, the real proof shall be the reproduction of elasticity phenomena known from the A340-300 flight test phase. Doing this successfully will provide confidence in the addressed APC prediction capabilities of the enhanced simulation tool. Because motion system performance decreases with increasing frequencies, and because the mode frequencies of the future large flexible a/c, such as A340-600 and A3XX, will be lower than of A340-300, there will be sufficient certainty.

At this stage preparation work (including hardware based FCL implementation) for the phenomenon reproduction in cooperation between AS, DA and TUB is nearly completed, and pilots soon will be invited for the according simulator sessions.

2.5 Early APC Avoidance

As introduced, ensuring that new aircraft-, FCS- and FCL-designs avoid tendencies for occurrence of APC due to elasticity, improved real time flight simulation shall provide experimental assistance. This support is regarded as highly efficient, because designs can be analyzed and optimized

already in early design phases, especially through the pilot in the loop capability before first flight. Within the aeroservoelastic design process, especially parameter tuning for acceptable elastic mode amplitudes and minimized loads in conjunction with good handling qualities can be judged and controlled by the feed-backs from flight simulator sessions. It also brings pilots' expertise into the design loop earlier. Future integral flight control laws can be optimized with respect to their effectiveness becoming interdisciplinary approved.

The current status of work is preparedness according to modeling and simulation setup process, as described in the following chapters. Impressive is, when flying the elastic A340-300 in the moving simulator, the FCL behavior with respect to elasticity can be felt hands-on. For example when flying an approach and trying to excite elastic modes on purpose via the side-stick (note: This is no APC!), and when passing through 500 ft R/A, an FCL internal switching, affecting elasticity becomes immediately obvious due to the motion impression. This capability for direct behavior identification, related to elasticity, is the driving factor for the described activities, targeting piloted motion flight simulator investigations. Additionally, such experiments should be avoided in the real aircraft because unnecessary loads would contribute to structural fatigue.

3. Aircraft Modeling

As indicated before, the achieved interdisciplinary a/c modeling is the joint outcome of contributions from flight mechanics as well as structural dynamics disciplines. The intention to couple the algorithms of rigid a/c movement and elastic modes by appropriate interfacing lead to a summary of the different traditional methodologies according to **table 1**.

Flight Mechanics & Maneuver Loads	**Aeroelastics & Gust Loads**
formulation in time domain	formulation in frequency domain
nonlinear equations of motion	linear equations of motion
absolute states	states as small deviations
nonlinear flight simulation	possibility of state space simulations after transformation into time domain
limited to motion of c/g, plus geometrical relations as for cockpit-, l/g- or tail-motion	direct access to motion of any grid point

Table 1: Different Methodologies

The following interdisciplinary methodology has been developed from the traditional ones within aeroelastics and flight mechanics. For the interfacing cooperation the agreed common coordinate system is body-fixed, originating in the c/g. The result is open for direct loads computation as well, but this is future work. Because formulation in time domain is a prerequisite for flight simulation, transformation of the aeroelastic mode equations from frequency domain into time domain is necessary, but was proven in the past.

Therefore the aeroelastic state space model formulation

$$\dot{\underline{x}}_e = \underline{\underline{A}}_{ee} \cdot \underline{x}_e + \underline{\underline{B}}_e \cdot \underline{u} \tag{2}$$

is one starting point. In order to present the formula easier to survey, gust disturbances are omitted here. Linearized 6 degrees of freedom rigid a/c motion can be written correspondingly:

$$\dot{\underline{x}}_r = \underline{\underline{A}}_{rr} \cdot \underline{x}_r + \underline{\underline{B}}_r \cdot \underline{u} \tag{3}$$

The vector $\underline{x}_r$ is part of the aeroelastic discipline's contribution. Per se it is not identical with the vector $\underline{x}_f$ within the flight mechanics formulation (see below). The vector $\underline{x}_r$ is the best possible approximation of $\underline{x}_f$. It results from inclusion of the rigid a/c modes into the structural dynamics tool called NASTRAN and from a specialized mode approximation supported vice versa by flight mechanics contributions of the exact modes. According to /3/ a coupled state space model is determined:

$$\begin{bmatrix} \dot{\underline{x}}_r \\ \dot{\underline{x}}_e \end{bmatrix} = \begin{bmatrix} \underline{\underline{A}}_{rr} & \underline{\underline{A}}_{re} \\ \underline{\underline{A}}_{er} & \underline{\underline{A}}_{ee} \end{bmatrix} \cdot \begin{bmatrix} \underline{x}_r \\ \underline{x}_e \end{bmatrix} + \begin{bmatrix} \underline{\underline{B}}_r \\ \underline{\underline{B}}_e \end{bmatrix} \cdot \underline{u} \tag{4}$$

Equation (3) can be rewritten for the exact flight mechanical behavior:

$$\dot{\underline{x}}_f = \underline{\underline{A}}_{ff} \cdot \underline{x}_f + \underline{\underline{B}}_f \cdot \underline{u} \tag{5}$$

Now the specialty of the cooperative interdisciplinary model is a transformation of equation (4) with two specified attributes:

- The vector $\underline{x}_r$ must follow stationary the path of $\underline{x}_f$.
- Therefore the coupling matrix $\underline{\underline{A}}_{re}$ (rigid due to elastic) may only lead to dynamic deviations of $\underline{x}_r$ around the path of $\underline{x}_f$ with frequencies upwards from the lowest frequency elastic mode.

The stationary effects of elasticity onto $\underline{x}_f$ and $\underline{x}_r$ have been found to be best incorporated by the flexible factors, which are part of the flight mechanical model contribution; here represented within $\underline{x}_f$. The transformation of equation (4), for which the aeroelastics specialists perform a special eigenvector calculation, leads to a formulation with $\dot{\underline{x}}_f$ as an additional input:

$$\begin{bmatrix} \dot{\underline{x}}_r \\ \dot{\underline{x}}_e \end{bmatrix} = \begin{bmatrix} 1 \\ \underline{\underline{\Phi L}}_{ef} \end{bmatrix} \cdot \dot{\underline{x}}_f + \begin{bmatrix} \underline{\underline{AL}}_{rr} & \underline{\underline{AL}}_{re} \\ \underline{\underline{AL}}_{er} & \underline{\underline{AL}}_{ee} \end{bmatrix} \cdot \begin{bmatrix} \underline{x}_r \\ \underline{x}_e \end{bmatrix} + \begin{bmatrix} \underline{\underline{BL}}_r \\ \underline{\underline{BL}}_e \end{bmatrix} \cdot \underline{u} \tag{6}$$

An output vector $\underline{y}$ results from integration of $\dot{\underline{x}}_r$ and $\dot{\underline{x}}_e$:

$$\underline{y} = \underline{\underline{\Phi L}}_{yf} \cdot \dot{\underline{x}}_f + \underline{\underline{CL}}_r \cdot \underline{x}_r + \underline{\underline{CL}}_e \cdot \underline{x}_e + \underline{\underline{DL}} \cdot \underline{u} \tag{7}$$

The output vector $\underline{y}$ gives cockpit accelerations, sensor signals, l/g above ground deviation due to elasticity and any other grid point motion needed for flight simulator application.

The main feature that $\underline{x}_f$ does not receive a backward coupling from the mode equations (6) and (7), allows for a replacement of $\dot{\underline{x}}_f$ from the linear equation (5) by the same vector being calculated nonlinear:

$$\dot{\underline{x}}_f = G_{nonlinear}\left(\underline{F}_{aero}, \underline{F}_{thrust}, \underline{F}_{weight}, \underline{F}_{gear}\right) \tag{8}$$

The function $G_{nonlinear}$ can be derived from the flight mechanical equations of motion; typical translatory equation:

$$\begin{bmatrix}\dot{u}_k\\ \dot{v}_k\\ \dot{w}_k\end{bmatrix}_f = \frac{1}{m}\begin{bmatrix}X^A\\ Y^A\\ Z^A\end{bmatrix}_f + \frac{1}{m}\begin{bmatrix}X^F\\ Y^F\\ Z^F\end{bmatrix}_f + \begin{bmatrix}-\sin\Theta\\ \sin\Phi\cos\Theta\\ \cos\Phi\cos\Theta\end{bmatrix}\cdot g - \begin{bmatrix}q_k w_k - r_k v_k\\ r_k u_k - p_k w_k\\ p_k v_k - q_k u_k\end{bmatrix}_f \tag{9}$$

And typical rotatory equation:

$$\begin{bmatrix}\dot{p}_k\\ \dot{q}_k\\ \dot{r}_k\end{bmatrix} = \underline{\underline{I}}_f^{-1}\cdot\left(\begin{bmatrix}L^A + L^F\\ M^A + M^F\\ N^A + N^F\end{bmatrix}_f - \begin{bmatrix}q_k r_k\left(I_z - I_y\right) - p_k q_k I_{zx}\\ r_k p_k\left(I_x - I_z\right) + \left(p_k^2 - r_k^2\right) I_{xz}\\ p_k q_k\left(I_y - I_x\right) + q_k r_k I_{xz}\end{bmatrix}_f\right) \tag{10}$$

with:

$$\underline{F}_{aero} = \left[X^A, Y^A, Z^A, L^A, M^A, N^A\right]^T \tag{11}$$

$$\underline{F}_{thrust} + \underline{F}_{gear} = \left[X^F, Y^F, Z^F, L^F, M^F, N^F\right]^T \tag{12}$$

$$\underline{F}_{weight} = \begin{bmatrix}-\sin\Theta\\ \sin\Phi\cos\Theta\\ \cos\Phi\cos\Theta\end{bmatrix}\cdot g \tag{13}$$

The equations (9) and (10) are typically implemented within flight simulators. They are the source for interfacing with the elasticity. But there is a significant distinction to be interpreted before deriving $\dot{\underline{x}}_f$ in equation (8) directly.

This distinction comes from the fact that the linear state space model (6) describes deviations from a single flight condition. Such a working point is defined by a certain (H, Ma) combination. Therefore $\dot{\underline{x}}_f$ in (8) corresponds with the absolute values in (9) and (10) being initialized at the mentioned flight condition and only the deviations being interfaced. For the reproduction of known elasticity phenomena in the flight simulators such proceeding can be sufficient.

Nevertheless for future investigations, focusing on APC due to elasticity, a wider simulation capability within the entire flight envelope is desirable. This will be achieved by consideration of larger numbers of flight condition related state space models and by sophisticated interpolation methodology. Related preparation work is documented in /5/, where the required computation power and the numerical complexity of this task are becoming visible (see also chapter 5).

The presented interdisciplinary modeling methodology is characterized by two peculiarities:

- Flight mechanics as well as structural dynamics disciplines can both implement the interdisciplinary model as an add-on to their traditional modeling. Flight mechanics interface the equations (6) and (7) via $\dot{\underline{x}}_f$, as described. Structural dynamics receive a linearized rigid a/c simulator-model according to equation (5), and then they can perform comparing off-line calculations in their proven environment.

- The interdisciplinary model features exactness at both ends of the common frequency regime. Stationary and low frequency rigid modes are dominated by the vector $\underline{x}_f$. Calculation of $\underline{x}_f$ is not influenced by the model upgrade. Higher elastic mode frequencies (vector $\underline{x}_e$) are correct as well, because the eigenvector calculation between equation (4) and (6) leaves them unchanged. Through parallel calculation of $\underline{x}_r$, also the intermediate frequency regime and the full rigid/elastic coupling is incorporated with best possible fidelity. The deviation of the c/g motion, due to elastic modes and due to the coupling, is permanently accessible by the difference $\underline{x}_r - \underline{x}_f$, which stationary fades to zero.

4. Work Process

The development of the interdisciplinary modeling methodology has been performed in close cooperation between flight mechanics and structural dynamics specialists. Comparative calculations where performed at all levels of progress. Automation of data generation and transfer as well as software code generation and transfer has been incorporated already from the beginning of the development. The process leads to piloted investigations in the six degrees of freedom, moving flight simulator located at TUB. Sessions in the moving flight simulator are slotted into it's main utilization as a training device. The limited accessibility and the higher costs per simulation hour lead to the decision, to develop and transfer fully tested models to Berlin.

Development and testing of the flight simulation software was carried out at DA's engineering flight simulator, featuring a fixed base generic cockpit with vision and sound. Here accessibility is better and costs are lower. This development simulation environment also has been used in parallel for off-line calculations. The automatic simulation test (AST) is a tool, which has been adapted especially for the checkout of the interdisciplinary modeling. It allows simulations to be run by scenarios predefined on a text file level and leads directly to specific plots.

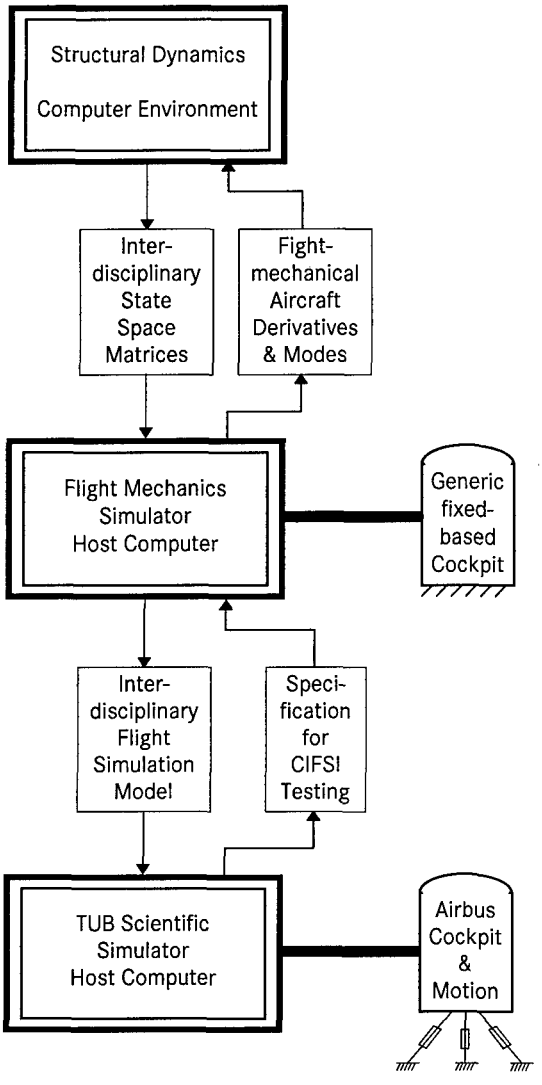

Figure 4: Cooperation and data/software transfers

From the point of view of flight mechanic the following steps belong to the creation of a running simulation, after a common decision for a flight condition to be investigated:

- Calculation of flight mechanic a/c derivatives and rigid a/c modes; delivery to structural dynamics in an agreed format.
  (Automation: Pressing a button and sending an e-mail)

- Structural dynamics specialists calculate the elastic modes and the full coupling (by a complex and intensive off-line computation), thereby generating the values of the matrices presented in the equations (6) and (7); delivery of these values back to flight mechanics in an agreed format.
  (Automation: Pressing a button, waiting and sending an e-mail)

- Real time capable coding of the equations (6) and (7).
  (Automation: Pressing a button and getting in return a FORTRAN subroutine ready for compilation)

- Implementation of this routine into DA's engineering flight simulator environment, where the a/c specific simulation and the necessary interfacing are ready for service.
  (Automation: Copy onto the simulator HOST computer, compilation and link)

- Intensive off-line automatic simulation testing (AST) and real-time tests in the development simulator with engineering pilots in the loop, widely covering the targeted model functionality and using CIFSI (see below) in order to ensure a seamless model transfer onto the moving flight simulator.

- Model transfer: TUB specific software adaptation, compressing extraction, centralization and final development simulator check.
  (Automation: Press a button and copy on a disk)

- Running the transferred model on the moving simulator and being prepared for piloted evaluations related to APC due to elasticity.
  (Automation: Read the software from disk, compile, link and run the simulation)

Software interfacing between the two simulation environments consists of two features (TUB interface and CIFSI). Cooperating specialists from TUB have prepared a FORTRAN interface, based on only two common blocks, which allows for a (now plug and play) integration of any a/c simulation model independently from the otherwise present A330/A340 related systems architecture and interdependence. The software environment of DA's development flight simulator has been connected with this interface in order to make the a/c modeling structure transferable. Initially the software could be switched for running in either environment.

But now, in a second step, the achieved status was further improved. A destined cockpit interface simulation (CIFSI) has been developed which replicates the moving simulator interface already within the development flight simulator. Using CIFSI means that DA's cockpit behaves virtually identically to the cockpit in Berlin. Finally it is this feature which allows for sufficient testing, including testing of the TUB specific interfacing before the model transfer. Besides the mentioned automation, this early, in depth testing capability is the real cost-saver featuring this process and allowing for the seamless a/c simulation model transfer.

5. Future Activities

5.1 Large Aircraft Flight Simulation Models

According to the presented methodologies flight simulation modeling shall be applied on new large flexible aircraft such as A340-600 and A3XX, permanently taking the latest specifications into account. These models shall respectively be transferred onto the moving flight simulator, allowing early detection of possible tendencies for APC due to elasticity and of according impacts on loads.

5.2 Further Modeling Improvements

As indicated before, flight simulation is most useful when the modeling is applicable within the entire flight envelope. The current status, to initialize the dynamic a/c elasticity modeling at certain flight conditions and then simulate nearby (with respect to altitude and Mach number variations), shall be overcome. Since the linear state space modeling of the elasticity part will remain the only one applicable in the foreseeable future, interpolations within a

larger number of state space models is the intended way to proceed.

Introducing investigations on the topic addressing interpolations of such specific state space models have been performed and documented in /5/. Besides the proper definition of absolute states and the related deviations from them, the challenge consists of an inherent coincidence. States and independent interpolation variables partially overlap. For example altitude is the one independent interpolation variable and in parallel it is a state within each single linear model. The other independent interpolation variable, the Mach number, is embedded within each single linear model with even more complexity. The states contain a/c velocity separated into body-fixed axes components, and the velocity of sound is dependent on altitude. Additionally the new interpolation methodology will require a huge amount of computation power for real time capable realization. That's why the presented openness of the involved flight simulation environments with respect to hardware upgrades is so welcome also in the future.

5.3 Work on Loads Control Functions

Special functionality for flight control laws, in order to keep loads at low levels, is under development at DA. Feasibility and value of these loads control functions shall also be validated by pilot-in-the-loop sessions utilizing the presented flight simulations within the multidisciplinary aeroservoelastic design process.

5.4 Implementation of interdisciplinary FCLs

Finally future flight control laws, improved for the needs of large flexible aircraft, shall prove their effectiveness with respect to the interdisciplinary requirements from structural dynamics and flight mechanics / handling qualities. Piloted flight simulations shall provide support within the design process from early phases onwards and confidence with respect to successful avoidance of APC tendencies due to elasticity, especially before first flight. The intermediate frequency regime, where the rigid a/c motion and the coupled elasticity are overlapping, and where the cooperating disciplines of structural dynamics and flight mechanics come parallel in touch, is the intended area for promising new flight simulation utilization, in particular pilot-in-the-loop simulation including cockpit motions.

6. Conclusions

This paper presented an approach to utilize pilot-in-the-loop flight simulation within the aeroservoelastic design process of large flexible aircraft. The intention is avoidance of APC due to elasticity and of excessive loads early during the development and especially before first flight. Successful interdisciplinary cooperation between structural dynamics and flight mechanics has been achieved. The cooperation found a modeling methodology, which can be considered in both disciplines as an add-on to their traditional approaches. It features exactness for rigid a/c motion as well as for the structural modes. In the intermediate frequency regime, where the phenomena are overlapping, highest possible fidelity of the model has been achieved through full coupling of rigid motion and elasticity. Two flight simulators are involved, each providing its advantages. An engineering flight simulator with a fixed base cockpit is the main software development tool with good accessibility and lower costs. And a special moving flight simulator with a scientific computation facility, allowing variable a/c modeling, is the target for the APC related piloted investigations. A proven model transfer from the development onto the moving flight simulator has been realized to a plug-and-play standard. The interdisciplinary cooperation process profits from automation, being widely designed into all data and software exchange steps from the beginning.

7. References

/1/ Koenig, K., Schuler, J.: *Integral Control of Large Flexible Aircraft*, Proceedings of RTA/AVT Meeting on Structural Aspects of Flexible Aircraft Control, Ottawa, Fall 1999

/2/ Kubica, F., Fath, D.: *Passenger Comfort Improvement by Integrated Control Law Design*, Proceedings of RTA/AVT Meeting on Structural Aspects of Flexible Aircraft Control, Ottawa, Fall 1999

/3/ Schuler, J.: *Flugregelung und aktive Schwingungsdämpfung für flexible Großraum-flugzeuge - Modellbildung und Simulation*, VDI Verlag, Düsseldorf, 1998, ISBN 3-18-368808-5

/4/ Karpel, M.: *Reduced-Order Aeroelastic Models via Dynamic Residualization*, Journal of Aircraft, Vol. 27, No. 5, May 1990

/5/ Massing, G.E.: *Untersuchungen zur Anwendbarkeit mehrdimensionaler linearer Interpolation auf Differentialgleichungen im Zustandsraum*, Diplomarbeit, Technical University Berlin, May 1999

Mobility Analysis of a Heavy Off-Road Vehicle Using a Controlled Suspension

M. Hönlinger, U. Glauch
Krauss-Maffei Wegmann GmbH&Co.KG
Krauss-Maffei- Straße 11
80997 Munich, Germany

Summary

Driving safety and ride comfort of cross-country vehicles can be improved with the help of a controlled spring/suspension system. The present paper describes the impact of a semiactive and partially active chassis system on the driving behaviour of a cross-country 8x8 wheeled vehicle. The mobility analysis is based on a multibody vehicle model used for simulating cross-country drives and handling. To start with, the fundamental "Skyhook"-principle is used for controlling; vertical accelerations and vehicle movements are clearly reduced on rough tracks and sine wave lanes.

1. Introduction

Especially for cross-country vehicles, the active chassis instead of a conventional chassis offers numerous advantages. Adjustment of the chassis to the road and to the driving situation offers numerous possibilities for improving the driving safety and the ride comfort and for reducing component wear and surface load, at the same time.

Upon closer examination of the total vehicle system from the point of view driving safety and ride comfort, next to the tyres the wheel suspension system has the greatest effects. Hence, interventions in this area will make sense in order to obtain fundamental improvements as regards driving safety and ride comfort.

Priority was given to this part of the investigation which was made with the help of a multibody simulation tool. Starting point was a cross-country 8x8 wheeled vehicle, fig. 1, which in the simulation was provided with a basic Skyhook chassis control and compared to the conventional chassis. With the help of vehicle simulations, the possibilities for mobility improvements with the help of controlled chassis were to be investigated.

As a rule, the mobility of a vehicle is determined by the possible maximum cross-country speed of the vehicle. On rough tracks and on good roads, maximum speed is mainly limited by the comfort of the ride, with due consideration of the driving safety. This is why the present investigation is mainly concentrating on the consequences for the comfort of the ride.

2. Controlled Chassis Systems

In chassis engineering, balancing of the chassis is a difficult and often quite demanding optimization task. For optimum ride comfort, spring and suspension rates should be as soft as possible. However, the related heavy body movements are detrimental for the driving safety. This is why for reasons of driving safety, the spring and suspension rates should be as hard as possible, in order to reduce body movements and dynamic wheel load deviations to a minimum. This will ensure good road contact and uniform load transmission of all wheels.

Fig. 2 is a graphic description of the target conflict between ride comfort and driving safety. If we take the body acceleration - as a measure for the ride comfort – in dependence on the dynamic wheel load – as a measure for the driving safety, a limiting curve of the physically possible can be derived for fixed pairs of shock absorbers and spring rigidity /1/. Due to the fixed characteristic curves, a vehicle with passive spring/suspension system can only cover one point on the envelopment curves, which will be either in favour of ride comfort or of driving safety, depending on the vehicle philosophy. In this context, the specific requirements of the vehicle, the expected road excitation and the driving situation must also be taken into consideration.

Active chassis systems are characterised by the fact that the loads between wheel and body are not created in dependence on the spring and damper rate, but can be applied according to requirements by means of external energy admission. By this means, the physical limits of passive wheel suspension systems shown in fig. 2 can be overcome.

Today, various systems are used for controlled chassis which can be subdivided into 3 groups, as can be seen from fig. 3 /2,3/:

- *Adaptive systems* are characterised by slowly adjustable spring-/suspension elements, the load characteristic of which can be adapted to the ride situation; i.e. in dependence on the speed, the driving manoeuvres or the condition of the road.
- *Semiactive systems* operated with rapidly adjustable spring/suspension elements, which facilitate controls

Paper presented at the RTO AVT Specialists' Meeting on "Structural Aspects of Flexible Aircraft Control", held in Ottawa, Canada, 18-20 October 1999, and published in RTO MP-36.

within the characteristic oscillation time of the body and/or the wheel.

- *Active systems* function essentially with hydraulic servo components, where the load is generated through external energy admission and controlled pursuant to a law of control /4/.

In chassis engineering, additional comfort through controlled chassis must always be seen in relation with the operational conditions, the higher purchase price and the additional power requirements. This is why vehicle simulations are an effective means for assessing possible improvements through controlled chassis as early as in the design phase

3. Model Description

3.1 Vehicle Model

To analyse the dynamic behaviour, a physical and a mathematical model is required. The entire vehicle model is built up in parameters with a multibody simulation tool (MBS) /5/. The necessary data have been taken from measurements, as far as possible, and compared to a test vehicle.

The MBS-total vehicle model, fig. 4, represents the following components and functions:

- chassis and wheel steering components
- axle- and steering kinematics
- drive train with all-wheel drive, longitudinal and transversal differentials
- wheels with internal emergency ring
- springs, passive and active shock absorbers
- hydraulic bump stop shock absorbers
- Skyhook control
- driver model
- road profiles, sine-wave lane, rough track, individual obstacles

3.2 Skyhook Control

The basic concept of the Skyhook control is the introduction of an additional shock absorber between the body and the inertia reference system, fig. 5. In this configuration, shock absorption counteracts the vertical acceleration of the body load independent of the influence of the wheel load. For technical realisation, an adjustable shock absorber is installed between wheel and body; the absorption capacity is controlled in dependence on the absolute velocity of the body v_a. External energy is required for this final control element. In the simulation model, the absorber force F_d between wheel and body is computed with the help of the following equation:

$$F_d = d_p * v_{rel} + d_a * v_a \quad (1)$$

The velocity of the body v_a is determined for each wheel station in the area of the chassis connection. In (1), the coefficients d_a correspond to active Skyhook suspension, d_p is the passive shock absorption and v_{rel} the velocity difference between wheel and body.

To represent the semiactive Skyhook control, and in contrast to active Skyhook suspension, no external energy is supplied to the system. This corresponds to an adjustable shock absorber; where the characteristic curve is controlled in dependence on the absolute velocity of the body v_a. In the simulation model the resulting absorption is computed as follows:

$$F_d = d_p * v_{rel} + d_a * v_a \quad \text{for } v_a * v_{rel} > 0 \quad (2)$$
$$F_d = d_p v_{rel} \quad \text{for } v_a * v_{rel} < 0 \quad (3)$$

Since Skyhook suspension is only controlled via the body velocity, the effect is unsatisfactory as regards intrinsic wheel frequency and higher frequencies /1/. This is why a frequency-dependent control is required for higher frequencies. For this purpose, an additional conventional shock absorber is used in the simulation.

4. Investigated Chassis Systems

The passive wheel suspension of the investigated vehicle consists of two spring/suspension elements for each wheel station. For hard shocks, a hydraulic bump stop shock absorber with high energy absorption has been installed on the hull which reacts after half of the spring travel, fig. 6. The bump stop absorber enables better tuning of the conventional shock absorbers and contributes to thermal relieve. In addition, the vehicle is equipped with a tyre pressure control system, to enable adapting the air pressure of the tyres to the condition of the road. The considerable mobility demands as regards quick traversing of obstacles, such as ramps, 10" individual TRAPEZOIDAL obstacle or 7 m sine-wave lane require a high energy absorption of the spring/suspension system, which can only be achieved through rigid tuning of the shock absorbers. In the following investigation, this standard configuration is called "rigid".

In the simulation model an adaptive, semiactive and a *partially active chassis system* are shown based on the passive chassis system. To determine the influence of an adaptive chassis control, a soft absorber characteristic is used, which corresponds to 50% of the standard design. The partially active chassis system is represented in the simulation model by means of an active Skyhook absorber replacing one of the two conventional shock absorbers. The essential objective of the Skyhook control is to stabilise long-wave body oscillations. The conventional shock absorber is used for the intrinsic wheel frequency, which is to be recommended also for real-time operation to ensure basic shock absorption in case of system failure. To reduce power requirements to a minimum, the passive spring elements are maintained for supporting the static body load. The total power consumption of the active actuator components is limited to 5% of the driving power. The semiactive chassis control takes place with a semiactive Skyhook shock absorber in accordance with the semiactive system.

5. Results of the Simulation

In the simulation typical test runs with various lanes, corrugated track, 7 m sine-wave lane and 10" individual

trapezoidal-obstacle are used for evaluating the ride comfort during cross-country driving. In the simulation, the possible maximum speed on the test runs is limited by the following quantities:

- Max. vertical acceleration in the driver's seat
  < 2,5 g for individual obstacles
- Max. vertical acceleration in the driver's seat
  < 1 g for sine-wave lane
- Pitch angle < 6°
- Power consumption in the driver's seat
  < 6 W

5.1 Corrugated Track

Fig. 7 shows the computed power consumption in the driver's seat for a typical corrugated track for different velocities. In the simulation a tyre pressure for road driving was selected. The effective value of oscillation power was computed as $m\ |a|\ |v|$, with v and a being the velocity and the acceleration. 80 kg were chosen for the vibrating load m. The results show the advantage of a soft-tuned or controlled absorber as compared to the standard configuration. With the help of a soft absorber (= adaptive control) maximum vibration in the driver's seat can be reduced in the area of the body natural frequency by 65% compared to the hard standard configuration. With semiactive and active dampers a reduction in power consumption of 64% and 77% is possible compared to the hard configuration.

The dynamic wheel load of a front wheel is shown in fig.8. A comparison of the different damper systems shows the advantage of the hard standard configuration for the areas around the natural frequencies of the wheel (~23 km/h) and the body (~5 km/h). With the help of a soft or controlled absorber the dynamic wheel load can be reduced in the area between the body and wheel natural frequency (around 10 km/h).

5.2 Sine-Wave Lane 7 m

Figs. 9-12 show the pitch angle, vertical acceleration and the wheel load during drive over the 7 m sine-wave lane as regards intrinsic body frequency. The results show that relatively small pitch angles (< 4 °, peak-peak) are achieved with the hard standard configuration. The essential advantage of the controlled chassis will be the reduction of the dynamic wheel load fluctuations.

Single Trapezoidal Obstacle (h = 250 mm)

Fig. 13 shows the vertical acceleration, the wheel load fluctuation and the pitch behaviour during drive over the individual trapezoidal obstacle. The shown vertical acceleration was filtered with a cut-off frequency of 16 Hz. The behaviour directly at the obstacle is hardly different, since it is mainly determined by the energy absorption of the hydraulic bump stop absorper. However, secondary vibrations are clearly reduced through active shock absorption. Compared to the standard configuration, vertical accelerations, pitch behaviour and wheel load fluctuations are reduced much faster.

5.4 ISO-Double Lane Changing

Fig. 14 shows the steering wheel angle, the roll angle and the wheel load during ISO-double lane changing at 70 km/h. The simulation results show that the transversal dynamics are hardly influenced by the various shock absorbers. However, the roll angle movement can clearly be influenced with the help of active absorption. But it is difficult to assess the related increase of comfort since this depends on subjective perception /6/. During this manoeuvre, reduction of wheel load fluctuation through controlled chassis is an advantage for improving the lateral guidance potential of the tyres /7/. For this purpose, a frequency-dependent control of the intrinsic wheel frequency is required.

6. Summary

This paper describes the investigations made with the help of dynamic driving simulations to improve the ride comfort of cross-country vehicles through controlled chassis. The investigations were based on a four-axle, all-wheel driven cross-country vehicle of the 33 t weight class, designed for high average speed on roads and in terrain. The spring/suspension system is characterised by its high energy absorption to enable rapid crossing of high individual obstacles, ramps and long ground humps. The individually installed hydraulic limit-stop shock absorbers absorb a large amount of the shock energy and by this means enable influencing the vibration absorbers as regards improvement of ride comfort.

Taking the example of the elementary Skyhook control, the simulation results show that on corrugated tracks and sine-wave lanes both the vibrational behaviour, the maximum vertical accelerations and the pitch movement can be noticeably reduced with the help of a controlled chassis. No negative consequences as regards increase of maximum vertical acceleration in case of individual obstacles could be found; this is essentially influenced by the separate hydraulic limit-stop shock absorbers.

As regards handling, the simulation results show that roll and pitch movements due to steering and braking can be considerably reduced with the help of the active control.

The high mobility requirements for the investigated vehicle in heavy terrain resulted in a relatively rigid tuning of the spring/suspension system. When looking at the typical operational profile of these vehicles it becomes clear that more than 90% of the rides take place on roads, tracks and rough tracks. A controlled chassis would ensure the same mobility in heavy terrain and improve the ride comfort both on bad road stretches and in easy terrain. By this means the average speed can be increased while reducing the stress for the crew at the same time. A high ride comfort is especially necessary for fatigue-free driving over long distances and will essentially contribute to the operational security for the crew.

It was only possible to deal with some aspects of chassis control in this preliminary investigation, this is why further investigations as regards mobility and control strategies will be required. The next step would be to design a controller for road and terrain operation to take also higher frequency excitations into account.

References

/1/ Mitschke M.; Dynamik der Kraftfahrzeuge, Bd B: Schwingungen; Springer Verlag; Berlin, 1997

/2/ Wallentowitz, H., Aktive Fahrwerktechnik, Fortschritte der Fahrzeugtechnik Bd. 10,Vieweg Verlag

/3/ Kallenbach, R.; Optimierung des Fahrzeugverhaltens mit semiaktiver Fahrwerkregelungen, VDI Bericht Nr. 699, 1988, Seite 121-134

/4/ Breuer, W.; Mechatronische Elemente bei der Untersuchung eines vierachsigen Geländefahrzeugs, VDI-Bericht Nr. 1293, 1996, Seite 585-601

/5/ ADAMS, Using Adams/Solver/Driver, Mechanical Dynamics, 1997/1998

/6/ Mitschke M.; Dynamik der Kraftfahrzeuge, Bd C: Fahrverhalten; Springer Verlag; Berlin, 1990

/7/ Alberti, V.; Beurteilung von Fahrzeugen mit adaptiver Fahrwerkdämpfung; VDI-Bericht Nr. 916, 1991, Seite 469-489

Fig. 1: 8x8- Off- Road Vehicle (33t)

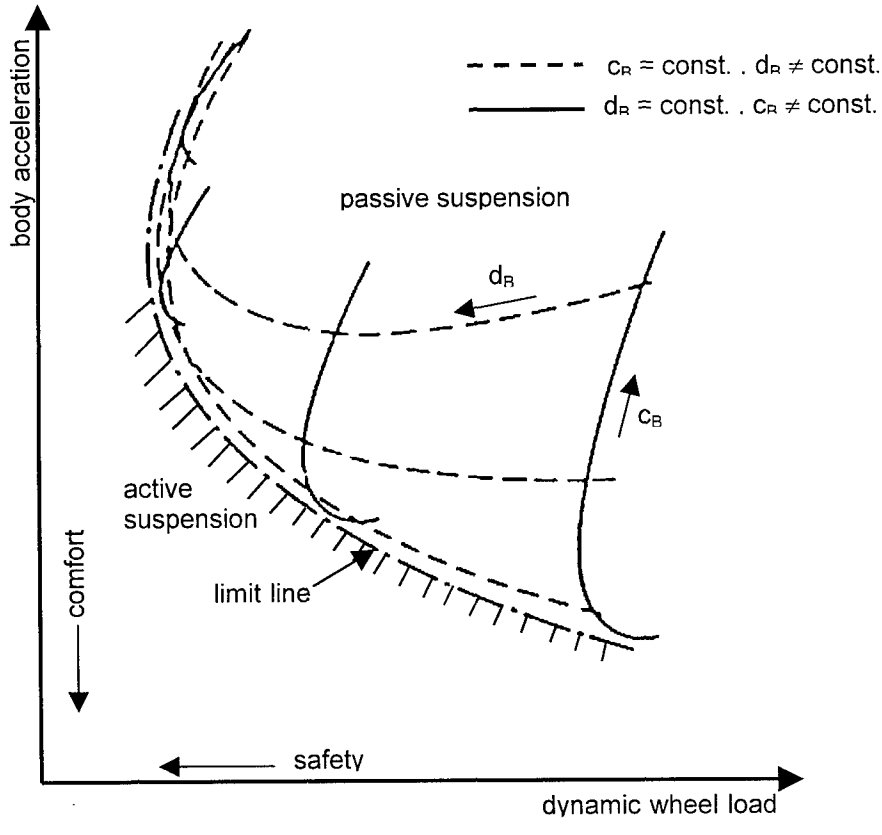

Fig. 2: Design of suspension systems

	Model	Force characteristic	Energy consumption	Control Frequency
passive	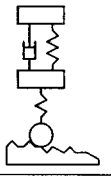	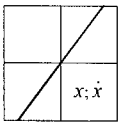		
adaptive	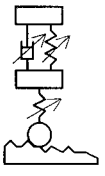	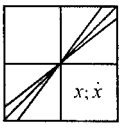	low	slower than the bodynatural frequency
semiactive		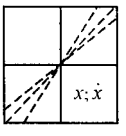	low	faster than the bodynatural frequency
active	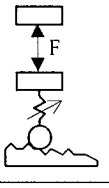	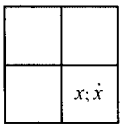	high	faster than the bodynatural frequency

Fig. 3: Classification of suspension systems

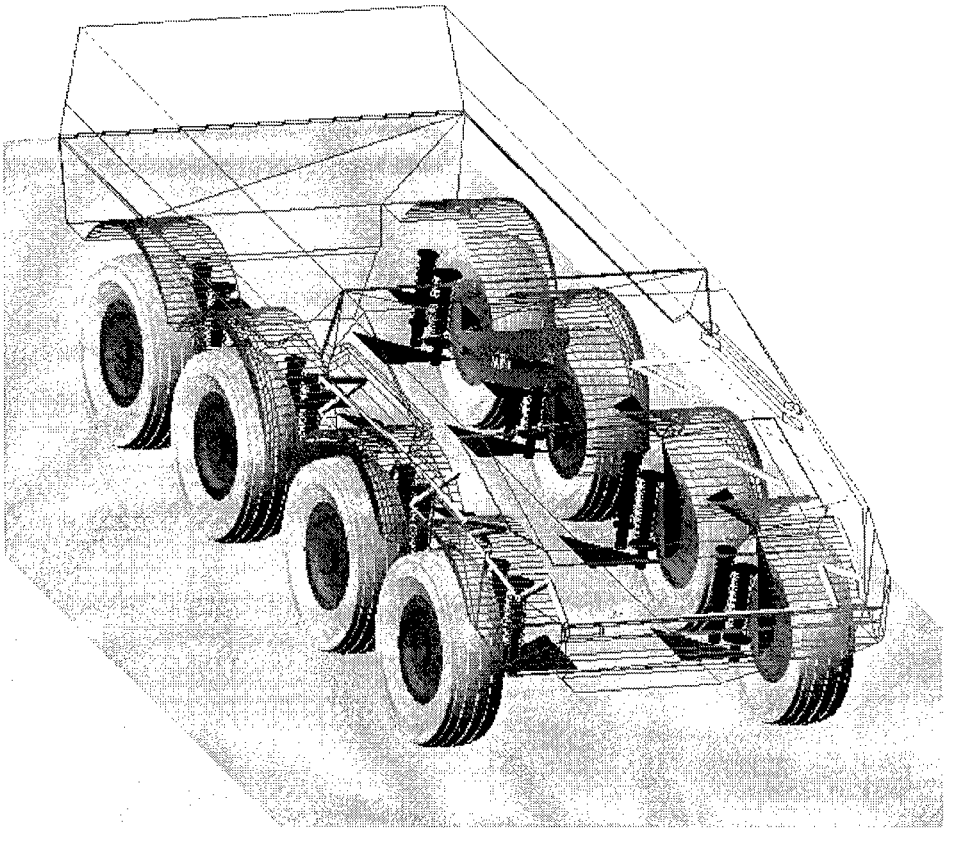

Fig. 4: MBS- Model 8x8 Off- Road Vehicle

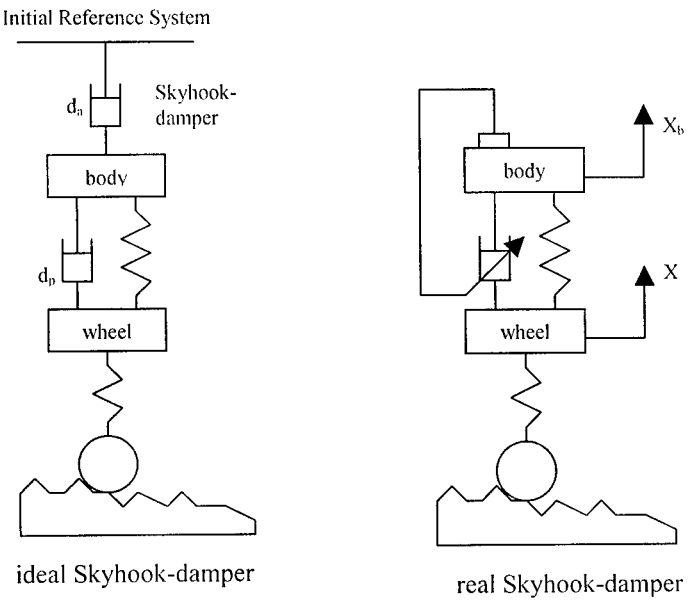

Fig. 5: Model of an active Skyhook-

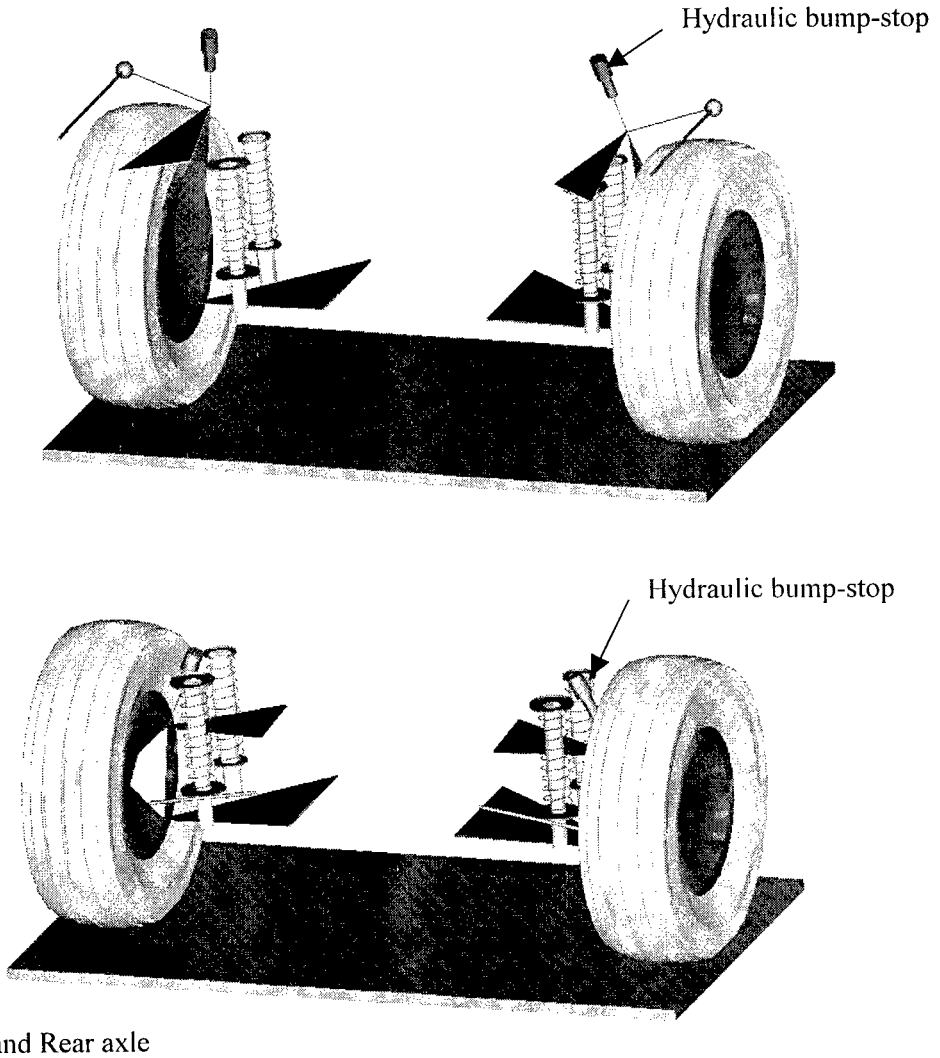

Fig. 6: Front and Rear axle

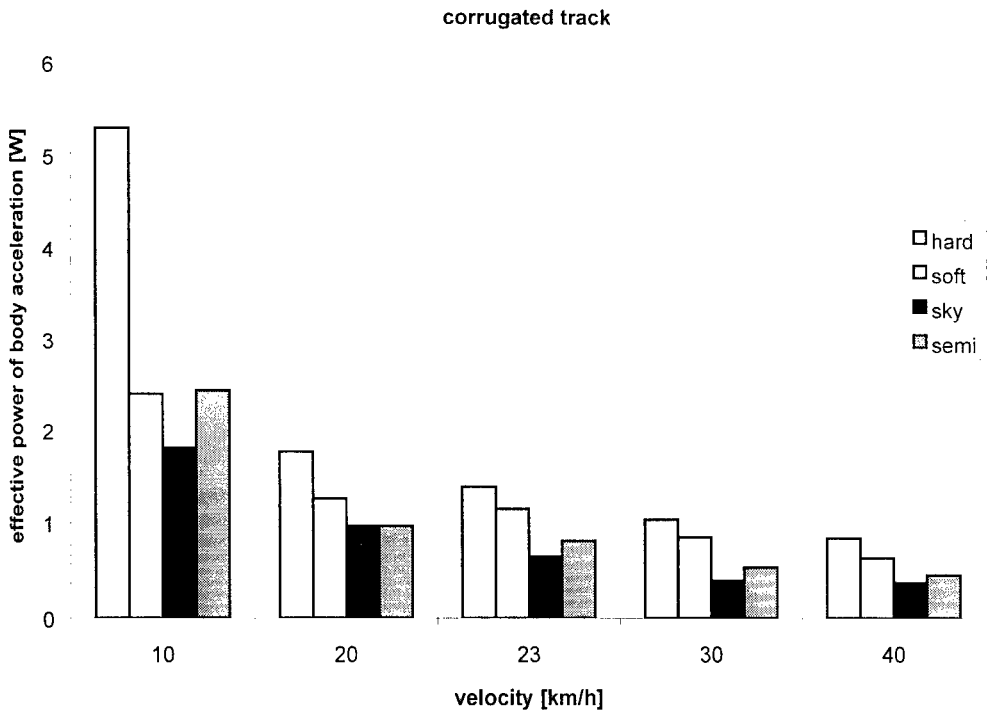

Fig. 7: Effective power of body vibration

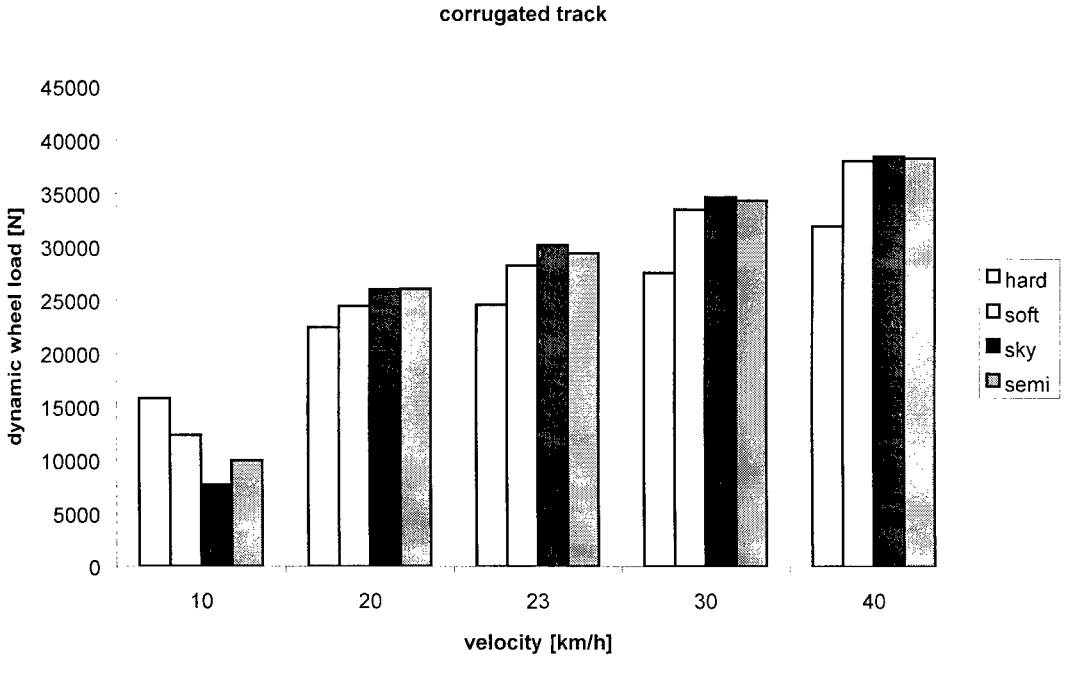

Fig. 8: Dynamic wheel load

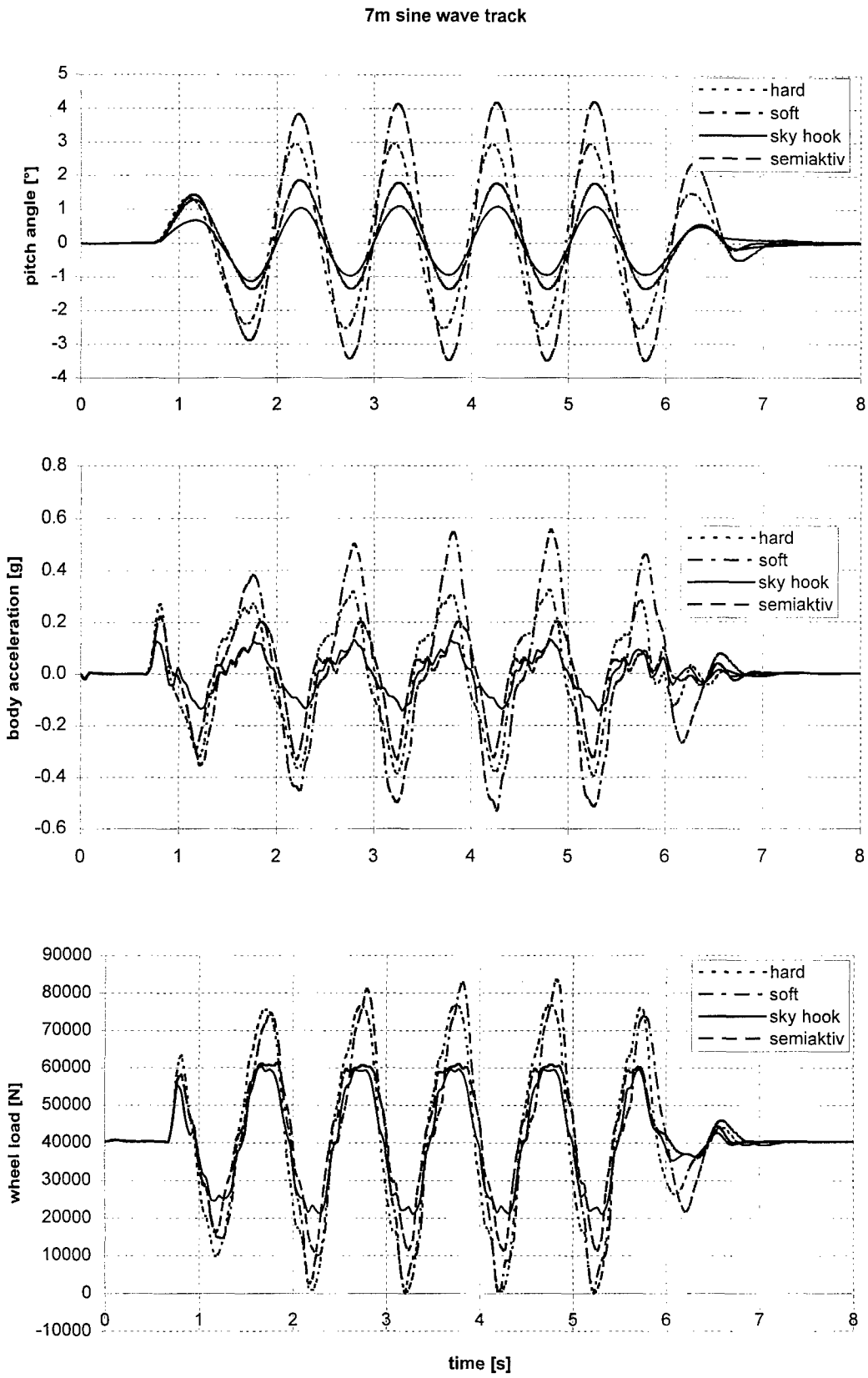

Fig. 9: Seven metre sine wave track at 25 km/h (Amplitude 100mm)

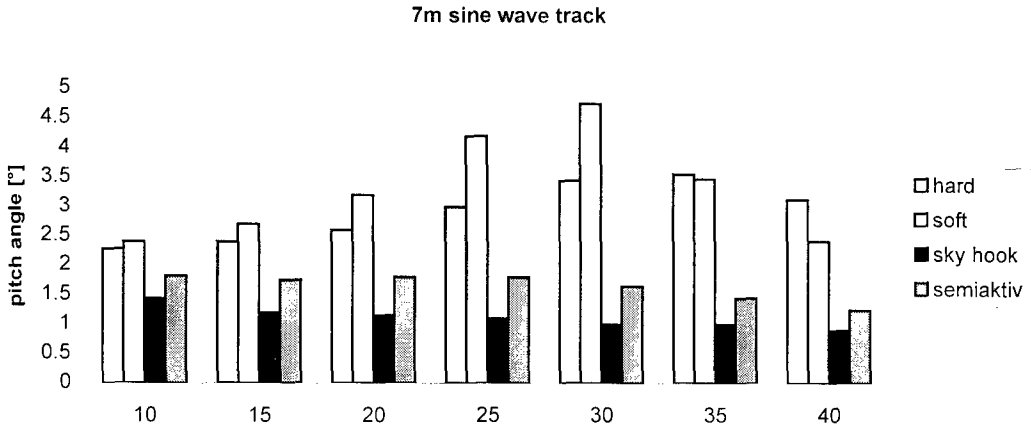

Fig. 10: Pitch angle with different damper systems

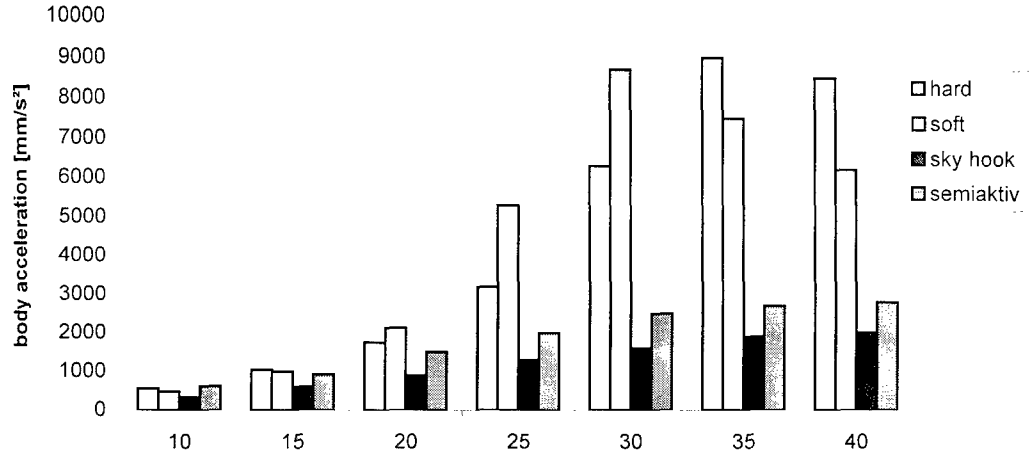

Fig. 11: Body acceleration with different damper systems

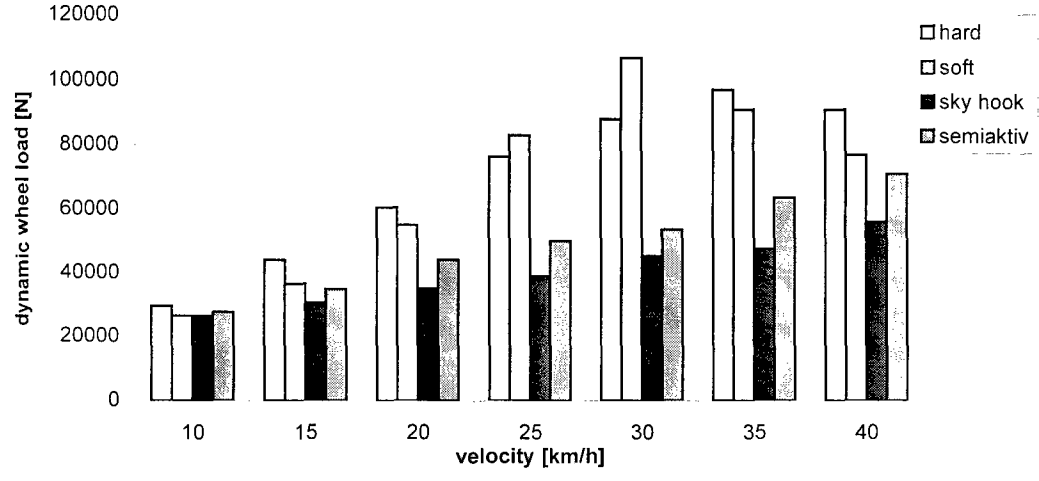

Fig. 12: Dynamic wheel load with different damper systems

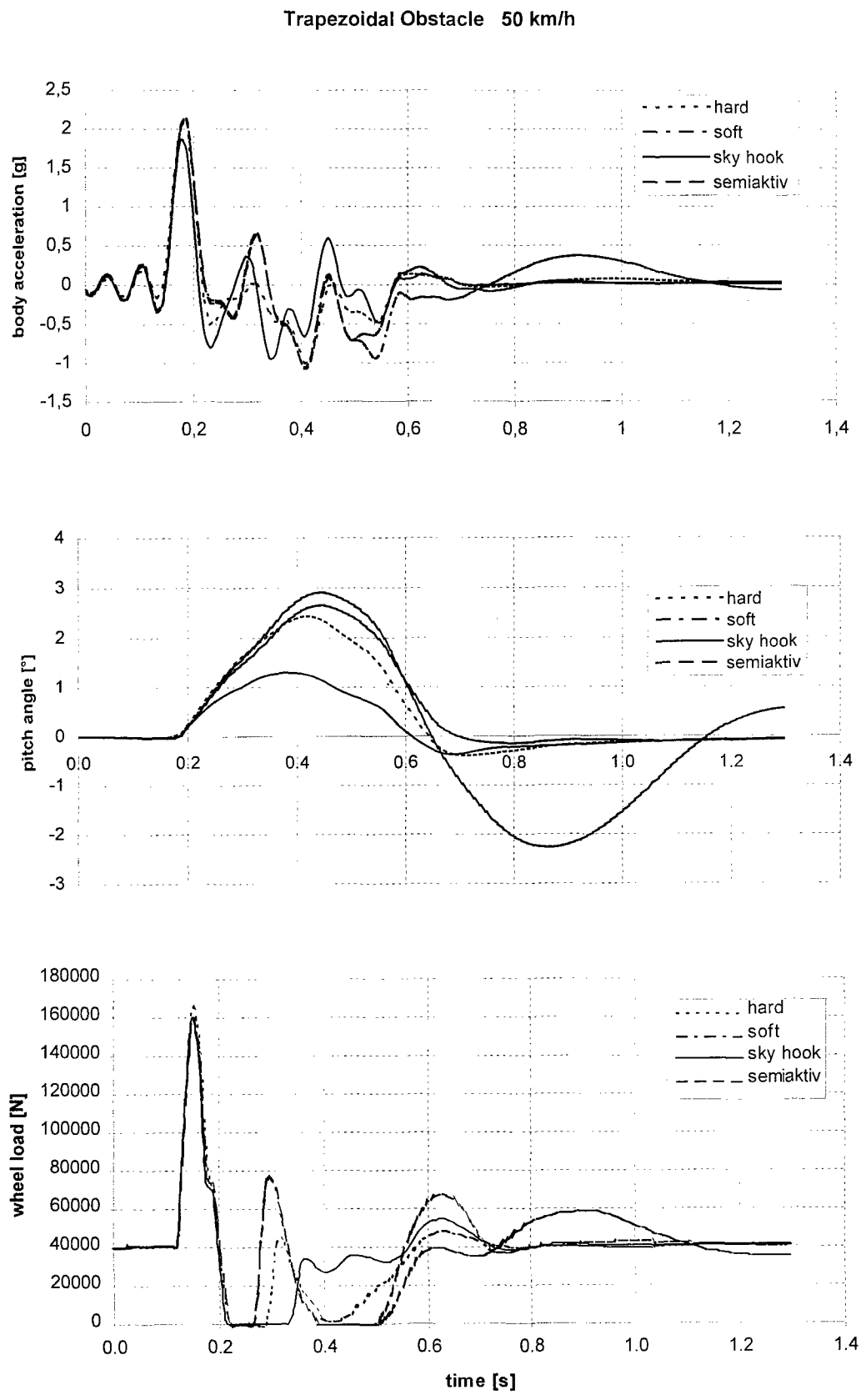

Fig.13: Trapezoidal obstacle clearance at 50 km/h (h=250 mm)

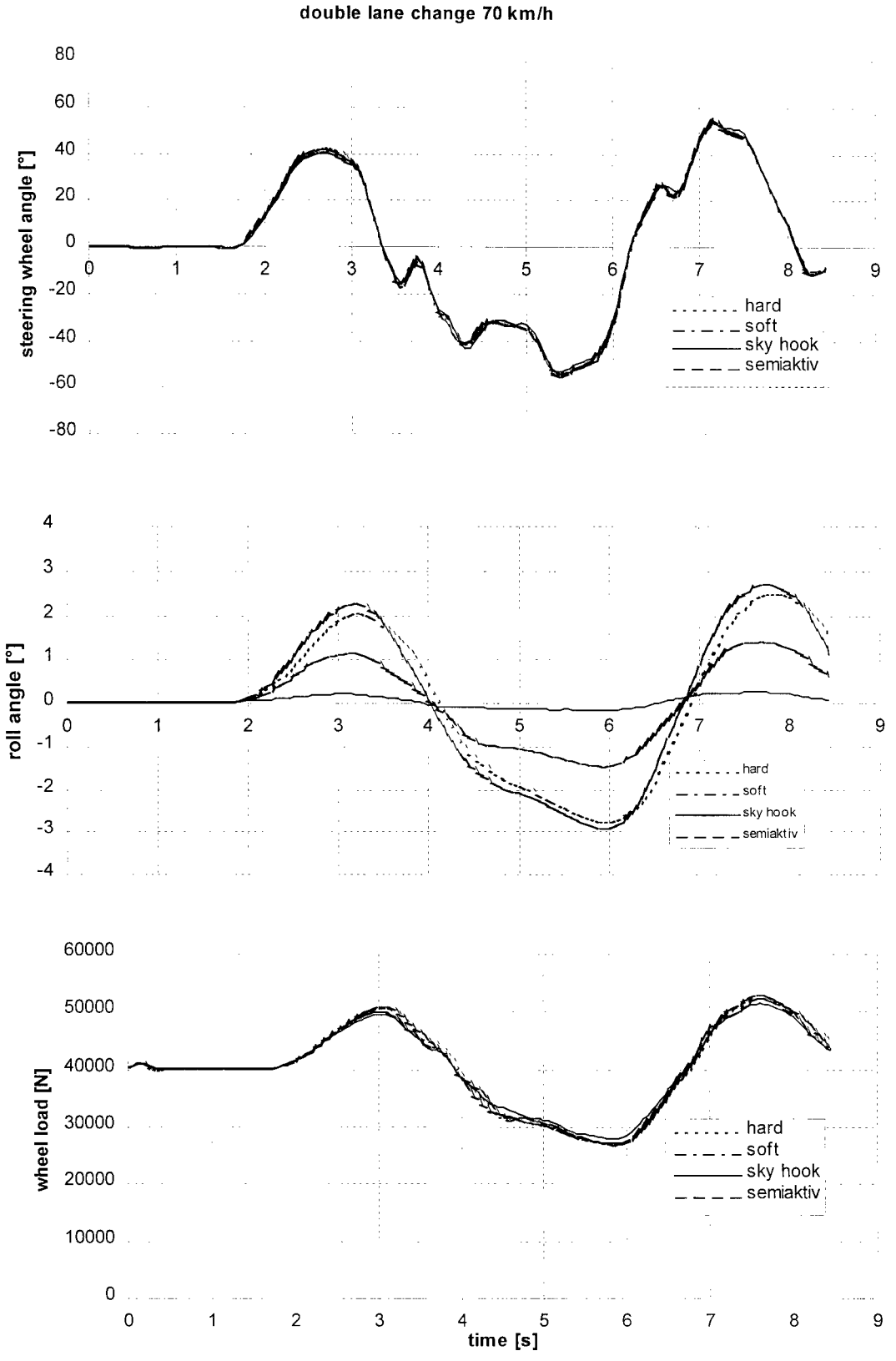

Fig.15: double lane change at 70 km/h

An integrated methodology for flexible aircraft control design
Une méthodologie globale de conception de lois de commande pour l'avion souple

D. Alazard, A. Bucharles, G. Ferreres, J.F. Magni, S. Prudhomme
Systems Control and Flight Dynamics Department,
ONERA-CERT, 2 avenue Edouard Belin, 31055 Toulouse Cedex, France

Abstract

This article details recent research activities of the *Systems Control and Flight Dynamics* department of ONERA in the field of flexible aircraft control. A long-term research program has been conducted for several years, with governmental funds, and with the technical support of AEROSPATIALE-Avions (Toulouse, France). Beyond the primary objectives of achieving various specifications for simultaneous aircraft motion and structural dynamics control, more fundamental questions are addressed, concerning the implications of rigid-structural dynamics coupling for the selection of suitable control law design methodologies.

Résumé

Cet article détaille les recherches récentes menées dans le domaine de la commande de l'avion souple au département de *Commande des Systèmes et Dynamique du Vol* de l'ONERA. Un programme de recherche d'envergure sur plusieurs années a été financé par le gouvernement français avec le soutien technique d'AEROSPATIALE-Avions (Toulouse, France). Au delà de la prise en compte des diverses spécifications relatives à la commande simultanée des dynamiques du vol et de la structure de l'avion, on aborde des questions plus fondamentales relatives à l'impact des couplages rigide-souple sur les méthodes de conception de lois de commande.

1 Introduction

For most aircraft of the past and present generations, control of the rigid and structural dynamics are considered as two distinct problems, as far as the frequencies of the structural modes do not overlap the frequency range of the rigid flight control. Generally, the rigid control is designed first, with low pass filtering of the outputs to avoid residual coupling with the structure, using a *passive control strategy* which leads to poor performance in perturbation rejection. Additionally, structural dynamics can be controlled using a specific feedback loop with appropriate filtering. This gives reasonably good results as long as the frequency separation assumption between rigid and flexible dynamics is valid. This is not any more the case for new generations of large transport [15] or supersonic aircraft [30] for which first structural modes show low frequencies and remain excited by the rigid control [4]. Filtering of measurements has limitations [10,11], generally leading to a loss of performance for the rigid dynamics, and unacceptable flight qualities. Control of such aircraft becomes a global rigid and flexible problem, and control laws must be designed in a global one-step procedure leading to a unique control loop with complex multivariable controllers [3]. First published developments in this research area of simultaneous rigid and flexible control are recent [5,6]. Some methodologies already have been proposed for civil aircraft applications [7,9,12,22]. As required performances on structural dynamics are very ambitious, an *active control strategy* is necessary. This is a real challenge, since the system model is of high order and subject to many uncertainties or unmeasured parameter variations against which the control laws must be robust. This article details a global methodology [34], developed in a long term research program COVAS[1] which has been conducted for several years, in the System Control and Flight Dynamics department of ONERA, as a solution for the flexible aircraft control problem. This research was funded by Direction des Programmes de l'Aviation Civile, via Service des Programmes Aéronautiques, with the technical support of AEROSPATIALE-Avions.

[1] COntrôle du Vol de l'Avion Souple, Flexible Aircraft Flight Control

Paper presented at the RTO AVT Specialists' Meeting on "Structural Aspects of Flexible Aircraft Control", held in Ottawa, Canada, 18-20 October 1999, and published in RTO MP-36.

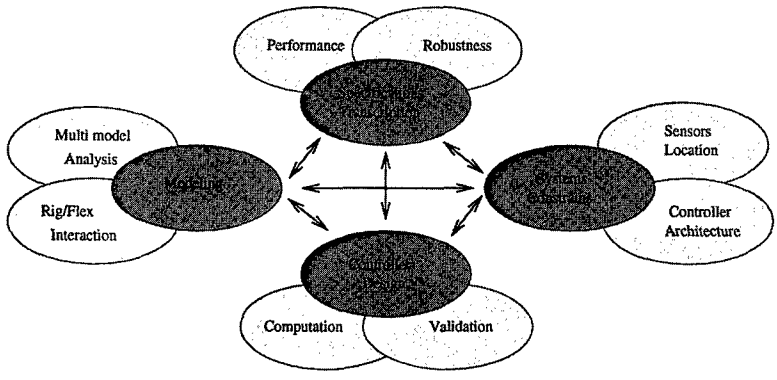

Figure 1: Related sub-problems for flexible aircraft control design

2 A multiobjective problem

Flexible aircraft control design is very challenging, because many issues are concerned as illustrated in figure 1. Most include considerations about rigid-structural interactions. This makes flexible aircraft control a multiobjective problem where different trades off are necessary.

2.1 Heterogeneous specifications

The selection of a methodology for solving this problem from the engineering point of view is strongly connected to the nature and the requirements of the control specifications. As summarized in table 1, specifications are heterogeneous, expressed either in time, frequency or parameter domain. The candidate design methodology must be able to simultaneously achieve these various specifications, for both rigid and structural dynamics.

Specs	Rigid	Flexible
Perf.	Time	Frequency
Robust.	Parameter	Frequency/Parameter

Table 1: Nature of control specifications.

Performance specifications: time and frequency domain

Performance specifications for the rigid dynamics are derived from required flight qualities and expressed in the time domain. These are settling times and decoupling constraints on the rigid states of the aircraft. The most natural control approach for achieving these specifications is eigenstructure assignment, which has proved efficiency for rigid aircraft [1,2]. However, applying this technique in its basic formulation to flexible aircraft leads to unacceptable coupling effects with the structure [22].

Performance specifications for the structural dynamics are mainly related to gust alleviation for load minimization and passenger comfort increasing [33], so that an active control strategy becomes necessary. These specifications are expressed in the frequency domain in terms of attenuation for acceleration responses to turbulence. Two competitive strategies are possible. The most natural one is explicit optimal control [23], trying to minimize the turbulence-to-acceleration transfer function in the frequency bandwidth where performance is needed. The second one is more physical. It consists in damping augmentation for modes that are the most significant for performance [22,24,25]. These two strategies have similar interpretations in terms of performance for high requirements in active control of the structure. It can be shown that optimal control naturally increases damping ratios, and that damping augmentation strategies can be interpreted in an optimal control scheme.

An additional specification is expressed in the frequency domain, namely the avoidance of pilot to structure coupling over a larger frequency domain than for rigid aircraft.

Robustness specifications: frequency and parameter domain

Standard robustness requirements for the rigid control are expressed in the parameter domain (robustness against aerodynamic coefficients variations, delays in the measurement or actuation loops, ...).

There are specific robustness specifications related to the structural dynamics. First, the model of the flexible aircraft is not so well known as the rigid model [8]. Highest frequency modes are generally neglected during modeling (normally called dynamical uncertainties), so that the control law must introduce convenient roll off. Moreover, there are several unmeasured parameters (mass, fuel distribu-

tion in the tanks, ...) in the flexible structure model parameters, leading to uncertainties against which the control law must be robust. This has motivated lots of research in the field of robustness analysis [16,17] and robust synthesis [18].

2.2 Systems constraints

Beyond the achievement of these primary objectives, the designed controllers should be easily adaptable to changes in the specifications and tuneable for refinements after flight tests. The control design methodology must provide a few *high level tuning parameter* with physical interpretation, and support some constraints for implementation considerations.

Low order control design for high order dynamics

As high performance is expected for structural control, a complex modeling of the dynamics is necessary (typically 50 to 80 states), which may lead to high order multivariable controller and violate order constraints related to real time implementation, and controller readability for adjustment during flight tests. The controllers must be as simple as possible, with physical interpretation. There is a need for lower order controller design. Among all possible strategies illustrated figure 2, direct design is the most complex, as the equations for the computation of optimal solution are untractable [20]. Multimodel modal control with a priori fixed controller dynamics gives a solution [22,31]. Alternatively, a low order model can be computed before control design. Model reduction is rather difficult, as the best reduction model for control design depends on the controller that is not yet known when reduction is computed [19,26]. The last strategy consists in computing a high order controller first, which may be difficult for high order model but guarantees a full information control design, and then reducing it, trying to recover known closed loop performance. However, reduction involves mathematical manipulations that may lead to unreadable multivariable controllers.

Sensors

Obviously, the more sensors are used in the control architecture, the better performance can be expected. However, for some practical reason related to implementation, particularly for redundancy [2], the amount of sensors should be strictly limited, which may lead to restrictions in performance. For a given number of sensors, a tricky selection of their location must then be undertaken, in order to reach the best trade off in performance and robustness.

[2] this problem is not addressed here

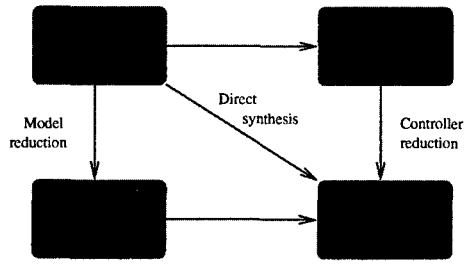

Figure 2: Strategies for low order controller design

3 Nominal model design and multimodel analysis

For rigid aircraft, control design can be performed chronologically within different steps: sensor selection, rigid control design, analysis of potential structural coupling, and structural filtering. As already mentioned, all steps must be considered in a one step control design for the flexible aircraft control case. However, for the sake of clarity, different levels of complexity are introduced in the sequel for presenting the methodology. They are illustrated in figure 3.

To complete the design process, various kinds of tools must be available: for selection of a convenient design model, for transcription of specifications, for computation of controllers, and for validation. Namely, the availability of multimodel analysis tools is a key point for having a good trade off in performance and robustness for flexible aircraft control laws.

3.1 Nominal model design with parameter uncertainty description

For controlling systems subject to parameter variations, multimodel control design techniques can be used [22] or other sophisticated techniques such as LPV (Linear Parameter Varying) [32] if an explicit description of parameter dependence is available. For flexible aircraft control, such a description of the structural dynamics is not always available. Modern control design techniques based on a single design model are used, with possible preliminary reduction to get a reasonable order, and less sophisticated description of parameter variations is used.

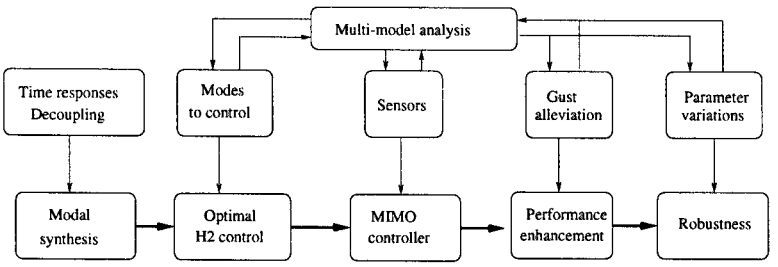

Figure 3: A strategy for flexible aircraft control design

Among strategies available for low order control design, a combination can be made between *preliminary open loop reduction* which brings the model to a reasonable order without removing any important information for control, and post synthesis *closed loop reduction*, keeping the least information for good control performance recovery on the true aircraft.

In the preliminary analysis of the control problem, multimodel analysis allows selection of a design model, and offers possible characterization of parameter variations on the structural modes in defining amplitudes of intervals in which parameters are expected to vary. This will be used for specifying robustness.

3.2 Generalized multimodel analysis

Indeed, multimodel analysis is useful for most control considerations, as illustrated in figure 3. It allows selection of modes to be controlled and sensors to retain for feedback. In the validation process of the control laws, it can detect *worst case* behaviors to be taken into account for performance and robustness improvement.

Selection of modes for active control

Modes to be controlled must be selected via a multimodel analysis of the open loop transfer from gust to acceleration, in order to achieve good robustness in gust alleviation performance, which is one of the most important control specification. An example is given figure 4 for the lateral dynamics of a conceptual aircraft, with analysis of transfer functions for different mass distribution configurations. A single model analysis would lead to forget some modes which are not significant for the corresponding configuration, but which should be retained as they significantly contribute to gust response for other configurations.

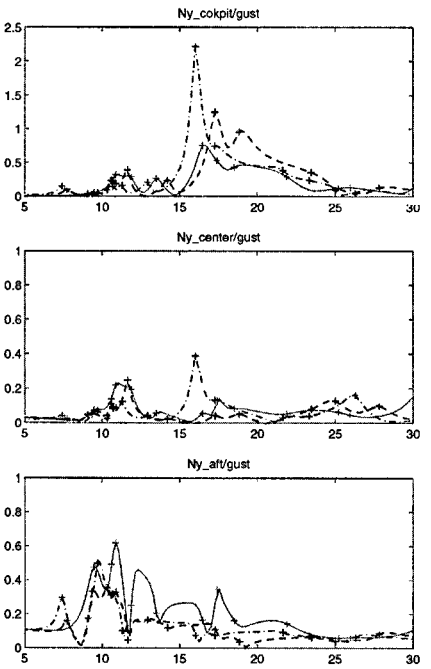

Figure 4: Multimodel analysis of modal contributions to gust response for selection of modes to be controlled

Selection of sensors

A major issue for control design is the capability of observing the dynamics of interest through the sensors. For rigid control purpose, sensors that are not polluted by the structural modes are generally preferred, in order to recover the best rigid performance and to limit the use of notch filtering. For high authority control of flexible structure, it becomes necessary to use outputs having a significant contribution from the structural modes to be controlled. As the modal contribution is very sensitive to measurement location, optimization of sensors location must be considered [13,14]. The selection of suitable sensors for control is also strongly dependent on the control objectives: sensors must be selected among those which contain the highest contribution of the structural modes to be controlled, but which are the least sensitive to variations on unmeasured parameters (especially mass distribution). For the lateral dynamics of a conceptual aircraft, figure 5 illustrates the energy of controlled structural modes which is contained in measurements at different locations along the fuselage, and a characterization of sensitivity to parameter variations. In this particular example, such an analysis would lead to select sensors ϕ and p at the center of the aircraft as at this location the highest energy and the smallest variations are obtained. On the contrary, sensors for N_y would be preferred at aft and those for r at front or aft.

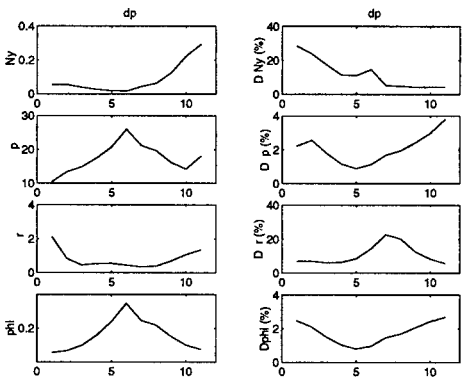

Figure 5: An illustration of sensors selection
Left: contribution of structural modes to output energy
Right: amplitude of variations due to parameter uncertainties
Sensor location: #1 cockpit, #6 center, #11 aft

4 Controller design

4.1 A generic architecture

A very generic controller architecture is used as shown figure 6, with feedforward H from pilot inputs to actuator signals which will include adequate filtering to prevent pilot/structure dynamical coupling, and with feedback K to control the closed loop dynamics and achieve perturbation rejection.

4.2 A standard formulation for transcription of specifications

The selected control design technique must allow simultaneous transcription of specifications of heterogeneous nature and the computation of the controller in one-step. For this, a convenient tool is the standard form of figure 7. First introduced by Doyle [21] in the context of robust control design, this formalism is now used for many applications. It uses an input to output linear representation of the nominal aircraft dynamics that is artificially augmented for transcription of dynamical specifications, with extensions for description of parameter uncertainties such as in 3.1. This leads to an augmented system, connecting generalized inputs to outputs and defining a mixed performance/robustness index. The control problem is now to design a feedback controller between measurements y and control signals u sent to the actuators, for minimizing the energy transmitted in closed loop from perturbations e on the aircraft, to regulated variables z. The control design technique must be suitable for robust stabilization of the aircraft, i.e. achieving specified performance of the nominal dynamics subject to all perturbations specified in the standard form.

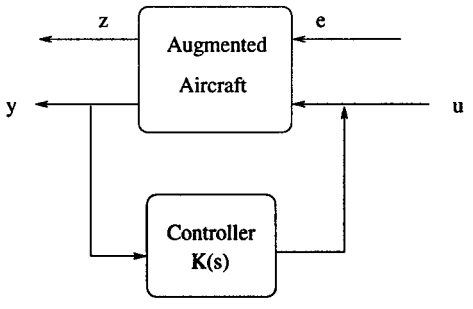

Figure 7: A general standard form for transcription of specifications

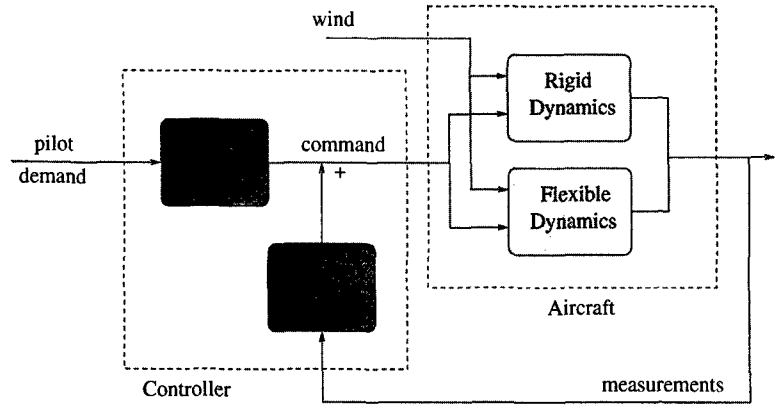

Figure 6: A generic architecture

4.3 High level tuning parameters

Figure 8 shows more details on a standard form that is used for flexible aircraft control. There are only a few blocks, for transcription of specifications, including both rigid and flexible control, roll off at higher frequencies (robustness against unmodelled dynamics), and for robustness against parameter variations using a perturbation approach. All these blocks only include a few adjustable parameters, which enables easy tuning of performance and robustness trade off. Such a standard form can be sophisticated for introducing more detailed specifications. Particularly, the nominal case description of the aircraft in figure 7 can be replaced by a more sophisticated modeling, using a specific block Δ for explicit dependence versus parameter variations, and another block $\Delta(s)$ for dynamical considerations, leading to an augmented description of the aircraft called LFT (Linear Fractional Transformation) illustrated figure 9.

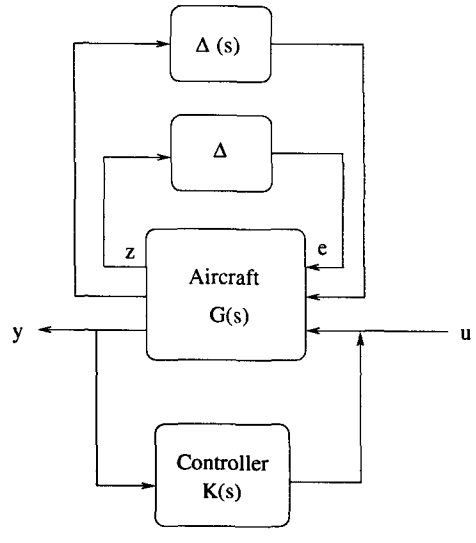

Figure 9: A generic LFT description for flexible aircraft control

4.4 Controller interpretation

The standard form naturally leads to optimal control (typically H_2 or H_∞), for minimizing the transfer functions between perturbations e and regulated outputs z, simultaneously achieving specified performance and robustness for rigid and structural control. As all blocks use input to output linear representations, the standard form and the associated optimal control design techniques are universal and remain useful for any order of the aircraft model. Only the parameter variation description block uses a specific state space representation of the aircraft.

Actually, H_2 is a generalization of optimal LQG control. Obtained controllers can be reformulated under an LQG like form, with state feedback and dynamical state estimation [27]. This justifies the transcription of parameter robustness specifications via a perturbation approach, using LTR and PRLQG extensions of LQG [28,29] in figure 8. Moreover, this interpretation leads to two-degrees-of-freedom controllers with feedback K and feedforward H in figure 6 having common dynamics. Figure 10 shows the transfer functions of the feedforward terms from pilot demand to actuator signals. It is clear that the dynamics lead to natural filtering of the pilot demand in order to avoid structural excitation and potential coupling. Feedforward can be improved via optimization within a multimodel framework.

4.5 Robustness assessment

Using the LFT description of nominal model with parameter variations such as in figure 9, robustness can be evaluated, using sophisticated analysis tools such as μ-analysis [35]. Analysing robustness in stability allows the computation of the parameter variations that can be supported bu the controller without destabilization of the closed loop. Analysing robust-

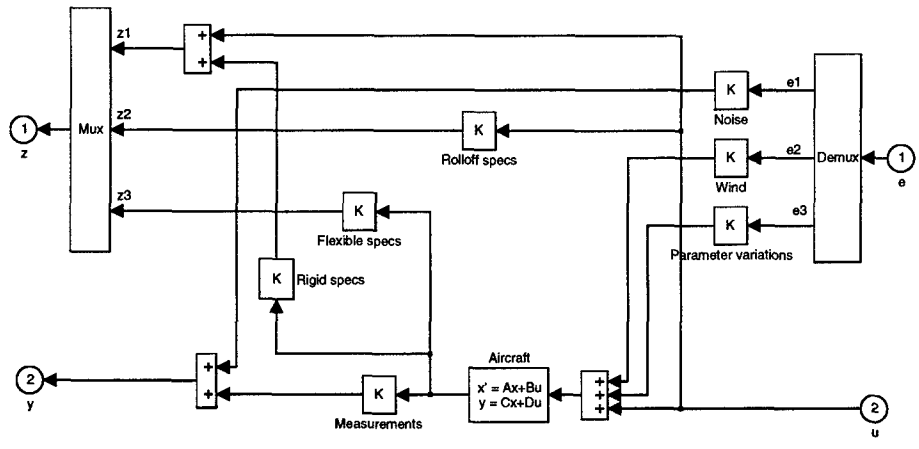

Figure 8: A specialized standard form for transcription of flexible aircraft control specifications

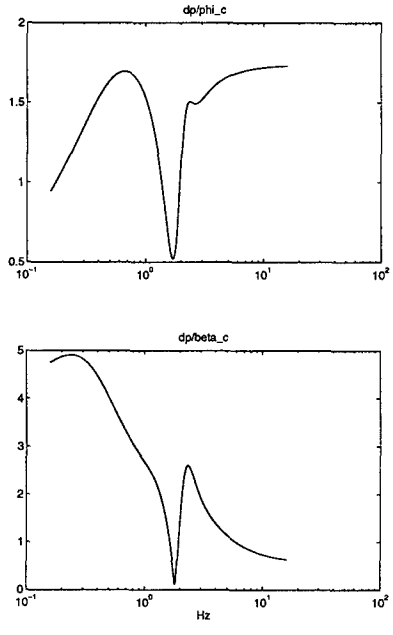

Figure 10: Dynamical feedforward

ness in performance indicates how closed loop rigid and flexible performance are modified by these parameter variations. There are difficult steps in this analysis. The first one is the construction of the LFT form. The second one is the computation of the μ norm [36], which can only be bounded. This is a difficult task for flexible aircraft having high order dynamics, with lowly damped modes.

5 Illustration for a conceptual flexible aircraft

The illustrative example is the lateral dynamics of a conceptual highly flexible aircraft, for which preliminary results have already been shown. All rigid and flexible specifications in performance and robustness have been transcribed into the formalism of the standard form, as shown figure 8. The control design technique is based on H_2. Though the dynamics of the aircraft is of very high order (about 80 states), the obtained controller is of low order (14 states), thanks to reduction. We now give a few more closed loop results, illustrated on next figures:

- Figure 11 shows time responses to standard demands in sideslip and roll, with a good robustness against large parameter variations on the rigid and flexible dynamics, and with low residual excitation of the structural modes.
- Figure 12 shows the frequency responses between gust and accelerations at various locations on the fuselage (front, center and aft) without and with active control of the structural dynamics. The achieved performance is about 50% reduction for all modal contributions below 3Hz.
- Figure 13 shows how pilot coupling transfer is

minimized in closed loop below 3Hz.

- Figure 14 illustrrates the analysis of robustness against uncertainties on flexible mode frequencies, using LFT representation and μ-analysis.

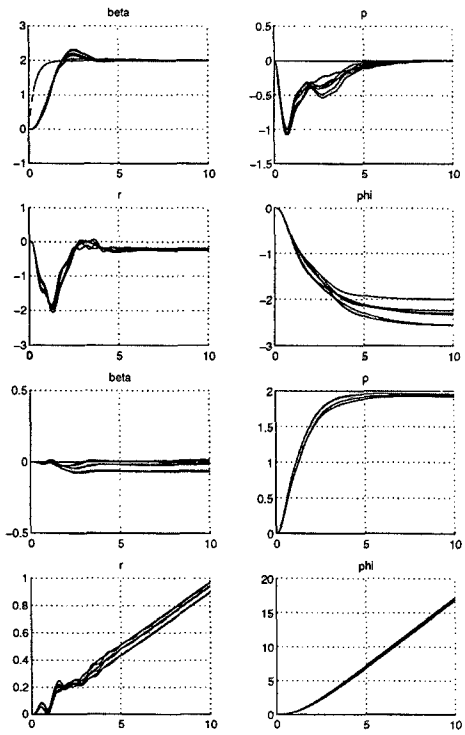

Figure 11: Illustration of robust performance for pilot demand in the time domain
Plots for 6 different mass distributions, light to heavy aircraft
Top 4 plots: 2^o sideslip demand with coordinated roll
Bottom 4 plots: $2^o/s$ roll rate demand with sideslip decoupling

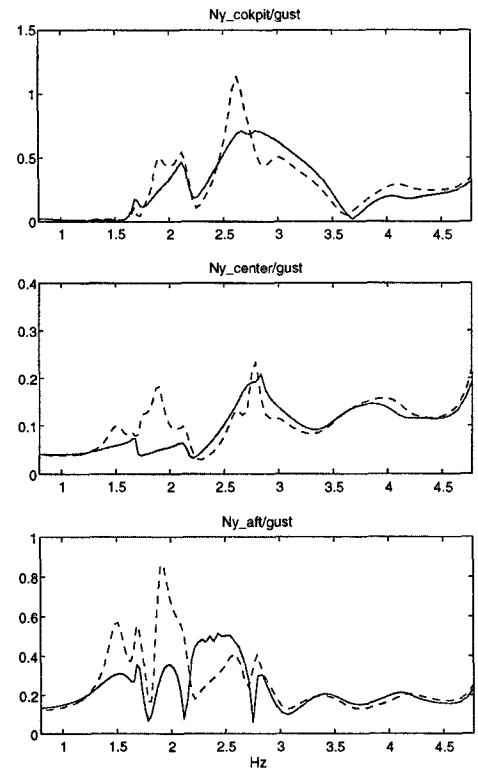

Figure 12: Illustration of gust alleviation performance in the frequency domain
Plots of lateral acceleration at various location along the fuselage:
- - open loop (no control),
- closed loop with active control

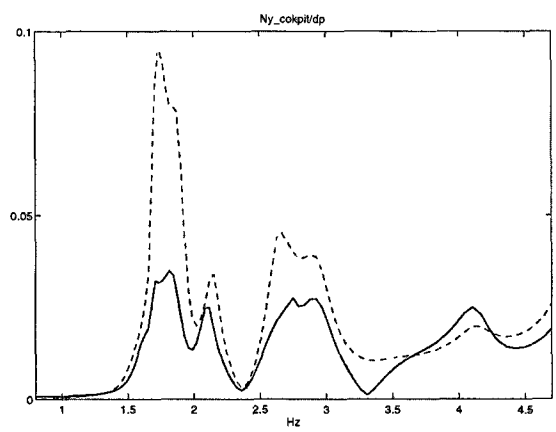

Figure 13: Minimization of pilot coupling transfer:
- - open loop (no control),
- closed loop with active control

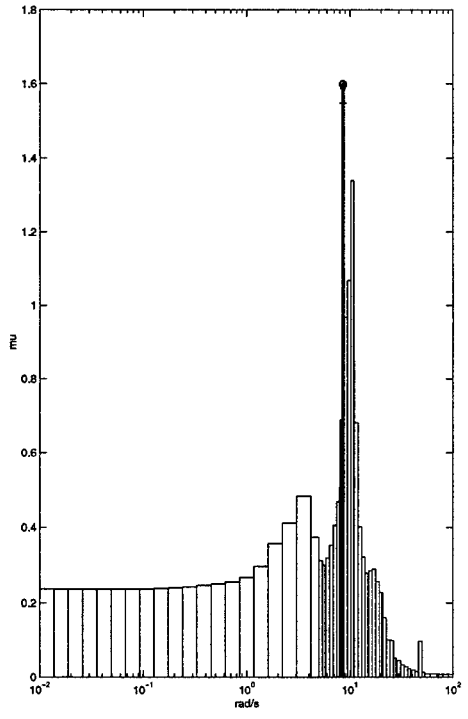

Figure 14: An example of robustness analysis using LFT representation and μ-analysis for uncertainties on flexible mode frequencies

6 Conclusion

As a result of the long-term research program COVAS in the Systems Control and Flight Dynamics department of ONERA, a methodology has been proposed and detailed in this article for flexible aircraft control. It is based on several sophisticated tools that allow:

- selection of a convenient design configuration, using multimodel analysis, and construction of a corresponding design model;
- transcription of heterogeneous specifications under a standard formulation, including standard rigid aircraft control performance specifications, more sophisticated specifications for active control of structural modes, and specifications for robustness;
- computation of controllers, using modern design and analysis techniques to achieve all rigid and flexible control specifications simultaneously ;
- validation and tuning of performance and robustness trade off, with very few *tuning parameters* for control optimization.

Research is under progress, in cooperation with AEROSPATIALE-avions, for modeling the explicit dependence of the aircraft dynamics versus structural parameters. This will allow enhancement in both performance and robustness, with possible introduction of parameter dependence in the structure of the controller.

References

[1] C. Favre, Fly-by-wire for commercial aircraft: the Airbus experience, Advances in aircraft flight control, Taylor and Francis, 1996

[2] J. Farineau, Lateral electric flight control laws of the A320 based upon eigenstructure assignment techniques, in Proceedings of the AIAA GNC conference, Boston, 1989

[3] J.M. Maciejowski, Multivariable feedback design, Electronic Systems Engineering Series, Addisson Wesley, 1989

[4] M.G. Gilbert, D.K. Schmidt and T.A.Weisshaar, Quadratic synthesis of integrated active control for an aeroelastic forward swept wing aircraft, Journal of Guidance Navigation and Control, 7-2, 1988

[5] M.G. Gilbert and D.K. Schmidt, Integrated structure/control law design by multilevel optimization, Journal of Guidance Navigation and Control, 14-5, 1991

[6] B. Newman and A. Kassem, Analytical relationships for linear quadratic aeroelastic flight control eigenvalues, Journal of Guidance Navigation and Control, 20-6, 1997

[7] F. Kubica, T. Livet, X. LeTron and A. Bucharles, Parameter robust flight control system for a flexible aircraft, Control Engineering Practice, 3-9, 1995

[8] K. Najmabadi, B. Fritchman and C. Tran, A process for model identification and validation of dynamical equations for a flexible aircraft, AGARD symposium on system identification for integrated development and flight testing, 1998

[9] I. Dardenne, Développement de méthodologies pour la synthèse de lois de commande d'un avion de transport souple, PhD thesis, SUPAERO, France, 1998

[10] S.Y. Chan, P.Y. Cheng and T. Myers, Advanced aeroservoelastic stabilization techniques for hypersonic flight vehicles, NASA Report 189702, 92

[11] B. Wie and K.W. Byun, New generalized structural filtering concept for active vibration control synthesis, Journal of Guidance Navigation and Control, 12-2, 1989

[12] F. Kubica and T. Livet, Flight control law synthesis for a flexible aircraft, In proceedings AIAA GNC conference, 1994

[13] W. Gawronski and K.B. Lim, Balanced actuator and sensor placement for flexible structures, In proceedings AIAA GNC, 1995

[14] B.S. Liebst, Accelerometer placement in active flutter suppression systems, Journal of Guidance Navigation and Control, 10-5, 1987

[15] J. Grouas, L'avion souple, Nouvelle Revue d'Aéronautique et d'Astronautique, 6, 1995

[16] D.K. Schmidt and B. Newman, Multivariable flight control synthesis and literal robustness analysis for an aeroelastic vehicle, In Proceeding AIAA GNC conference, 1990
[17] M.R. Anderson, Robustness evaluation of a flexible aircraft control system, In Proceeding AIAA GNC conference, 1990
[18] D.K. Schmidt and T.K. Chen, Frequency domain synthesis of a robust flutter suppression control law, Journal of Guidance Navigation and Control, 9-3, 1986
[19] S. Prudhomme, Reduction for aeroelastic aircraft control design: a practical approach, in Proceeding AIAA GNC conference, 1995
[20] D.C. Hyland and D.S. Bernstein, Explicit optimality conditions for fixed order dynamic compensation, in Proceedings IEEE Conference on Decision and Control, 1983
[21] J.C. Doyle, Analysis of feedback systems with structured uncertainties, in IEE Proceedings, part D, 129, 1982
[22] Y. Le Gorrec, Commande modale robuste et synthèse de gains autoséquencés, Approche multimodèle, PhD thesis, SUPAERO, France, 1998
[23] C. Hwang and W.S. Pi, Optimal control applied to aircraft flutter suppression, Journal of Guidance Navigation and Control, 7, 1984,
[24] W.E. Hopkins and J. Medanic and W.R. Perkins, Output feedback pole placement in the design of suboptimal linear quadratic, International Journal of Control, 34-3, 1981
[25] M.H. Amin, Optimal pole shifting for continuous multivariable linear systems, International Journal of Control, 41-3, 1985
[26] P.M.R. Wortelboer and O.H. Bosgra, Generalized frequency weighted balanced reduction, in Proceedings Conference on Decision and Control, 1992
[27] D. Alazard, P. Apkarian, Observer based structures of arbitrary compensators, International Journal of Robust and Nonlinear Control, 1999
[28] G. Stein and M. Athans, The LQG/LTR procedure for multivariable feedback control design , IEEE Transactions in Automatic Control, 32-2, 1987
[29] J. Douglas and M. Athans, Robust linear quadratic design with real parameter uncertainty, IEEE Transations on Automatic Control, 39-1, 1994
[30] D.K. Schmidt, Dynamics and control of hypersonic aeropropulsive aeroelastic vehicules, in Proceedings AIAA GNC conference, 1992
[31] J.F. Magni, Multimodel eigenstructure assignment in flight control design, Aerospace Science and Technology, volume 3, 1999
[32] J.M. Biannic, Commande robuste des systèmes à paramètres variables, PhD thesis, SUPAERO, France, 1996
[33] K. Seyffarth, M. Lacabanne, K Konig and H. Cassan, Comfort in turbulence for a large civil aircraft, Forum International Aéroélasticité et Dynamique de Structures, Strasbourg, France, 1993
[34] D. Alazard, A. Bucharles, G. Ferreres, J.F. Magni, S. Prudhomme, Towards a global methodology for flexible aircraft control design, ONERA-DLR Aerospace Symposium, Paris, France, 1999
[35] C. Doll, G. Ferreres, J. F. Magni, μ-Tools for Flight Control Robustness Assessment, Aerospace Science and Technology (Special Issue : flight control law design), 1998
[36] G. Ferreres, J.M. Biannic, A μ analysis technique without frequency gridding, American Control Conference, 1998

REPORT DOCUMENTATION PAGE

1. Recipient's Reference	2. Originator's References	3. Further Reference	4. Security Classification of Document
	RTO-MP-36 AC/323(AVT)TP/17	ISBN 92-837-0014-7	UNCLASSIFIED/ UNLIMITED

5. Originator Research and Technology Organization
North Atlantic Treaty Organization
BP 25, 7 rue Ancelle, F-92201 Neuilly-sur-Seine Cedex, France

6. Title
Structural Aspects of Flexible Aircraft Control

7. Presented at/sponsored by
the Specialists' Meeting of the RTO Applied Vehicle Technology Panel (AVT) held in Ottawa, Canada, 18-20 October 1999.

8. Author(s)/Editor(s)	9. Date
Multiple	May 2000
10. Author's/Editor's Address	**11. Pages**
Multiple	292

12. Distribution Statement There are no restrictions on the distribution of this document. Information about the availability of this and other RTO unclassified publications is given on the back cover.

13. Keywords/Descriptors

Flight control
Military aircraft
Flexibility
Aeroelasticity
Servomechanisms
Structural properties
Design
Static loads
Dynamic loads
Flutter
Mathematical models
Integrated systems
Control equipment
Transport aircraft
Flexible structures

14. Abstract

The Specialists' Meeting dealt with Design Issues and more specifically Structural Aspects of Flexible Aircraft Control.

Twenty six papers and a Keynote address were presented with the following objective: How the design methods used in the development of military fighter aircraft can be improved, and applied to transport aircraft design applications.

There were three sessions covering the following topics:

- Aeroservoelasticity
- Active Control of Flexible Structure I
- Active Control of Flexible Structure II

NORTH ATLANTIC TREATY ORGANIZATION

RESEARCH AND TECHNOLOGY ORGANIZATION
BP 25 • 7 RUE ANCELLE
F-92201 NEUILLY-SUR-SEINE CEDEX • FRANCE
Télécopie 0(1)55.61.22.99 • E-mail mailbox@rta.nato.int

DIFFUSION DES PUBLICATIONS
RTO NON CLASSIFIEES

L'Organisation pour la recherche et la technologie de l'OTAN (RTO), détient un stock limité de certaines de ses publications récentes, ainsi que de celles de l'ancien AGARD (Groupe consultatif pour la recherche et les réalisations aérospatiales de l'OTAN). Celles-ci pourront éventuellement être obtenues sous forme de copie papier. Pour de plus amples renseignements concernant l'achat de ces ouvrages, adressez-vous par lettre ou par télécopie à l'adresse indiquée ci-dessus. Veuillez ne pas téléphoner.

Des exemplaires supplémentaires peuvent parfois être obtenus auprès des centres nationaux de distribution indiqués ci-dessous. Si vous souhaitez recevoir toutes les publications de la RTO, ou simplement celles qui concernent certains Panels, vous pouvez demander d'être inclus sur la liste d'envoi de l'un de ces centres.

Les publications de la RTO et de l'AGARD sont en vente auprès des agences de vente indiquées ci-dessous, sous forme de photocopie ou de microfiche. Certains originaux peuvent également être obtenus auprès de CASI.

CENTRES DE DIFFUSION NATIONAUX

ALLEMAGNE
Streitkräfteamt / Abteilung III
Fachinformationszentrum der Bundeswehr, (FIZBw)
Friedrich-Ebert-Allee 34
D-53113 Bonn

BELGIQUE
Coordinateur RTO - VSL/RTO
Etat-Major de la Force Aérienne
Quartier Reine Elisabeth
Rue d'Evère, B-1140 Bruxelles

CANADA
Directeur - Recherche et développement - Communications et gestion de l'information - DRDCGI 3
Ministère de la Défense nationale
Ottawa, Ontario K1A 0K2

DANEMARK
Danish Defence Research Establishment
Ryvangs Allé 1, P.O. Box 2715
DK-2100 Copenhagen Ø

ESPAGNE
INTA (RTO/AGARD Publications)
Carretera de Torrejón a Ajalvir, Pk.4
28850 Torrejón de Ardoz - Madrid

ETATS-UNIS
NASA Center for AeroSpace Information (CASI)
Parkway Center
7121 Standard Drive
Hanover, MD 21076-1320

FRANCE
O.N.E.R.A. (ISP)
29, Avenue de la Division Leclerc
BP 72, 92322 Châtillon Cedex

GRECE (Correspondant)
Hellenic Ministry of National Defence
Defence Industry Research & Technology General Directorate
Technological R&D Directorate
D.Soutsou 40, GR-11521, Athens

HONGRIE
Department for Scientific Analysis
Institute of Military Technology
Ministry of Defence
H-1525 Budapest P O Box 26

ISLANDE
Director of Aviation
c/o Flugrad
Reykjavik

ITALIE
Centro documentazione tecnico-scientifica della Difesa
Via Marsala 104
00185 Roma

LUXEMBOURG
Voir Belgique

NORVEGE
Norwegian Defence Research Establishment
Attn: Biblioteket
P.O. Box 25, NO-2007 Kjeller

PAYS-BAS
NDRCC
DGM/DWOO
P.O. Box 20701
2500 ES Den Haag

POLOGNE
Chief of International Cooperation Division
Research & Development Department
218 Niepodleglosci Av.
00-911 Warsaw

PORTUGAL
Estado Maior da Força Aérea
SDFA - Centro de Documentação
Alfragide
P-2720 Amadora

REPUBLIQUE TCHEQUE
VTÚL a PVO Praha / Air Force Research Institute Prague
Národní informační středisko obranného výzkumu (NISČR)
Mladoboleslavská ul., 197 06 Praha 9

ROYAUME-UNI
Defence Research Information Centre
Kentigern House
65 Brown Street
Glasgow G2 8EX

TURQUIE
Millî Savunma Başkanliği (MSB)
ARGE Dairesi Başkanliği (MSB)
06650 Bakanliklar - Ankara

AGENCES DE VENTE

NASA Center for AeroSpace Information (CASI)
Parkway Center
7121 Standard Drive
Hanover, MD 21076-1320
Etats-Unis

The British Library Document Supply Centre
Boston Spa, Wetherby
West Yorkshire LS23 7BQ
Royaume-Uni

Canada Institute for Scientific and Technical Information (CISTI)
National Research Council
Document Delivery
Montreal Road, Building M-55
Ottawa K1A 0S2, Canada

Les demandes de documents RTO ou AGARD doivent comporter la dénomination "RTO" ou "AGARD" selon le cas, suivie du numéro de série (par exemple AGARD-AG-315). Des informations analogues, telles que le titre et la date de publication sont souhaitables. Des références bibliographiques complètes ainsi que des résumés des publications RTO et AGARD figurent dans les journaux suivants:

Scientific and Technical Aerospace Reports (STAR)
STAR peut être consulté en ligne au localisateur de ressources uniformes (URL) suivant:
http://www.sti.nasa.gov/Pubs/star/Star.html
STAR est édité par CASI dans le cadre du programme NASA d'information scientifique et technique (STI)
STI Program Office, MS 157A
NASA Langley Research Center
Hampton, Virginia 23681-0001
Etats-Unis

Government Reports Announcements & Index (GRA&I)
publié par le National Technical Information Service
Springfield
Virginia 2216
Etats-Unis
(accessible également en mode interactif dans la base de données bibliographiques en ligne du NTIS, et sur CD-ROM)

Imprimé par le Groupe Communication Canada Inc.
(membre de la Corporation St-Joseph)
45, boul. Sacré-Cœur, Hull (Québec), Canada K1A 0S7

NORTH ATLANTIC TREATY ORGANIZATION

RESEARCH AND TECHNOLOGY ORGANIZATION
BP 25 • 7 RUE ANCELLE
F-92201 NEUILLY-SUR-SEINE CEDEX • FRANCE
Telefax 0(1)55.61.22.99 • E-mail mailbox@rta.nato.int

DISTRIBUTION OF UNCLASSIFIED
RTO PUBLICATIONS

NATO's Research and Technology Organization (RTO) holds limited quantities of some of its recent publications and those of the former AGARD (Advisory Group for Aerospace Research & Development of NATO), and these may be available for purchase in hard copy form. For more information, write or send a telefax to the address given above. **Please do not telephone.**

Further copies are sometimes available from the National Distribution Centres listed below. If you wish to receive all RTO publications, or just those relating to one or more specific RTO Panels, they may be willing to include you (or your organisation) in their distribution.

RTO and AGARD publications may be purchased from the Sales Agencies listed below, in photocopy or microfiche form. Original copies of some publications may be available from CASI.

NATIONAL DISTRIBUTION CENTRES

BELGIUM
Coordinateur RTO - VSL/RTO
Etat-Major de la Force Aérienne
Quartier Reine Elisabeth
Rue d'Evère, B-1140 Bruxelles

CANADA
Director Research & Development
Communications & Information
Management - DRDCIM 3
Dept of National Defence
Ottawa, Ontario K1A 0K2

CZECH REPUBLIC
VTÚL a PVO Praha /
Air Force Research Institute Prague
Národní informační středisko
obranného výzkumu (NISČR)
Mladoboleslavská ul., 197 06 Praha 9

DENMARK
Danish Defence Research
Establishment
Ryvangs Allé 1, P.O. Box 2715
DK-2100 Copenhagen Ø

FRANCE
O.N.E.R.A. (ISP)
29 Avenue de la Division Leclerc
BP 72, 92322 Châtillon Cedex

GERMANY
Streitkräfteamt / Abteilung III
Fachinformationszentrum der
Bundeswehr, (FIZBw)
Friedrich-Ebert-Allee 34
D-53113 Bonn

GREECE (Point of Contact)
Hellenic Ministry of National
Defence
Defence Industry Research &
Technology General Directorate
Technological R&D Directorate
D.Soutsou 40, GR-11521, Athens

HUNGARY
Department for Scientific
Analysis
Institute of Military Technology
Ministry of Defence
H-1525 Budapest P O Box 26

ICELAND
Director of Aviation
c/o Flugrad
Reykjavik

ITALY
Centro documentazione
tecnico-scientifica della Difesa
Via Marsala 104
00185 Roma

LUXEMBOURG
See Belgium

NETHERLANDS
NDRCC
DGM/DWOO
P.O. Box 20701
2500 ES Den Haag

NORWAY
Norwegian Defence Research
Establishment
Attn: Biblioteket
P.O. Box 25, NO-2007 Kjeller

POLAND
Chief of International Cooperation
Division
Research & Development
Department
218 Niepodleglosci Av.
00-911 Warsaw

PORTUGAL
Estado Maior da Força Aérea
SDFA - Centro de Documentação
Alfragide
P-2720 Amadora

SPAIN
INTA (RTO/AGARD Publications)
Carretera de Torrejón a Ajalvir, Pk.4
28850 Torrejón de Ardoz - Madrid

TURKEY
Millî Savunma Başkanliği (MSB)
ARGE Dairesi Başkanliği (MSB)
06650 Bakanliklar - Ankara

UNITED KINGDOM
Defence Research Information
Centre
Kentigern House
65 Brown Street
Glasgow G2 8EX

UNITED STATES
NASA Center for AeroSpace
Information (CASI)
Parkway Center
7121 Standard Drive
Hanover, MD 21076-1320

SALES AGENCIES

NASA Center for AeroSpace Information (CASI)
Parkway Center
7121 Standard Drive
Hanover, MD 21076-1320
United States

The British Library Document Supply Centre
Boston Spa, Wetherby
West Yorkshire LS23 7BQ
United Kingdom

Canada Institute for Scientific and Technical Information (CISTI)
National Research Council
Document Delivery
Montreal Road, Building M-55
Ottawa K1A 0S2, Canada

Requests for RTO or AGARD documents should include the word 'RTO' or 'AGARD', as appropriate, followed by the serial number (for example AGARD-AG-315). Collateral information such as title and publication date is desirable. Full bibliographical references and abstracts of RTO and AGARD publications are given in the following journals:

Scientific and Technical Aerospace Reports (STAR)
STAR is available on-line at the following uniform resource locator:
http://www.sti.nasa.gov/Pubs/star/Star.html
STAR is published by CASI for the NASA Scientific and Technical Information (STI) Program
STI Program Office, MS 157A
NASA Langley Research Center
Hampton, Virginia 23681-0001
United States

Government Reports Announcements & Index (GRA&I)
published by the National Technical Information Service
Springfield
Virginia 22161
United States
(also available online in the NTIS Bibliographic Database or on CD-ROM)

Printed by Canada Communication Group Inc.
(A St. Joseph Corporation Company)
45 Sacré-Cœur Blvd., Hull (Québec), Canada K1A 0S7

ISBN 92-837-0014-7